Avoiding tumor resistance – different approaches for new chemotherapeutic agents and their mechanistic assessment

DISSERTATION

von

Madeleine Johanna Maria Gold

Bayreuth, 2020

UNIVERSITÄT
BAYREUTH

UNIVERSITÄT BAYREUTH

Avoiding tumor resistance – different approaches for new chemotherapeutic agents and their mechanistic assessment

DISSERTATION

zur Erlangung des akademischen Grades einer Doktorin der Naturwissenschaften (Dr. rer. nat.)
in der Bayreuther Graduiertenschule für Mathematik und Naturwissenschaften (BayNAT)
der Universität Bayreuth

vorgelegt von

Madeleine Johanna Maria Gold

aus Pegnitz

Bayreuth, 2020

Die vorliegende Arbeit wurde in der Zeit von April 2017 bis Oktober 2020 in Bayreuth am Lehrstuhl für Organische Chemie I unter Betreuung von Herrn Professor Dr. Rainer Schobert angefertigt.

Vollständiger Abdruck der von der Bayreuther Graduiertenschule für Mathematik und Naturwissenschaften (BayNAT) der Universität Bayreuth genehmigten Dissertation zur Erlangung des akademischen Grades einer Doktorin der Naturwissenschaften (Dr. rer. nat.).

Dissertation eingereicht am:	20.11.2020
Zulassung durch das Leitungsgremium:	07.12.2020
Wissenschaftliches Kolloquium:	23.07.2021

Amtierender Direktor:	Prof. Dr. Markus Lippitz

Prüfungsausschuss:

Prof. Dr. Rainer Schobert	(Gutachter)
Prof. Dr. Katharina Pachmann	(Gutachterin)
Prof. Dr. Klaus Ersfeld	(Vorsitz)
Prof. Dr. Matthias Ullmann	

(Weitere Gutachter: Prof. Dr. Michael Höpfner)

“Success is not final, failure is not fatal: it is the courage to continue that counts.”

— Winston Churchill

Abkürzungsverzeichnis

5-FU	5-Fluoruracil
ABC	*ATP-binding cassette transporter*
ADP	Adenosindiphosphat
AML	akute, myeloische Leukämie
Apaf-1	*apoptosis protease-activating factor-1*
AraC	*cytosine arabinoside*
ATP	Adenosintriphosphat
Bak	*Bcl-2 homologous antagonist killer*
Bax	*Bcl-2-associated X protein*
Bcl-2	*B-cell lymphoma 2*
BCRP	*breast cancer resistance protein*
CAM	Chorioallantoismembran
CA4	Combretastatin A-4
C(E)TC	*circulating (epithelial) tumor cell*
CDDP	Cisplatin; cis-Diammindichloridoplatin
CDK1	Cyclin-abhängige Kinase 1
c-FLIP	*cellular-FLICE inhibitory protein*
CPT	Camptothecin(e)
CTLA4	*cytotoxic T-lymphocyte-associated protein 4*
DLC	*delocalized lipophilic cation*
DISC	*death-inducing signalling complex*
DMF	Dimethylformamid
DMSO	Dimethylsulfoxid
DNA	Desoxyribonukleinsäure

DR5	*death receptor 5*
EMSA	*electrophoretic mobility shift assay*
EMT	Epithelial-mesenchymale Transition
EpCAM	*epithelial cell adhesion molecule*
ERCC1	*excision repair cross-complementing protein 1*
EZM	extrazelluläre Matrix
GSH	Glutathion
GST	Glutathion-S-Transferase
IAP	*inhibitors of apoptosis protein*
IC_{50}	halbmaximale, inhibitorische Konzentration
MBA	*microtubule binding agent*
MDR	*multidrug resistance*
MDR1	*multidrug resistance protein 1*
MET	Mesenchymal-epitheliale Transition
MOMP	*mitochondrial outer membrane permeabilisation*
MRD	*minimal residual disease*
MRP1	*multidrug resistance-associated protein 1*
MTA	*microtubule targeting agents*
MTT	3-(4,5-Dimethylthiazol-2-yl)-2,5-diphenyltetrazoliumbromid
NHC	*N*-heterozyklische Carbene
oc	*open circular*
P-gp	P-Glykoprotein
P_i	anorganisches Phosphat
PD-1	*programmed cell death protein 1*
PD-L1	*programmed cell death ligand 1*

PET-CT	Positronenemissionstomographie-Computertomographie
PI	Propidiumiodid
Puma	*p53 upregulated modulator of apoptosis*
Rb	*retinoblastoma protein*
ROS	reaktive Sauerstoffspezies
SA-ßgal	*senescence-associated ß-galactosidase*
sc	*supercoiled*
SI	Selektivitätsindex
SIV	subintestinale Venen
TIS	Therapie-induzierte Seneszenz
TopoI	Topoisomerase I
TopoII	Topoisomerase II
TMD	Transmembrandomäne
TME	Tumor-*Microenviroment*
TSZ	Tumorstammzelle(n)
VDA	*vascular disrupting agent*
VEGF	*vascular endothelial growth factor*
VTA	*vascular targeting agent*
ZPD	zytoplasmatische Domäne

Bei allen weiteren Abkürzungen handelt es sich um gängige Abkürzungen und SI-Einheiten, welche laut ihrer Definition verwendet wurden.

Summary

With growing biochemical knowledge and the development of targeted therapies since the beginning of the 21st century, the individualization of therapy for every single patient and their tumor has taken center stage in cancer research. Despite all advancements in this field, in 90% of cases chemoresistance is responsible for the failure of antitumoral therapy. For this reason there is a considerable demand for new therapeutic agents, selectively addressing resistant tumor cells, but also for new biomarkers enabling an early detection of existing or imminent resistance.

In the first section of this work, some preclinical studies of new potential drug candidates, which were designed to avoid chemoresistance in different ways, are described. Moreover, the assessment of their particular mechanisms of action on a molecular level was in the focus.

Two new series of drugs aimed at the circumvention of p53-related chemoresistance. As p53 plays a key role in the induction of apoptosis, cells with p53 mutations are significantly less sensitive or even resistant against apoptosis-inducing stimuli, e.g. chemotherapeutic agents. In this work, new ruthenium(II) and gold(I) complexes inducing apoptosis in a p53-independent way were investigated.

A benzochromene ruthenium(II) complex derived from lawsone (2-hydroxy-1,4-naphthoquinone), the pigment and active ingredient of the henna plant, avoids p53-dependency by induction of cellular senescence. Therapy-induced senescence represents one alternative to conventional cytotoxic chemotherapy and implicates even more advantages. As its aim is not to eliminate malignant cells, but to irreversible inhibit their proliferation, side effects for the patient could be reduced especially in the longtime treatment of specific cancer types.

Also [1,3-diethyl-4,5-diarylimidazol-2-yliden](L) gold(I) complexes showed activity against tumor cells independent from their p53 mutational status. By confocal microscopy with 518A2 melanoma cells, organelle-specific cellular uptake of those complexes was observed. Whereas, mainly the nature of ligand L, responsible for the complex charge, size and lipophilicity, was decisive for the site of cellular accumulation. This concept of controlling the intracellular distribution of metallodrugs by choice of secondary ligands and the complex charge could be exploited in a rational design of drugs particularly active against resistant tumor cells.

Topoisomerase I inhibitors are established antitumoral agents mainly applied within combination regimens. The high rate of chemoresistance development also represents a big issue for this kind of therapy. To date, the camptothecin family agents, like topotecan or irinotecan, are the only topoisomerase I-specific drugs with clinical approval. With camptothecin resistance often significantly depending on the molecular structure of the agent, the implementation of a novel, structural-independent class of topoisomerase I inhibitors may contribute to bypass this problem. In the scope of this work, three topoisomerase I inhibiting copper(II) complexes with Schiff base-like ligands were identified. In contrast to established copper complexes with topoisomerase I inhibiting activity, neither an interaction

with DNA nor an impact on the intracellular concentration of reactive oxygen species was observed. The new copper(II) complexes with Schiff base-like ligands are potentially interesting drug candidates for further studies.

Another possibility for the avoidance of tumor resistance are pleiotropic agents that address more than one cellular target at a time. Derived from the concept of polychemotherapy - to date the most successful approach to prevent the development of chemoresistance - these agents aim to reduce side effects, as well as pharmacokinetic discrepancies between individual combinational drugs. In this work, a series of multimodal thienopyrimidone derivatives were tested regarding their antitumoral properties. From a structural point of view, these substances combine the ß-tubulin binding 3,4,5-trimethoxyphenyl fragment with the biologically active thieno[2,3-*d*]pyrimidone pharmacophore. By means of different *in vitro* and *in vivo* assays, one derivative with improved activity and tolerability compared to the reported lead structures was identified within the series.

In the second part of this work, a potential monitoring tool for the early detection of therapy response in patients with colorectal cancer was investigated via a clinical *proof-of-principle* study.

Circulating tumor cells are an important link between the primary tumor and distant metastasis and are readily accessible from the blood of cancer patients. Moreover, they reflect changes of the tumor cells on a translational, transcriptional, or genetic level in real-time, enabling the early realization of upcoming resistances. Different studies have already demonstrated that the longitudinal monitoring of the number and properties of circulating tumor cells provide valuable information on therapy response and disease progression. In the case of non-metastatic colorectal cancer patients, the detection rate via established techniques is too low to further analyze potential correlations. This work demonstrates that the Maintrac® method is appropriate for the monitoring of circulating tumor cells during therapy in patients with colorectal cancer of all stages. Although this study´s results confirm reported trends, further studies with bigger patients´ collectives have to show, which conclusions for therapy decisions may be implicated from the profile of circulating tumor cells during therapy of colorectal cancer patients.

Zusammenfassung

Mit immer weiter fortschreitendem biochemischen Verständnis, sowie der Entwicklung von zielgerichteten Therapien, steht seit Beginn des 21. Jahrhunderts nunmehr die Individualisierung der Tumortherapie für den jeweiligen Patienten und dessen Tumor im Fokus der Krebsforschung. Trotz aller Fortschritte sind in 90% der Fälle Chemoresistenzen für das Scheitern einer Therapie verantwortlich. Aus diesem Grund besteht ein enormer Bedarf an neuen Wirkstoffen, welche insbesondere resistente Tumorzellen adressieren, aber auch an neuartigen Biomarkern, welche ein frühzeitiges Erkennen be- oder entstehender Resistenzen ermöglichen.

Im ersten Teil dieser Arbeit wurden präklinische Untersuchungen neuer, potentieller Wirkstoffkandidaten durchgeführt, welche jeweils in unterschiedlicher Weise für die Umgehung von Chemoresistenzen konzipiert worden waren. Auch die Aufklärung der jeweiligen Wirkmechanismen auf molekularer Ebene stand hierbei im Fokus.

Zwei neuartige Wirkstoffserien hatten hierbei die Umgehung der durch p53-Mutation hervorgerufenen Chemoresistenz zum Ziel. Da p53 eine Schlüsselrolle in der Einleitung von Apoptose zukommt, sind betroffene Zellen wesentlich insensitiver bis resistent gegen Apoptose-induzierende Stimuli, wie beispielsweise chemotherapeutische Wirkstoffe. In dieser Arbeit werden neuartige Ruthenium(II)- und Gold(I)-Komplexe untersucht, die p53-unabhängig Apoptose induzieren können.

Ein von Lawson (2-Hydroxy-1,4-naphthoquinon), dem Farb- und Wirkstoff der Hennapflanze, abgeleiteter Benzochromen-Ruthenium(II)-Komplex umgeht hierbei die p53-Abhängigkeit durch die Induktion zellulärer Seneszenz. Die Therapie-induzierte Seneszenz stellt eine potentielle Alternative zur konventionellen, zytotoxischen Chemotherapie dar und birgt weitere Vorteile: da ihr Ziel nicht die Elimination maligner Zellen, sondern die irreversible Inhibition ihrer Proliferation ist, könnten so insbesondere in der Langzeitbehandlung bestimmter Krebsarten Nebenwirkungen für den Patienten reduziert werden.

Auch [1,3-diethyl-4,5-diarylimidazol-2-yliden](L)-Gold(I)-NHC-Komplexe überzeugten durch ihre vom p53-Mutationsstatus unabhängige Wirksamkeit gegen Tumorzellen. Durch konfokalmikroskopische Studien an 518A2 Melanomzellen konnte ihre Organell-spezifische Aufnahme beobachtet werden, welche hauptsächlich von der Natur des Liganden L bzw. von diesem bestimmt, von der Ladung, Größe und Lipophilie der Komplexe abhängig ist. Diese Erkenntnisse könnten für das rationale Design von Target-spezifischen metallbasierten Wirkstoffen mit besonderer Effektivität gegen Apoptose-resistente Tumore von großer Bedeutung sein.

Topoisomerase I-Inhibitoren sind etablierte antitumorale Wirkstoffe, die klinisch vor allem im Rahmen von Kombinationsregimen eingesetzt werden. Eine große Problematik stellt auch in diesem Fall die hohe Rate der Resistenzentwicklung dar. Wirkstoffe der Camptothecin-Familie, wie Topotecan oder Irinotecan, sind aktuell die einzigen Topoisomerase I-spezifischen Substanzen mit klinischer Zulassung. Da Camptothecin-Resistenz in vielen Fällen maßgeblich von der Struktur des Wirkstoffes abhängig ist,

kann diese potentiell durch die Einführung einer strukturell neuartigen Klasse an Topoisomerase I-Inhibitoren umgangen werden. Im Rahmen dieser Arbeit konnten innerhalb einer Serie von Kupfer(II)-Komplexen mit Schiff-Base ähnlichen Liganden durch Zytotoxizitätstests drei besonders aktive Verbindungen identifiziert werden, welche das Enzym Topoisomerase I inhibieren. Da diese Verbindungen, im Gegensatz zu bereits bekannten Kupferkomplexen mit Topoisomerase I-inhibierender Wirkung, weder eine Interaktion mit DNA, noch einen Einfluss auf die intrazelluläre Konzentration an reaktiven Sauerstoffspezies zeigten, stellen sie interessante Wirkstoffkandidaten für weitere Studien dar.

Eine weitere Möglichkeit zur Umgehung von Chemoresistenzen sind pleiotrope Wirkstoffe, das heißt Substanzen, die mehrere zelluläre Targets gleichzeitig adressieren. Abgeleitet vom bisher erfolgreichsten Konzept zur Vermeidung von Resistenzen - der Polychemotherapie - sollen diese Wirkstoffe zur Vermeidung starker Nebenwirkungen, sowie pharmakokinetischer Diskrepanzen zwischen den einzelnen Kombinationswirkstoffen beitragen. In dieser Arbeit wurde eine Serie an multimodalen Thienopyrimidon-Derivaten bezüglich ihrer antitumoralen Eigenschaften untersucht. Strukturell vereinen diese Verbindungen das 3,4,5-Trimethoxyphenyl-Fragment, welches an ß-Tubulin bindet, mit dem biologisch aktiven Thieno[2,3-*d*]pyrimidon-Pharmakophor. Mittels verschiedener *in vitro* und *in vivo* Tests konnte innerhalb der getesteten Serie neuartiger Verbindungen ein Derivat identifiziert werden, welches mit verbesserter Aktivität und Verträglichkeit eine Weiterentwicklung der literaturbekannten Leitstruktur darstellt.

Im zweiten Teil dieser Arbeit wurde mit Hilfe einer klinischen *proof-of-principle* Studie ein potentielles Monitoring-Verfahren zur frühzeitigen Erkennung des Therapieansprechens bei Patienten mit kolorektalem Karzinom untersucht. Zirkulierende Tumorzellen stellen das Bindeglied zwischen Primärtumor und Fernmetastasen dar, und können im Blut von Tumorpatienten relativ einfach quantifiziert und charakterisiert werden. Darüber hinaus spiegeln sie Veränderungen des Tumors auf translationaler, transkriptionaler oder genetischer Ebene in Echtzeit wieder, wodurch auch entstehende Resistenzen frühzeitig erkannt werden können. Zahlreiche Studien haben gezeigt, dass die longitudinale Überwachung der Anzahl und Eigenschaften der zirkulierenden Tumorzellen im Blut von Krebspatienten wertvolle Informationen bezüglich des Ansprechens einer Therapie oder dem Fortschreiten der Erkrankung beisteuern kann. Im Falle nicht metastasierter Patienten mit kolorektalem Karzinom, jedoch, ist die Detektionsrate unter Verwendung etablierter Methoden zu gering um mögliche Zusammenhänge zu untersuchen. In dieser Arbeit konnte nachgewiesen werden, dass die Maintrac®-Methode ein geeignetes Verfahren für das Stadien-unabhängige Monitoring zirkulierender Tumorzellen im Therapieverlauf bei Patienten mit kolorektalem Karzinom darstellt. Obwohl die gewonnenen Ergebnisse bereits in der Literatur beschriebene Trends bestätigen, müssen weitere Studien mit größeren Patientenkollektiven zeigen, welche Schlussfolgerungen aus dem CETC-Verlauf der Patienten für Therapieentscheidungen gezogen werden könnten.

1. Einleitung

1.1. Tumorresistenzen in der Chemotherapie

Mitte des 20. Jahrhunderts fanden die ersten Chemotherapeutika (wie Stickstoffloste[1] oder Aminopterin[2]) ihren Weg in die klinische Anwendung und es konnten zunächst gute Erfolge bei der Behandlung maligner Tumore erzielt werden. Allerdings stellte man schnell fest, dass nicht alle Patienten gleichermaßen auf die Therapien ansprachen, und dass die Erkrankung häufig nach einer anfänglichen Remission aufgrund von Resistenzentwicklung rezidivierte. Die ersten Lösungsansätze konnten hierbei aus der Mikrobiologie, wo man auch mit Wirkstoffresistenzen zu kämpfen hatte, abgeleitet werden: man ging von der Monotherapie mit nur einem einzigen Wirkstoff, zur Kombinations-, bzw. Polychemotherapie über, bei welcher mehrere Wirkstoffe mit verschiedenen zellulären Angriffspunkten gleichzeitig oder nacheinander verabreicht wurden.[3] Da dieser Ansatz für verschiedene Formen des Lymphoms, sowie Brust- und Hodenkrebs erstaunlich gut funktionierte,[4] wurde die Kombinationstherapie zum neuen Paradigma der Chemotherapie und es entwickelten sich von da an immer komplexere und ausgefeiltere Therapieregime. Zu Beginn des 21. Jahrhunderts begann die Weiterentwicklung der Polychemotherapie zu stagnieren und es entstanden mit zunehmendem biochemischen Verständnis erste zielgerichtete Strategien zur Behandlung von Krebs, welche auf die sogenannten *Hallmarks of Cancer* abzielten.[5,6] Allerdings profitierten nur einige, wenige Patienten mit bestimmten genetischen Merkmalen von diesen zielgerichteten Therapien, und auch in diesen Fällen war die Entstehung von Resistenzen kein seltenes Phänomen.[7] Einen noch jüngeren Ansatz in der Krebsmedizin stellt die Immuntherapie dar, bei der monoklonale Antikörper, beispielsweise anti-CTLA4[8] oder anti-PD-1/PD-L1,[9] verwendet werden um negative Regulationsmechanismen des adaptiven Immunsystems aufzuheben, wodurch dieses wieder dazu befähigt wird, die maligne entarteten Zellen zu erkennen und zu eliminieren. Im Rahmen klinischer Studien zeigte die Immuntherapie bereits gute Ansprechraten, sowie eine deutliche Verlängerung des progressionsfreien Überlebens für bestimmte Patientengruppen.[10] Die initiale Resistenz einiger Tumoren, sowie die Entstehung von Resistenzen in anfänglich sensitiven Tumoren stellt auch im Falle der Immuntherapie das Hauptproblem dar, welches oft zum Scheitern der Behandlung führt.[11]

Demnach ist offensichtlich, dass die Aufklärung der zahlreichen Resistenzmechanismen einerseits, aber auch die Suche nach neuen Wirkstoffen, die entweder Aktivität gegen ebendiese resistenten Tumorzellen zeigen oder Resistenz-vermeidende Wirkmechanismen besitzen wichtige Aspekte der modernen Krebsforschung darstellen.

1.2. Mechanismen der Resistenzentwicklung

Ist ein Tumor resistent gegen ein bestimmtes Chemotherapeutikum, so können dieser Resistenz verschiedene Mechanismen auf systemischem, regionalem oder lokalem Niveau zu Grunde liegen (siehe Abb. 1). Unter systemischer oder pharmakokinetischer Resistenz fasst man Resistenzmechanismen zusammen, die ihren Ursprung in der Absorption (Aufnahme), Distribution (Verteilung), dem Metabolismus oder der Exkretion (Ausscheidung) eines Wirkstoffes im oder aus dem Organismus haben.[12] Der Begriff »Regionale Resistenzmechanismen« beschreibt Aspekte, welche die Interaktion zwischen Tumor und Wirtsorganismus betreffen, wie beispielsweise die Morphologie der regional vorhandenen Vaskulatur oder die Blutviskosität.[12] Sowohl systemische, als auch regionale Resistenzmechanismen stehen in direktem Zusammenhang mit dem Wirtsorganismus selbst und können in präklinischen Studien nicht berücksichtigt werden. Bei der Suche nach neuen Wirkstoffen spielen deshalb zunächst lokale, vom Tumor oder Tumor-*Microenvironment* (TME) ausgehende Resistenzen eine Rolle, da sie unter *in vitro*-Bedingungen (z. B. durch Tumorzelllinien) simuliert werden können. Die wichtigsten lokalen Resistenzmechanismen sollen in den nachfolgenden Abschnitten genauer betrachtet werden.

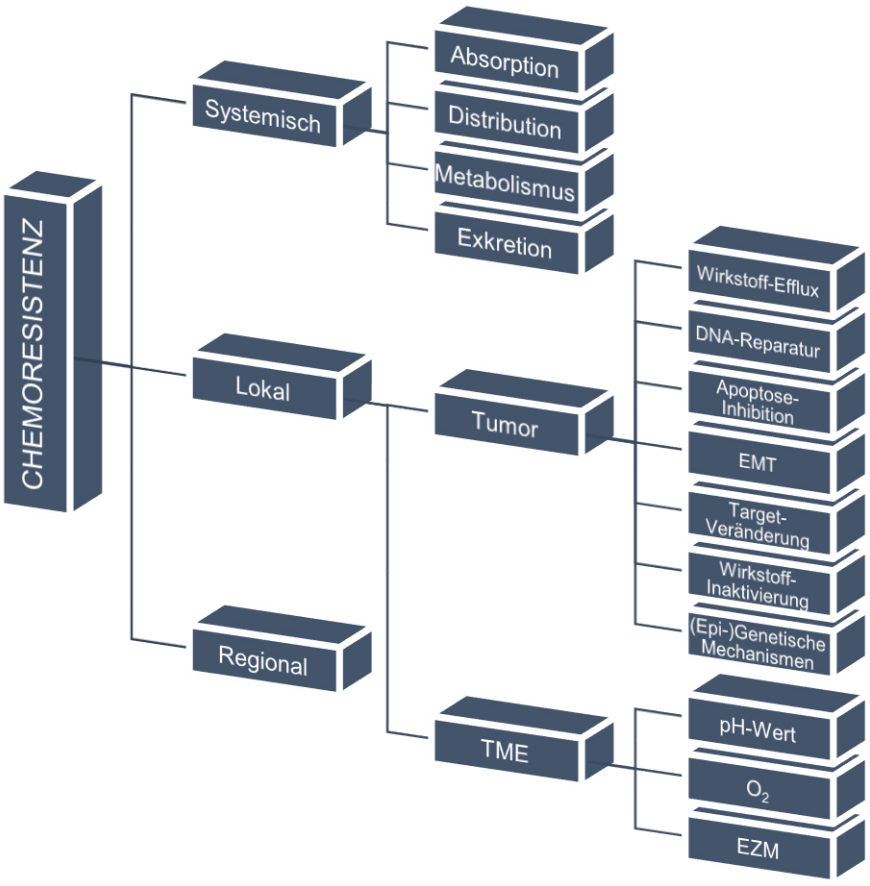

Abbildung 1. Übersicht über die wichtigsten Resistenzmechanismen. Diese können auf systemischem, regionalem und lokalem Level entstehen. TME = Tumor-*Microenvironment*; EMT = Epithelial-Mesenchymale Transition, EZM = Extrazelluläre Matrix. (Eigene Darstellung nach Alfarouk *et al.* 2015.[12])

1.2.1. Tumor-bedingte Resistenzmechanismen

Neben pharmakokinetischen oder anderen vom Wirtsorganismus beeinflussten Ursachen, kann eine Chemoresistenz auch direkt in den Tumorzellen selbst entstehen. Tumor-bedingte Resistenzmechanismen haben ihren Ursprung in genetischen, epigenetischen, metabolischen oder anderweitigen Veränderungen der Tumorzellen selbst. Im Folgenden sollen die in Abb. 1 aufgeführten lokalen, Tumor-bedingten Resistenzmechanismen genauer beschrieben werden.

1.2.1.1. Wirkstoff-Efflux

Der wohl bekannteste und am besten erforschte Resistenzmechanismus ist die Fähigkeit bestimmter Tumorzellen, Wirkstoffe relativ unspezifisch aus der Zelle auszuschleusen. Dafür verantwortlich sind Transmembranproteine der Familie der *ATP-binding cassette* (ABC)-Transporter, deren physiologische Funktion im Schutz der Zelle vor Toxinen liegt.[13] Strukturell bestehen ABC-Transporter aus zwei zytoplasmatischen Domänen (ZPD), die für die Bindung von ATP verantwortlich sind, sowie zwei relativ variablen transmembranen Domänen (TMD).[13] Bindet nun ein passendes Substrat an die TMD des Enzyms, so kommt es durch Hydrolyse von ATP zu einer Konformationsänderung des Proteins und das Substrat wird in den Extrazellulärraum entlassen (siehe Abb. 2).[14] Insbesondere drei ABC-Transporter – *multidrug resistance protein 1* (MDR1), *multidrug resistance-associated protein 1* (MRP1), und *breast cancer resistance protein* (BCRP) – werden in Tumorzellen überexprimiert. Ihnen allen gemeinsam ist ihre geringe Substratspezifität, die den Efflux einer ganzen Reihe strukturell verschiedener Wirkstoffe (Taxane, Alkaloide, Kinase-Inhibitoren, u.a.) ermöglicht.[15] Durch den kontinuierlichen Abtransport der Wirkstoffe aus dem Zytoplasma kann die intrazelluläre Wirkstoffkonzentration gering gehalten und die zytotoxische Effizienz teilweise bis hin zum absoluten Wirkungsverlust herabgesetzt werden.

1.2.1.2. DNA-Reparaturmechanismen

DNA-Reparaturmechanismen spielen eine wichtige Rolle bei der Entstehung von Resistenzen gegen Wirkstoffe, deren direktes oder indirektes zelluläres Target die DNA ist. Durch die (übermäßige) Aktivierung bestimmter Signalwege können die durch den Wirkstoff hervorgerufenen DNA-Läsionen rückgängig gemacht werden und die Tumorzelle kann der Wirkung des Chemotherapeutikums entfliehen.[15] Platin-basierte Agenzien, wie beispielsweise Cisplatin (CDDP), verursachen DNA *crosslinks*, was schließlich zur Induktion von Apoptose führt. In vielen CDDP-resistenten Tumorzellen wird ERCC1 (*excision repair cross-complementing protein 1*) überexprimiert, wodurch es zu einer erhöhten Aktivität der Nukleotidexzisionsreparatur kommt und die DNA-Läsionen durch nachfolgende homologe Rekombination behoben werden können.[16] Im therapeutischen Kontext kann die Inhibition bestimmter Signalwege des DNA-Reparatursystems auch zur Sensibilisierung resistenter Tumore genutzt werden.[17]

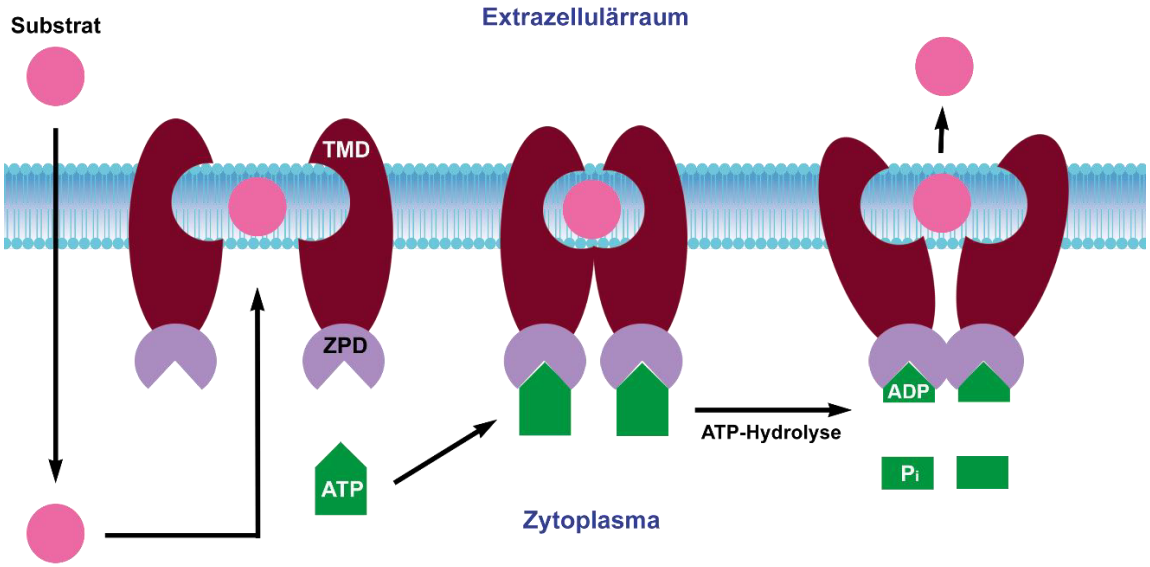

Abbildung 2. Funktionsweise eines ABC-Transporters. ABC-Transporter sind Energie-abhängige Transportproteine; im Zuge der Substratbindung und ATP-Hydrolyse durchlaufen sie eine Konformationsänderung, welche den Transport des Substrates vom Zytoplasma in den Extrazellulärraum vermittelt. TMD = Transmembrandomäne; ZPD = zytoplasmatische Domäne; ATP = Adenosintriphosphat; ADP = Adenosindiphosphat; P_i = anorganisches Phosphat; (Eigene Darstellung nach Chen *et al.* 2016;[18])

1.2.1.3. Apoptose-Inhibition

Viele antitumorale Wirkstoffe (z. B. CDDP, Doxorubicin) führen letztlich zur Induktion des »programmierten Zelltodes«, der sogenannten Apoptose.[19] Apoptose kann einerseits durch die Zelle selbst über diverse interne Schadensdetektoren eingeleitet werden, was als intrinsischer Signalweg bezeichnet wird. Andererseits spricht man von extrinsischer Apoptose, wenn deren Induktion durch die Interaktion einer geschädigten Zelle mit Immunzellen über spezielle, in der Zytoplasmamembran lokalisierte Todesrezeptoren resultiert (Abb. 3).[20] Eine Schlüsselrolle bei der Regulation beider Signalwege fällt dem Tumorsuppressorprotein p53 zu, dessen codierendes Gen in circa 50% aller Tumore mutiert ist.[21,22] Resultiert die Mutation in einem funktionsunfähigen oder funktional eingeschränkten Proteinprodukt, nimmt die Sensitivität der Tumorzellen für pro-apoptotische Signale, z. B. nach DNA-Schädigung durch einen antitumoralen Wirkstoff, ab. Darüber hinaus kann auch der Verlust anderer pro-apoptotischer Faktoren (z. B. Bax) oder die Überexpression anti-apoptotischer Signalproteine, beispielsweise Bcl-2 oder IAPs (*inhibitors of apoptosis proteins*), zu einer auf Apoptose-Inhibition basierenden Chemoresistenz beitragen.[19]

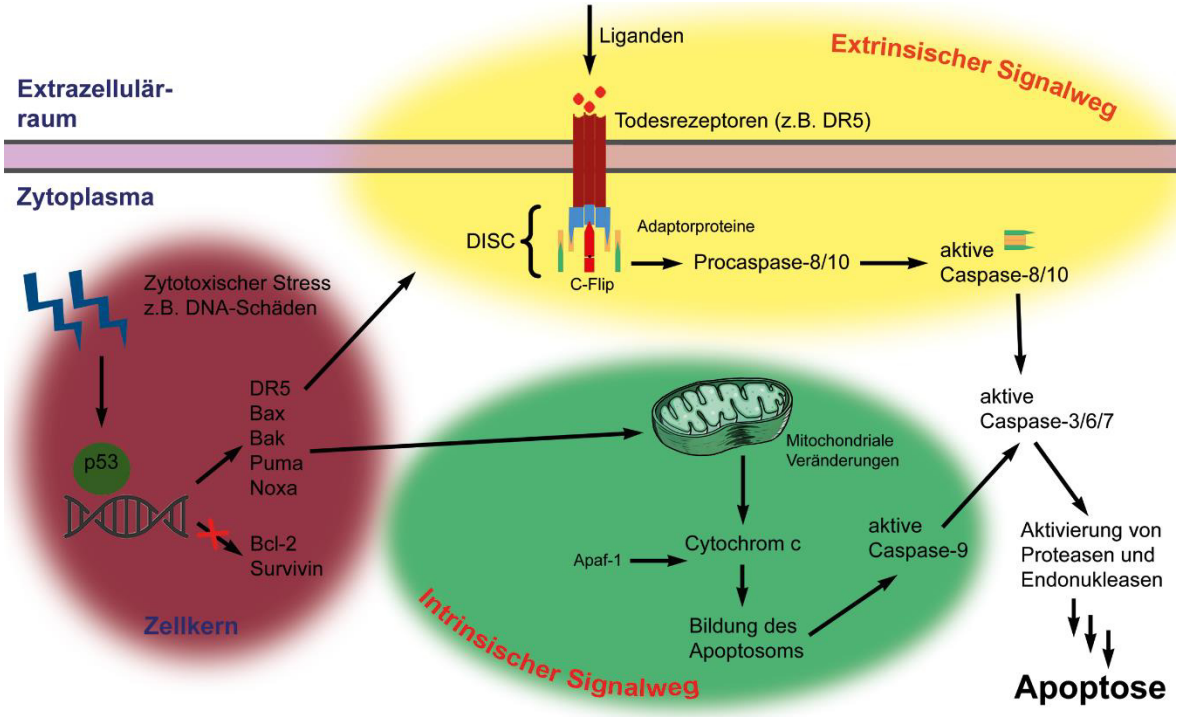

Abbildung 3. Schematische Darstellung von extrinsischem und intrinsischem Apoptose-Signalweg. Der extrinsische Signalweg beginnt mit der Bindung extrazellulärer Liganden an die extrazelluläre Domäne eines Todesrezeptors (z.B. *death receptor 5*, DR5), woraufhin an der zytoplasmatischen Seite des Rezeptors der DISC (*death-inducing signalling complex*) entsteht. DISC führt zur auto-katalytischen Aktivierung der Pro-Caspasen-8 und 10, welche in ihrer aktiven Form die Effektor-Caspasen-3/6/7 aktivieren. C-Flip (*cellular-FLICE inhibitory protein*) ist ein wichtiger Inhibitor des extrinsischen Apoptose-Signalweges. Zytotoxische Reize, wie z.B. DNA-Schädigung, führen zu einer Aktivierung von p53, wodurch die Expression pro-apoptotischer Faktoren erhöht, und die anti-apoptotischer Faktoren inhibiert wird. Vermittelt durch in etwa 25 verschiedene pro- und anti-apoptotische Proteine (z.B. Bax, Bak), beginnt intrinsische Apoptose mit MOMP (*mitochondrial outer membrane permeabilisation*) und resultiert letztlich in der Freisetzung von Cytochom c ins Zytoplasma. Cytochrom c und Apaf-1 (*apoptosis protease-activating factor-1*) bilden das sogenannte Apoptosom, welches Caspase-9 aktiviert und diese wiederum die Effektor-Caspasen-3/6/7.[23] (Eigene Darstellung nach Goldar *et al.* 2015; Haupt *et al.* 2003.[23,24])

1.2.1.4. Epithelial-mesenchymale Transition

Die Epithelial-mesenchymale Transition (EMT) ist ein physiologischer Prozess, der während der Embryonalentwicklung und in adultem Gewebe während der Wundheilung eine Rolle spielt. Man versteht darunter eine schnelle und meist reversible Veränderung des Zell-Phänotyps: epitheliale Zellen lösen ihre Zell-Zell-Kontakte, verlieren ihre Polarität und es kommt zu einer Umstrukturierung des Zytoskeletts.[25] Letztlich entsteht eine Zelle mit mesenchymalen Eigenschaften, sowie invasivem Potential.[25] In den frühen 90-iger Jahren wurde erstmals die Hypothese aufgestellt, dass die EMT eine entscheidende Rolle im Metastasierungsprozess spielen könnte.[26] Dieser Hypothese zufolge durchlaufen bestimmte Tumorzelle eine EMT, wodurch sie mesenchymale Eigenschaften erhalten, die

sie wiederrum zur Migration innerhalb des Organismus und zur Bildung von Fernmetastasen befähigen.[27] Mittlerweile ist bekannt, dass Tumorpatienten, welche nicht auf eine Chemotherapie ansprechen, in der Regel immer Fernmetastasen bilden.[28] Dies legt die Vermutung nahe, dass die Prozesse der Metastasierung und der Chemoresistenz miteinander verknüpft sind, wobei möglicherweise die EMT die Basis beider Prozesse darstellt. Verschiedene Studien haben gezeigt, dass Tumorzellen mit EMT-typischen Eigenschaften primär resistenter gegen chemotherapeutische Wirkstoffe sind,[29] aber auch, dass anfänglich sensitive Tumorzellen durch den Prozess der EMT Resistenzen entwickeln können.[30] Darüber hinaus steht die EMT in engem Zusammenhang mit den unter 1.3.4. und 1.3.5. diskutierten Einflussfaktoren auf die Entwicklung von Resistenzen: den Tumorstammzellen und den zirkulierenden Tumorzellen. Bis heute sind die der EMT zugrunde liegenden Mechanismen nicht vollständig aufgeklärt und auch die Rolle, welche die EMT im Tumorgeschehen spielt oder bei der Tumortherapie spielen könnte, ist noch immer Gegenstand der Forschung.

1.2.1.5. Target-Veränderung

Im Laufe einer Chemotherapie kann es passieren, dass sich ein Zielprotein durch gewisse Umstände verändert, oder dass die zelluläre Konzentration eines Targetmoleküls soweit abnimmt, dass dessen Manipulation keinen weitreichenden Effekt mehr auf die Zelle erlaubt. Strukturell veränderte Targetproteine resultieren in der Regel aus genetischen Mutationen. Begründet in der intratumoralen Heterogenität ist vor allem in Tumoren mit hoher Mutationslast die Wahrscheinlichkeit hoch, dass es eine Subpopulation an resistenten Tumorzellen gibt. Die resistente Subpopulation trägt in diesem Fall eine Mutation, welche zu einem Proteinprodukt mit voller Funktionsfähigkeit, aber veränderten stereochemischen Eigenschaften führt, sodass der jeweilige Wirkstoff nicht mehr binden kann. Durch Mutation im zugrundeliegenden Gen strukturell veränderte Targetproteine sind ein häufiger Mechanismus der Resistenzentwicklung bei Topoisomerase II-Inhibitoren (z. B. Doxorubicin).[31] Auch der zweite Aspekt der Targetveränderung spielt im Falle der Topoisomerase-Inhibitoren eine Rolle: eine reduzierte Expressionsrate des Targets am jeweiligen Wirkort, wodurch kein Angriffspunkt für den Wirkstoff mehr vorhanden ist.[31] Dieses Beispiel macht darüber hinaus deutlich, dass Chemoresistenz meist ein komplexes Phänomen ist, bei dem verschiedene zelluläre Resistenzmechanismen zusammenlaufen und/oder ineinander übergehen.

1.2.1.6. Wirkstoff-Inaktivierung

Chemoresistenz kann auch durch die Inaktivierung eines antitumoralen Wirkstoffes auf seinem Weg zur oder in der Tumorzelle selbst verursacht werden. Die erste Möglichkeit hierfür ist eine Überaktivität des zellulären Entgiftungssystems, welches dafür verantwortlich ist die Zelle vor durch toxische Metaboliten oder Xenobiotika verursachten Schäden zu schützen. Ein Beispiel für ein häufig an

Resistenzmechanismen beteiligtes Enzym des zellulären Entgiftungssystems ist die Glutathion-S-Transferase (GST), welche die Bindung potentiell schädlicher Moleküle an Glutathion (GSH) katalysiert. Die an GSH gebundenen Metaboliten oder Xenobiotika können anschließend weiter metabolisiert und aus der Zelle, bzw. dem Organismus ausgeschieden werden. Chemoresistente Tumorzellen weisen oft eine erhöhte Expression an GST auf, was zur Folge hat, dass ein größerer Anteil des Wirkstoffs durch die Bindung an GSH inaktiviert und ausgeschieden werden kann.[32]

Eine weitere Möglichkeit der Wirkstoff-Inaktivierung ergibt sich im weitesten Sinne im Falle von sogenannten *Prodrugs*. Das heißt im Falle von antitumoralen Wirkstoffen, die erst durch Enzyme metabolisch zum aktiven Wirkstoff modifiziert werden müssen. Hier kann eine verringerte Wirkstoffeffizienz durch eine reduzierte Aktivierung des *Prodrugs* verursacht werden. Beispielsweise der für die Behandlung von akuter myeloischer Leukämie (AML) verwendete Wirkstoff AraC (Cytarabin) muss durch das Enzym Desoxycytidinkinase mehrfach phosphoryliert werden, um seine aktive Form zu erreichen. Im Falle eines Funktionsverlustes dieses Enzyms, zum Beispiel durch Mutation, wird die Aktivierung, und damit auch die Aktivität dieses Wirkstoffes entscheidend herabgesetzt.[33]

1.2.1.7. (Epi-)Genetische Mechanismen

Die Genamplifikation ist ein genetisches Phänomen, welches in circa 10% aller Tumore vorkommt und verschiedenen Formen der Chemoresistenz zugrunde liegen kann.[34] Hierbei kommt es zur selektiven Replikation einer bestimmten Chromosomenregion, wodurch multiple Kopien eines Gens entstehen. Ein Beispiel hierfür ist die durch Genamplifikation hervorgerufene Resistenz gegen Methotrexat: durch erhöhte Expression des Targetproteins kommt es bei limitierter Wirkstoffkonzentration zum Verlust der zytotoxischen Wirkung.[35]

Auch epigenetische Mechanismen spielen eine wichtige Rolle bei der Entstehung verschiedener Chemoresistenzen. Die zwei wichtigsten Arten der epigenetischen Veränderungen sind erstens die DNA-Methylierung und zweitens die Modifizierung von Histonproteinen. DNA-Methylierung findet an Cytosin-Basen innerhalb von Promotorregionen der DNA statt, wobei Hypermethylierung eines Promotors zur Inaktivierung der Expression des betreffenden Gens führt. Modifizierungen an Histonproteinen regulieren die Genexpression indem sie zur Veränderung der Chromatinstruktur beitragen: Acetylierung von Histonproteinen öffnet die DNA und aktiviert dadurch die Genexpression, Deacetylierung führt zu einer Kondensation des Chromatins und zur Inaktivierung der Gene der jeweiligen DNA-Region.[15] Durch erhöhten Wirkstoffefflux hervorgerufene *Multidrug*-Resistenzen können beispielsweise durch Demethylierung des MDR1 Promotors und daraus resultierender Überexpression der MDR1-Transporterproteins ausgelöst werden.[36]

1.2.2. Tumor-*Microenvironment*

Eine möglichst homogene Verteilung innerhalb eines Tumors stellt eine wichtige Voraussetzung für die effektive Wirkung eines chemotherapeutischen Wirkstoffes dar. Hierbei müssen Wirkstoffe immer das direkt an den Tumor angrenzende Gewebe – das sogenannte Tumor-*Microenvironment* (TME) – durchqueren. Das TME besteht aus den umgebenden Blutgefäßen, Immunzellen, Fibroblasten, Signalmolekülen, sowie der extrazellulären Matrix (EZM).[37] Tumor und TME stehen in einem engen Zusammenhang und beeinflussen sich gegenseitig, wodurch Veränderungen im TME auf verschiedene Weisen zu einer Chemoresistenz beitragen können.

1.2.2.1. pH-Wert

Hypoxie und hohe Glykolyseraten sind typische Charakteristika solider Tumore, die zu einer erhöhten Produktion und Exkretion von Laktat und H^+ in den die Tumorzellen umgebenden Extrazellulärraum führen.[38,39] In der Tumor-Mikroumgebung herrschen deshalb häufig leicht saure Bedingungen vor (pH 6.5-6.9), während der pH-Wert im Zytoplasma der Tumorzellen im neutralen bis schwach basischen Bereich bleibt.[38] Es resultiert ein in normalem Gewebe nicht vorkommender pH-Gradient, der für das Phänomen des sogenannten *Ion trapping* verantwortlich ist. Viele antitumorale Wirkstoffe sind entweder schwache Basen oder schwache Säuren (siehe Tab. 1). Ungeladene, ionisierbare schwache Basen, wie Doxorubicin, können frei durch die Plasmamembran diffundieren. Weist jedoch das TME einen leicht sauren pH-Wert auf, so werden sie protoniert und dadurch positiv geladen. Infolge dessen sinkt ihre Zellpermeabilität und die ionisierten Wirkstoffmoleküle können ihr Target innerhalb der Zelle nicht mehr erreichen. Im Gegensatz dazu, reichern sich schwache Säuren in einer leicht basischen Umgebung, wie dem Zytoplasma, an, wodurch ihre Aufnahme und Effektivität gesteigert wird.[40] Darüber hinaus spielt die im TME vorherrschende Azidität auch eine wichtige Rolle bei der Progression der Erkrankung, beispielsweise durch die Stimulation des Tumorzellwachstums, sowie metastatischer Prozesse.[39,41]

Tabelle 1. pKa-Werte einiger klinisch-etablierter antitumoraler Wirkstoffe.[42]

Wirkstoff	pKa	Ionisationsverhalten
Doxorubicin	8.3	Schwache Base
Paclitaxel	Zwitterion	
5-FU	7.76	Schwache Säure*
CDDP	5.06	Schwache Säure

*Trotz des relativ hohen pKa-Wertes zählt man 5-FU (5-Fluoruracil) aufgrund seiner durch das Fluoratom bedingten Elektronen-ziehenden Eigenschaften zu den schwachen Säuren.[42]

1.2.2.2. Sauerstoff

Ein weiteres Charakteristikum maligner Tumore ist ihre hohe Proliferationsrate. In Kombination mit fehlender bzw. unzureichender Vaskularisierung können daraus Regionen im Tumor entstehen, in denen permanent oder zeitweise hypoxische Bedingungen vorliegen.[43] Ein hypoxisches TME kann in verschiedener Hinsicht zur Chemoresistenz beitragen:

- Für die Vermittlung der pro-apoptotischen Wirkung vieler antitumoraler Wirkstoffe sind freie Radikale unabdingbar. In Abwesenheit von Sauerstoff kommt es deshalb zu einem Aktivitätsverlust dieser Medikamente.[44]
- Hypoxie stimuliert die Expression von ABC-Transportern und damit die Entstehung von *Multidrug*-Resistenzen.[45]
- Einige Stoffwechselenzyme, die für die Aktivierung von Wirkstoffen notwendig sind, weisen unter hypoxischen Bedingungen eine reduzierte Aktivität auf.[46]

1.2.2.3. Extrazelluläre Matrix

Der Begriff »extrazelluläre Matrix« (EZM) beschreibt die Gesamtheit aller Makromoleküle im Interzellularraum. Sie besteht hauptsächlich aus Glycoproteinen, Proteinen und Proteoglycanen, wobei ihre Zusammensetzung und Struktur exakt an die Bedürfnisse der umgebenden Zellen angepasst ist. Neben ihrer physikalischen Gerüstfunktion, ist die EZM ein wichtiger Bestandteil bei der Übermittlung von Wachstums-, Migrations- und Differenzierungssignalen.[37] Aufgrund der im Vergleich zu nicht-malignem Gewebe abweichenden Eigenschaften von Tumorgewebe (z. B. Azidität, Hypoxie), unterscheidet sich auch die EZM innerhalb des TME stark von der in gesundem Gewebe.[47] Tumore mit hohem EZM-Anteil weisen eine schlechtere Prognose, sowie eine höhere Resistenzwahrscheinlichkeit auf. Letzteres ist darin begründet, dass die EZM eine physikalische Barriere bildet, welche die Wirkstoffaufnahme verzögern, reduzieren oder sogar verhindern kann.[48]

1.3. Weitere Einflussfaktoren auf die Entwicklung von Resistenzen

Wie im vorausgehenden Abschnitt deutlich wurde, ist »Chemoresistenz« eine äußerst komplexe Thematik, bei der die einzelnen Mechanismen schwer voneinander abgrenzbar sind und zum Teil auch ineinander übergreifen. Im Folgenden sollen deshalb weitere Einflussfaktoren beschrieben werden, die zwar *per se* keinen Resistenzmechanismus darstellen, allerdings durchaus großen Einfluss auf die Entstehung von resistenten Tumorzellen ausüben können. Auch im Hinblick auf die Entwicklung neuer Strategien zur Umgehung von Chemoresistenzen sind die nachfolgend dargelegten Einflussfaktoren wichtig, da sie einerseits neue Angriffspunkte liefern, andererseits auch potentielle Risiken aufdecken können.

1.3.1. Wachstumsrate und Tumormasse

Die Goldie-Coldman Hypothese ist ein mathematisches Modell, welches den Zusammenhang zwischen Tumormasse, Mutationsrate und Wahrscheinlichkeit einer Resistenzentwicklung eines Tumors beschreibt.[49] Diesem Modell zufolge nimmt die Wahrscheinlichkeit, dass ein Tumor Wirkstoff-resistente Zellen enthält, mit der Tumormasse und der intrinsischen, genetischen Instabilität der Tumorzellen zu.

Da sich die Wachstumsrate eines Tumors direkt auf die Tumormasse auswirkt, sollte auch diese bei Überlegungen bezüglich Resistenzentwicklung eingeschlossen werden. Tumorwachstum erfolgt sigmoidal, das heißt exponentiell schneller bei geringeren Tumormassen, während sich die Wachstumsrate bei größeren Zellzahlen einem Plateau nähert.[50] Da eine Chemotherapie die Tumorgröße in der Regel verringert, können potentiell im Patienten verbliebene Tumorzellen zu ihrer exponentiellen Wachstumsphase zurückkehren, sobald die Therapie beendet wird. Dieser Beobachtung entspringt der Ansatz der sogenannten *Dose dense*-Therapie, bei der die behandlungsfreien Zeiträume möglichst kurz gehalten werden.[51]

1.3.2. Tumorheterogenität

Der Begriff »Tumorheterogenität« fasst im Allgemeinen die Heterogenität zwischen verschiedenen Tumorarten, verschiedenen Patienten innerhalb einer Tumorentität, Primärtumor(en) und Metastase(n) innerhalb ein und desselben Patienten, sowie zwischen den Zellen innerhalb eines einzigen Tumors zusammen. Während die Heterogenität zwischen verschiedenen Tumorarten und Patienten zwar ein wichtiger Faktor ist, der die Entwicklung einer umfassenden Therapiemethode gegen Krebs erschwert, stellen insbesondere die Heterogenität der Tumorzellen innerhalb eines Patienten, bzw. eines einzigen Tumors wichtige Kriterien für die Entwicklung von Resistenzen gegen Chemotherapeutika dar.[52] Hierbei kann Heterogenität sowohl auf genetischer, epigenetischer, proteomischer oder metabolischer Ebene, als auch in Bezug auf das TME vorhanden sein.

Diversität auf genetischem Level kommt vor allem durch Mutationen, Genamplifikationen, Deletionen, chromosomale Neuanordnungen, Transpositionen genetischer Elemente oder ähnliche Prozesse zustande. Der ausschlaggebende Punkt hierbei ist die Geschwindigkeit mit der diese Prozesse ablaufen; die sogenannte Tumormutationslast. Tumore mit einer geringen genetischen Mutationslast entwickeln generell später Resistenzen, als genetisch instabile Tumore.[52] Epigenetische, proteomische und metabolische Unterschiede können teilweise auf primäre genetische Veränderungen zurückgeführt werden, allerdings zählt man auch Unterschiede in Bezug auf die Zellzyklusphase, stochastische Unterschiede zwischen den Zellen oder eine hierarchische Organisation innerhalb der Zellpopulation in Form von beispielsweise Tumorstammzellen (TSZ) dazu.[53] Ein weiterer zur Heterogenität beitragender Faktor ist das TME.[54] Wie unter 1.2.2. beschrieben, kann durch bestimmte Eigenschaften der genannten

Einzelbestandteile der TME ebenfalls eine Wirkstoffresistenz vermittelt werden. Behinderung der Wirkstoffresorption oder parakrine Wachstumsstimulation sind nur zwei Beispiele.[55]

1.3.3. Therapeutische Selektion

Aufgrund der intratumoralen Heterogenität ist es – abhängig von der Tumormasse, sowie der Mutationslast – mehr oder weniger wahrscheinlich, dass es initial Tumorzellen mit Resistenzen gegen bestimmte Chemotherapeutika gibt. Aufgrund dessen reichern sich während einer Chemotherapie exakt diese Zellen an und, darüber hinaus, wird durch die Elimination der übrigen Tumorzellen noch mehr Raum für das Wachstum der resistenten Zellen geschaffen, wodurch ein anfänglich gutes Ansprechen des Tumors auf eine Therapie häufig eine aggressivere Progression der Erkrankung zur Folge hat.[56] Um dieses Phänomen so weit wie möglich zu vermeiden, verwendet man heute fast ausschließlich Kombinationsregime aus zwei oder mehr verschiedenen Wirkstoffen, sodass die Wahrscheinlichkeit von zurückbleibenden resistenten Zellen und damit auch für den häufig daraus resultierenden Progress der Erkrankung minimiert wird.[56] Für den Einsatz in Kombinationsregimen besteht deshalb ein kontinuierlicher Bedarf an neuen Wirkstoffen mit Aktivität gegen resistente Tumorzellen.

1.3.4. Tumorstammzellen – *Survival of the smartest*

Die Tumorstammzell-Hypothese erwuchs ursprünglich aus der Beobachtung einer histologischen Ähnlichkeit zwischen Tumorgewebe und embryonalem Gewebe, welche beide aus verschiedenen, heterogenen Zellpopulationen bestehen. TSZ stellen eine relativ kleine Population innerhalb eines Tumors dar, die sich neben der Expression zahlreicher Stammzellmarker durch Quieszenz (Verharren in der G0-Phase des Zellzyklus) und die Fähigkeit zur Selbsterneuerung auszeichnet und in der Lage ist zu proliferationsfähigen Tumorzellen, welche den Großteil der Tumormasse bilden, zu differenzieren.[57,58]

Die Isolation von TSZ wurde erstmals im Jahr 1994 für Leukämie beschrieben.[59] In den darauffolgenden Jahren auch für diverse andere Tumorarten, wie z. B. Brust-, Darm-, Lungen-, oder Prostatakrebs.[60] Klinische Bedeutung bekamen diese Zellen erst als erste Patientenstudien zur *Minimal Residual Disease* (MRD) veröffentlicht wurden. Der Ausdruck MRD beschreibt eine kleine Anzahl von Tumorzellen, die nach einer Behandlung im Patienten zurückbleiben und die Hauptursache für Rückfälle darstellen. Die Problematik der MRD kann sehr gut durch die Tumorstammzell-Hypothese erklärt werden: das initiale Ansprechen auf die Behandlung, was die Reaktion der aktiv-proliferierenden Tumorzellen widerspiegelt, und einen späteren Progress der Erkrankung, da die quieszenten, häufig multi-resistenten TSZ zurückbleiben.[61] Ob TSZ aus normalen Stammzellen oder aus Nicht-Stammzellen entstehen und was die treibende Kraft im Transformationsprozess darstellt, ist zum aktuellen Zeitpunkt noch Gegenstand der Forschung.[57] Man geht jedoch davon aus, dass sowohl die Störung des physiologischen Gleichgewichts zwischen Protoonkogenen und Tumorsuppressorgenen,

als auch die EMT (siehe 1.2.1.4.) eine wichtige Rolle spielen.[62] Studien zufolge sind TSZ auch ein ausschlaggebender Faktor bei der Entstehung von Resistenzen gegenüber verschiedenen Chemotherapeutika, wie beispielsweise Cisplatin, Paclitaxel,[63] Etoposid,[64] sowie Doxorubicin und Methotrexat.[65] Obwohl aktuell nicht alle Mechanismen im Detail verstanden sind, weiß man mittlerweile, dass TSZ eine ganze Reihe an verschiedenen Strategien einsetzen können um sich gegen chemotherapeutische Wirkstoffe zu schützen (siehe Abb. 4).

Abbildung 4. Die vielschichtigen Resistenzmechanismen von Tumorstammzellen. TSZ vereinen verschiedenste Mechanismen der Chemoresistenz in sich: Zunächst wird durch die Lokalisation in TSZ-Nischen innerhalb des TME oder die Expression von ABC-Transportern die Exposition des Wirkstoffes vermieden. Versagt diese Strategie, so werden auf transkriptioneller oder epigenetischer Ebene weitere Schutzmechanismen, wie eine Überaktivierung der DNA-Reparaturmaschinerie oder die Inhibition von Apoptose, aktiviert. (Eigene Darstellung nach Zhao *et al.* 2016.[57])

Zunächst sind TSZ in sogenannten TSZ-Nischen lokalisiert, das heißt an speziellen Stellen innerhalb der TME, an denen sie physikalisch abgeschirmt sind und dadurch einer zellulären Wirkstoffexposition entgehen können.[57] Gelangt ein Wirkstoff trotz allem in das Zytoplasma einer TSZ, so werden weitere Mechanismen aktiviert, um letale Folgen der Exposition zu vermeiden. Viele TSZ exprimieren deshalb transmembrane Effluxpumpen, wie ABC-Transporter, die den Wirkstoff im »Ernstfall« wieder aus der Zelle herausschleusen können.[66] Darüber hinaus sind TSZ in der Lage zelluläre Targets von Wirkstoffen zu eliminieren, beispielsweise durch die dynamische Anpassung der Expression bestimmter für die Wirkung/Inaktivierung eines Chemotherapeutikums notwendiger Enzyme.[57] Aber auch durch

Quieszenz entziehen sie sich dem Einfluss einer Chemotherapie, die häufig nur auf proliferierende Zellen abzielt.[67] Vor allem bei DNA-interagierenden Wirkstoffen, wie Platinderivaten oder Topoisomerase-Inhibitoren, kann die Resistenz von TSZ auch durch nachträgliche Reparatur zellulärer Schäden vermittelt werden, da in vielen TSZ DNA-Reparaturmechanismen übermäßig stark aktiviert sind.[68] Aber auch Target-unabhängig führen durch Chemotherapeutika verursachte Schäden in TSZ nicht immer zum gewünschten Effekt – dem programmierten Zelltod – da anti-apoptotische Signalwege übermäßig stark aktiviert und pro-apoptotische Signalwege herunter reguliert sind.[57] Letztlich wird deutlich, dass TSZ viele der in den vorherigen Kapiteln beschriebenen Mechanismen der Chemoresistenz in sich vereinen, was sie zu einem besonders schwer adressierbaren Target, und somit zu einer großen Herausforderung für die chemotherapeutische Forschung macht.

1.3.5. Zirkulierende Tumorzellen

Zirkulierende Tumorzellen (*circulating tumor cells*, CTCs) sind Zellen, die aus soliden Tumoren freigesetzt, anschließend über Körperflüssigkeiten, wie zum Beispiel Blut oder Lymphe, im Organismus verteilt werden, und sich letztlich an einer anderen Stelle des Körpers festsetzen und zu Fernmetastasen heranwachsen können (siehe Abb. 5). Der Entstehungsprozess von CTCs ist aktuell noch nicht vollständig verstanden. Allerdings weiß man, dass EMT (siehe 1.2.1.4.) im Falle epithelialer Tumore (circa 90%) eine wichtige Rolle spielt. Während der EMT entsteht aus einer polarisierten, epithelialen Zelle, die normalerweise in der Basalmembran verankert ist, durch diverse biochemische Veränderungen eine Zelle mit mesenchymalen, bzw. stammzellartigen Eigenschaften, unter anderem erhöhter Migrationsfähigkeit, Invasivität, und Apoptoseresistenz.[69,70] Darüber hinaus nimmt man an, dass insbesondere die zirkulierenden, epithelialen Tumorzellen (*circulating epithelial tumor cells*, CETCs), das heißt solche Zellen, die sowohl epitheliale, als auch mesenchymale Eigenschaften aufweisen und sich sozusagen mitten im EMT-Prozess befinden, ein ganz besonders hohes metastatisches Potential aufweisen.[70,71] Aufgrund der durch die EMT verliehenen Eigenschaften, ähneln C(E)TCs in vieler Hinsicht den unter 1.3.4. beschriebenen TSZ, vor allem bezüglich ihrer erhöhten Resistenz gegenüber verschiedener Chemotherapeutika oder anderer antitumoraler Therapien.[72]

Die Detektion und Quantifizierung von C(E)TCs im Rückenmark oder Blut von Tumorpatienten kann auf verschiedene Weise erfolgen. Viele Methoden beginnen zunächst mit einem Anreicherungsschritt, um die Konzentration dieser seltenen Zellen zu steigern und damit ihren Nachweis zu erleichtern. In diesem Zusammenhang unterscheidet man positive und negative Anreicherungsverfahren auf der Basis biologischer (z.B. Expression bestimmter Oberflächen-Antigene) oder physikalischer Eigenschaften (z.B. Zellgröße, Dichte, Verformbarkeit). Die Selektivität der Anreicherung kann hierbei durch die Kombination aus biologischen und physikalischen Determinanten gesteigert werden.[73] Eine mögliche Methode zur Anreichung mittels physikalischer Charakteristika stellt die Dichtegradienten-

Zentrifugation dar, wobei es hier durch diverse Waschschritte zu einem erheblichen Verlust der relevanten Zellen kommen kann.[74] Auch die *Magnetic Bead*-Anreicherung (mittels spezieller auf magnetischen Partikeln immobilisierten Antikörpern) kann zu einer immensen Schädigung der Zellen führen und somit die Ergebnisse der CTC-Quantifizierung beeinträchtigen.[75] Eine weitere Möglichkeit zum Nachweis von CETCs ist die sogenannte MAINTRAC®-Methode, welche auf jegliche Anreicherungsschritte verzichtet und dadurch deutlich bessere Detektionsraten verzeichnet.[76] Dieses fluoreszenz-basierte Verfahren nutzt einen für epitheliale Zellen spezifischen Antikörper (anti-EpCAM; *epithelial cell adhesion molecule*) zur Detektion der CETCs in Patientenblut, kombiniert mit einem Vitalitätsmarker (PI; Propidiumiodid) für den Ausschluss avitaler Tumorzellen.

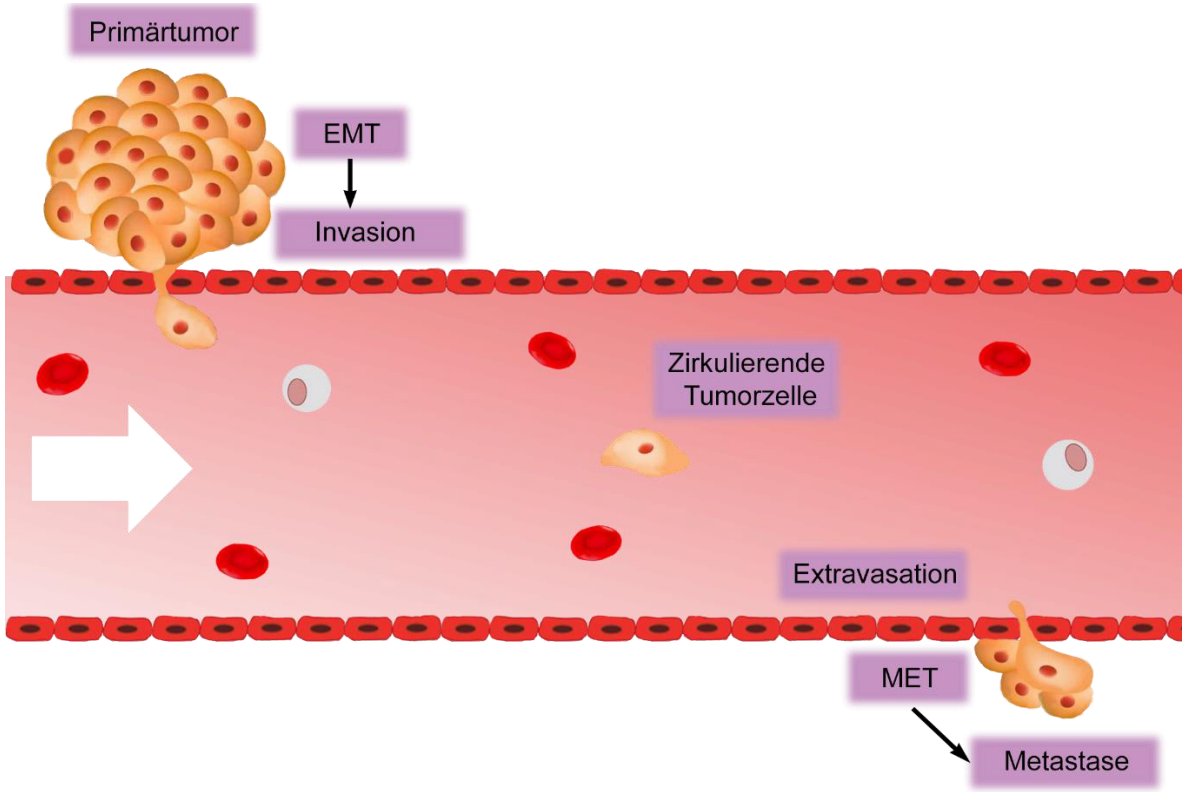

Abbildung 5. Zirkulierende (epitheliale) Tumorzellen. Bestimmte Bedingungen können dazu führen, dass Tumorzellen im Primärtumor den Prozess der EMT durchlaufen und durch aktive Invasion in den Blutkreislauf oder in angrenzende Lymphgefäße gelangen. Dort können die C(E)TCs für unbestimmte Zeit persistieren, bevor sie sich an einer anderen Stelle im Organismus festsetzen und zu wachsen beginnen. EMT = Epithelial-mesenchymale Transition; MET = Mesenchymal-epitheliale Transition. (Eigene Darstellung nach Chot *et al.* 2018; Lozar *et al.* 2019.[77])

1.4. Verschiedene Ansätze zur Resistenzumgehung

Da man die für Chemoresistenzen verantwortlichen Mechanismen immer besser versteht, gibt es mittlerweile diverse Ansätze um entweder die Resistenzentstehung initial zu vermeiden, oder aber um

die resistenten Tumorzellen trotzdem mit antitumoralen Wirkstoffen erreichen zu können. Der erste und bis heute erfolgreichste Ansatz in diesem Zusammenhang ist die Polychemotherapie, bei der verschiedene Wirkstoffe gleichzeitig oder nacheinander verabreicht werden. Bei der Behandlung von Brust- oder Hodenkarzinomen, sowie kolorektalen Karzinomen können auf diese Weise nach wie vor gute Erfolge erzielt werden.[4,35,78] Die Auswahl der Kombinationswirkstoffe muss hierbei mit großer Sorgfalt erfolgen: es sollten Wirkstoffe ausgewählt werden, die sowohl unterschiedliche Wirkmechanismen, als auch Wirkorte besitzen, sodass synergistische, statt additive Effekte resultieren. Auch potentielle Nebenwirkungen und Wirkstoffinteraktionen müssen berücksichtigt werden.[35] Da Polychemotherapien auch starke Nebenwirkungen hervorrufen können, verfolgt die moderne Forschung zielgerichtetere Ansätze: Beispielsweise werden Wirkstoffe für Kombinationsregime entwickelt, die bestimmte, häufig für *multidrug*-Resistenzen verantwortliche ABC-Transporter inhibieren.[79] Im Nachfolgenden sollen die im Rahmen dieser Dissertation behandelten Ansätze für die Umgehung von Chemoresistenzen genauer beschrieben werden.

1.4.1. Induktion von zellulärer Seneszenz

Zelluläre Seneszenz ist ein Phänomen durch welches Zellen die Fähigkeit zur aktiven Proliferation verlieren. Seneszente Zellen sind vital und metabolisch aktiv, allerdings dauerhaft und irreversibel in der G1- oder G2/M-Phase des Zellzyklus arretiert.[80] Man unterscheidet zwei grundsätzliche Formen der Seneszenz: erstens die replikative, durch kürzer werdende Telomere bedingte Seneszenz,[81] und zweitens die prämature, durch oxidativen Stress, DNA-Schäden oder andere Stressfaktoren akut induzierbare Seneszenz.[80] Physiologisch gesehen, stellt die zelluläre Seneszenz einen Tumorsuppressormechanismus dar, dessen Funktion im Schutz der Zelle vor malignen Veränderungen besteht.[82] Konventionelle Tumortherapie baut in der Regel auf zytotoxische Strategien, deren Ziel die Elimination der Tumorzellen darstellt. Ein großer Nachteil hierbei sind die häufig starken Nebenwirkungen der zytotoxischen Agenzien, sowie die Entstehung von Resistenzen, welche wiederrum zu einem Progress der Erkrankung bzw. Rezidiven führen können.[80] In der Langzeitbehandlung bestimmter Tumorarten könnte deshalb auch die Induktion Therapie-induzierter Seneszenz (TIS) und die daraus resultierende Zytostasis der Tumorzellen eine Alternative darstellen. Besonders erwähnenswert ist in diesem Zusammenhang, dass verschiedene Seneszenz-induzierende Wirkstoffe auch Aktivität gegenüber Apoptose-resistenten Tumorzellen mit p53- und/oder p16-Mutationen zeigen.[82]

1.4.2. Topoisomerase I-Inhibition

Topoisomerasen sind Enzyme, welche die Topologie doppelsträngiger DNA-Moleküle verändern können. Sie sind für die Replikation und Transkription der DNA essentiell, indem sie die Superhelizität

der DNA-Moleküle lokal auflösen, wodurch die DNA für die Enzymmaschinerien der Replikation oder Transkription zugänglich wird. Man unterscheidet hierbei grundsätzlich zwei Enzymtypen:

- die Topoisomerase I (TopoI), welche durch Bildung einer Phosphodiesterbindung zwischen einem Tyrosinrest im aktiven Zentrum des Enzyms und dem DNA-Molekül einen Einzelstrangbruch verursacht, durch welchen der intakte Einzelstrang anschließend hindurch geführt wird.[83]
- Topoisomerase II (TopoII), welche durch die Bildung zweier Phosphodiesterbindungen einen Doppelstrangbruch verursacht, durch welchen dann ein intakter DNA-Doppelstrang hindurch geführt wird. Insgesamt ist für die Funktion der TopoII die Energie aus der Hydrolyse von einem Molekül ATP notwendig.[83]

Da Topoisomerasen maßgeblich an der Zellproliferation beteiligt sind, stellen sie gute Targets für chemotherapeutische Wirkstoffe dar. Auf molekularer Ebene bilden die meisten Topoisomerase-Inhibitoren einen stabilen Tertiärkomplex mit dem DNA-Strang und dem Enzym, wodurch es zur Arretierung der Replikations-/Transkriptionsgabel und zum Bruch des DNA-Stranges kommt. Durch die Schädigung der DNA wird letztlich Apoptose induziert. In Tabelle 2 sind einige, klinisch etablierte Topoisomerase-Inhibitoren und ihre Indikationen zusammengefasst.

Tabelle 2. Beispiele klinisch-etablierter Topoisomerase-Inhibitoren. Die Wirkstoffe gehören unterschiedlichen Substanzklassen an und besitzen Spezifität für Topoisomerase Typ I oder II.[83]

Wirkstoff	**Substanzklasse**	**Target**	**Indikation**
Doxorubicin	Anthracycline	TopoIIA	Mammakarzinom (in Kombinationsregimen); akute lymphoblastische und myeloblastische Leukämie; Hodgkin/Nicht-Hodgkin Lymphome; versch. solide Tumore in der metastasierten Situation;
Mitoxantron	Anthracendion	TopoIIA	Chron. multiple Sklerose; Prostatakarzinom;
Etoposid	Epipodophyllotoxin	TopoIIA	Hodentumore; kleinzelliges Bronchialkarzinom;
Topotecan	Camptothecin	TopoIB	Kleinzelliges Bronchialkarzinom; Zervixkarzinome (nur Stadium IVB);

Während die TopoII-spezifischen Inhibitoren strukturell relativ stark variieren, sind die Camptothecine (CPT; z. B. Topotecan oder Irinotecan) aktuell die einzige TopoI-spezifische Substanzklasse mit klinischer Zulassung. Trotz guter Aktivität und relativ guter Verträglichkeit, entwickeln viele Tumore im Laufe der Therapie Resistenzen gegen diese Wirkstoffe.[84] Die häufigsten Ursachen für CPT-Resistenz sind Wirkstoff-Efflux durch Überexpression von ABC-Transportern (z. B. MDR1 oder P-gp), sowie genetische Mutationen, die zu einem strukturell veränderten, voll funktionsfähigen Proteinprodukt führen, an welches der Wirkstoff nicht mehr binden kann.[84] Da sowohl die

Substratspezifität der ABC-Effluxpumpen, als auch die Bindung an die TopoI maßgeblich von der Struktur des Wirkstoffes beeinflusst wird, kann die Chemoresistenz in diesem Fall zum Beispiel durch die Einführung einer strukturell neuartigen Klasse an TopoI-Inhibitoren umgangen werden.

1.4.3. Pleiotrope Wirkmechanismen

Wie bereits erwähnt, ist die Polychemotherapie noch immer der in der klinischen Anwendung vorherrschende Ansatz um Chemoresistenzen zu vermeiden bzw. zu umgehen. Beispielsweise durch den Einsatz von Irinotecan oder Cisplatin in Kombinationsregimen konnte die Ansprechrate und auch das progressionsfreie Überleben von Patienten mit metastasierten Tumorerkrankungen deutlich verbessert werden.[85] Allerdings zählen nicht nur häufige und starke Nebenwirkungen zu den Nachteilen der Kombinationstherapie, sondern auch unterschiedliche Löslichkeit und pharmakokinetische Eigenschaften der verschiedenen Wirkstoffe.[86] Eine vielversprechende Alternative zur konventionellen Kombinationstherapie ist das Design und die Entwicklung neuer Hybridmoleküle, welche zwei oder mehr biologisch aktive Pharmakophore in sich vereinen und dadurch mehrere zelluläre Targets gleichzeitig adressieren können.[87] Auf diese Weise können sowohl Chemoresistenzen vermieden, als auch Nebenwirkungen und pharmakokinetische Diskrepanzen minimiert werden.[88] Das wohl bekannteste antitumorale Hybridmolekül ist das aus *Streptomyces verticillus* isolierbare Glycopeptid Bleomycin (siehe Abb. 6).

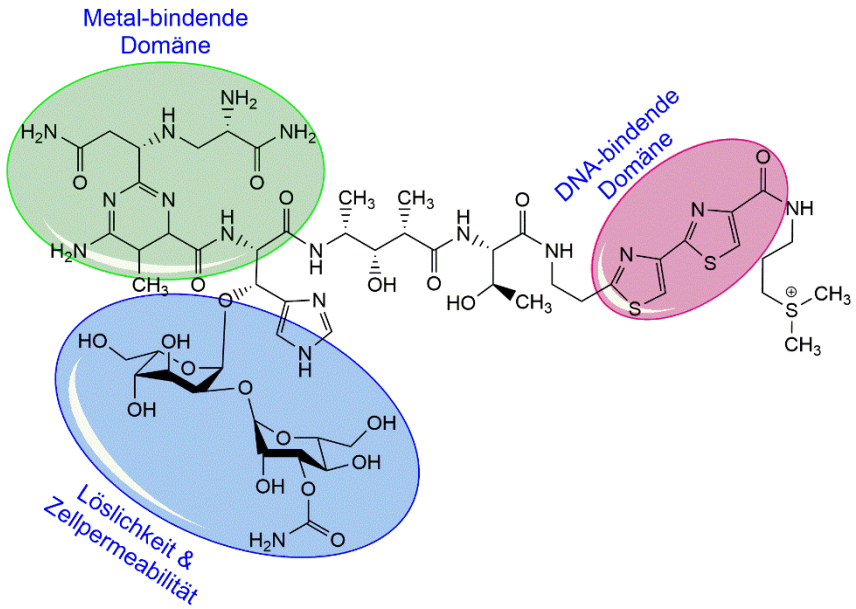

Abbildung 6. Struktur des klinisch-etablierten, antitumoralen Wirkstoffes Bleomycin. Bleomycin vereint drei Strukturmotive mit jeweils unterschiedlicher, biologischer Aktivität: einen Kohlenhydratanteil, welcher für Löslichkeit und Zellpermeabilität verantwortlich ist (blau), eine DNA-bindende Domäne (violett), sowie eine Amin-reiche Domäne für die Chelatisierung von Metallionen (grün).[89] (Eigene Darstellung nach Avendano und Menendez 2015.[89])

Dieses Molekül vereint drei strukturelle Domänen mit jeweils eigener biologischer Aktivität: den Kohlenhydratanteil, welcher die Löslichkeit verbessert und für die Aufnahme in die Zellen verantwortlich ist, ein DNA-bindendes Motiv, sowie eine Amin-reiche Domäne, welche redoxaktive Metallionen chelatisieren und dadurch die Entstehung von DNA-Strangbrüchen vermitteln kann.[87]

1.4.4. p53-unabhängige Apoptoseinduktion

Wie bereits unter 1.2.1.3. beschrieben, zählt die Mutation im TP53-Tumorsuppressorgen zu den häufigsten in Tumoren vorkommenden genetischen Veränderungen.[21,22] Da viele Chemotherapeutika ihre Aktivität durch die Induktion von Apoptose vermitteln, führt fehlende Expression eines funktionsfähigen p53-Proteins häufig zu Resistenzen, da die mutierten Zellen nicht mehr oder nur noch in geringem Maße in der Lage sind konventionelle, p53-gesteuerte Apoptose zu induzieren.[90] Insbesondere die Wirkeffizienz DNA-schädigender Wirkstoffe ist stark abhängig vom p53-Status der Tumorzellen. Beispielsweise konnte durch *in vitro*-Studien gezeigt werden, dass die Inaktivierung von p53 in Kolonkarzinomzellen mit Wildtyp p53 zu einer ausgeprägten Resistenz gegenüber Oxaliplatin führt.[91] Ein möglicher Ansatz für die Umgehung von derartigen Resistenzen sind Wirkstoffe, die die p53-Wildtypkonformation wieder herstellen können. Einige Substanzen mit dieser Eigenschaft sind bereits beschrieben, unter anderem die von Yu *et al.* untersuchten Thiosemicarbazon-Derivate (NSC319725, NSC319726, NSC328784): ihre Bindung an bestimmte p53-Mutanten macht die für die Funktionalität des Proteins wichtige Koordination von Zink-Ionen – eine Fähigkeit, die durch die Mutation verloren ging – wieder möglich.[92] Ein weiterer Ansatz für das Targeting von p53-mutanten, resistenten Tumorzellen sind Substanzen, die unabhängig von p53 die Apoptose-Maschinerie aktivieren können.[93,94] Die erst kürzlich veröffentlichte Studie von Anaya-Eugenio *et al.* beispielweise, beschreibt den aus *Penicillium aurantiacobrunneum* isolierten Naturstoff Auransterol, welcher unabhängig von der p53-Funktionalität Apoptose in HT-29 Kolonkarzinomzellen induzieren kann.[93] Im Gegensatz zu p53-reaktivierenden, besitzen p53-unabhängige Wirkstoffe ein breiteres Wirkungsspektrum, da sie in ihrer Wirksamkeit nicht auf spezielle Mutationsvarianten beschränkt sind.

1.4.5. *Realtime*-Monitoring mittels CETCs

Eine Methode zur Überwachung der Therapieeffizienz in Echtzeit könnte die aktuelle Tumortherapie deutlich verbessern, da schneller auf potentielle Veränderungen, wie zum Beispiel die Entstehung von Resistenzen, reagiert werden könnte. Konventionell wird das Ansprechen eines Tumors über Röntgenaufnahmen zu verschiedenen Zeitpunkten der Therapie bestimmt, wobei ausschließlich Größenveränderungen berücksichtigt werden. Auch funktionelle Darstellungen mittels Röntgen oder PET-CT während der therapeutischen Intervention werden für manche Tumorarten durchgeführt.[95] Das Vorliegen einer Therapie-induzierten Resistenz wird in der Regel durch eine einzelne Biopsie des Primärtumors oder der behandelten Metastase(n) bestätigt.[95] Die Problematik bei dieser

Vorgehensweise liegt einerseits darin, dass die Tumorheterogenität nicht berücksichtigt wird, und andererseits werden im Blut zirkulierende Tumorzellen (CTCs, siehe Kapitel 1.3.5.), welche für die Entstehung von Metastasen verantwortlich sind, nicht einbezogen. Darüber hinaus spiegeln CTCs die Heterogenität eines Tumors in Echtzeit wieder, das heißt auch potentielle Veränderungen auf genetischer, epigenetischer, transkriptioneller oder translationaler Ebene können nachgewiesen werden.[96] Diese - auch als *Liquid Biopsy* bezeichnete - Methode bringt zusätzliche Vorteile (wie z.B. geringe Kosten, geringer Aufwand, nicht-invasiv) mit sich und stellt deshalb einen vielversprechenden Ansatz zur Individualisierung der Tumortherapie dar. Insbesondere könnte das *Realtime*-Monitoring mittels CTCs eine Hilfestellung für Mediziner darstellen, um für eine bestimmte Therapie geeignete Patienten zu selektieren, und im Gegenzug, andere Patienten vor unnötigen Behandlungen und den damit verbundenen Nebenwirkungen zu schützen. Die klinische Bedeutung dieser Methode wurde in der Vergangenheit bereits durch verschiedene Studien untersucht. Studien von Rudiger *et al.*,[97] Inhestern *et al.*[98] und Pachmann *et al.*[99] belegen, dass das CTC-Profil im Laufe der Erkrankung bei Patienten mit Mamma-, Eierstock-, sowie Kopf- und Halskarzinomen möglicherweise eine Alternative zur invasiven Biopsie darstellt. Eine konstante oder abnehmende Anzahl an CTCs im Blut korreliert hierbei mit einer guten Prognose, während steigende CTC-Zahlen mit einem erhöhten Risiko der Metastasierung in Verbindung gebracht werden konnten.[100]

2. Zielsetzung

Das immer weiter fortschreitende biochemische Verständnis und die Entwicklung zielgerichteter Therapien haben seit Beginn des 21. Jahrhunderts zu enormen Fortschritten in der Tumortherapie beigetragen.[101] Darüber hinaus steht die Individualisierung der Therapie für den jeweiligen Patienten und dessen Tumor nunmehr im Fokus.[102] Trotz aller Fortschritte ist die Prognose für Patienten mit einer Krebserkrankung, insbesondere im Falle fortgeschrittener Stadien, oftmals schlecht und Therapien führen nicht zu einer Heilung, sondern lediglich zu einer Verlängerung der Lebenserwartung.[103] Das Scheitern der Therapie steht dabei in circa 90% der Fälle mit der Entstehung von resistenten Tumorzellen in Zusammenhang.[34] Aus diesem Grund besteht ein enormer Bedarf an neuen Wirkstoffen, welche insbesondere resistente Tumorzellen adressieren, aber auch an neuartigen Biomarkern, welche ein frühzeitiges Erkennen be- oder entstehender Resistenzen ermöglichen.

Im Rahmen dieser Arbeit werden präklinische Untersuchungen neuer, potentieller Wirkstoffkandidaten bezüglich deren antitumoraler Effektivität durchgeführt. Auch die Aufklärung der jeweiligen Wirkmechanismen auf molekularer Ebene steht hierbei im Fokus. Bei den untersuchten Substanzen handelt es sich um verschiedene Metallkomplexe, sowie eine Serie von Thienopyrimidon-Derivaten, welche alle für sich mögliche Ansätze zur Adressierung chemoresistenter Tumore darstellen. Die Untersuchung der Wirksamkeit der neuen Verbindungen, sowie die Aufklärung ihrer Wirkmechanismen erfolgt sowohl *in vitro* durch Experimente an humanen Zelllinien, als auch durch *in vivo*-Testsysteme (Hühnerei und Zebrafischembryo).

Weiterhin wird im Rahmen einer klinischen *proof-of-principle* Studie ein Monitoring-Verfahren untersucht, welches sowohl die Individualisierung der Therapie verbessern, als auch ein frühzeitiges Erkennen von Resistenzen ermöglichen könnte. Hierbei werden 22 Patienten mit kolorektalem Karzinom bezüglich der Anzahl und Eigenschaften ihrer zirkulierenden Tumorzellen im Blut evaluiert. Besonderes Augenmerk wird hierbei auf den Einfluss der jeweiligen Therapieverfahren in der neoadjuvanten oder adjuvanten Situation gelegt.

Insgesamt sollen die Erkenntnisse aus den präklinischen, sowie klinischen Studien die Grundlage zur Entwicklung neuer Ansätze, aber auch zum Ausbau und zur Optimierung etablierter Ansätze zur Umgehung von Chemoresistenzen bilden.

3. Synopsis

3.1. Übersicht der Teilprojekte

Die vorliegende kumulative Dissertation beinhaltet fünf Publikationen, in denen mögliche Konzepte für die Umgehung verschiedener Chemoresistenzen untersucht wurden.

Aufgrund der in vielen Tumoren vorkommenden *loss-of-function* Mutation im TP53-Tumorsuppressorgen, stellen neuartige Substanzen, die p53-unabhängige Arten des Zelltodes hervorrufen, eine Möglichkeit dar diese resistenten Tumorzellen zu adressieren. Die Publikationen I und IV beschreiben neuartige Ruthenium(II)-, bzw. Gold(I)-Komplexe, die diese Kriterien erfüllen und demnach potentiell zur Verbesserung der Ansprechrate in Tumoren mit p53-Mutation beitragen könnten.

Ein weiterer Ansatzpunkt zur Vermeidung bzw. Umgehung von Resistenzen sind Wirkstoffe, die sich von klinisch-etablierten Wirkstoffen strukturell unterscheiden, aber dasselbe zelluläre Target adressieren, wodurch bestimmte pharmakokinetische Resistenzmechanismen, sowie solche, die durch angepasste Genexpression der Tumorzellen begründet werden, umgangen werden können. Dieser Ansatz wird in Publikation II verfolgt, in der eine Serie neuartiger, antitumoraler Cu(II)-Komplexe beschrieben wird.

Auch Substanzen, die mehrere antitumorale Strukturmotive in sich vereinen, wodurch sie mehr als ein Target in der Zelle angreifen, besitzen gutes Potential für den Einsatz bei der Behandlung von chemoresistenten Tumoren. Die in Publikation III beschriebenen Thienopyrimidon-Derivate vereinen zwei etablierte antitumorale Strukturmotive und ein multimodaler Wirkmechanismus (anti-angiogen, vaskular-destruktiv, Kinase-Inhibition) konnte durch verschiedene *in vitro*-Studien belegt werden.

Darüber hinaus stellt auch die frühzeitige Erkennung von bestehenden oder entstehenden Chemoresistenzen eine wirkungsvolle Strategie zu deren Umgehung dar. Im Blut zirkulierende Tumorzellen, beispielsweise, sind ein einfach zugänglicher Biomarker, welcher in direktem Zusammenhang mit der Prognose des jeweiligen Patienten steht. In Publikation V werden die Ergebnisse einer prospektiven *proof-of-principle* Studie vorgestellt, deren Fokus auf dem Monitoring von CETCs während der Therapie von Patienten mit kolorektalem Karzinom mittels Maintrac®-Methode lag.

Alle im Rahmen dieser Arbeit untersuchten Testsubstanzen wurden an chemischen Lehrstühlen der Universität Bayreuth synthetisiert. Zum Teil wurden die Untersuchungen der Wirkmechanismen der Testverbindungen in Kooperation mit dem Institut für Biophysik der *Academy of Science of the Czech Republic* in Brünn (Tschechien), dem Lehrstuhl für Biophysik der Wissenschaftlichen Fakultät der *Palacky Universität Olmütz* (Tschechien), dem Lehrstuhl für Chemie des *Abeda Inamdar Senior College* in Pune (Indien), dem Lehrstuhl für Anorganische Chemie IV der Universität Bayreuth, dem *Research Center for Integrated Analysis and Territorial Management* der Universität Bukarest (Rumänien), sowie dem Lehrstuhl für *Cancer Biology* der *University of Kansas Medical Center* (Kansas, USA) durchgeführt. Die in Publikation V diskutierten klinischen Daten wurden in Zusammenarbeit mit dem Klinikum Bayreuth (Deutschland), sowie der Simfo GmbH (Bayreuth, Deutschland) generiert.

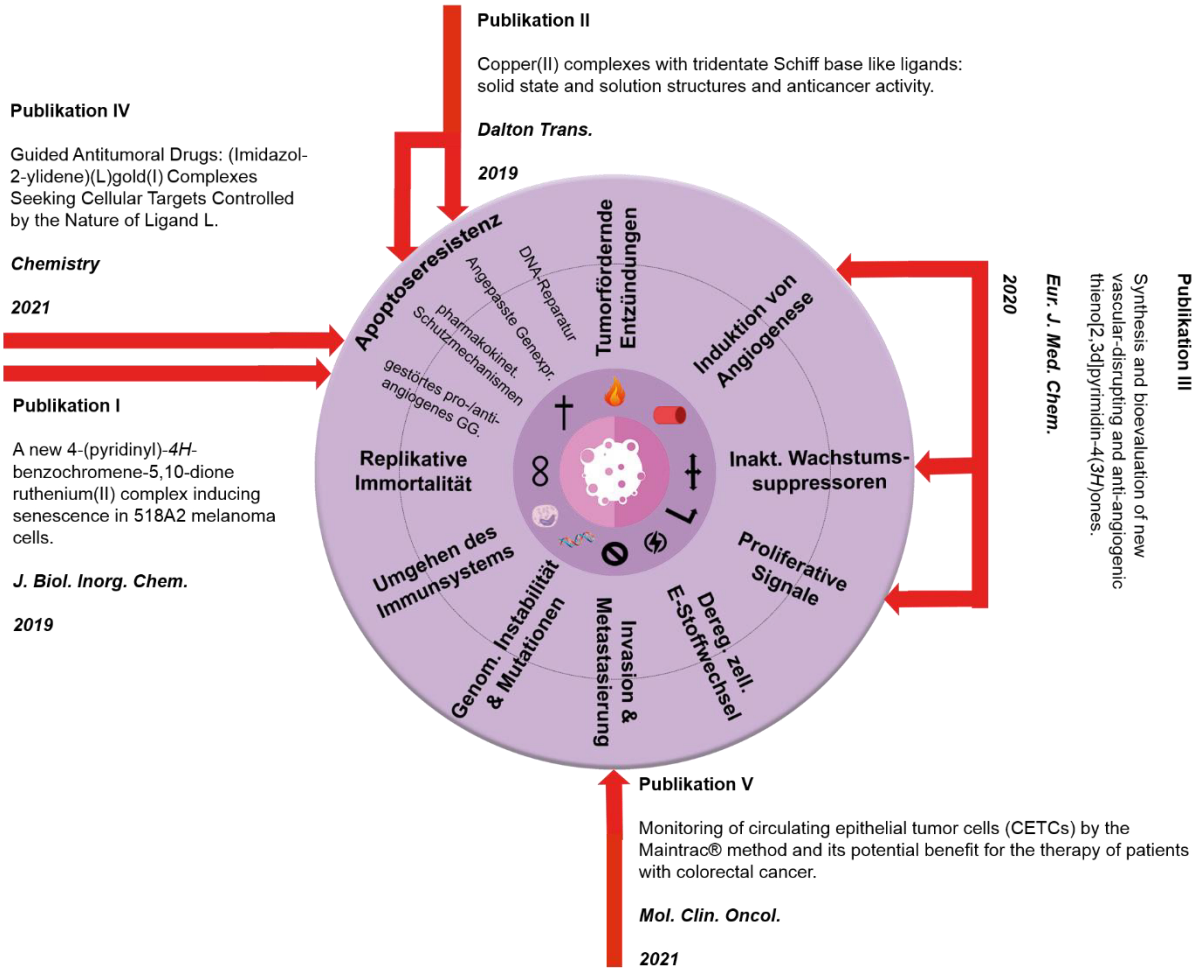

Abbildung 7. Die sogenannten *Hallmarks of Cancer*[6] können in verschiedener Weise für das Vorhandensein bzw. die Entstehung von Chemoresistenzen verantwortlich sein. Die einzelnen Publikationen wurden hierbei den jeweiligen Angriffspunkten für die Umgehung eben dieser Resistenzen zugeordnet. Im Rahmen dieser Arbeit wurden verschiedene Projekte bearbeitet, die sich mit der Umgehung von Chemoresistenzen beschäftigen. Publikation I beschreibt einen neuartigen Ruthenium(II)-Komplex der in der Lage ist in p53-defizienten Melanomzellen Seneszenz statt herkömmlicher Apoptose zu induzieren. Auch die in Publikation IV beschriebenen Gold(I)-NHC-Komplexe adressieren p53-mutierte Tumorzellen indem sie eine von p53-unabhängige Art des Zelltodes hervorrufen. In Publikation II geht es um neuartige Kupfer(II)-Komplexe, welche eine strukturell von etablierten Topoisomerase I-Inhibitoren verschiedene Wirkstoffklasse darstellen, und somit zur Umgehung pharmakokinetischer und durch veränderte Genexpression bedingter Resistenzen beitragen können. Die in Publikation III beschriebenen Thienopyrimidon-Derivate mit multimodalen Wirkmechanismus können sowohl anti-angiogen, als auch vaskular-destruktiv, sowie als Kinase-Inhibitoren wirken, und so chemoresistente Tumorzellen angreifen. In Publikation V wird eine potentielle Methode zur frühzeitigen Erkennung des Therapieansprechens beschrieben, bei welcher die für die Metastasierung verantwortlichen Tumorzellen (CETCs) im Blut von Patienten mit kolorektalem Karzinom mittels Maintrac®-Methode überwacht werden.

3.2. Ein neuartiger, Seneszenz-induzierender 4-(pyridinyl)-4*H*-benzo[*g*]chromene-5,10-dion Ruthenium(II)-Komplex

Der erste im Rahmen dieser Dissertation veröffentlichte Artikel behandelt einen neuartigen Ruthenium(II) *piano stool*-Komplex, der sich durch seine Selektivität auszeichnet und - statt herkömmlicher Apoptose - zelluläre Seneszenz induziert, was insbesondere für die Behandlung Apoptose-resistenter Tumoren einen interessanten Ansatz darstellt.

Das maligne Melanom zählt zu den aggressivsten Arten des Hautkrebses. Die 5-Jahres-Überlebensrate von Patienten mit metastasierten Erkrankungen (Stadium IV) liegt zwischen 9 und 28%.[104] Obwohl der Großteil dieser Patienten mittlerweile von Immuntherapien oder anderen zielgerichteten Wirkstoffen profitiert, sind diese häufig mit starken Nebenwirkungen verbunden. Für Stadium IV-Patienten, welche nicht auf zielgerichtete Therapien ansprechen, ist die konventionelle, zytotoxische Chemotherapie die einzig mögliche Option, wobei hier die Ansprechrate eher gering und die Wahrscheinlichkeit einer Resistenzentwicklung hoch ist.

Der in dieser Studie untersuchte Benzochromen-Ruthenium(II)-Komplex (Abb. 8) zeigt eine mit Cisplatin vergleichbare Selektivität für humane, Bcl-2-überexprimierende[105] und p53-mutierte[106] 518A2 Melanomzellen, verbunden mit einer geringeren Toxizität gegenüber nicht-malignen humanen Hautfibroblasten. Da die antitumoralen Eigenschaften vieler Rutheniumverbindungen auf deren Affinität zu DNA beruhen, wurde auch der neuartige Rutheniumkomplex auf eine solche hin untersucht. Anhand drei verschiedener Versuche, sowie Aufnahmestudien konnte die DNA als zelluläres Target des Metallkomplexes identifiziert werden. Da weiterhin für Cisplatin und Ruthenium-basierte Wirkstoffe bekannt ist, dass diese unter anderem in den Redoxstoffwechsel der Zellen eingreifen können, wurde auch dies für den Ruthenium(II)-Komplex überprüft. Und in der Tat konnte nach Behandlung von 518A2 Melanomzellen mit dem Metallkomplex ein, im Vergleich zu Cisplatin und dem Liganden, fünfmal stärkerer Anstieg der intrazellulären Konzentration an reaktiven Sauerstoffspezies (ROS) beobachtet werden. Mit Hilfe von Zyklovoltammetrie-Studien wurden darüber hinaus die Redoxeigenschaften des Rutheniumkomplexes, sowie des Liganden im zellfreien Kontext untersucht. Hierbei konnte die Reversibilität des Elektronentransfers, welche nur für den Metallkomplex, nicht aber für den Liganden nachgewiesen werden konnte, für die unterschiedlich starken Effekte auf die ROS-Konzentration verantwortlich gemacht werden.

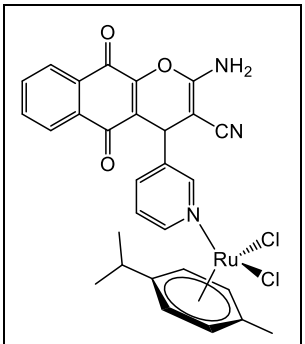

Abbildung 8. Struktur des Benzochromen-Ru(II)-Komplexes.

Eine mögliche Erklärung für die selektivere Wirkung des Rutheniumkomplexes im Vergleich zum Liganden könnte einerseits in seiner grundsätzlich höheren und spezifischeren Aufnahme begründet sein. Andererseits zeigten sowohl die Zytotoxizitätsmessungen, als auch Zellzyklusstudien eine un-

spezifischere Aktivität des Liganden, welche vermutlich auf eine generelle Schädigung von Biomolekülen durch höhere Reaktivität und Instabilität zurückzuführen ist. Das Ruthenium-Fragment scheint demzufolge das Naphthoquinon-System bezüglich seiner Redoxeigenschaften zu stabilisieren, was höchstwahrscheinlich zu einem komplett unterschiedlichen zellulären Wirkmechanismus führt.
Da anhand von Zellzyklusstudien und einer Messung der Caspase-3/7 Aktivität eine maßgebliche Beteiligung von Apoptose, als auch Nekrose am Wirkmechanismus des Benzochromen-Rutheniumkomplexes ausgeschlossen werden konnte, rückten nun alternative Arten des Zelltodes oder Wachstumsarrests in den Fokus der Untersuchungen. In diesem Zusammenhang konnte nach Behandlung mit dem Komplex mit Hilfe eines Seneszenz-assoziierten ß-Galaktosidase (SA-ßgal) Aktivitätstests ein deutlich erhöhter Anteil an seneszenten Zellen nachgewiesen werden.
Eine mögliche Alternative für die konventionelle, zytotoxische Chemotherapie, bei der das Hauptziel in der Elimination von malignen Zellen liegt, stellt die sogenannte Therapie-induzierte Seneszenz (TIS) dar.[80,107] Da das Ziel der TIS die irreversible Inhibition der Tumorzellproliferation und nicht der Tumorzelltod ist, stellt sie einen vielversprechenden Ansatz für die Reduktion der Nebenwirkungen in der Langzeitbehandlung mancher Krebsarten dar. Ein weiterer Vorteil von TIS-induzierenden Chemotherapeutika liegt in ihrer Wirksamkeit gegenüber Krebszellen, die resistent gegenüber Apoptose-induzierenden Stimuli sind.[107] Allerdings gibt es auch kontroverse Studien, die belegen, dass ein erhöhter Anteil an seneszenten Zellen unter gewissen Umständen zur Tumorprogression beitragen kann, weshalb spezifisch Seneszenz-induzierende Wirkstoffe, wie der in dieser Studie beschriebene Ruthenium(II)-Komplex, einen wertvollen Beitrag zur weiteren Forschung in diesem Bereich leisten können.

Weitere Details in: M. Gold, Y. Mjahid, K. Ahmed, H. Kostrhunova, J. Kasparkova, V. Brabec, B. Biersack, R. Schobert.

A new 4-(pyridinyl)-4H-benzo[g]chromene-5,10-dione ruthenium(II) complex inducing senescence in 518A2 melanoma cells.

J. Biol. Inorg. Chem. **2019** *24*,647-657.

[Publikation I]

3.3. Kupfer(II)-Komplexe mit Schiff-Base ähnlichen Liganden: Festphasenstruktur, Struktur in Lösung, sowie antitumorale Aktivität

Die zweite im Rahmen dieser Dissertation veröffentlichte Arbeit behandelt eine Serie von 18 Kupfer(II)-Komplexen mit konzentrationsabhängiger, zytotoxischer Wirkung gegenüber verschiedenen Tumorzelllinien. Für die aktivsten Verbindungen konnte eine Inhibition der Topoisomerase I als Wirkmechanismus nachgewiesen werden.

Topoisomerase I-Inhibitoren, wie Camptothecin, Topotecan und Irinotecan, sind etablierte chemotherapeutische Wirkstoffe und werden klinisch insbesondere in Kombinationsregimen für die Therapie von Eierstockkarzinomen und kolorektalen Karzinomen eingesetzt.[108] Eine große Problematik beim Einsatz dieser Wirkstoffe ist die hohe Rate der Resistenzentwicklung,[109] was möglicherweise durch Wirkstoffe umgangen werden könnte, die nicht zur Camptothecin-Familie gehören und eine komplett andere Struktur aufweisen.

Im Rahmen dieser Studie wurden 18 Kupfer(II)-Komplexe mit Schiff-Base ähnlichen Liganden synthetisiert, welche in ihren Substituenten (R, R‘, R‘‘) variiert wurden um die elektronische Umgebung des Metallzentrums zu verändern (Abb. 9). Mittels Kristallstrukturanalyse wurden neun Komplexe genauer untersucht: Komplexe ohne Substitution am Pyrimidinring kristallisierten als dimere oder polymere Komplexe, während Derivate mit substituiertem Pyrimidinring zu einer quadratisch-planaren Festphasenstruktur führten. Die Struktur in Lösung, sowie das Löslichkeitsverhalten und die Stabilität der Kupferkomplexe wurden mittels UV/Vis-Spektroskopie und Zyklovoltammetrie analysiert und in nachfolgenden biochemischen Tests berücksichtigt. Mit Hilfe von MTT-Assays wurde zunächst die Zytotoxizität aller Komplexe, sowie Kupfersulfat und einem Liganden gegenüber verschiedenen Tumorzelllinien bestimmt. Hier stellten sich insbesondere die Komplexe mit Elektronen-schiebenden Substituenten am Pyridinring (**10** und **14**, Abb. 9) als sehr aktiv heraus, während sich eine Substitution mit Elektronen-ziehenden Gruppen am Pyridinring negativ auf die zytotoxische Aktivität auswirkte. Die Behandlung der Tumorzelllinien mit reinem Liganden resultierte in keinerlei zytotoxischem Effekt. Interessanterweise zeigte der Kupfer(II)-Komplex **10** zusätzlich eine gute Selektivität für Tumorzellen (Selektivitätsindex: 4.8; Cisplatin: 3.0). Nachdem sowohl eine Interaktion mit DNA, als auch ein Einfluss auf die intrazelluläre Konzentration an reaktiven Sauerstoffspezies als Wirkmechanismus für die drei aktivsten Komplexe **1**, **10** und **14** ausgeschlossen werden konnte, sollte noch deren Wirkung auf ein weiteres für Kupferkomplexe typisches

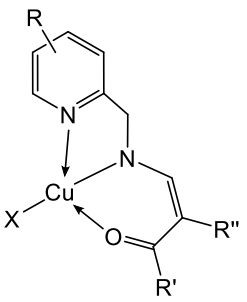

#	R	R‘	R“	X
1	-4-H	-Me	-COOEt	NO_3^-
10	-4-OMe	-OEt	-COOEt	Br^-
14	-4-Me	-OEt	-COOEt	Br^-

Abbildung 9. Übersichtsstruktur der Kupferkomplexe mit Schiff-Base ähnlichen Liganden mit den Substituenten R, R‘ und R‘‘.

Target – das Enzym Topoisomerase I – untersucht werden.[110,111] Topoisomerasen sind Enzyme, die topologische DNA-Isomere durch Änderung des Grades an Superhelizität ineinander umwandeln und insbesondere für die Replikation und Transkription der DNA obligatorisch sind. Da zyklische Plasmid-DNA in Lösung hauptsächlich in superhelikaler (sc = *supercoiled*) Form vorliegt, bewirkt die Inkubation mit Topoisomerase I eine Relaxation dieser Plasmide hin zur offenkettigen (oc = *open circular*) Form. Diese beiden Formen, sowie Intermediate können aufgrund ihrer unterschiedlichen elektrophoretischen Mobilität in einem Agarosegel voneinander getrennt werden. Für die Komplexe **1** und **10** konnte eine starke, für Komplex **14** eine moderate Inhibition der Topoisomerase I-Aktivität nachgewiesen werden (Abb. 10), welche zumindest teilweise zur biologischen Aktivität dieser Verbindungen beitragen dürfte. Dieser spezifische Wirkmechanismus unterscheidet die in dieser Studie beschriebenen Verbindungen von bereits bekannten Kupferkomplexen mit Topoisomerase I inhibierender Wirkung, welche zusätzliche Effekte auf das oxidative Gleichgewicht der Zellen, sowie eine DNA-Interaktion zeigen.[110]

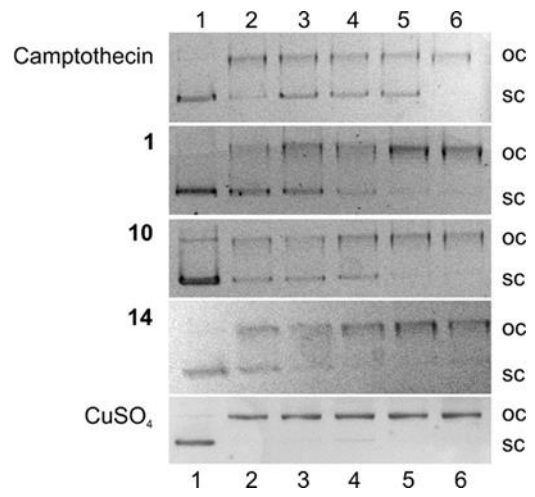

Abbildung 10. Inhibition der Topoisomerase I durch die Kupfer(II)-Komplexe **1**, **10** und **14**. Spalte 1: 100 µM, kein Enzym; Spalten 2-6: 100, 50, 25, 10, 5 µM mit Enzym; oc = open circular, sc = supercoiled.

Weitere Details in: K. Dankhoff, M. Gold, L. Kober, F. Schmitt, L. Pfeiffer, A. Dürrmann, H. Kostrhunova, M. Rothemund, V. Brabec, R. Schobert, B. Weber.

Copper(II) complexes with tridentate Schiff base-like ligands: solid state and solution structures and anticancer activity.

Dalton Trans. **2019** *48*, 15220-15230.

[Publikation II]

3.4. Synthese und Bioevaluation neuartiger vaskular-disruptiver und anti-angiogener Thieno[2,3-*d*]pyrimidin-4(3*H*)-one

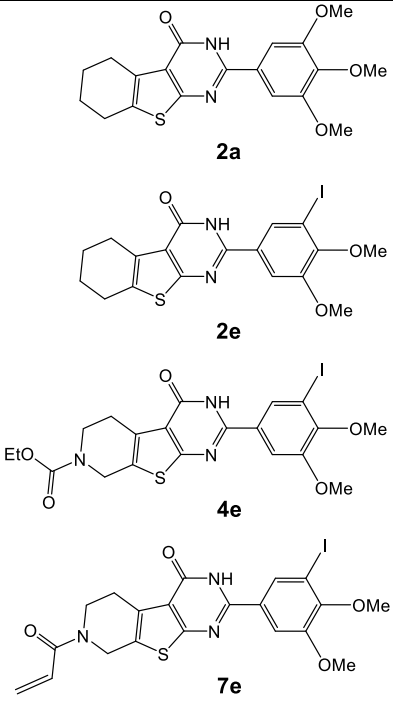

Abbildung 11. Strukturen der Leitverbindung **2a**, sowie der aktivsten Derivate **2e, 4e** und **7e**.

Aufgrund der entgleisten Expression von pro- und anti-angiogenen Faktoren, unterscheiden sich Tumorblutgefäße morphologisch, sowie funktionell deutlich von normalen Blutgefäßen: es fehlt jegliche strukturelle Ordnung und die sogenannten Tumorendothelzellen sind nur locker und diskontinuierlich mit der Basalmembran verknüpft.[112] Diese und andere Alleinstellungsmerkmale machen Tumorblutgefäße zu einem interessanten Target für die Chemotherapie,[113] z. B. mit Mikrotubuli-bindenden Wirkstoffen (*Microtubule binding agents*, MBA), die in der Mitosephase des Zellzyklus angreifen. Ein wichtiges Strukturmotiv vieler MBA ist das 3,4,5-Trimethoxyphenyl-Fragment, welches an die ß-Untereinheit von Tubulin-Polymeren bindet.[114] Eine Möglichkeit um der Resistenzentwicklung, welche beim Einsatz von MBA in Kombinationsregimen relativ häufig vorkommt, entgegenzuwirken, ist die kovalente Verknüpfung des Trimethoxyphenyl-Motivs mit anderen biologisch aktiven Strukturmotiven, um Wirkstoffe mit multimodalen Wirkmechanismen zu erhalten. Die dritte Publikation im Rahmen dieser Dissertation befasst sich mit einer Serie von 46 Arylthienopyrimidonen, welche an die von Rabindran *et al.*[115] veröffentlichte Leitstruktur **2a** (Abb. 11) angelehnt sind. Sie verbinden das Trimethoxyphenyl-Motiv mit dem Thieno[2,3-*d*]pyrimidon-Pharmakophor und zeigen sowohl *in vitro*, als auch *in vivo* vaskular-disruptive und anti-angiogene Effekte.

Zunächst konnte im Rahmen von Zytotoxizitätsstudien beobachtet werden, dass eine 3-Bromo-4,5-dimethoxyphenyl (Motiv **c**) und 3-Iodo-4,5-dimethoxyphenyl-Substitution (Motiv **e**) zu einer deutlichen Steigerung der Wirksamkeit im Vergleich zur Leistruktur **2a** führte. Diese

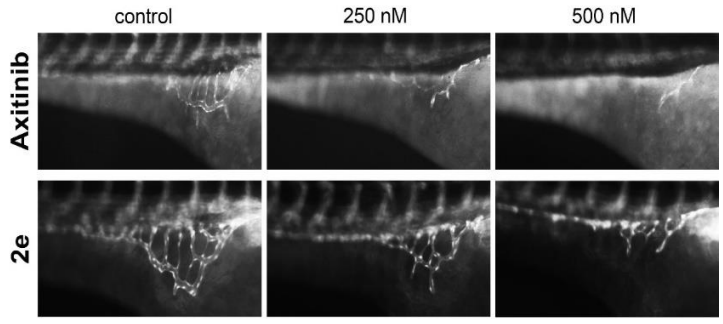

Abbildung 12. Anti-angiogene Effekte der Testsubstanz **2e** in Zebrafisch-Angiogenese-Tests. Hierfür wurden 24 h alte, transgene *Tg(fli1a:EGFP)* Zebrafischembryonen mit 250 bzw. 500 nM an Testsubstanz **2e** inkubiert und anschließend die Fläche der subintestinalen Venen (SIV) densitometrisch analysiert. Der bekannte anti-angiogene Wirkstoff Axitinib diente als Positivkontrolle (6.3× Vergrößerung).

Verbindungen (**2e**, **4e** und **7e**; Abb. 11) waren zudem in der Lage die Polymerisation von isoliertem Tubulin zu inhibieren. Die beiden aktivsten Verbindungen **2e** und **4e** wurden für weiterführende mechanistische Studien ausgewählt. Nachdem der nach Behandlung von Endothelhybridzellen mit **2e** und **4e** beobachtete G2/M-Arrest sogar ausgeprägter war als bei der Tubulin-bindenden Referenzverbindung Combretastatin-A4 (CA4) konnte nachgewiesen werden, dass zusätzliche Effekte durch das Thienopyrimidon-Fragment (CDK1 Inhibition) dafür verantwortlich sind. Genau wie die Referenzverbindung CA4, zeigten die Test-substanzen **2e** und **4e** konzentrations-abhängig sowohl vaskular-disruptive, als auch anti-angiogene Effekte in *Tube Formation*-Assays (Abb. 13), CAM-Assays und Zebrafisch-Angiogenese-Tests (Abb. 12). Besonders interessant bezüglich einer potentiellen klinischen Anwendung war in diesem Zusammenhang die Beobachtung, dass die durch Verbindung **2e** hervorgerufene Destruktion der Blutgefäße in CAM-Assays reversibel war und die Blutgefäße in der Lage waren sich wieder zu regenerieren. Generell erwies sich vor allem Verbindung **2e** als potentieller Wirkstoffkandidat, da sowohl in CAM-Assays, als auch in Zebrafisch-Angiogenese-Assays eine gute Verträglichkeit beobachtet wurde. Derivat **4e** und Referenz-verbindung CA4 konnten aufgrund ihrer starken Toxizität nicht im Zebrafischembryo-Model getestet werden.

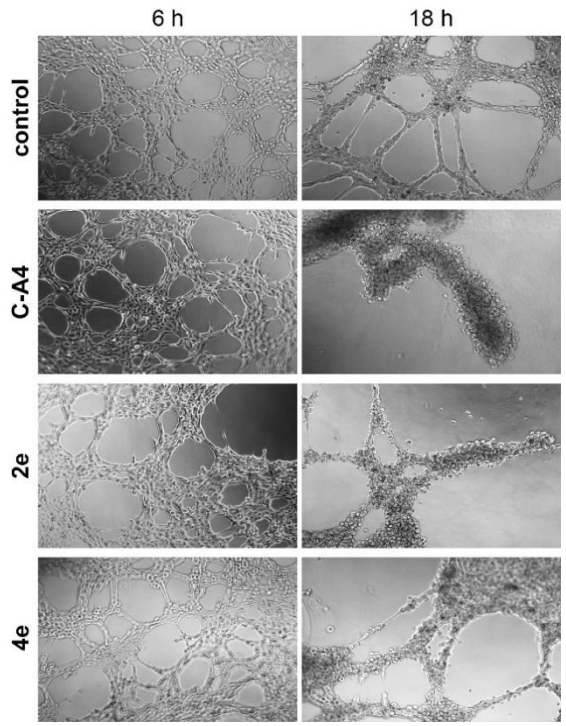

Abbildung 13. Vaskular-disruptive Effekte der Derivate **2e** und **4e** in *Tube Formation*-Assays mit EA.hy926 Endothelhybridzellen in Matrigel. CA4 diente als Positiv-kontrolle. Die Negativkontrollen wurden mit der entsprechenden Menge an DMSO behandelt (Vergrößerung 60×).

Weitere Details in:

M. Gold, L. Köhler, C. Lanzloth, I. Andronache, S. Anant, P. Dandawate, B. Biersack, R. Schobert.

Synthesis and bioevaluation of new vascular-targeting and anti-angiogenic thieno[2,3-d]pyrimidin-4(3H)-ones.

Eur. J. Med. Chem. **2020** *189*, 112060-112076.

[Publikation III]

3.5. Antitumorale [1,3-diethyl-4,5-diarylimidazol-2-yliden](L) Gold(I)-Komplexe mit zellulären Targets basierend auf den Eigenschaften des Liganden L

Fast die Hälfte aller Tumore (42%) weisen eine Mutation im Tumorsuppressorgen TP53, welches den Transkriptionsfaktor p53 codiert, auf.[116] Das Tumorsuppressorprotein p53 (auch als »Wächter des Genoms« bezeichnet) wird durch zellulären Stress, wie z.B. DNA-Schäden oder Onkogene, aktiviert und beeinflusst in Folge dessen verschiedene Signalwege, die situationsbedingt zu Zellzyklusarrest, Seneszenz oder Apoptose führen können.[116] Die Zelle wird dadurch vor neoplastischer Entartung geschützt. Fehlt hingegen funktionsfähiges p53 in der Zelle, so können sich Schäden anhäufen und eine Karzinogenese wird begünstigt. Darüber hinaus hat der p53-Status auch einen großen Einfluss auf die Chemosensitivität von Tumorzellen: Tumorzellen mit p53-Mutation sind resistent(er) gegenüber Wirkstoffen, die hauptsächlich über p53-vermittelte Induktion von Apoptose wirken, wie z.B. Oxaliplatin[117] oder Doxorubicin.[118] Um eine Verbesserung der Ansprechrate auf eine Chemotherapie zu erreichen, sind deshalb neuartige Wirkstoffe gefragt, die unabhängig von p53 wirken.

Die vierte Veröffentlichung im Rahmen dieser Dissertation beschäftigt sich mit der intrazellulären Lokalisation und dem antitumoralen Wirkmechanismus verschiedener, zum Teil neuartiger [1,3-diethyl-4,5-diarylimidazol-2-yliden](L)Gold(I)-NHC-Komplexe, welche eine vom p53-Mutationsstatus unabhängige Wirksamkeit besitzen.

Die untersuchten Komplexe sind hierbei an die von Muenzner *et al.*[119] bereits publizierte Leitstruktur **6a** (L = derselbe NHC-Ligand; Abb. 14) angelehnt und unterscheiden sich von dieser nur durch den jeweiligen Liganden L (**4a**: L = Cl; **5a**: L = PPh_3; Abb. 14). Zusätzlich zu den Komplexen **4a-6a** wurden die Anthracenyl-Analoga **4b-6b** synthetisiert und aufgrund ihrer autofluoreszenten Eigenschaften für intrazellulären Lokalisationsstudien herangezogen.

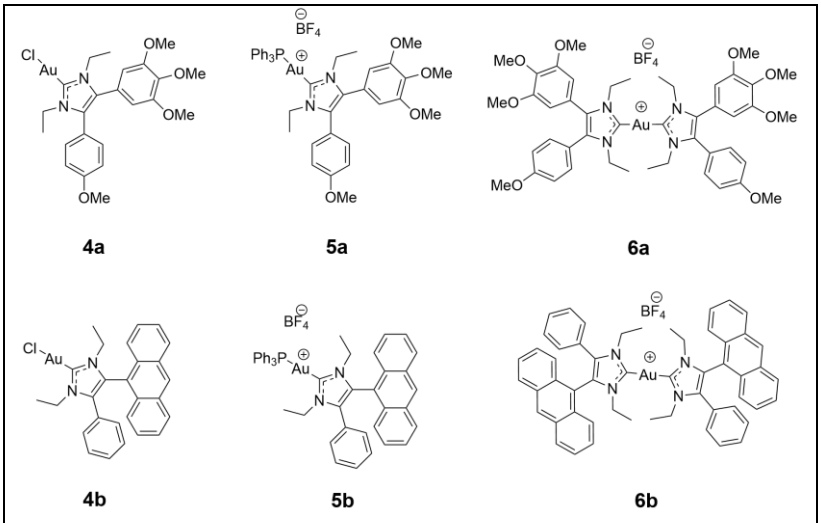

Abbildung 14. Strukturen der antitumoralen [1,3-diethyl-4,5-diarylimidazol-2-yliden](L)Gold(I)-Komplexe **4-6**.

Alle Komplexe **4-6** zeigten in MTT-Tests p53-unabhängig antiproliferative Eigenschaften gegenüber verschiedenen Tumorzelllinien. Innerhalb beider Serien **a** und **b** beobachtete man eine mit zunehmendem DLC-Charakter steigende Aktivität der Verbindungen (**4 < 5 < 6**), was einen ersten Hinweis auf eine vergleichbare zelluläre Aufnahme und Wirkung der jeweils analogen Komplexpaare **a** und **b** darstellt. Die Komplexe **4b-6b** wurden ursprünglich als leicht in der Zelle zu lokalisierende

Analoga der Verbindungen **4a-6a** synthetisiert. Letztere enthalten statt dem fluoreszenten Anthracenyl-Liganden, das für die antitumorale Substanz CA4 typische 3,4,5-Trimethoxyphenyl-Motif. Nach Behandlung von 518A2 Melanomzellen konnte der neutrale Komplex **4b** mittels konfokaler Fluoreszenzmikroskopie im Nukleus und in geringerem Ausmaß im Zytoplasma der Zellen nachgewiesen werden. Der kationische Triphenylphosphan-Komplex **5b**, reicherte sich spezifisch in den Mitochondrien der Tumorzellen an, wohingegen der bis-NHC-Komplex **6b** überwiegend in den Lysosomen lokalisiert werden konnte (siehe Abb. 15). Basierend auf den Ergebnissen der Lokalisationsstudien wurde anschließend mittels verschiedener biochemischer Assays auf Kompartiment-spezifische Aktivitäten der Gold(I)-NHC-Komplexpaare **4**, **5** und **6** getestet. Aufgrund der Nukleotrophie des neutralen Komplexes **4b**, wurden die Verbindungen **4a/b** auf eine potentielle Interaktion mit DNA hin untersucht. Wie bereits für andere neutrale Gold(I)-NHC-Komplexe mit leicht austauschenden Liganden (z.B. Cl^-) bekannt,[120] konnte für die Komplexe **4** eine nicht-kovalente Interaktion mit DNA nachgewiesen werden. Die in den Mitochondrien vermuteten Komplexe **5** zeigten eine sogar stärkere Inhibition des Enzyms Thioredoxinreduktase (TrxR) als der klinisch etablierte Goldkomplex Auranofin. Auch eine aus der Ansammlung von oxidiertem Thioredoxin (Trx) und reaktiven Sauerstoffspezies in den Mitochondrien resultierende Reduktion des mitochondrialen Membranpotentials konnte für beide Komplexe **5a** und **5b** nachgewiesen werden. Für die bis-NHC-Komplexe **6** konnte, passend zu ihrer Anreicherung in den Lysosomen der Tumorzellen, eine zeitabhängige Abnahme des Lysosomenmembranpotentials beobachtet werden.

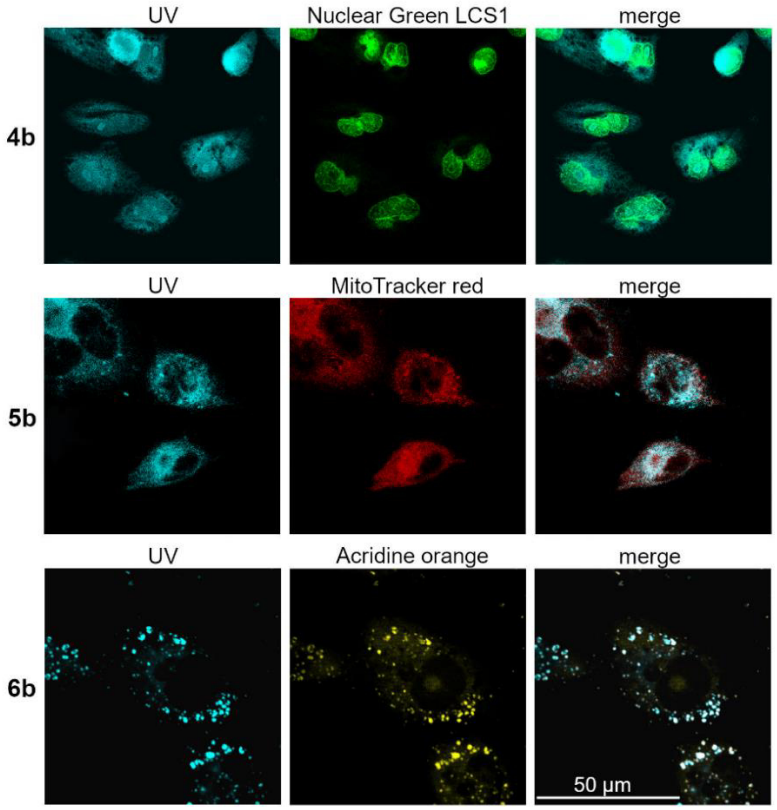

Abbildung 15. Fluoreszenzmikroskopische Lokalisationsstudien der Komplexe **4b-6b** in 518A2 Melanomzellen. Emission der Gold(I)-NHC-Komplexe im UV-Bereich (linke Spalte), Gegenfärbung der jeweiligen zellulären Kompartimente mit spezifischen Farbstoffen (mittlere Spalte), *merge* (rechte Spalte). Vergrößerung 2000×.

Insgesamt konnte die Annahme, dass sich die jeweiligen Komplexpaare der Serien **a** und **b** in ihrer zellulären Aufnahme und Wirkungsweise ähneln, sowohl durch vergleichbare Ergebnisse in Zytotoxizitätsstudien, als auch in mechanistischen Studien bestätigt werden. Die für die intrazelluläre Lokalisation ausschlaggebende Faktoren scheinen letztlich vor allem der Ligand L, und von diesem bestimmt, die Ladung, Größe und Lipophilie der Komplexe zu sein. Diese Erkenntnisse könnten für das rationale Design von Target-spezifischen metallbasierten Wirkstoffen von großer Bedeutung sein.

Weitere Details in: S.I. Bär, M. Gold, T. Rehm, S.W. Schleser, A. Bär, L. Köhler, L.R. Carnell, B. Biersack, R. Schobert.

Guided Antitumoral Drugs: (Imidazol-2-ylidene)(L)gold(I) Complexes Seeking Cellular Targets Controlled by the Nature of Ligand L

Chemistry **2021** *27*, 5003-5010.

[Publikation IV]

3.6. Monitoring von zirkulierenden, epithelialen Tumorzellen (CETCs) mittels Maintrac®-Methode und dessen potentieller klinischer Nutzen für die Therapie von Patienten mit kolorektalem Karzinom

Das kolorektale Karzinom ist weltweit für 9.2% aller tumor-bedingten Sterbefälle verantwortlich und belegt damit, nach dem Bronchialkarzinom, Platz zwei der tumor-bedingten Todesursachen.[121] Durch die Einführung von Screening-Programmen, sowie neuen Wirkstoffen konnte das Gesamtüberleben von Patienten mit kolorektalem Karzinom in den letzten 30 Jahren deutlich verbessert werden.[122] Während die konventionelle zytotoxische Chemotherapie noch immer die Basis der Behandlung von Kolorektalkarzinomen darstellt, sind in den letzten Jahren zielgerichtete Therapien, für welche die Selektion geeigneter Patienten über bestimmte genetischer Marker erfolgen kann, in den Vordergrund gerückt.[123] Allerdings profitiert nur ein relativ kleines Patientenkollektiv von diesem Therapieansatz, da die Wirksamkeit auf spezifischen genetischen Eigenschaften der Tumorzellen basiert. Obwohl auch für das Ansprechen einer konventionellen Chemotherapie bereits prognostische Biomarker existieren, werden diese aus zeit- und kostentechnischen Gründen, sowie unzureichender Validierung in der Praxis meist nicht eingesetzt.[123,124] Zirkulierende Tumorzellen stellen das Bindeglied zwischen dem Primärtumor und Fernmetastasen dar, und können aus Blutproben von Krebspatienten relativ einfach quantifiziert und charakterisiert werden.

Eine etablierte Methode zur Detektion dieser Zellen im Blut von Tumorpatienten ist das CellSearch-System, bei welchem nach einem Anreicherungsschritt eine immunologische Färbung zur Identifikation der zirkulierenden Tumorzellen erfolgt.[125] Im Falle von Patienten mit metastasiertem kolorektalem Karzinom liefert die CellSearch-Methode gute Ergebnisse,[126,127] bei nicht-metastasierten Patienten allerdings, ist die Detektionsrate mittels CellSearch zu gering um potentielle Zusammenhänge zwischen zirkulierenden Tumorzellen und Patientencharakteristika oder Therapieverlauf zu untersuchen.[128] In dieser prospektiven *proof-of-principle* Studie wurde die Maintrac®-Methode zur Quantifizierung und Charakterisierung der zirkulierenden, epithelialen Tumorzellen (*circulating epithelial tumor cells*,

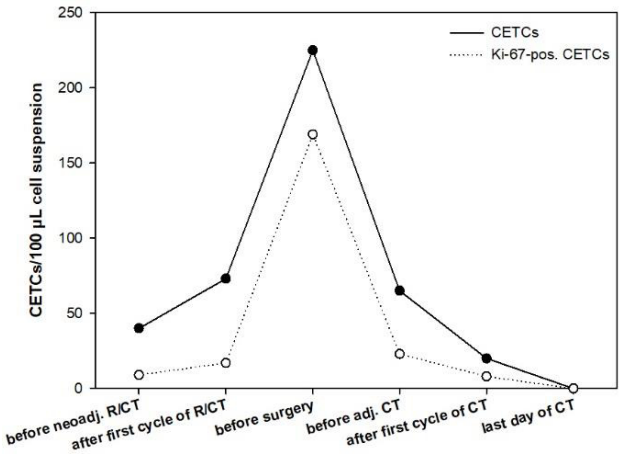

Abbildung 16. Verlauf der Anzahl an zirkulierenden, epithelialen Tumorzellen (CETCs), sowie Ki-67-positiven CETCs im Blut eines Patienten mit Rektumkarzinom während der neoadjuvanten R/CT, sowie der anschließenden adjuvanten CT. Dieser Patient scheint sowohl von der Operation, als auch von der zusätzlichen adjuvanten Therapie zu profitieren.

CETCs) bei 22 Patienten mit kolorektalem Karzinom aller Stadien verwendet, welche mit neoadjuvanter und/oder adjuvanter (Radio-)Chemotherapie (R/CT) behandelt wurden.

Mit Hilfe der Maintrac®-Methode konnten im Blut aller 22 Patienten unabhängig vom Tumorstadium CETCs detektiert werden. Zusätzlich zu den epithelialen Eigenschaften, konnten einigen CETCs proliferative Aktivität, sowie Stammzelleigenschaften nachgewiesen werden. Außerdem konnten literaturbekannte Zusammenhänge reproduziert werden, was einen weiteren Hinweis für die Funktionalität der eingesetzten Methode in diesem Kontext darstellt. Studien von Zitt, sowie Sun *et al.* zeigten übereinstimmend, dass bei Patienten mit gutem Ansprechen auf die Therapie die Anzahl an zirkulierenden Tumorzellen abfällt, während bei schlechtem Ansprechen keine nennenswerten Veränderungen zu verzeichnen waren.[129,130] Diese Ergebnisse konnten auch durch weitere Studien bestätigt werden.[131,132] Im Rahmen dieser Studie zeigte sich ebenfalls ein Zusammenhang zwischen dem Ansprechen der Rektumkarzinom-Patienten auf eine neoadjuvante R/CT ermittelt nach histologischen und bildgebenden Kriterien und dem Verlauf der CETC-Zahl. Bei Patienten mit gutem Ansprechen auf die Therapie kam es zu einer Abnahme der CETC-Zahl im Blut, während eine Zunahme der CETCs mit einem schlechten Ansprechen korrelierte.

Im Gegensatz zur heterogenen Reaktion der CETC-Zahl in der neoadjuvanten Situation, führte die adjuvante CT zu einer konstanten Abnahme der CETCs im Blut der Patienten. Eine potentielle Erklärung für diese Beobachtung ist die in der adjuvanten Situation geringere Tumorlast. Darüber hinaus ist die Wahrscheinlichkeit, dass initial resistente Zellen enthalten sind, im Falle der mikroskopischen Restgewebe in der adjuvanten Situation geringer. Auf der Grundlage dieser Beobachtung wären weitere Studien interessant, um die Fragestellung zu klären, ob und wann einzelne Rektumkarzinompatienten von einer zusätzlichen adjuvanten CT nach einer neoadjuvanten R/CT profitieren würden.

Alle beschriebenen Trends konnten anhand eines Fallbeispiels veranschaulicht werden: Ein 63-jähriger Rektumkarzinom-Patient (Stadium III) verzeichnete einen drastischen Anstieg der CETCs im Laufe der neoadjuvanten R/CT auf welche er schlecht ansprach. Erst nach der operativen Entfernung des Tumors und der anschließenden adjuvanten CT fiel die Anzahl an CETCs im Blut ab, bis am letzten Tag der Therapie keine CETCs mehr nachweisbar waren (Abb. 16).

Weitere Details in: M. Gold, K. Pachmann, A. Kiani, R. Schobert

Monitoring of circulating epithelial tumor cells (CETCs) by the Maintrac® method and its potential benefit for the therapy of patients with colorectal cancer

Mol. Clin. Oncol. **2021** *15*, 201.

[Publikation V]

4. Literaturverzeichnis

[1] LS Goodman, MM Wintrobe **(1946)** Nitrogen mustard therapy; use of methyl-bis (beta-chloroethyl) amine hydrochloride and tris (beta-chloroethyl) amine hydrochloride for Hodgkin‘s disease, lymphosarcoma, leukemia and certain allied and miscellaneous disorders. *J Am Med Assoc*, **132**:*126–132*.

[2] S Farber, LK Diamond **(1948)** Temporary remissions in acute leukemia in children produced by folic acid antagonist, 4-aminopteroyl-glutamic acid. *N Engl J Med*, **238**:*787–793*.

[3] J Crofton **(1959)** Chemotherapy of pulmonary tuberculosis. *Br Med J*, **1**:*1610–1614*.

[4] VT DeVita, RM Simon, SM Hubbard, RC Young, CW Berard, *et al.* **(1980)** Curability of advanced Hodgkin‘s disease with chemotherapy. Long-term follow-up of MOPP-treated patients at the National Cancer Institute. *Ann Intern Med*, **92**:*587–595*.

[5] D Hanahan, RA Weinberg **(2000)** The Hallmarks of Cancer. *Cell*, **100**:*57–70*.

[6] D Hanahan, RA Weinberg **(2011)** Hallmarks of cancer: the next generation. *Cell*, **144**:*646–674*.

[7] LM Ellis, DJ Hicklin **(2009)** Resistance to Targeted Therapies: Refining Anticancer Therapy in the Era of Molecular Oncology. *Clin Cancer Res*, **15**:*7471–7478*.

[8] DR Leach, MF Krummel, JP Allison **(1996)** Enhancement of antitumor immunity by CTLA-4 blockade. *Science*, **271**:*1734–1736*.

[9] Y Iwai, M Ishida, Y Tanaka, T Okazaki, T Honjo, *et al.* **(2002)** Involvement of PD-L1 on tumor cells in the escape from host immune system and tumor immunotherapy by PD-L1 blockade. *Proc Natl Acad Sci U S A*, **99**:*12293–12297*.

[10] A Ribas, JD Wolchok **(2018)** Cancer immunotherapy using checkpoint blockade. *Science*, **359**:*1350–1355*.

[11] CM Fares, EM van Allen, CG Drake, JP Allison, S Hu-Lieskovan **(2019)** Mechanisms of Resistance to Immune Checkpoint Blockade: Why Does Checkpoint Inhibitor Immunotherapy Not Work for All Patients? *Am Soc Clin Oncol Educ Book*, **39**:*147–164*.

[12] KO Alfarouk, CM Stock, S Taylor, M Walsh, AK Muddathir, *et al.* **(2015)** Resistance to cancer chemotherapy: failure in drug response from ADME to P-gp. *Cancer Cell Int*, **15**:*71*.

[13] A Tamaki, C Ierano, G Szakacs, RW Robey, SE Bates **(2011)** The controversial role of ABC transporters in clinical oncology. *Essays Biochem*, **50**:*209–232*.

[14] ZE Sauna, SV Ambudkar **(2001)** Characterization of the catalytic cycle of ATP hydrolysis by human P-glycoprotein. The two ATP hydrolysis events in a single catalytic cycle are kinetically similar but affect different functional outcomes. *J Biol Chem*, **276**:*11653–11661*.

[15] G Housman, S Byler, S Heerboth, K Lapinska, M Longacre, *et al.* **(2014)** Drug resistance in cancer: an overview. *Cancers*, **6**:*1769–1792*.

[16] L Bonanno, A Favaretto, R Rosell **(2014)** Platinum drugs and DNA repair mechanisms in lung cancer. *Anticancer Res*, **34**:*493–501*.

[17] S Madhusudan, ID Hickson **(2005)** DNA repair inhibition: a selective tumour targeting strategy. *Trends Mol Med*, **11**:*503–511*.

[18] Z Chen, T Shi, L Zhang, P Zhu, M Deng, *et al.* **(2016)** Mammalian drug efflux transporters of the ATP binding cassette (ABC) family in multidrug resistance: A review of the past decade. *Cancer Lett*, **370**:*153–164*.

[19] JJG Marin, MR Romero, P Martinez-Becerra, E Herraez, O Briz **(2009)** Overview of the molecular bases of resistance to chemotherapy in liver and gastrointestinal tumours. *Curr Mol Med*, **9**:*1108–1129*.

[20] MS D'Arcy **(2019)** Cell death: a review of the major forms of apoptosis, necrosis and autophagy. *Cell Biol Int*, **43**:*582–592*.

[21] B Vogelstein, D Lane, AJ Levine **(2000)** Surfing the p53 network. *Nature*, **408**:*307–310*.

[22] AJ Levine **(1997)** p53, the Cellular Gatekeeper for Growth and Division. *Cell*, **88**:*323–331*.

[23] S Goldar, MS Khaniani, SM Derakhshan, B Baradaran **(2015)** Molecular mechanisms of apoptosis and roles in cancer development and treatment. *Asian Pac J Cancer Prev*, **16**:*2129–2144*.

[24] S Haupt, M Berger, Z Goldberg, Y Haupt **(2003)** Apoptosis - the p53 network. *J Cell Sci*, **116**:*4077–4085*.

[25] A Singh, J Settleman **(2010)** EMT, cancer stem cells and drug resistance: an emerging axis of evil in the war on cancer. *Oncogene*, **29**:*4741–4751*.

[26] ED Hay **(1990)** Role of cell-matrix contacts in cell migration and epithelial-mesenchymal transformation. *Cell Differ Dev*, **32**:*367–375*.

[27] JT Nauseef, MD Henry **(2011)** Epithelial-to-mesenchymal transition in prostate cancer: paradigm or puzzle? *Nat Rev Urol*, **8**:*428–439*.

[28] Y Shang, X Cai, D Fan **(2013)** Roles of epithelial-mesenchymal transition in cancer drug resistance. *Curr Cancer Drug Targets*, **13**:*915–929*.

[29] a) T Arumugam, V Ramachandran, KF Fournier, H Wang, L Marquis, *et al.* **(2009)** Epithelial to mesenchymal transition contributes to drug resistance in pancreatic cancer. *Cancer Res*, **69**:*5820–5828*; b) A Kumar, J Xu, S Brady, H Gao, D Yu, *et al.* **(2010)** Tissue transglutaminase promotes drug resistance and invasion by inducing mesenchymal transition in mammary epithelial cells. *PLoS ONE*, **5**:*e13390*; c) J Liu, AN Eischeid, X-M Chen **(2012)** Col1A1 production and apoptotic resistance in TGF-β1-induced epithelial-to-mesenchymal transition-like phenotype of 603B cells. *PLoS ONE*, **7**:*e51371*.

[30] a) N Ahmed, K Abubaker, J Findlay, M Quinn **(2010)** Epithelial mesenchymal transition and cancer stem cell-like phenotypes facilitate chemoresistance in recurrent ovarian cancer. *Curr Cancer Drug Targets*, **10**:*268–278*; b) B Aktas, M Tewes, T Fehm, S Hauch, R Kimmig, *et al.* **(2009)** Stem cell and epithelial-mesenchymal transition markers are frequently overexpressed in circulating tumor cells of metastatic breast cancer patients. *Breast Cancer Res*, **11**:*R46*; c) H van Malenstein, J Dekervel, C Verslype, E van Cutsem, P Windmolders, *et al.* **(2013)** Long-term exposure to sorafenib of liver cancer cells induces resistance with epithelial-to-mesenchymal transition, increased invasion and risk of rebound growth. *Cancer Lett*, **329**:*74–83*.

[31] WT Beck, SE Morgan, Y-Y Mo, UG Bhat **(1999)** Tumor cell resistance to DNA topoisomerase II inhibitors: new developments. *Drug Resist Updat*, **2**:*382–389*.

[32] MP Gamcsik, GR Dubay, BR Cox **(2002)** Increased rate of glutathione synthesis from cystine in drug-resistant MCF-7 cells. *Biochem Pharmacol*, **63**:*843–851*.

[33] AP Stegmann, MW Honders, A Hagemeijer, B Hoebee, R Willemze, *et al.* **(1995)** In vitro-induced resistance to the deoxycytidine analogues cytarabine (AraC) and 5-aza-2‘-deoxycytidine (DAC) in a rat model for acute myeloid leukemia is mediated by mutations in the deoxycytidine kinase (dck) gene. *Ann Hematol*, **71**:*41–47*.

[34] B Mansoori, A Mohammadi, S Davudian, S Shirjang, B Baradaran **(2017)** The Different Mechanisms of Cancer Drug Resistance: A Brief Review. *Adv Pharm Bull*, **7**:*339–348*.

[35] YA Luqmani **(2005)** Mechanisms of drug resistance in cancer chemotherapy. *Med Princ Pract*, **14**:*35–48*.

[36] P Kantharidis, A El-Osta, M deSilva, DM Wall, XF Hu, *et al.* **(1997)** Altered methylation of the human MDR1 promoter is associated with acquired multidrug resistance. *Clin Cancer Res*, **3**:*2025–2032*.

[37] DA Senthebane, A Rowe, NE Thomford, H Shipanga, D Munro, *et al.* **(2017)** The Role of Tumor Microenvironment in Chemoresistance: To Survive, Keep Your Enemies Closer. *Int J Mol Sci*, **18**:*1586–1616*.

[38] AI Hashim, X Zhang, JW Wojtkowiak, GV Martinez, RJ Gillies **(2011)** Imaging pH and metastasis. *NMR Biomed*, **24**:*582–591*.

[39] RA Gatenby, RJ Gillies **(2008)** A microenvironmental model of carcinogenesis. *Nat Rev Cancer*, **8**:*56–61*.

[40] KO Alfarouk, D Verduzco, C Rauch, AK Muddathir, AHH Bashir, *et al.* **(2015)** Erratum: Glycolysis, tumor metabolism, cancer growth and dissemination. A new pH-based etiopathogenic perspective and therapeutic approach to an old cancer question. *Oncoscience*, **2**:*317*.

[41] JS Fang, RD Gillies, RA Gatenby **(2008)** Adaptation to hypoxia and acidosis in carcinogenesis and tumor progression. *Semin Cancer Biol*, **18**:*330–337*.

[42] BP Mahoney, N Raghunand, B Baggett, RJ Gillies **(2003)** Tumor acidity, ion trapping and chemotherapeutics. *Biochem Pharmacol*, **66**:*1207–1218*.

[43] J Pouysségur, F Dayan, NM Mazure **(2006)** Hypoxia signalling in cancer and approaches to enforce tumour regression. *Nature*, **441**:*437–443*.

[44] K Sakata, TT Kwok, BJ Murphy, KR Laderoute, GR Gordon, *et al.* **(1991)** Hypoxia-induced drug resistance: comparison to P-glycoprotein-associated drug resistance. *Br J Cancer*, **64**:*809–814*.

[45] KM Comerford, TJ Wallace, J Karhausen, NA Louis, MC Montalto, *et al.* **(2002)** Hypoxia-inducible factor-1-dependent regulation of the multidrug resistance (MDR1) gene. *Cancer Res*, **62**:*3387–3394*.

[46] C Legendre, T Hori, P Loyer, C Aninat, S Ishida, *et al.* **(2009)** Drug-metabolising enzymes are down-regulated by hypoxia in differentiated human hepatoma HepaRG cells: HIF-1alpha involvement in CYP3A4 repression. *Eur J Cancer*, **45**:*2882–2892*.

[47] E Henke, R Nandigama, S Ergün **(2019)** Extracellular Matrix in the Tumor Microenvironment and Its Impact on Cancer Therapy. *Front Mol Biosci*, **6**:*160*.

[48] M Schober, R Jesenofsky, R Faissner, C Weidenauer, W Hagmann, *et al.* **(2014)** Desmoplasia and chemoresistance in pancreatic cancer. *Cancers*, **6**:*2137–2154*.

[49] JH Goldie, AJ Coldman **(1979)** A mathematic model for relating the drug sensitivity of tumors to their spontaneous mutation rate. *Cancer Treat Rep*, **63**:*1727–1733*.

[50] L Norton, R Simon, HD Brereton, AE Bogden **(1976)** Predicting the course of Gompertzian growth. *Nature*, **264**:*542–545*.

[51] R Gray, R Bradley, J Braybrooke, Z Liu, R Peto, *et al.* **(2019)** Increasing the dose intensity of chemotherapy by more frequent administration or sequential scheduling: a patient-level meta-analysis of 37 298 women with early breast cancer in 26 randomised trials. *Lancet*, **393**:*1440–1452*.

[52] D Wu, DC Wang, Y Cheng, M Qian, M Zhang, *et al.* **(2017)** Roles of tumor heterogeneity in the development of drug resistance: A call for precision therapy. *Semin Cancer Biol*, **42**:*13–19*.

[53] a) PB Gupta, CM Fillmore, G Jiang, SD Shapira, K Tao, *et al.* **(2011)** Stochastic state transitions give rise to phenotypic equilibrium in populations of cancer cells. *Cell*, **146**:*633–644*; b) C Gasch, B Ffrench, JJ O'Leary, MF Gallagher **(2017)** Catching moving targets: cancer stem cell hierarchies, therapy-resistance & considerations for clinical intervention. *Mol Cancer*, **16**:*43-58*.

[54] MB Meads, RA Gatenby, WS Dalton **(2009)** Environment-mediated drug resistance: a major contributor to minimal residual disease. *Nat Rev Cancer*, **9**:*665–674*.

[55] P Sharma, S Hu-Lieskovan, JA Wargo, A Ribas **(2017)** Primary, Adaptive, and Acquired Resistance to Cancer Immunotherapy. *Cell*, **168**:*707–723*.

[56] D Sun, S Dalin, MT Hemann, DA Lauffenburger, B Zhao **(2016)** Differential selective pressure alters rate of drug resistance acquisition in heterogeneous tumor populations. *Sci Rep*, **6**:*36198*.

[57] J Zhao **(2016)** Cancer stem cells and chemoresistance: The smartest survives the raid. *Pharmacol Ther*, **160**:*145–158*.

[58] a) PB Gupta, CL Chaffer, RA Weinberg **(2009)** Cancer stem cells: mirage or reality? *Nat Med*, **15**:*1010–1012*; b) NY Frank, T Schatton, MH Frank **(2010)** The therapeutic promise of the cancer stem cell concept. *J Clin Invest*, **120**:*41–50*.

[59] T Lapidot, C Sirard, J Vormoor, B Murdoch, T Hoang, *et al.* **(1994)** A cell initiating human acute myeloid leukaemia after transplantation into SCID mice. *Nature*, **367**:*645–648*.

[60] C Tang, BT Ang, S Pervaiz **(2007)** Cancer stem cell: target for anti-cancer therapy. *FASEB J*, **21**:*3777–3785*.

[61] LV Nguyen, R Vanner, P Dirks, CJ Eaves **(2012)** Cancer stem cells: an evolving concept. *Nat Rev Cancer*, **12**:*133–143*.

[62] SA Mani, W Guo, M-J Liao, EN Eaton, A Ayyanan, *et al.* **(2008)** The epithelial-mesenchymal transition generates cells with properties of stem cells. *Cell*, **133**:*704–715*.

[63] a) M Cojoc, K Mäbert, MH Muders, A Dubrovska **(2015)** A role for cancer stem cells in therapy resistance: cellular and molecular mechanisms. *Semin Cancer Biol*, **31**:*16–27*; b) N Shafee, CR Smith, S Wei, Y Kim, GB Mills, *et al.* **(2008)** Cancer stem cells contribute to cisplatin resistance in Brca1/p53-mediated mouse mammary tumors. *Cancer Res*, **68**:*3243–3250*.

[64] G Liu, X Yuan, Z Zeng, P Tunici, H Ng, *et al.* **(2006)** Analysis of gene expression and chemoresistance of CD133+ cancer stem cells in glioblastoma. *Mol Cancer*, **5**:*67-79*.

[65] a) C Yan, L Luo, CY Guo, S Goto, Y Urata, *et al.* **(2017)** Doxorubicin-induced mitophagy contributes to drug resistance in cancer stem cells from HCT8 human colorectal cancer cells. *Cancer Lett*, **388**:*34–42*; b) N Zhang, R Li, KS Tao, DY Cao, Z-Y Ti, *et al.* **(2010)** Characterization of a stem-like population in hepatocellular carcinoma MHCC97 cells. *Oncol Rep*, **23**:*827–831*.

[66] A Shervington, C Lu **(2008)** Expression of multidrug resistance genes in normal and cancer stem cells. *Cancer Invest*, **26**:*535–542*.

[67] S Buczacki, RJ Davies, DJ Winton **(2011)** Stem cells, quiescence and rectal carcinoma: an unexplored relationship and potential therapeutic target. *Br J Cancer*, **105**:*1253–1259*.

[68] P Bouwman, J Jonkers **(2012)** The effects of deregulated DNA damage signalling on cancer chemotherapy response and resistance. *Nat Rev Cancer*, **12**:*587–598*.

[69] R Kalluri, RA Weinberg **(2009)** The basics of epithelial-mesenchymal transition. *J Clin Invest*, **119**:*1420–1428*.

[70] MA Nieto, RYJ Huang, RA Jackson, JP Thiery **(2016)** EMT: 2016. *Cell*, **166**:*21–45*.

[71] MA Papadaki, G Stoupis, PA Theodoropoulos, D Mavroudis, V Georgoulias, *et al.* **(2019)** Circulating Tumor Cells with Stemness and Epithelial-to-Mesenchymal Transition Features Are Chemoresistant and Predictive of Poor Outcome in Metastatic Breast Cancer. *Mol Cancer Ther*, **18**:*437–447*.

[72] M Saxena, MA Stephens, H Pathak, A Rangarajan **(2011)** Transcription factors that mediate epithelial-mesenchymal transition lead to multidrug resistance by upregulating ABC transporters. *Cell Death Dis*, **2**:*e179*.

[73] C Alix-Panabières, K Pantel **(2014)** Challenges in circulating tumour cell research. *Nat Rev Cancer*, **14**:*623–631*.

[74] TA Fleisher, GE Marti **(2001)** Detection of unseparated human lymphocytes by flow cytometry. *Curr Protoc Immunol*, **8**:*7.9.1-7.9.7*.

[75] FAW Coumans, CJM Doggen, G Attard, JS de Bono, LWMM Terstappen **(2010)** All circulating EpCAM+CK+CD45- objects predict overall survival in castration-resistant prostate cancer. *Ann Oncol*, **21**:*1851–1857*.

[76] K Pachmann, JH Clement, C-P Schneider, B Willen, O Camara, *et al.* **(2005)** Standardized quantification of circulating peripheral tumor cells from lung and breast cancer. *Clin Chem Lab Med*, **43**:*617–627*.

[77] a) H Cho, J Kim, H Song, KY Sohn, M Jeon, *et al.* **(2018)** Microfluidic technologies for circulating tumor cell isolation. *Analyst*, **143**:*2936–2970*; b) T Lozar, K Gersak, M Cemazar, CG Kuhar, T Jesenko **(2019)** The biology and clinical potential of circulating tumor cells. *Radiol Oncol*, **53**:*131–147*.

[78] JY Douillard, D Cunningham, AD Roth, M Navarro, RD James, *et al.* **(2000)** Irinotecan combined with fluorouracil compared with fluorouracil alone as first-line treatment for metastatic colorectal cancer: a multicentre randomised trial. *Lancet*, **355**:*1041–1047*.

[79] S Karthikeyan, SL Hoti **(2015)** Development of Fourth Generation ABC Inhibitors from Natural Products: A Novel Approach to Overcome Cancer Multidrug Resistance. *Anticancer Agents Med Chem*, **15**:*605–615*.

[80] JA Ewald, JA Desotelle, G Wilding, DF Jarrard **(2010)** Therapy-induced senescence in cancer. *J Natl Cancer Inst*, **102**:*1536–1546*.

[81] L Hayflick, PS Moorhead **(1961)** The serial cultivation of human diploid cell strains. *Exp Cell Res*, **25**:*585–621*.

[82] IB Roninson, EV Broude, BD Chang **(2001)** If not apoptosis, then what? Treatment-induced senescence and mitotic catastrophe in tumor cells. *Drug Resist Updat*, **4**:*303–313*.

[83] K Hevener, TA Verstak, KE Lutat, DL Riggsbee, JW Mooney **(2018)** Recent developments in topoisomerase-targeted cancer chemotherapy. *Acta Pharm Sin B*, **8**:*844–861*.

[84] ZA Rasheed, EH Rubin **(2003)** Mechanisms of resistance to topoisomerase I-targeting drugs. *Oncogene*, **22**:*7296–7304*.

[85] a) D Cunningham, Y Humblet, S Siena, D Khayat, H Bleiberg, *et al.* **(2004)** Cetuximab monotherapy and cetuximab plus irinotecan in irinotecan-refractory metastatic colorectal cancer. *N Engl J Med*, **351**:*337–345*; b) Y Ergun, NY Ozdemir, EK Guner, E Esin, MA Sendur, *et al.* **(2018)** Comparison of Gemcitabine monotherapy with Gemcitabine and Cisplatin combination in metastatic pancreatic cancer: a retrospective analysis. *J BUON*, **23**:*116–121*.

[86] a) A Anighoro, J Bajorath, G Rastelli **(2014)** Polypharmacology: challenges and opportunities in drug discovery. *J Med Chem*, **57**:*7874–7887*; b) J-U Peters **(2013)** Polypharmacology - foe or friend? *J Med Chem*, **56**:*8955–8971*.

[87] B Meunier **(2008)** Hybrid molecules with a dual mode of action: dream or reality? *Acc Chem Res*, **41**:*69–77*.

[88] AR de Lera, A Ganesan **(2016)** Epigenetic polypharmacology: from combination therapy to multitargeted drugs. *Clin Epigenetics*, **8**:*105-126*.

[89] C Avendano, JC Menendez **(2015)** Medicinal Chemistry of Anticancer Drugs. *Elsevier Science*, Burlington, 2nd edn.

[90] DB Longley, J Boyer, WL Allen, T Latif, PR Ferguson, *et al.* **(2002)** The role of thymidylate synthase induction in modulating p53-regulated gene expression in response to 5-fluorouracil and antifolates. *Cancer Res*, **62**:*2644–2649*.

[91] D Arango, AJ Wilson, Q Shi, GA Corner, MJ Arañes, *et al.* **(2004)** Molecular mechanisms of action and prediction of response to oxaliplatin in colorectal cancer cells. *Br J Cancer*, **91**:*1931–1946*.

[92] G D'Orazi, D Givol **(2012)** p53 reactivation: the link to zinc. *Cell Cycle*, **11**:*2581–2582*.

[93] GD Anaya-Eugenio, CY Tan, LH Rakotondraibe, EC Carcache de Blanco **(2020)** Tumor suppressor p53 independent apoptosis in HT-29 cells by auransterol from Penicillium aurantiacobrunneum. *Biomed Pharmacother*, **127**:*110124*.

[94] a) J-Z Qin, L Stennett, P Bacon, B Bodner, MJC Hendrix, *et al.* **(2004)** p53-independent NOXA induction overcomes apoptotic resistance of malignant melanomas. *Mol Cancer Ther*, **3**:*895–902*; b) LM McNamee, MH Brodsky **(2009)** p53-independent apoptosis limits DNA damage-induced aneuploidy. *Genetics*, **182**:*423–435*.

[95] N Vasan, J Baselga, DM Hyman **(2019)** A view on drug resistance in cancer. *Nature*, **575**:*299–309*.

[96] M Tellez-Gabriel, M-F Heymann, D Heymann **(2019)** Circulating Tumor Cells as a Tool for Assessing Tumor Heterogeneity. *Theranostics*, **9**:*4580–4594*.

[97] N Rudiger, E-L Stein, E Schill, G Spitz, C Rabenstein, *et al.* **(2013)** Chemosensitivity Testing of Circulating Epithelial Tumor Cells (CETC) in Vitro: Correlation to in Vivo Sensitivity and Clinical Outcome. *JCT*, **4**:*597–605*.

[98] J Inhestern, K Oertel, V Stemmann, H Schmalenberg, A Dietz, *et al.* **(2015)** Prognostic Role of Circulating Tumor Cells during Induction Chemotherapy Followed by Curative Surgery Combined with Postoperative Radiotherapy in Patients with Locally Advanced Oral and Oropharyngeal Squamous Cell Cancer. *PLOS ONE*, **10**:*e0132901*.

[99] K Pachmann, O Camara, A Kavallaris, S Krauspe, N Malarski, *et al.* **(2008)** Monitoring the response of circulating epithelial tumor cells to adjuvant chemotherapy in breast cancer allows detection of patients at risk of early relapse. *J Clin Oncol*, **26**:*1208–1215*.

[100] K Pachmann, R Dengler, K Lobodasch, F Fröhlich, T Kroll, *et al.* **(2008)** An increase in cell number at completion of therapy may develop as an indicator of early relapse: quantification of circulating epithelial tumor cells (CETC) for monitoring of adjuvant therapy in breast cancer. *J Cancer Res Clin Oncol*, **134**:*59–65*.

[101] DB Longley, PG Johnston **(2005)** Molecular mechanisms of drug resistance. *J Pathol*, **205**:*275–292*.

[102] D Hanahan **(2014)** Rethinking the war on cancer. *Lancet*, **383**:*558–563*.

[103] KD Miller, L Nogueira, AB Mariotto, JH Rowland, KR Yabroff, *et al.* **(2019)** Cancer treatment and survivorship statistics, 2019. *CA: Cancer J Clin*, **69**:*363–385*.

[104] FC Svedman, D Pillas, A Taylor, M Kaur, R Linder, *et al.* **(2016)** Stage-specific survival and recurrence in patients with cutaneous malignant melanoma in Europe - a systematic review of the literature. *Clin Epidemiol*, **8**:*109–122*.

[105] L Benimetskaya, K Ayyanar, N Kornblum, D Castanotto, J Rossi, *et al.* **(2006)** Bcl-2 protein in 518A2 melanoma cells in vivo and in vitro. *Clin Cancer Res*, **12**:*4940–4948*.

[106] SF Zerp, A van Elsas, LT Peltenburg, PI Schrier **(1999)** p53 mutations in human cutaneous melanoma correlate with sun exposure but are not always involved in melanomagenesis. *Br J Cancer*, **79**:*921–926*.

[107] C Nardella, JG Clohessy, A Alimonti, PP Pandolfi **(2011)** Pro-senescence therapy for cancer treatment. *Nat Rev Cancer*, **11**:*503–511*.

[108] P Pan, Y Li, H Yu, H Sun, T Hou **(2013)** Molecular principle of topotecan resistance by topoisomerase I mutations through molecular modeling approaches. *J Chem Inf Model*, **53**:*997–1006*.

[109] GL Beretta, L Gatti, P Perego, N Zaffaroni **(2013)** Camptothecin resistance in cancer: insights into the molecular mechanisms of a DNA-damaging drug. *Curr Med Chem*, **20**:*1541–1565*.

[110] Z-F Chen, M-X Tan, L-M Liu, Y-C Liu, H-S Wang, *et al.* **(2009)** Cytotoxicity of the traditional chinese medicine (TCM) plumbagin in its copper chemistry. *Dalton Trans,* **28**:*10824–10833*.

[111] a) Z Yu, JA Cowan **(2017)** Catalytic Metallodrugs: Substrate-Selective Metal Catalysts as Therapeutics. *Chemistry*, **23**:*14113–14127*; b) F Tisato, C Marzano, M Porchia, M Pellei, C Santini **(2010)** Copper in diseases and treatments, and copper-based anticancer strategies. *Med Res Rev*, **30**:*708–749*.

[112] H Hashizume, P Baluk, S Morikawa, JW McLean, G Thurston, *et al.* **(2000)** Openings between Defective Endothelial Cells Explain Tumor Vessel Leakiness. *Am J Pathol*, **156**:*1363–1380*.

[113] a) K Hida, Y Hida, M Shindoh **(2008)** Understanding tumor endothelial cell abnormalities to develop ideal anti-angiogenic therapies. *Cancer Sci*, **99**:*459–466*; b) AME Abdalla, L Xiao, MW Ullah, M Yu, C Ouyang, *et al.* **(2018)** Current Challenges of Cancer Anti-angiogenic Therapy and the Promise of Nanotherapeutics. *Theranostics*, **8**:*533–548*.

[114] ON Zefirova, AG Diikov, NV Zyk, NS Zefirov **(2007)** Ligands of the colchicine site of tubulin: A common pharmacophore and new structural classes. *Russ Chem Bull*, **56**:*680–688*.

[115] YD Wang, S Johnson, D Powell, JP McGinnis, M Miranda, *et al.* **(2005)** Inhibition of tumor cell proliferation by thieno[2,3-d]pyrimidin-4(1H)-one-based analogs. *Bioorg Med Chem Lett*, **15**:*3763–3766*.

[116] VJN Bykov, SE Eriksson, J Bianchi, KG Wiman **(2018)** Targeting mutant p53 for efficient cancer therapy. *Nat Rev Cancer*, **18**:*89–102*.

[117] a) RL Hayward, JS Macpherson, J Cummings, BP Monia, JF Smyth, *et al.* **(2004)** Enhanced oxaliplatin-induced apoptosis following antisense Bcl-xl down-regulation is p53 and Bax dependent: Genetic evidence for specificity of the antisense effect. *Mol Cancer Ther*, **3**:*169–178*; b) J Boyer, EG McLean, S Aroori, P Wilson, A McCulla, *et al.* **(2004)** Characterization of p53 wild-type and null isogenic colorectal cancer cell lines resistant to 5-fluorouracil, oxaliplatin, and irinotecan. *Clin Cancer Res*, **10**:*2158–2167*.

[118] D Dart, S Picksley, P Cooper, J Double, M Bibby **(2004)** The role of p53 in the chemotherapeutic responses to cisplatin, doxorubicin and 5-fluorouracil treatment. *Int J Oncol*, **24**:*115-125*.

[119] JK Muenzner, B Biersack, H Kalie, IC Andronache, L Kaps, *et al.* **(2014)** Gold(I) biscarbene complexes derived from vascular-disrupting combretastatin A-4 address different targets and show antimetastatic potential. *Chem Med Chem*, **9**:*1195–1204*.

[120] Ö Karaca, SM Meier-Menches, A Casini, FE Kühn **(2017)** On the binding modes of metal NHC complexes with DNA secondary structures: implications for therapy and imaging. *Chem Comm*, **53**:*8249–8260*.

[121] F Bray, J Ferlay, I Soerjomataram, RL Siegel, LA Torre, *et al.* **(2018)** Global cancer statistics 2018: GLOBOCAN estimates of incidence and mortality worldwide for 36 cancers in 185 countries. *CA: Cancer J Clin*, **68**:*394–424*.

[122] S Boussios, MA Ozturk, M Moschetta, A Karathanasi, N Zakynthinakis-Kyriakou, *et al.* **(2019)** The Developing Story of Predictive Biomarkers in Colorectal Cancer. *J Pers Med*, **9**:*12*.

[123] a) CJA Punt, M Koopman, L Vermeulen **(2017)** From tumour heterogeneity to advances in precision treatment of colorectal cancer. *Nature Rev Clin Oncol*, **14**:*235–246*. b) CG Moertel, TR Fleming, JS Macdonald, DG Haller, JA Laurie, *et al.* **(1990)** Levamisole and fluorouracil for adjuvant therapy of resected colon carcinoma. *N Engl J Med*, **322**:*352–358*.

[124] a) AA Friedman, A Letai, DE Fisher, KT Flaherty **(2015)** Precision medicine for cancer with next-generation functional diagnostics. *Nat Rev Cancer*, **15**:*747–756*; b) MJ Garnett, EJ Edelman, SJ Heidorn, CD Greenman, A Dastur, *et al.* **(2012)** Systematic identification of genomic markers of drug sensitivity in cancer cells. *Nature*, **483**:*570–575*; c) MPA Ebert, M Tänzer, B Balluff, E Burgermeister, AK Kretzschmar, *et al.* **(2012)** TFAP2E-DKK4 and chemoresistance in colorectal cancer. *N Engl J Med*, **366**:*44–53*.

[125] L Wang, P Balasubramanian, AP Chen, S Kummar, YA Evrard, *et al.* **(2016)** Promise and limits of the CellSearch platform for evaluating pharmacodynamics in circulating tumor cells. *Semin Oncol*, **43**:*464–475*.

[126] SJ Cohen, CJA Punt, N Iannotti, BH Saidman, KD Sabbath, *et al.* **(2008)** Relationship of circulating tumor cells to tumor response, progression-free survival, and overall survival in patients with metastatic colorectal cancer. *J Clin Oncol*, **26**:*3213–3221*.

[127] J Tol, M Koopman, MC Miller, A Tibbe, A Cats, *et al.* **(2010)** Circulating tumour cells early predict progression-free and overall survival in advanced colorectal cancer patients treated with chemotherapy and targeted agents. *Ann Oncol*, **21**:*1006–1012*.

[128] J Sastre, ML Maestro, J Puente, S Veganzones, R Alfonso, *et al.* **(2008)** Circulating tumor cells in colorectal cancer: correlation with clinical and pathological variables. *Ann Oncol*, **19**:*935–938*.

[129] M Zitt, M Zitt, HM Müller, AJ Dinnewitzer, V Schwendinger, *et al.* **(2006)** Disseminated tumor cells in peripheral blood: a novel marker for therapy response in locally advanced rectal cancer patients undergoing preoperative chemoradiation. *Dis Colon Rectum*, **49**:*1484–1491*.

[130] W Sun, G Li, J Wan, J Zhu, W Shen, *et al.* **(2016)** Circulating tumor cells: A promising marker of predicting tumor response in rectal cancer patients receiving neoadjuvant chemo-radiation therapy. *Oncotarget,* **7**:*69507–69517*.

[131] E Magni, E Botteri, PS Ravenda, MC Cassatella, E Bertani, *et al.* **(2014)** Detection of circulating tumor cells in patients with locally advanced rectal cancer undergoing neoadjuvant therapy followed by curative surgery. *Int J Colorectal Dis*, **29**:*1053–1059.*

[132] S Hinz, C Röder, J Tepel, A Hendricks, C Schafmayer, *et al.* **(2015)** Cytokeratin 20 positive circulating tumor cells are a marker for response after neoadjuvant chemoradiation but not for prognosis in patients with rectal cancer. *BMC Cancer*, **15**:*953.*

5. Publikationen

5.1. Darstellung des Eigenanteils

Die in dieser Arbeit vorgestellten Publikationen wurden in Kooperation mit anderen Mitarbeitern der Universität Bayreuth, sowie mit Arbeitsgruppen anderer Institutionen erarbeitet. Hierzu zählen das Institut für Biophysik der *Academy of Science of the Czech Republic* in Brünn (Tschechien), der Lehrstuhl für Biophysik der Wissenschaftlichen Fakultät der Palacky Universität Olmütz (Tschechien), der Lehrstuhl für Chemie des *Abeda Inamdar Senior College* in Pune (Indien), der Lehrstuhl für Anorganische Chemie IV der Universität Bayreuth, das *Research Center for Integrated Analysis and Territorial Management* der Universität Bukarest (Rumänien), der Lehrstuhl für *Cancer Biology* der *University of Kansas Medical Center* (Kansas, USA), das Institut für Hämatologie und Onkologie des Klinikums Bayreuth (Bayreuth, Deutschland), sowie die Simfo GmbH (Bayreuth, Deutschland).

Es folgt eine detaillierte Darstellung der Beiträge der Co-Autoren zu den jeweiligen Publikationen.

5.1.1. Eigenanteil: Publikation I

Die Ergebnisse zu diesem Thema wurden im ***Journal of Biological Inorganic Chemistry*** mit dem folgenden Titel veröffentlicht (DOI: 10.1007/s00775-019-01677-y):

„A new 4-(pyridinyl)-4H-benzochromene-5,10-dione ruthenium(II) complex inducing senescence in 518A2 melanoma cells“

von den Autoren

Madeleine Gold, Yusufi Mujahid, Khursheed Ahmed, Hana Kostrhunova, Jana Kasparkova, Viktor Brabec, Bernhard Biersack, Rainer Schobert.

Eigenanteil: NMR-Stabilitätsstudien;
Konzeption, Durchführung und Auswertung der biologischen Assays:
MTT-Assay, Herstellung der Zell- und Zellkern-Lysate für die Studien zur zellulären Aufnahme, Ethidiumbromidsättigungs-Assay, EMSA, DCFH-DA-Assay, ROS/Superoxide Assay, Zellzyklusanalyse, Nachweis der Seneszenz-asoziierten ß-Galaktosidase-Aktivität, Caspase-3/7 Assay;
Verfassen des Manuskriptes inklusive Diskussion und Interpretation der Ergebnisse, sowie Korrektur und Revision des Manuskriptes, graphische Repräsentation und Bearbeitung der Abbildungen.

Y. Mujahid: Cyclovoltammetrie.

K. Ahmed: Cyclovoltammetrie.

H. Kostrhunova: ICP-MS-Messungen für die Aufnahme- und DNA-Bindungsstudien.

J. Kasparkova: ICP-MS-Messungen für die Aufnahmestudien.

V. Brabec: ICP-MS-Messungen für die Aufnahme- und DNA-Bindungsstudien, Diskussion des Manuskriptes.

B. Biersack: Synthese, Aufreinigung und Charakterisierung der Testverbindungen; Verfassen entsprechender Manuskriptpassagen, Diskussion und Korrektur des Manuskriptes.

R. Schobert: Manuskriptkonzeption, Diskussion und Korrektur des Manuskriptes.

5.1.2. Eigenanteil: Publikation II

Die Ergebnisse zu diesem Thema wurden im Journal ***Dalton Transactions*** mit dem folgenden Titel veröffentlicht (DOI: 10.1039/C9DT02571E):

„Copper(II) complexes with tridentate Schiff base-like ligands: solid state and solution structures and anticancer activity.“

von den Autoren

Katja Dankhoff, Madeleine Gold, Luisa Kober, Florian Schmitt, Lena Pfeiffer, Andreas Dürrmann, Hana Kostrhunova, Matthias Rothemund, Viktor Brabec, Rainer Schobert, Birgit Weber.

Eigenanteil: Konzeption, Durchführung und Auswertung der biologischen Assays: MTT-Assay, EtBr-Sättigungs-Assay, EMSA, TopoI- Aktivitätsmessung Verfassen des Manuskriptes inklusive Diskussion und Interpretation der Ergebnisse, sowie Korrektur und Revision des Manuskriptes, graphische Repräsentation und Bearbeitung der Abbildungen.

K. Dankhoff: Synthese, Aufreinigung und Charakterisierung der getesteten Verbindungen (inklusive Röntgenstrukturanalyse); Verfassen des Manuskriptes inklusive Diskussion und Interpretation der Ergebnisse, sowie Korrektur und Revision des Manuskriptes, graphische Repräsentation und Bearbeitung der Abbildungen.

L. Kober: Hilfe bei der Durchführung von MTT-Assays und TopoI-Aktivitätsmessungen im Rahmen einer Bachelorarbeit (betreut durch M. Gold und R. Schobert).

F. Schmitt: Durchführung von MTT-Assays und NBT-Assays.

L. Pfeiffer: Hilfe bei der Synthese, Aufreinigung und Charakterisierung der getesteten Verbindungen.

A. Dürrmann: Hilfe bei der Synthese, Aufreinigung und Charakterisierung der getesteten Verbindungen.

H. Kostrhunova: ICP-MS-Messungen für die Aufnahmestudien.

M. Rothemund: Durchführung von MTT-Assays.

V. Brabec: Diskussion des Manuskriptes.

R. Schobert: Diskussion und Korrektur des Manuskriptes.

B. Weber: Manuskriptkonzeption, Diskussion und Korrektur des Manuskriptes.

5.1.3. Eigenanteil: Publikation III

Die Ergebnisse zu diesem Thema wurden im ***European Journal of Medicinal Chemistry*** mit dem folgenden Titel veröffentlicht (DOI: 10.1016/j.ejmech.2020.112060):

„Synthesis and bioevaluation of new vascular-targeting and anti-angiogenic thieno[2,3-d]pyrimidin-4(3H)-ones."

von den Autoren

Madeleine Gold, Leonhard Köhler, Clarissa Lanzloth, Ion Andronache, Shrikant Anant, Prasad Dandawate, Bernhard Biersack, Rainer Schobert.

Eigenanteil: Konzeption, Durchführung und Auswertung der biologischen Assays:
MTT-Assay, Tubulinpolymerisations-Assay, Zellzyklusanalyse, Immunofluoreszenzfärbungen des Zytoskeletts, CDK1-Aktivitätsmessung, *Tube formation*-Assay, CAM-Assay, Zebrafisch-Angiogenese-Assay, Caspase-3/7-Assay;
Verfassen des Manuskriptes inklusive Diskussion und Interpretation der Ergebnisse, sowie Korrektur und Revision des Manuskriptes, graphische Repräsentation und Bearbeitung der Abbildungen.

L. Köhler: Hilfe bei der Durchführung von MTT-Assay und *Tube formation*-Assay; Durchführung der CDK1-Aktivitätsmessung im Rahmen eines Mitarbeiterpraktikums und eines Forschungsmoduls (betreut durch M. Gold und R. Schobert).

C. Lanzloth: Hilfe bei der Durchführung des Zebrafisch-Angiogenese-Assays im Rahmen eines Forschungsmoduls (betreut durch M. Gold und R. Schobert).

I. Andronache: Fraktalanalyse der Blutgefäßveränderungen im CAM-Assay; Diskussion und Korrektur des Manuskriptes.

S. Anant: Durchführung und Auswertung der Docking-Studien; Verfassen entsprechender Manuskriptpassagen.

P. Dandawate: Durchführung und Auswertung der Docking-Studien.

B. Biersack: Synthese, Aufreinigung und Charakterisierung der getesteten Verbindungen; Verfassen entsprechender Manuskriptpassagen; Diskussion und Korrektur des Manuskriptes.

R. Schobert: Konzeption, Diskussion und Korrektur des Manuskriptes.

5.1.4. Eigenanteil: Publikation IV

Die Ergebnisse zu diesem Thema wurden im Journal ***Chemistry – A European Journal*** mit dem folgenden Titel veröffentlicht (DOI: 10.1002/chem.202005451):

„Guided Antitumoral Drugs: (Imidazol-2-ylidene)(L)gold(I) Complexes Seeking Cellular Targets Controlled by the Nature of Ligand L.“

von den Autoren

Sofia I. Bär, Madeleine Gold, Sebastian W. Schleser, Tobias Rehm, Alexander Bär, Leonhard Köhler, Lucas R. Carnell, Bernhard Biersack, Rainer Schobert.

Eigenanteil: Konzeption, Durchführung und Auswertung der biologischen Assays:
MTT-Assay, Caspase-3/7-Assay, Ethidiumbromidsättigungs-Assay, Thioredoxinreduktase-Aktivitäts-Assay;
Verfassen des Manuskriptes inklusive Diskussion und Interpretation der Ergebnisse, sowie Korrektur und Revision des Manuskriptes, graphische Repräsentation und Bearbeitung der Abbildungen.

S. Bär: Konzeption, Durchführung und Auswertung von biologischen Assays:
MTT-Assay, Lokalisationsstudien, Zellzyklusanalyse, Untersuchung des Mitochondrienmembranpotentials, DCFH-DA-Assay, Immunofluoreszenzfärbung des Zytoskeletts, Untersuchung der Lysosomenaktivität;
Manuskriptkonzeption, inklusive Korrektur und Revision des Manuskriptes, graphische Repräsentation und Bearbeitung der Abbildungen.

A. Bär: Synthese, Aufreinigung und Charakterisierung der getesteten Verbindungen; Verfassen entsprechender Manuskriptpassagen mit graphischer Repräsentation.

B. Biersack: Synthese der getesteten Verbindungen; Verfassen entsprechender Manuskriptpassagen.

T. Rehm: Synthese, Aufreinigung und Charakterisierung der getesteten Verbindungen.

L. Köhler: Durchführung des EMSA.

L. Kober: Hilfe bei der Durchführung von MTT-Assay, Tubulinpolymerisations-Assay und Immunofluoreszenzfärbung des Zytoskeletts im Rahmen eines Mitarbeiterpraktikums (betreut durch S. Bär und R. Schobert).

M. Rothemund: Vorarbeiten zur biologischen Aktivität der Testsubstanzen.

R. Schobert: Konzeption, Diskussion und Korrektur des Manuskriptes.

5.1.5. Eigenanteil: Publikation V

Die Ergebnisse zu diesem Thema wurden im Journal ***Molecular and Clinical Oncology*** unter dem folgenden Titel veröffentlicht (DOI: 10.3892/mco.2021.2363):

„Monitoring of circulating epithelial tumor cells (CETCs) by the Maintrac® method and its potential benefit for the therapy of patients with colorectal cancer.“

von den Autoren

Madeleine Gold, Katharina Pachmann, Alexander Kiani, Rainer Schobert.

Eigenanteil: Vorbereitung, Konzeption und Durchführung der klinischen Studie: Verfassen von Studienprotokoll und Ethikantrag, Dokumentation;
Konzeption, Durchführung und Auswertung der biologischen und biochemischen Assays:
CETC-Quantifizierung mittels Maintrac®-Methode, Kultivierung von Tumorsphären aus Patientenblut, sowie aus Primärtumorgewebe, weitere immunologische Charakterisierung von CETCs und Tumorsphären;
Statistische Auswertung der Daten mittels Sigmaplot;
Verfassen des Manuskriptes inklusive Diskussion und Interpretation der Ergebnisse, sowie Korrektur und Revision des Manuskriptes, graphische Repräsentation und Bearbeitung der Abbildungen.

K. Pachmann: Konzeption biochemischer und biologischer Assays, Interpretation der Daten, Korrektur und Revision des Manuskriptes.

A. Kiani: Konzeption und Durchführung der klinischen Studie als Studienarzt, Interpretation der Daten, Korrektur und Revision des Manuskriptes.

R. Schobert: Vorbereitung und Konzeption der klinischen Studie und der biochemischen Assays, Interpretation der Daten, Korrektur und Revision des Manuskriptes.

5.2. Publikation I

A new 4-(pyridinyl)-4H-benzochromene-5,10-dione ruthenium(II) complex inducing senescence in 518A2 melanoma cells

Madeleine Gold,[a] Yusufi Mujahid,[b] Khursheed Ahmed,[b] Hana Kostrhunova,[c] Jana Kasparkova,[c,d] Viktor Brabec,[c] Bernhard Biersack,[a] Rainer Schobert*[a]

[a] *Organic Chemistry Laboratory, University of Bayreuth, Universitaetsstrasse 30, 95440 Bayreuth, Germany*

[b] *Department of Chemistry, Abeda Inamdar Senior College, 2390-B, K.B. Hidayatullah Road, Pune, 411001, India*

[c] *Institute of Biophysics, Czech Academy of Sciences, Kralovopolska 135, 61265, Brno, Czech Republic*

[d] *Department of Biophysics, Faculty of Science, Palacky University, Slechtitelu 27, 78371, Olomouc, Czech Republic*

* Corresponding author, Email address: Rainer.schobert@uni-bayreuth.de

J. Biol. Inorg. Chem. **2019**, 24, 647-657.

JBIC Journal of Biological Inorganic Chemistry (2019) 24:647–657
https://doi.org/10.1007/s00775-019-01677-y

ORIGINAL PAPER

A new 4-(pyridinyl)-4*H*-benzo[*g*]chromene-5,10-dione ruthenium(II) complex inducing senescence in 518A2 melanoma cells

Madeleine Gold[1] · Yusufi Mujahid[2] · Khursheed Ahmed[2] · Hana Kostrhunova[3] · Jana Kasparkova[3,4] · Viktor Brabec[3] · Bernhard Biersack[1] · Rainer Schobert[1]

Received: 2 May 2019 / Accepted: 6 June 2019 / Published online: 19 June 2019

Abstract
2-Amino-5,10-dihydro-5,10-dioxo-4(pyridine-3-yl)-4*H*-benzo[*g*]chromene-3-carbonitrile **5**, a cytotoxic lawsone derivative, was reacted with [Ru(*p*-cymene)Cl_2]$_2$ to afford a new Ru(II) 'piano-stool' complex **6** which differed from its ligand **5** by a greater selectivity for highly invasive 518A2 melanoma cells over human dermal fibroblasts in MTT cytotoxicity assays, and by inducing senescence rather than apoptosis in the former. DNA is a likely cellular target of complex **6** as it bound, presumably non-covalently, to linear and circular double-stranded DNA in vitro and as ruthenium was found in the lysate of nuclei of treated 518A2 melanoma cells. It also caused a fivefold increase of reactive oxygen species in these cells, originating from a more persistent redox cycling as visualised by cyclic voltammetry.

Keywords Naphthoquinone · Lawsone · Ruthenium(II) complex · Melanoma · Anticancer agents · Senescence

Introduction

Cutaneous melanoma is one of the most aggressive skin cancer types. In contrast to other cancer entities, melanoma does not respond well to cytotoxic chemotherapy. However, cytotoxic drugs such as cisplatin (CDDP, cis-[$Pt^{II}(NH_3)_2Cl_2$]) and carboplatin are frequently used for palliative therapy of advanced cutaneous melanoma to mitigate symptoms, e.g., in combination regimes with dacarbazine, an alkylating triazene derivative [1]. In comparison with single agent therapies, established combinatorial therapies result in slightly increased response rates, which, unfortunately, do not normally translate into extended overall survival of the patients [2]. This emphasizes the need for alternative agents suitable for systemic treatment of metastatic melanoma, especially for patients not responding to immunotherapy, or those living in regions, where the latter is not available.

Although a host of platinum compounds, including such with less pronounced side effects, had been synthesized and tested over the last few decades, only oxaliplatin and carboplatin were approved by the FDA and registered worldwide for clinical use. However, severe side effects and resistance to platinum-based cancer chemotherapy could not be eliminated entirely. One line of further improvement is the use of metals other than platinum. Ruthenium, a transition metal of the platinum group, attracted particular attention [3], with three complexes, NAMI-A, KP1019, and IT-139, reaching clinical trials [4–6]. Three properties of ruthenium compounds are particularly meaningful for their medical usage. First, most Ru(II) and Ru(III) complexes exhibit (slow) ligand exchange kinetics similar to that of Pt(II) compounds, rendering them kinetically stable and preventing rapid equilibration reactions [3, 7]. Second, all oxidation states [Ru(II), Ru(III), Ru(IV)] are accessible under physiological conditions [3, 7]. Finally, ruthenium may mimic iron in binding to serum transferrin and albumin, and so accumulate in rapidly dividing cancer cells, which often overexpress transferrin receptors due to their raised iron demand

Electronic supplementary material The online version of this article (https://doi.org/10.1007/s00775-019-01677-y) contains supplementary material, which is available to authorized users.

✉ Rainer Schobert
Rainer.schobert@uni-bayreuth.de

[1] Organic Chemistry Laboratory, University of Bayreuth, Universitaetsstrasse 30, 95440 Bayreuth, Germany

[2] Department of Chemistry, Abeda Inamdar Senior College, 2390-B, K.B. Hidayatullah Road, Pune 411001, India

[3] Institute of Biophysics, Czech Academy of Sciences, Kralovopolska 135, 61265 Brno, Czech Republic

[4] Department of Biophysics, Faculty of Science, Palacky University, Slechtitelu 27, 78371 Olomouc, Czech Republic

[3]. Besides ruthenium(III) complexes, such as NAMI-A, which are supposed to act as prodrugs being reduced to the biologically more active ruthenium(II) forms only inside the tumor cells [7], the "piano-stool" (arene)ruthenium(II) complexes (basic structure RuPy **1,** Scheme 1) are also considered potential anticancer agents, featuring the bioactive Ru(II) state in a particularly stabilized form [8]. Numerous structural variations with anticancer effects have been described [8–11]. While it was long-known that the coordination of certain bioactive ligands to ruthenium(II) leads to complexes with enhanced toxicity in and selectivity for neoplastic cells, we could even observe pleiotropic, synergistic, and additive effects [10, 12]. Lawsone (2-hydroxy-1,4-naphthoquinone, Scheme 1) **2**, a pigment constituent and active principle of the Henna plant (*Lawsonia inermis*) [13], has been prescribed in ayurvedic medicine mainly for the treatment of skin and hair disease [14]. The lawsone motif is also part of other biologically active *p*-quinones, such as α-lapachone **3** and β-lapachone **4** (Scheme 1). β-Lapachone **4** in particular has been an object of antitumor drug research, lately. The cellular mechanisms of its antitumoral effects are not fully understood, although the induction of p53- and caspase-independent cell death in cancer cells seems to play an important role [15]. Magedov et al. [16] synthesized a library of naphthoquinones and evaluated their in vitro activity against human cancer cells. They found that 2-amino-5,10-dihydro-5,10-dioxo-4-(pyridin-3-yl)-4*H*-benzo[*g*]chromene-3-carbonitrile **5** (Scheme 2) is highly antiproliferative with IC_{50} values in the single-digit micromolar range, inducing apoptosis in human leukemia cells. We now combined the beneficial aspects of the lawsone and Ru(II) "piano-stool" complex motifs in a new complex **6** of pyridinylnaphthoquinone **5**, and investigated in vitro its biological and anti-melanoma effects.

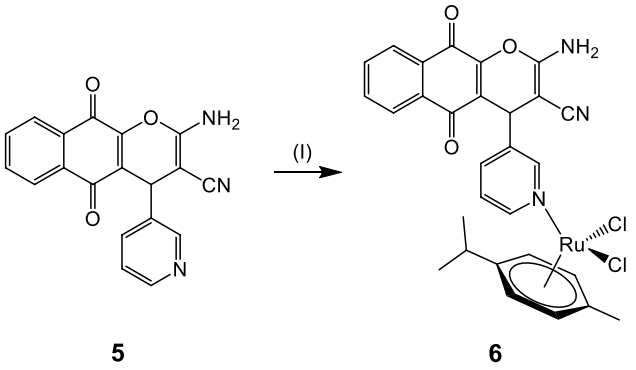

5 **6**

Scheme 2 Reagents and conditions: (I) [Ru(*p*-cymene)Cl_2]$_2$, acetone, rt, 30 min, 100%

Materials and methods

Chemical synthesis

General

All starting compounds were purchased from Sigma-Aldrich. Compound **5** was prepared according to a literature procedure [16].

The melting range was determined with a Gallenkamp apparatus and is uncorrected. IR spectra were recorded on a Perkin–Elmer One FT-IR spectrophotometer. Magnetic resonance (NMR) spectra were recorded under conditions as indicated on a Bruker Avance 300 spectrometer. Chemical shifts (δ) are given in parts per million downfield from TMS as internal standard. Mass spectra were recorded using a Varian 1200L Q3 (ESI). Elemental analyses were carried out with a Perkin–Elmer 2400 CHN elemental analyzer. Satisfactory microanalyses (C, ± 0.2; H, ± 0.1) were obtained for both tested compounds. For example, for **5**: Anal. Calcd. for $C_{19}H_{11}N_3O_3$ (M = 329.31): C, 69.30; H, 3.37; N, 12.76. Found: C, 69.10; H, 3.35; N, 12.92%. Cyclic voltammograms were recorded in DMSO on a Bioanalytical System BASi EPSILON Model instrument with X–Y recorder using a three electrode system with a platinum working electrode, Ag^+/AgCl as the reference electrode and a platinum wire as the auxiliary electrode in 0.1 M *t*-Bu_4NClO_4 (tetrabutylammonium perchlorate) as supporting electrolyte. Ferrocene served as internal standard.

(3-(2-Amino-3-cyano-5,10-dihydro-5,10-dioxo-4*H*-benzo[g]chromen-4-yl)pyridine)(dichlorido)(η^5-*p*-cymene)ruthenium(II) 6

Compound **5** (75 mg, 0.23 mmol) and [Ru(*p*-cymene)Cl_2]$_2$ (70 mg, 0.12 mmol) were dissolved in acetone (10 mL).

Scheme 1 Structures of "piano-stool" complex RuPy **1**, lawsone **2**, α-lapachone **3**, and β-lapachone **4**

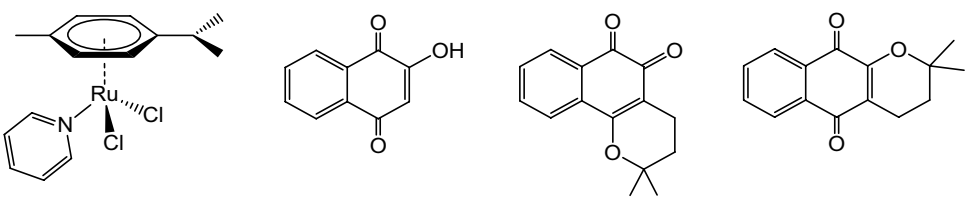

1 **2** **3** **4**

The reaction mixture was vigorously stirred for 30 min. The formed precipitate was collected, washed with acetone and n-hexane, and dried in vacuum. Yield: 143 mg (0.23 mmol, 100%); amber solid of m.p. > 170 °C (dec.). Anal. Calcd. for $C_{29}H_{25}Cl_2N_3O_3Ru$ ($M = 635.5$): C, 54.81; H, 3.97; N, 6.61. Found: C, 54.65; H, 4.01; N, 6.58%. υ_{max}(ATR)/cm^{-1} 3318, 3194, 2961, 2190, 1698, 1667, 1630, 1612, 1592, 1578, 1475, 1432, 1402, 1365, 1332, 1302, 1244, 1201, 1090, 1075, 1058, 1027, 954, 870, 799, 767, 734, 714, 700; ^{1}H NMR (300 MHz, $CDCl_3$) δ 1.2–1.3 (6 H, m), 2.09 (3 H, s), 2.9–3.0 (1 H, m), 4.89 (1 H, s), 5.2–5.5 (6 H, m), 7.2–7.3 (1 H, m), 7.7–7.8 (3 H, m), 7.9–8.0 (1 H, m), 8.0–8.1 (1 H, m), 8.8–8.9 (1 H, m), 9.06 (1 H, s); ^{13}C NMR (75.5 MHz, $CDCl_3$) δ 18.1, 22.2, 30.9, 34.3, 54.9, 82.8, 85.4, 99.6, 109.0, 113.4, 121.5, 126.8, 130.2, 133.4, 134.9, 137.0, 142.4, 155.1, 157.4, 166.5, 179.1, 184.0; *m/z* (ESI) 600.2 [M$^+$–Cl] (4), 465.5 (8), 366.5 (8), 282.4 (100), 256.4 (25).

Biological evaluation

Cell lines and culture conditions

The human melanoma cell line 518A2 was a gift from the University Hospital Vienna, Austria (Department of Radiotherapy and Radiology). The human colon carcinoma cell line HCT-116 (ACC-581), and its p53 knockout mutant HCT-116$^{p53-/-}$ were purchased from The German Collection of Microorganisms and Cell Cultures (DSMZ, Braunschweig). The cells were grown in Dulbecco´s Modified Eagle Medium (DMEM; Biochrom) high glucose supplemented with 10% (*v*/*v*) fetal bovine serum (FBS; Biochrom.) and 1% (*v*/*v*) antibiotic–antimycotic solution (Thermo Scientific). Human dermal fibroblasts HDFa (ATCC® PCS-201-012™) were grown in DMEM supplemented with 10% (*v*/*v*) FBS, 1% (*v*/*v*) antibiotic–antimycotic, and 2 mM glutamine (Biochrom). All cells were incubated at 37 °C, 5% CO_2, 95% humidified atmosphere. They were serially passaged following trypsinization using 0.05% trypsin/0.02% EDTA (*w*/*v*; Biochrom GmbH, Berlin, Germany). Mycoplasma contamination was frequently monitored, and only mycoplasma-free cultures were used.

Inhibition of cell growth (MTT assay)

3-(4,5-Dimethylthiazol-2-yl)-2,5-diphenyltetrazolium bromide (MTT; ABCR) was used to identify viable cells which reduce it to a violet formazan. 518A2 melanoma cells, colon carcinoma cells HCT-116 and HCT-116$^{p53-/-}$ (5×10^4 cells mL^{-1}, 100 µL well^{-1}), as well as HDFa cells (10×10^4 cells mL^{-1}, 100 µL well^{-1}) were seeded in 96-well tissue culture plates and cultured for 24 h at 37 °C, 5% CO_2 and 95% humidity. After treatment with the test compounds (dilution series ranging from 100 µM to 5 pM in ddH_2O), incubation of cells was continued for 72 h. Blank and solvent controls were treated identically. After the addition of a 5 mg mL^{-1} stock solution of MTT in phosphate buffered saline (PBS), microplates were incubated for 2 h, centrifuged at 300 g, 4 °C for 5 min and the supernatant medium was discarded. The precipitate of formazan crystals was then redissolved in a 10% (*w*/*v*) solution of sodium dodecylsulfate (SDS; Carl Roth) in DMSO containing 0.6% (*v*/*v*) acetic acid. To ensure complete dissolution of formazan, microplates were incubated for at least 1 h in the dark. Finally, the absorbance at $\lambda = 570$ and 630 nm (background) was measured using a microplate reader (Tecan F200). All experiments were carried out in quadruplicate and the percentage of viable cells was calculated as the mean ± SD with controls set to 100%.

Cellular and nuclear uptake

Cellular accumulation of ruthenium was measured in 518A2 melanoma cells cultured in DMEM supplemented with 10% FBS. The cells were seeded in 6-well plates (1.5×10^5 cells well^{-1}), were allowed to adhere for 24 h (37 °C, 5% CO_2, 95% humidity), and then incubated with solvent (DMSO), or varying concentration of complex **6** (10, 25, and 50 µM) for 24 h under cell-culture conditions. The adherent cells were washed twice with PBS, detached by trypsinization, and washed twice with ice cold PBS.

Whole cell lysates were obtained by resuspension of the cell pellet in lysis buffer 1 (0.1 M Tris/HCl, 0.2% Triton X-100, 200 kIU Aprotinin mL^{-1}, pH 7.4) and incubation for 20 min on ice. After centrifugation (5 min, $800 \times g$, 4 °C), the supernatant was used for measurements.

For nuclear lysates, the cell pellet was resuspended in lysis buffer 2 (200 mM HEPES, 10 mM KCl, 0.1 mM EDTA, 0.1 mM EGTA, 1.5 mM $MgCl_2$, 0.05 mM DTT, 200 kIU Aprotinin/mL, pH 7.4), digested mechanically, and incubated on ice for 20 min. By centrifugation (1 min, $1200 \times g$, 4 °C), nuclei were pelleted and the supernatant containing cytosolic fraction was discarded. The nuclei were washed thrice in PBS and lysed in lysis buffer 2 plus 0.2% Triton X-100 for following analysis. Protein concentration of all samples was determined using Bradford test.

To give fully homogenised solutions, samples were digested by a high-pressure microwave digestion system (MARS5, CEM) with HCl, and the content of ruthenium was determined by ICP-MS (Agilent 7500, Agilent, Japan).

Ethidium bromide staining assay

DNA interaction was assessed by a fluorescence-based ethidium bromide (EtBr) staining assay. Salmon sperm DNA (SS-DNA, Sigma-Aldrich) or pBR322 plasmid DNA (Thermo Scientific) was pipetted into a black 96-well plate in TE buffer to reach a final amount of 1 µg/100 µL assay volume and incubated with varying concentrations of test compounds for 2 h at 37 °C. Afterwards, 100 µL of a 10 µg mL^{-1} EtBr solution in TE buffer was added to each well. After 5 min of incubation, the fluorescence ($\lambda_{ex} = 535$ nm, $\lambda_{em} = 595$ nm) was detected using a microplate reader (Tecan F200). Each fluorescence value was corrected for possible intrinsic compound and EtBr background fluorescence. As all experiments were carried out in triplicate, the relative EtBr fluorescence was calculated as mean ± SD with solvent controls set to 100%. A decreased fluorescence indicates an interaction between DNA and test compound which prevents the intercalation of EtBr molecules into the DNA.

Analysis of intracellular ROS levels

For DCFH-DA assays, 518A2 melanoma cells (1×10^5 cells mL^{-1}, 100 µL $well^{-1}$) were seeded in black 96-well tissue culture plates and incubated for 24 h (37 °C, 5% CO_2, and 95% humidity). Then, the culture medium was replaced by serum-free medium containing 20 µM 2′,7′-dichlorofluorescin diacetate (DCFH-DA; Sigma-Aldrich) and the cells were incubated for 30 min (37 °C, 5% CO_2, and 95% humidity). After cells had been washed with PBS twice, serum-free medium (100 µL $well^{-1}$) was added and the cells were treated with different concentrations of the test compounds or solvent for 1 h (37 °C, 5% CO_2, and 95% humidity). Finally, the fluorescence intensity was measured at an emission wavelength of 535 nm (excitation wavelength: 485 nm) using a microplate reader (Tecan F200). All experiments were carried out in triplicate and the percentage of intracellular ROS levels calculated as the mean ± SD with controls set to 100%.

For a more differentiated assessment of ROS, the Cellular ROS/Superoxide Detection Assay Kit (abcam) was used. 518A2 melanoma cells (1×10^5 cells mL^{-1}, 100 µL $well^{-1}$) were seeded in black 96-well tissue culture plates with clear bottom and incubated for 24 h (37 °C, 5% CO_2, 95% humidity). The cells were washed with 1 × wash buffer, loaded with ROS/superoxide detection reagent with the addition of either the vehicle, test compounds, or positive control (pyocyanin) and incubated for 1 h (37 °C, 5% CO_2, and 95% humidity) with periodic shaking in the dark. Finally, the fluorescence intensities were measured at an emission wavelength of 520 nm (green) and 610 nm (orange; excitation wavelengths: 485 nm and 550 nm), respectively, using a microplate reader (Tecan F200). To consider cytotoxicity of the applied concentrations of the test compounds or solvent, MTT assays were performed simultaneously with an identically treated 96-well plate. All experiments were carried out in sextuplicate and the percentage of intracellular ROS and superoxide levels calculated as the mean ± SD with controls set to 100%.

Cell-cycle analysis

518A2 melanoma cells (3 mL $well^{-1}$; 5×10^4 cells mL^{-1}) were grown on 6-well tissue culture plates for 24 h (37 °C, 5% CO_2, 95% humidity). After treatment with different concentrations of the test compounds or solvent, the cells were incubated for another 24 h (37 °C, 5% CO_2, 95% humidity). After fixation in 70% EtOH (1 h, 4 °C), cells were washed with PBS and incubated with propidium iodide (PI; Carl Roth) staining solution (50 µg mL^{-1} PI, 0.1% sodium citrate, and 50 µg mL^{-1} RNAse A in PBS) for 30 min at 37 °C. The fluorescence intensity of 10 000 single cells was measured at $\lambda_{em} = 570$ nm ($\lambda_{ex} = 488$ nm laser source) with a Beckmann Coulter Cytomics FC500 flow cytometer. The distribution (%) of cells over the different phases of the cell cycle (sub-G1, G1, S, and G2/M phases) was determined by the CXP software (Beckmann Coulter).

Senescence-associated β-galactosidase staining

For the determination of the senescence-associated β-galactosidase (SA-βgal) activity, a cytochemical assay based on the conversion of the chromogenic substrate 5-bromo-4-chloro-3-indoyl-β-D-galactopyranoside (X-gal) at pH 6.0 was applied. 518A2 melanoma cells were grown on coverslips (4×10^4 cells mL^{-1}) in 24-well plates for 24 h (37 °C, 5% CO_2, and 95% humidity), treated with different concentrations of the test compounds or solvent and subsequently incubated for a further 72 h (37 °C, 5% CO_2, and 95% humidity). The supernatant medium was discarded, and cells were washed in 1 × PBS, and fixed with 4% formaldehyde for 5 min at room temperature. Then, 500 µL of SA-βgal-staining solution (20 µM citric acid, 40 µM disodium hydrogenphosphate, 5 mM potassium ferricyanide, 5 mM potassium ferrocyanide, 150 mM sodium chloride, 2 mM magnesium chloride, and 1 mg mL^{-1} X-gal) was added to each well and conversion of the substrate was performed in an incubator without CO_2 supply at 37 °C for 16 h. The coverslips were mounted in Mowiol 4-88-based mounting medium containing 2.5% (*w*/*v*) DABCO and 1 µg mL^{-1} DAPI (4′,6-diamidino-2-phenyl-indole) for counterstaining the nuclei. SA-βgal-positive cells were detected with brightfield microscopy, and nuclei were documented by fluorescence microscopy (ZEISS Axiovert 135 and AxioCam MRc5). For each concentration, a minimum of 400 cells from at least four different pictures were counted

(AxioVision software) and the percentage of senescent cells was calculated as the ratio of SA-ßgal-positive cells (bright-field: blue/green) to the total number of counted cells.

Results

Synthesis and characterization

Naphthoquinone **5** was synthesized by a base-catalyzed one-pot reaction of malononitrile with pyridine-3-aldehyde and lawsone **2** as previously described [16]. Its reaction with [Ru(*p*-cymene)Cl_2]$_2$ afforded the corresponding Ru(II) complex **6** as an amber solid in 100% yield (Scheme 2). Its stability in aqueous solution (with 50% D_2O plus 0.9% NaCl) over at least 72 h was ascertained by ^{1}H-NMR spectroscopy (*cf.* Supporting Information, Fig. 1).

Biological evaluation

Inhibition of cancer cell proliferation

The ligand **5** and its complex **6** were screened for their inhibitory effects on the growth of human cancer cells of different entities (melanoma, colon, mamma, and cervix carcinoma) and of non-malignant adult human dermal fibroblasts (HDFa), and a selectivity index (SI) was calculated (Table 1).

Compounds **5** and **6** showed IC_{50} values in the micromolar range against cells of 518A2 melanoma, HT-29 colon carcinoma, and multi-drug resistant MCF-7^{Topo} mamma and KB-V1^{Vbl} cervix carcinoma. IC_{50} data from Magedov et al. [16] for the ligand **5** (HeLa: 14.2 ± 1.0 µM, MCF-7/AZ: 3.4 ± 0.8 µM, Jurkat: 20.4 ± 5.8 µM) roughly match with our findings. Compared to CDDP, the lawsone derivatives **5** and **6** were less active against HT-29, MCF-7^{Topo} and KB-V1^{Vbl} carcinoma cells, but showed a similar activity against highly invasive, Bcl-2 overexpressing [17] and p53-mutated [18] 518A2 melanoma cells. In contrast, ruthenium(II) pyridine complex **1** did not show any inhibitory effect against these cancer cell lines or HDFa. Complex **6** was quite selective for the melanoma cells with an SI of 4.6. While CDDP was slightly more selective with an SI of 5.2, it was also more generally cytotoxic.

Cellular and nuclear uptake

Via ICP-MS, we quantified the overall uptake of complex **6** into 518A2 melanoma cells by measuring the amount of Ru taken up by the whole cells in comparison with lysed purified nuclei, comprised of nuclear DNA plus all nucleus- and DNA-associated proteins. In a concentration-dependent manner, the metal content of the whole cell lysates rose from 45 over 76 to 200 ng Ru/mg total protein upon incubation with 10 µM, 25 µM, or 50 µM of complex **6**. For the nuclear lysates, the corresponding figures showed a similar increase from 5 over 16 to 24 ng Ru/mg (*cf.* Supporting Information, Fig. 2). This is proof of the complex **6** reaching the cytoplasm as well as the nuclei of 518A2 melanoma cells in a quantity sufficient to contribute to its observed biological effects.

Interaction with DNA

The antitumoral properties of ruthenium complexes are believed to originate in part from their affinity to DNA [19]. Complex **6** was scrutinized for DNA interaction by means of a fluorescence-based microplate assay. First, double-stranded, linear salmon sperm DNA was incubated with either ligand **5** or complex **6**, subsequently stained with ethidium bromide (EtBr), and at last the fluorescence of potential EtBr/DNA adducts was measured (Fig. 1). As the fluorescence of EtBr molecules multiplies when intercalated in double-stranded DNA, a decrease in fluorescence intensity implies an interaction of the test compound with DNA in such a way as to prevent EtBr molecules from intercalating. Upon treatment of DNA with increasing concentrations of ligand **5,** no appreciable change in fluorescence intensity

Table 1 Inhibitory concentrations IC_{50}^{a} [µM] of CDDP, RuPy **1**, **5**, and **6** when applied to cells of human 518A2 melanoma, HT-29 colon carcinoma, mdr MCF-7^{Topo} mamma carcinoma, mdr KB-V1^{Vbl} cervix carcinoma, and human adult dermal fibroblast cell line HDFa; selectivity indices (SI) calculated as IC_{50} (HDFa)/IC_{50} (518A2)

	IC50[µM]					SI (HDFa/518A2)
	518A2	HT-29	MCF-7^{Topo}	KB-V1^{Vbl}	HDFa	
CDDP	7.8 ± 1.1	16.4 ± 1.3	12.9 ± 3.0	2.2 ± 0.3	41.0 ± 4.0	5.2
1	> 100	> 100	> 100	> 100	> 100	–
5	12.9 ± 1.9	26.1 ± 5.1	12.6 ± 2.1	27.3 ± 4.4	17.9 ± 3.1	1.4
6	13.5 ± 0.5	41.2 ± 3.4	17.0 ± 2.3	35.6 ± 3.2	62.4 ± 5.0	4.6

[a]Values are derived from dose–response curves obtained by measuring the percentage of vital cells of treated wells relative to untreated controls after 72 h of incubation using MTT assays. Values are mean ± SD of four independent experiments

was detected. In contrast, complex **6** induced a significant, concentration-dependent reduction of fluorescence intensity, which exceeded even that caused by CDDP. With circular pBR322 plasmid DNA, virtually the same effect was observed only to a somewhat lesser extent in the case of **6** (*cf.* Supporting Information, Fig. 3).

In electrophoretic mobility shift assays (EMSA), circular plasmid DNA, which naturally occurs in a negative supercoiled topology conferring it a high electrophoretic mobility, was treated with a dilution series of compounds **5** and **6** or CDDP and then subjected to agarose gel electrophoresis (*cf.* Supporting Information, Fig. 4). When chemicals bind to, or intercalate into double-stranded DNA, this supercoiled form is relaxed and electrophoretic mobility decreases. However, no such effect was observed, neither for ligand **5**, nor its complex **6**. We assume that interactions between complex **6** and circular plasmid DNA are too weak (possibly non-covalent) and/or are disrupted by the applied electrophoretic potential.

This assumption was supported by ICP-MS analyses of purified, genomic DNA from 518A2 melanoma cells treated with different concentrations (10 and 20 µM) of complex **6** for up to 24 h. The content of ruthenium associated with DNA (0.15 ± 0.05 to 0.33 ± 0.04 pg Ru/µg DNA) was markedly lower not only than that we had found for the nuclear extracts of 518A2 cells consisting of DNA plus associated protein (*cf.* Supporting Information, Fig. 2), but also lower than metalation degrees reported in the literature for cisplatin under similar conditions (e.g., 5 pg Pt/µg DNA in HeLa cells) [20]. This is another hint at ruthenium being only loosely bound to DNA and partly getting lost in the course of the purification process.

However, DNA seems to be a conceivable cellular target of complex **6**, but not of the ligand **5**.

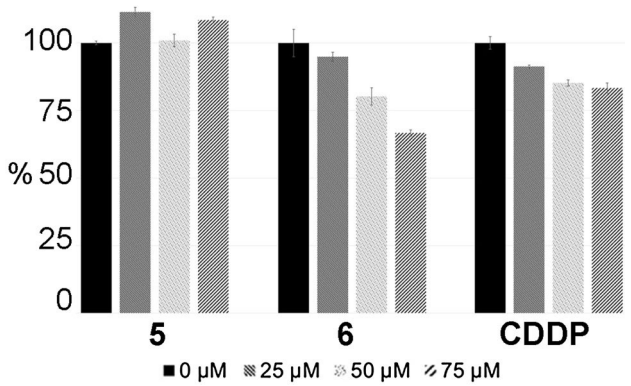

Fig. 1 Effects of ligand **5** and its complex **6**, as well as CDDP, on the relative fluorescence intensity (negative control set to 100%) of ethidium bromide in intercalating assays with salmon sperm DNA. Values ± SD were calculated as the means of at least three independent experiments

Increase of intracellular ROS levels

Cytotoxic effects of CDDP are primarily ascribed to its formation of nuclear DNA adducts, eventually leading to programmed cell death, especially in cells with high mitotic activity. However, DNA interaction per se is not a sufficient explanation for the high antitumor activity of CDDP. Various studies have identified a CDDP mediated rise in the intracellular concentration of reactive oxygen species (ROS) as another important factor. The detailed mechanism of ROS generation by CDDP is, however, still a controversial issue [21]. Ruthenium complexes are also thought to influence intracellular ROS concentrations. Keppler's KP1019 induced apoptosis in HT-29 colon carcinoma cells primarily by intracellular generation of ROS [22]. β-Lapachone **4** was also found to induce multiple, caspase-independent cell death mechanisms in cancer cells via elevated ROS concentrations [23].

We determined the influence of ligand **5** and its complex **6** on the intracellular ROS concentration of 518A2 melanoma cells, in comparison with CDDP, by means of a fluorescence-based staining assay (Fig. 2).

Treatment of 518A2 melanoma cells with CDDP, in line with other studies [23], led to a ca 50% increase of the intracellular ROS concentration, as did ligand **5**. Interestingly, treatment with complex **6** almost quintupled the ROS concentration, indicating the importance of ROS for its mechanism of action. The effect of complex **6** on the intracellular ROS level of 518A2 melanoma cells could be countered by addition of the ROS scavenger *N*-acetyl-L-cysteine in DCFH-DA assays and confirmed using another fluorescence-based detection assay which allows the differentiated detection of the entire cellular ROS and of cellular superoxide ($O_2^{\bullet-}$) only. While 518A2 melanoma cells treated with the known ROS inducer pyocyanin were found to have increased cellular levels of both overall ROS and $O_2^{\bullet-}$, cells treated with complex **6** showed an increase in overall ROS concentration in combination with a slight decrease of $O_2^{\bullet-}$ levels (*cf.* Supporting Information, Fig. 5). A similar, though less pronounced, trend was also observed for CDDP treated melanoma cells. A speculative explanation of this phenomenon would be that these complexes of Ru(II) and Pt(II) to some extent catalyse the conversion of $O_2^{\bullet-}$ into other reactive oxygen species such as O_2, H_2O_2, and finally H_2O.

The redox properties of ligand **5** and complex **6** in a cell-free context were studied by cyclic voltammetry (*cf.* Supporting Information, Fig. 6). Ligand **5** gave rise to a pair of peaks at − 493 mV (i_{pc} 9.4 µA) and − 411 mV (i_{pa} 1.0 µA) indicative of a one-electron transfer redox couple. When run in cathodic direction, this pair of peaks was embedded in a series of smaller peaks of other irreversible reduction steps. This cyclic voltammogram is more complex than that of the parent compound lawsone which features only a single

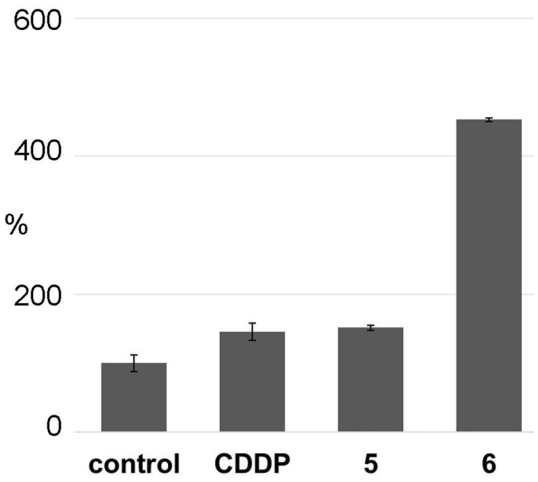

Fig. 2 Relative increase of the intracellular concentration of reactive oxygen species in 518A2 melanoma cells after treatment with solvent (DMSO: control) or 50 µM of CDDP or the lawsone derivatives **5** and **6** for 1 h. All experiments were performed in sextuplicate. The ROS level was calculated as mean ± SD with respect to untreated control set to 100%

pair of peaks at − 320 mV and − 100 mV. Interestingly, the cyclic voltammogram of complex **6** appeared much tidier than that of **5** with a single pair of redox peaks at − 481 mV (i_{pc} 4.2 µA)/− 392 mV (i_{pa} 1.7 µA), indicative of a more reversible electron transfer than that of ligand **5**. This more perfect and persistent redox cycling of complex **6** when compared to that of ligand **5** might contribute to its greater ROS producing effect in 518A2 melanoma cells.

Effects on the cell cycle

Since we had observed DNA interaction, as well as an increase of intracellular ROS levels upon treatment of 518A2 melanoma cells with ruthenium(II) complex **6**, we also ascertained its effect on the cell cycle, as well as a potential induction of apoptosis.

To this end, 518A2 melanoma cells were treated for 24 h with complex **6** in a concentration below its IC_{50} value for 518A2 melanoma cells (5 µM) and in a concentration slightly above the IC_{50} value (25 µM), then fixed and subjected to cell-cycle analysis via flow cytometry (Fig. 3). A negative control run with cells treated with equivalent amounts of DMSO gave the normal distribution of 518A2 melanoma cells in the different cell-cycle phases.

518A2 melanoma cells treated with 5 µM of the known apoptosis-inducing drug CDDP showed a significant increase of the sub-G1 fraction, representing cell fragments likely resulting from apoptotic cell death. Treatment with complex **6** resulted in a minor increase of the sub-G1 peak, so neither apoptosis nor necrosis seem to play a major role in its mechanism of action, although Magedov et al. had reported ligand **5** to induce apoptosis in HL-60 leukemia cells [16]. We confirmed the negative results of our cell-cycle analyses by assaying the caspase-3/7 activity in 518A2 melanoma cells treated with CDDP or complex **6** (*cf.* Supporting Information, Fig. 7).

Moreover, 518A2 cells were arrested in the G2/M phase of the cell cycle when treated with sub-IC_{50} concentrations of complex **6**, whereas treatment with concentrations above the IC_{50} value led to a shift of the cell-cycle arrest from G2/M- to G1-phase concomitant with a slight increase of the sub-G1 fraction. In summary, we could exclude a caspase-dependent, apoptotic cell death as a major aspect of the mode of action of complex **6** in 518A2 melanoma cells, yet observed their concentration-dependent arrest in G2/M phase of the cell cycle upon treatment with **6**.

Induction of senescence in melanoma cells

Cellular senescence was first described by Hayflick and Moorhead [24] as a state of irreversible growth arrest of normal human fibroblasts after serial cultivation in vitro. The therapeutic induction of senescence (TIS) offers a way to cytostasis of rapidly dividing cancer cells. Senescence is also called replicative or cellular ageing, and manifests itself in two major types: intrinsic, telomere-dependent replicative senescence and extrinsic, stress-induced premature senescence (SIPS) [25, 26]. The former is caused mainly by the progressive loss of telomeric DNA with each cell division, whereas there are conceivable stressors which can lead to SIPS such as DNA damage and oxidative stress, among others [25, 27]. The senescence-like phenotype is defined by its permanent growth arrest and the absence of proliferation markers, and by morphological changes like enlarged and flattened cell shape, and by the senescence-associated secretory phenotype (SASP) [28, 29]. Histochemically, senescent cells can be detected by staining for senescence-associated ß-galactosidase (SA-ßgal) [30], which we did for 518A2 melanoma cells treated with complex **6** (Fig. 4).

Untreated 518A2 melanoma cells showed normal morphology and a confluent cell layer after 72 h incubation under cell-culture conditions. No blue-stained cells were detected after staining of the fixed cells with X-gal-staining solution at pH 6. After treatment of the cells with 10 µM CDDP, 4.3% of the cells were positive for SA-ß-galactosidase, whereas higher concentrations (25 µM) led to a drastically decreased cell number with 9.2% SA-ßgal-positive 518A2 melanoma cells. After treatment with increasing concentrations of ligand **5** a decrease of cell density, no meaningful percentage of blue cells was observed (10 µM: 0.4%, 25 µM: 3.5%). Only few of the melanoma cells treated with 10 µM **6** for 72 h showed a blueish hue under bright field microscopy (5%). However, the cell layer was clearly less dense when compared to the negative control, and also

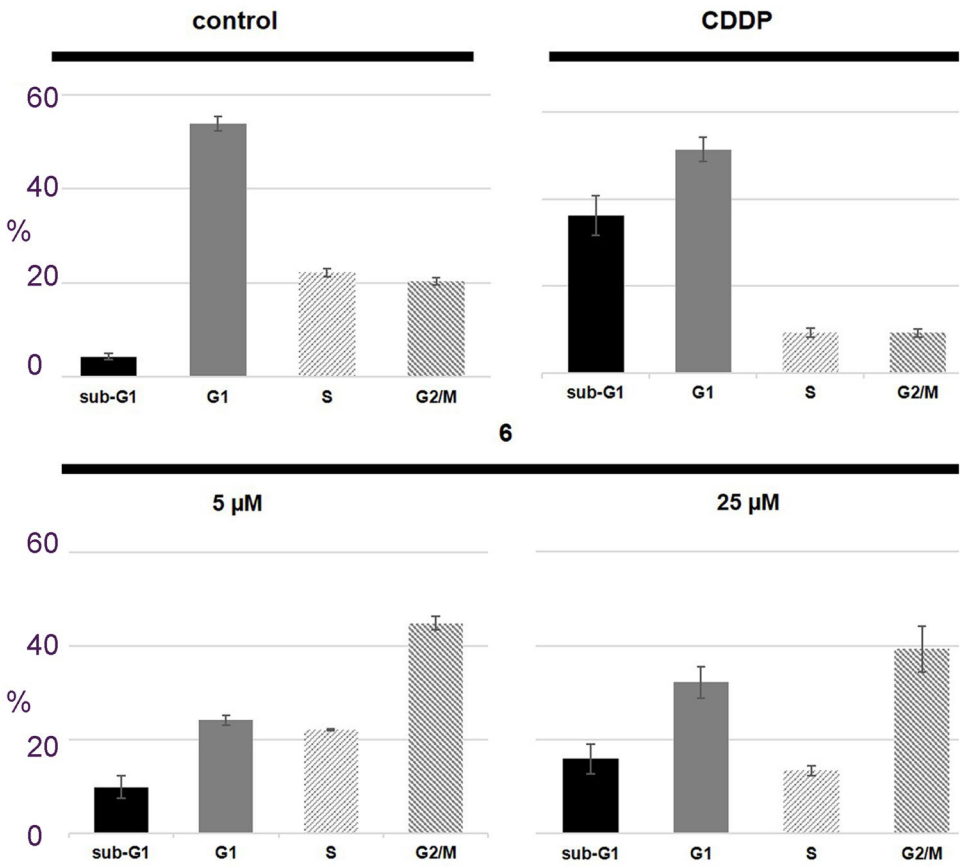

Fig. 3 Effect on the cell-cycle progression of 518A2 melanoma cells after 24 h incubation with vehicle (control), or 5 µM of CDDP, or 5 µM and 25 µM of complex **6**. Percentage of 518A2 melanoma cells in G1, S, and G2/M cell-cycle phases and the proportion of potentially apoptotic cells (sub-G1) as determined by flow cytometry. Values are the mean ± SD of three independent experiments

a change in cell shape could be observed: cells appeared bigger in volume and flattened, which are both morphological signs of cellular senescence [29]. When treated with 25 µM of complex **6** ca. 65% of the 518A2 melanoma cells appeared blue under bright field microscopy, also showing the typical senescent morphology.

Discussion

The 5-year overall survival (OS) rate for patients with metastatic melanoma (stage IV) lies between 9 and 28% [31]. Today, the majority of these patients benefit from immune and targeted therapies. For instance, cytokine therapy with interleukin-2 (IL-2) increases their OS significantly, yet is associated with severe side effects. For stage IV patients not responding to targeted therapy, conventional chemotherapy is the only available option yielding low response rates at a high risk of resistance induction.

The new ruthenium(II) complex **6** was comparable to CDDP in terms of specificity for human melanoma cells over non-malignant human dermal fibroblasts with the added bonus of a lower general toxicity against normal cells. We also identified DNA as a likely cellular target of **6**.

518A2 melanoma cells were arrested in G2/M phase, a consequence of DNA damage by complex **6**. In contrast to CDDP, complex **6** did neither induce a major increase of the sub-G1 cell fraction nor of the activity of effector caspases 3 and 7. Thus, apoptosis and necrosis appear to play no major role in its mechanism of action.

Like apoptosis and transient growth arrest, cellular senescence is a distinct tumor suppressor mechanism, limiting the proliferation of cells at different stages of mutagenesis. Which of these three lines is taken, depends on the cell type, and on the kind and the level of stress. Several cell types undergo SIPS when exposed to sub-lethal stress, essentially DNA damage and/or oxidative stress, to prevent cancerogenesis [32]. As senescence is an irreversible process, chemotherapy could possibly benefit from substances inducing SIPS in tumor cells, and studies have already revealed DNA-damaging agents being able to do so [33, 34]. High rates of senescent cells were detected after treatment of cells with doxorubicin, aphidicolin, and CDDP in vitro [35]. Moreover, it was shown that tumor cell senescence is not only an in vitro phenomenon as, for example, SA-βgal activity was found distinctly increased in tumor sections of mamma carcinoma patients who had undergone doxorubicin-based neoadjuvant chemotherapy in comparison with patients without the previous chemotherapy [36].

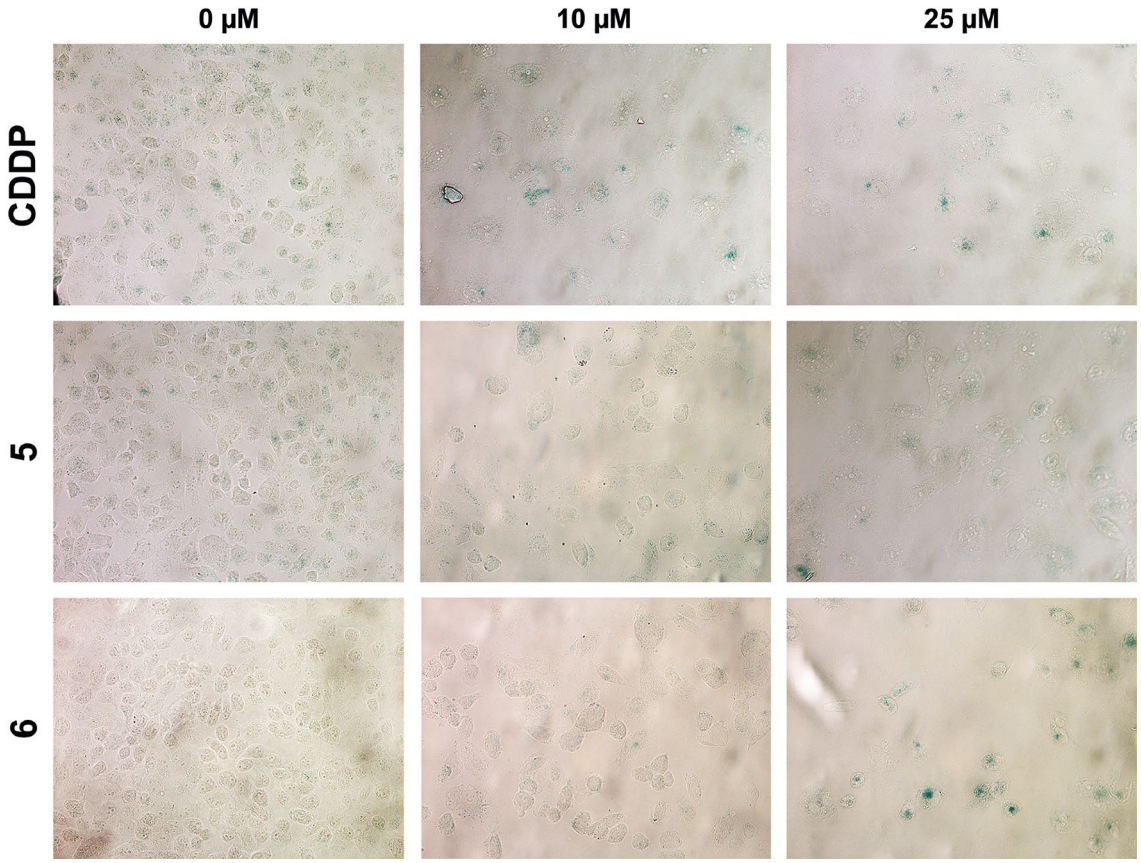

Fig. 4 Senescence-associated β-galactosidase staining of 518A2 melanoma cells treated with CDDP, and compounds **5** or **6**. Cells were seeded on glass coverslips, incubated with indicated concentrations for 72 h at 37 °C, 5% CO_2, and 95% humidity, stained with X-Gal-staining solution (pH 6) for 16 h and embedded in Mowiol 4-88-based mounting medium. Images are representative of four independent experiments

Our data show that CDDP induced apoptotic cell death rather than SIPS in 518A2 melanoma cells, whereas senescence-typical SA-βgal activity of 518A2 melanoma cells was significantly increased after treatment with complex **6**, without noticeable apoptosis. 518A2 melanoma cells treated with complex **6** showed a typical senescent morphology. Even the tremendous increase of intracellular ROS levels in 518A2 melanoma cells treated with **6** can, at least partly, be ascribed to the induction of senescence, as earlier studies had shown that senescent cells produce high levels of downstream ROS such as H_2O_2 [37].

Various studies pointed out that therapy-induced senescence (TIS) might be a potential alternative to conventional chemotherapy which aims at eliminating transformed cancer cells via apoptosis or necrosis [38, 39]. TIS seeks to induce tumor cell stasis rather than tumor cell death, and so probably constitutes a more promising approach for the long-term management of some cancers when compared to side effect associated therapies with cytotoxic agents. TIS should also be applicable to tumors resistant to apoptotic stimuli [38]. Schmitt et al. postulated an improved prognosis and treatment outcome for mice bearing tumors amenable to drug-induced senescence, in comparison with mice bearing tumors with defects retarding the onset of senescence [40]. Results from animal studies also indicated that the cellular senescence program in vivo can activate the immune system, leading to the clearance of malignant cells [41]. Te Poele et al. showed that the neoadjuvant application of DNA-damaging agents could induce senescence in human mamma tumors in vivo and that this induction is an important prognostic factor [34]. The effectiveness and gentleness of cytostatic therapies in comparison with the cytotoxic approach were also demonstrated in clinical studies [42, 43].

However, there are also observations, indicating that senescent tumor cells contribute to tumor progression under certain conditions. Although growth-arrested, senescent cells of the so-called senescence-associated secretory phenotype (SASP) [44] can express secretory proteins such as cytokines, chemokines, growth factors, and matrix-remodeling associated proteases which may affect the tumor micro-environment in an autocrine and/or paracrine

manner. Secreted matrix-remodeling factors (e.g., MMPs) are thought to enhance tumor angiogenesis and metastasis [45]. Pro-inflammatory cytokines secreted by senescent cells are thought to boost tumor cell proliferation in a paracrine way, whereas these pro-inflammatory messengers activate the immune response leading to a recruitment of immune cells to the tumor tissue [46]. SASP also leads to autocrine effects which may contribute to the maintenance of the senescence growth arrest [44]. The nature of cellular effects of SASP is pleiotropic and seems to be cell-type dependent [44]. The SASP of senescent melanoma cells is still largely unexplored.

Recent studies demonstrated that specific melanoma cells retain the ability to senesce in response to certain stimuli and that most melanoma cells are highly resistant to cytotoxic, apoptosis-inducing chemotherapy [47]. Interestingly, most melanoma cells have a powerful pro-senescence signaling via activation of BRAF or NRAS [48]. Other studies proved that senescence represents a protective physiological process in human naevi, benign tumors of melanocytes. In vivo senescence markers (e.g., SA-βgal) were found to be present at a high degree in naevi, whereas these markers were absent in dysplastic naevi or early melanoma [49, 50]. There is also evidence that clinically established drugs for the treatment of metastatic melanoma induce senescence, such as, for example, the DNA-alkylating agent temozolomide (TMZ), a first-line drug for the chemotherapy of metastatic melanoma [51].

One explanation for the greater cancer cell selectivity of complex **6** when compared to its ligand **5** might lie in its generally higher and cancer cell-specific cellular uptake. Moreover, our cyclic voltammetry and cell-cycle studies suggest that the unspecific cytotoxicity of ligand **5** may result from its higher reactivity and instability causing unspecific damage to biomolecules. The ruthenium fragment appears to stabilize the naphthoquinone system in terms of redox cycling and ROS production to the effect of an altogether different cellular mechanism of action.

Acknowledgements R. S. thanks the Deutsche Forschungsgemeinschaft (DFG) for a grant (Scho 402/12-2), H. K., J. K. and V. B. were supported by the Czech Science Foundation (Grant 17–05302S).

Funding Deutsche Forschungsgemeinschaft Grant Scho 402/12; Czech Science Foundation Grant 17–05302S.

Compliance with ethical standards

Conflicts of interest There are no conflicts of interest.

References

1. Garbe C, Peris K, Hauschild A, Saiag P, Middleton M, Bastholt L et al (2016) Diagnosis and treatment of melanoma. European consensus-based interdisciplinary guideline—update 2016. Eur J Cancer 63:201–217
2. Pasquali S, Hadjinicolaou AV, Chiarion Sileni V, Rossi CR, Mocellin S (2018) Systemic treatments for metastatic cutaneous melanoma. Cochrane Database Syst Rev 2:CD011123
3. Antonarakis ES, Emadi A (2010) Ruthenium-based chemotherapeutics: are they ready for prime time? Cancer Chemother Pharmacol 66:1–9
4. Rademaker-Lakhai JM, van den Bongard D, Pluim D, Beijnen JH, Schellens JH (2004) A phase I and pharmacological study with imidazolium-trans-DMSO-imidazole-tetrachlororuthenate, a novel ruthenium anticancer agent. Clin Cancer Res 10:3717–3727
5. Hartinger CG, Jakupec MA, Zorbas-Seifried S, Groessl M, Egger A, Berger W et al (2008) KP1019 a new redox-active anticancer agent—preclinical development and results of a clinical phase I study in tumor patients. Chem Biodivers 5:2140–2155
6. Burris HA, Bakewell S, Bendell JC, Infante J, Jones SF, Spigel DR et al (2016) Safety and activity of IT-139, a ruthenium-based compound, in patients with advanced solid tumours: a first-in-human, open-label, dose-escalation phase I study with expansion cohort. ESMO Open 1:e000154
7. Allardyce CS, Dyson PJ (2001) Ruthenium in medicine: current clinical uses and future prospects. Platin Metals Rev 45:62–69
8. Biersack B (2016) Anticancer activity and modes of action of (arene) ruthenium(II) complexes coordinated to C-, N-, and O-ligands. Mini Rev Med Chem 16:804–814
9. Pettinari R, Petrini A, Marchetti F, Pettinari C, Riedel T, Therrien B et al (2017) Arene-ruthenium(II) complexes with bioactive ortho-hydroxydibenzoylmethane ligands: synthesis, structure, and cytotoxicity. Eur J Inorg Chem 12:1800–1806
10. Schmitt F, Kasparkova J, Brabec V, Begemann G, Schobert R, Biersack B (2018) New (arene)ruthenium(II) complexes of 4-aryl-4*H*-naphthopyrans with anticancer and anti-vascular activities. J Inorg Biochem 184:69–78
11. Thota S, Rodrigues DA, Crans DC, Barreiro EJ (2018) Ru(II) compounds: next-generation anticancer metallotherapeutics? J Med Chem 61:5805–5821
12. Biersack B, Zoldakova M, Effenberger K, Schobert R (2010) (Arene)Ru(II) complexes of epidermal growth factor receptor inhibiting tyrophostins with enhanced selectivity and cytotoxicity in cancer cells. Eur J Med Chem 45:1972–1975
13. Pradhan R, Dandawate P, Vyas A, Padhye S, Biersack B, Schobert R et al (2012) From body art to anticancer activities: perspectives on medical properties of henna. Curr Drug Target 13:1777–1798
14. Nadkarni KM (1908) Indian plants and drugs, 1st edn. Nortan & Co., Madras
15. Park EJ, Min KJ, Lee TJ, Yoo YH, Kim YS, Kwon TK (2014) β-Lapachone induces programmed necrosis through the RIP1-PARP-AIF-dependent pathway in human hepatocellular carcinoma SK-Hep1 cells. Cell Death Dis 5:e1230
16. Magedov IV, Kireev AS, Jenkins AR, Evdokimov NM, Lima DT, Tongwa P et al (2012) Structural simplification of bioactive natural products with multicomponent synthesis. 4H-pyrano-[2,3-b] naphthoquinones with anticancer activity. Bioorg Med Chem Lett 22:5195–5198
17. Benimetskaya L, Ayyanar K, Kornblum N, Castanotto D, Rossi J, Wu S et al (2006) Bcl-2 protein in 518A2 melanoma cells in vivo and in vitro. Clin Cancer Res 12:4940–4948
18. Zerp SF, Van Elsas A, Peltenburg LTC, Schrier PI (1999) p53 mutations in human cutaneous melanoma correlate with sun exposure but are not always involved in melanomagenesis. Br J Cancer 79:921–926
19. Brabec V, Novakova O (2006) DNA binding mode of ruthenium complexes and relationship to tumor cell toxicity. Drug Resist Update 9:111–122

20. Intini FP, Zajac J, Novohradsky V, Saltarella T, Pacifico C et al (2017) Novel antitumor platinum(II) conjugates containing the nonsteroidal anti-inflammatory agent diclofenac: synthesis and dual mechanism of antiproliferative effects. Inorg Chem 56:1483–1497
21. Marullo R, Werner E, Degtyareva N, Moore B, Altavilla G, Ramalingam SS et al (2013) Cisplatin induces a mitochondrial-ROS response that contributes to cytotoxicity depending on mitochondrial redox status and bioenergetic functions. PLoS One 8:e81162
22. Kapitza S, Jakupec MA, Uhl M, Keppler BK, Marian B (2005) The heterocyclic ruthenium(III) complex KP1019 (FFC14A) causes DNA damage and oxidative stress in colorectal tumor cells. Cancer 226:115–121
23. Park EJ, Choi KS, Kwon TK (2011) β-Lapachone-induced reactive oxygen species (ROS) generation mediates autophagic cell death in glioma U87 MG cells. Chem Biol Interact 189:37–44
24. Hayflick L, Moorhead PS (1961) The serial cultivation of human diploid cell strains. Exp Cell Res 25:585–621
25. Itahana K, Campisi J, Dimri GP (2004) Mechanisms of cellular senescence in human and mouse cells. Biogerontology 5:1–10
26. Debacq-Chainiaux F, Ameur RB, Bauwens E, Dumortier E, Toutfaire M, Toussaint O (2016) Stress-induced (premature) senescence. In: Rattan S, Hayflick L (eds) Cellular ageing and replicative senescence. Healthy Ageing and longevity, 4th edn. Springer, Cham, pp 243–262
27. Okada H, Mak TW (2004) Pathways of apoptotic and non-apoptotic death in tumour cells. Nat Rev Cancer 4:592–603
28. Gire V, Dulic V (2015) Senescence from G2 arrest, revisited. Cell Cycle 14:297–304
29. Sikora E, Mosieniak G, Sliwinska MA (2016) Morphological and functional characteristics of senescent cells. Curr Drug Targets 17:377–387
30. Kurz DJ, Decary S, Hong Y, Erusalimsky JD (2000) Senescence-associated (beta)-galactosidase reflects an increase in lysosomal mass during replicative ageing of human endothelial cells. J Cell Sci 113:3613–3622
31. Svedman FC, Pillas D, Taylor A, Kaur M, Linder R, Hansson J (2016) Stage-specific survival and recurrence in patients with cutaneous malignant melanoma in Europe—a systematic review of the literature. Clin Epidemiol 8:109–122
32. Toussaint O, Royer V, Salmon M, Remacle J (2002) Stress-induced premature senescence and tissue ageing. Biochem Pharmacol 64:1007–1009
33. Berns A (2002) Senescence: a companion in chemotherapy? Cancer Cell 1:309–311
34. te Poele RH, Okorokov AL, Jardine L, Cummings J, Joel SP (2002) DNA damage is able to induce senescence in tumor cells in vitro and in vivo. Cancer Res 62:1876–1883
35. Chang BD, Broude EV, Dokmanovic M, Zhu H, Ruth A, Xuan Y et al (1999) A senescent-like phenotype distinguishes tumor cells that undergo terminal proliferation arrest after exposure to anticancer agents. Cancer Res 59:3761–3767
36. Roninson IB, Broude EV, Chang BD (2001) If not apoptosis, then what? Treatment-induced senescence and mitotic catastrophe in tumor cells. Drug Resist Update 4:303–313
37. Chen Q, Fischer A, Reagan JD, Yan LJ, Ames BN (1995) Oxidative DNA damage and senescence of human diploid fibroblast cells. Proc Natl Acad Sci USA 92:4337–4341
38. Ewald JA, Desotelle JA, Wilding G, Jarrard DF (2010) Therapy-induced senescence in cancer. J Natl Cancer Inst 102:1536–1546
39. Nardella C, Clohessy JG, Alimonti A, Pandolfi PP (2011) Pro-senescence therapy for cancer treatment. Nat Rev Cancer 11:503–511
40. Schmitt CA, Fridman JS, Yang M, Lee S, Baranov E, Hoffman RM, Lowe SW (2002) A senescence program controlled by p53 and p16INK4a contributes to the outcome of cancer therapy. Cell 109:335–346
41. Xue W, Zender L, Miething C, Dickins RA, Hernando E, Krizhanovsky V et al (2007) Senescence and tumor clearance is triggered by p53 restoration in murine liver carcinomas. Nature 445:656–660
42. Martin L, Schilder RJ (2006) Novel non-cytotoxic therapy in ovarian cancer: current status and future prospects. J Natl Comp Cancer Netw 4:955–966
43. Winquist E, Waldron T, Berry S, Ernst DS, Hotte S, Lukka H (2006) Non-hormonal systemic therapy in men with hormone-refractory prostate cancer and metastases: a systemic review from the cancer care Ontario program in evidence-based care's genitourinary cancer disease site group. BMC Cancer 6:112
44. Coppe JP, Desprez PY, Krtolica A, Campisi J (2010) The senescence-associated secretory phenotype: the dark side of tumor suppression. Annu Rev Pathol 5:99–118
45. Lee M, Lee JS (2014) Exploiting tumor cell senescence in anticancer therapy. BMB Rep 47:51–59
46. Freund A, Orjalo V, Desprez PY, Campisi J (2010) Inflammatory networks during cellular senescence: causes and consequences. Trends Mol Med 16:238–246
47. Soengas MS, Lowe SW (2003) Apoptosis and melanoma chemoresistance. Oncogene 22:3138–3151
48. Zhuang D, Mannava S, Grachtchouk V, Tang WH, Patil S, Wawrzyniak JA et al (2008) C-MYC overexpression is required for continuous suppression of oncogene-induced senescence in melanoma cells. Oncogene 27:6623–6634
49. Gray-Schopfer VC, Cheong SC, Chong H, Chow J, Moss T, Abdel-Malek ZA et al (2006) Cellular Senescence in Naevi and immortalization in melanoma: a role for p16? Br J Cancer 95:496–505
50. Michaloglou C, Vredeveld L, Soengas M, Denoyelle C, Kuilman T, van der Horst C et al (2005) BRAFE600-associated senescence-like cell cycle arrest of human naevi. Nature 436:720–724
51. Mhaidat NM, Zhang XD, Allen J, Avery-Kiejda KA, Scott RJ, Hersey P (2007) Temozolomide induces senescence but not apoptosis in human melanoma cells. Br J Cancer 97:1225–1233

-Supplementary data-
A new 4-(pyridinyl)-4*H*-benzo[*g*]chromene-5,10-dione ruthenium(II) complex inducing senescence in 518A2 melanoma cells

Madeleine Gold[1], Yusufi Mujahid[2], Khursheed Ahmed[2], Hana Kostrhunova[3], Jana Kasparkova[3,4], Viktor Brabec[3], Bernhard Biersack[1], and Rainer Schobert[1]

[1]Organic Chemistry Laboratory, University of Bayreuth, Universitaetsstrasse 30, 95440 Bayreuth, Germany.

[2]Department of Chemistry, Abeda Inamdar Senior College, 2390-B, K.B. Hidayatullah Road, Pune 411001, India.

[3]Institute of Biophysics, Czech Academy of Sciences, Kralovopolska 135, CZ-61265 Brno, Czech Republic.

[4]Department of Biophysics, Faculty of Science, Palacky University, Slechtitelu 27, CZ-78371 Olomouc, Czech Republic.

Corresponding Author: Rainer Schobert, Tel.: +49 921/552679, Email: Rainer.schobert@uni-bayreuth.de

Table of content

Biological assays

Electrophoretic mobility shift assay (EMSA)

Circular pBR322 plasmid DNA (0.5 µg mL^{-1}; Thermo Scientific) was incubated with different concentrations (0, 25, 50, 75, 100 µM) of the test compounds or cisplatin in TE-buffer (10 mM Tris-HCl, 1 mM EDTA, pH 8.5) for 24 h at 37 °C. Afterwards the DNA samples were subjected to electrophoresis using 1 % agarose gel in 0.5× TBE-buffer (89 mM Tris, 89 mM boric acid, 25 mM EDTA, pH 8.3) and stained with an ethidium bromide solution (10 µg mL^{-1} in 0.5× TBE-buffer) for 30 minutes. Finally DNA bands were visualized via UV excitation. All experiments were performed at least in duplicate.

Determination of the Ru content of genomic DNA

518A2 melanoma cells were seeded at a density of 2×10^5 cells/dish, grown overnight and treated with ruthenium complex **6** at the concentration of 10 µM for 24 h and 20 µM for 6 h under standard cell culture conditions (37 °C, 5 % CO_2 and 95 % humidity). The cells were then washed with PBS, harvested and pelleted. Cell pellets were lysed with DNAzol^{TM} reagent (Invitrogen) according to the manufacturer's instruction to isolate the nuclear DNA. The purified DNA was dissolved in ddH_2O and the DNA concentration was determined spectrophotometrically. The ruthenium content was assessed with ICP-MS.

Caspase-3/7 activation

For caspase activity measurements the Apo-ONE® Homogenous Caspase-3/7 Assay Kit (Promega Corp., Wisconsin, USA) was used. Therefore 518A2 melanoma cells (1.35×10^4 cells/well) were grown in black 96-well plates for 24 h (37 °C, 5 % CO_2 and 95 % humidity) and subsequently incubated with different concentrations of the test compounds or solvent for further 24 h under cell culture conditions. Afterwards 1× caspase-3/7 substrate solution was added to each well and the substrate transformation by potentially activated caspase-3/7 was performed for 60 min at rt. Finally the fluorescence intensity (λ_{ex}: 485 ± 20 nm, λ_{em}: 530 ± 25 nm) was measured using a microplate reader (Tecan F200). For an incorporation of a potential loss of cell viability after the incubation with the test compounds, a MTT-assay was performed equally (as described above). All experiments were carried out in quadruplicate, blank values (caspase-3/7 substrate solution plus test compounds/solvent) were subtracted to reduce background signals, and the caspase-3/7 activity of the remaining vital cells was calculated as means ± SD with solvent controls set to 100%.

Results

Stability testing via ^{1}H-NMR spectroscopy

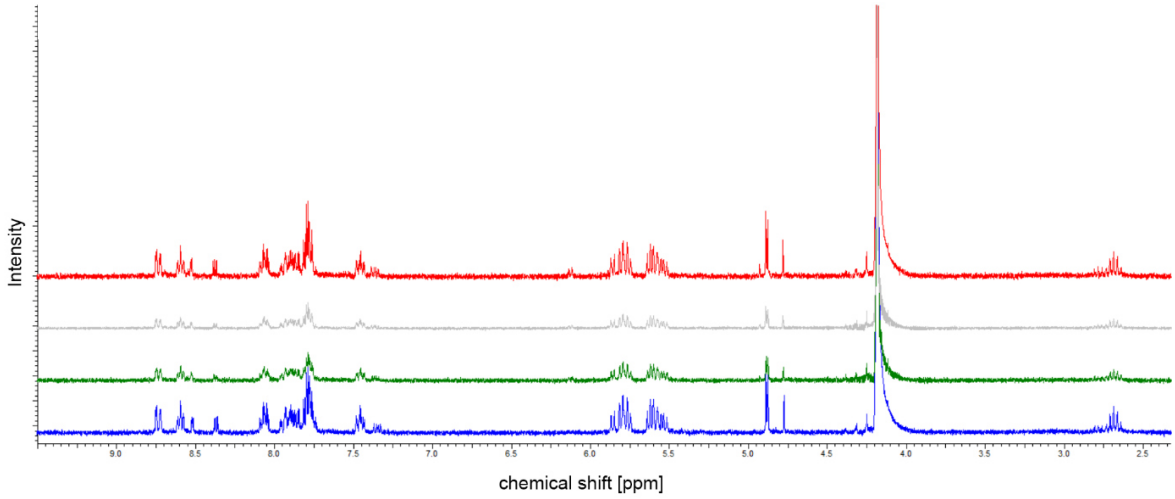

Figure 1. ^{1}H NMR spectra of ruthenium(II) complex **6** after 0 h (blue), 24 h (green), 48 h (grey) and 72 h (red), dissolved in 50% D_2O with 0.9% NaCl.

Cellular and nuclear uptake

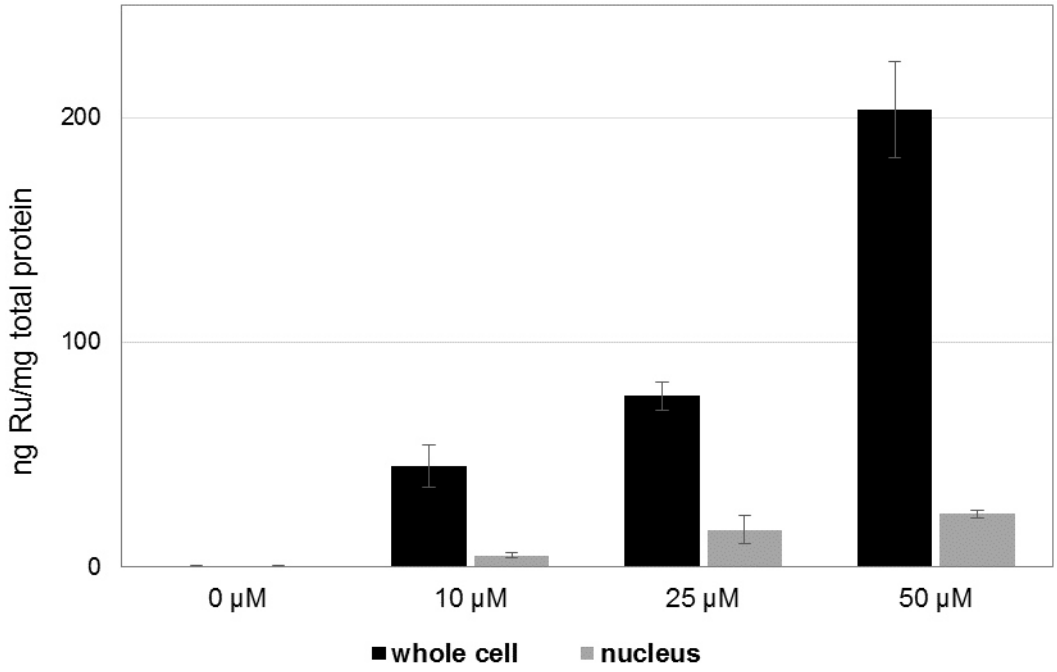

Figure 2. Ruthenium content (ng Ru / mg total protein) in whole cell lysates and nuclear lysates of 518A2 cells treated with 10 µM, 25 µM or 50 µM of complex **6**, determined by ICP-MS (three independent experiments). The Ru content was standardized to total protein content of whole cell or nuclear samples after lysis.

Interaction with pBR322 plasmid DNA (ethidium bromide assay)

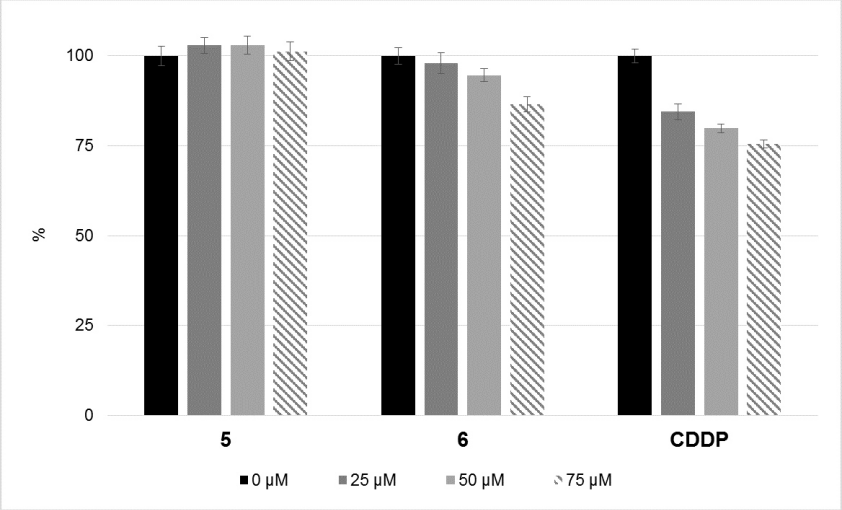

Figure 3. Effects of ligand **5** and its complex **6**, as well as CDDP, on the relative fluorescence intensity (negative control set to 100%) of ethidium bromide in intercalating assays with circular pBR322 plasmid DNA. Values ± SD were calculated as the means of at least three independent experiments.

Interaction with pBR322 plasmid DNA (EMSA)

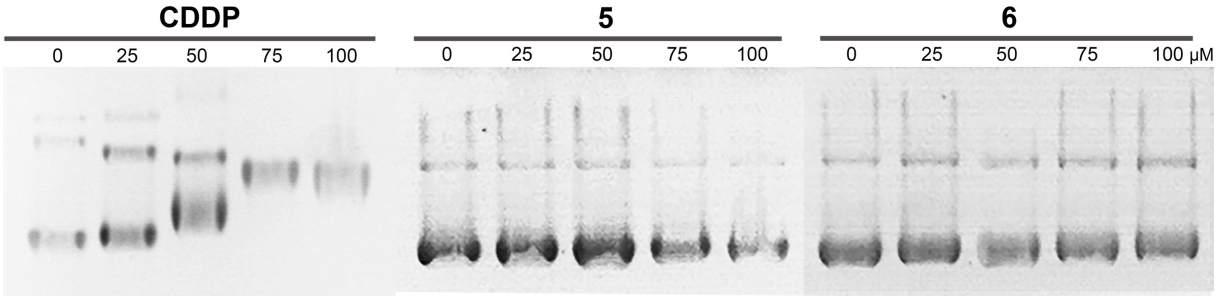

Figure 4. Interaction with circular pBR322 plasmid DNA as observed by EMSA after 24 h incubation with test compounds **5** and **6**, as well as CDDP. Pictures are representative for at least two independent experiments.

Effect on intracellular ROS and superoxide concentrations

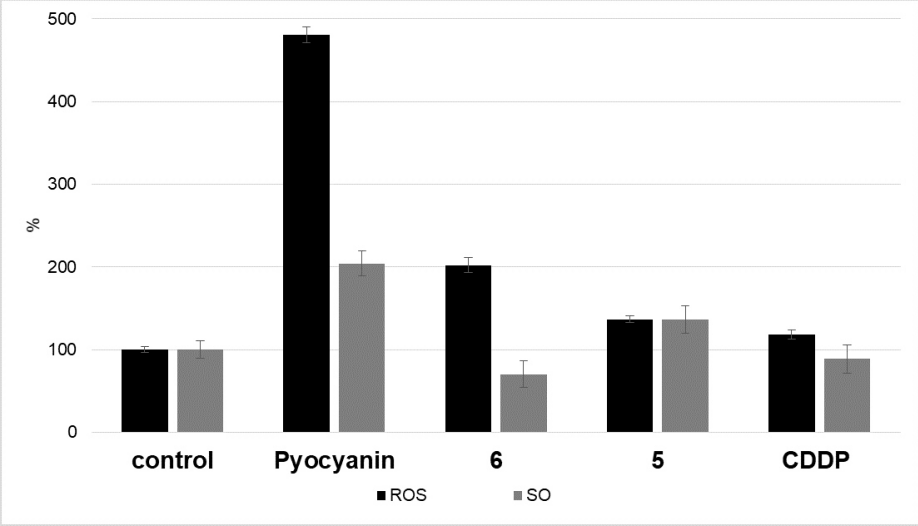

Figure 5. Intracellular ROS and superoxide (SO) levels in 518A2 melanoma cells after 1 h treatment with solvent (control), or 100 µM each of pyocyanin (positive control), complex **6**, ligand **5** or CDDP. Values ± SD were calculated as the means of at least six independent experiments.

Redox properties in a cell-free context

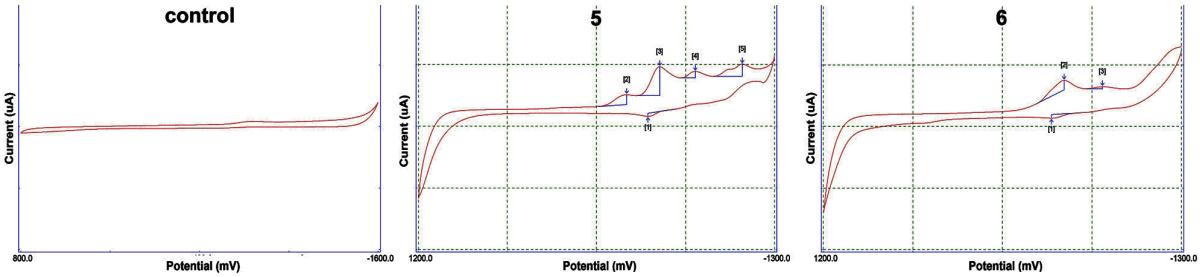

Figure 6. Cyclic voltammetry of test compounds **5** and **6** in a cell-free context.

Induction of apoptosis in 518A2 melanoma cells

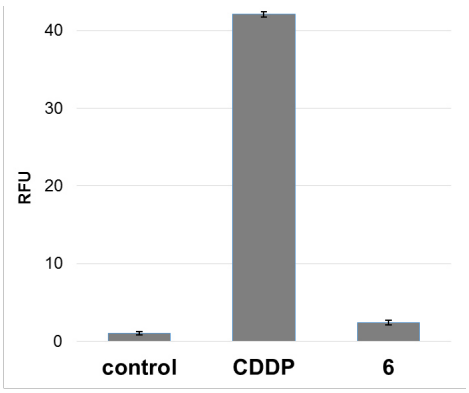

Figure 7. Caspase-3/7 activity in melanoma cells after treatment with **CDDP** or **6**. 518A2 cells were incubated for 24 h at 37 °C, 5% CO_2 and 95% humidity with 5 µM of **CDDP** or **6**, respectively. Control samples were treated with similar amounts of solvent (DMSO). The caspase-3/7 activity was measured using Apo-ONE® Homogenous Caspase-3/7 Assay. All date are expressed as mean ± SD of four independent experiments as ratios to control values.

5.3. Publikation II

Copper(II) complexes with tridentate Schiff base-like ligands: solid state and solution structures and anticancer activity

Katja Dankhoff,[a] Madeleine Gold,[b] Luisa Kober,[b] Florian Schmitt,[b] Lena Pfeiffer,[a] Andreas Dürrmann,[a] Hana Kostrhunova,[c] Matthias Rothemund,[b] Viktor Brabec,[c] Rainer Schobert,*[b] Birgit Weber*[a]

[a] Department of Chemistry, Inorganic Chemistry IV, University of Bayreuth, Universitaetsstrasse 30, 95447 Bayreuth, Germany

[b] Department of Chemistry, Organic Chemistry I, University of Bayreuth, Universitaetsstrasse 30, 95447 Bayreuth, Germany

[c] Czech Academy of Sciences, Institute of Biophysics, Kralovopolska 135, 61265 Czech Republic

* Corresponding author, Email address: weber@uni-bayreuth.de

Dalton Trans. **2019**, 48, 15220-15230.

Dalton Transactions

PAPER

View Article Online
View Journal | View Issue

Cite this: *Dalton Trans.*, 2019, **48**, 15220

Copper(II) complexes with tridentate Schiff base-like ligands: solid state and solution structures and anticancer activity†

Katja Dankhoff,‡[a] Madeleine Gold,‡[b] Luisa Kober,[b] Florian Schmitt,[b] Lena Pfeifer,[a] Andreas Dürrmann,[a] Hana Kostrhunova,[c] Matthias Rothemund,[b] Viktor Brabec,[c] Rainer Schobert *[b] and Birgit Weber *[a]

Received 18th June 2019,
Accepted 17th September 2019

DOI: 10.1039/c9dt02571e

rsc.li/dalton

We report 15 new Cu(II) complexes with tridentate *NNO* β-acylenamino ligands derived from 2-picolylamine and bearing up to three alkyl, alkoxy, alkoxycarbonyl, or (pseudo)halide substituents. The structures of nine complexes were elucidated by single crystal X-ray diffraction analysis. Complexes with an unsubstituted pyridine ring crystallised with a square pyramidal coordination sphere, whereas substitution of the pyridine ring led to a square planar coordination sphere around the metal centre. The solution structures and properties of the complexes were characterised by UV-Vis spectroscopy and cyclic voltammetry. They were also tested for their cytotoxic effect on four human cancer cell lines. Two complexes were identified that were highly active with single-digit IC_{50} values, exceeding those of cisplatin by far. A tentative structure–activity relationship was proposed as well as topoisomerase I inhibition as a possible mode of action, while any significant interference with DNA and the level of reactive oxygen species could be excluded.

Introduction

The incidence and economic burden of cancer rise at an alarming rate. While the field of medicinal inorganic chemistry could in principle offer many avenues for the development of new therapeutic agents against cancer, the research is still dominated by platinum and ruthenium complexes.[1] Cisplatin, carboplatin, and oxaliplatin are customarily used for the treatment of various cancer entities such as testicular or colon cancer. These three complexes share a similar structure and mechanism of action. Despite their high efficacy, their clinical applicability is limited by serious side effects, originating from their high toxicity, and by the frequent occurrence of intrinsic or acquired resistance of tumours to platinum compounds.[2]

However, anti-cancer active complexes of metals other than platinum, including copper, became the focus of research interest in recent years.[3] Copper is essential for the development of organisms as it plays an important role as part of the active site of various metalloproteins such as tyrosinase, catecholase, or hemocyanin.[4] Therefore its complexes have been investigated under the assumption that endogenous metals may be less toxic to normal cells than to cancer cells. Nevertheless, copper is toxic at higher concentrations as it is redox-active and can displace other metal ions.[5] Anti-cancer active copper complexes may act in various ways, *e.g.* by DNA binding, apoptosis induction *via* reactive oxygen species (ROS) generation, and by inhibition of topoisomerase I.[6]

Cu(II) complexes with tridentate NNO-chelating Schiff base ligands were only occasionally evaluated for biological activity, and mostly for antibacterial effects.[7] For a few of them an interaction with DNA was observed.[8] However, to the best of our knowledge, there are no studies on their antiproliferative impact on cancer cells, in contrast to the related, yet well-investigated tridentate NNS-chelated thiosemicarbazone complexes.[9]

Here we present a series of 18 Cu(II) complexes with tridentate Schiff base-like ligands that bear different substituents (R, R′, and R″) to alter the electronic environment of the metal centre. The impact of the substituents on the properties of the corresponding complexes was already successfully demonstrated for the corresponding Fe(II/III) and Zn(II) complexes.[10] Here, single crystal X-ray structures of nine Cu(II) complexes were obtained and are discussed. All compounds were tested

[a]*Department of Chemistry, Inorganic Chemistry IV, University of Bayreuth, Universitätsstr. 30, 95447 Bayreuth, Germany. E-mail: weber@uni-bayreuth.de*
[b]*Department of Chemistry, Organic Chemistry I, University of Bayreuth, Universitätsstr. 30, 95447 Bayreuth, Germany*
[c]*Czech Academy of Sciences, Institute of Biophysics, Kralavopolska 135, CZ-61256 Czech Republic*

†Electronic supplementary information (ESI) available. CCDC 1566628–1566632 and 1915614–1915617. For ESI and crystallographic data in CIF or other electronic format see DOI: 10.1039/c9dt02571e

‡These authors contributed equally to this work.

with regard to their cytotoxic activity against different cancer cell lines. The underlying modes of action were investigated.

Results and discussion

Synthesis

The complexes were synthesised in three steps (Scheme 1). First, the tridentate ligands were synthesised by a condensation reaction between the amine and the respective β-acylenol ether. The synthesis of **HL1–HL6** was carried out as described previously.[10a] The substituted 2-picolylamines were synthesised using the synthetic procedures described by Karlin *et al.*[11] In order to obtain the corresponding Cu(II) complexes, $CuSO_4$, sodium methoxide, which acts as a base for the deprotonation of the ligand, and the respective tridentate ligand were heated to reflux in methanol, resulting in a dark blue or dark green solution. The use of a water-free base is important to avoid the formation of $Cu(OH)_2$/CuO during synthesis. The Cu(II) complexes **1–18** were precipitated with an aqueous solution of the sodium salt of the anion. They were obtained as crystalline, blue to green powders and their purity was confirmed by means of elemental analysis, mass spectrometry, and IR spectroscopy. Complexes **1–3** were described previously.[10a] An overview of all complexes described in this work is given in Table 1.

X-ray structure analysis

Crystals suitable for single crystal X-ray structure analysis were obtained for compounds **4**, **5**, **7**, **8**, **9**, **12**, **15**, **17**, and **18** by liquid–liquid diffusion of the precursor complex solution and an aqueous sodium bromide solution at room temperature. The crystallographic data were obtained at 133 K and are summarised in Table S1.† Selected bond lengths and angles of the coordination sphere are given in Table S2.† All complexes crystallised with one anion and one tridentate ligand per metal centre. The structures of **4**, **7**, and **17** are shown in Fig. 1 as representative examples, the remaining structures can be found in the ESI, Fig. S1.† Complexes **4**, **5**, **8**, and **9** crystallised as μ-bridged dimers, with the bromide ions connecting the two Cu(II) centres and the ligands orientated *trans* to one another. Complex **7** crystallised as a one dimensional coordination polymer with the anions bridging the metal centres to form an infinite chain, as described previously by us for complexes of this type.[10a] The metal centre has a square pyramidal coordination sphere.

Table 1 Overview of the structures of copper complexes **1–18**. Complexes **1–3** were described previously[10a]

Complex	Ligand	R	R′	R″	X^-	Solid state structure
1	**HL1**	-4-H	-Me	-COOEt	NO_3^-	Dimer[10a]
2	**HL1**	-4-H	-Me	-COOEt	Cl^-	Dimer[10a]
3	**HL1**	-4-H	-Me	-COOEt	NCS^-	Polymer[10a]
4	**HL1**	-4-H	-Me	-COOEt	Br^-	Dimer
5	**HL2**	-4-H	-Me	-COMe	Br^-	Dimer
6	**HL3**	-4-H	-OEt	-COOEt	Br^-	Unknown
7	**HL4**	-4-H	-OEt	-CN	Br^-	Polymer
8	**HL5**	-4-H	-Ph	-COOEt	Br^-	Dimer
9	**HL6**	-4-H	-Me	-COOMe	Br^-	Dimer
10	**HL7**	-4-OMe	-OEt	-COOEt	Br^-	Unknown
11	**HL8**	-4-OMe	-OEt	-CN	Br^-	Unknown
12	**HL9**	-4-Cl	-OEt	-COOEt	Br^-	Monomer
13	**HL10**	-4-Cl	-OEt	-CN	Br^-	Unknown
14	**HL11**	-4-Me	-OEt	-COOEt	Br^-	Unknown
15	**HL12**	-4-Me	-OEt	-CN	Br^-	Monomer
16	**HL13**	-6-Me	-OEt	-CN	Br^-	Unknown
17	**HL14**	-5-Me	-OEt	-COOEt	Br^-	Monomer
18	**HL15**	-5-Me	-OEt	-CN	Br^-	Monomer

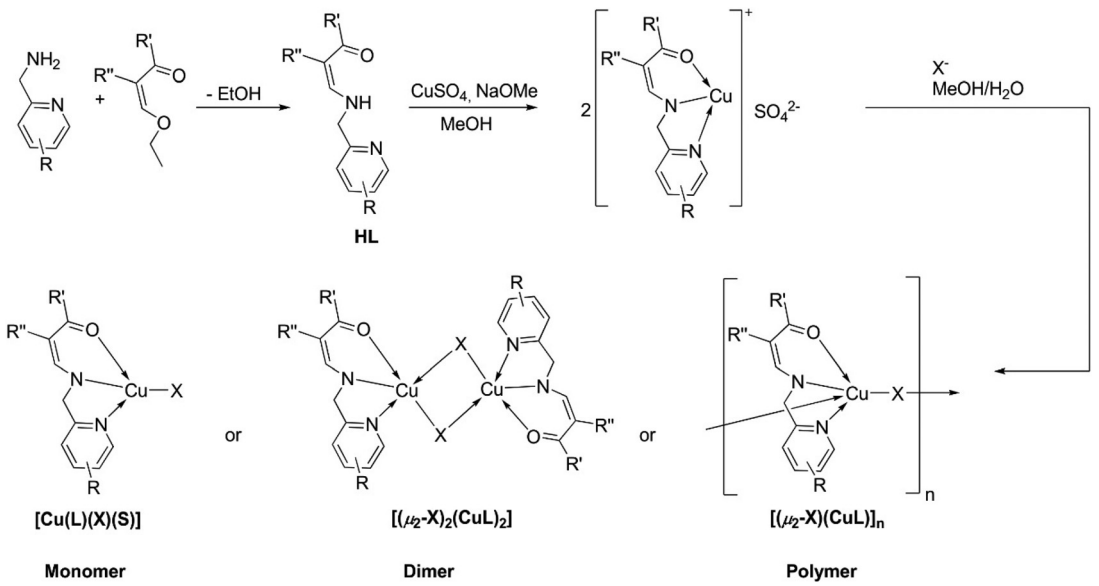

Scheme 1 General synthesis of the tridentate ligands **HL1–15** and their Cu(II) complexes **1–18**. The organic substituents R, R′, and R″ and the anions X^- are specified in Table 1. Complexes **1–3** were obtained as described previously.[10a]

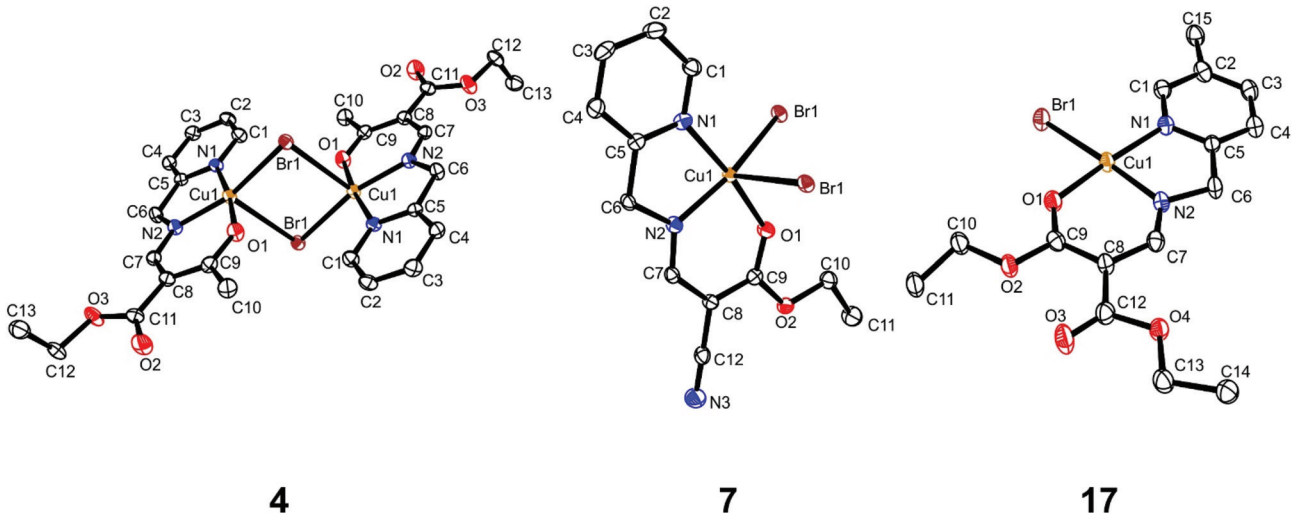

Fig. 1 Structures of **4** (left), **7** (middle), and **17** (right). Thermal ellipsoids were drawn at 50% probability level. Hydrogen atoms were omitted for clarity.

Complexes **12**, **15**, **17**, and **18** show a square planar coordination of the Cu(II) centre, yet do not form dimers or polymers, or coordinate additional solvent molecules, unlike previously described complexes. For all square planar Cu(II) complexes M···π and π···π interactions involving the centroids (5-ring and 6-ring) around the metal centre were observed, leading to a stacking of the planar complexes. Details on all intermolecular interactions can be found in the ESI, Tables S3–S5.† Interactions between keto oxygen and aromatic C–H groups were also observed for all complexes.

Powder X-ray diffraction analyses were done to confirm that the complexes obtained from synthesis and the single crystals had the same structure. The diffraction patterns are given in the ESI, Fig. S2 and S3.† Except for complexes **5** and **12**, the patterns are identical. Small differences visible in the patterns of the other complexes can be explained with the different temperatures and methods used for the measurements.

The magnetism of compounds **4–18** was investigated, the magnetic behaviour of complexes **1–3** was described previously.[10a] Measurements down to 2 K were performed for the dimeric complexes **4** and **9** and for the monomeric compound **15**. The other substances were investigated down to 50 K. The $\chi_M T$ *vs.* T plots are presented in Fig. S4–S6,† the magnetic moments are summarised in Table S6.† The room temperature moment is within the expected range for dimeric or monomeric copper(II) complexes. Only weak ferromagnetic interactions ($J < 10$ cm^{-1}) are observed in case of the dimeric complexes. This is in agreement with previously described complexes of this type.[10a] In the case of the monomeric complex **15** very weak antiferromagnetic interactions are observed that were not analysed any further.

UV-Vis spectroscopy and cyclic voltammetry

UV-Vis spectra of the complexes were recorded in water (**1**) and DMSO (**2–18**); they can be found in the ESI, Fig. S7–S9,† the absorption maxima and the logarithm of the extinction coefficient are summarised in Table 2. Complex **1** is not stable in DMSO solution with its colour quickly changing from light blue to dark red/brown. Absorption maxima (in DMSO) between 624 and 676 nm were observed for all complexes except **16** (764 nm), possibly due to the 6-methyl group on the pyridine ring being rather close to the metal centre. Complexes **11–18** featured a second absorption maximum between 390 and 442 nm. In aqueous solution the absorption maxima are slightly blue-shifted. The complexes **3**, **8**, and **11** were not completely soluble in water. The extinction coefficient ε indicates a d–d transition and no charge transfer responsible for the colour. The spectra were recorded over 72 h to investigate the stability of the compounds in solution (**1** in water, the remaining in DMSO). No change of the position of the absorption maxima was seen, however, for complexes **2**, **3**, **4**, **5**, **8**, **9**, **12**, and **13** a decrease of extinction took place. In order to determine whether or not the anion still coordinates the Cu(II) centre conductivity measurements were carried out (Table 2). This is especially of interest regarding the dimeric or polymeric species. The conductivity of the solution used for the UV-Vis measurements was measured three times to obtain a mean value. The observed values indicate that the anion is no longer coordinated to the metal centre but is most likely replaced by a solvent molecule. This indicates that in solution probably only monomeric species exist, unlike in the solid state.

The electrochemical behaviour of the compounds was investigated using cyclic voltammetry. The voltammograms are presented in the ESI, Fig. S10–S12,† the reduction and oxidation potentials are summarised in Table 2. All complexes show irreversible reduction peaks between −0.4 and −0.8 V corresponding to the reduction of Cu(II) to Cu(I). The exception is again compound **16** with a reduction potential of −0.26 V. The anodic processes are not very well-defined and correspond to oxidation processes of the ligand, taking place above 0.7 V.

Table 2 Absorption maxima λ_{max}, log ε, molar conductivity σ, and electrochemical properties (in acetonitrile, 0.1 M NBu_4PF_6, *vs.* $Ag/AgNO_3$, 50 mV s^{-1}) of the complexes discussed in this work

	λ_{max} [nm] (log ε)		σ [10^3 µS cm^{-1} M^{-1}]			
	Water	DMSO	Water	DMSO	E_{red} [V]	E_{ox} [V]
1	624 (2.07)	Not stable	89	Not stable	−0.71	1.42
2	630 (2.06)	668 (2.18)	85	17	−0.8	1.01
						1.39
3	Not completely soluble	639 (2.17)	Not completely soluble	19	−0.71	−0.55
					0.24	0.67
						0.81
4	626 (2.04)	638 (2.17)	89	30	−0.66	0.76
					0.43	
					0.65	
5	626 (2.06)	640 (2.17)	101	29	−0.62	0.86
						1.38
6	641 (1.90)	661 (2.05)	97	29	−0.6	0.86
					0.43	
7	656 (1.85)	674 (1.99)	97	29	−0.46	0.72
					0.45	1.35
8	Not completely soluble	644 (2.15)	Not completely soluble	27	−0.62	0.82
					0.44	
					0.66	
9	624 (2.06)	640 (2.13)	96	28	−0.64	0.84
					0.43	
10	636 (2.04)	654 (2.08)	95	27	−0.64	0.84
	372 (2.56)				0.43	
11	Not completely soluble	673 (2.01)	Not completely soluble	29	−0.48	0.62
		411 (2.09)			0.44	0.76
						1.38
12	645 (2.01)	664 (2.04)	102	27	−0.54	0.86
	391 (2.18)	409 (2.15)			0.47	
13	655 (1.94)	676 (2.00)	101	27	−0.42	0.78
	401 (2.09)	407 (2.12)				1.44
14	639 (2.03)	650 (1.82)	100	17	−0.59	0.84
	386 (2.34)	395 (2.06)			0.45	
15	659 (2.03)	667 (1.99)	110	19	−0.46	0.75
	398 (2.16)	408 (2.14)				1.37
16	698 (1.95)	746 (1.96)	98	27	−0.26	0.75
	429 (2.11)	442 (2.06)				1.36
17	638 (2.03)	659 (2.06)	96	29	−0.62	0.77
	390 (2.19)	406 (2.17)			0.38	1.17
18	647 (1.98)	674 (2.00)	97	29	−0.5	0.7
	401 (2.11)	412 (2.09)				1.3

Cytotoxicity

All complexes were tested for their structure-dependent antiproliferative activity against cells of human 518A2 melanoma, HT-29, HCT-116^{wt}, and HCT-116$^{p53-/-}$ colon carcinoma, and the cervix carcinoma cell line HeLa using the standard MTT assay (Table 3 and Fig. 2). The complexes **1–4** share the same chelate ligand **HL1**, yet differ in their counter anions. The other complexes own the same counter anion (Br^-) but carry different substituents either on the β-acylenamino fragment (**5–9**) or on the latter and the pyridine ring (**10–18**). The free ligand **HL11** and $CuSO_4$ were investigated as well. The solubility of compounds **3**, **8**, and **11** (not fully soluble in water) in PBS was confirmed by diluting a 2 mM DMSO solution to 100 µM in PBS. No precipitate occurred and the UV-Vis spectra are presented in Fig. S13.†

All compounds showed dose-dependent growth inhibition of all cell lines, exceeding that of $CuSO_4$ in most cases. Complexes **11–13** and **15** proved least active against all cell lines with IC_{50} values greater 40 µM on average. Complexes **1–4**, differing only in their counter anions, were of comparable, moderate activity. Also, the spread in the IC_{50} values for complexes **4–9**, sharing an unsubstituted pyridine ring while differing in substituents R′ and R″, was only marginal. In contrast, complexes **10** (R = 4-OMe) and **14** (R = 4-Me) which both have electron donating substituents R in 4-position of the pyridine ring and are identical in substituents R′ (= OEt), R″ (= COOEt) and counter anion (= Br^-) showed the highest activity of all tested compounds, including the clinical established drug cisplatin, with single-digit micromolar IC_{50} values against all cancer cell lines. Interestingly, the couple of complexes **11** (R = 4-OMe) and **15** (R = 4-Me), identical to **10**/**14** in terms of substituents R and R′ yet carrying a cyanide instead of a COOEt substituent R″ were virtually inactive against all cell lines. So, a tentative SAR assumption is that the cytotoxicity of such copper complexes might be enhanced by sticking electron donors on the pyridine ring and by avoiding strongly electron withdrawing substituents R″ such as cyanide. The free ligand **HL11** of compound **14** was also

Table 3 Growth inhibitory concentrations IC_{50} (μM; 72 h) of complexes **1–18**, ligand **HL11**, $CuSO_4$, and cisplatin for cells of human melanoma 518A2, colon carcinomas HT-29, HCT-116^{wt} and HCT-116$^{p53-/-}$, cervix carcinoma HeLa, as well as non-cancerous human dermal fibroblasts (adult) HDFa. Selectivity index (SI) was calculated as IC_{50}(HDFa)/øIC_{50} (all tested cancer cell lines)

	518A2	HT-29	HCT-116^{wt}	HCT-116$^{p53-/-}$	HeLa	HDFa	SI
$CuSO_4$	34.0 ± 1.3	>50	49.8 ± 3.0	>50	>50		
Cisplatin[13]	7.8 ± 1.1	8.5 ± 0.3	12.0 ± 1.1	27.0 ± 4.1		41.0 ± 4.0	3.0
1	8.2 ± 0.5	17.2 ± 0.1	8.7 ± 0.5	20.1 ± 2.6	38.8 ± 1.2	15.6 ± 1.9	0.8
2	13.8 ± 2.4	18.2 ± 4.8	20.4 ± 1.9	34.1 ± 0.7	17.3 ± 0.5		
3	15.2 ± 1.7	15.8 ± 1.3	7.7 ± 1.3	17.6 ± 1.0	18.0 ± 1.7		
4	15.1 ± 0.2	19.4 ± 1.2	27.8 ± 1.6	18.1 ± 1.4	15.8 ± 2.5		
5	17.1 ± 1.1	23.2 ± 1.1	38.0 ± 4	27.5 ± 1.2	30.0 ± 1.2		
6	17.6 ± 1.6	25.1 ± 0.5	21.0 ± 1.9	18.6 ± 1.5	22.0 ± 2.2		
7	18.4 ± 2.3	17.5 ± 1.7	19.5 ± 0.7	25.6 ± 2.6	18.4 ± 1.1		
8	11.4 ± 0.7	27.7 ± 3.7	9.7 ± 0.8	10.0 ± 0.4	15.1 ± 1.8		
9	23.7 ± 1.3	27.0 ± 1.7	14.5 ± 1.2	19.3 ± 0.7	20.1 ± 0.6		
10	5.9 ± 0.4	2.2 ± 0.3	4.7 ± 0.1	2.2 ± 0.3	4.0 ± 0.3	18.4 ± 0.4	4.8
11	>50	>50	44.0 ± 1.0	34.9 ± 1.2	>50		
12	>50	>50	49.7 ± 2.1	16.9 ± 0.8	47.7 ± 1.6		
13	>50	>50	49.5 ± 3.7	>50	>50		
14	8.3 ± 0.5	4.0 ± 0.2	8.1 ± 0.9	2.3 ± 0.2	9.0 ± 0.8	18.3 ± 1.1	2.9
15	>100	>50	>50	>50	>50		
16	15.9 ± 0.6	40.8 ± 4.9	16.7 ± 0.6	20.1 ± 1.4	43.7 ± 5.5		
17	15.1 ± 1.2	30.7 ± 2.4	11.0 ± 0.7	20.8 ± 1.4	17.8 ± 0.6		
18	17.4 ± 0.8	26.4 ± 2.7	50.5 ± 3.9	29.1 ± 9.8	37.4 ± 5.4		
HL11	>100	>100	>100	>100	>100		
$CuSO_4$ + HL11 (1 : 1)	23.5 ± 1.3	16.8 ± 1.2	9.9 ± 0.1	7.6 ± 0.3	38.8 ± 6.4		

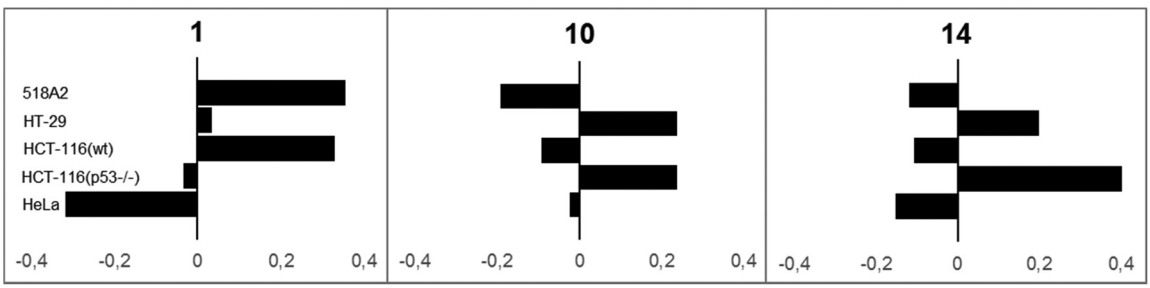

Fig. 2 Cell line specificities of copper complexes **1** (left), **10** (middle) and **14** (right) as deviations of the log(IC_{50}) for individual cells lines from the mean log(IC_{50}) value over all cell lines. Negative values indicate lower and positive values higher than average activities. Mean log(IC_{50}) values are 1.3 for complex **1**, 0.58 for complex **10**, and 0.80 for complex **14**.

tested inactive. Mixtures of ligand **HL11** and $CuSO_4$ (1 : 1) were less cytotoxic against all cancer cell lines in comparison to the corresponding complex **14**. What little activity we found for these mixtures can probably be ascribed to a spontaneous, partial complex formation, as solutions of **HL11** and $CuSO_4$ turned immediately greenish (like solutions of pure complex **14**) after mixing.

The selectivity for tumour cells of the most active complexes **1**, **10**, and **14** can be estimated by comparison of their cytotoxicities against cancer cell lines and non-cancerous cells (HDFa). In this context, complex **10** showed a very high selectivity with a selectivity index (SI = 4.8) higher than that of cisplatin (SI = 3.0). The stability of those compounds in PBS solution (100 μM) was investigated at 37 °C over 72 h using UV-Vis spectroscopy (Fig. S14†). No change can be seen indicating that the complexes are stable under these conditions.

Moreover, the uptake of the most active complexes **1**, **10** and **14** into HCT-116^{wt} colon carcinoma cells was quantified using ICP-MS (Table 4). These three complexes appear to have about the same intrinsic cytotoxic activity against this particular cancer cell line. The differences in their IC_{50} values nicely

Table 4 Copper content in HCT-116^{wt} colon carcinoma cells (ng per 10^6 cells) after treatment with 4 μM of the test compounds **1**, **10** and **14**, as well as $CuSO_4$ and mixtures of the latter with ligand **HL11** for 24 h under standard cell culture conditions. The copper content of untreated cells (0.76 ± 0.31 ng Cu per 10^6 cells) has already been subtracted from the presented values

Compound	Copper content in cell lysates [ng per 10^6 cells]	IC_{50} values for HCT-116^{wt} [μM]
1	5.70 ± 1.08	8.7 ± 0.5
10	11.78 ± 0.77	4.7 ± 0.1
14	7.94 ± 1.65	8.1 ± 0.9
$CuSO_4$	3.96 ± 0.79	49.8 ± 3.0
$CuSO_4$ + **HL11** (1 : 1)	4.46 ± 0.71	9.9 ± 0.1

correlate with their intracellular concentrations. It is remarkable that the structurally different couple **1** and **14** exhibit very similar uptake rates and IC_{50} values, while the structurewise closely related pair **10** and **14** differ by a factor of *circa* 2 in both. The cellular copper content in cells after treatment with $CuSO_4$ alone was significantly lower compared to that of cells treated with complexes **1**, **10** or **14**.

Treatment with mixtures of $CuSO_4$ and ligand **HL11** led to values between those of $CuSO_4$ and the corresponding complex **14**, confirming the assumption of spontaneous, partial formation of complex **14** in solution. It should be noted, though, that this might be different for cell lines other than HCT-116^{wt}. As the cytotoxic effect of copper complexes may originate from DNA binding[5,12] we investigated the interaction of complexes **1**, **10**, and **14** both with linear salmon sperm DNA using an ethidium bromide intercalation assay (*cf.* ESI, Fig. S15†) and with circular pBR322 plasmid DNA in electrophoretic mobility shift assays (EMSA, Fig. S16†). No significant effects were observed in either assay. An alternative mode of action is the generation of reactive oxygen species (ROS).[12,14] Therefore the complexes, $CuSO_4$, and free ligand **HL11** were investigated with respect to their influence on the ROS level in 518A2 melanoma cells using NBT assays after 24 h incubation (Fig. S17†). The cells were treated with the test compounds (1 and 10 μM) or vehicle. All compounds including $CuSO_4$ and **HL11** led to a small rise in cellular ROS levels. There is no stringent correlation between the rise in ROS and the cytotoxicity exhibited by the complexes, indicating the generation of ROS not to be the dominant mode of action.

Another type of clinical important targets for anticancer drugs are the topoisomerase enzymes[6] which catalyse the supercoiling of the DNA. As copper complexes have been shown to be able to inhibit these enzymes,[5] complexes **1**, **10**, **14**, and $CuSO_4$ were tested for inhibition of topoisomerase I (Fig. 3). Compounds **1** and **10** showed a similar inhibition of the enzyme (setting in from 25 μM), whereas **14** inhibited topoisomerase I only at concentrations of at least 50 μM. Addition of $CuSO_4$ to the reaction mixture had no influence on the activity of topoisomerase I. This confirms that the inhibitory effect stems from the intact complexes rather than copper salts from decomposition.

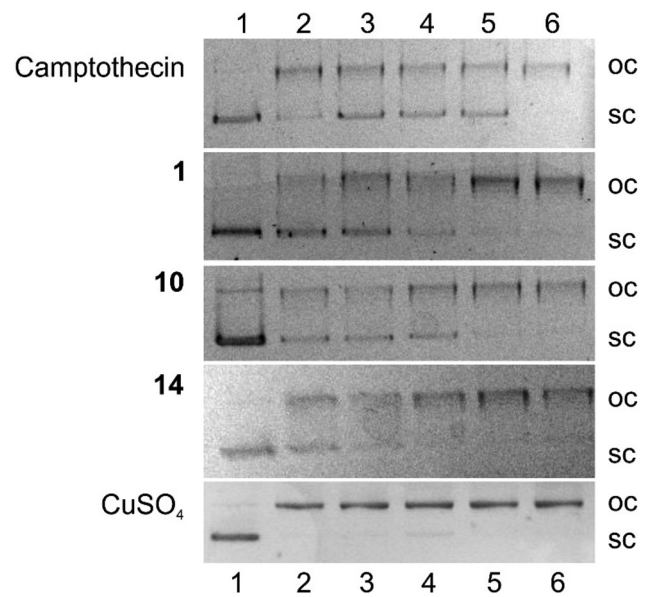

Fig. 3 Inhibition of topoisomerase I by Camptothecin, complexes **1**, **10**, **14**, and $CuSO_4$. Lane 1: 100 μM substance without enzyme; lane 2–6: 100, 50, 25, 10, and 0 μM with enzyme. Top: Open circular form (oc) generated by active topoisomerase I, bottom: supercoiled form (sc).

Experimental

Complexes **1–3**, ligands **HL1–HL6**, 2-aminomethyl-4-methoxypyridine, 2-aminomethyl-4-chloropyridine, 2-amino-methyl-4-methylpyridine, 2-aminomethyl-5-methylpyridine, and 2-aminomethyl-6-methylpyridine were synthesised by previously described procedures.[10,11] Methanol used for the complex synthesis was distilled over magnesium under argon. All other chemicals were commercially available and used as received. ^{1}H NMR spectra were measured at room temperature and 300 MHz with a Varian INOVA 300. Elemental analysis were measured with a Vario EL III from Elementar Analysen-Systeme with acetanilide as standard. The samples were placed in a small tin boat. Mass spectra were recorded with a Finnigan MAT 8500 with a data system MASPEC II. IR spectra were recorded with a PerkinElmer Spectrum 100 FT-IR spectrometer. Conductivity was measured with a FiveGo F3 portable meter from Mettler Toledo.

HL7. 2-Aminomethyl-4-methoxypyridine (0.6 g, 4.3 mmol, 1 eq.) was diluted in ethanol (5 mL) and diethylethoxymethylene-malonate (1.2 g, 5.2 mmol, 1.2 eq.) was added, resulting in an orange solution. This mixture was heated to reflux for 1 h. After cooling to room temperature, the solvent was removed under reduced pressure, yielding a dark orange oil. After one week at −28 °C, the now orange solid was suspended in ice-cold diethyl ether (3 mL), filtered, washed with ice-cold diethyl ether (5 mL), and dried in air. Yield: 0.86 g (308.33 g mol^{-1}, 64%). Elemental analysis ($C_{15}H_{20}N_2O_5{\cdot}0.3H_2O$, %) found C 57.17, H 6.84, N 8.57; calcd C 57.32, H 6.63, N 8.91. ^{1}H NMR (298 K, $CDCl_3$, 300 MHz): δ = 9.6 (1 H, m, –N*H*), 8.42 (1 H, m, 6-Py*H*), 8.11 (1 H, d, ^3J = 14.1 Hz, =C*H*), 6.78 (2 H, m, 2-&4-Py*H*), 4.62 (2 H, d, ^3J = 6.1 Hz, 2-Py–CH_2), 4.23 (4 H, m, –O–CH_2–CH$_3$), 3.87 (3 H, s, –O–CH_3), 1.34 (6 H, m, –O–CH$_2$–CH_3) ppm. MS (EI, pos.) *m*/*z* (%): 308 ($C_{15}H_{20}N_2O_5$, 20), 262 ($C_{13}H_{15}N_2O_4$, 100), 123 (C_7H_8NO, 85). IR: ν = 3275 (m, N–H), 1684 (s, C=O), 1630 (s, C=O) cm^{-1}.

HL8. 2-Aminomethyl-4-methoxypyridine (0.5 g, 3.6 mmol, 1 eq.) was diluted in ethanol (5 mL) and ethyl(ethoxymethylene)-cyanoacetate (0.73 g, 4.3 mmol, 1.2 eq.) was added, resulting in a yellow suspension. This mixture was heated to reflux for 1 h. After cooling to room temperature white needles precipitated. Those were filtered, washed with ethanol, and dried in air. Yield: 0.34 g (261.28 g mol^{-1}, 36%). Elemental analysis ($C_{13}H_{15}N_3O_3$, %) found C 59.60, H 5.50, N 16.00; calcd C 59.76,

H 5.79, N 16.08. ^{1}H NMR (298 K, $CDCl_3$, 300 MHz): δ = 9.43 (1 H, m, –N*H*), 8.43 (1 H, d, ^3J = 5.8 Hz, 6-Py*H*), 7.48 (1 H, d, ^3J = 13.8 Hz, =C*H*), 6.85 (2 H, m, 3-&5-Py*H*), 4.63 (2 H, d, ^3J = 5.9 Hz, 2-Py–CH_2), 4.22 (2 H, q, ^3J = 7.3 Hz, –O–CH_2–CH$_3$), 3.92 (3 H, s, –O–CH_3), 1.29 (3 H, t, ^3J = 7.1 Hz, –O–CH$_2$–CH_3) ppm. MS (EI, pos.) *m*/*z* (%): 261 ($C_{13}H_{15}N_3O_3$, 100), 232 ($C_{11}H_{10}N_3O_3$, 25), 215 ($C_{11}H_{10}N_3O_2$, 65), 188 ($C_{10}H_{10}N_3O$, 45), 149 ($C_8H_{10}N_2O$, 60), 123 (C_7H_8NO, 100). IR: ν = 3202 (m, N–H), 2206 (s, C≡N), 1683 (s, C=O) cm^{-1}.

HL9. 2-Aminomethyl-4-chloropyridine (0.5 g, 3.5 mmol, 1 eq.) was diluted in ethanol (5 mL) and diethylethoxymethylene-malonate (0.91 g, 4.2 mmol, 1.2 eq.) was added, resulting in a yellow solution. The mixture was heated to reflux for 1 h. After cooling to room temperature approximately half of the solvent was removed under reduced pressure. A light yellow solid precipitated, which was filtered, washed with ethanol, and dried in air. Yield: 0.7 g (312.75 g mol^{-1}, 63%). Elemental analysis ($C_{14}H_{17}ClN_2O_4$, %) found C 53.71, H 5.32, N 8.94; calcd C 53.77, H 5.48, N 8.96. ^{1}H NMR (298 K, $CDCl_3$, 300 MHz): δ = 9.62 (1 H, m, –N*H*), 8.52 (1 H, m, 6-Py*H*), 8.09 (1 H, d, ^3J = 13.8 Hz, =C*H*), 7.37 (2 H, m, 2-&4-Py*H*), 4.75 (2 H, d, ^3J = 6.2 Hz, 2-Py–CH_2), 4.22 (4 H, m, –O–CH_2–CH$_3$), 1.33 (6 H, m, –O–CH$_2$–CH_3) ppm. MS (EI, pos.) *m*/*z* (%): 312 ($C_{14}H_{17}ClN_2O_4$, 30), 266 ($C_{12}H_{12}ClN_2O_3$, 100), 153 ($C_7H_7ClN_2$, 100), 127 (C_6H_5ClN, 100). IR: ν = 3281 (m, N–H), 1680 (s, C=O), 1640 (s, C=O) cm^{-1}.

HL10. 2-Aminomethyl-4-chloropyridine (0.5 g, 3.5 mmol, 1 eq.) was diluted in ethanol (5 mL) and ethyl(ethoxymethylene)-cyanoacetate (0.71 g, 4.2 mmol, 1.2 eq.) was added, resulting in a yellow solution. This mixture was heated to reflux for 1 hour. After cooling to room temperature and storing at −28 °C, a solid was isolated by filtration, washed with ice-cold diethyl ether, and recrystallised in methanol (5 mL). The white, crystalline precipitate was filtered, washed with methanol, and dried in air. Yield: 0.42 g (265.70 g mol^{-1}, 46%). Elemental analysis ($C_{12}H_{12}ClN_3O_2$, %) found C 54.05, H 4.49, N 15.83; calcd C 54.25, H 4.55, N 15.82. ^{1}H NMR (298 K, $CDCl_3$, 300 MHz): δ = 9.43 (1 H, m, –N*H*), 8.52 (1 H, d, ^3J = 5.3 Hz, 6-Py*H*), 7.46 (1 H, d, ^3J = 13.8 Hz, =C*H*), 7.30 (1 H, dd, ^3J = 5.3 Hz, ^4J = 2.0 Hz, 5-Py*H*), 7.27 (1 H, d, ^3J = 1.7 Hz, 3-Py*H*), 4.61 (2 H, d, ^3J = 6.1 Hz, 2-Py–CH_2), 4.23 (2 H, q, ^3J = 7.1 Hz, –O–CH_2–CH$_3$), 1.32 (3 H, t, ^3J = 7.1 Hz, –O–CH$_2$–CH_3) ppm. MS (EI, pos.) *m*/*z* (%): 265 ($C_{12}H_{12}ClN_3O_2$, 75), 219 ($C_{10}H_7ClN_3O$, 80), 153 ($C_7H_7ClN_2$, 100), 127 (C_6H_5ClN, 100). IR: ν = 3288 (m, N–H), 2208 (s, C≡N), 1679 (s, C=O) cm^{-1}.

HL11. 2-Aminomethyl-4-methylpyridine (0.75 g, 6.1 mmol, 1 eq.) was diluted in ethanol (5 mL) and diethylethoxymethylene-malonate (1.59 g, 7.4 mmol, 1.2 eq.) was added, resulting in a yellow solution. This mixture was heated to reflux for 1 hour. After cooling to room temperature the solvent was removed under reduced pressure resulting in an orange oil. This was stored at −28 °C for 1 day. The now orange solid was suspended in ice-cold diethyl ether (5 mL), filtered, washed with ice cold diethyl ether (5 mL), and dried in air. Yield: 0.71 g (292.14 g mol^{-1}, 39%). Elemental analysis ($C_{15}H_{20}N_2O_4{\cdot}H_2O$, %) found C 57.84, H 7.19, N 8.73; calcd C 58.05, H 7.15, N 9.03. ^{1}H NMR (298 K, $CDCl_3$, 300 MHz): δ = 9.55 (1 H, m, –N*H*), 8.45 (1 H, d, ^3J = 5.1 Hz, 6-Py*H*), 8.09 (1 H, d, ^3J = 13.8 Hz, =C*H*), 7.21 (2 H, m, 2-&4-Py*H*), 4.77 (2 H, d, ^3J = 6.0 Hz, 2-Py–CH_2), 4.21 (4 H, m, –O–CH_2–CH$_3$), 2.44 (3 H, s, 4-Py–CH_3), 1.30 (6 H, m, –O–CH$_2$–CH_3) ppm. MS (EI, pos.) *m*/*z* (%): 292 ($C_{15}H_{20}N_2O_4$, 45), 246 ($C_{13}H_{14}N_2O_3$, 100), 219 ($C_{12}H_{15}N_2O_2$, 55), 133 ($C_8H_9N_2$, 100), 107 (C_7H_9N, 100). IR: ν = 3262 (m, N–H), 1675 (s, C=O), 1636 (s, C=O) cm^{-1}.

HL12. 2-Aminomethyl-4-methylpyridine (0.5 g, 4.1 mmol, 1 eq.) was diluted in ethanol (5 mL) and ethyl(ethoxymethylene)-cyanoacetate (0.68 g, 4.9 mmol, 1.2 eq.) was added, resulting in a yellow solution. The mixture was heated to reflux for 1 hour. After cooling to room temperature the solvent was removed under reduced pressure and the dark yellow oil was stored at −28 °C for 3 days. The now yellow solid was suspended in ice-cold diethyl ether (5 mL), filtered, and washed with ice cold diethyl ether (5 mL). The crude product was recrystallised from methanol to yield a white, crystalline solid. Yield: 0.51 g (245.12 g mol^{-1}, 50%). Elemental analysis ($C_{13}H_{15}N_3O_2{\cdot}0.25$ H_2O, %) found C 62.84, H 6.17, N 16.84; calcd C 62.51, H 6.25, N 16.82. ^{1}H NMR (298 K, $CDCl_3$, 300 MHz): δ = 9.43 (1 H, m, –N*H*), 8.48 (1 H, d, ^3J = 5.1 Hz, 6-Py*H*), 7.48 (1 H, d, ^3J = 13.8 Hz, =C*H*), 7.17 (2 H, m, 3-&5-Py*H*), 4.67 (2 H, d, ^3J = 5.7 Hz, 2-Py–CH_2), 4.25 (2 H, m, –O–CH_2–CH$_3$), 2.43 (3 H, s, 4-Py–CH_3), 1.32 (3 H, t, ^3J = 7.1 Hz, –O–CH$_2$–CH_3) ppm. MS (EI, pos.) *m*/*z* (%): 245 ($C_{13}H_{15}N_3O_2$, 80), 199 ($C_{11}H_{10}N_3O$, 50), 172 ($C_{10}H_{10}N_3$, 55), 133 ($C_7H_9N_2$, 100), 107 (C_7H_7N, 100). IR: ν = 3280 (m, N–H), 2204 (s, C≡N), 1673 (s, C=O) cm^{-1}.

HL13. 2-Aminomethyl-6-methylpyridine (1 g, 8.2 mmol, 1 eq.) was diluted in ethanol (5 mL) and ethyl(ethoxymethylene)-cyanoacetate (1.66 g, 9.8 mmol, 1.2 eq.) was added, resulting in a yellow solution. The mixture was heated to reflux for 1 hour. After cooling to room temperature the solvent was removed under reduced pressure, yielding a dark yellow oil. After 3 days at −28 °C the now dark yellow solid was suspended in ice-cold diethyl ether (5 mL), filtered, and washed with ice-cold diethyl ether (10 mL). Recrystallisation from methanol gave a white solid. Yield: 0.27 g (245.12 g mol^{-1}, 14%). Elemental analysis ($C_{13}H_{15}N_3O_2{\cdot}0.5$ H_2O, %) found C 62.25, H 6.86, N 16.34; calcd C 61.40, H 6.34, N 16.52. ^{1}H NMR (298 K, $CDCl_3$, 300 MHz): δ = 9.42 (1 H, m, –N*H*), 8.43 (1 H, d, ^3J = 5.8 Hz, 6-Py*H*), 7.48 (1 H, d, ^3J = 13.8 Hz, =C*H*), 6.85 (2 H, m, 3-&5-Py*H*), 4.63 (2 H, d, ^3J = 5.9 Hz, 2-Py–CH_2), 4.22 (2 H, q, ^3J = 7.3 Hz, –O–CH_2–CH$_3$), 3.92 (3 H, s, –O–CH_3), 1.29 (3 H, t, ^3J = 7.1 Hz, –O–CH$_2$–CH_3) ppm. MS (EI, pos.) *m*/*z* (%): 245 ($C_{13}H_{15}N_3O_2$, 100), 199 ($C_{11}H_{10}N_3O$, 65), 172 ($C_{10}H_{10}N_3$, 55), 133 ($C_7H_9N_2$, 100), 107 (C_7H_7N, 100). IR: ν = 3269 (m, N–H), 2204 (s, C≡N), 1694 (s, C=O) cm^{-1}.

HL14. 2-Aminomethyl-5-methylpyridine (1 g, 8.2 mmol, 1 eq.) was diluted in ethanol (5 mL) and diethylethoxymethylene-malonate (2.13 g, 9.8 mmol, 1.2 eq.) was added, resulting in a yellow solution. This mixture was heated to reflux for 1 hour. After cooling to room temperature the solvent was removed under reduced pressure yielding a yellow oil. This oil was stored at −28 °C for 1 week. The now yellow solid was suspended in ice-cold diethyl ether (5 mL), filtered, washed with

ice-cold diethyl ether (10 mL), and dried in air. Yield: 1.36 g (292.14 g mol^{-1}, 57%). Elemental analysis ($C_{15}H_{20}N_2O_4{\cdot}0.5EtOH{\cdot}0.5H_2O$, %) found C 59.47, H 7.34, N 8.23; calcd C 59.24, H 7.46, N 8.64. ^{1}H NMR (298 K, $CDCl_3$, 300 MHz): δ = 9.6 (1 H, m, –N*H*), 8.43 (1 H, m, 6-Py*H*), 8.11 (1 H, d, ^3J = 14.0 Hz, =C*H*), 7.60 (1 H, m, 4-Py*H*), 7.22 (1 H, d, ^3J = 7.9 Hz, 3-Py*H*), 4.68 (2 H, d, ^3J = 6.1 Hz, 2-Py–CH_2), 4.21 (4 H, m, –O–CH_2–CH$_3$), 2.36 (3 H, s, 5-Py–CH$_3$), 1.29 (6 H, m, –O–CH$_2$–CH_3) ppm. MS (EI, pos.) *m*/*z* (%): 292 ($C_{15}H_{20}N_2O_4$, 45), 246 ($C_{13}H_{15}N_2O_3$, 100), 133 ($C_8H_{10}N_2$, 100), 107 (C_7H_8N, 100). IR: ν = 3307 (m, N–H), 1682 (s, C=O), 1617 (s, C=O) cm^{-1}.

HL15. 2-Aminomethyl-5-methylpyridine (1 g, 8.2 mmol, 1 eq.) was diluted in ethanol (5 mL) and ethyl(ethoxymethylene)-cyanoacetate (1.66 g, 9.8 mmol, 1.2 eq.) was added, resulting in a yellow solution. This mixture was heated to reflux for 1 hour. After cooling to room temperature the solvent was removed under reduced pressure, yielding an orange oil. This was stored at −28 °C for 1 day, suspended in ice-cold diethyl ether (5 mL), filtered, and washed with ice-cold diethyl ether (10 mL). Recrystallisation from THF gave a white, crystalline solid. Yield: 0.38 g (245.12 g mol^{-1}, 19%). Elemental analysis ($C_{13}H_{15}N_3O_2$, %) found C 63.52, H 6.33, N 17.13; calcd C 63.66, H 6.16, N 17.13. ^{1}H NMR (298 K, $CDCl_3$, 300 MHz): δ = 8.41 (1 H, d, ^4J = 0.7 Hz, 6-Py*H*), 8.03 (1 H, d, ^3J = 15.2 Hz, =C*H*), 7.43 (1 H, dd, ^3J = 7.82 Hz, ^4J = 0.86 Hz, 4-Py*H*), 7.15 (1 H, d, ^3J = 8.0 Hz, 3-Py*H*), 7.01 (1 H, m, –N*H*), 4.61 (2 H, d, ^3J = 5.6 Hz, 2-Py–CH_2), 4.21 (2 H, q, ^3J = 7.3 Hz, –O–CH_2–CH$_3$), 2.35 (3 H, s, 5-Py–CH_3), 1.29 (3 H, t, ^3J = 7.1 Hz, –O–CH$_2$–CH_3) ppm. MS (EI, pos.) *m*/*z* (%): 245 ($C_{13}H_{15}N_3O_2$, 100), 199 ($C_{11}H_{10}N_3O$, 70), 133 ($C_8H_{10}N_2$, 100), 107 (C_7H_8N, 100). IR: ν = 3269 (m, N–H), 2204 (s, C≡N), 1694 (s, C=O) cm^{-1}.

General procedure for the synthesis of the Cu(II) complexes

0.2 g of the corresponding ligand, $CuSO_4$ (1.2 eq.), and sodium methoxide (1.2 eq.) were dissolved in methanol (20 mL) under argon atmosphere and heated to reflux for 1 h, resulting in a dark blue or green solution. After cooling to RT the excess of $CuSO_4$ and sodium methoxide was removed by filtration. All further steps were carried out in air. The Cu(II) complexes were precipitated with an aqueous solution of the corresponding sodium or potassium salt of the anion (4 eq. in 20 mL). If no precipitate occurred, the solvent was removed under reduced pressure until a solid could be isolated. This solid was washed with water and methanol and dried in air.

[(μ-Br)$_2$(CuL1)$_2$] (4). Yield: 0.20 g green, crystalline powder (781.45 g mol^{-1}, 32%). Elemental analysis ($C_{26}H_{30}Br_2Cu_2N_4O_6$, %) found C 40.07, H 3.72, N 7.20; calcd C 39.96, H 3.87, N 7.17. MS (EI, pos.) *m*/*z* (%): 391 ($C_{15}H_{18}BrCuN_2O_3$, 14), 309 ($C_{13}H_{15}CuN_2O_3$, 52), 248 ($C_{13}H_{15}N_2O_3$, 14), 93 (C_6H_6N, 100). IR: ν = 1685 (s, C=O), 1604 (s, C=O) cm^{-1}.

[(μ-Br)$_2$(CuL2)$_2$] (5). Yield: 0.12 g green needles (721.40 g mol^{-1}, 18%). Elemental analysis ($C_{24}H_{26}Br_2Cu_2N_4O_4$, %) found C 39.96, H 3.88, N 7.74; calcd C 39.96, H 3.63, N 7.77. MS (EI, pos.) *m*/*z* (%): 361 ($C_{12}H_{13}BrCuN_2O_2$, 1), 279 ($C_{12}H_{13}CuN_2O_2$, 9), 218 ($C_{12}H_{13}N_2O_2$, 42), 93 (C_6H_6N, 100). IR: ν = 1649 (s, C=O), 1613 (s, C=O) cm^{-1}.

[CuL3Br] (6). Yield: 0.16 g green powder (420.75 g mol^{-1}, 13%). Elemental analysis ($C_{14}H_{17}BrCuN_2O_4$, %) found C 39.99, H 4.28, N 6.91; calcd C 39.97, H 4.07, N 6.66. MS (EI, pos.) *m*/*z* (%): 421 ($C_{14}H_{17}BrCuN_2O_4$, 25), 340 ($C_{14}H_{17}CuN_2O_4$, 29), 93 (C_6H_6N, 100). IR: ν = 1685 (s, C=O), 1623 (s, C=O) cm^{-1}.

[(μ-Br)(CuL4)]$_n$ (7). Yield: 0.14 g green powder (373.70 g mol^{-1}, 43%). Elemental analysis ($C_{12}H_{12}CuN_3O_2$, %) found C 38.70, H 3.48, N 11.26; calcd C 38.57, H 3.24, N 11.24. MS (EI, pos.) *m*/*z* (%): 374 ($C_{12}H_{12}CuBrN_3O_2$, 2), 293 ($C_{12}H_{12}CuN_3O_2$, 4), 231 ($C_{12}H_{12}N_3O_2$, 23), 93 (C_6H_6N, 100). IR: ν = 2201 (s, C≡N), 1627 (s, C=O) cm^{-1}.

[(μ-Br)$_2$(CuL5)$_2$] (8). Yield: 0.20 g dark green needles (905.59 g mol^{-1}, 35%). Elemental analysis ($C_{36}H_{34}Br_2Cu_2N_4O_6$, %) found C 48.09, H 3.98, N 6.23; calcd C 47.75, H 3.78, N 6.19. MS (EI, pos.) *m*/*z* (%): 310 ($C_{18}H_{17}N_2O_3$, 16), 93 (C_6H_6N, 100). IR: ν = 1671 (s, C=O), 1602 (s, C=O) cm^{-1}.

[(μ-Br)$_2$(CuL6)$_2$] (9). Yield: 0.20 g dark blue, crystalline powder (753.39 g mol^{-1}, 31%). Elemental analysis ($C_{24}H_{26}Br_2Cu_2N_4O_6$, %) found C 38.19, H 3.18, N 7.22; calcd C 38.26, H 3.48, N 7.44. MS (EI, pos.) *m*/*z* (%): 376 ($C_{12}H_{13}BrCuN_2O_3$, 6), 295 ($C_{12}H_{13}CuN_2O_3$, 24), 234 ($C_{12}H_{13}N_2O_3$, 22), 93 (C_6H_6N, 100). IR: ν = 1687 (s, C=O), 1613 (s, C=O) cm^{-1}.

[CuL7Br] (10). Yield: 0.09 g dark green powder (450.78 g mol^{-1}, 31%). Elemental analysis ($C_{15}H_{19}BrCuN_2O_5$, %) found C 39.43, H 4.27, N 6.38; calcd C 39.97, H 4.25, N 6.21. MS (EI, pos.) *m*/*z* (%): 451 ($C_{15}H_{19}BrCuN_2O_5$, 5), 370 ($C_{15}H_{19}CuN_2O_5$, 5), 308 ($C_{15}H_{19}N_2O_5$, 52), 262 ($C_{13}H_{14}N_2O_4$, 100), 123 (C_7H_8NO, 100). IR: ν = 1662 (s, C=O), 1618 (s, C=O) cm^{-1}.

[CuL8Br] (11). Yield: 0.25 dark green, crystalline powder (403.72 g mol^{-1}, 81%). Elemental analysis ($C_{13}H_{14}BrCuN_3O_3$, %) found C 39.27, H 3.98, N 10.63; calcd C 38.68, H 3.50, N 10.41. MS (EI, pos.) *m*/*z* (%): 404 ($C_{13}H_{14}BrCuN_3O_3$, 5), 323 ($C_{13}H_{14}CuN_3O_3$, 15), 261 ($C_{13}H_{14}N_3O_3$, 100), 123 (C_7H_8NO, 100). IR: ν = 2207 (s, C≡N), 1616 (s, C=O) cm^{-1}.

[CuL9Br] (12). Yield: 0.12 g dark green, crystalline powder (455.19 g mol^{-1}, 41%). Elemental analysis ($C_{14}H_{16}BrClCuN_2O_4$, %) found C 37.03, H 3.52, N 6.13; calcd C 36.94, H 3.54, N 6.15. MS (EI, pos.) *m*/*z* (%): 455 ($C_{14}H_{16}BrClCuN_2O_4$, 15), 375 ($C_{14}H_{16}ClCuN_2O_4$, 15), 266 ($C_{12}H_{12}ClN_2O_3$, 100), 127 (C_6H_5ClN, 100). IR: ν = 1664 (s, C=O), 1596 (s, C=O) cm^{-1}.

[CuL10Br] (13). Yield: 0.18 g dark green, crystalline powder (408.14 g mol^{-1}, 59%). Elemental analysis ($C_{12}H_{11}BrClCuN_3O_2$, %) found C 35.18, H 2.55, N 10.27, calcd C 35.31, H 2.72, N 10.30. MS (EI, pos.) *m*/*z* (%): 408 ($C_{12}H_{11}BrClCuN_3O_2$, 10), 327 ($C_{11}H_{12}ClCuN_3O_2$, 20), 265 ($C_{11}H_{12}ClN_3O_2$, 60), 219 ($C_{10}H_6ClN_3O$, 80), 127 (C_6H_5ClN, 100). IR: ν = 2209 (s, C≡N), 1616 (s, C=O) cm^{-1}.

[CuL11Br] (14). Yield: 0.13 g dark green, crystalline powder (434.78 g mol^{-1}, 35%). Elemental analysis ($C_{15}H_{19}BrCuN_2O_4{\cdot}MeOH$, %) found C 40.26, H 4.40, N 6.27; calcd C 39.79, H 4.67, N 6.19. MS (EI, pos.) *m*/*z* (%): 435 ($C_{15}H_{19}BrCuN_2O_4$, 15), 354 ($C_{15}H_{19}CuN_2O_4$, 20), 246 ($C_{13}H_{14}N_2O_3$, 100), 133 ($C_8H_9N_2$, 100), 107 (C_7H_9N, 100). IR: ν = 1673 (s, C=O), 1599 (s, C=O) cm^{-1}.

[CuL12Br] (15). Yield: 0.20 g dark green, crystalline powder (387.72 g mol^{-1}, 65%). Elemental analysis ($C_{13}H_{14}BrCuN_3O_2$,

%) found C 40.37, H 3.63, N 10.68; calcd C 40.27, H 3.64, N 10.84. MS (EI, pos.) *m*/*z* (%): 388 ($C_{13}H_{14}BrCuN_3O_2$, 10), 307 ($C_{13}H_{14}CuN_3O_2$, 20), 245 ($C_{13}H_{14}N_3O_2$, 80), 107 (C_7H_9N, 100). IR: ν = 2208 (s, C≡N), 1620 (s, C═O) cm^{-1}.

[CuL13Br] (16). Yield: 0.09 g dark green, crystalline powder (387.72 g mol^{-1}, 29%). Elemental analysis ($C_{13}H_{14}BrCuN_3O_2{\cdot}H_2O$, %) found C 38.38, H 4.01, N 10.31; calcd C 38.48, H 3.97, N 10.36. MS (EI, pos.) *m*/*z* (%): 245 ($C_{13}H_{14}N_3O_2$, 100), 199 ($C_{11}H_9N_3O$, 85), 133 ($C_8H_9N_2$, 100), 107 (C_7H_8N, 100). IR: ν = 2216 (s, C≡N), 1635 (s, C═O) cm^{-1}.

[CuL14Br] (17). Yield: 0.15 g dark green, crystalline powder (434.78 g mol^{-1}, 50%). Elemental analysis ($C_{15}H_{19}BrCuN_2O_4$, %) found C 41.51, H 4.45, N 6.37; calcd C 41.44, H 4.41, N 6.44. MS (EI, pos.) *m*/*z* (%): 435 ($C_{15}H_{19}BrCuN_2O_4$, 20), 353 ($C_{15}H_{19}CuN_2O_4$, 20), 292 ($C_{15}H_{19}N_2O_4$, 20), 246 ($C_{13}H_{14}N_2O_3$, 100), 133 ($C_8H_9N_2$, 100), 107 (C_7H_8N, 100). IR: ν = 1684 (s, C═O), 1606 (s, C═O) cm^{-1}.

[CuL15Br] (18). Yield: 0.17 g dark green, crystalline powder (387.72 g mol^{-1}, 54%). Elemental analysis ($C_{13}H_{14}BrCuN_3O_2$, %) found C 40.18, H 3.50, N 10.72; calcd C 40.27, H 3.64, N 10.84. MS (EI, pos.) *m*/*z* (%): 388 ($C_{13}H_{14}BrCuN_3O_2$, 5), 307 ($C_{13}H_{14}CuN_3O_2$, 10), 245 ($C_{13}H_{14}N_3O_2$, 70), 133 ($C_8H_9N_2$, 100), 107 (C_7H_8N, 100). IR: ν = 2204 (s, C≡N), 1622 (s, C═O) cm^{-1}.

X-ray diffraction on single crystals

The X-ray analysis of all crystals was performed with a Stoe StadiVari diffractometer using graphite-monochromated MoKα radiation. The data were corrected for Lorentz and polarization effects. The structures were solved by direct methods (SIR-2014)[15] and refined by fullmatrix least-square techniques against $F_o^2 - F_c^2$ (SHELXL-97).[16] All hydrogen atoms were calculated in idealised positions with fixed displacement parameters. ORTEP-III[17] was used for the structure representation. CCDC 1566628–1566632 and 1915614–1915617† contain the supplementary crystallographic data for this paper.

Powder X-ray diffraction

Powder diffractograms were measured with a STOE StadiP Powder Diffractometer (STOE, Darmstadt) using Cu[Kα1] radiation with a Ge Monochromator, and a Mythen 1K Stripdetector in transmission geometry.

Magnetic measurements

Magnetic measurements on the compounds were carried out using a SQUID MPMS-XL5 from Quantum Design with an applied field of 5000 G, and in the temperature range from 300 to 50 K (or 2 K). The sample was prepared in a gelatine capsule held in a plastic straw. The raw data were corrected for the diamagnetic part of the sample holder and the diamagnetism of the organic ligand using tabulated Pascal's constants.[18]

Optical properties

Absorbance spectra were obtained using an Agilent UV-Vis spectrophotometer 8453 (Agilent Technologies, USA) operating in a spectral range of 190–1100 nm. The spectra were measured at 298 K in quartz cells with 1 cm lightpath (Hellma, Germany).

Cyclic voltammetry

Redox potentials were obtained using a CH Instruments Electrochemical Analyser (610E) in 0.1 M NBu_4PF_6/MeCN with a platinum electrode, referenced to 0.01 M $AgNO_3$ at room temperature with a scan rate of 50 mV s^{-1}.

Cell culture

The human melanoma cell line 518A2, and the human colon carcinoma cell lines HT-29, HCT-116^{wt}, and HCT-116$^{p53-/-}$, and the cervix carcinoma cell line HeLa were cultivated in Dulbecco's Modified Eagle Medium supplemented with 10% FBS, and 1% antibiotic–antimycotic at 37 °C, 5% CO_2 and 95% humidity. Only mycoplasma-free cultures were used.

MTT assay

The cytotoxicity of the compounds was studied *via* the MTT-based proliferation assay[19] on cells of 518A2 melanoma (obtained from the department of Radiotherapy and Radiobiology, University Hospital Vienna, Austria), HT-29 (DSMZ ACC-299) and HCT-116^{wt} (DSMZ ACC-581) colon carcinomas, HeLa (DSMZ ACC-57) cervix carcinoma, and human dermal fibroblasts (adult) HDFa (ATCC® PCS-201-012™). Briefly, cells (100 µL per well; 5×10^4 cells per mL) were grown in 96-well plates for 24 h and then treated with varying concentrations of the test compound or solvent control (DMSO) for 72 h. After centrifugation of the plates (300*g*, 5 min, 4 °C), the supernatant was discarded and 50 µL per well of a 0.05% MTT solution in PBS was added to the wells and incubated for 2 h. After another centrifugation step the supernatant was discarded and the formazan precipitate was dissolved in 25 µL DMSO containing 10% SDS and 0.6% acetic acid for at least 1 h at 37 °C and the absorbance of formazan (570 nm) and background (630 nm) was measured with a microplate reader (Tecan). The IC_{50} values were calculated as the mean ± standard deviation of four independent experiments.

Cellular uptake

For measurement of the cellular uptake of the copper complexes into colon carcinoma cells ICP-MS analysis of cell lysates was carried out. Therefore, HCT-116^{wt} cells were seeded at a density of 2×10^6 cells per dish and grown over night. The cells were subsequently treated with 4 µM of the test compounds under cell culture conditions. After 24 h the cells were washed with 1× PBS, harvested, counted and pelleted. The cells were lysed using the microwave acid (HCl) digestion system (CEM Mars®). Copper content was determined using ICP-MS (Agilent 7000, Japan). The copper content of untreated cells (0.76 ± 0.31 ng Cu per 10^6 cells) has already been subtracted from the presented values.

Ethidium bromide saturation assay

Salmon sperm DNA (SS-DNA, Sigma-Aldrich) was pipetted into a black 96-well plate in TE buffer (10 mM Tris-HCl, 1 mM

EDTA, pH 8.5) to reach a final amount of 1 μg per 100 μL and incubated with varying concentrations of complexes **1**, **10**, **14** and $CuSO_4$ for 2 h at 37 °C. Afterwards, 100 μL of a 10 μg mL^{-1} ethidium bromide solution in TE buffer was added to each well. After 5 min of incubation, the fluorescence (λ_{ex} = 535 nm, λ_{em} = 595 nm) was detected using a microplate reader (Tecan F200). Each fluorescence value was corrected by possible intrinsic compound and ethidium bromide background fluorescence. As all experiments were carried out in triplicate, the relative ethidium bromide fluorescence was calculated as mean ± SD with solvent controls set to 100%.

Electrophoretic mobility shift assay

Circular plasmid DNA pBR322 (1.5 μg, Thermo Scientific) in TE buffer (10 mM Tris-HCl, 1 mM EDTA, pH 8.5) was incubated with dilution series of cisplatin (CDDP) or complexes **1**, **10**, and **14** (0, 5, 10, 25, 50 μM) at 37 °C for 24 h (20 μL total sample volume). Then, samples were subjected to gel electrophoresis using 1% agarose gels in 0.5× TBE buffer (89 mM Tris, 89 mM boric acid, 25 mM EDTA, pH 8.3). After staining the gels with ethidium bromide (10 μg mL^{-1}), DNA bands were documented using UV excitation. Experiments were carried out at least in duplicate.

NBT assay

The effect of the test compounds on the relative levels of reactive oxygen species (ROS) was studied by using the NBT assay.[20] 518A2 melanoma cells (100 μL per well, 1 × 10^5 cells per mL) were seeded in 96 well plates and allowed to adhere for 24 h. Then, the cells were treated with the test compounds (1 and 10 μM) or vehicle (DMSO) for 24 h. After centrifugation (300*g*, 5 min, 4 °C) the supernatant was discarded and the cells were incubated with 25 μL of a 0.1% NBT solution in PBS for 4 h at 37 °C. Then, the cells were centrifuged again (300*g*, 5 min, 4 °C) and the NBT solution was withdrawn. The precipitated formazan was dissolved for 30 min by adding first 25 μL of a 2 M KOH solution and then 33 μL DMSO. Then, the absorbance of formazan (630 nm) and background (405 nm) was measured with a microplate reader (Tecan). The formazan absorbance of the vehicle treated control cells was set as 100% ROS generation. All experiments were performed in sextuplicate resulting in the relative ROS generation as the mean ± standard deviation.

Topoisomerase I inhibition assay

To detect a potential inhibition of topoisomerase I a relaxation assay with supercoiled plasmid DNA was performed. Therefore, nuclear extracts containing topoisomerase type I and II enzymes were prepared from HT-29 colon carcinoma cells by differential centrifugation. Briefly, 0.5 μg pBR322 supercoiled plasmid DNA (Carl Roth) was incubated with the nuclear enzyme extracts in assay buffer (50 mM Tris/HCl, 100 mM KCl, 1 mM DTT, 1 mM EDTA, 5 μg mL^{-1} acetylated bovine serum albumin, pH 7.5) with varying concentrations of the test compounds for 30 min at 37 °C. The absence of ATP in the reaction mixture prevented the activity of topoisomerase type II enzymes and the DMSO concentration was standardized to 1% for all samples to exclude influence of the solvent. Reaction products were extracted with phenol–chloroform–isoamyl alcohol mixture (49.5 : 49.5 : 1; Sigma Aldrich), mixed with 5 μL of 5× loading dye, loaded onto a 1% agarose gel and electrophoresis was carried out at 66 V for 3.5 h. Gels were stained with ethidium bromide (10 μg mL^{-1}) for 30 min, washed with ddH_2O and photographed under UV light.

Conclusions

We presented 15 new Cu(II) complexes with different tridentate Schiff base-like ligands bearing varying substituents on the pyridine ring and the chelate cycle. Single crystal X-ray structures of nine complexes were obtained and discussed. Compounds with no substituents on the pyridine ring crystallised as dimeric or polymeric complexes, with the metal centres being bridged by the anions. The introduction of substituents on the pyridine ring led to the crystallisation of square planar compounds with short M···π and π···π interactions. The compounds were tested for their cytotoxic activity towards various cancer cell lines. Three previously described complexes with the same tridentate ligand (**HL1**) but different anions were investigated as well to rule out a potential influence of the anion. Most compounds were moderately active with IC_{50} values >10 μM. Two complexes (**10** and **14**) bearing only ester side chains on the chelate perimeter and electron-releasing methoxy or methyl groups in 4-position of the pyridine ring showed IC_{50} values in the low single-digit micromolar range. The respective complexes with a cyanide side chain instead of an ester group (**11** and **15**) were inactive (IC_{50} > 50 μM). The counter anion of the complexes does not seem to be crucial for the antiproliferative effect. These observations provide an entry point for future drug optimisations. In terms of the mode of action and the biological targets of the active copper complexes we could exclude the involvement of reactive oxygen species and any significant DNA interaction, but confirmed the inhibition of topoisomerase I to at least contribute to their anticancer effect. This sets them apart from other known topoisomerase I inhibitory Cu(II) complexes that already carry anticancer active ligands such as plumbagin,[6b] and that interfere with ROS levels and bind to DNA.

Conflicts of interest

There are no conflicts to declare.

Acknowledgements

RS thanks the Deutsche Forschungsgemeinschaft (DFG) for a grant (Scho 402/12-2), HK and VB were supported by the Czech Science Foundation (Grant 17-05302S). KD thanks the University of Bayreuth Graduate School (BayNAT program) for financial support. Florian Puchtler (ACI, Department of Chemistry, University of Bayreuth) is thanked for the powder X-ray diffraction.

Notes and references

1 (*a*) T. C. Johnstone, K. Suntharalingam and S. J. Lippard, *Chem. Rev.*, 2016, **116**, 3436–3486; (*b*) D. Wang and S. J. Lippard, *Nat. Rev. Drug Discovery*, 2005, **4**, 307–320; (*c*) L. Kelland, *Nat. Rev. Cancer*, 2007, **7**, 573–584; (*d*) E. Alessio, G. Mestroni, A. Bergamo and G. Sava, *Curr. Top. Med. Chem.*, 2004, **4**, 1525–1535; (*e*) J. Hildebrandt, H. Görls, N. Häfner, G. Ferraro, M. Dürst, I. B. Runnebaum, W. Weigand and A. Merlino, *Dalton Trans.*, 2016, **45**, 12283–12287; (*f*) C. G. Hartinger, M. A. Jakupec, S. Zorbas-Seifried, M. Groessl, A. Egger, W. Berger, H. Zorbas, P. J. Dyson and B. K. Keppler, *Chem. Biodiversity*, 2008, **5**, 2140–2155; (*g*) A. Casini and J. Reedijk, *Chem. Sci.*, 2012, **3**, 3135–3144.

2 Y. Jung and S. J. Lippard, *Chem. Rev.*, 2007, **107**, 1387–1407.

3 (*a*) S. Tardito and L. Marchiò, *Curr. Med. Chem.*, 2009, **16**, 1325–1348; (*b*) M. Tacke, *J. Organomet. Chem.*, 2015, **782**, 17–21; (*c*) D. M. Griffith, B. Szőcs, T. Keogh, K. Y. Suponitsky, E. Farkas and P. Buglyó, *J. Inorg. Biochem.*, 2011, **105**, 763–769; (*d*) M. Buczkowskar, A. Bodtke, U. Lindequist, M. Gdaniec and P. J. Bednarski, *Arch. Pharm. Chem. Life Sci.*, 2011, **344**, 605–616; (*e*) L. Oehninger, R. Rubbiani and I. Ott, *Dalton Trans.*, 2013, **42**, 3269–3284.

4 (*a*) E. I. Solomon, D. E. Heppner, E. M. Johnston, J. W. Ginsbach, J. Cirera, M. Qayyum, M. T. Kieber-Emmons, C. H. Kjaergaard, R. G. Hadt and L. Tian, *Chem. Rev.*, 2014, **114**, 3659–3853; (*b*) C. Citek, S. Herres-Pawlis and T. D. P. Stack, *Acc. Chem. Res.*, 2015, **48**, 2424–2433; (*c*) J. N. Hamann, B. Herzigkeit, R. Jurgeleit and F. Tuczek, *Coord. Chem. Rev.*, 2017, **334**, 54–66; (*d*) A. Hoffmann, S. Binder, A. Jesser, R. Haase, U. Flörke, M. Gnida, M. Salomone Stagni, W. Meyer-Klaucke, B. Lebsanft, L. E. Grünig, S. Schneider, M. Hashemi, A. Goos, A. Wetzel, M. Rübhausen and S. Herres-Pawlis, *Angew. Chem.*, 2014, **126**, 305–310; (*e*) C. Wilfer, P. Liebhäuser, A. Hoffmann, H. Erdmann, O. Grossmann, L. Runtsch, E. Paffenholz, R. Schepper, R. Dick, M. Bauer, M. Dürr, I. Ivanović-Burmazović and S. Herres-Pawlis, *Chem. – Eur. J.*, 2015, **21**, 17639–17649.

5 C. Santini, M. Pellei, V. Gandin, M. Porchia, F. Tisato and C. Marzano, *Chem. Rev.*, 2014, **114**, 815–862.

6 (*a*) F. Tisato, C. Marzano, M. Porchia, M. Pellei and C. Santini, *Med. Res. Rev.*, 2010, **30**, 708–749; (*b*) Z.-F. Chen, M.-X. Tan, L. M. Liu, Y.-C. Liu, H.-S. Wang, B. Yang, Y. Peng, H.-G. Liu, H. Liang and C. Orvig, *Dalton Trans.*, 2009, 10824–10833; (*c*) Z. Yu and J. A. Cowan, *Chem. – Eur. J.*, 2017, **23**, 14113–14127.

7 (*a*) Z. H. Chohan and S. Kausar, *Chem. Pharm. Bull.*, 1993, **41**, 951–953; (*b*) M. K. Panda, M. M. Shaikh, R. J. Butcher and P. Ghosh, *Inorg. Chim. Acta*, 2011, **372**, 145–151.

8 (*a*) B.-T. Ko, C.-C. Chang, S.-L. Lai, F.-J. Lai and C.-C. Lin, *Polyhedron*, 2012, **45**, 49–54; (*b*) L. H. A. Rahman, A. M. Abu-Dief, S. K. Hamdan and A. A. Seleem, *Int. J. Nano. Chem.*, 2015, **1**, 65–77.

9 J. Easmon, G. Pürstinger, G. Heinisch, T. Roth, H. H. Fiebig, W. Holzer, W. Jäger, M. Jenny and J. Hofmann, *J. Med. Chem.*, 2001, **44**, 2164–2171.

10 (*a*) K. Dankhoff and B. Weber, *CrystEngComm*, 2018, **20**, 818–828; (*b*) K. Dankhoff, S. Schneider, R. Nowak and B. Weber, *Z. Anorg. Allg. Chem.*, 2018, **644**, 1839–1848; (*c*) K. Dankhoff and B. Weber, *Dalton Trans.*, 2019, DOI: 10.1039/C9DT00846B; (*d*) P. M. Schäfer, K. Dankhoff, M. Rothemund, A. N. Ksiazkiewicz, A. Pich, R. Schobert, B. Weber and S. Herres-Pawlis, *ChemistryOpen*, 2019, **8**, 1020–1026.

11 (*a*) A. Nanthakumar, S. Fox, N. M. Murthy and K. D. Karlin, *J. Am. Chem. Soc.*, 1997, **119**, 3898–3906; (*b*) C. X. Zhang, S. Kaderli, M. Costas, E. Kim, Y.-M. Neuhold, K. D. Karlin and A. D. Zuberbühler, *Inorg. Chem.*, 2003, **42**, 1807–1824.

12 D. Denoyer, S. Masaldan, S. La Fontaine and M. A. Cater, *Metallomics*, 2015, **7**, 1459–1476.

13 T. Rehm, M. Rothemund, J. K. Muenzner, A. Noor, R. Kempe and R. Schobert, *Dalton Trans.*, 2016, **45**, 15390–15398.

14 (*a*) C. Duncan and A. R. White, *Metallomics*, 2012, **4**, 127–138; (*b*) Z.-Y. Ma, X. Qiao, C.-Z. Xie, J. Shao, J.-Y. Xu, Z.-Y. Qiang and J.-S. Lou, *J. Inorg. Biochem.*, 2012, **117**, 1–9; (*c*) A. Sîrbu, O. Palamarciuc, M. V. Babak, J. M. Lim, K. Ohui, E. A. Enyedy, S. Shova, D. Darvasiová, P. Rapta, W. H. Ang and V. B. Arion, *Dalton Trans.*, 2017, **46**, 3833–3847.

15 A. Altomare, M. C. Burla, M. Camalli, G. L. Cascarano, C. Giacovazzo, A. Guagliardi, A. G. G. Moliterni, G. Polidori and R. Spagna, *J. Appl. Crystallogr.*, 1999, **32**, 115–119.

16 G. Sheldrick, *Acta Crystallogr., Sect. A: Found. Crystallogr.*, 2008, **64**, 112–122.

17 (*a*) C. K. Johnson and M. N. Burnett, *ORTEP-III*, Oak-Ridge National Laboratory, Oak-Ridge, TN, 1996; (*b*) L. Farrugia, *J. Appl. Crystallogr.*, 1997, **30**, 565.

18 O. Kahn, *Molecular Magnetism*, VCH, New York, N.Y, 1993.

19 T. Mosmann, *J. Immunol. Methods*, 1983, **65**, 55–63.

20 J. K. Muenzner, B. Biersack, A. Albrecht, T. Rehm, U. Lacher, W. Milius, A. Casini, J.-J. Zhang, I. Ott, V. Brabec, O. Stuchlikova, I. C. Andronache, L. Kaps, D. Schuppan and R. Schobert, *Chem. – Eur. J.*, 2016, **22**, 18953–18962.

Supporting Information for:

Copper(II) complexes with tridentate Schiff base-like ligands: solid state and solution structures and anticancer activity

Katja Dankhoff[+],[a] Madeleine Gold[+],[b] Luisa Kober,[b] Florian Schmitt,[b] Lena Pfeifer,[a] Andreas Dürrmann,[a] Hana Kostrhunova,[c] Matthias Rothemund,[b] Viktor Brabec,[c] Rainer Schobert,*[b] and Birgit Weber*[a]

[a] Department of Chemistry, Inorganic Chemistry IV, Universität Bayreuth, Universitätsstr. 30, 95447 Bayreuth, Germany, e-mail: weber@uni-bayreuth.de

[b] Department of Chemistry, Organic Chemistry I, Universität Bayreuth, Universitätsstr. 30, 95447 Bayreuth, Germany

[c] Czech Academy of Sciences, Institute of Biophysics, Kralovopolska 135, CZ-61265 Czech Republic

[+] These authors contributed equally to this work.

Table S1. Crystallographic data of the complexes discussed in this work.

	4	**5**	**7**	**8**	**9**
CCDC	1566628	1566629	1566630	1566631	1566632
formula	$[(\mu_2\text{–Br})_2(\text{CuL1})_2]$	$[(\mu_2\text{–Br})_2(\text{CuL2})_2]$	$[(\mu_2\text{–Br})(\text{CuL4})]_n$	$[(\mu_2\text{–Br})_2(\text{CuL5})_2]$	$[(\mu_2\text{–Br})_2(\text{CuL6})_2]$
sum formula	$C_{26}H_{30}Br_2Cu_2N_4O_6$	$C_{24}H_{26}Br_2Cu_2N_4O_4$	$C_{12}H_{12}BrCuN_3O_2$	$C_{36}H_{34}Br_2Cu_2N_4O_6$	$C_{24}H_{26}Br_2Cu_2N_4O_6$
M/ g mol^{-1}	781.44	721.39	373.70	905.57	753.38
crystal system	triclinic	triclinic	monoclinic	monoclinic	triclinic
space group	P–1	P–1	$P2_1/c$	$P2_1/n$	P–1
crystal description	blue green block	blue block	green plate	green block	blue green prism
a/ Å	7.7302(4)	7.9933(7)	7.6905(4)	10.5383(6)	8.0566(4)
b/ Å	9.2879(5)	9.2785(11)	24.3476(14)	9.5476(5)	8.4259(4)
c/ Å	10.2517(5)	9.4396(10)	7.7833(4)	17.4636(12)	11.1094(5)
α/ °	94.782(4)	90.031(9)	90	90	75.675(4)
β/ °	94.310(4)	98.575(7)	113.207(4)	100.791(5)	86.846(4)
γ/ °	108.849(4)	111.440(8)	90	90	68.045(4)
V/ Å^3	690.07(6)	643.21(12)	1339.46(13)	1726.04(18)	677.12(6)
Z	1	1	4	2	1
ρ_{calcd}/ g cm^{-3}	1.880	1.862	1.853	1.742	1.848
μ/ mm^{-1}	4.485	4.798	4.614	3.600	4.567
crystal size/ mm	0.090×0.070×0.065	0.110×0.105×0.097	0.110×0.102×0.093	0.104×0.097×0.093	0.099×0.084×0.075
F(000)	390	358	740	908	374
T/ K	133(2)	133(2)	133(2)	133(2)	133(2)
λ/ Å	Mo-K_α 0.71073	Mo-K_α 0.71073	Mo-K_α 0.71073	Mo-K_α 0.71073	Mo-K_α 0.71073
Θ range/ °	2.00–28.50	2.2–28.6	1.68–28.67	2.11–28.47	1.9–28.4
Reflns. collected	3242	7822	3151	4145	3198
Indep. reflns.(R_{int})	2709 (0.0317)	3021 (0.1611)	2226 (0.0608)	2693 (0.1860)	2677 (0.0299)
Parameters	181	163	172	226	172
$R1$ (all data)	0.0266 (0.0361)	0.0814 (0.1116)	0.0404 (0.0654)	0.0733 (0.1115)	0.0241 (0.0332)
$wR2$	0.0628	0.2878	0.1099	0.2261	0.0560
GooF	0.985	1.064	0.960	1.011	0.997

Table S1. (continued)

	12	**15**	**17**	**18**
CCDC	1915615	1915614	1915617	1915616
formula	[CuL9Br]	[CuL12Br]	[CuL14Br]	[CuL15Br]
sum formula	$C_{14}H_{16}BrClCuN_2O_4$	$C_{13}H_{14}BrCuN_3O_2$	$C_{15}H_{19}BrCuN_2O_4$	$C_{13}H_{14}BrCuN_3O_2$
M/ g mol^{-1}	455.19	387.72	434.77	387.72
crystal system	triclinic	triclinic	monoclinic	triclinic
space group	P–1	P–1	$P2_1/a$	P–1
crystal description	green cube	green plate	green plate	green plate
a/ Å	8.0351(3)	7.8986(4)	7.9002(3)	7.5494(2)
b/ Å	9.6830(3)	8.2689(3)	18.0037(6)	8.2358(3)
c/ Å	11.4547(4)	11.3892(4)	11.3870(5)	12.3671(4)
α/ °	98.869(3)	85.890(3)	90	107.000(3)
β/ °	102.321(3)	78.823(3)	94.962(4)	96.398(3)
γ/ °	104.864(3)	81.476(3)	90	102.191(3)
V/ Å^3	820.70(5)	720.98(5)	1613.54(11)	706.30(4)
Z	2	2	4	2
ρ_{calcd}/ g cm^{-3}	1.842	1.786	1.790	1.823
μ/ mm^{-1}	3.947	4.289	3.851	4.378
crystal size/ mm	0.095×0.076×0.065	0.119×0.117×0.098	0.079×0.052×0.037	0.085×0.045×0.032
F(000)	454	386	876	386
T/ K	133(2)	133(2)	133(2)	133(2)
λ/ Å	Mo-K_α 0.71073	Mo-K_α 0.71073	Mo-K_α 0.71073	Mo-K_α 0.71073
Θ range/ °	1.9–28.5	1.8–29.1	1.6–28.4	1.8–28.5
Reflns. collected	12083	8912	12531	10623
Indep. reflns.(R_{int})	3966 (0.030)	3350 (0.028)	3900 (0.058)	3406 (0.027)
Parameters	208	181	208	181
R1 (all data)	0.0368 (0.0504)	0.0296 (0.0431)	0.0430 (0.0642)	0.0272 (0.0400)
wR2	0.0995	0.0741	0.1137	0.0659
GooF	1.04	1.034	1.04	1.05

Table S2. Selected bond lengths/Å and angles/° of the complexes discussed in this work.

	Cu–N_{py}	Cu–N	Cu–O	Cu–X	Cu–X–Cu	X–Cu–X
4	2.0126(19)	1.928(2)	1.9363(18)	2.4316(4) 2.8919(4)	91.15(1)	88.85(1)
5	1.993(7)	1.924(8)	1.926(6)	2.4419(14) 2.9264(15)	91.16(4)	88.84(4)
7	1.995(3)	1.949(3)	1.951(3)	2.4153(6) 2.8131(6)	95.92(2)	96.08(2)
8	1.994(6)	1.945(5)	1.918(4)	2.4330(12) 2.9152(12)	86.70(4)	93.30(3)
9	2.0001(17)	1.9316(17)	1.9256(17)	2.4281(3) 2.9752(4)	91.17(1)	88.83(1)
12	1.995(3)	1.930(3)	1.923(3)	2.3787(5)	/	/
15	2.026(2)	1.976(2)	1.9730(18)	2.4174(4)	/	/
17	1.990(3)	1.936(3)	1.940(2)	2.3770(6)	/	/
18	2.005(2)	1.928(3)	1.9481(16)	2.3588(4)	/	/

Figure S1. Structures of **5**(top left), **8** (top middle), **9** (top right), **12** (bottom left), **15** (bottom middle), and **18** (bottom right). Ellipsoids were drawn at 50 % probability level. Hydrogen atoms were omitted for clarity.

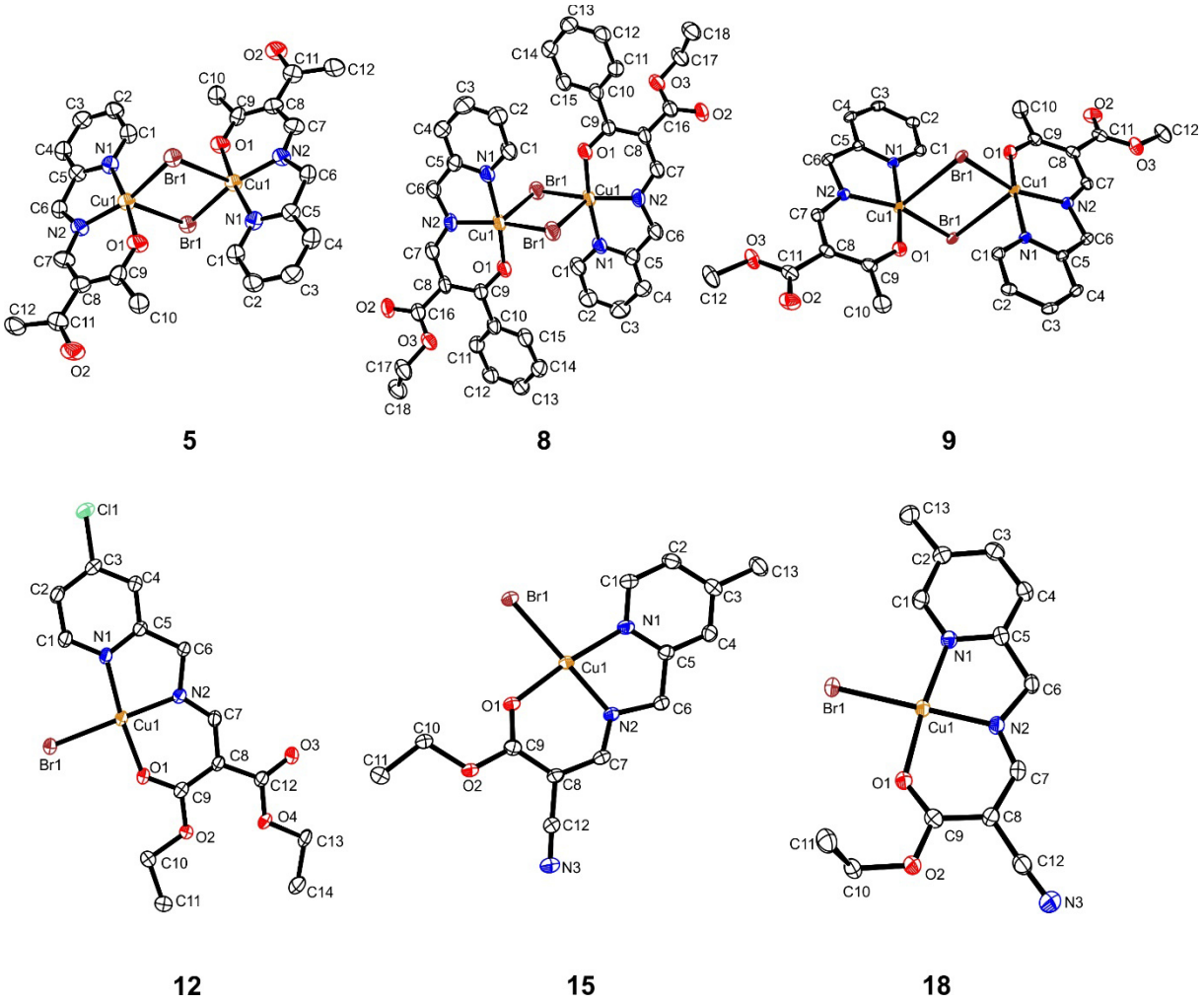

Table S3. Summary of the C–H···π / X–Y···π interactions of the complexes presented in this work.

		C_g	H···C_g/Å Y···C_g/Å	X–H···C_g/° X–Y···C_g/°	X···C_g/Å
5	C12–H12A	Cu1–O1–C9–C8–C7–N2[a]	2.83	141	3.644(11)
7	C6–H6A	Cu1–O1–C9–C8–C7–N2[b]	2.66	141	3.485(4)
	C10–H10B	N1–C1–C2–C3–C4–C5[c]	2.81	141	3.634(5)
12	C3–Cl1	Cu1–N1–C5–C6–N2[d]	3.3478(14)	84.40(11)	3.614(3)
17	C10–H10A	N1–C1–C2–C3–C4–C5[e]	2.98	132	3.709(4)
	Cu1–Br1	Cu1–N1–C5–C6–N2[f]	3.3662(14)	83.37(3)	3.8900(14)
	Cu1–Br1	N1–C1–C2–C3–C4–C5[f]	3.8784(15)	118.56(3)	5.4320(15)

a: −3−x, −y, −z; b: x, 3/2−y, 1/2+z; c: x, 3/2−y, −1/2+z; d: 1−x, −y, 2−z; e: −1/2+x, 1/2−y, z; f: 1/2+x, 1/2−y, z.

Table S4. Selected distances and angles of the π– π and M– π interactions of the complexes presented in this work. C_g(I) is the centroid of the ring number I, α is the dihedral angle between the rings, β is the angle between the vector C_g(I) → C_g(J) and the normal to ring I, γ is the angle between the vector C_g(I) → C_g(J) and the normal to ring J.

	C_g(I)	C_g(J)	C_g–C_g/Å	α/°	β/°	γ/°
4	Cu1–O1–C9–C8–C7–N2	N1–C1–C2–C3–C4–C5[a]	3.9305(14)	2.29(11)	25.5	24.0
9	N1–C1–C2–C3–C4–C5	Cu1[b]	3.982	0	29.86	0
12	Cu1–N1–C5–C6–N2	Cu1–O1–C9–C8–C7–N2[b]	3.3580(16)	2.53(12)	9.6	9.8
	N1–C1–C2–C3–C4–C5	N1–C1–C2–C3–C4–C5[c]	3.4951(18)	0.02(15)	17.4	17.4
	Cu1–N1–C5–C6–N2	Cu1[b]	3.544	0	22.30	0
	Cu1–O1–C9–C8–C7–N2	Cu1[b]	3.707	0	28.89	0
15	Cu1–N1–C5–C6–N2	Cu1–O1–C9–C8–C7–N2[d]	3.2977(14)	3.99(10)	11.6	11.9
	Cu1–N1–C5–C6–N2	N1–C1–C2–C3–C4–C5[a]	3.6338(14)	0.81(12)	19.5	18.7
	Cu1–N1–C5–C6–N2	Cu1[d]	3.635	0	30.33	0
	Cu1–O1–C9–C8–C7–N2	Cu1[d]	3.423	0	20.86	0
	N1–C1–C2–C3–C4–C5	Cu1[a]	3.570	0	16.69	0
17	Cu1–N1–C5–C6–N2	Cu1–O1–C9–C8–C7–N2[e]	3.5852(18)	4.02(14)	21.8	18.6
	Cu1–N1–C5–C6–N2	Cu1[f]	3.890	0	32.59	0
	Cu1–O1–C9–C8–C7–N2	Cu1[f]	3.444	0	16.48	0
18	Cu1–N1–C5–C6–N2	Cu1–N1–C5–C6–N2[g]	3.5980(14)	0.02(11)	20.0	20.0
	Cu1–N1–C5–C6–N2	Cu1–O1–C9–C8–C7–N2[h]	3.4963(13)	1.40(10)	22.6	23.6
	Cu1–N1–C5–C6–N2	N1–C1–C2–C3–C4–C5[g]	3.6748(13)	3.91(11)	22.6	22.3
	Cu1–O1–C9–C8–C7–N2	N1–C1–C2–C3–C4–C5[g]	3.5589(13)	2.74(10)	17.7	18.0
	Cu1–N1–C5–C6–N2	Cu1[h]	3.650	0	28.30	0
	Cu1–N1–C5–C6–N2	Cu1[g]	3.907	0	30.19	0
	Cu1–O1–C9–C8–C7–N2	Cu1[h]	3.322	0	14.07	0
	N1–C1–C2–C3–C4–C5	Cu1[g]	3.548	0	21.11	0

a: 1–x, 1–y, –z; b: 1–x, 1–y, 2–z; c: 1–x, –y, 2–z; d: 1–x, –y, –z; e: 1/2+x, 1/2–y, z; f: –1/2+x, 1/2–y, z; g: 2–x, –y, 1–z; h: 1–x, –y, 1–z.

Table S5. Hydrogen bonds and angles of the complexes presented in this work.

	Donor	Acceptor	D–H/Å	H···A/Å	D···A/Å	D–H···A/°
4	C3–H3	Br1[a]	0.95	2.82	3.606(3)	140
	C6–H6B	Br1[b]	0.99	2.77	3.652(3)	149
5	C2–H2	O2[c]	0.95	2.48	3.203(12)	133
	C6–H6A	Br1[d]	0.99	2.83	3.730(9)	151
	C6–H6B	O2[e]	0.99	2.56	3.378(11)	140
7	C6–H6B	Br1[f]	0.99	2.88	3.766(4)	149
	C7–H7	Br1[g]	0.95	2.84	3.744(4)	159
8	C7–H7	O2[h]	0.95	2.39	3.318(9)	164
9	C3–H3	Br1[i]	0.95	2.90	3.602(2)	132
	C6–H6B	Br1[j]	0.99	2.92	3.829(2)	153
12	C2–H2	Br1[k]	0.95	2.91	3.842(3)	167
	C4–H4	O3[l]	0.95	2.30	3.142(4)	148
15	C6–H6A	Br1[m]	0.99	2.88	3.747(3)	147
17	C4–H4	O3[o]	0.95	2.42	3.370(5)	173
18	C7–H7	Br1[a]	0.95	2.85	3.622(2)	139
	C13–H13C	Br1[p]	0.98	2.91	3.832(3)	157

a: x, –1+y, z; b: 1–x, 1–y, –z; c: 1+x, 1+y, 1+z; d: –3–x, –y, 1–z; e: –3–x, –y, –z; f: 1+x, 3/2–y, 1/2+z; g: 1+x, y, 1+z; h: 2–x, –y, 1–z; i: –1+x, 1+y, z; j: 1–x, 1–y, 2–z; k: –x, –y, 2–z; l: 2–x, 1–y, 2–z; m: 1+x, y, z; o: –1/2–x, 1/2+y, –z; p: 2–x, 1–y, 1–z.

Figure S2. Powder X-ray diffraction patterns and calculated pattern of **4**, **5**, **7**, **8**, and **9**. Calculated patterns were obtained at 133 K, measured at room temperature.

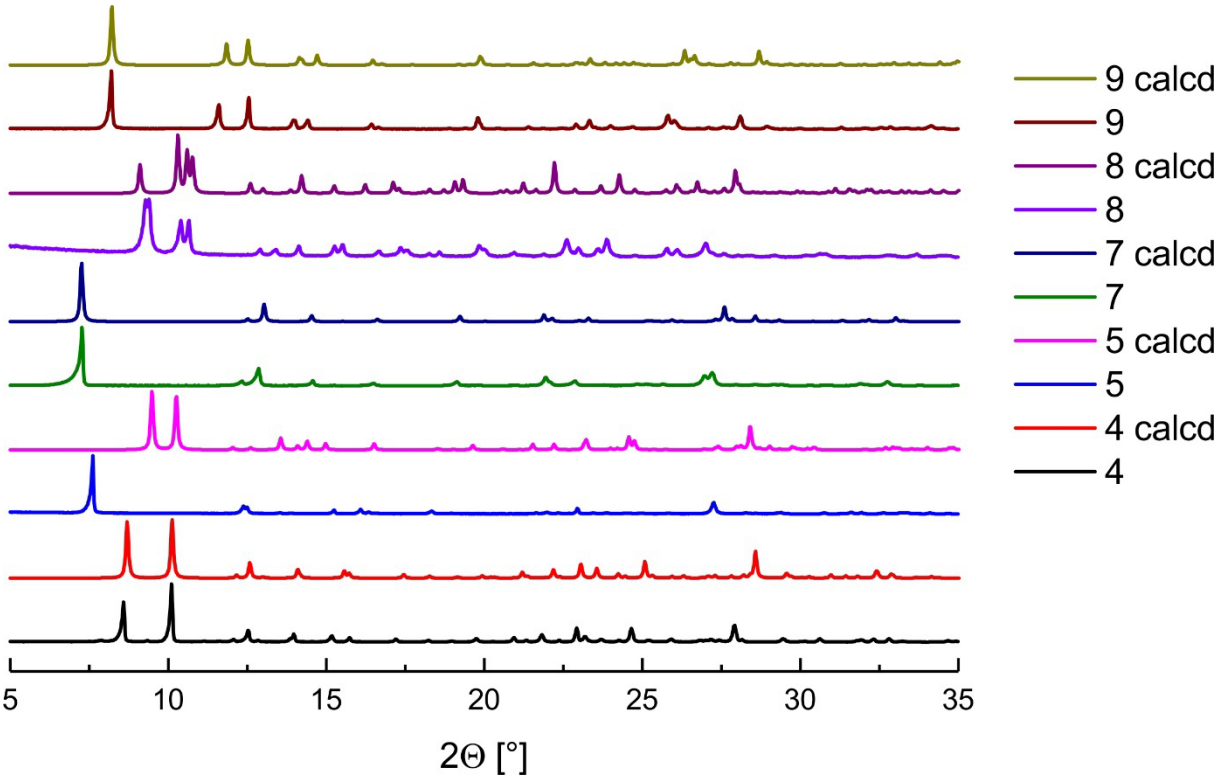

Figure S3. Powder X-ray diffraction patterns and calculated patterns of **12**, **15**, **17**, and **18**. Calculated patterns were obtained at 133 K, measured at room temperature.

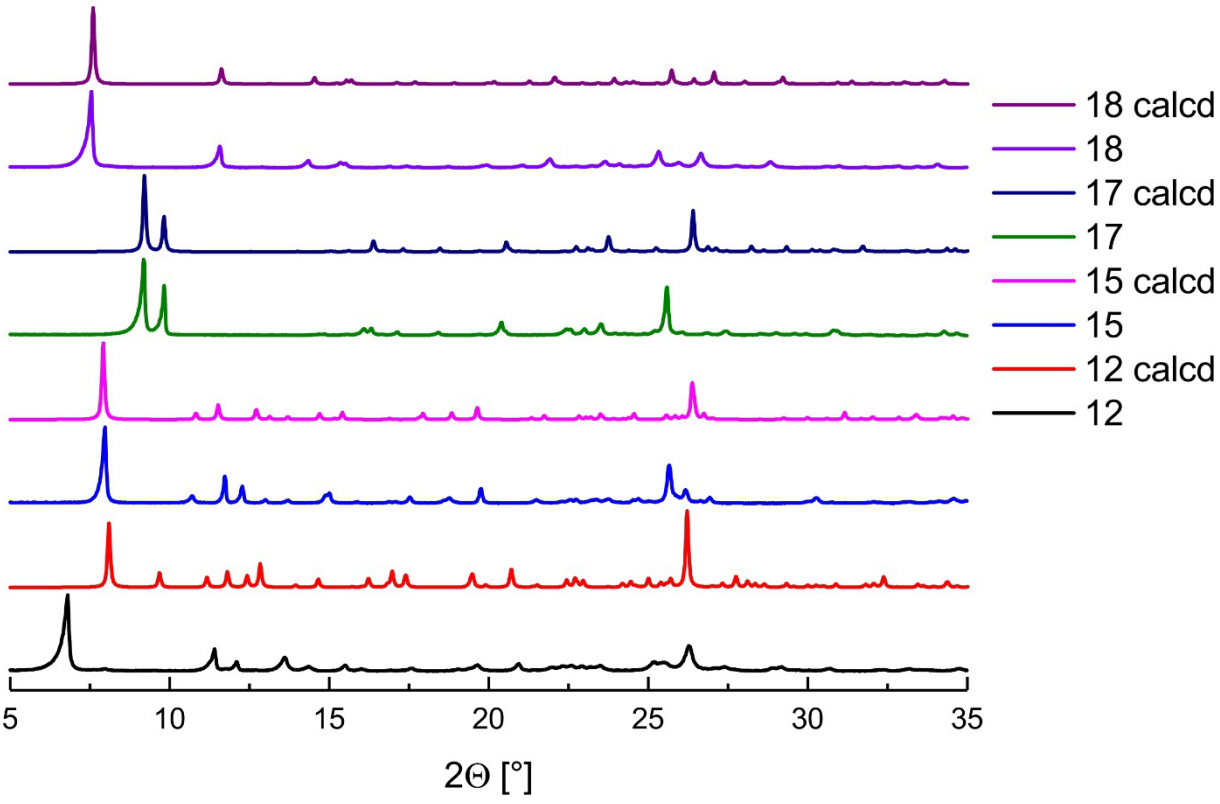

Figure S4. $\chi_M T$ vs. T plots of compounds **4**, **5**, **6**, **7**, **8**, and **9**.

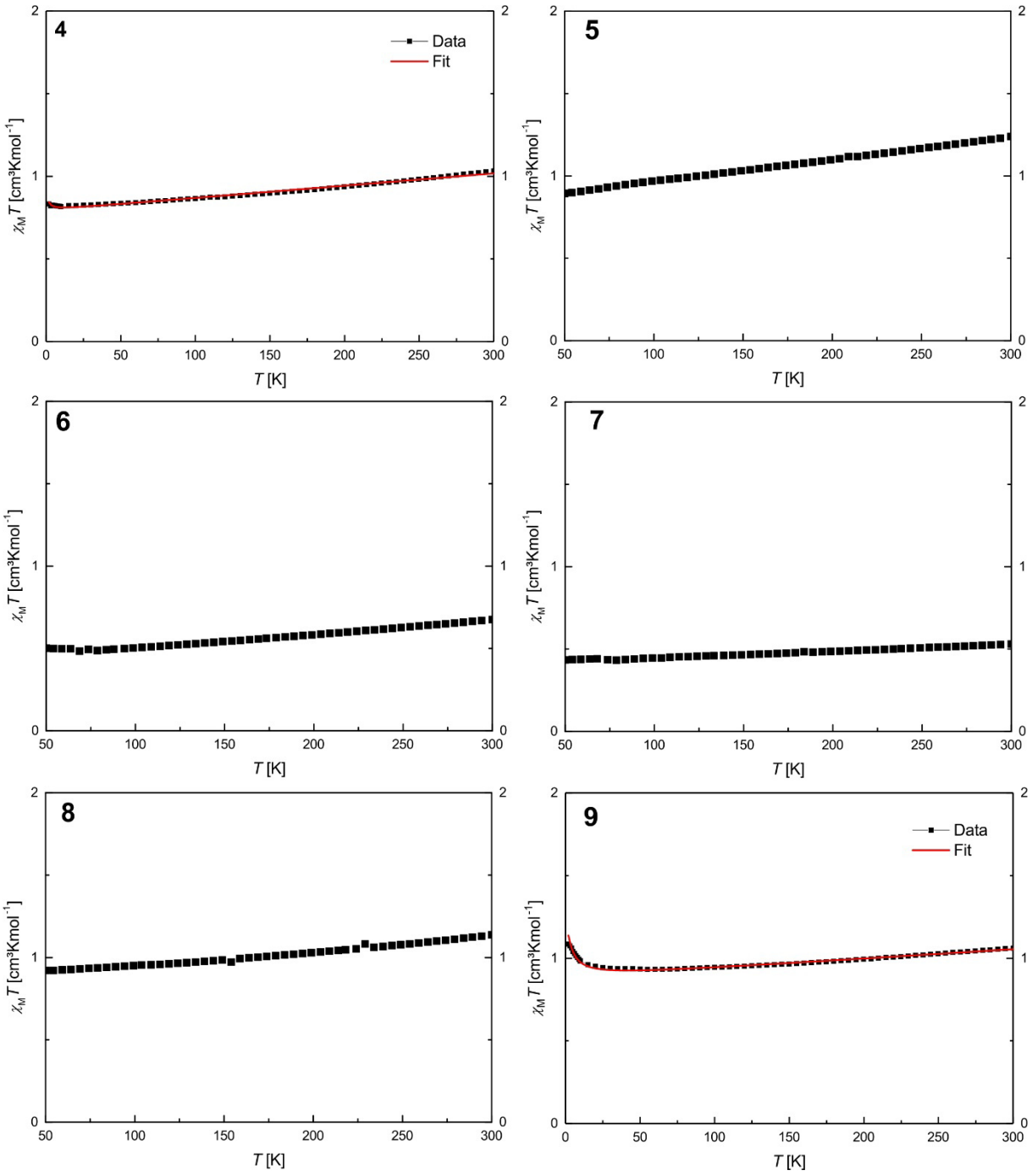

Figure S5. $\chi_M T$ vs. T plots of compounds **10**, **11**, **12**, **13**, **14**, and **15**.

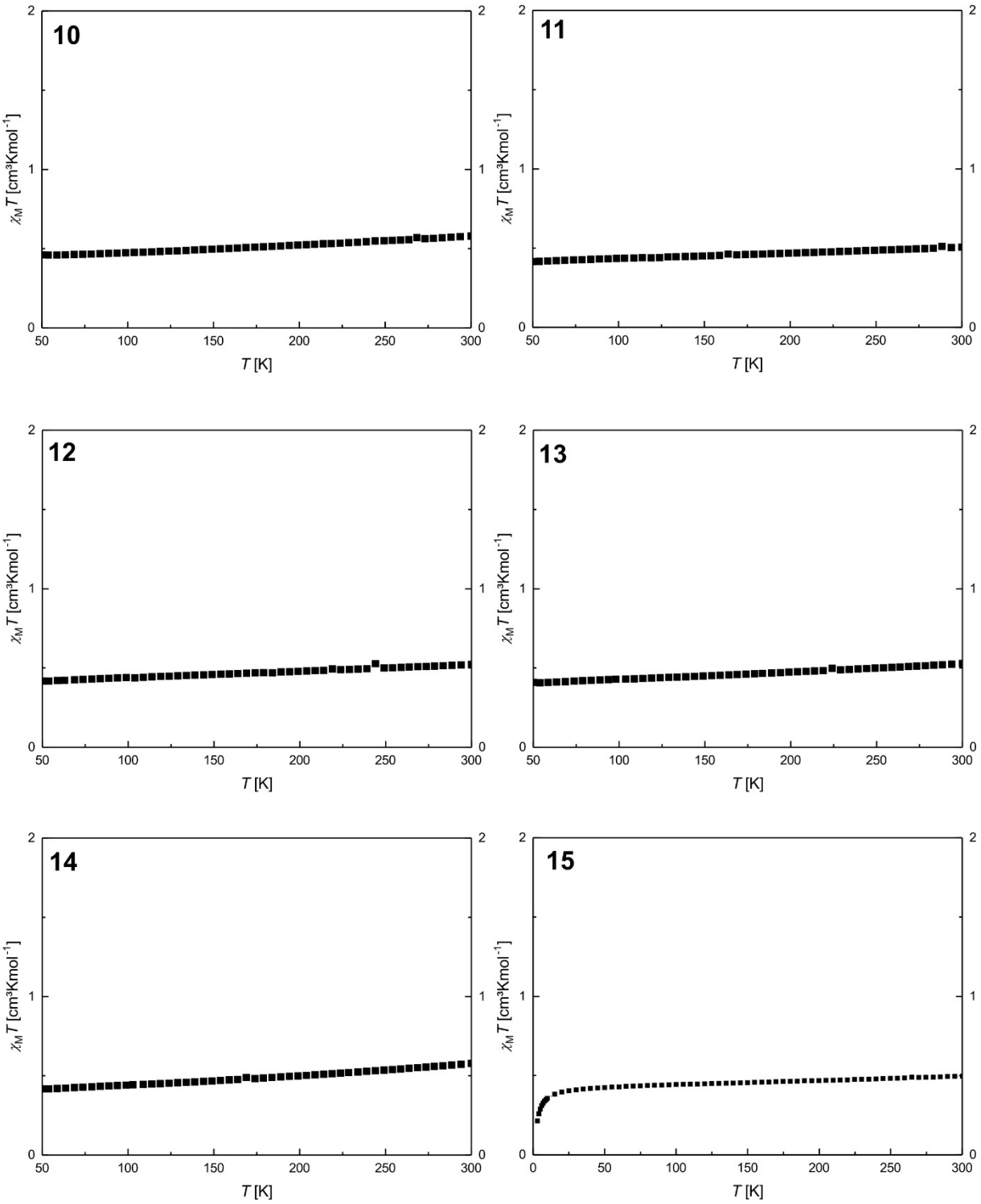

Figure S6. $\chi_M T$ vs. T plots of compounds **16**, **17**, and **18**.

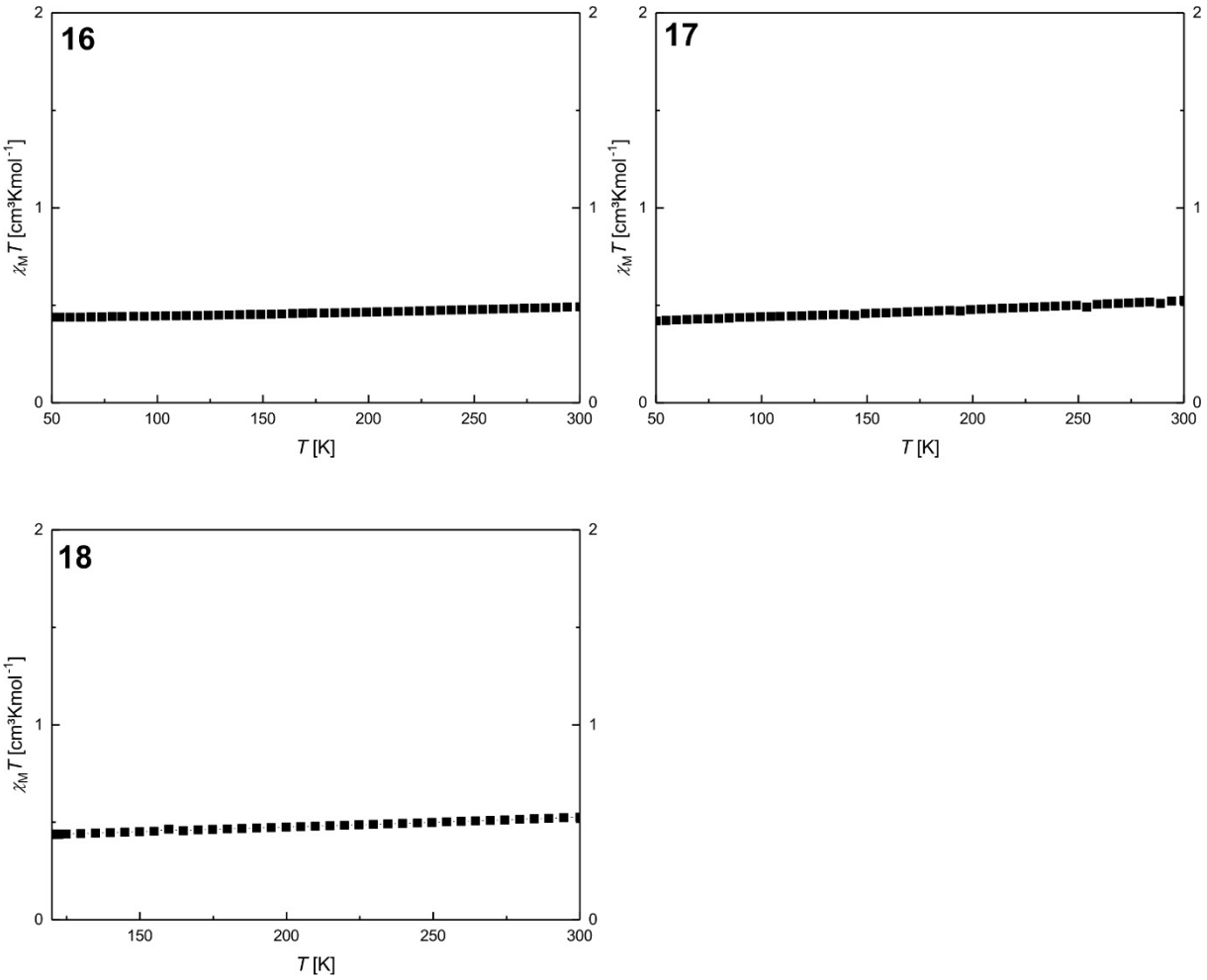

Table S6. Data of the magnetic measurements with μ_{eff} at 300 K, $\chi_M T$ at 300 K, 50 K, and, if measured, 2 K, and, if determined, the coupling constant J, g, and TIP.

	μ_{eff} [μ_B] (300 K)	$\chi_M T$ [$cm^3K^{-1}mol^{-1}$] (300 K)	$\chi_M T$ [$cm^3K^{-1}mol^{-1}$] (50 K)	$\chi_M T$ [$cm^3K^{-1}mol^{-1}$] (2 K)	J [cm^{-1}]	g	TIP [cm^3mol^{-1}]
4	2.88	1.04	0.84	0.83	0.38(5)	2.057(3)	$7.45(11)\cdot10^{-4}$
5	3.15	1.24	0.89				
6	2.33	0.68	0.50				
7	2.06	0.53	0.43				
8	3.02	1.14	0.92				
9	2.90	1.05	0.93	1.09	3.38(19)	2.163(4)	$5.79(17)\cdot10^{-4}$
10	2.16	0.58	0.46				
11	2.01	0.51	0.42				
12	2.05	0.52	0.42				
13	2.06	0.53	0.41				
14	2.15	0.58	0.42				
15	1.99	0.50	0.42	0.21			
16	1.99	0.49	0.44				
17	2.05	0.53	0.42				
18	2.05	0.53	0.44 (120 K)*				

*due to technical difficulties this complex was only measured down to 120 K.

Figure S7. UV-Vis spectra of **1**–**6** (**1** in H_2O, **2**–**6** in DMSO) at the indicated time points.

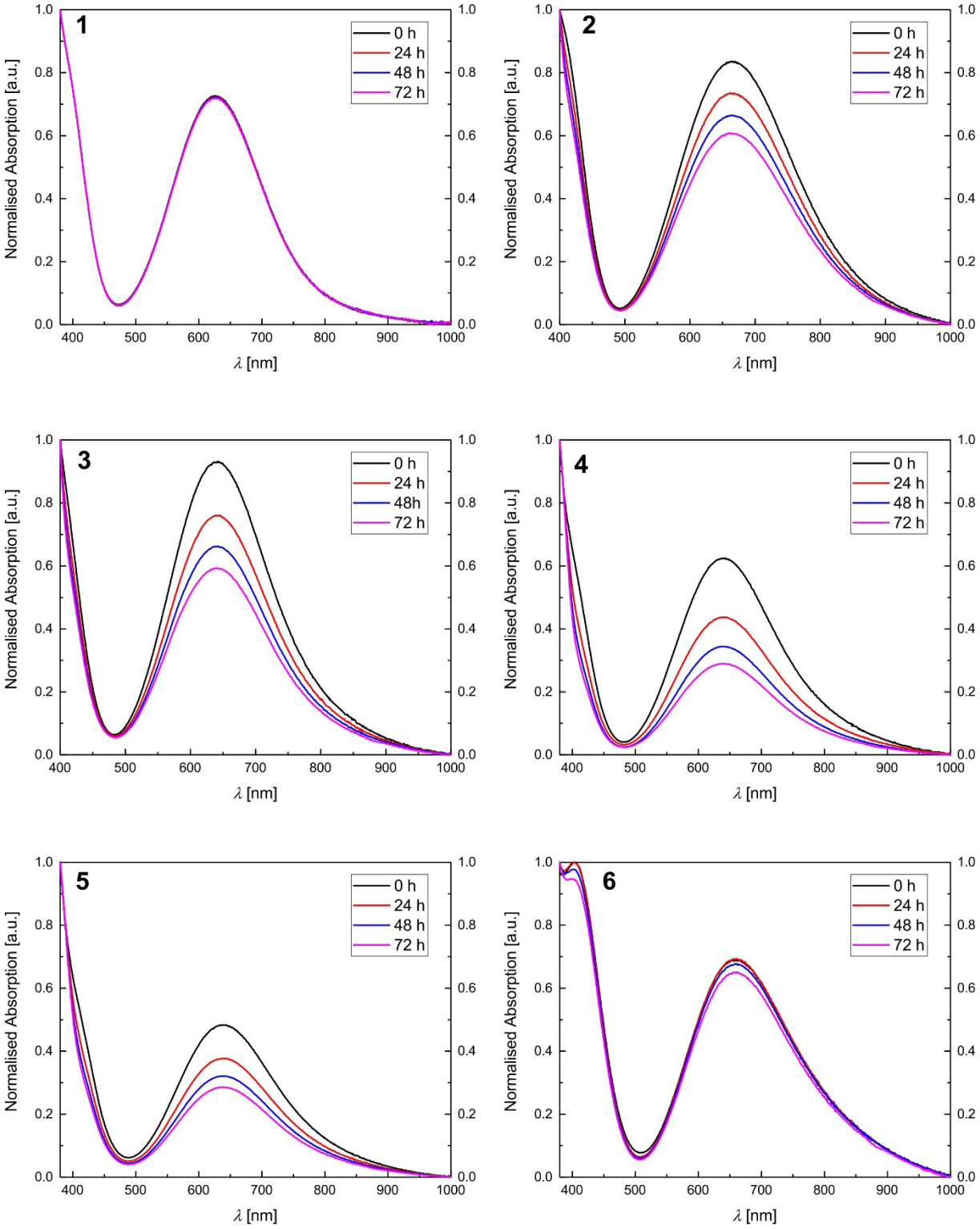

Figure S8. UV-Vis spectra of **7–12** (DMSO) at the indicated time points.

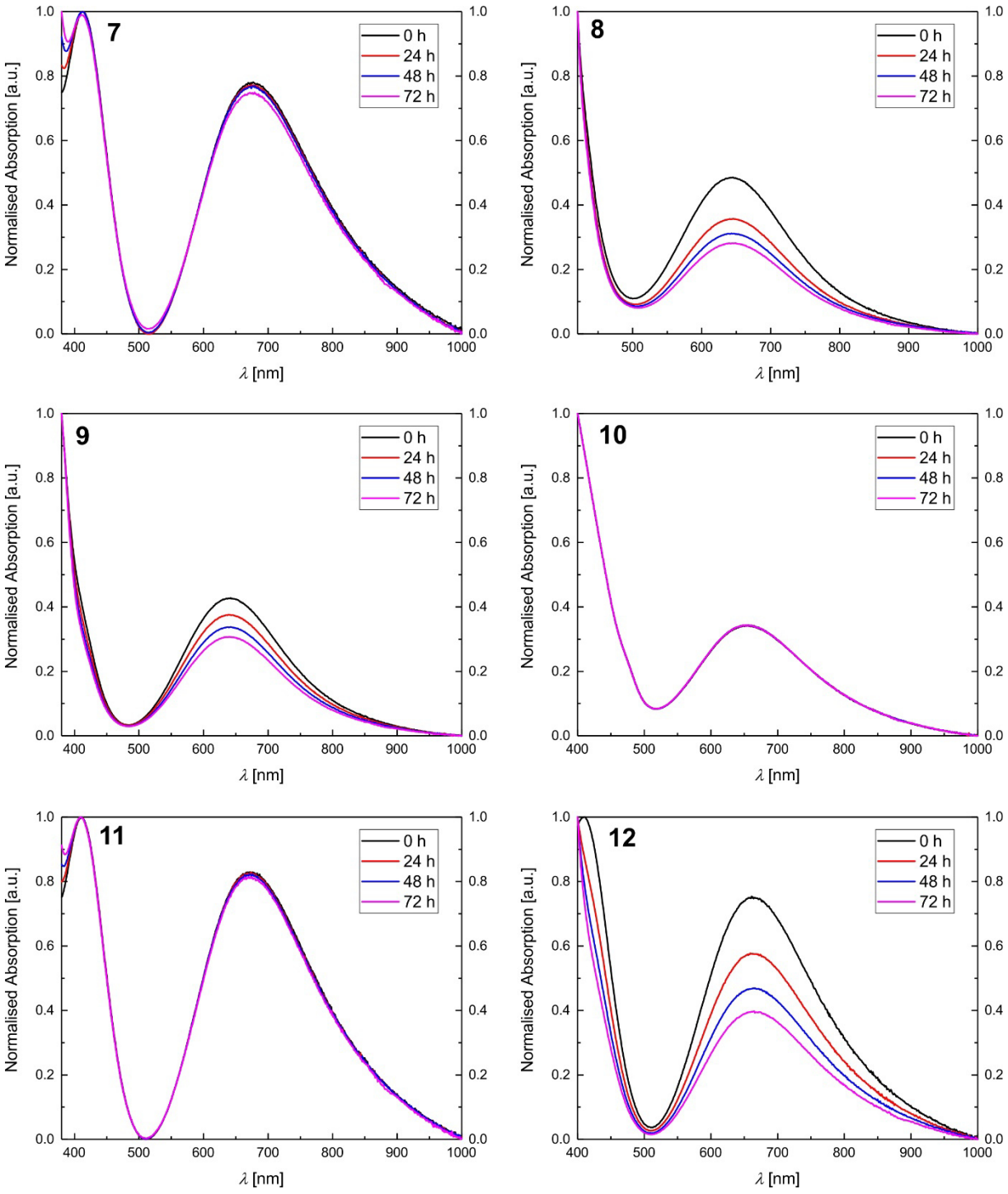

Figure S9. UV-Vis spectra of **13–18** (DMSO) at the indicated time points.

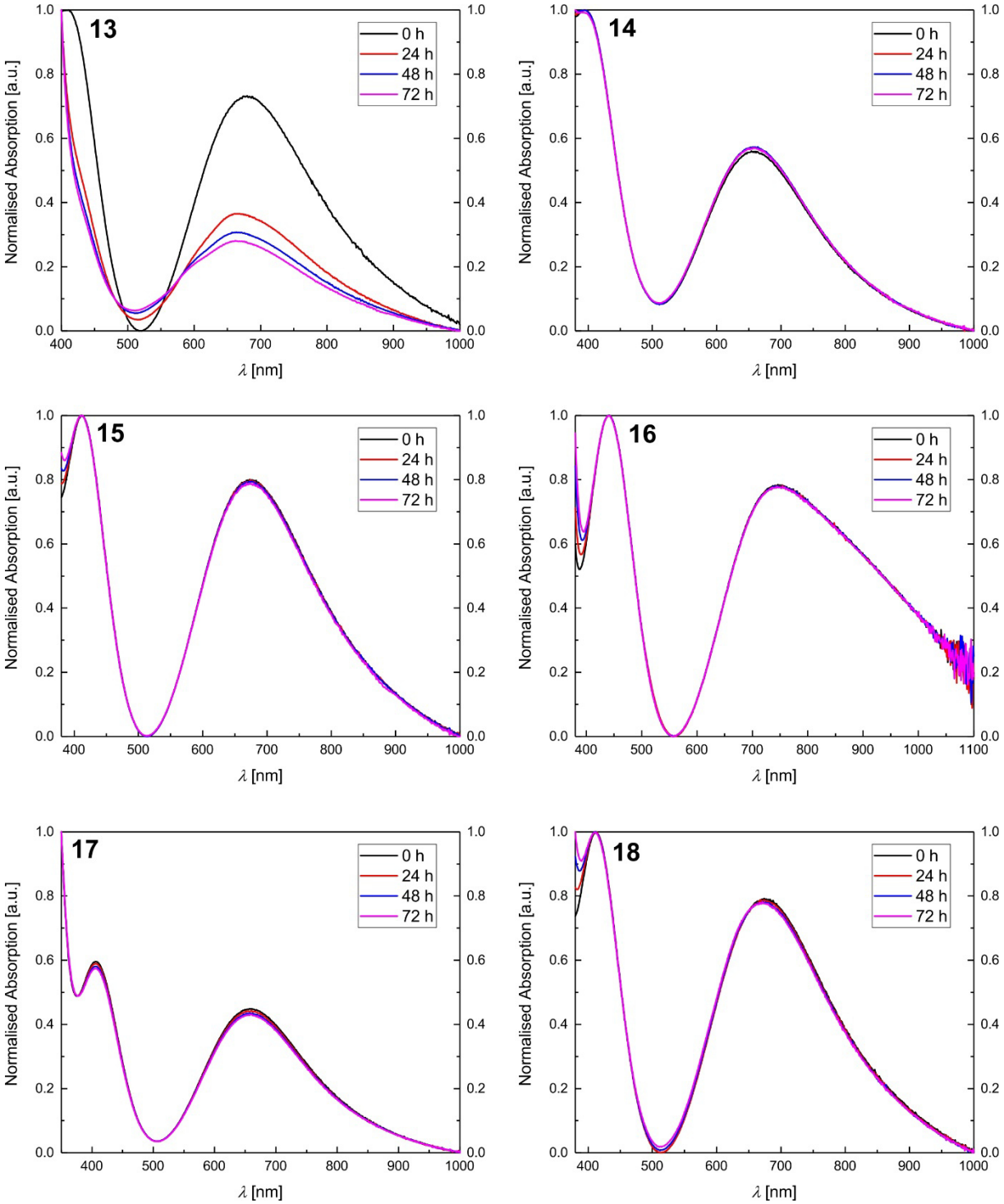

Figure S10. Cyclic voltammograms (MeCN, 0.1 M NBu_4PF_6, vs. $Ag/AgNO_3$, 50 mV/s) of **1**–**6**.

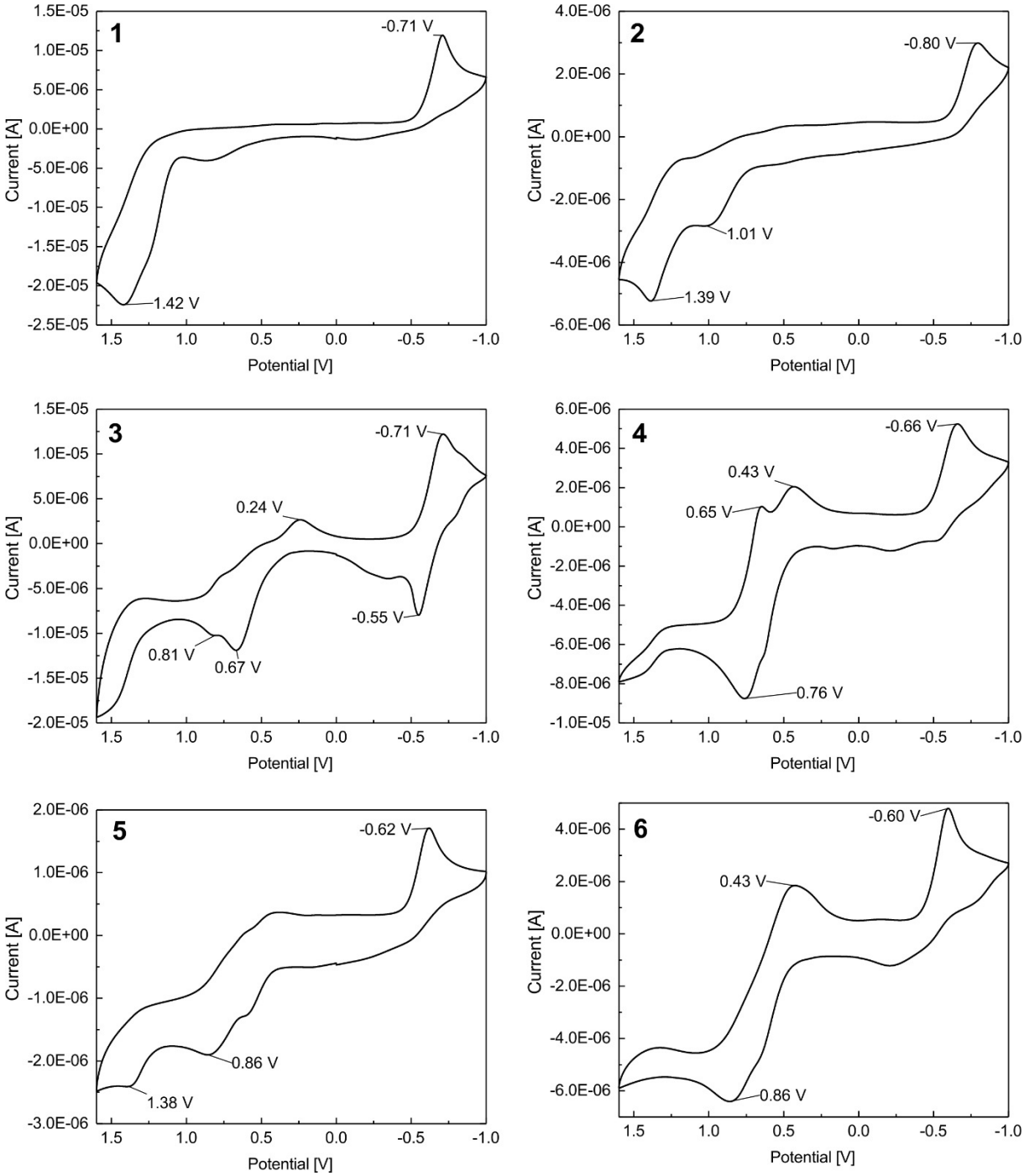

Figure S11. Cyclic voltammograms (MeCN, 0.1 M NBu_4PF_6, vs. $Ag/AgNO_3$, 50 mV/s) of **7**–**12**.

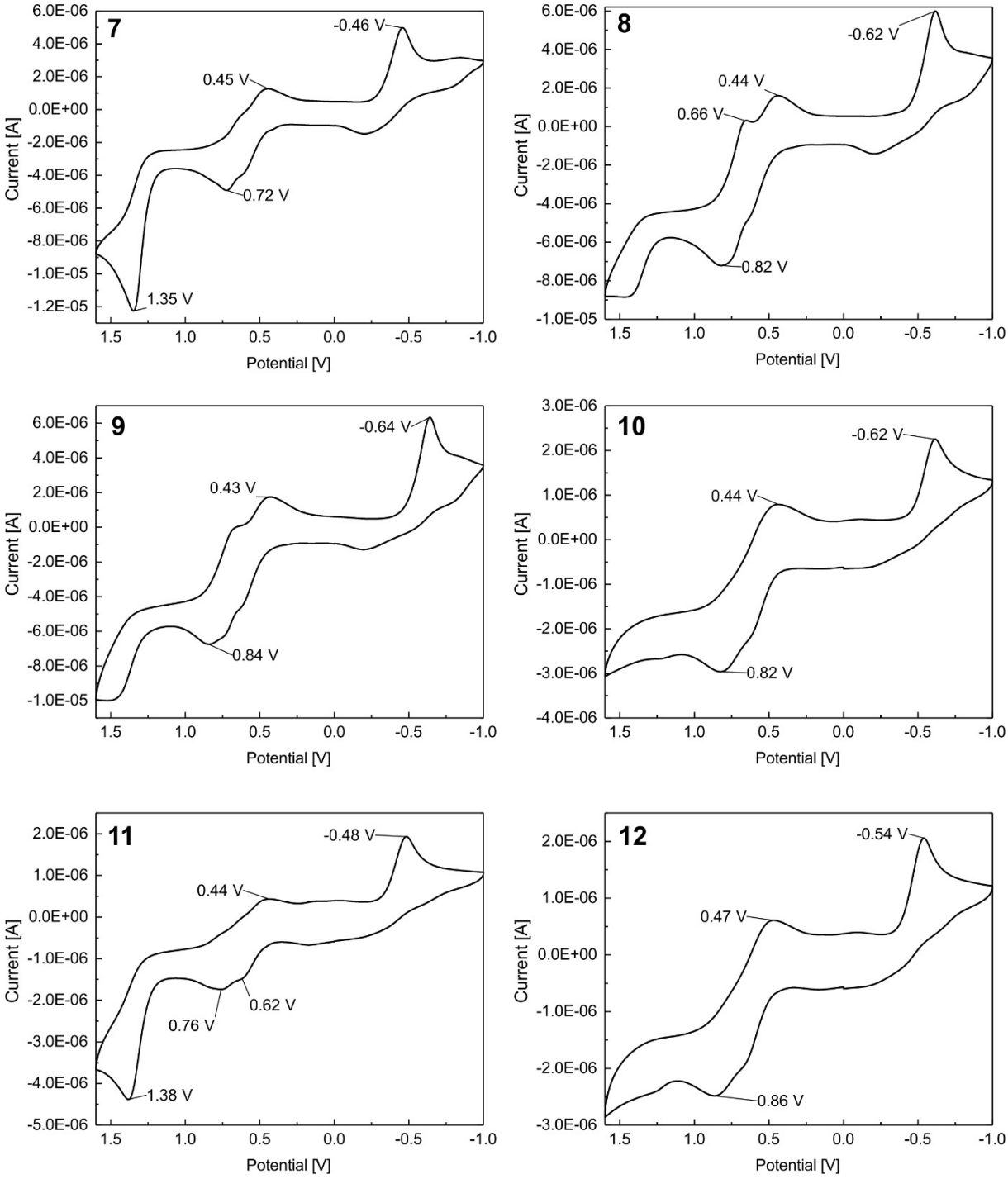

Figure S12. Cyclic voltammograms (MeCN, 0.1 M NBu_4PF_6, vs. $Ag/AgNO_3$, 50 mV/s) of **13**–**18**.

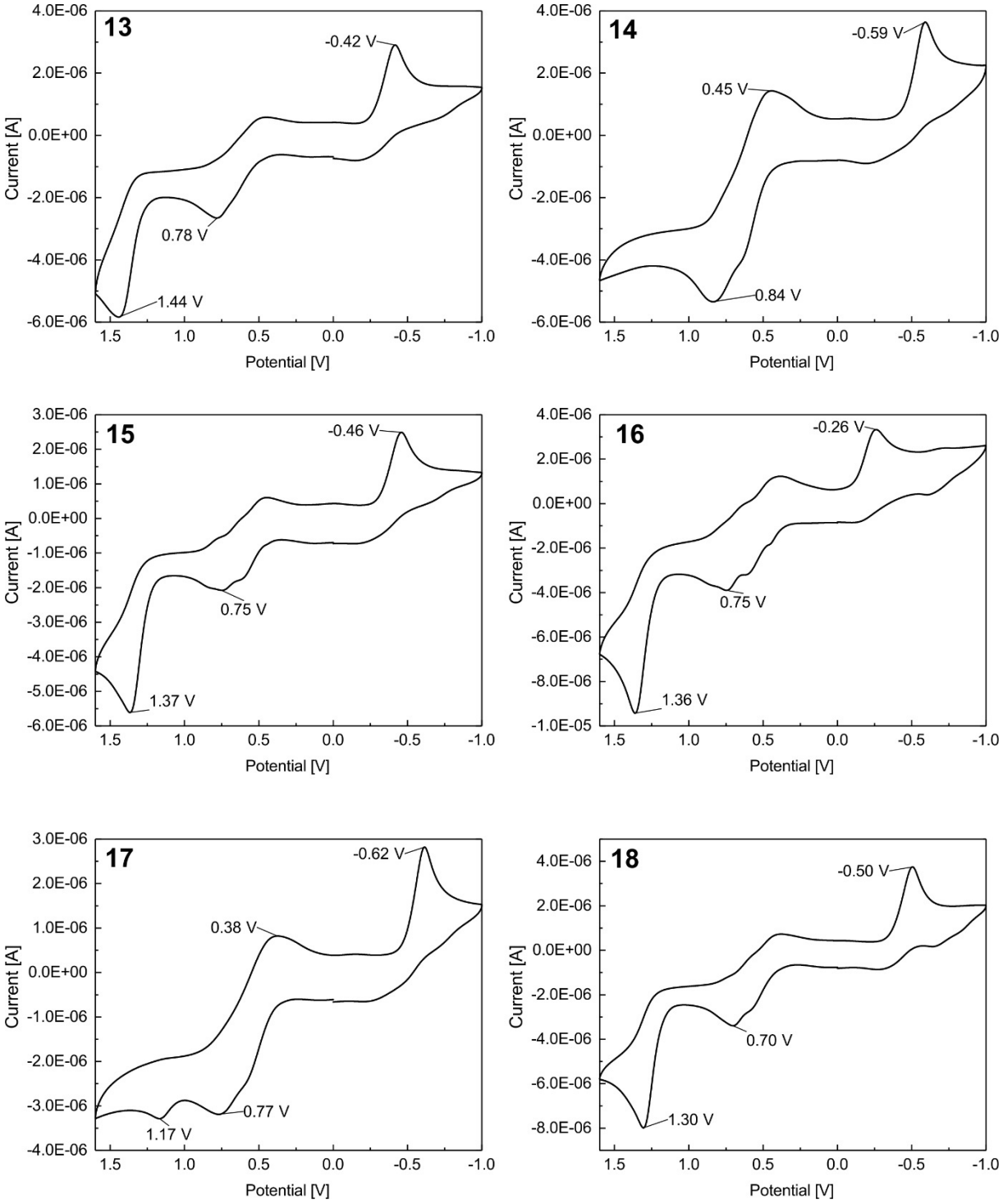

Figure S13. UV-Vis spectra of **3**, **8**, and **11** in PBS.

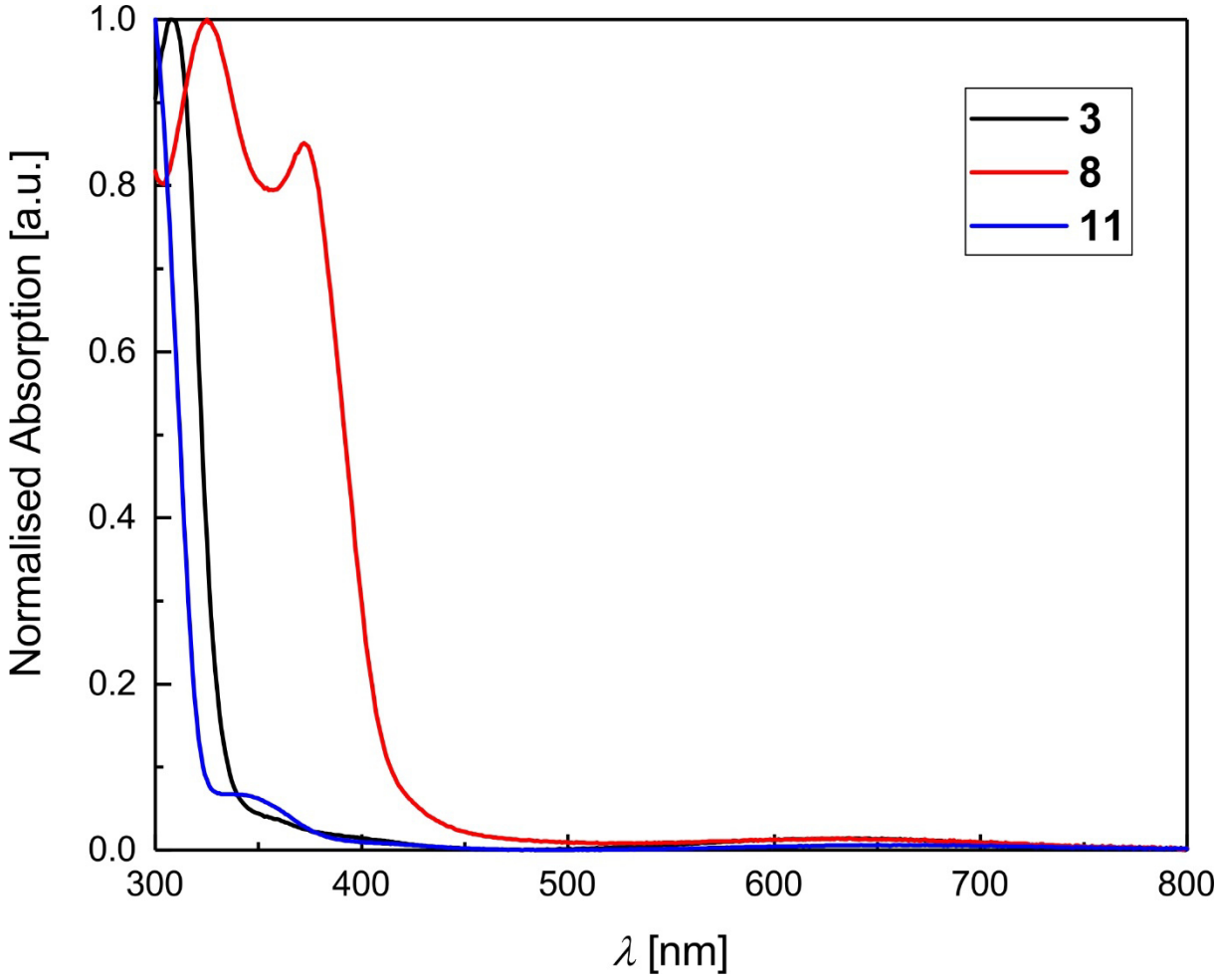

Figure S14. UV-Vis spectra of compounds **1**, **10**, and **14** (100 µM) in PBS at 37 °C at the indicated time points.

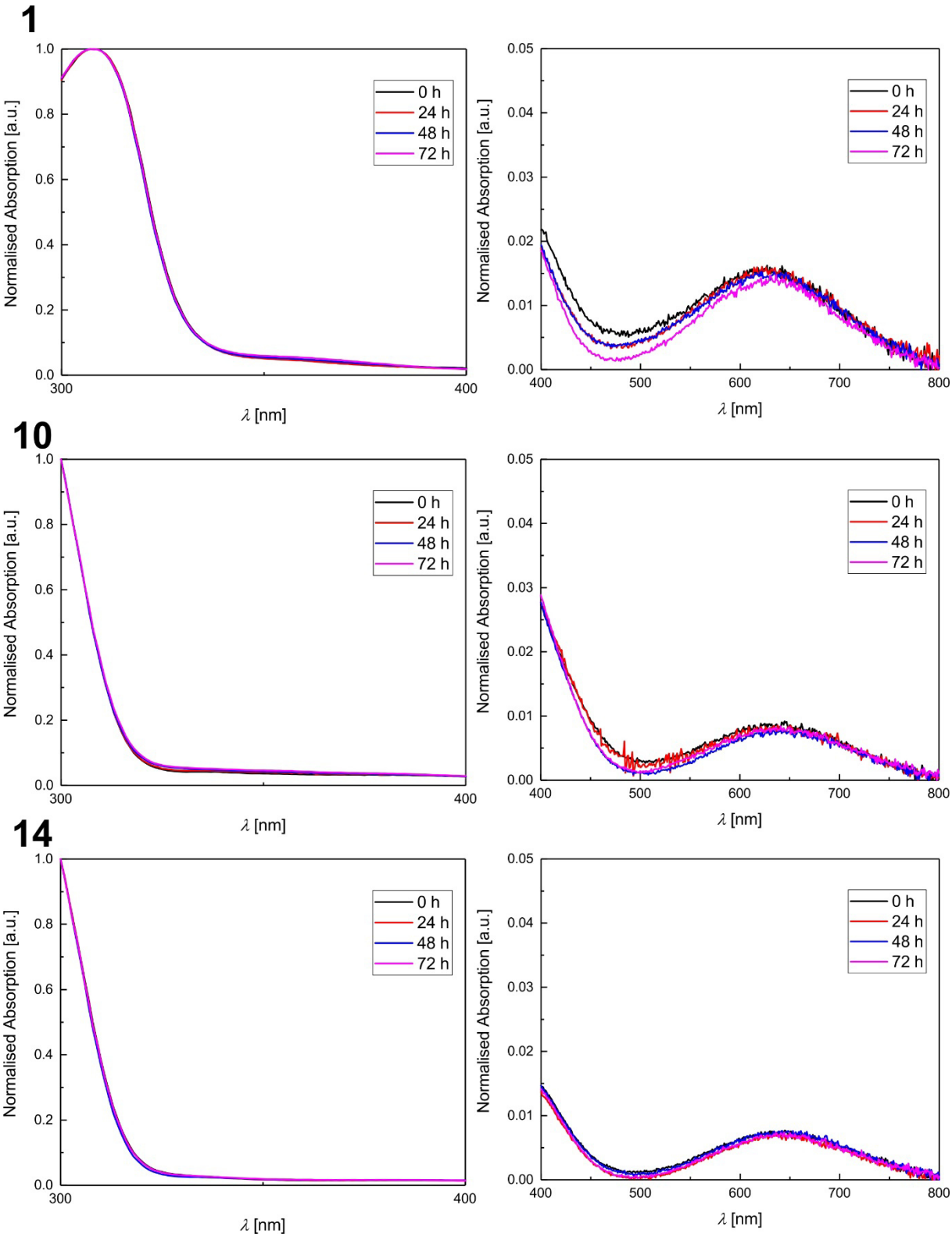

Figure S15. Relative ethidium bromide–DNA adduct fluorescence after pre-incubation with vehicle (0 µM) of **1**, **10**, **14**, and $CuSO_4$ (25, 50, 75, 100 µM) for 2 h. A decreased fluorescence indicates an interaction between DNA and test compound which prevents the intercalation of ethidium bromide molecules between the double-stranded SS-DNA. Values ± SD derived from at least three independent experiments with controls set to 100 %.

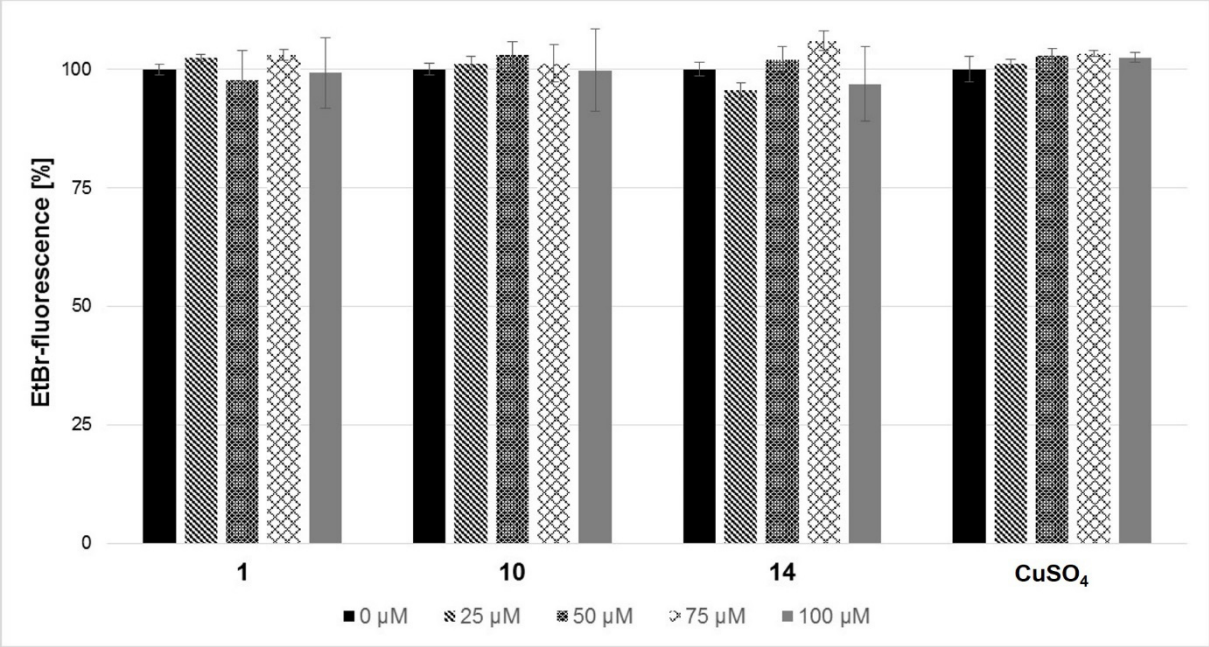

Figure S16. Electrophoretic mobility shift assay (EMSA) with circular pBR322 DNA. DNA was incubated with cis-platin (CDDP, top left), **1** (top right), **10** (bottom left), or **14** (bottom right) (0, 5, 10, 25, 50 µM) for 24 h and subjected to agarose gel electrophoresis followed by ethidium bromide staining. Supercoiled form (top) and open circular form (bottom). Pictures are representative for at least two independent experiments.

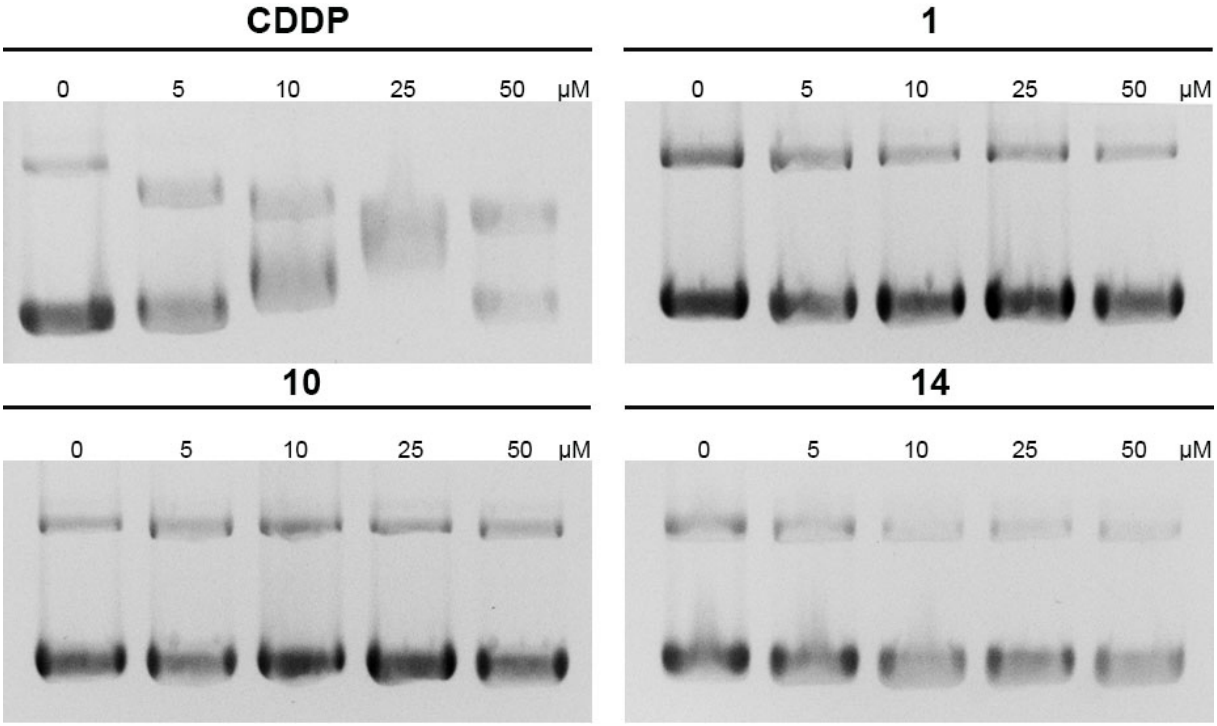

Figure S17. Effect of copper complexes **1–18**, $CuSO_4$, and HL11 on the relative superoxide levels in 518A2 melanoma cells after 24 h incubation as determined by NBT assays. The ROS production (%) was obtained as the mean ± standard deviation of six independent experiments with respect to untreated control cells set to 100 %.

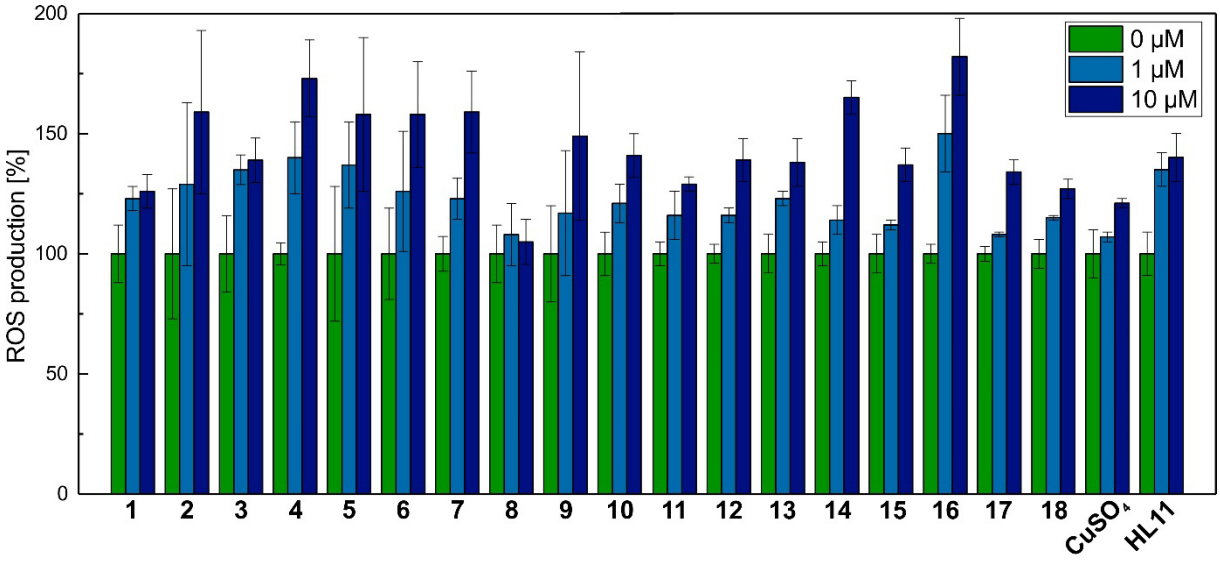

Figure S18. Mass spectrum (DIP, EI, pos.) of **4**.

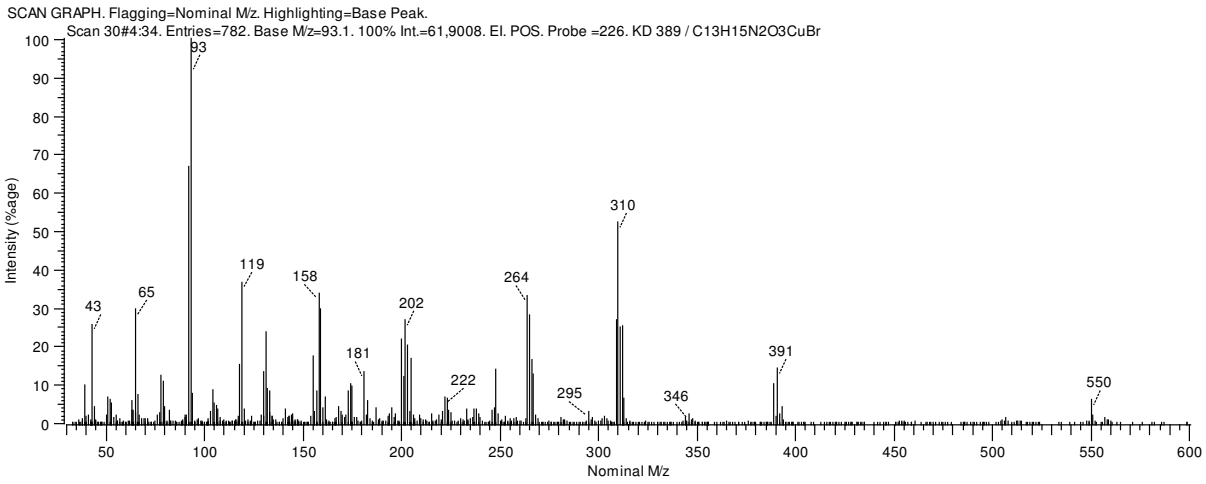

Figure S19. Mass spectrum (DIP, EI, pos.) of **5**.

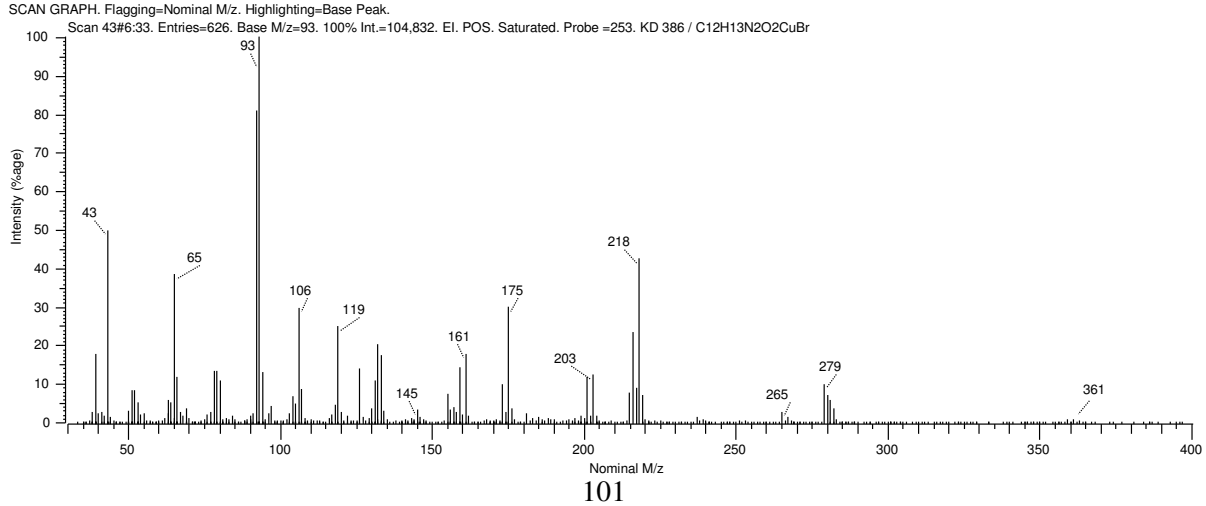

Figure S20. Mass spectrum (DIP, EI, pos.) of **6**.

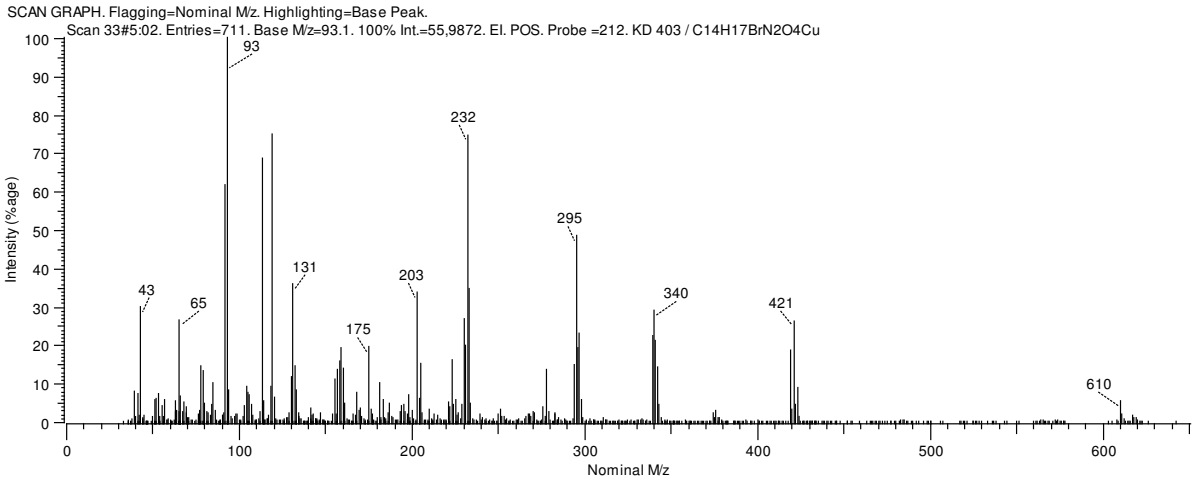

Figure S21. Mass spectrum (DIP, EI, pos.) of **7**.

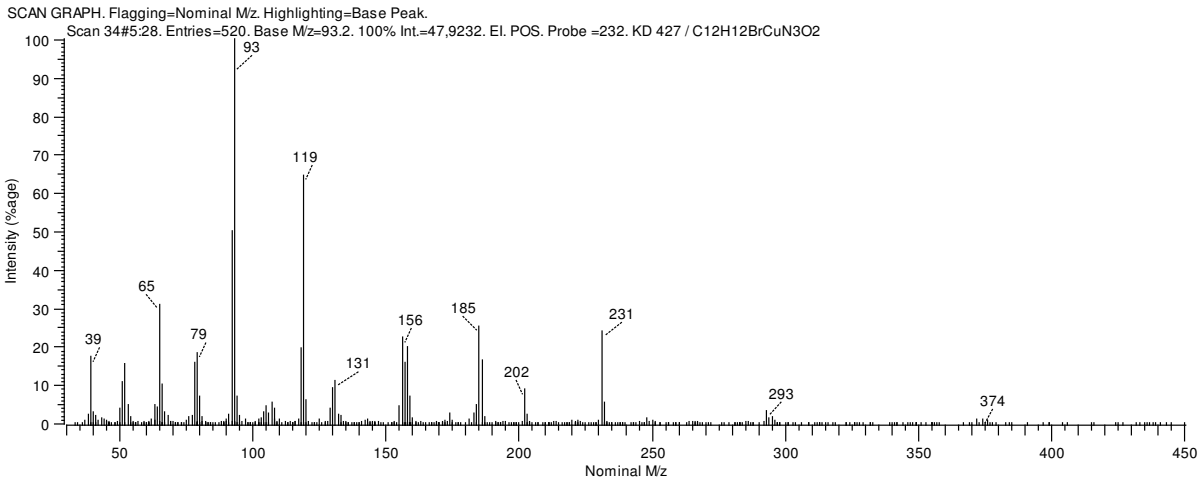

Figure S22. Mass spectrum (DIP, EI, pos.) of **8**.

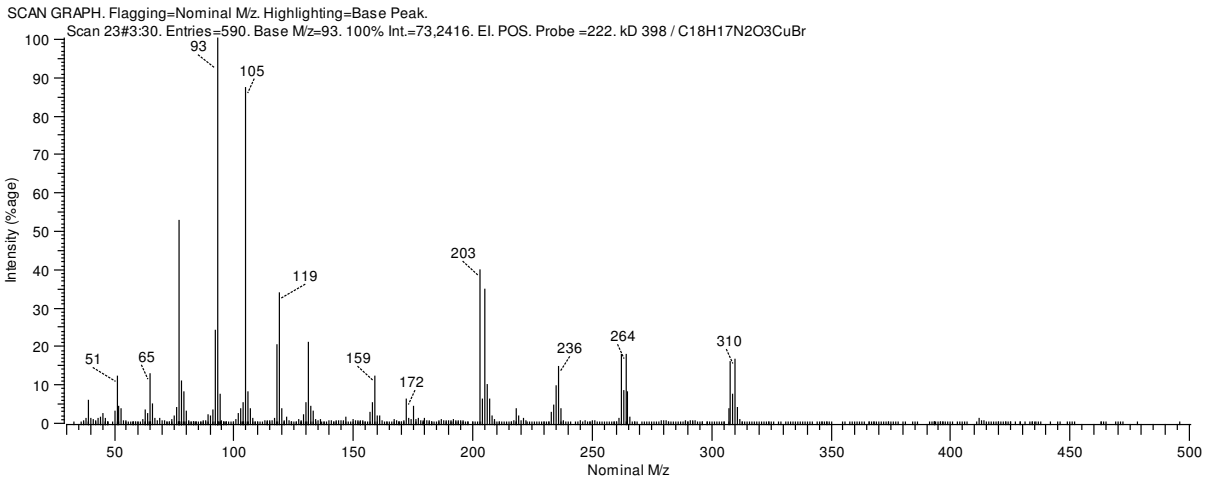

Figure S23. Mass spectrum (DIP, EI, pos.) of **9**.

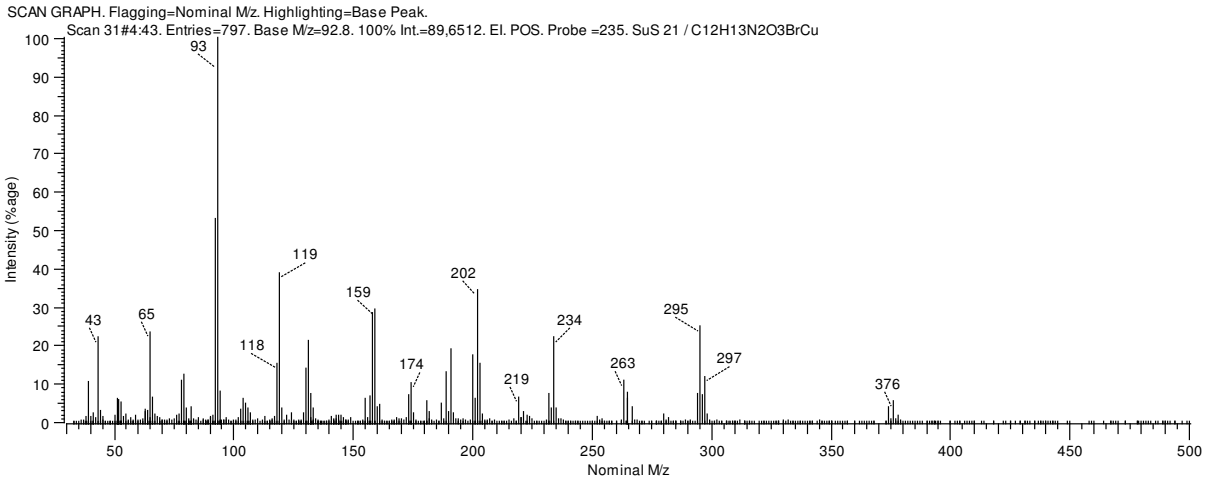

Figure S24. Mass spectrum (DIP, EI, pos.) of **10**.

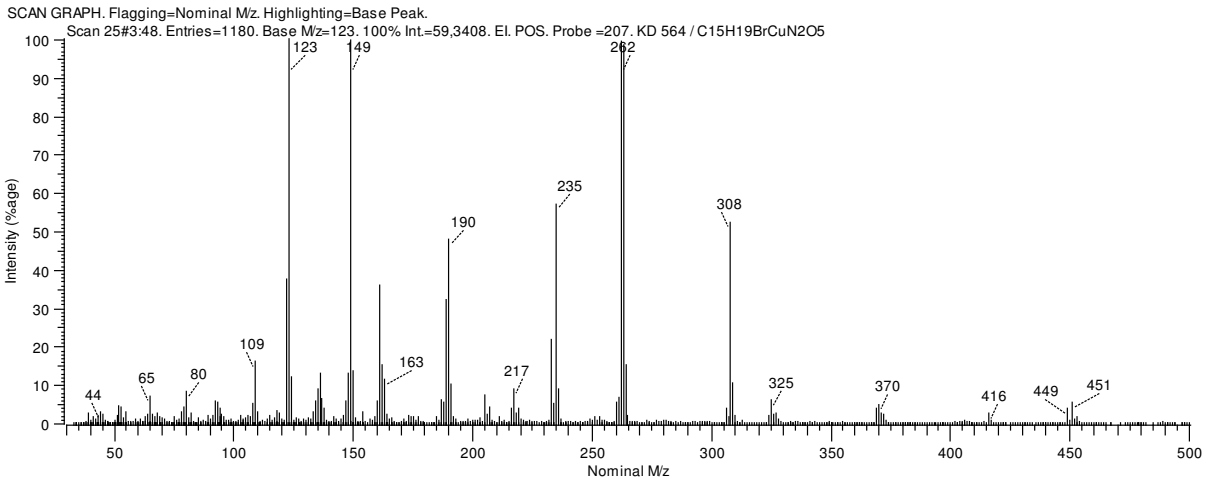

Figure S25. Mass spectrum (DIP, EI, pos.) of **11**.

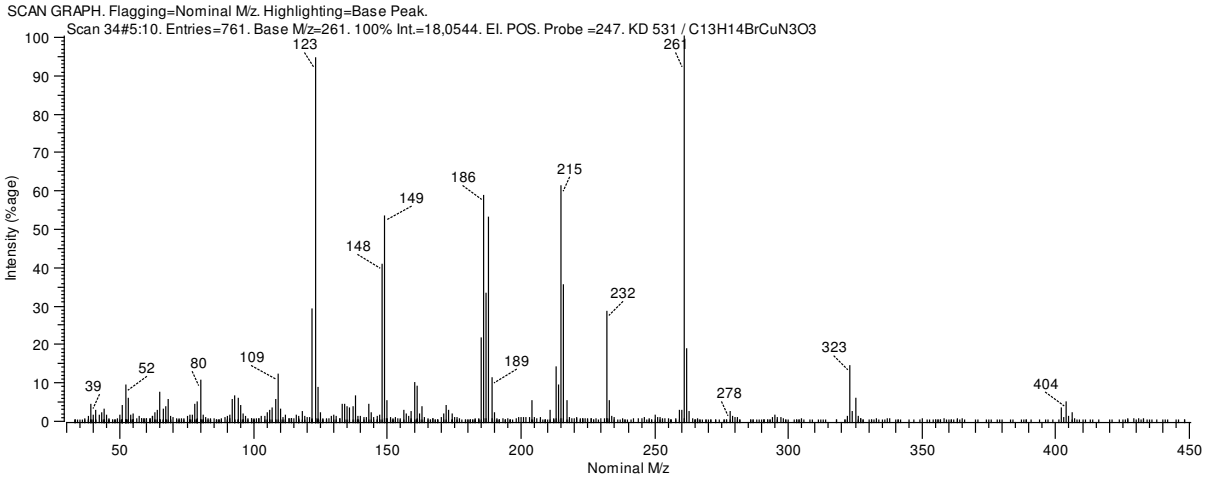

Figure S26. Mass spectrum (DIP, EI, pos.) of **12**.

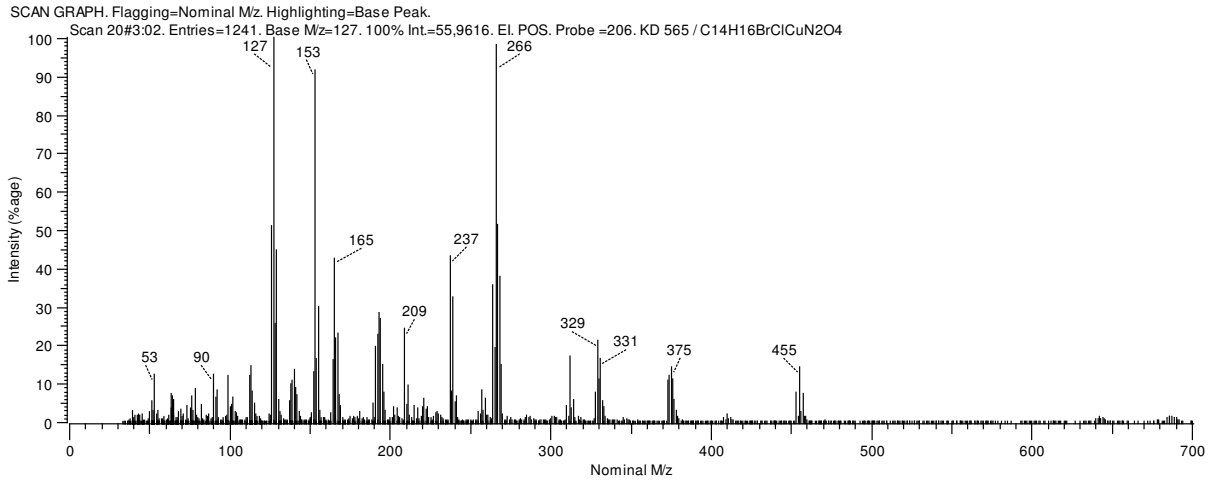

Figure S27. Mass spectrum (DIP, EI, pos.) of **13**.

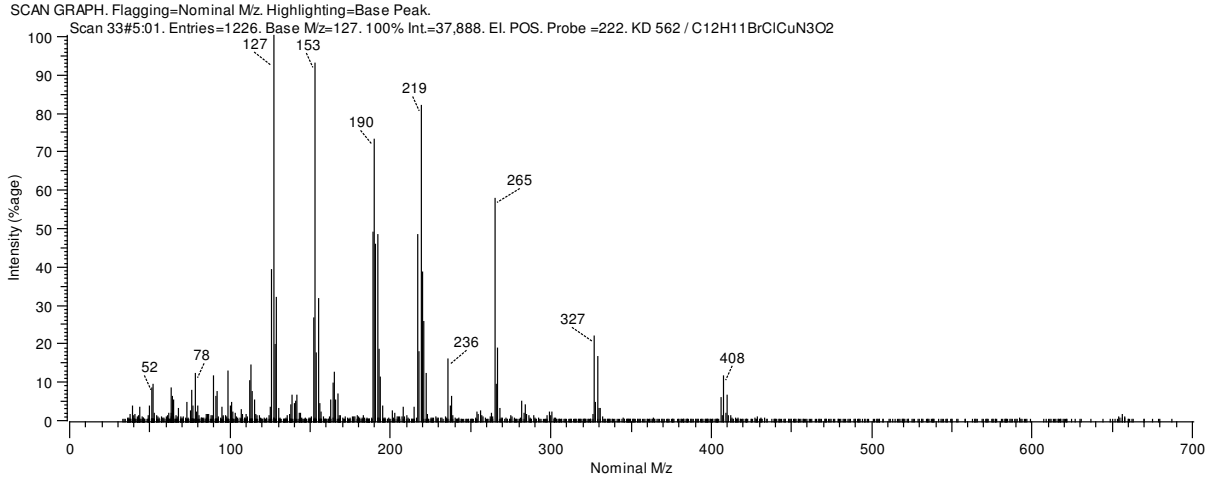

Figure S28. Mass spectrum (DIP, EI, pos.) of **14**.

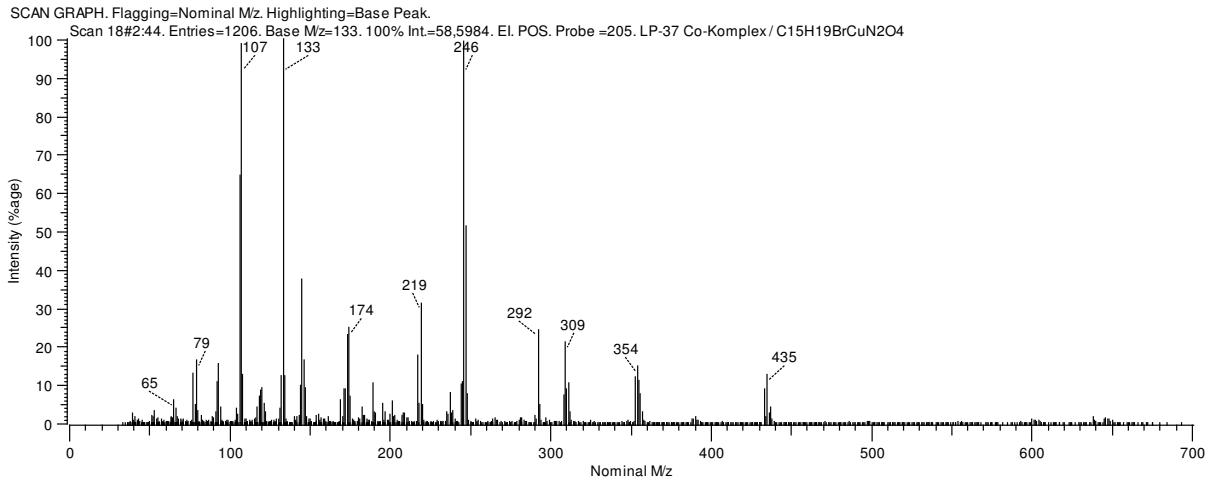

Figure S29. Mass spectrum (DIP, EI, pos.) of **15**.

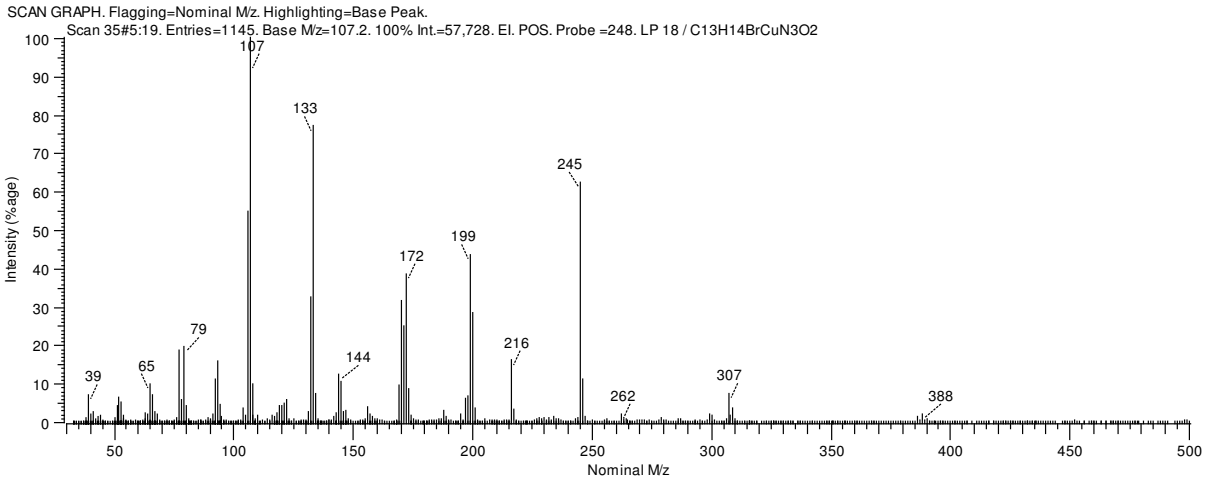

Figure S30. Mass spectrum (DIP, EI, pos.) of **16**.

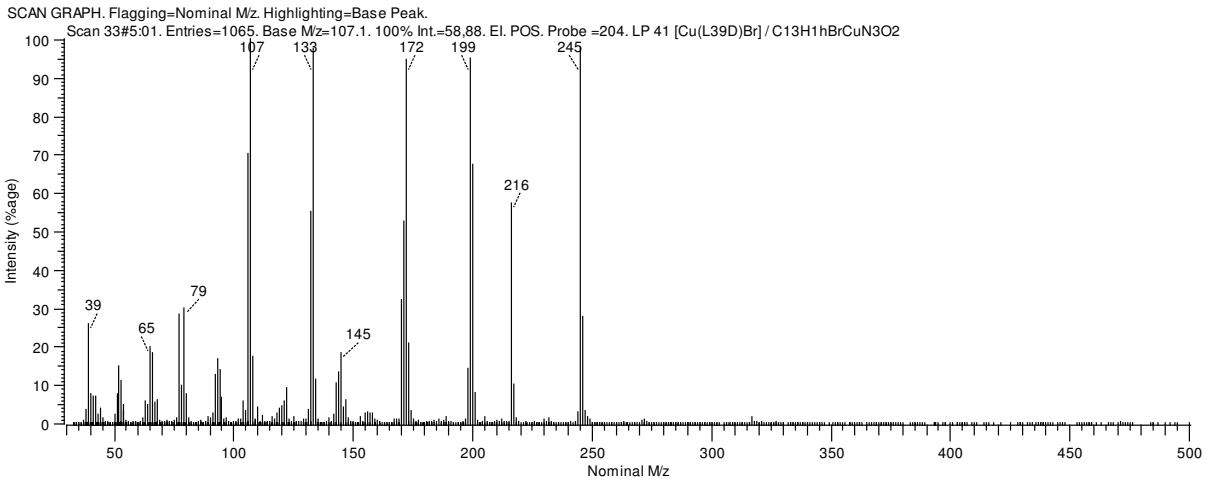

Figure S31. Mass spectrum (DIP, EI, pos.) of **17**.

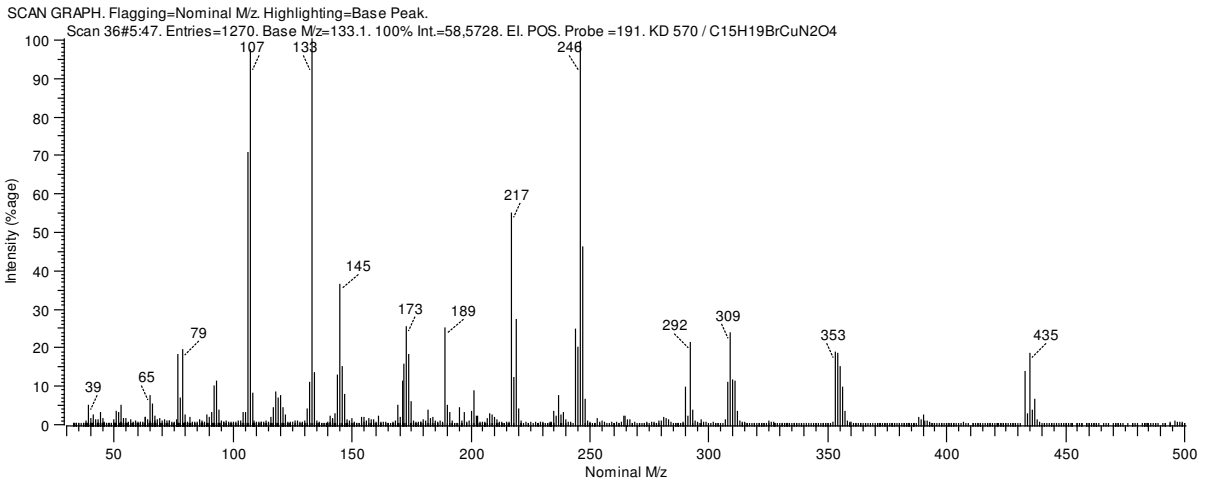

Figure S32. Mass spectrum (DIP, EI, pos.) of **18**.

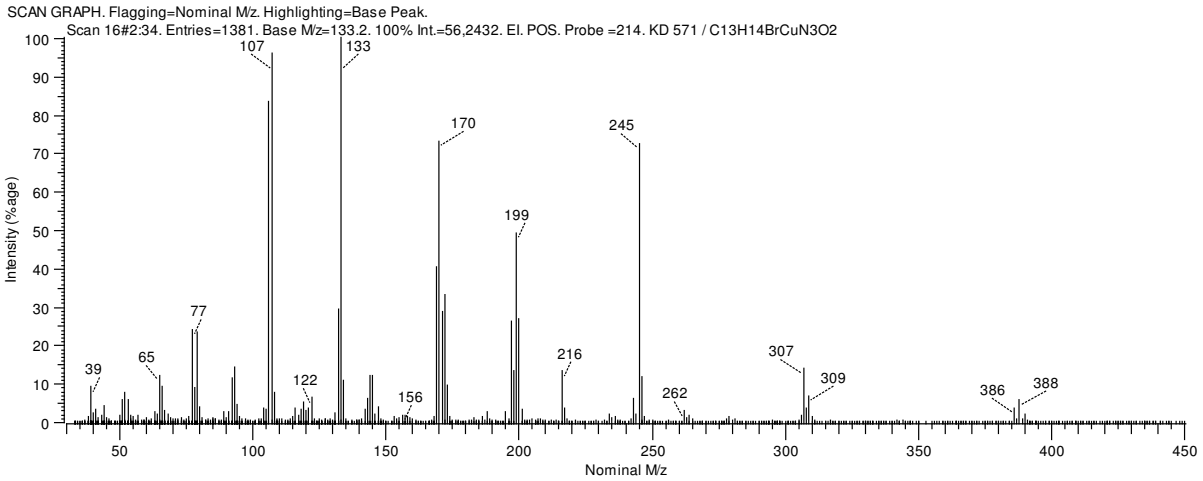

5.4. Publikation III

Synthesis and bioevaluation of new vascular-targeting and anti-angiogenic thieno [2,3-*d*]pyrimidin-4(*3H*)-ones

Madeleine Gold,[a] Leonhard Köhler,[a] Clarissa Lanzloth,[a] Ion Andronache,[b] Shrikant Anant,[c] Prasad Dandawate,[c] Bernhard Biersack,[a] Rainer Schobert*[a]

[a] Organic Chemistry Laboratory, University of Bayreuth, Universitaetsstrasse 30, 95440 Bayreuth, Germany

[b] Research Center for Integrated Analysis and Territorial Management, University of Bucharest, 4-12, Regina Elisabeta Avenue, Bucharest, 3rd District, 030018, Romania

[c] Department of Cancer Biology, University of Kansas Medical Center, 3901 Rainbow Boulevard, Kansas City, KS, 66160, USA

* Corresponding author, Email address: Rainer.Schobert@uni-bayreuth.de

Eur. J. Med. Chem. **2020**, 189, 112060-112075.

European Journal of Medicinal Chemistry 189 (2020) 112060

Contents lists available at ScienceDirect

European Journal of Medicinal Chemistry

journal homepage: http://www.elsevier.com/locate/ejmech

Research paper

Synthesis and bioevaluation of new vascular-targeting and anti-angiogenic thieno[2,3-*d*]pyrimidin-4(3*H*)-ones

Madeleine Gold [a], Leonhard Köhler [a], Clarissa Lanzloth [a], Ion Andronache [b], Shrikant Anant [c], Prasad Dandawate [c], Bernhard Biersack [a], Rainer Schobert [a, *]

[a] Organic Chemistry Laboratory, University Bayreuth, Universitaetsstrasse 30, 95440, Bayreuth, Germany
[b] Research Center for Integrated Analysis and Territorial Management, University of Bucharest, 4-12, Regina Elisabeta Avenue, Bucharest, 3rd District, 030018, Romania
[c] Department of Cancer Biology, University of Kansas Medical Center, 3901 Rainbow Boulevard, Kansas City, KS, 66160, USA

ARTICLE INFO

Article history:
Received 11 December 2019
Received in revised form
8 January 2020
Accepted 8 January 2020
Available online 9 January 2020

Keywords:
Thienopyrimidine
Microtubule binding agents
Vascular-disruptive agents
Anti-angiogenesis
Anticancer drugs

ABSTRACT

A series of forty-six 5,6-annulated 2-arylthieno [2,3-*d*]pyrimidin-4(3*H*)-ones were prepared as potentially pleiotropic anticancer drugs with variance in the tubulin-binding trimethoxyphenyl motif at C-2 of a thieno [2,3-*d*]pyrimidine fragment, enlarged by additional rings of different size and substitution. By assessing their cytotoxicity against various cancer cells, their influence on the polymerization of neat tubulin and the dynamics of microtubule and F-actin cytoskeletons, and their vascular-disrupting and anti-angiogenic activities *in vitro* and *in vivo*, structure-activity relations were identified which suggest the 3-iodo-4,5-dimethoxyphenyl substituted thienopyrimidine **2e** as a promising anticancer drug candidate for further research. 2020 Elsevier Ltd. All rights reserved.

1. Introduction

Tumor angiogenesis is a key step in the process of tumor growth and metastasis. As the survival of mammalian cells depends on a constant supply of oxygen and nutrients, they have to be located within 100–200 μm (the diffusion limit of oxygen) of a blood vessel [1]. Tumors, too, have to recruit (or create) new blood vessels by angiogenesis (or comparable, pathological processes) for growing beyond this size. Angiogenesis is regulated by a dynamic equilibrium of pro- and anti-angiogenic stimuli [2]. It is now widely believed that the extent of shifting it towards the pro-angiogenic side is, among other criteria, responsible for the rate of tumor growth [3]. Due to the imbalanced expression of angiogenic and anti-angiogenic factors, tumor blood vessels display an abnormal morphology and function and, therefore, differ from normal blood vessels. This makes them an interesting target for anti-tumoral therapy [4,5]. The morphological abnormalities of tumor vasculature mainly result from tumor endothelial cells (TEC) lacking organization as they are only loosely and discontinuously attached to the inner wall of the vessels without a real barrier-like function [6]. Tumor blood vessels were long considered to consist of normal, diploid endothelial cells recruited from neighboring vessels. However, recent studies confirmed that TEC feature several cytogenetic abnormalities, such as aneuploidy and abnormal centrosomes [7], which could explain the often observed resistance of TEC to chemotherapeutic agents [8]. The origin of these cytogenetically different TEC is still unknown. Transdifferentiation (common progenitor cell → TEC), fusion of tumor and endothelial cells, dedifferentiation (tumor cell → TEC), or gene transfer are conceivable explanations [5]. As a consequence of their abnormal morphology (leakiness, lack of pericytes and basement membrane) tumor blood vessels are more fragile and dependent on the cytoskeleton to maintain cell shape and polarization, making them more susceptible to microtubule-binding agents (MBA) [9]. MBA are widely employed in curative and palliative chemotherapies [10]. Microtubule stabilizing as well as destabilizing agents interfere with the regular formation and function of the mitotic spindle and, accordingly, block cell proliferation which is most detrimental for highly proliferating tumor cells. Preclinically, MBA can be identified by their vascular-disrupting and anti-angiogenic effects *in vitro* and *in vivo* [11–13]. An early observation was the sensitivity of

* Corresponding author.
E-mail address: Rainer.Schobert@uni-bayreuth.de (R. Schobert).

https://doi.org/10.1016/j.ejmech.2020.112060
0223-5234/

endothelial cells of growing capillaries to the toxic effects of colchicine [14]. A salient structural motif among the microtubule destabilizing agents that bind to the colchicine binding site is the 1,2,3-trimethoxyphenyl fragment as occurring in natural products such as combretastatin A-4 (CA4), podophyllotoxin, or steganacin, as well as synthetic ligands modelled on them [15,16]. A recent trend in optimizing antitumoral tubulin binders is their covalent conjugation with other antitumoral pharmacophores to afford pleiotropic drugs which are cheaper to make and less prone to unwanted drug-drug interference and resistance attrition when compared to combinatorial regimens. An example from our group were conjugates of CA4-analogues with hydroxamates that combine tubulin interference with histone deacetylase (HDAC) inhibition [17]. In the current paper we report on conjugates of the thieno[2,3-*d*]pyrimidone pharmacophore carrying variants of the archetypical tubulin binding oligomethoxyphenyl motif [18,19]. Thieno[2,3-*d*]pyrimidines have shown a broad range of therapeutically useful properties including antimicrobial [20,21], antiviral [22], antiinflammatory[23] [23], antianxiety [24]. and cancer cell autophagy inducing effects [25]. Fig. 1 depicts examples of highly antitumoral 2-arylthieno[2,3-*d*]pyrimidin-4(3*H*)-ones.

2. Results and discussion

2.1. Synthesis and characterization

Compounds **2a-j**, **3b-e**, **3g**, and **3i-j** were prepared by reaction of cyclohexyl- (**1a**) and cycloheptyl-thiophene derivatives (**1b**) and the respective aryl aldehydes according to literature procedures [26,27]. Similarly, reaction of *N*-ethoxycarbonylpiperidine derivative **1c** with the respective aryl aldehydes afforded compounds **4a-g**, **4j** [28], and **4k** [29] (Scheme 1).

N-Benzyloxycarbonylpiperidines **5a-c**, **5e**, **5i-j**, and **5l-m** were obtained by reacting **1d** with aryl aldehydes (Scheme 2). Their treatment with TFA and thioanisole afforded the piperidinium salts **6a-c**, **6e**, **6i-j**, and **6l-m**. The reaction of **6c** or **6e** with acryloyl chloride led to the acryl amides **7c** and **7e** while reaction with acetyl chloride gave the acetamides **8c** and **8e**.

2.2. Biological evaluation

Stock solutions of all test compounds were prepared at 10 mM in DMSO and stored for at most one week at −20 °C. They were, depending on the respective assay, diluted in ddH_2O, cell culture medium, or buffer. Compounds **2f**, **2h-j**, **4b**, **4d**, and **5a-c**, **5e**, **5i-j**, **5l-m** were not completely soluble in water, and thus excluded from *in vitro* and *in vivo* assays.

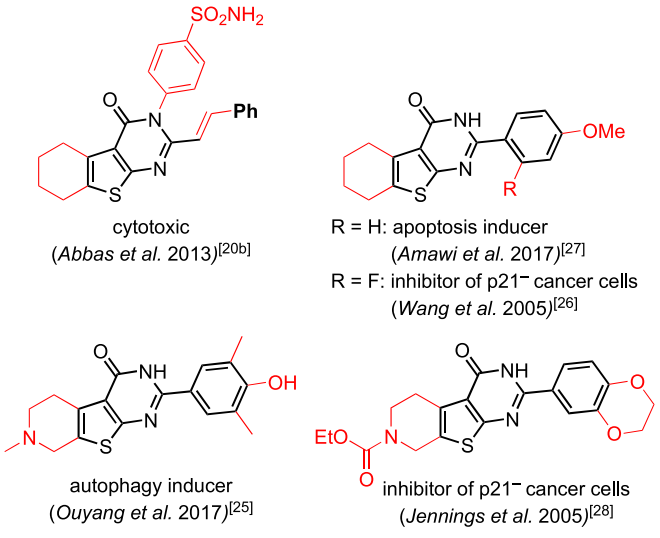

Fig. 1. Antitumoral 2-arylthieno[2,3-*d*]pyrimidin-4(3*H*)-ones.

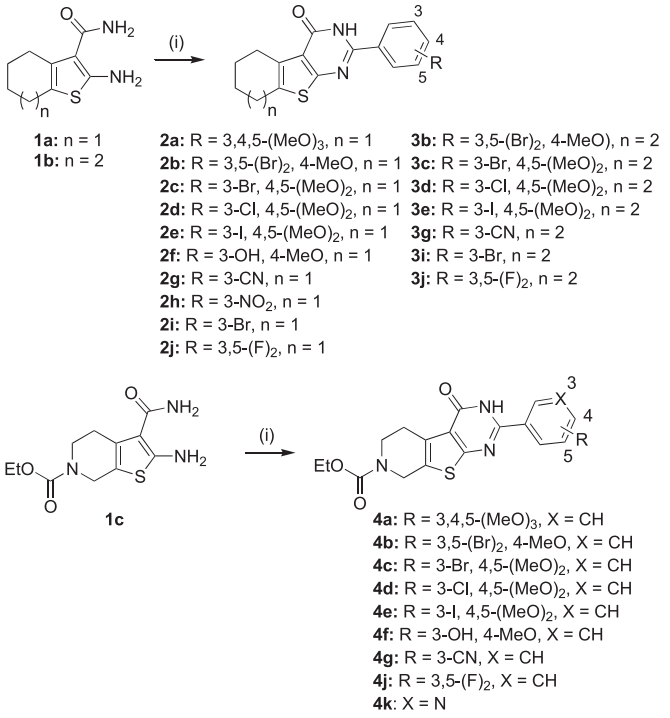

Scheme 1. Synthesis of 5,6-annulated 2-arylthieno [2,3-*d*]pyrimidin-4(3*H*)-ones **2**–**4**. Reagents and conditions: (i) aryl aldehyde, HCl, *n*-BuOH, 80 °C, 1 h, 30–92% (**2**, **3**) and 30–56% (**4**).

2.2.1. Inhibition of cancer cell proliferation

The thienopyrimidones were tested for their potential to inhibit the growth of a panel of four cancer cell lines from three different entities and one endothelial hybrid cell line (EA.hy926) using MTT assays. The most active compounds were also screened for toxic effects on non-malignant human adult dermal fibroblasts (HDFa) to estimate their selectivity for tumor cells. Table 1 summarizes their IC_{50} values including those obtained for the known antimitotic combretastatin A-4 (CA4) and vascular disruptive/anti-angiogenic axitinib. With the exception of compounds **3i**, **3j**, and **6a**, all thieno[2,3-*d*]pyrimidones gave dose-dependent inhibitory curves for the whole panel of malignant cell lines with IC_{50} values in the three-digit nanomolar to low micromolar concentration range. The structural parameters, i.e. the residues on the phenyl ring, the size of the cycloalkane in **2** and **3**, and the N-substituents in the piperidines **4**–**8**, were found to have a different bearing on the antiproliferative effect of the new thieno[2,3-*d*]pyrimidones. The substituents on the phenyl ring proved most important, with the **e** (3-iodo-4,5-dimethoxy) and **c** (3-bromo-4,5-dimethoxy) motifs leading to highly active compounds in all combinations with other structural features and against most of the tested cell lines, with the exception of **6c**. Substitution pattern **g** (3-cyano) in compound series **3** and **4**, as well as pattern **j** (3,5-difluoro) in series **3**, **4** and **6**, gave poor results. The replacement of the phenyl ring with pyridine as in **4k** abolished the cytotoxic effect. The size of the cycloalkyl ring in compound classes **2** (n = 1) and **3** (n = 2) was less decisive than the phenyl substitution with the exception of **3g** which is an outlier and far less active than **2g**. The N-substituent on the piperidine ring

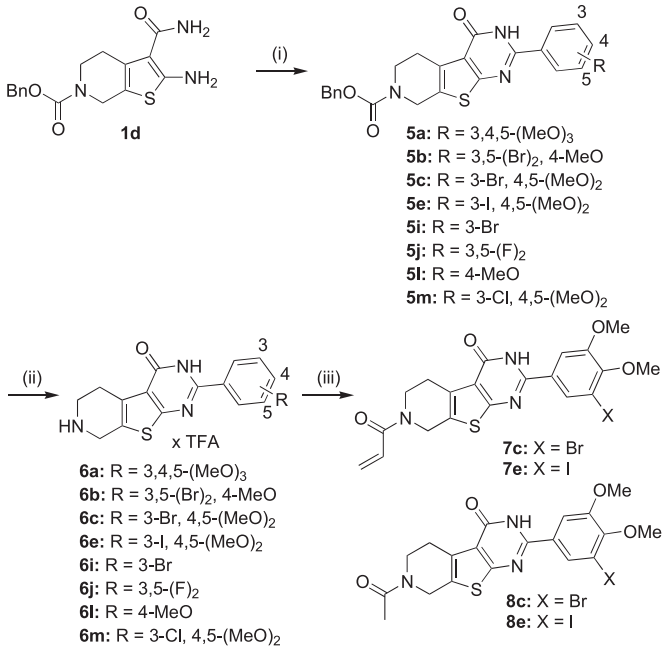

Scheme 2. Synthesis of 5,6-annulated 2-arylthieno [2,3-*d*]pyrimidin-4(3*H*)-ones **5**–**8**. Reagents and conditions: (i) aryl aldehyde, HCl, *n*-BuOH, 80 °C, 1 h, 30–58%; (ii) TFA, thioanisole, rt, 3 h, 41–89%; (iii) CH_2=CH–COCl (for **7c**, **7e**) or AcCl (for **8c**, **8e**), aqueous K_2CO_3, acetone, rt, 24 h, 42–94%.

of compounds **4** (-COEt), **7** (-HC=CHCO), and **8** (-COMe) appears to only slightly influence their cytotoxicity, as **4c**, **7c** and **8c**, like **4e**, **7e** and **8e** were of comparable activity in individual cell lines.

2.2.2. Inhibition of tubulin dynamics

Microtubules are hollow, tubular structures, which consist of α- and β-tubulin monomers. They are involved in numerous cellular processes including intracellular transport, cell motility, mechanical solidity, and mitosis [30]. As the disruption of the cellular tubulin dynamics interferes with the regular formation of an intact mitotic spindle, highly proliferating cells are hit hardest by MBA which are thus attractive antitumoral agents. A good deal of the new thieno[2,3-*d*]pyrimidones carry phenyl rings with substitution patterns derived from the trimethoxyphenyl motif present in various natural tubulin binders such as colchicine or CA4. They were screened for a potential interference with tubulin dynamics using purified pig brain tubulin (SI, Figs. 1S-5S). The most potent inhibitors of tubulin polymerization were, once more, those compounds with substitution pattern **e** (3-iodo-4,5-dimethoxy) at the phenyl ring (Fig. 2). Compounds **2e** and **4e** were selected for further mechanistic studies. The well performing compound **7e** was excluded for the moment only on grounds of its slightly lesser cytotoxicity.

2.2.3. Influence on the microtubule and actin cytoskeleton

The effect of compounds **2e** and **4e** on the microtubule cytoskeleton of EA.hy926 endothelial hybrid cells was assessed by

Table 1
Inhibitory concentrations IC_{50}[a] [μM] of compounds **2a-8e** when applied to EA.hy926 endothelial hybrid cells, cells of 518A2 melanoma, HT-29 and HCT-116 ^{wt} colon carcinomas, HCT-116$^{p53-/-}$ knockout mutant colon carcinoma, mdr KB-V1^{Vbl} cervix carcinoma, and human adult dermal fibroblasts HDFa.

	IC_{50} [μM]					
	EA.hy926	518A2	HCT-116 ^{wt}	HCT-116$^{p53-/-}$	KB-V1^{Vbl}	HDFa
2a	0.4 ± 0.03	0.2 ± 0.02	5.5 ± 0.9	0.3 ± 0.05	0.2 ± 0.02	>100
2b	1.0 ± 0.1	2.4 ± 0.3	0.8 ± 0.03	0.7 ± 0.1	0.7 ± 0.03	
2c	0.3 ± 0.01	0.3 ± 0.02	0.4 ± 0.02	0.5 ± 0.01	0.3 ± 0.04	
2d	0.4 ± 0.02	0.4 ± 0.01	0.5 ± 0.03	1.0 ± 0.1	0.3 ± 0.02	
2e	0.2 ± 0.01	0.1 ± 0.003	0.2 ± 0.05	0.1 ± 0.01	0.1 ± 0.01	>100
2g	1.2 ± 0.2	0.3 ± 0.02	0.7 ± 0.05	0.2 ± 0.02	1.9 ± 0.2	
3b	1.0 ± 0.1	0.4 ± 0.03	0.9 ± 0.1	1.0 ± 0.1	1.4 ± 0.2	
3c	0.3 ± 0.03	0.2 ± 0.02	0.8 ± 0.07	0.3 ± 0.02	0.3 ± 0.06	
3d	0.2 ± 0.03	0.7 ± 0.02	0.3 ± 0.03	0.8 ± 0.02	0.7 ± 0.01	
3e	0.2 ± 0.02	0.2 ± 0.01	0.3 ± 0.03	0.2 ± 0.04	0.6 ± 0.06	
3g	13.1 ± 1.7	9.4 ± 0.9	3.8 ± 0.7	1.0 ± 0.1	18.2 ± 2.6	
3i	>100	>100	>100	>100	>100	
3j	>100	>100	>100	>100	>100	
4a	0.2 ± 0.02	0.2 ± 0.01	0.6 ± 0.02	0.5 ± 0.04	0.8 ± 0.1	
4c	0.2 ± 0.03	0.5 ± 0.02	0.4 ± 0.02	0.5 ± 0.04	0.3 ± 0.03	
4e	0.1 ± 0.01	0.1 ± 0.01	0.3 ± 0.01	0.1 ± 0.01	0.1 ± 0.1	13.1 ± 1.7
4f	4.5 ± 0.6	2.3 ± 0.1	1.8 ± 0.1	5.6 ± 0.5	2.2 ± 0.3	
4g	12.5 ± 1.7	4.1 ± 0.2	4.9 ± 0.03	4.3 ± 0.1	7.1 ± 0.6	
4j	4.0 ± 0.4	5.2 ± 0.7	1.6 ± 0.2	4.2 ± 0.5	5.3 ± 0.4	
4k	>100	80.0 ± 2.0	32.5 ± 5.3	39.1 ± 5.2	35.2 ± 6.3	
6a	>100	>100	>100	>100	>100	
6b	1.0 ± 0.2	5.8 ± 0.2	1.5 ± 0.03	1.5 ± 0.1	6.2 ± 0.6	
6c	11.5 ± 0.8	9.3 ± 0.2	10.6 ± 0.6	7.4 ± 0.9	2.0 ± 0.2	
6e	1.0 ± 0.1	1.4 ± 0.2	1.0 ± 0.01	0.8 ± 0.05	2.5 ± 0.2	
6i	1.6 ± 0.1	1.7 ± 0.2	1.6 ± 0.1	1.4 ± 0.07	2.2 ± 0.2	
6j	5.4 ± 0.2	5.7 ± 0.2	6.9 ± 0.5	3.6 ± 0.2	6.5 ± 0.5	
6l	3.8 ± 0.2	3.8 ± 0.4	4.0 ± 0.2	2.2 ± 0.3	6.7 ± 0.3	
6m	6.3 ± 0.2	16.4 ± 1.2	>100	10.8 ± 1.2	17.0 ± 1.3	
7c	0.9 ± 0.03	0.7 ± 0.09	4.3 ± 0.7	4.6 ± 0.5	1.9 ± 0.2	
7e	0.4 ± 0.02	0.2 ± 0.01	2.0 ± 0.2	0.7 ± 0.05	1.2 ± 0.1	
8c	0.9 ± 0.03	0.5 ± 0.04	0.4 ± 0.03	0.5 ± 0.03	2.8 ± 0.7	
8e	0.1 ± 0.01	0.3 ± 0.03	0.2 ± 0.02	0.4 ± 0.03	0.6 ± 0.03	
CA4	0.01 ± 0.002[b]	0.02 ± 0.001[b]	0.003 ± 0.0002[b]	0.002 ± 0.0002	0.004 ± 0.0001	>100
Axitinib	6.1 ± 0.1	4.4 ± 0.2	1.5 ± 0.1	1.6 ± 0.3	12.9 ± 0.5	>100

[a] Values are the means ± SD determined in four independent experiments and derived from dose-response curves after 72 h incubation using the MTT assay.
[b] Schmitt et al. [17].

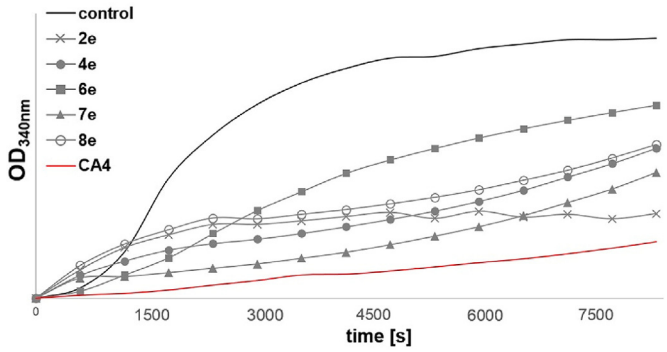

Fig. 2. Inhibition of tubulin polymerization by the 3-iodo-4,5-dimethoxyphenyl-substituted compounds **2e, 4e, 6e, 7e** and **8e** (10 μM each) as determined by a turbidimetric cell-free tubulin assay. CA4 (10 μM) was used as a positive control. Negative controls were treated with an equivalent amount of vehicle (DMSO). Data are representative of at least two independent experiments.

immunofluorescence staining (Fig. 3). The solvent-treated control cells showed well defined microtubules, while CA4 had a distinct destabilizing effect, even at concentrations as low as 25 nM. There were no tubular structures left, with most of the tubulin evenly spread throughout the cytoplasm. At higher concentrations (50 nM) most of the cells showed characteristic signs of apoptosis such as nuclear breakdown and blebbing. Surprisingly, treatment with the trimethoxyphenyl-substituted derivative **2a** did not affect the microtubule cytoskeleton. Upon treatment with lower concentrations of the 3-iodo-4,5-dimethoxyphenyl compounds **2e** and **4e** the microtubules appeared even more intense, but also shorter in comparison to the solvent-treated control cells. At higher concentrations, this fragmentary structure of the microtubules was even more obvious and the number of multinucleated cells (indicating the induction of a *mitotic catastrophe*) increased rapidly.

The cellular effects of MBA are not limited to the destruction of microtubules and the resulting mitotic block or vascular disrupting effects, they also affect the cellular motility [31]. The depolymerization of microtubules leads to an increased activation of RhoA, resulting in the formation of so-called actin *Stress Fibers,* which provide an additional morphological stabilization for the cells, yet reduce their mobility [32,33]. Results from immunofluorescence staining of the actin cytoskeleton of EA.hy926 endothelial hybrid cells treated with CA4, **2a**, **2e** or **4e** (Fig. 4) are consistent with those from staining of the tubulin cytoskeleton. After treatment with sublethal doses of CA4, **2e** and **4e** EA.hy926 cells showed distinct actin *Stress Fibers*, whereas treatment with the same concentration of reference compound **2a** did not alter the cytoskeletal arrangement.

2.2.4. Influence on the cell cycle

During the cell cycle, microtubules alternate between periods of growth and shrinkage via exchange of tubulin subunits, with the turnover being particularly high at the onset of mitosis [34]. Destabilizing MBA bind to cognate binding sites of α- or β-tubulin and prevent the formation of specific microtubule contacts. As a result, the mitotic spindle cannot form correctly, the cell cycle arrests in the G2/M-phase, and cells may consequently undergo apoptosis. We examined the influence of **2e** and **4e** on the cell cycle progress of EA.hy926 endothelial hybrid cells by FACS analysis (Fig. 5). Both compounds led to an arrest of the cell cycle in G2/M phase which in the case of **4e** exceeded even that by CA4 in magnitude. As the interference of **2e** and **4e** with neat tubulin (Fig. 2) and with cellular microtubules (Fig. 3) was less distinct

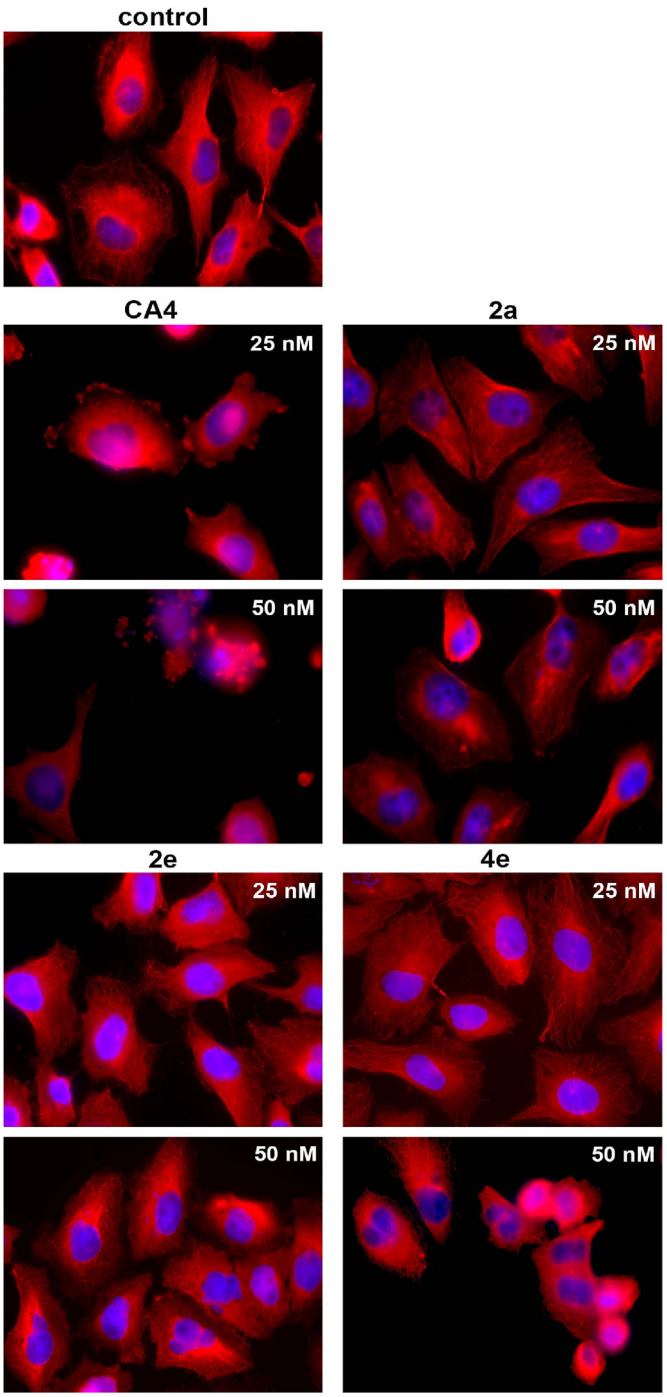

Fig. 3. Effect of compounds **2a**, **2e**, and **4e** on the microtubule cytoskeleton of EA.hy926 endothelial hybrid cells after 24 h of treatment under cell culture conditions. CA4 was used as a positive control, and the negative controls were treated with an equivalent amount of the solvent DMSO. Images are representative of at least five independent assays. Magnification 630 × .

when compared with that of CA4, other factors beyond microtubule destabilization might contribute to their pronounced G2/M arrest of EA.hy926 endothelial hybrid cells. Like CA4, **2e** and **4e** led to a concentration-dependent increase of apoptotic cells (sub-G1 fraction), which we identified as an apoptotic event by means of caspase-3/7 activation assays (*cf.* SI, Fig. 6S).

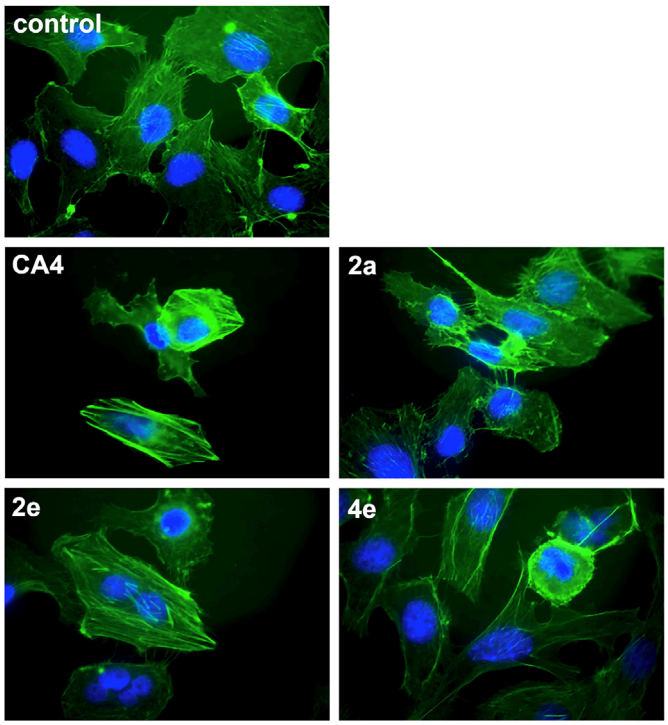

Fig. 4. Effect of compounds **2a**, **2e**, and **4e** (50 nM each) on the actin cytoskeleton of EA.hy926 endothelial hybrid cells. Negative controls were treated with an equivalent amount of solvent (DMSO), CA4 (50 nM) served as a positive control. Images are representative of at least five independent assays. Magnification 630 × .

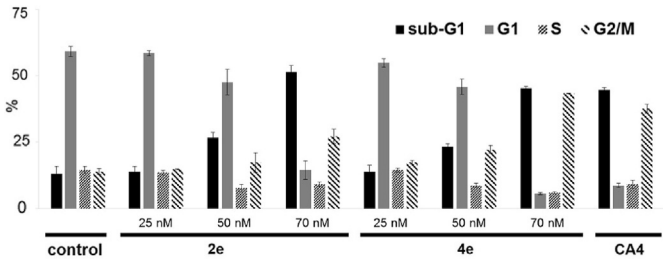

Fig. 5. Concentration-dependent effects of **2e** and **4e** on the cell cycle progress of EA.hy926 endothelial hybrid cells after 24 h of treatment. Positive control: CA4 (70 nM for 24 h); negative control: cells treated with an equivalent volume of DMSO. Values are the means ± SD of three independent experiments.

2.2.5. *Molecular docking into the colchicine binding site of β-tubulin*

To explore reasons for their different tubulin interaction and cytotoxicity on a molecular level, we docked the compounds **2a**, **2e**, **4e**, and CA4 into the colchicine binding site of β-tubulin (Table 2, Fig. 7S), based on the X-ray structure of β-tubulin (PDB ID: 1SA0). The docking results were inconclusive insofar as they did not mirror the distinctly different effects of the four compounds on microtubules, the F-actin cytoskeleton and on the overall viability of tumor and endothelial cells. Even with an error margin of ca. ± 1 kcal/mol, the calculated binding energies for **2a**, **2e**, and **4e** exceeded that of CA4.

2.2.6. *Inhibition of CDK1*

Thienopyrimidones, related to those studied here, were shown to inhibit kinases [35–38], and in particular cyclin-dependent kinases [19,39], a family of highly conserved serine/threonine protein kinases present in all known eukaryotes, and essential for cell cycle regulation, gene transcription, mRNA processing and other cellular events [40,41]. CDK require the association with a regulatory cyclin-subunit for activity [41]. Three CDK (1, 2, and 4) and their activating cyclins (A, B, D, and E) are essential for the mammalian cell cycle [42]. CDK4/cyclin D and CDK2/cyclin E/A complexes are essential for the passage through G1 and S phase of the cell cycle, whereas CDK1/cyclin A/B complexes trigger the onset of G2 and M phase [43]. CDK1 is the only non-redundant CDK which can cover for all other CDK in case of loss or inhibition, making it an interesting target for antitumor therapy [44–46]. Titration of the active enzyme/cyclin complex with increasing concentrations of thienopyrimidones **2e** and **4e** (Fig. 6) revealed a kinase inhibitory effect which, though inferior to that of staurosporine, is significant and might contribute to their biological effects and their strong G2/M arrest in particular.

Table 2
Results from molecular docking of **2a**, **2e**, and **4e** into the colchicine binding site of β-tubulin (PDB ID: 1SA0) by means of Autodock Vina software.

cmpd	binding energy [kcal/mol]	No. of H-bonds	amino acids involved
CA4	−5.4	4	Asp26 Glu27 Gln43
2a	−6.9	1	Leu248
2e	−7.2	1	Leu248
4e	−6.6	3	Lys352 Asn349

2.2.7. *Vascular-disruptive effects*

Due to its disorganized structure and hyperpermeability, tumor vasculature is a unique target for chemotherapeutic agents [47], which either inhibit the formation of new tumor blood vessels (anti-angiogenic effect), or disrupt existing ones (vascular-disruptive effect). CA4 exerts both effects [48–53]. As the thienopyrimidones **2e** and **4e** maintain the 4′,5′-dimethoxyphenyl motif of CA4, we also tested them for vascular-disrupting effects *in vitro* and *in ovo*. Both compounds **2e** and **4e** showed vascular-disrupting

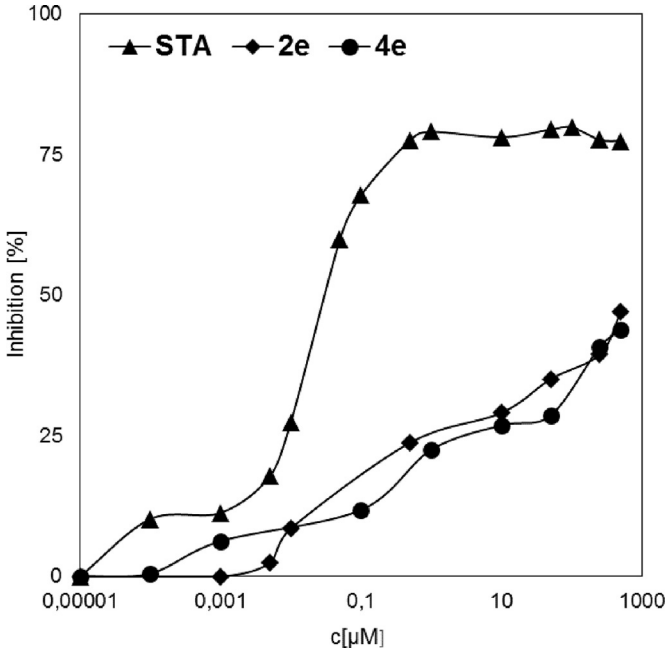

Fig. 6. Inhibition of kinase activity of CDK1/CyclinA2 complex by compounds **2e** and **4e**, determined via luminescence-based ADP-Glo™ Kinase-Assay (Promega). The known CDK1 inhibitor staurosporine (STA) was used as a positive control. Negative controls treated with the solvent were set to 100% activity, and relative inhibition (100 [%] - activity [%]) was calculated. All experiments were carried out at least in duplicate.

effects on vessel-like structures formed by EA.hy926 endothelial hybrid cells grown on a matrigel matrix (Fig. 7). In tests on the vasculature in the chorioallantoic membrane of fertilized hen eggs (CAM assays) derivative **2e** led to interesting effects (Fig. 8). After incubation with **2e** for 6 h, hemorrhage, mainly of smaller vessels and capillaries was observed. However, the membrane eventually recovered within 24 h after application. CA4, in contrast, led to a complete, irreversible shutdown of the developing vasculature by 24 h post application, and to a >90% mortality rate of the chicken embryos. There was also a weak vascular-disrupting effect detectable upon treatment with **4e** for 24 h.

2.2.8. *Anti-angiogenic effects*

Quite a few classic MBA, e.g. taxol, 2-methoxyestradiol, colchicine or CA4, show anti-angiogenic activity *in vitro* and *in vivo* [54–58], which often requires lower, non-cytotoxic concentrations when compared to those initiating vascular-disrupting effects [59,60]. The cellular mechanisms of the anti-angiogenic effect of MBA are not fully understood. But as tumor-neovascularization occurs primarily by sprouting, a process particularly dependent on endothelial cell-adhesion, migration, and cell-cell interactions, it is likely due to their ability to disturb at least one of these processes, which strongly depend on the reliability of the cellular tubulin dynamics [59–61]. Others suppose the inhibition of specific signaling pathways to be responsible for anti-angiogenic effects of MBA [62–64]. Since thienopyrimidones are known inhibitors of protein kinases, including such involved in angiogenesis, like Tie-2 or VEGF [37,65], we tested compounds **2e** and **4e** for inhibitory effects on the formation of vessel-like structures from EA.hy926 endothelial hybrid cells on matrigel, as well as on the angiogenesis in the chorioallantoic membrane of fertilized chicken embryos and of transgenic zebrafish embryos. Both compounds **2e** and **4e** showed anti-angiogenic effects in tube formation assays with EA.hy926 endothelial hybrid cells seeded on matrigel (Fig. 9) and in CAM-assays (Fig. 10). In both assays anti-angiogenic effects could be observed at lower concentrations than vascular-disruptive effects (Figs. 7 and 8; tube formation assay: 150 nM vs. 250 nM, CAM assay: 5 nmol vs. 15 nmol). An anti-angiogenic effect of compound **2e** was also confirmed by an *in vivo* assay using transgenic zebrafish embryos. Upon treatment with **2e**, the relative area of SIV, which develops via angiogenic processes between 24 hpf and 72 hpf, was concentration-dependently reduced by 18% (250 nM), or 28% (500 nM) in comparison to the SIV area of solvent-treated control embryos (Fig. 11). Compound **4e** was too toxic to be tested, as was CA4. Therefore the known angiogenesis inhibitor axitinib had to be used as a positive control, despite its different mechanism of action (selective VEGF inhibitor).

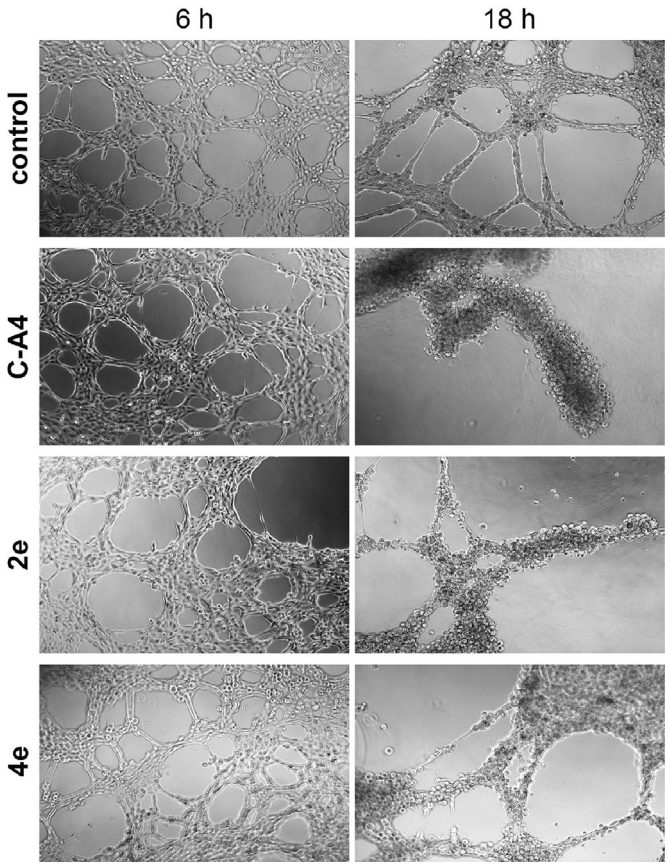

Fig. 7. Disruptive effects of **2e** and **4e** (250 nM each) on vessel-like structures formed by EA.hy926 endothelial hybrid cells grown in Endothelial Cell Growth Medium 2 (PromoCell) on matrigel for 6 h before incubation with the test compounds for 12 h. Negative controls were treated with DMSO. Positive control: CA4 (250 nM). Images are representative of three independent experiments. Vitality of the treated cells was >80% compared to DMSO treated control cells. Magnification 100 × .

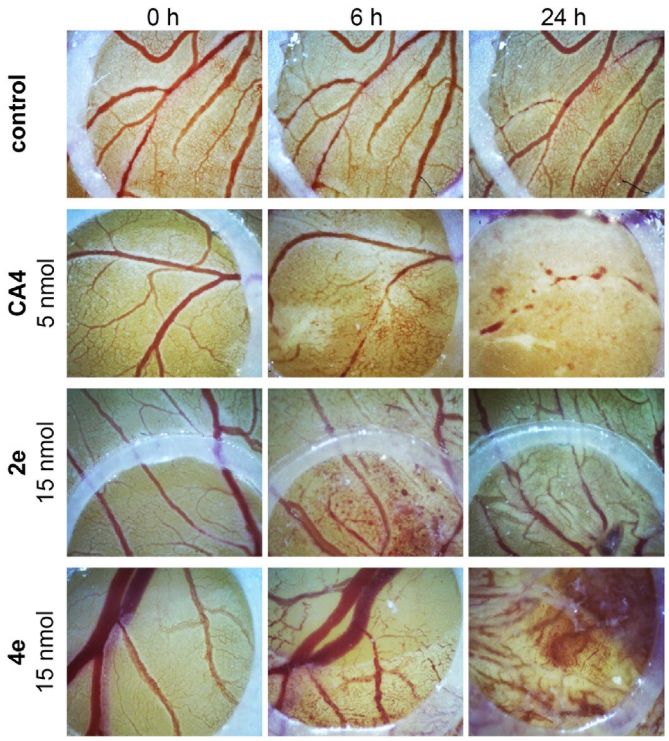

Fig. 8. Vascular-disruptive effects of **2e** and **4e** (15 nmol), and CA4 (5 nmol), topically applied on the blood vessels of the chorioallantoic membrane of fertilized chicken eggs inside a ring of silicon foil (ø 5 mm) after 0 h, 6 h, and 24 h. Negative controls were incubated with DMSO. Images are representative of three independent assays. Magnification 60 × . (For interpretation of the references to color in this figure legend, the reader is referred to the Web version of this article.)

3. Conclusions

The intention of this study was the covalent conjugation of a cytotoxic thieno[2,3-*d*]pyrimidone fragment with the oligomethoxyphenyl motif, typical of tubulin binders such as combretastatin A4 (CA4) and colchicine, to achieve multimodal drugs. A conclusion we can draw from the observed structure-activity relations is that the original 3,4,5-trimethoxyphenyl pattern, present in these two lead compounds, does not give the best results in

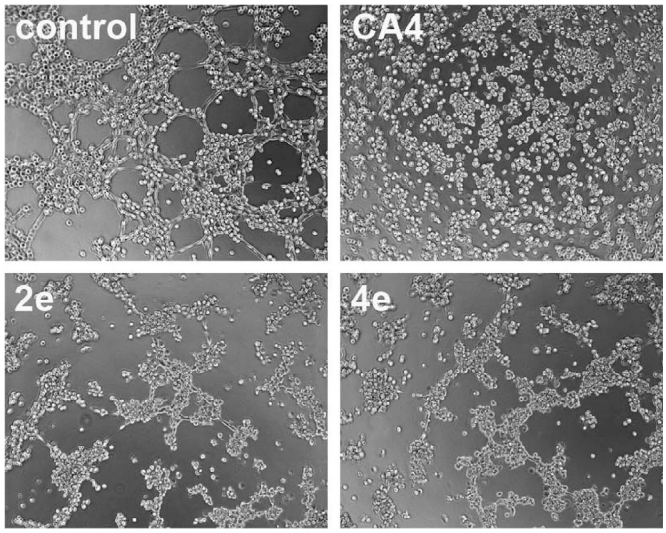

Fig. 9. Effects of compounds **2e** and **4e** (150 nM) on the formation of tubular, blood vessel-like structures by EA.hy926 endothelial hybrid cells when grown on thin layers of matrigel for 6 h. Negative controls were treated with DMSO. Positive control: CA4 (100 nM). Images are representative of at least three independent experiments. Vitality of the treated cells was >95% compared to DMSO treated cells. Magnification 100 × .

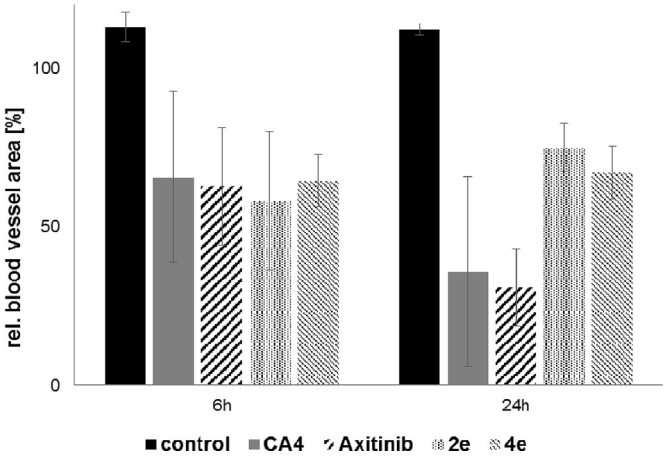

Fig. 10. Relative blood vessel area of the chorioallantoic membrane of fertilized chicken eggs after treatment with CA4 (2.5 nmol), axitinib (5 nmol), or **2e** and **4e** (5 nmol each) after 6 h and 24 h as determined by fractal analysis. Negative controls were treated with DMSO. Vessel area at t = 0 was set to 100%. Values ± SD are derived from at least three independent runs.

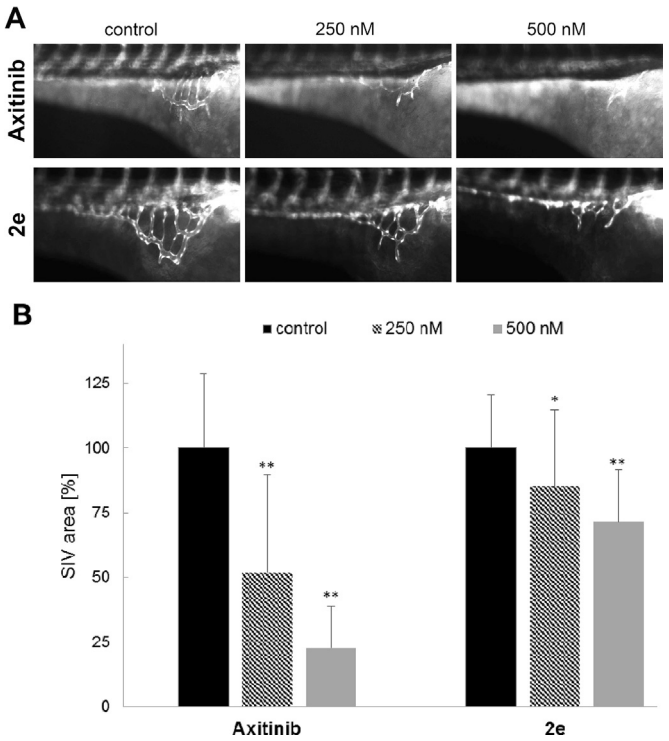

Fig. 11. Effect of **2e** in a zebrafish angiogenesis assay. 24 h post fertilization (hpf) old transgenic *Tg(fli1a:EGFP)* zebrafish embryos were exposed to 250 nM or 500 nM of **2e** or the positive control axitinib for 48 h at 28 °C in embryo medium. **A**: Images are representative of at least 20 independent experiments (magnification 6.3 ×). **B**: The area covered by subintestinal veins (SIV) was quantified using ImageJ software. The SIV area of zebrafish treated with an equivalent amount of DMSO was set to 100%. Values ± SD are derived from at least 20 independent experiments. Significant deviations from control data were determined using a *t*-test. *p > 0.01, **p > 0.001.

conjugates with 5,6-annulated thieno [2,3-*d*]pyrimidin-4(3*H*)-ones. Conjugate **2a**, for instance, cannot even be considered a bimodal drug, as it exhibited none of the typical effects on the microtubule and F-actin cytoskeletons of endothelial cells. Its cytotoxicity is likely to originate mainly from the thienopyrimidone moiety. The general trend in cytotoxicities across the structural subclasses of the new conjugates is that 3-bromo-4,5-dimethoxyphenyl (motif **c**) and 3-iodo-4,5-dimethoxyphenyl (motif **e**) substitution at C-2 of the thieno [2,3-*d*]pyrimidin-4(3*H*)-one leads to derivatives with distinctly submicromolar IC_{50} values in all tested cell lines. These compounds are also potent inhibitors of the polymerization of neat tubulin (e.g. **2e**, **4e**, **7e**), they induce alterations in the microtubule and F-actin cytoskeletons (e.g. **2e**, **4e**) and they cause a G2/M cell cycle arrest, which is more pronounced than that initiated by CA4, probably due to additional effects typical of thienopyrimidones [66], such as the observed inhibition of CDK1/cyclin A. The lead compound CA4 exhibits vascular-disruptive, as well as anti-angiogenic effects [48–52]. The thienopyrimidones **2e** and **4e** also showed such effects in tube formation and CAM assays, as well as in zebrafish angiogenesis assays. It is worthy of note that the destruction of blood vessels and capillaries in the CAM of fertilized chicken eggs caused by compound **2e** was reversible. It might be used for replacing irregular tumor vasculature by normal blood vessels in order to better apply chemotherapeutics. When applied in lower concentrations, compounds **2e** and **4e** also showed anti-angiogenic effects in tube formation and in CAM assays, derivative **2e** additionally in transgenic zebrafish embryos. This compound is proof of the validity of the concept to generate pleiotropic drugs by covalent combination of individual pharmacophores, albeit with the potential necessity to structurally optimise the latter, but also with the option to obtain genuinely new effects. Compounds **2e** and **4e** might thus serve as a starting point for the next generation of multimodal thienopyrimidone drugs.

4. Experimental

4.1. Chemistry

Compounds **2a**, **2h**, **3i**, **4a**, **4k**, **5a**, and **5l** are known and were prepared according to literature procedures [25–29]. Analytical data of these compounds were in agreement with the published data. The starting compounds and pure solvents were purchased from the usual sources and were used without further purification. Melting points: Gallenkamp apparatus (uncorrected). Absorption

and fluorescence measurements were run using a plate reader. Cell cycle analysis was done using a flow cytometer. Fluorescence images were obtained using Zeiss Imager A1 AX10 (microtubules, actin) and Leica MZ10F (zebrafish) microscopes. IR spectra were measured on a PerkinElmer Spectrum One FT-IR spectrophotometer equipped with an ATR sampling unit. NMR spectra were run on a Bruker Avance 300 spectrometer. Chemical shifts are given in parts per million (δ) downfield from Me_4Si as internal standard and coupling constants (*J*) are given in Hz. Mass spectra were measured on a Varian MAT 311A (EI). Elemental analyses were performed with an Elementar UNICUBE (Elementar Analysensysteme GmbH).

4.1.1. 2-(3,5-Dibromo-4-methoxyphenyl)-5,6,7,8-tetrahydrobenzothieno [2,3-d]pyrimidin-4(3H)-one, $C_{17}H_{14}Br_2N_2O_2S$, (2b)

3-Amino-4,5,6,7-tetrahydrobenzo [*b*]thiophene-2-carboxamide (294 mg, 1.5 mmol) and 3,5-dibromo-4-methoxybenzaldehyde (293 mg, 1.0 mmol) were dissolved in 1-butanol (10 mL) and conc. HCl (0.1 mL) was added. After stirring for 1 min at 80 °C a precipitate was formed and more 1-butanol (10 mL) was added to the suspension whereupon the precipitate dissolved. The reaction mixture was stirred at 80 °C for 1 h. After cooling, the precipitate was collected, washed with 1-butanol and water and dried in vacuum. Yield: 280 mg (0.60 mmol, 60%); off-white solid of m.p. 348 °C; υ_{max} (ATR)/cm^{-1} 3005, 2935, 2856, 1652, 1589, 1567, 1552, 1526, 1505, 1477, 1463, 1420, 1385, 1346, 1334, 1298, 1267, 1254, 1196, 1175, 1155, 1109, 1067, 1016, 988, 964, 888, 871, 848, 817, 805, 781, 746, 715, 665, 638, 618; ^{1}H NMR (300 MHz, $CDCl_3$/DMSO-d_6) δ 1.7–1.9 (4 H, m), 2.6–2.7 (2 H, m), 2.9–3.0 (2 H, m), 3.84 (3 H, s), 8.37 (2 H, s), 12.3–12.4 (1 H, br s); ^{13}C NMR (75.5 MHz, $CDCl_3$/DMSO-d_6) δ 21.6, 22.3, 24.6, 25.0, 60.1, 117.6, 121.0, 130.3, 130.8, 131.5, 133.0, 148.3, 155.4, 158.8, 162.6; *m/z* (%) 472 (54) [M^+], 470 (100) [M^+], 468 (51) [M^+], 444 (17), 442 (38), 440 (18); Anal. Calcd. for $C_{17}H_{14}Br_2N_2O_2S$: C, 43.43; H, 3.00; N, 5.96; S, 6.82. Found: C, 43.59; H, 3.02; N, 5.91; S, 6.97.

4.1.2. 2-(3-Bromo-4,5-dimethoxyphenyl)-5,6,7,8-tetrahydrobenzothieno [2,3-d]pyrimidin-4(3H)-one, $C_{18}H_{17}BrN_2O_3S$, (2c)

3-Amino-4,5,6,7-tetrahydrobenzo [*b*]thiophene-2-carboxamide (294 mg, 1.5 mmol) and 3-bromo-4,5-dimethoxybenzaldehyde (245 mg, 1.0 mmol) were dissolved in 1-butanol (10 mL) and conc. HCl (0.1 mL) was added. The reaction mixture was stirred at 80 °C for 1 h. After cooling down, the formed precipitate was collected, washed with 1-butanol and water and dried in vacuum. Yield: 185 mg (0.44 mmol, 44%); pale yellow solid of m.p. 328 °C; ^{1}H NMR (300 MHz, $CDCl_3$) δ 1.8–1.9 (4 H, m), 2.7–2.8 (2 H, m), 3.0–3.1 (2 H, m), 3.91 (3 H, s), 3.98 (3 H, s), 7.74 (1 H, s), 8.00 (1 H, s), 12.6–12.7 (1 H, br s); ^{13}C NMR (75.5 MHz, $CDCl_3$) δ 22.2, 23.0, 25.3, 25.9, 56.5, 60.7, 111.6, 117.9, 121.1, 123.8, 129.2, 131.6, 134.0, 149.2, 150.0, 153.8, 160.8, 164.7; *m/z* (%) 422 (100) [M^+], 420 (99) [M^+], 407 (15), 405 (16), 394 (38), 392 (39), 171 (24); Anal. Calcd. for $C_{18}H_{17}BrN_2O_3S$: C, 51.31; H, 4.07; N, 6.65; S, 7.61. Found: C, 51.45; H, 4.10; N, 6.43; S, 7.64.

4.1.3. 2-(3-Chloro-4,5-dimethoxyphenyl)-5,6,7,8-tetrahydrobenzothieno [2,3-d]pyrimidin-4(3H)-one, $C_{18}H_{17}ClN_2O_3S$, (2d)

Compound **2d** was prepared analogously to **2c** from 3-amino-4,5,6,7-tetrahydrobenzo [*b*]thiophene-2-carboxamide (147 mg, 0.75 mmol) and 3-chloro-4,5-dimethoxybenzaldehyde (100 mg, 0.5 mmol). Yield: 103 mg (0.27 mmol, 54%); off-white solid of m.p. 315–316 °C; υ_{max} (ATR)/cm^{-1} 2936, 2837, 1645, 1579, 1557, 1532, 1508, 1485, 1471, 1428, 1417, 1393, 1349, 1315, 1302, 1257, 1233, 1196, 1176, 1151, 1098, 1070, 1052, 1017, 997, 965, 924, 877, 861, 846, 804, 776, 748, 721, 695, 662, 639, 625, 603; ^{1}H NMR (300 MHz, $CDCl_3$) δ 1.8–1.9 (4 H, m), 2.6–2.7 (2 H, m), 3.0–3.1 (2 H, m), 3.92 (3 H, s), 3.98 (3 H, s), 7.74 (1 H, s), 7.94 (1 H, s), 12.7–12.8 (1 H, br s); ^{13}C NMR (75.5 MHz, $CDCl_3$) δ 22.2, 23.0, 25.3, 25.9, 56.5, 60.8, 110.9, 120.9, 121.2, 128.5, 128.7, 131.7, 134.0, 148.2, 150.0, 153.9, 160.9, 164.7; *m/z* (%) 378 (38) [M^+], 376 (100) [M^+], 350 (8), 348 (27); Anal. Calcd. for $C_{18}H_{17}ClN_2O_3S$: C, 57.37; H, 4.55; N, 7.43; S, 8.51. Found: C, 57.38; H, 4.55; N, 7.50; S, 8.63.

4.1.4. 2-(3-Iodo-4,5-dimethoxyphenyl)-5,6,7,8-tetrahydrobenzothieno [2,3-d]pyrimidin-4(3H)-one, $C_{18}H_{17}IN_2O_3S$, (2e)

Compound **2e** was prepared analogously to **2c** from 3-amino-4,5,6,7-tetrahydrobenzo [*b*]thiophene-2-carboxamide (147 mg, 0.75 mmol) and 3-iodo-4,5-dimethoxybenzaldehyde (146 mg, 0.5 mmol). Yield: 70 mg (0.15 mmol, 30%); pale yellow solid of m.p. 334–335 °C; υ_{max} (ATR)/cm^{-1} 2933, 2837, 1653, 1591, 1570, 1552, 1537, 1506, 1481, 1462, 1443, 1425, 1393, 1345, 1331, 1301, 1252, 1234, 1195, 1148, 1136, 1102, 1069, 1044, 1015, 998, 964, 926, 892, 865, 851, 823, 783, 741, 720, 680, 664, 626; ^{1}H NMR (300 MHz, $CDCl_3$) δ 1.8–1.9 (4 H, m), 2.7–2.8 (2 H, m), 3.0–3.1 (2 H, m), 3.89 (3 H, s), 3.97 (3 H, s), 7.71 (1 H, s), 8.09 (1 H, s), 12.2–12.3 (1 H, br s); ^{13}C NMR (75.5 MHz, $CDCl_3$) δ 22.2, 23.0, 25.3, 26.0, 56.4, 60.6, 92.4, 112.6, 121.1, 129.4, 130.0, 131.6, 134.1, 149.8, 151.7, 152.6, 160.6, 164.6; *m/z* (%) 468 (100) [M^+], 440 (21).

4.1.5. 2-(3-Hydroxy-4-methoxyphenyl)-5,6,7,8-tetrahydrobenzothieno [2,3-d]pyrimidin-4(3H)-one, $C_{17}H_{16}N_2O_3S$, (2f)

Compound **2f** was prepared analogously to **2c** from 3-amino-4,5,6,7-tetrahydrobenzo [*b*]thiophene-2-carboxamide (147 mg, 0.75 mmol) and isovanillin (76 mg, 0.5 mmol). Yield: 73 mg (0.22 mmol, 44%); pale yellow solid of m.p. 339–340 °C; υ_{max} (ATR)/cm^{-1} 3100, 2933, 2839, 1701, 1643, 1594, 1517, 1491, 1434, 1337, 1260, 1203, 1159, 1087, 1023, 964, 929, 849, 815, 763, 733, 708, 654, 642, 619; ^{1}H NMR (300 MHz, $CDCl_3$/MeOD) δ 1.8–1.9 (4 H, m), 2.7–2.8 (2 H, m), 2.9–3.0 (2 H, m), 3.91 (3 H, s), 6.95 (1 H, d, $J = 8.5$ Hz), 7.49 (1 H, s), 7.50 (1 H, d, $J = 8.5$ Hz); ^{13}C NMR (75.5 MHz, $CDCl_3$/MeOD) δ 22.6, 23.3, 25.5, 25.8, 56.3, 111.7, 114.2, 120.3, 121.3, 124.4, 131.6, 134.2, 147.0, 151.4, 152.6, 160.1; *m/z* (%) 328 (100) [M^+], 313 (20), 300 (72).

4.1.6. 2-(3-Cyanophenyl)-5,6,7,8-tetrahydrobenzothieno [2,3-d] pyrimidin-4(3H)-one, $C_{17}H_{13}N_3OS$, (2g)

Compound **2g** was prepared analogously to **2c** from 3-Amino-4,5,6,7-tetrahydrobenzo [*b*]thiophene-2-carboxamide (147 mg, 0.75 mmol) and 3-cyanobenzaldehyde (66 mg, 0.5 mmol). Yield: 87 mg (0.28 mmol, 57%); pale yellow solid of m.p. 354 °C; υ_{max} (ATR)/cm^{-1} 3062, 3036, 2933, 2854, 2231, 1634, 1583, 1553, 1537, 1506, 1480, 1458, 1438, 1407, 1331, 1299, 1278, 1258, 1237, 1195, 1176, 1152, 1101, 1068, 1013, 997, 964, 931, 909, 848, 820, 803, 778, 765, 755, 710, 676, 652, 632, 623; ^{1}H NMR (300 MHz, DMSO-d_6) δ 1.7–1.9 (4 H, m), 2.7–2.8 (2 H, m), 2.9–3.0 (2 H, m), 7.7–7.8 (1 H, m), 8.04 (1 H, d, $J = 8.9$ Hz), 8.42 (1 H, d, $J = 8.1$ Hz), 8.54 (1 H, s), 12.70 (1 H, s); *m/z* (%) 307 (100) [M^+], 279 (76).

4.1.7. 2-(3-Bromophenyl)-5,6,7,8-tetrahydrobenzothieno [2,3-d] pyrimidin-4(3H)-one, $C_{16}H_{13}BrN_2OS$, (**2i**)

Compound **2i** was prepared analogously to **2c** from 3-amino-4,5,6,7-tetrahydrobenzo [*b*]thiophene-2-carboxamide (147 mg, 0.75 mmol) and 3-bromobenzaldehyde (92 mg, 0.5 mmol). Yield: 60 mg (0.17 mmol, 34%); pale yellow solid of m.p. 355 °C; υ_{max} (ATR)/cm^{-1} 3095, 29283 2850, 1651, 1575, 1554, 1537, 1506, 1477, 1463, 1446, 1397, 1348, 1334, 1289, 1254, 1204, 1174, 1158, 1137, 1103, 1071, 1009, 994, 963, 913, 871, 791, 776, 715, 701, 676, 653, 621; ^{1}H

NMR (300 MHz, DMSO-d_6) δ 1.7–1.9 (4 H, m), 2.7–2.8 (2 H, m), 2.9–3.0 (2 H, m), 7.4–7.5 (1 H, m), 7.7–7.8 (1 H, m), 8.1–8.2 (1 H, m), 8.32 (1 H, s), 12.60 (1 H, s); *m/z* (%) 362 (100) [M^+], 360 (97) [M^+], 334 (61), 332 (60).

4.1.8. 2-(3,5-Difluorophenyl)-5,6,7,8-tetrahydrobenzothieno [2,3-d] pyrimidin-4(3H)-one, $C_{16}H_{12}F_2N_2OS$, (2j)

Compound **2j** was prepared analogously to **2c** from 3-amino-4,5,6,7-tetrahydrobenzo [*b*]thiophene-2-carboxamide (147 mg, 0.75 mmol) and 3,5-difluorobenzaldehyde (71 mg, 0.5 mmol). Yield: 50 mg (0.13 mmol, 32%); pale yellow solid of m.p. 389 °C; υ_{max} (ATR)/cm^{-1} 3091, 2949, 2857, 1652, 1634, 1622, 1601, 1543, 1509, 1476, 1459, 1446, 1432, 1407, 1347, 1325, 1294, 1254, 1219, 1201, 1173, 1149, 1124, 1091, 1069, 1030, 988, 964, 929, 887, 876, 851, 817, 802, 778, 742, 722, 659; ^{1}H NMR (300 MHz, DMSO-d_6) δ 1.7–1.9 (4 H, m), 2.7–2.8 (2 H, m), 2.9–3.0 (2 H, m), 7.4–7.6 (1 H, m), 7.8–7.9 (2 H, m), 12.6–12.7 (1 H, br s); *m/z* (%) 318 (100) [M^+], 303 (21), 290 (82), 140 (16).

4.1.9. 2-(3,5-Dibromo-4-methoxyphenyl)-5,6,7,8-tetrahydro-4H-cyclohepta[b]thienopyrimidin-4(3H)-one, $C_{18}H_{16}Br_2N_2O_2S$, (3b)

Compound **3b** was prepared analogously to **2c** from 2-amino-5,6,7,8-tetrahydro-4*H*-cyclohepta [*b*]thiophene-3-carboxamide (157 mg, 0.75 mmol) and 3,5-dibromo-4-methoxybenzaldehyde (146 mg, 0.5 mmol). Yield: 90 mg (0.19 mmol, 38%); brown solid of m.p. 328–329 °C; υ_{max} (ATR)/cm^{-1} 3062, 2912, 2844, 1641, 1560, 1549, 1520, 1498, 1472, 1459, 1439, 1419, 1376, 1357, 1295, 1255, 1219, 1198, 1161, 1136, 1091, 1014, 994, 966, 936, 898, 886, 826, 800, 781, 771, 744, 714, 667, 655, 641, 610; ^{1}H NMR (300 MHz, $CDCl_3$/MeOD) δ 1.5–1.6 (4 H, m), 1.7–1.8 (2 H, m), 2.6–2.7 (2 H, m), 3.1–3.2 (2 H, m), 3.76 (3 H, s), 8.07 (2 H, s); ^{13}C NMR (75.5 MHz, $CDCl_3$/MeOD) δ 26.9, 27.3, 27.6, 29.9, 32.1, 60.4, 118.4, 121.8, 130.4, 131.3, 136.7, 138.9, 148.1, 156.2, 159.9, 162.0; *m/z* (%) 486 (52) [M^+], 484 (100) [M^+], 482 (48) [M^+], 469 (17), 456 (22).

4.1.10. 2-(3-Bromo-4,5-dimethoxyphenyl)-5,6,7,8-tetrahydro-4H-cyclohepta[b]thienopyrimidin-4(3H)-one, $C_{19}H_{19}BrN_2O_3S$, (3c)

Compound **3c** was prepared analogously to **2c** from 2-amino-5,6,7,8-tetrahydro-4*H*-cyclohepta [*b*]thiophene-3-carboxamide (315 mg, 1.5 mmol) and 3-bromo-4,5-dimethoxybenzaldehyde (245 mg, 1.0 mmol). Yield: 130 mg (0.30 mmol, 30%); brown solid of m.p. 304–305 °C; υ_{max} (ATR)/cm^{-1} 3089, 2913, 2841, 1631, 1575, 1560, 1532, 1505, 1477, 1463, 1425, 1410, 1393, 1354, 1320, 1299, 1265, 1233, 1199, 1167, 1152, 1101, 1073, 1047, 1017, 1007, 965, 933, 905, 881, 848, 830, 781, 751, 720, 687, 657, 615; ^{1}H NMR (300 MHz, $CDCl_3$) δ 1.6–1.8 (4 H, m), 1.8–1.9 (2 H, m), 2.8–2.9 (2 H, m), 3.3–3.4 (2 H, m), 3.92 (3 H, s), 3.98 (3 H, s), 7.68 (1 H, s), 7.97 (1 H, s), 12.3–12.4 (1 H, br s); ^{13}C NMR (75.5 MHz, $CDCl_3$) δ 27.3, 27.7, 28.2, 30.1, 32.5, 56.4, 60.8, 111.3, 118.0, 121.7, 123.8, 129.1, 137.0, 138.5, 149.1, 149.7, 153.8, 161.0, 163.0; *m/z* (%) 436 (99) [M^+], 434 (100) [M^+], 421 (30), 419 (30), 408 (35), 406 (34).

4.1.11. 2-(3-Chloro-4,5-dimethoxyphenyl)-5,6,7,8-tetrahydro-4H-cyclohepta[b]thienopyrimidin-4(3H)-one, $C_{19}H_{19}ClN_2O_3S$, (3d)

Compound **3d** was prepared analogously to **2c** from 2-amino-5,6,7,8-tetrahydro-4*H*-cyclohepta [*b*]thiophene-3-carboxamide (78 mg, 0.375 mmol) and 3-chloro-4,5-dimethoxy-benzaldehyde (50 mg, 0.25 mmol). Yield: 90 mg (0.23 mmol, 92%); brown solid of m.p. 298–299 °C; υ_{max} (ATR)/cm^{-1} 2913, 2841, 1635, 1582, 1537, 1506, 1480, 1465, 1427, 1412, 1394, 1351, 1320, 1303, 1271, 1235, 1199, 1140, 1103, 1051, 1020, 1008, 966, 933, 903, 881, 858, 825, 781, 753, 721, 698, 661, 612, 602; ^{1}H NMR (300 MHz, $CDCl_3$) δ 1.7–1.8 (4 H, m), 1.8–1.9 (2 H, m), 2.8–2.9 (2 H, m), 3.3–3.4 (2 H, m), 3.93 (3 H, s), 3.98 (3 H, s), 7.66 (1 H, s), 7.86 (1 H, s), 12.23 (1 H, s); ^{13}C NMR (75.5 MHz, $CDCl_3$) δ 27.3, 27.7, 28.2, 30.1, 32.5, 56.5, 60.9, 110.5, 121.1, 121.8, 128.5, 128.8, 137.0, 138.5, 148.1, 149.8, 154.0, 161.0, 163.0; *m/z* (%) 392 (62) [M^+], 390 (100) 377 (14), 375 (33), 193 (31), 185 (27).

4.1.12. 2-(3-Iodo-4,5-dimethoxyphenyl)-5,6,7,8-tetrahydro-4H-cyclohepta[b]thienopyrimidin-4(3H)-one, $C_{19}H_{19}IN_2O_3$, (**3e**)

Compound **3e** was prepared analogously to **2c** from 2-amino-5,6,7,8-tetrahydro-4*H*-cyclohepta [*b*]thiophene-3-carboxamide (157 mg, 0.75 mmol) and 3-iodo-4,5-dimethoxybenzaldehyde (146 mg, 0.5 mmol). Yield: 80 mg (0.17 mmol, 34%); brown solid of m.p. 165–167 °C; υ_{max} (ATR)/cm^{-1} 2918, 2846, 1645, 1559, 1572, 1539, 1477, 1462, 1424, 1409, 1300, 1273, 1232, 1196, 1139, 1103, 1041, 1018, 998, 967, 856, 821, 784, 751, 720, 681, 662, 622; ^{1}H NMR (300 MHz, DMSO-d_6) δ 1.6–1.8 (4 H, m), 1.8–1.9 (2 H, m), 2.8–2.9 (2 H, m), 3.6–3.7 (2 H, m) 3.78 (3 H, s), 3.93 (3 H, s), 7.82 (1 H, s), 8.15 (1 H, s), 12.51 (1 H, s); ^{13}C NMR (75.5 MHz, DMSO-d_6) δ 26.8, 27.2, 27.3, 29.1, 31.9, 55.8, 56.3, 59.8, 60.0, 92.7, 112.3, 121.4, 128.2, 129.2, 129.4, 136.5, 137.0, 149.8, 150.6, 152.0, 159.2, 161.6; *m/z* (%) 482 (100) [M^+], 467 (37), 454 (33), 440 (12), 428 (13).

4.1.13. 2-(3-Cyanophenyl)-5,6,7,8-tetrahydro-4H-cyclohepta[b] thienopyrimidin-4(3H)-one, $C_{18}H_{15}N_3OS$, (**3g**)

Compound **3g** was prepared analogously to **2c** from 2-amino-5,6,7,8-tetrahydro-4*H*-cyclohepta [*b*]thiophene-3-carboxamide (157 mg, 0.75 mmol) and 3-cyanobenzaldehyde (66 mg, 0.5 mmol). Yield: 85 mg (0.22 mmol, 45%); brown solid of m.p. 320–321 °C; υ_{max} (ATR)/cm^{-1} 3094, 3007, 2928, 2850, 2231, 1638, 1546, 1505, 1478, 1465, 1445, 1400, 1361, 1342, 1298, 1263, 1220, 1200, 1159, 1146, 1097, 1072, 1048, 1017, 999, 985, 968, 936, 915, 901, 846, 824, 807, 794, 780, 737, 715, 676, 667, 655, 621; ^{1}H NMR (300 MHz, DMSO-d_6) δ 1.5–1.7 (4 H, m), 1.8–1.9 (2 H, m), 2.8–2.9 (2 H, m), 3.2–3.3 (2 H, m), 7.7–7.8 (1 H, m), 8.0–8.1 (1 H, m), 8.3–8.4 (1 H, m), 8.52 (1 H, s), 12.65 (1 H, s); ^{13}C NMR (75.5 MHz, DMSO-d_6) δ 26.8, 27.1, 27.3, 29.1, 31.9, 60.3, 111.8, 118.1, 121.9, 129.9, 131.2, 132.2, 133.1, 134.4, 136.6, 137.6, 149.9, 159.0, 160.9; *m/z* (%) 321 (100) [M^+], 306 (35), 293 (42), 279 (16), 267 (18), 129 (21), 102 (13).

4.1.14. 2-(3,5-Difluorophenyl)-5,6,7,8-tetrahydro-4H-cyclohepta[b] thienopyrimidin-4(3H)-one, $C_{17}H_{14}F_2N_2OS$, (**3j**)

Compound **3j** was prepared analogously to **2c** from 2-amino-5,6,7,8-tetrahydro-4*H*-cyclohepta [*b*]thiophene-3-carboxamide (157 mg, 0.75 mmol) and 3,5-difluorobenzaldehyde (71 mg, 0.5 mmol). Yield: 70 mg (0.21 mmol, 42%); brown solid of m.p. 385–386 °C; υ_{max} (ATR)/cm^{-1} 3095, 2991, 2929, 2852, 1652, 1625, 1601, 1549, 1506, 1471, 1446, 1431, 1401, 1354, 1329, 1297, 1254, 1227, 1200, 1156, 1124, 1092, 1072, 1048, 1028, 990, 970, 934, 907, 878, 854, 825, 791, 780, 764, 729, 719, 660; ^{1}H NMR (300 MHz, DMSO-d_6) δ 1.6–1.7 (4 H, m), 1.8–1.9 (2 H, m), 2.8–2.9 (2 H, m), 3.3–3.4 (2 H, m), 7.4–7.5 (1 H, m), 7.8–7.9 (2 H, m), 12.61 (1 H, s); *m/z* (%) 332 (100) [M^+], 317 (43), 304 (42), 290 (16), 278 (20), 140 (18).

4.1.15. 2-(3,5-Dibromo-4-methoxyphenyl)-7-ethoxycarbonyl-5,6,7,8-tetrahydropyridylthieno [2,3-d]pyrimidin-4(3H)-one, $C_{19}H_{17}Br_2N_3O_4S$, (**4b**)

Compound **4b** was prepared analogously to **2c** from ethyl 2-amino-3-carbamoyl-4,5-dihydrothieno [2,3-*c*]pyridine-6(7*H*)-carboxylate (202 mg, 0.75 mmol) and 3,5-dibromo-4-methoxybenzaldehyde (146 mg, 0.5 mmol). Yield: 80 mg (0.15 mmol, 30%); colorless solid of m.p. 357 °C; υ_{max} (ATR)/cm^{-1} 3080, 3000, 2968, 2930, 2861, 1698, 1651, 1594, 1571, 1531, 1504, 1479, 1465, 1431, 1412, 1384, 1374, 1351, 1300, 1267, 1257, 1232, 1204, 1167, 1098, 1068, 1050, 1020, 990, 954, 905, 889, 869, 837, 819, 793, 781, 769, 744, 714, 688, 671, 639, 616; ^{1}H NMR (300 MHz, DMSO-d_6) δ 1.22 (3 H, t, J = 7.1 Hz), 2.9–3.0 (2 H, m), 3.6–3.7 (2 H, m), 3.87 (3 H, s), 4.10 (2 H, q, J = 7.1 Hz), 4.66 (2 H, s), 8.43 (2 H, s), 12.6–12.7

(1 H, br s); ^{13}C NMR (75.5 MHz, DMSO-d_6) δ 14.5, 25.2, 42.9, 60.6, 61.1, 117.7, 120.2, 129.5, 130.4, 132.0, 154.8, 155.8, 158.6, 163.6; *m/z* (%) 545 (14) [M$^+$], 543 (25) [M$^+$], 541 (11) [M$^+$], 516 (92), 514 (100), 512 (89), 472 (11), 470 (22), 468 (13).

*4.1.16. 2-(3-Bromo-4,5-dimethoxyphenyl)-7-ethoxycarbonyl-5,6,7,8-tetrahydropyridylthieno [2,3-d]pyrimidin-4(3H)-one, $C_{20}H_{20}BrN_3O_5S$, (**4c**)*

Compound **4c** was prepared analogously to **2c** from ethyl 2-amino-3-carbamoyl-4,5-dihydrothieno [2,3-*c*]pyridine-6(7*H*)-carboxylate (404 mg, 1.5 mmol) and 3-bromo-4,5-dimethoxybenzaldehyde (245 mg, 1.0 mmol). Yield: 150 mg (0.30 mmol, 30%); colorless solid of m.p. 317 °C; υ_{max} (ATR)/cm^{-1} 2983, 2941, 1707, 1662, 1595, 1578, 1546, 1508, 1487, 1463, 1427, 1399, 1385, 1346, 1334, 1305, 1291, 1262, 1231, 1203, 1170, 1155, 1104, 1044, 1018, 992, 960, 943, 928, 867, 845, 829, 793, 779, 767, 758, 752, 723, 696, 675, 626, 601; ^{1}H NMR (300 MHz, DMSO-d_6) δ 1.22 (3 H, t, J = 7.1 Hz), 2.9–3.0 (2 H, m), 3.6–3.7 (2 H, m), 3.82 (3 H, s), 3.95 (3 H, s), 4.10 (2 H, q, J = 7.1 Hz), 4.66 (2 H, s), 7.84 (1 H, s), 8.00 (1 H, s), 12.66 (1 H, s); ^{13}C NMR (75.5 MHz, DMSO-d_6) δ 14.5, 25.3, 42.9, 56.4, 60.3, 61.1, 111.7, 116.8, 120.3, 123.7, 128.6, 129.0, 129.4, 148.2, 150.8, 153.2, 154.8, 158.6, 163.6; *m/z* (%) 495 (23) [M$^+$], 493 (21) [M$^+$], 466 (100), 464 (92), 422 (8), 420 (9).

*4.1.17. 2-(3-Chloro-4,5-dimethoxyphenyl)-7-ethoxycarbonyl-5,6,7,8-tetrahydropyridylthieno [2,3-d]pyrimidin-4(3H)-one, $C_{20}H_{20}ClN_3O_5S$, (**4d**)*

Compound **4d** was prepared analogously to **2c** from ethyl 2-amino-3-carbamoyl-4,5-dihydrothieno [2,3-*c*]pyridine-6(7*H*)-carboxylate (202 mg, 0.75 mmol) and 3-chloro-4,5-dimethoxybenzaldehyde (100 mg, 0.5 mmol) were dissolved in 1-butanol (5 mL) and conc. HCl (0.1 mL) was added. Yield: 70 mg (0.16 mmol, 32%); colorless solid of m.p. 311–312 °C; υ_{max} (ATR)/cm^{-1} 2987, 2944, 1706, 1664, 1583, 1552, 1509, 1489, 1462, 1445, 1427, 1400, 1386, 1346, 1307, 1294, 1264, 1232, 1204, 1172, 1105, 1048, 1022, 996, 960, 929, 867, 848, 834, 812, 779, 768, 754, 724, 707, 680, 627, 602; ^{1}H NMR (300 MHz, DMSO-d_6) δ 1.22 (3 H, t, J = 7.1 Hz), 2.9–3.0 (2 H, m), 3.6–3.7 (2 H, m), 3.83 (3 H, s), 3.95 (3 H, s), 4.10 (2 H, q, J = 7.1 Hz), 4.66 (2 H, s), 7.81 (1 H, s), 7.87 (1 H, s), 12.67 (1 H, s); ^{13}C NMR (75.5 MHz, DMSO-d_6) δ 14.5, 25.3, 42.9, 56.4, 60.4, 61.1, 111.0, 120.9, 127.2, 128.0, 129.4, 147.1, 150.9, 153.4, 154.7, 158.6, 163.6; *m/z* (%) 451 (9) [M$^+$], 449 (26) [M$^+$], 422 (36), 420 (100), 376 (13).

*4.1.18. 2-(3-Iodo-4,5-dimethoxyphenyl)-7-ethoxycarbonyl-5,6,7,8-tetrahydropyridylthieno [2,3-d]pyrimidin-4(3H)-one, $C_{20}H_{20}IN_3O_5S$, (**4e**)*

Compound **4e** was prepared analogously to **2c** from ethyl 2-amino-3-carbamoyl-4,5-dihydrothieno [2,3-*c*]pyridine-6(7*H*)-carboxylate (202 mg, 0.75 mmol) and 3-iodo-4,5-dimethoxybenzaldehyde (146 mg, 0.5 mmol). Yield: 87 mg (0.16 mmol, 32%); colorless solid of m.p. 295 °C; υ_{max} (ATR)/cm^{-1} 2977, 2937, 2904, 2862, 2829, 1704, 1661, 1591, 1574, 1542, 1508, 1485, 1460, 1445, 1423, 1397, 1384, 1344, 1304, 1292, 1258, 1231, 1202, 1185, 1167, 1104, 1041, 1015, 995, 960, 928, 887, 868, 850, 836, 822, 806, 779, 767, 749, 722, 694, 673, 647, 625, 601; ^{1}H NMR (300 MHz, DMSO-d_6) δ 1.22 (3 H, t, J = 7.1 Hz), 2.9–3.0 (2 H, m), 3.6–3.7 (2 H, m), 3.78 (3 H, s), 3.93 (3 H, s), 4.10 (2 H, q, J = 7.1 Hz), 4.66 (2 H, s), 7.83 (1 H, s), 8.17 (1 H, s), 12.6–12.7 (1 H, br s); ^{13}C NMR (75.5 MHz, DMSO-d_6) δ 14.5, 25.3, 42.9, 56.3, 60.0, 61.1, 92.7, 112.4, 120.3, 128.8, 129.3, 129.4, 150.8, 152.0, 154.7, 158.7, 163.6; *m/z* (%) 541 (100) [M$^+$], 512 (100), 468 (20), 452 (8); Anal. Calcd. for $C_{20}H_{20}IN_3O_5S$: C, 44.37; H, 3.72; N, 7.76; S, 5.92. Found: C, 44.33; H, 3.68; N, 7.65; S, 6.05.

*4.1.19. 2-(3-Hydroxy-4-methoxyphenyl)-7-ethoxycarbonyl-5,6,7,8-tetrahydropyridylthieno [2,3-d]pyrimidin-4(3H)-one, $C_{19}H_{19}N_3O_5S$, (**4f**)*

Compound **4f** was prepared analogously to **2c** from ethyl 2-amino-3-carbamoyl-4,5-dihydrothieno [2,3-*c*]pyridine-6(7*H*)-carboxylate (202 mg, 0.75 mmol) and isovanillin (76 mg, 0.5 mmol). Yield: 70 mg (0.17 mmol, 35%); off-white solid of m.p. 318–320 °C; υ_{max} (ATR)/cm^{-1} 3383, 2986, 2943, 2846, 1641, 1553, 1521, 1493, 1467, 1436, 1389, 1375, 1353, 1331, 1298, 1271, 1231, 1203, 1187, 1137, 1123, 1090, 1050, 1013, 985, 947, 880, 832, 819, 795, 764, 732, 710, 681, 658, 617^{1}H NMR (300 MHz, DMSO-d_6) δ 1.22 (3 H, t, J = 7.1 Hz), 2.9–3.0 (2 H, m), 3.6–3.7 (2 H, m), 3.85 (3 H, s), 4.10 (2 H, q, J = 7.1 Hz), 4.63 (2 H, s), 7.02 (1 H, d, J = 8.5 Hz), 7.6–7.7 (2 H, m), 9.34 (1 H, s), 12.38 (1 H, s); ^{13}C NMR (75.5 MHz, DMSO-d_6) δ 14.5, 25.3, 42.9, 55.7, 61.1, 111.6, 114.6, 119.4, 124.1, 127.8, 129.4, 146.5, 150.8, 152.5, 154.8, 158.7, 164.1;; *m/z* (%) 401 (61) [M$^+$], 372 (100), 328 (34), 313 (18); Anal. Calcd. for $C_{19}H_{19}N_3O_5S$: C, 56.85; H, 4.77; N, 10.47; S, 7.99. Found: C, 56.62; H, 4.77; N, 10.74; S, 8.39.

*4.1.20. 2-(3-Cyanophenyl)-7-ethoxycarbonyl-5,6,7,8-tetrahydropyridylthieno [2,3-d]pyrimidin-4(3H)-one, $C_{19}H_{16}N_4O_3S$, (**4g**)*

Compound **4g** was prepared analogously to **2c** from ethyl 2-amino-3-carbamoyl-4,5-dihydrothieno [2,3-*c*]pyridine-6(7*H*)-carboxylate (202 mg, 0.75 mmol) and 3-cyanobenzaldehyde (66 mg, 0.5 mmol). Yield: 105 mg (0.28 mmol, 56%); colorless solid of m.p. 342–344 °C; υ_{max} (ATR)/cm^{-1} 3046, 2982, 2957, 2234, 1708, 1656, 1582, 1571, 1542, 1509, 1486, 1454, 1409, 1384, 1374, 1358, 1348, 1303, 1285, 1265, 1234, 1200, 1172, 1108, 1038, 1013, 975, 954, 904, 856, 841, 813, 768, 717, 678, 669, 660, 636, 626; ^{1}H NMR (500 MHz, DMSO-d_6) δ 1.22 (3 H, t, J = 7.1 Hz), 2.9–3.0 (2 H, m), 3.6–3.7 (2 H, m), 4.10 (2 H, q, J = 7.1 Hz), 4.67 (2 H, s), 7.6–7.7 (1 H, m), 8.0–8.1 (1 H, m), 8.4–8.5 (1 H, m), 8.58 (1 H, s), 12.83 (1 H, br s); *m/z* (%) 380 (13) [M$^+$], 351 (100), 307 (33), 279 (8), 129 (9); Anal. Calcd. for $C_{19}H_{16}N_4O_3S$: C, 59.99; H, 4.24; N, 14.73; S, 8.43. Found: C, 59.73; H, 4.20; N, 14.66; S, 8.80.

*4.1.21. 2-(3,5-Difluorophenyl)-7-ethoxycarbonyl-5,6,7,8-tetrahydropyridylthieno [2,3-d]pyrimidin-4(3H)-one, $C_{18}H_{15}F_2N_3O_3S$, (**4j**)*

Compound **4j** was prepared analogously to **2c** from ethyl 2-amino-3-carbamoyl-4,5-dihydrothieno [2,3-*c*]pyridine-6(7*H*)-carboxylate (202 mg, 0.75 mmol) and 3,5-difluorobenzaldehyde (71 mg, 0.5 mmol). Yield: 66 mg (0.17 mmol, 34%); colorless solid of m.p. 335–336 °C; υ_{max} (ATR)/cm^{-1} 3089, 2982, 2869, 1709, 1652, 1625, 1604, 1547, 1509, 1485, 1467, 1424, 1376, 1348, 1329, 1300, 1257, 1233, 1206, 1190, 1171, 1158, 1123, 1111, 1100, 1092, 1045, 1030, 1006, 990, 956, 932, 878, 850, 780, 767, 756, 723, 679, 662, 627;^{1}H NMR (300 MHz, DMSO-d_6) δ 1.22 (3 H, t, J = 7.1 Hz), 2.9–3.0 (2 H, m), 3.6–3.7 (2 H, m), 4.10 (2 H, q, J = 7.1 Hz), 4.67 (2 H, s), 7.4–7.6 (1 H, m), 7.8–7.9 (2 H, m), 12.7–12.8 (1 H, br s); *m/z* (%) 391 (17) [M$^+$], 362 (100), 318 (33), 290 (13), 140 (14); Anal. Calcd. for $C_{18}H_{15}F_2N_3O_3S$: C, 55.24; H, 3.86; N, 10.74; S, 8.19. Found: C, 55.17; H, 3.89; N, 10.79; S, 8.67.

*4.1.22. 2-(3,5-Dibromo-4-methoxyphenyl)-7-benzoxycarbonyl-5,6,7,8-tetrahydropyridylthieno [2,3-d]pyrimidin-4(3H)-one, $C_{24}H_{19}Br_2N_3O_4S$, (**5b**)*

Compound **5b** was prepared analogously to **2c** from benzyl 2-amino-3-carbamoyl-4,5-dihydrothieno [2,3-*c*]pyridine-6(7*H*)-carboxylate (248 mg, 0.75 mmol) and 3,5-dibromo-4-methoxybenzaldehyde (146 mg, 0.5 mmol). Yield: 90 mg (0.15 mmol, 30%); off-white solid of m.p. 316–317 °C; υ_{max} (ATR)/cm^{-1} 3070, 3006, 2958, 2864, 1702, 1660, 1588, 1568, 1530, 1506, 1478, 1467, 1448, 1417, 1385, 1343, 1300, 1264, 1254, 1233, 1204,

1187, 1095, 1080, 1067, 1044, 1022, 978, 931, 912, 889, 873, 827, 795, 777, 766, 756, 748, 740, 715, 695, 670, 640, 608; ^{1}H NMR (300 MHz, DMSO-d_6) δ 2.9–3.0 (2 H, m), 3.7–3.8 (2 H, m), 3.87 (3 H, s), 4.71 (2 H, s), 5.14 (2 H, s), 7.3–7.4 (5 H, m), 8.43 (2 H, s), 12.7–12.8 (1 H, br s); ^{13}C NMR (75.5 MHz, DMSO-d_6) δ 43.1, 60.6, 66.5, 117.3, 120.6, 127.6, 127.9, 128.4, 129.5, 130.8, 132.0, 136.7, 148.6, 154.6, 155.8, 158.6, 163.6; *m/z* (%) 605 (1) [M$^+$], 515 (100), 471 (18), 224 (13), 91 (49), 44 (13).

4.1.23. 2-(3-Bromo-4,5-dimethoxyphenyl)-7-benzoxycarbonyl-5,6,7,8-tetrahydropyridylthieno [2,3-d]pyrimidin-4(3H)-one, $C_{25}H_{22}BrN_3O_5S$, (**5c**)

Compound **5c** was prepared analogously to **2c** from benzyl 2-amino-3-carbamoyl-4,5-dihydrothieno [2,3-*c*]pyridine-6(7*H*)-carboxylate (497 mg, 1.5 mmol) and 3-bromo-4,5-dimethoxybenzaldehyde (245 mg, 1.0 mmol). Yield: 211 mg (0.38 mmol, 38%); colorless solid of m.p. 300 °C; υ_{max} (ATR)/cm^{-1} 3098, 2938, 2829, 1699, 1651, 1590, 1574, 1563, 1529, 1488, 1471, 1416, 1393, 1383, 1345, 1318, 1296, 1257, 1228, 1202, 1192, 1170, 1157, 1108, 1093, 1045, 1016, 994, 950, 920, 878, 837, 818, 776, 761, 718, 699, 659, 647, 624; ^{1}H NMR (300 MHz, DMSO-d_6) δ 3.0–3.1 (2 H, m), 3.7–3.8 (2 H, m), 3.82 (3 H, s), 3.95 (3 H, s), 4.7–4.8 (2 H, m), 5.15 (2 H, s), 7.3–7.4 (5 H, m), 7.84 (1 H, s), 8.00 (1 H, s), 12.6–12.7 (1 H, br s); ^{13}C NMR (75.5 MHz, DMSO-d_6) δ 43.1, 56.4, 60.3, 66.5, 111.7, 116.8, 120.3, 123.7, 127.6, 127.9, 128.4, 128.6, 129.4, 136.7, 148.2, 150.8, 153.2, 154.6, 158.6, 163.6; *m/z* (%) 557 (2) [M$^+$], 555 (2) [M$^+$], 466 (100), 464 (100), 422 (13), 420 (13), 277 (12), 151 (16), 91 (37).

4.1.24. 2-(3-Iodo-4,5-dimethoxyphenyl)-7-benzoxycarbonyl-5,6,7,8-tetrahydropyridylthieno [2,3-d]pyrimidin-4(3H)-one, $C_{25}H_{22}IN_3O_5S$, (**5e**)

Compound **5e** was prepared analogously to **2c** from benzyl 2-amino-3-carbamoyl-4,5-dihydrothieno [2,3-*c*]pyridine-6(7*H*)-carboxylate (248 mg, 0.75 mmol) and 3-iodo-4,5-dimethoxybenzaldehyde (146 mg, 0.5 mmol). Yield: 175 mg (0.29 mmol, 58%); colorless solid of m.p. 282–283 °C; υ_{max} (ATR)/cm^{-1} 2940, 2856, 2831, 1699, 1663, 1574, 1544, 1505, 1486, 1458, 1415, 1397, 1383, 1345, 1304, 1251, 1231, 1213, 1198, 1187, 1150, 1100, 1041, 1015, 995, 974, 945, 930, 905, 864, 849, 832, 811, 794, 778, 769, 745, 723, 697, 673, 649, 602; ^{1}H NMR (300 MHz, $CDCl_3$/DMSO-d_6) δ 3.0–3.1 (2 H, m), 3.7–3.8 (2 H, m), 3.78 (3 H, s), 3.90 (3 H, s), 4.65 (2 H, s), 5.10 (2 H, s), 7.2–7.3 (5 H, m), 7.76 (1 H, s), 8.16 (1 H, s), 12.4–12.5 (1 H, br s); ^{13}C NMR (75.5 MHz, $CDCl_3$/DMSO-d_6) δ 41.9, 54.9, 58.8, 65.6, 90.8, 111.0, 119.3, 126.3, 126.6, 127.0, 128.2, 128.5, 135.2, 149.4, 149.6, 150.8, 153.5, 157.8, 162.8; *m/z* (%) 603 (2) [M$^+$], 512 (100), 468 (20), 91 (41); Anal. Calcd. for $C_{25}H_{22}IN_3O_5S$: C, 49.76; H, 3.67; N, 6.96; S, 5.31. Found: C, 49.73; H, 3.55; N, 6.95; S, 5.21.

4.1.25. 2-(3-Bromophenyl)-7-benzoxycarbonyl-5,6,7,8-tetrahydropyridylthieno [2,3-d]pyrimidin-4(3H)-one, $C_{23}H_{18}BrN_3O_3S$, (**5i**)

Compound **5i** was prepared analogously to **2c** from benzyl 2-amino-3-carbamoyl-4,5-dihydrothieno [2,3-*c*]pyridine-6(7*H*)-carboxylate (248 mg, 0.75 mmol) and 3-bromobenzaldehyde (93 mg, 0.5 mmol). Yield: 90 mg (0.18 mmol, 36%); colorless solid of m.p. 280–281 °C; υ_{max} (ATR)/cm^{-1} 3009, 2947, 2891, 1710, 1660, 1580, 1548, 1498, 1481, 1464, 1413, 1384, 1352, 1299, 1271, 1235, 1204, 1187, 1168, 1097, 1075, 1047, 1022, 1010, 987, 973, 949, 926, 910, 876, 865, 820, 804, 794, 778, 767, 748, 724, 709, 697, 676, 651, 617; ^{1}H NMR (300 MHz, DMSO-d_6) δ 3.0–3.1 (2 H, m) 3.7–3.8 (2 H, m), 4.70 (2 H, s), 5.15 (2 H, s), 7.3–7.5 (6 H, m), 7.77 (1 H, d, J = 8.0 Hz), 8.13 (1 H, d, J = 8.9 Hz), 8.32 (1 H, s), 12.7 (1 H, s); ^{13}C NMR (75.5 MHz, DMSO-d_6) δ 24.5, 43.1, 58.4, 66.5, 120.3, 121.9, 126.8, 127.6, 127.9, 128.4, 129.5, 130.3, 130.8, 134.1, 136.7, 145.7, 151.2, 154.6, 158.5, 163.8; *m/z* (%) 496 (4) [M$^+$], 494 (4) [M$^+$], 406 (100), 404 (99), 362 (33), 360 (36), 91 (92).

4.1.26. 2-(3,5-Difluorophenyl)-7-benzoxycarbonyl-5,6,7,8-tetrahydropyridylthieno [2,3-d]pyrimidin-4(3H)-one, $C_{23}H_{17}F_2N_3O_3$, (**5j**)

Compound **5j** was prepared analogously to **2c** from benzyl 2-amino-3-carbamoyl-4,5-dihydrothieno [2,3-*c*]pyridine-6(7*H*)-carboxylate (248 mg, 0.75 mmol) and 3,5-difluorobenzaldehyde (71 mg, 0.5 mmol). Yield: 70 mg (0.15 mmol, 30%); colorless solid of m.p. 346–347 °C; υ_{max} (ATR)/cm^{-1} 3092, 3066, 2960, 2885, 1699, 1654, 1624, 1598, 1561, 1546, 1511, 1496, 1482, 1447, 1433, 1410, 1385, 1346, 1322, 1301, 1261, 1235, 1206, 1177, 1155, 1125, 1088, 1079, 1041, 1030, 1003, 989, 965, 928, 915, 886, 876, 856, 826, 789, 779, 769, 756, 725, 699, 680, 660, 631, 603; ^{1}H NMR (300 MHz, DMSO-d_6) δ 3.0–3.1 (2 H, m), 3.7–3.8 (2 H, m), 4.71 (2 H, s), 7.3–7.4 (5 H, m), 7.4–7.6 (1 H, m), 7.8–7.9 (2 H, m), 12.75 (1 H, s); *m/z* (%) 453 (1) [M$^+$], 362 (100%), 318 (42), 91 (34).

4.1.27. 2-(3-Chloro-4,5-dimethoxyphenyl)-7-benzoxycarbonyl-5,6,7,8-tetrahydropyridylthieno [2,3-d]pyrimidin-4(3H)-one, $C_{25}H_{22}ClN_3O_5S$, (**5 m**)

Compound **5m** was prepared analogously to **2c** from benzyl 2-amino-3-carbamoyl-4,5-dihydrothieno [2,3-*c*]pyridine-6(7*H*)-carboxylate (248 mg, 0.75 mmol) and 3-chloro-4,5-dimethoxybenzaldehyde (100 mg, 0.5 mmol). Yield: 130 mg (0.25 mmol, 50%); colorless solid of m.p. 309 °C; υ_{max} (ATR)/cm^{-1} 3104, 2999, 2963, 2830, 1704, 1654, 1581, 1562, 1534, 1511, 1486, 1475, 1453, 1415, 1394, 1383, 1346, 1321, 1297, 1260, 1230, 1203, 1174, 1155, 1106, 1093, 1052, 1020, 997, 936, 915, 877, 861, 830, 797, 776, 765, 753, 719, 710, 696, 671, 663, 649, 625, 613, 599; ^{1}H NMR (300 MHz, $CDCl_3$/DMSO-d_6) δ 3.0–3.1 (2 H, m) 3.7–3.8 (2 H, m), 3.82 (3 H, s), 3.93 (3 H, s), 4.66 (2 H, s), 5.11 (2 H, s), 7.2–7.4 (5 H, m), 7.75 (1 H, s), 7.85 (1 H, s), 12.4–12.5 (1 H, br s); ^{13}C NMR (75.5 MHz, $CDCl_3$/DMSO-d_6) δ 23.9, 41.6, 54.8, 58.8, 65.2, 109.1, 119.0, 119.7, 126.0, 126.2, 126.5, 126.8, 128.0, 135.0, 145.8, 149.4, 151.9, 153.1, 157.4, 162.4; *m/z* (%) 511 (2) [M$^+$], 422 (63), 420 (100), 376 (17), 91 (38).

4.1.28. 2-(3,4,5-Trimethoxyphenyl)-5,6,7,8-tetrahydropyridylthieno [2,3-d]pyrimidin-4(3H)-one × CF_3COOH, $C_{20}H_{20}F_3N_3O_6S$, (**6a**)

5a (47 mg, 0.093 mmol) was dissolved in TFA (2.06 mL, 27 mmol) and treated with thioanisole (588 µL, 5 mmol). The reaction mixture was stirred at room temperature for 3 h. The excess of TFA was evaporated and the residue was recrystallized from EtOH/*n*-hexane. Yield: 25 mg (0.051 mmol, 55%); colorless solid of m.p. 289–290 °C; υ_{max} (ATR)/cm^{-1} 3004, 2945, 2836, 1667, 1597, 1548, 1514, 1489, 1470, 1450, 1421, 1351, 1335, 1285, 1276, 1229, 1201, 1178, 1125, 1019, 997, 929, 888, 860, 847, 836, 798, 782, 756, 722, 690, 647, 630; ^{1}H NMR (300 MHz, DMSO-d_6) δ 3.2–3.3 (2 H, m) 3.4–3.5 (2 H, m), 3.74 (3 H, s), 3.89 (6 H, s), 4.43 (2 H, s), 7.52 (2 H, s), 9.3–9.4 (2 H, br s), 12.7–12.8 (1 H, br s); ^{13}C NMR (75.5 MHz, DMSO-d_6) δ 22.5, 41.6, 56.2, 60.2, 105.3, 119.6, 124.0, 126.5, 128.2, 140.5, 152.8, 152.9, 158.7, 164.4; *m/z* (%) 373 (100) [M$^+$], 344 (60), 152 (20).

4.1.29. 2-(3,5-Dibromo-4-methoxyphenyl)-5,6,7,8-tetrahydropyridylthieno [2,3-d]pyrimidin-4(3H)-one × CF_3CO_2H, $C_{18}H_{14}Br_2F_3N_3O_4S$, (**6b**)

Compound **6b** was prepared analogously to **6a** from **5b** (40 mg, 0.066 mmol). Yield: 20 mg (0.034 mmol, 52%); colorless solid of m.p. > 290 °C; υ_{max} (ATR)/cm^{-1} 2957, 2836, 2623, 1639, 1566, 1522, 1505, 1471, 1426, 1382, 1296, 1268, 1187, 1129, 1069, 1016, 988, 887, 831, 796, 779, 741, 718, 669, 658, 634, 618; ^{1}H NMR (300 MHz, DMSO-d_6) δ 3.1–3.2 (2 H, m) 3.4–3.5 (2 H, m), 3.87 (3 H, s), 4.43 (2 H, s), 8.44 (2 H, s); ^{13}C NMR (75.5 MHz, DMSO-d_6) δ 22.5, 41.7,

60.7, 117.8, 120.1, 125.0, 128.3, 128.4, 130.3, 132.1, 151.0, 155.9, 158.5, 163.9; *m/z* (%) 473 (26) [M^+], 471 (52) [M^+], 430 (57), 428 (100), 426 (53), 350 (13), 348 (14), 278 (13), 151 (15), 91 (21), 42 (15).

4.1.30. 2-(3-Bromo-4,5-dimethoxyphenyl)-5,6,7,8-tetrahydropyridylthieno [2,3-d]pyrimidin-4(3H)-one × CF_3CO_2H, $C_{19}H_{17}BrF_3N_3O_5S$, (**6c**)

Compound **6c** was prepared analogously to **6a** from **5c** (56 mg, 0.1 mmol). Yield: 32 mg (0.06 mmol, 60%); colorless solid of m.p. 298 °C; υ_{max} (ATR)/cm^{-1} 3004, 2937, 2831, 1705, 1656, 1594, 1578, 1543, 1505, 1486, 1477, 1463, 1428, 1399, 1353, 1301, 1261, 1238, 1197, 1180, 1124, 1104, 1047, 1019, 1003, 980, 928, 891, 864, 834, 798, 781, 750, 722, 667, 643, 629, 602; ^{1}H NMR (300 MHz, DMSO-d_6) δ 3.1–3.2 (2 H, m) 3.4–3.5 (2 H, m), 3.83 (3 H, s), 3.95 (3 H, s), 4.43 (2 H, s), 7.85 (1 H, s), 8.02 (1 H, s), 9.3–9.5 (2 H, br s), 12.6–12.9 (1 H, br s); ^{13}C NMR (75.5 MHz, DMSO-d_6) δ 22.4, 41.6, 56.5, 60.3, 111.8, 116.9, 119.8, 123.9, 124.4, 128.2, 128.4, 148.3, 151.5, 153.2, 157.6, 158.6, 164.1;; *m/z* (%) 423 (97) [M^+], 421 (100) [M^+], 394 (82), 392 (78), 152 (33).

4.1.31. 2-(3-Iodo-4,5-dimethoxyphenyl)-5,6,7,8-tetrahydropyridylthieno [2,3-d]pyrimidin-4(3H)-one × CF_3COOH, $C_{19}H_{17}F_3IN_3O_5S$, (**6e**)

Compound **6e** was prepared analogously to **6a** from **5e** (60 mg, 0.1 mmol). Yield: 47 mg (0.081 mmol, 81%); colorless solid of m.p. 298 °C; υ_{max} (ATR)/cm^{-1} 2963, 2935, 2831, 1704, 1656, 1590, 1573, 1538, 1485, 1473, 1460, 1425, 1396, 1386, 1350, 1298, 1259, 1237, 1195, 1177, 1122, 1103, 1044, 1017, 1000, 980, 927, 865, 826, 797, 780, 748, 720, 683, 664, 642, 629, 600; ^{1}H NMR (300 MHz, DMSO-d_6) δ 3.1–3.3 (2 H, m) 3.4–3.5 (2 H, m), 3.79 (3 H, s), 3.93 (3 H, s), 4.43 (2 H, s), 7.84 (1 H, s), 8.18 (1 H, s), 9.29 (2 H, s), 12.7–12.8 (1 H, br s); ^{13}C NMR (75.5 MHz, DMSO-d_6) δ 22.4, 41.6, 56.3, 60.1, 92.7, 112.5, 119.7, 124.3, 125.9, 128.2, 128.9, 129.1, 129.6, 151.0, 151.4, 152.0, 158.6, 164.2; *m/z* (%) 469 (100) [M^+], 440 (67), 152 (11).

4.1.32. 2-(3-Bromophenyl)-5,6,7,8-tetrahydropyridylthieno [2,3-d] pyrimidin-4(3H)-one × CF_3COOH, $C_{17}H_{13}BrF_3N_3O_3S$, (**6i**)

Compound **6i** was prepared analogously to **6a** from **5i** (50 mg, 0.1 mmol). Yield: 40 mg (0.084 mmol, 84%); colorless solid of m.p. >290 °C (dec.); υ_{max} (ATR)/cm^{-1} 2993, 2825, 2633, 1650, 1579, 1537, 1510, 1488, 1465, 1428, 1404, 1391, 1303, 1287, 1198, 1174, 1128, 1076, 1011, 993, 979, 888, 834, 797, 775, 652, 637; ^{1}H NMR (300 MHz, DMSO-d_6) δ 3.1–3.2 (2 H, m) 3.4–3.5 (2 H, m), 4.53 (2 H, s), 7.5–7.6 (1 H, m), 7.8–7.9 (1 H, m), 8.1–8.2 (1 H, m), 8.33 (1 H, s); ^{13}C NMR (75.5 MHz, DMSO-d_6) δ 22.4, 41.6, 120.1, 121.9, 124.7, 126.8, 128.3, 128.4, 129.5, 130.4, 130.8, 133.9, 134.3, 151.9, 158.5, 164.0; *m/z* (%) 363 (92) [M^+], 361 (91) [M^+], 334 (99), 332 (100), 184 (15), 182 (16), 151 (13).

4.1.33. 2-(3,5-Difluorophenyl)-5,6,7,8-tetrahydropyridylthieno [2,3-d]pyrimidin-4(3H)-one × CF_3COOH, $C_{17}H_{12}F_5N_3O_3S$, (**6j**)

Compound **6j** was prepared analogously to **6a** from **5j** (41 mg, 0.09 mmol). Yield: 24 mg (0.055 mmol, 61%); colorless solid of m.p. >300 °C; υ_{max} (ATR)/cm^{-1} 3070, 2999, 2861, 1645, 1598, 1548, 1513, 1488, 1462, 1450, 1436, 1419, 1396, 1359, 1333, 1305, 1262, 1202, 1171, 1136, 1123, 1028, 990, 980, 925, 878, 855, 831, 798, 779, 750, 720, 663; ^{1}H NMR (300 MHz, DMSO-d_6) δ 3.1–3.3 (2 H, m) 3.4–3.5 (2 H, m), 4.44 (2 H, s), 7.5–7.6 (1 H, m), 7.8–8.0 (2 H, m), 9.2–9.5 (2 H, br s), 12.6–12.9 (1 H, br s); ^{13}C NMR (75.5 MHz, DMSO-d_6) δ 22.4, 41.6, 106.7–107.3 (m), 111.0–111.3 (m), 120.4, 125.2, 125.9, 128.3, 135.1, 151.0, 158.5, 160.6–160.8 (m), 163.7–163.9 (m), 164.1; *m/z* (%) 319 (99) [M^+], 318 (98) [M^+], 290 (100), 151 (25), 140 (47), 113 (28), 91 (20).

4.1.34. 2-(4-Methoxyphenyl)-5,6,7,8-tetrahydropyridylthieno [2,3-d]pyrimidin-4(3H)-one × CF_3COOH, $C_{18}H_{16}F_3N_3O_4S$, (**6l**)

Compound **6l** was prepared analogously to **6a** from **5l** (45 mg, 0.1 mmol). Yield: 38 mg (0.089 mmol, 89%); colorless solid of m.p. 312–313 °C; υ_{max} (ATR)/cm^{-1} 2999, 2946, 2846, 1651, 1606, 1543, 1521, 1492, 1442, 1427, 1402, 1389, 1319, 1292, 1261, 1201, 1182, 1123, 1030, 1002, 979, 883, 838, 797, 782, 742, 721, 692, 649, 598; ^{1}H NMR (300 MHz, DMSO-d_6) δ 3.1–3.2 (2 H, m) 3.4–3.5 (2 H, m), 3.85 (3 H, s), 4.41 (2 H, s), 7.08 (2 H, d, J = 9.0 Hz), 8.14 (2 H, d, J = 9.0 Hz), 9.4–9.5 (2 H, br s), 12.5–12.7 (1 H, br s); ^{13}C NMR (75.5 MHz, DMSO-d_6) δ 22.5, 41.5, 55.5, 114.1, 119.2, 123.4, 123.7, 128.2, 129.4, 153.0, 158.7, 162.1, 164.7; *m/z* (%) 313 (100) [M^+], 312 (92), 284 (97), 134 (28), 91 (16).

4.1.35. 2-(3-Chloro-4,5-dimethoxyphenyl)-5,6,7,8-tetrahydropyridylthieno [2,3-d]pyrimidin-4(3H)-one × CF_3COOH, $C_{19}H_{17}ClF_3N_3O_5S$, (**6 m**)

Compound **6m** was prepared analogously to **6a** from **5m** (51 mg, 0.1 mmol). Yield: 20 mg (0.041 mmol, 41%); colorless solid of m.p. 296 °C; υ_{max} (ATR)/cm^{-1} 3000, 2943, 2836, 1657, 1582, 1542, 1508, 1479, 1429, 1400, 1353, 1304, 1264, 1236, 1199, 1175, 1130, 1104, 1050, 1021, 996, 926, 863, 834, 798, 781, 753, 722, 702, 664; ^{1}H NMR (300 MHz, DMSO-d_6) δ 3.1–3.2 (2 H, m) 3.4–3.5 (2 H, m), 3.84 (3 H, s), 3.96 (3 H, s), 4.43 (2 H, s), 7.82 (1 H, s), 7.89 (1 H, s), 9.2–9.4 (2 H, br s), 12.7–12.9 (1 H, br s); ^{13}C NMR (75.5 MHz, DMSO-d_6) δ 22.4, 41.6, 56.5, 60.5, 111.2, 115.3, 119.8, 121.1, 124.4, 127.2, 127.8, 128.2, 128.4, 147.3, 151.6, 153.4, 158.6, 164.1; *m/z* (%) 377 (100) [M^+], 350 (36), 348 (92), 152 (23).

4.1.36. 2-(3-Bromo-4,5-dimethoxyphenyl)-7-acryloyl-5,6,7,8-tetrahydropyridylthieno [2,3-d]pyrimidin-4(3H)-one, $C_{20}H_{18}BrN_3O_4S$, (**7c**)

Compound **6c** (33 mg, 0.062 mmol) was suspended in acetone and treated with acryloyl chloride (35 μL, 0.43 mmol). K_2CO_3 (197 mg, 1.43 mmol, dissolved in 2 mL H_2O) was added and the reaction mixture was stirred at room temperature for 24 h. Water (20 mL) was added and the formed precipitate was collected, washed with water and dried in vacuum. Yield: 20 mg (0.042 mmol, 68%); colorless solid of m.p. 298–299 °C; υ_{max} (ATR)/cm^{-1} 2938, 2831, 1651, 1614, 1595, 1578, 1544, 1505, 1487, 1470, 1428, 1397, 1357, 1303, 1260, 1218, 1194, 1147, 1103, 1063, 1043, 1018, 994, 974, 947, 926, 866, 836, 818, 786, 751, 723, 694, 674, 659, 602; ^{1}H NMR (300 MHz, DMSO-d_6) δ 3.0–3.1 (2 H, m) 3.82 (3 H, s), 3.8–3.9 (2 H, m), 3.95 (3 H, s), 4.8–5.0 (2 H, m), 5.7–5.8 (1 H, m), 6.1–6.2 (1 H, m), 6.9–7.0 (1 H, m), 7.84 (1 H, s), 8.00 (1 H, s), 12.6–12.7 (1 H, br s); ^{13}C NMR (75.5 MHz, DMSO-d_6) δ 26.5, 41.4, 42.3, 56.4, 60.3, 111.7, 116.8, 120.3, 123.7, 127.8, 128.2, 128.4, 129.2, 129.5, 130.6, 148.2, 150.8, 153.2, 158.6, 164.9, 165.6; *m/z* (%) 477 (100) [M^+], 475 (97) [M^+], 420 (43), 394 (21), 392 (19), 152 (13), 55 (34).

4.1.37. 2-(3-Iodo-4,5-dimethoxyphenyl)-7-acryloyl-5,6,7,8-tetrahydropyridylthieno [2,3-d]pyrimidin-4(3H)-one, $C_{20}H_{18}IN_3O_4S$, (**7e**)

Compound **7e** was prepared analogosuly to **7c** from **6e** (47 mg, 0.081 mmol), acryloyl chloride (46 μL, 0.56 mmol) and K_2CO_3 (257 mg, 1.87 mmol). Yield: 40 mg (0.076 mmol, 94%); colorless solid of m.p. 292–293 °C; υ_{max} (ATR)/cm^{-1} 2926, 2872, 2846, 1664, 1650, 1587, 1568, 1552, 1537, 1505, 1485, 1473, 1438, 1394, 1358, 1332, 1301, 1256, 1239, 1219, 1192, 1152, 1103, 1066, 1048, 1018, 973, 948, 926, 881, 861, 846, 828, 806, 788, 751, 723, 688, 670, 644, 635, 620; ^{1}H NMR (300 MHz, DMSO-d_6) δ 2.5–2.6 (2 H, m) 2.9–3.1 (2 H, m), 3.77 (3 H, s), 3.8–3.9 (2 H, m), 3.92 (3 H, s), 4.7–4.9 (2 H, m), 5.7–5.8 (1 H, m), 6.16 (1 H, d, J = 15.3 Hz), 6.8–7.0 (1 H, m), 7.83 (1 H, s), 8.16 (1 H, s), 12.65 (1 H, s); *m/z* (%) 523 (100) [M^+], 468 (36),

452 (22), 440 (30), 340 (9), 152 (12), 55 (19).

4.1.38. 2-(3-Bromo-4,5-dimethoxyphenyl)-7-acetyl-5,6,7,8-tetrahydropyridylthieno [2,3-d]pyrimidin-4(3H)-one, $C_{19}H_{18}BrN_3O_4S$, (**8c**)

Compound **8c** was prepared analogously to **7c** from **6c** (33 mg, 0.062 mmol), acetyl chloride (31 μL, 0.43 mmol) and K_2CO_3 (197 mg, 1.43 mmol). Yield: 12 mg (0.026 mmol, 42%); colorless solid of m.p. 292–294 °C; υ_{max} (ATR)/cm^{-1} 2945, 2831, 1666, 1650, 1593, 1575, 1543, 1506, 1487, 1475, 1431, 1395, 1361, 1351, 1303, 1260, 1232, 1205, 1194, 1170, 1152, 1105, 1045, 1015, 986, 949, 925, 878, 861, 835, 818, 791, 782, 752, 723, 693, 674, 631, 611; ^{1}H NMR (300 MHz, DMSO-d_6) δ 2.0–2.1 (3 H, m), 2.9–3.1 (2 H, m) 3.7–3.8 (2 H, m), 3.82 (3 H, s), 3.95 (3 H, s), 4.7–4.8 (2 H, m), 7.84 (1 H, s), 8.01 (1 H, s), 12.68 (1 H, s); ^{13}C NMR (75.5 MHz, DMSO-d_6) δ 21.2, 21.8, 25.2, 26.1, 42.8, 44.7, 56.4, 60.3, 111.7, 116.8, 120.4, 123.7, 128.4, 128.6, 129.4, 129.5, 148.2, 150.8, 153.2, 158.6, 164.8, 168.7; *m/z* (%) 465 (100) [M$^+$], 463 (97) [M$^+$], 422 (43), 420 (43), 406 (36), 404 (32), 394 (33), 392 (31), 179 (16), 152 (29), 91 (10), 43 (47).

4.1.39. 2-(3-Iodo-4,5-dimethoxyphenyl)-7-acetyl-5,6,7,8-tetrahydropyridylthieno [2,3-d]pyrimidin-4(3H)-one, $C_{19}H_{18}IN_3O_4S$, (**8e**)

Compound **8e** was prepared analogously to **7c** from **6e** (31 mg, 0.053 mmol), acetyl chloride (31 μL, 0.43 mmol) and K_2CO_3 (197 mg, 1.43 mmol). Yield: 22 mg (0.043 mmol, 81%); colorless solid of m.p. 217–218 °C; υ_{max} (ATR)/cm^{-1} 2944, 2877, 2841, 1701, 1665, 1650, 1589, 1571, 1540, 1507, 1485, 1469, 1446, 1434, 1422, 1394, 1347, 1304, 1256, 1232, 1202, 1168, 1152, 1103, 1042, 1015, 986, 947, 926, 888, 863, 848, 830, 807, 780, 770, 746, 723, 698, 672, 649, 631, 611, 601; ^{1}H NMR (300 MHz, DMSO-d_6) δ 2.0–2.1 (3 H, m), 3.0–3.1 (2 H, m) 3.7–3.8 (2 H, m), 3.78 (3 H, s), 3.93 (3 H, s), 4.7–4.8 (2 H, m), 7.84 (1 H, s), 8.17 (1 H, s), 12.67 (1 H, s); *m/z* (%) 511 (100) [M$^+$], 468 (37), 452 (24), 440 (13), 326 (7), 152 (4), 43 (5); Anal. Calcd. for $C_{19}H_{18}IN_3O_4S$: C, 44.63; H, 3.55; N, 8.22; S, 6.27. Found: C, 46.52; H, 3.68; N, 8.05; S, 6.31.

4.2. Biological evaluation

4.2.1. Cell lines and culture conditions

EA.hy926 (ATCC® CRL-2922™) endothelial hybrid cells, 518A2 (Department of Radiotherapy and Radiobiology, University Hospital Vienna) human melanoma cells, HCT-116 (ACC-581) human colon carcinoma cells, as well as its p53 knockout mutant cell line HCT-116$^{p53-/-}$, KB-V1^{Vbl} resistant cervix carcinoma cells, and HDFa (ATCC® PCS-201-012™) human dermal fibroblasts were grown in Dulbecco's Modified Eagle Medium (DMEM; Biochrom) high glucose supplemented with 10% (v/v) fetal bovine serum (FBS; Biochrom.) and 1% (v/v) Antibiotic-Antimycotic solution (Thermo Scientific). All cells were incubated at 37 °C, 5% CO_2, 95% humidified atmosphere and were serially passaged following trypsinization by using 0.05% trypsin/0.02% EDTA (w/v; Biochrom GmbH, Berlin, Germany). The maximum-tolerated dose of vinblastine was added to the cell culture medium 24 h after every cell passage to keep the KB-V1^{Vbl} cells resistant. For a more detailed assessment of the effect of the most active derivatives on human cancer-associated endothelial cells we used the endothelial hybrid cell line EA.hy926, which is easier to passage and cultivate than primary endothelial cells such as human umbilical vein endothelial cells (HUVEC). Mycoplasma contamination was frequently monitored, and only mycoplasma-free cultures were used.

4.2.2. Inhibition of cell growth (MTT assay)

The tetrazolium salt 3-(4,5-dimethylthiazol-2-yl)-2,5-diphenyltetrazolium bromide (MTT; ABCR) was used to identify viable cells which reduce it to a violet formazan. EA.Hy926 endothelial hybrid cells, 518A2 melanoma cells, colon carcinoma cells HCT-116 and HCT-116$^{p53-/-}$, KB-V1^{Vbl} cervix carcinoma cells (5×10^4 cells mL^{-1}, 100 μL/well), as well as HDFa cells (10×10^4 cells mL^{-1}, 100 μL/well) were seeded in 96-well tissue culture plates and cultured for 24 h at 37 °C, 5% CO_2 and 95% humidity. After treatment with the test compounds incubation of cells was continued for 72 h. Blank and solvent (DMSO) controls were treated identically. After addition of a 5 mg/mL MTT stock solution in phosphate buffered saline (PBS), the microplates were incubated for 2 h at 37 °C, centrifuged at 300 g, 4 °C for 5 min and the supernatant medium was discarded. The precipitate of formazan crystals was redissolved in a 10% (w/v) solution of sodium dodecylsulfate (SDS; Carl Roth) in DMSO containing 0.6% (v/v) acetic acid. To ensure complete dissolution of formazan, the microplates were incubated for at least 1 h in the dark. Finally the absorbance at λ = 570 and 630 nm (background) was measured using a microplate reader (Tecan F200). All experiments were carried out in quadruplicate and the percentage of viable cells was calculated as the mean ± SD with controls set to 100%.

4.2.3. Cell cycle analysis

EA.hy926 endothelial hybrid cells (3 mL/well; 5×10^4 cells mL^{-1}) were grown on 6-well tissue culture plates for 24 h (37 °C, 5% CO_2, 95% humidity). After treatment with different concentrations of the test compounds or DMSO, the cells were incubated for another 24 h (37 °C, 5% CO_2, 95% humidity). After fixation in 70% EtOH (1 h, 4 °C), cells were washed with PBS and incubated with propidium iodide (PI; Carl Roth) staining solution (50 μg/mL PI, 0.1% sodium citrate, 50 μg/mL RNAse A in PBS) for 30 min at 37 °C. The fluorescence intensity of 10 000 single cells, respectively, was measured at λ_{em} = 570 nm (λ_{ex} = 488 nm laser source) with a Beckmann Coulter Cytomics FC500 flow cytometer. The distribution (%) of cells in the different phases of the cell cycle (sub-G1, G1, S and G2/M phase) was determined by CXP software (Beckmann Coulter).

4.2.4. Tubulin polymerization assay

50 μL of Brinkley's Buffer 80 (BRB80) containing 20% glycerol and 3 mM GTP was pipetted in a 96-well half-area plate. After the test compounds or solvent (DMSO) were added to the wells to reach a final concentration of 10 μM, 50 μL of porcine brain tubulin in BRB80 (10 mg/mL) was pipetted into each well, respectively. The microplate was immediately placed in the pre-heated microplate reader (Tecan F200) and polymerization was measured turbidimetrically at 37 °C by recording the absorption at 340 nm for 2 h in intervals of 20 s. All experiments were performed at least in duplicate.

4.2.5. Fluorescence labeling of microtubules

EA.hy926 endothelial hybrid cells (500 μL/well, 1×10^5 cells/well) were seeded on glass coverslips in 24-well plates and incubated under cell culture conditions for 24 h. The cells were treated with various concentrations of the test compounds or solvent (DMSO) and incubated for another 24 h. After fixation in 3.7% formaldehyde solution (in PBS) for 20 min at rt, cells were incubated in 1% BSA, 0.1% Triton X-100 in PBS for 30 min at rt for blocking and permeabilisation. Immunostaining of microtubules was performed by treating the cells first with a primary antibody against alpha-tubulin (anti alpha-tubulin, mouse monoclonal antibody) followed by incubation with a secondary antibody conjugated to AlexaFluor®-546 (goat anti-mouse IgG-AlexaFluor®-546, Invitrogen) for 1 h in the dark. Then, the glass coverslips were mounted in ProLong™ Gold Antifade Mountant (Invitrogen) containing 1 μg/mL DAPI (4′,6-diamidino-2-phenylindole) for

counterstaining of the nuclei. Alterations of the microtubule cytoskeleton were documented by fluorescent microscopy using a Zeiss Imager A1 AX10 (630 × magnification).

4.2.6. Molecular docking studies

The Autodock vina program was used to study the binding of the test compounds in the colchicine binding site of β-tubulin [67]. The Autodock vina software was developed at Molecular Graphics Lab at The Scripps Research Institute, is established for its accuracy and speed, and is optimized for drug screening. The structure of β-tubulin was downloaded from protein data bank (PDB ID: 1sa0) [68]. The protein was prepared by selecting chain B and deleting all other chains, ligands and water molecules from PDB. Colchicine is known to bind to Cys241, therefore the 3D-gridbox was created containing all amino acids surrounding Cys241 with a grid spacing of 1.0 Å and 60 × 60 × 60 point size. Total Kollman and Gasteiger charges were applied to ligands and protein before docking. Lamarckian GA was used to predict the top ligand-protein bound conformations. About 10 conformations for each ligand-protein complex were obtained and the most stable conformation was selected based on the scoring, hydrogen bonding and the lowest binding energy. The structure of ligand-protein complex was visualized using Pymol [69].

4.2.7. Fluorescence labeling of actin filaments

For staining of the F-actin filaments, EA.hy926 endothelial hybrid cells were seeded on glass coverslips (500 μL/well, 5×10^4 cells/mL), incubated for 24 h under cell culture conditions (37 °C, 5% CO_2, 95% humidity) and subsequently treated with different concentrations of test compounds or DMSO for another 3 h. The cells were washed with pre-warmed PBS, fixed in 3.7% formaldehyde in PBS (pH 7.0) for 10 min at rt, permeabilized in 0.5% Triton X-100 in PBS for 5 min at rt and finally stained with Acti-Stain™ 488 phalloidin (100 nM in PBS; Cytoskeleton) for 30 min at rt in the dark. The cells were washed three times with PBS and the coverslips were mounted in ProLong™ Gold Antifade Mountant (Invitrogen) containing 1 μg/mL DAPI (4′,6-diamidino-2-phenylindole) for counterstaining of the nuclei. Documentation of actin filaments was carried out by fluorescence microscopy (Zeiss Imager A1 AX10×, 630 × magnification).

4.2.8. Tube formation assay

EA.hy926 endothelial hybrid cells (100 μL/well, 5×10^5 cells/mL) were seeded on thin layers of basement membrane-like matrix Matrigel® (Corning) in 96 well plates in Endothelial Cell Growth Medium 2 (PromoCell GmbH). Potentially formed tubular networks were documented via light microscopy (Zeiss Axiovert 135×, 100 × magnification). For determination of anti-angiogenic effects, treatment with solvent (DMSO), positive control combretastatin-A4 (CA4) or various concentrations of the test compounds was carried out immediately after seeding of the cells on matrigel and the formation of tubular structures was observed after 6 h of incubation under cell culture conditions (37 °C, 5% CO_2, 95% humidity). For determination of vascular-destructive effects, the cells were first incubated for 6 h under cell culture conditions (37 °C, 5% CO_2, 95% humidity) and the formed vessel-like structures were then treated with solvent, CA4 or the test compounds for 12 h under cell culture conditions. Cell viability was confirmed by MTT-assays to be higher than 80% with negative control set to 100%. All experiments were carried out at least in triplicate.

4.2.9. Chorioallantoic membrane (CAM) assay in fertilized chicken embryos

Fertilized white leghorn chicken eggs (SPF eggs, VALO Biomedia) were incubated until day 5 past fertilization (37 °C, 50–60% humidity) and opened on day six past fertilization by cutting a window of 2–3 cm diameter into the more rounded pole of the eggshell, which was sealed with tape again. After another 24 h incubation, rings of silicon foil (5 mm diameter) were placed onto the developing CAM vessels and test compounds (5 or 15 nmol) or equivalent amounts of solvent (DMSO) were pipetted into the silicon ring. The effects were documented after 0 h, 6 h, and 24 h post application using a light microscope (60 × magnification, Traveller).

The quantitative evaluation of a potential antiangiogenic effect was performed on image sections taken from the light microscope pictures and the area covered by blood vessels was determined by fractal analysis using IQM 3.50 [70], and Fractal Analysis System 3.4.7 [71], and validated by Vessel Segmentation Tool 0.1.4 [72]. The blood vessel area at 0 h (before treatment) was set to 100% and the relative alteration of the blood vessel area after 6 and 24 h was determined. All experiments were carried out at least in triplicate.

4.2.10. Zebrafish angiogenesis assay

Tg(fli1a:EGFP) transgenic zebrafish with a casper background were raised under standard conditions at 27–28 °C [73,74]. Embryos were manually dechorionated 24–26 hpf, transferred into 6-well plates [5 embryos/well in 5 mL E3 medium (5 mM NaCl, 0.17 mM KCl, 0.33 mM $CaCl_2$, 0.33 mM $MgSO_4$, 0.01% methylene blue, pH 7.2)] and treated with different concentrations of the test compounds, or vehicle (DMSO) for 48 h at 27–28 °C. The development of the vascular system of the embryos, especially the SIV (subintestinal veins) area, was documented by fluorescence microscopy (λ_{ex} = 488 nm, λ_{em} = 509 nm; Leica MZ10F with Zeiss AxioCam MRrc and Mrc-ZEN pro 2012 software). The length of SIV of at least 20 identically treated embryos was quantified as means ± SD with vehicle control set to 100%. Significance of results was determined using a *t*-test. *: $p < 0.001$, **: $p < 0.01$.

4.2.11. CDK1/CyclinA2 kinase assays

The kinase assays were run by using full-length recombinant CDK1/CyclinA2 protein complexes co-expressed by baculovirus in Sf9 insect cells (Promega). Activity of the CDK1/CyclinA2 kinase complexes was measured by the luminescence-based ADP-Glo™ Kinase Assay (Promega) in a 96-well-format. Individual reactions were set up in a final volume of 25 μL with 2 ng of active CDK1/CyclinA2 and 5 μg of histone H1 substrate in reaction buffer (40 mM Tris-HCl, 20 mM $MgCl_2$, 0.1 mg/mL BSA, 50 μM DTT, pH 7.5). Kinase reactions were initiated by addition of 5 μL 250 μM ATP solution and incubated at 30 °C for 15 min under constant agitation. The reaction was terminated and the remaining ATP was depleted by addition of 25 μL of ADP-Glo™ reagent to each well. After an additional incubation time of 40 min with shaking, 50 μL of kinase detection reagent was added, followed by another 30 min of incubation at rt. The luminescence was measured using a FLUOstar microplate reader (Omega). To estimate the amount of ADP produced by the CDK1 kinase reaction, an ATP-to-ADP percent conversion curve was prepared using ultra-pure ADP and ATP. All experiments were carried out at least in duplicate.

Abbreviations

518A2	Human melanoma cell line
ATR	Attenuated total reflection
BRB80	Brinkley's Buffer 80
CA4	Combretastatin A-4
CAM	Chorioallantoic membrane
CDK	Cyclin-dependent kinase
DAPI	4′,6-diamidino-2-phenylindole
EA.hy926	Human endothelial hybrid cell line

EI	Electron ionization
FACS	Fluorescence assisted cell sorting
FBS	Fetal bovine serum
FT-IR	Fourier-transform infrared spectroscopy
HCT-116	Human colon carcinoma cell line
HCT-116$^{p53-/-}$	Knockout mutant cell line, lacking functional p53 protein
HDAC	Histone deacetylase
HDFa	Human dermal fibroblasts, adult
hpf	Hours post fertilization
HUVEC	Human umbilical vein endothelial cells
IC_{50}	Half maximum inhibitory concentration
KB-V1^{Vbl}	Multi-drug resistant cervix carcinoma cell line
MBA	Microtubule binding agent
MTT	3-(4,5-dimethylthiazol-2-yl)-2,5-diphenyl tetrazolium bromide
NMR	Nuclear magnetic resonance
p	Probability value
PDB	Protein data bank
SIV	Subintestinal veins
SPF	Specific pathogen free
STA	Staurosporine
TEC	Tumor endothelial cell
VEGF	Vascular growth factor

Appendix A. Supplementary data

Supplementary data to this article can be found online at https://doi.org/10.1016/j.ejmech.2020.112060.

References

[1] P. Carmeliet, R.K. Jain, Angiogenesis in cancer and other diseases, Nature 407 (2000) 249–257.
[2] L.M. Iruela-Arispe, H.F. Dvorak, Angiogenesis: a dynamic balance of stimulators and inhibitors, Thromb. Haemost. 78 (1997) 672–677.
[3] J. Folkman, Angiogenesis in cancer, vascular, rheumatoid and other disease, Nat. Med. 1 (1995) 27–31.
[4] A.M.E. Abdalla, L. Xiao, M.W. Ullah, M. Yu, C. Ouyang, et al., Current challenges of cancer anti-angiogenic therapy and the promise of nanotherapeutics, Theranostics 8 (2018) 533–548.
[5] K. Hida, Y. Hida, Shindoh M Understanding tumor endothelial cell abnormalities to develop ideal anti-angiogenic therapies, Cancer Sci. 99 (2007) 459–466.
[6] H. Hashizume, P. Baluk, S. Morikawa, J.W. McLean, G. Thurston, et al., Openings between defective endothelial cells explain tumor vessel leakiness, Am. J. Pathol. 156 (2000) 1363–1380.
[7] P.P. Lin, O. Gires, D.D. Wang, L. Li, H. Wang, Comprehensive in situ co-detection of aneuploid circulating endothelial and tumor cells, Sci. Rep. 7 (2017) 1–10.
[8] Y.Q. Xiong, H.C. Sun, W. Zhang, X.D. Zhu, P.Y. Zhuang, et al., Human hepatocellular carcinoma tumor-derived endothelial cells manifest increased angiogenesis capability and drug resistance compared with normal endothelial cells, Clin. Cancer Res. 15 (2009) 4838–4846.
[9] D.W. Siemann, The unique characteristics of tumor vasculature and preclinical evidence for its selective disruption by tumor-vascular disrupting agents, *Cancer* Treat Rev. 37 (2011) 63–74.
[10] M.A. Jordan, L. Wilson, Microtubules as a target for anticancer drugs, Nat. Rev. Cancer 4 (2004) 253–265.
[11] D. Belotti, V. Vergani, T. Drudis, P. Borsotti, M.R. Pitelliet, et al., The microtubule-affecting drug paclitaxel has antiangiogenic activity, Clin. Cancer Res. 2 (1996) 1843–1849.
[12] G.G. Dark, S.A. Hill, V.E. Prise, G.M. Tozer, G.R. Pettit, et al., Combretastatin A-4, an agent that displays potent and selective toxicity toward tumor vasculature, Cancer Res. 57 (1997) 1829–1834.
[13] B. Pourroy, S. Honoré, E. Pasquier, Bourgarel-Rey, A. Kruczynski, et al., Antiangiogenic concentrations of vinflunine increase the interphase microtubule dynamics and decrease the motility of endothelial cells, Cancer Res. 66 (2006) 3256–3263.
[14] R.J. Ludford, Colchicine in the experimental chemotherapy of cancer, J. Natl. Cancer Inst. 6 (1945) 89–101.
[15] O.N. Zefirova, A.G. Diikov, N.V. Zyk, N.S. Zefirov, Ligands of the colchicine binding site of tubulin: a common pharmacophore and new structural classes, Rus. Chem. Bull. IE 56 (2007) 680–688.
[16] R.M. Lee, D.A. Gewirtz, Colchicine site inhibitors of microtubule integrity as vascular disrupting agents, Drug Dev. Res. 69 (2008) 352–358.
[17] F. Schmitt, L.C. Gosch, A. Dittmer, M. Rothemund, T. Mueller, et al., Oxazole-bridged combretastatin A-4 derivatives with tethered hydroxamic acids: structure-activity relations of new inhibitors of HDAC and/or tubulin function, Int. J. Mol. Sci. 20 (2019) 383.
[18] K.M. Al-Taisan, H.M.A. Al-Hazimi, S.S. Al-Shihry, Synthesis, characterization and biological studies of some novel thieno[2,3-d]pyrimidines, Molecules 15 (2010) 3932–3957.
[19] T. Horiuchi, M. Nagata, M. Kitagawa, K. Akahane, K. Uoto, Discovery of novel thieno [2,3-*d*] pyrimidin-4-yl hydrazone-based inhibitors of cyclin D1-CDK4: synthesis, biological evaluation and structure-activity relationships, Part 2, Bioorg. Med. Chem. 17 (2009) 7850–7860.
[20] a) B.V. Ashalatha, B. Narayana, K.K.V. Raj, N.S. Kumari, Synthesis of some new bioactive 3-amino-2-mercapto-5,6,7,8-tetrahydro-1-benzothieno[2,3-*d*]pyrimidin-4(3H)-one derivatives, Eur. J. Med. Chem. 42 (2007) 719–728;
b) S.E. Abbas, N.M.A. Gawad, R.F. George, Y.A. Akar, Synthesis, antitumor and antibacterial activities of some novel tetrahydrobenzo[4,5]thieno[2,3-d]pyrimidine derivatives, Eur. J. Med. Chem. 65 (2013) 195–204.
[21] M.B. Dewal, A.S. Wani, C. Vidaillac, D. Oupicky, M.J. Rybak, et al., Thieno[2,3-d] pyrimidinedione derivatives as antibacterial agents, Eur. J. Med. Chem. 51 (2012) 145–153.
[22] A.E. Rashad, M.A. Ali, Synthesis and antiviral screening of some thieno 2,3-*d* pyrimidine nucleosides, Nucleos. Nucleot. Nucl. 25 (2006) 17–28.
[23] a) V. Alagarsamy, S. Meena, K.V. Ramseshu, V.R. Solomon, K. Thirumurugan, et al., Synthesis, analgesic, anti-inflammatory, ulcerogenic index and antibacterial activities of novel 2-methylthio-3-substituted-5,6,7,8-tetrahydrobenzo(b) thieno 2,3-*d* pyrimidin-4(3*H*)-ones, Eur. J. Med. Chem. 41 (2006) 1293–1300;
b) Y. Zhang, L. Luo, C. Han, H. Lv, D. Chen, Design, synthesis, and biological activity of tetrahydrobenzo[4,5]thieno[2,3-*d*]pyrimidine derivatives as anti-inflammatory agents, Molecules 22 (2017) 1960–1981.
[24] M. Modica, M. Santagati, F. Russo, L. Parotti, L. De Gioia, et al., [[(Arylpiperazinyl)alkyl]thio]thieno[2,3-d]pyrimidone derivatives as high-affinity, selective 5-HT1A receptor ligands, J. Med. Chem. 40 (1997) 574–585.
[25] L. Ouyang, L. Zhang, J. Liu, L. Fu, D. Yao, et al., Discovery of a small-molecule bromodomain-containing protein 4 (BRD4) inhibitor that induces AMP-activated protein kinase-modulated autophagy-associated cell death in breast cancer, J. Med. Chem. 60 (2017) 9990–10012.
[26] Y.D. Wang, S. Johnson, D. Powell, J.P. McGinnis, M. Miranda, S.K. Rabindran, Inhibition of tumor cell proliferation by thieno[2,3-d]pyrimidin-4(1H)-one-based analogs, Bioorg. Med. Chem. Lett 15 (2005) 3763–3766.
[27] H. Amawi, C. Karthikeyan, R. Pathak, N. Hussein, R. Christman, et al., Thienopyrimidine derivatives exert their anticancer efficacy via apoptosis induction, oxidative stress and mitotic catastrophe, Eur. J. Med. Chem. 138 (2017) 1053–1065.
[28] D. Jennings, S.L. Kincaid, Y.D. Wang, G. Krishnamurthy, C.F. Beyer, et al., Parallel synthesis and biological evaluation of 5,6,7,8-tetrahydrobenzothieno[2,3-*d*]pyrimidin-4(3H)-one cytotoxic agents selective for p21-deficient cells, Bioorg. Med. Chem. Lett 15 (2005) 4731–4735.
[29] H. Yamada, et al., to Nippon Soda Co Ltd. Tokyo (Jpn). Thienopyrimidine Compounds and Salts Thereof and Process for the Preparation of the Same, 2000. EP1323719A1, WO59912A1.
[30] K.J. Verhey, J. Gaertig, The tubulin code, Cell Cycle 6 (2007) 2152–2160.
[31] D. Bates, A. Eastman, Microtubule destabilising agents: far more than just antimitotic anticancer drugs: MDA mechanism of action, Br. J. Clin. Pharmacol. 83 (2017) 255–268.
[32] K. Chitaley, R. Webb, Microtubule depolymerization facilitates contraction of vascular smooth muscle via increased activation of RhoA/Rho-kinase, Med. Hypotheses 56 (2001) 381–385.
[33] B.P. Liu, M. Chrzanowska-Wodnicka, K. Burridge, Microtubule depolymerization induces stress fibers, focal adhesions, and DNA synthesis via the GTP-binding protein Rho, Cell Adhes. Commun. 5 (1998) 249–255.
[34] Y. Zhai, P.J. Kronebusch, P.M. Simon, G.G. Borisy, Microtubule dynamics at the G2/M transition: abrupt breakdown of cytoplasmic microtubules at nuclear envelope breakdown and implications for spindle morphogenesis, J. Cell Biol. 135 (1996) 201–214.
[35] S. Bugge, S.J. Kaspersen, S. Larsen, U. Nonstad, G. Bjørkøy, et al., Structure-activity study leading to identification of a highly active thienopyrimidine based EGFR inhibitor, Eur. J. Med. Chem. 75 (2014) 354–374.
[36] R.W.A. Luke, P. Ballard, D. Buttar, L. Campell, J. Curwen, et al., Novel thienopyrimidine and thiazolopyrimidine kinase inhibitors with activity against Tie-2 in vitro and in vivo, Bioorg. Med. Chem. Lett 19 (2009) 6670–6674.
[37] Y. Dai, Y. Guo, R.R. Frey, Z. Ji, M.L. Curtin, et al., Thienopyrimidine ureas as novel and potent multitargeted receptor tyrosine kinase inhibitors, J. Med. Chem. 48 (2005) 6066–6083.
[38] W.J. McClellan, Y. Dai, C. Abad-Zapatero, D.H. Albert, J.J. Bouska, et al., Discovery of potent and selective thienopyrimidine inhibitors of Aurora kinases, Bioorg. Med. Chem. Lett 21 (2011) 5620–5624.
[39] T. Horiuchi, Y. Takeda, N. Haginoya, M. Miyazaki, M. Nagata, et al., Discovery of novel thieno[2,3-*d*]pyrimidin-4-yl hydrazone-based cyclin-dependent kinase 4 inhibitors: synthesis, biological evaluation and structure-activity relationships, Chem. Pharm. Bull. 59 (2011) 991–1002.
[40] T. Hunter, J. Pines, Cyclins and cancer II: cyclin D and CDK inhibitors come of age, Cell 79 (1994) 573–582.
[41] D.O. Morgan, Cyclin-dependent kinases: engines, clocks, and microprocessors, Annu. Rev. Cell Dev. Biol. 13 (1997) 261–291.

[42] D.O. Morgan, Principles of CDK regulation, Nature 374 (1995) 131–134.
[43] L.T. Vassilev, C. Tovar, S. Chen, D. Knezevic, X. Zhao, et al., Selective small-molecule inhibitor reveals critical mitotic functions of human CDK1, Proc. Natl. Acad. Sci. 103 (2006) 10660–10665.
[44] A. Satyanarayana, P. Kaldis, Mammalian cell-cycle regulation: several Cdks, numerous cyclins and diverse compensatory mechanisms, Oncogene 28 (2009) 2925–2939.
[45] O. Tetsu, F. McCormick, Proliferation of cancer cells despite CDK2 inhibition, Cancer Cell 3 (2003) 233–245.
[46] C.J. Sherr, J.M. Roberts, Living with or without cyclins and cyclin-dependent kinases, Genes Dev. 18 (2004) 2699–2711.
[47] D. Siemann, The unique characteristics of tumor vasculature and preclinical evidence for its selective disruption by tumor-vascular disrupting agents, Cancer Treat Rev. 37 (2011) 63–74.
[48] G.M. Tozer, C. Kanthou, C.S. Parkins, S.A. Hill, The biology of the combretastatins as vascular targeting agents, Int. J. Exp. Pathol. 83 (2002) 21–38.
[49] E. Porcù, A. Salvador, I. Primac, S. Mitola, R. Ronca, et al., Vascular disrupting activity of combretastatin analogues, Vasc. Pharmacol. 83 (2016) 78–89.
[50] M. Su, J. Huang, S. Liu, Y. Xiao, X. Qin, et al., The anti-angiogenic effect and novel mechanisms of action of Combretastatin A-4, Sci. Rep. 6 (2016), 28139.
[51] Y.W. Shi, W. Yuan, X. Wang, J. Gong, S.X. Zhu, et al., Combretastatin A-4 efficiently inhibits angiogenesis and induces neuronal apoptosis in zebrafish, Sci. Rep. 6 (2016), 30189.
[52] B.C. Baguley, K.M. Holdaway, L.L. Thomsen, L. Zhuang, L.J. Zwi, Inhibition of growth of colon-38 adenocarcinoma by vinblastine and colchicines: evidence for a vascular mechanism, Eur. J. Cancer 27 (1991) 482–487.
[53] S.A. Hill, J. Lonergan, J. Denekamp, D.J. Chaplin, Vinca alkaloids: anti-vascular effects in a murine tumour, Eur. J. Cancer 9 (1993) 1320–1324.
[54] N. Klauber, S. Parangi, E. Flynn, E. Hamel, R.J. D'Amato, Inhibition of angiogenesis and breast cancer in mice by the microtubule inhibitors 2-methoxyestradiol and taxol, Cancer Res. 57 (1997) 81–86.
[55] D.S. Grant, T.L. Williams, M. Zahaczewsky, A.P. Dicker, Comparison of the antiangiogenic activities using paclitaxel (taxol) and docetaxel (taxotere), Int. J. Cancer 104 (2003) 121–129.
[56] S.J. Stafford, J. Schwimer, C.T. Anthony, J.L. Thomson, Y.Z. Wang, et al., Colchicine and 2-methoxyestradiol inhibit human angiogenesis, J. Surg. Res. 125 (2005) 104–108.
[57] Y.W. Shi, W. Yuan, X. Wang, J. Gong, S.X. Zhu, et al., Combretastatin A-4 efficiently inhibits angiogenesis and induces neuronal apoptosis in zebrafish, Sci. Rep. 6 (2016), 30189.
[58] M. Su, J. Huang, S. Liu, Y. Xiao, X. Qin, et al., The anti-angiogenic effect and novel mechanisms of action of Combretastatin A-4, Sci. Rep. 6 (2016) 28139.
[59] M.N.A. Bijman, G.P. van Nieuw Amerongen, N. Laurens, V.W.M. van Hinsbergh, E. Boven, Microtubule-targeting agents inhibit angiogenesis at subtoxic concentrations, a process associated with inhibition of Rac1 and Cdc42 activity and changes in the endothelial cell cytoskeleton, Mol. Cancer Ther. 5 (2006) 2348–2357.
[60] B. Ahmed, L.I. Van Eijk, J.C. Bouma-Ter Steege, D.W.J. van der Schaft, A.M. van Esch, et al., Vascular targeting effect of combretastatin A-4 phosphate dominates the inherent angiogenesis inhibitory activity, Int. J. Cancer 105 (2003) 20–25.
[61] D.S. Grant, T.L. Williams, M. Zahaczewsky, A.P. Dicker, Comparison of the antiangiogenic activities using paclitaxel (taxol) and docetaxel (taxotere), Int. J. Cancer 104 (2003) 121–129.
[62] H. Lu, J. Murtagh, E.L. Schwartz, The microtubule binding drug laulimalide inhibits vascular endothelial growth factor-induced human endothelial cell migration and is synergistic when combined with docetaxel (taxotere), Mol. Pharmacol. 69 (2006) 1207–1215.
[63] L. Vincent, P. Kermani, L.M. Young, J. Cheng, F. Zhang, et al., Combretastatin A4 phosphate induces rapid regression of tumor neovessels and growth through interference with vascular endothelial-cadherin signaling, J. Clin. Investig. 115 (2005) 2992–3006.
[64] M. Su, J. Huang, S. Liu, Y. Xiao, X. Qin, et al., The anti-angiogenic effect and novel mechanisms of action of Combretastatin A-4, Sci. Rep. 6 (2016) 28139.
[65] R.W.A. Luke, P. Ballard, D. Buttar, L. Campbell, J. Curwen, et al., Novel thienopyrimidine and thiazolopyrimidine kinase inhibitors with activity against Tie-2 in vitro and in vivo, Bioorg. Med. Chem. Lett 19 (2009) 6670–6674.
[66] E.Z. Elrazaz, R.A.T. Serya, N.S.M. Ismail, D.A. Abou El Ella, K.A.M. Abouzid, Thieno[2,3-*d*]pyrimidine based derivatives as kinase inhibitors and anticancer agents, FJPS 1 (2015) 33–41.
[67] O. Trott, A.J. Olson, AutoDock Vina: improving the speed and accuracy of docking with a new scoring function, efficient optimization, and multithreading, J. Comput. Chem. 31 (2010) 455–461.
[68] R.B. Ravelli, B. Gigant, P.A. Curmi, I. Jourdain, S. Lachkar, et al., Insight into tubulin regulation from a complex with colchicine and a stathmin-like domain, Nature 428 (2004) 198–202.
[69] N. Alexander, N. Woetzel, J. Meiler, bcl::Cluster: a method for clustering biological molecules coupled with visualization in the Pymol Molecular Graphics System, IEEE Int. Conf. Comput. Adv. Bio. Med. Sci. (2011) 13–18.
[70] P. Kainz, M. Mayrhofer-Reinhartshuber, H. Ahammer, IQM: an extensible and portable open source application for image and signal analysis in Java, PLoS One 10 (2015) 1.
[71] L.M. Kirchner, S.P. Schmidt, B.S. Gruber, Quantitation of angiogenesis in the chick chorioallantoic membrane model using fractal analysis, Microvasc. Res. 51 (1996) 2–14.
[72] Condurache AP, Aach T, Grzybowski S, Machens H. Vessel segmentation and analysis in laboratory skin transplant micro-angiogram. in Proceedings of the 18th IEEE Symposium on CBMS-2005, pp. 21-26, IEEE, Dublin, Ireland, June 23-24.
[73] N.D. Lawson, B.M. Weinstein, In vivo imaging of embryonic vascular development using transgenic zebrafish, Dev. Biol. 248 (2002) 307–318.
[74] R.M. White, A. Sessa, C. Burke, T. Bowman, J. LeBlanc, et al., Transparent adult zebrafish as a tool for in vivo transplantation analysis, Cell Stem Cell 2 (2008) 183–189.

-Supplementary data-

Synthesis and bioevaluation of new vascular-targeting and anti-angiogenic thieno[2,3-*d*]pyrimidin-4(3*H*)-ones

Madeleine Gold[1], Leonhard Köhler[1], Clarissa Lanzloth[1], Ion Andronache[2], Shrikant Anant[3], Prasad Dandawate[3], Bernhard Biersack[1], Rainer Schobert[1]

[1]Organic Chemistry Laboratory, University of Bayreuth, Universitaetsstrasse 30, 95440 Bayreuth, Germany.

[2]Research Center for Integrated Analysis and Territorial Management, University of Bucharest, 4-12, Regina Elisabeta Avenue, Bucharest, 3rd District, 030018, Romania.

[3]Department of Cancer Biology, University of Kansas Medical Center, 3901 Rainbow Boulevard, Kansas City, KS 66160, USA.

Corresponding author: Rainer Schobert, Fax: +49 921/552671
Email: Rainer.schobert@uni-bayreuth.de

Table of content

Biological assays

Caspase-3/7 activation

For caspase activity measurements the Apo-ONE® Homogenous Caspase-3/7 Assay Kit (Promega Corp., Wisconsin, USA) was used. Therefore EA.hy926 endothelial hybrid cells (1.35×10^4 cells/well) were grown in black 96-well plates for 24 h (37 °C, 5% CO_2 and 95% humidity) and subsequently incubated with different concentrations of the test compounds or solvent for further 24 h under cell culture conditions. Afterwards 1× caspase-3/7 substrate solution was added to each well and the substrate transformation by potentially activated caspase-3/7 was performed for 60 min at rt. Finally the fluorescence intensity (λ_{ex}: 485 ± 20 nm, λ_{em}: 530 ± 25 nm) was measured using a microplate reader (Tecan F200). For an incorporation of a potential loss of cell viability after the incubation with the test compounds, a MTT-assay was performed equally (as described above). All experiments were carried out in quadruplicate, blank values (caspase-3/7 substrate solution plus test compounds/solvent) were subtracted to reduce background signals, and the caspase-3/7 activity of the remaining vital cells was calculated as means ± SD with solvent controls set to 100%.

Results

Inhibition of tubulin dynamics

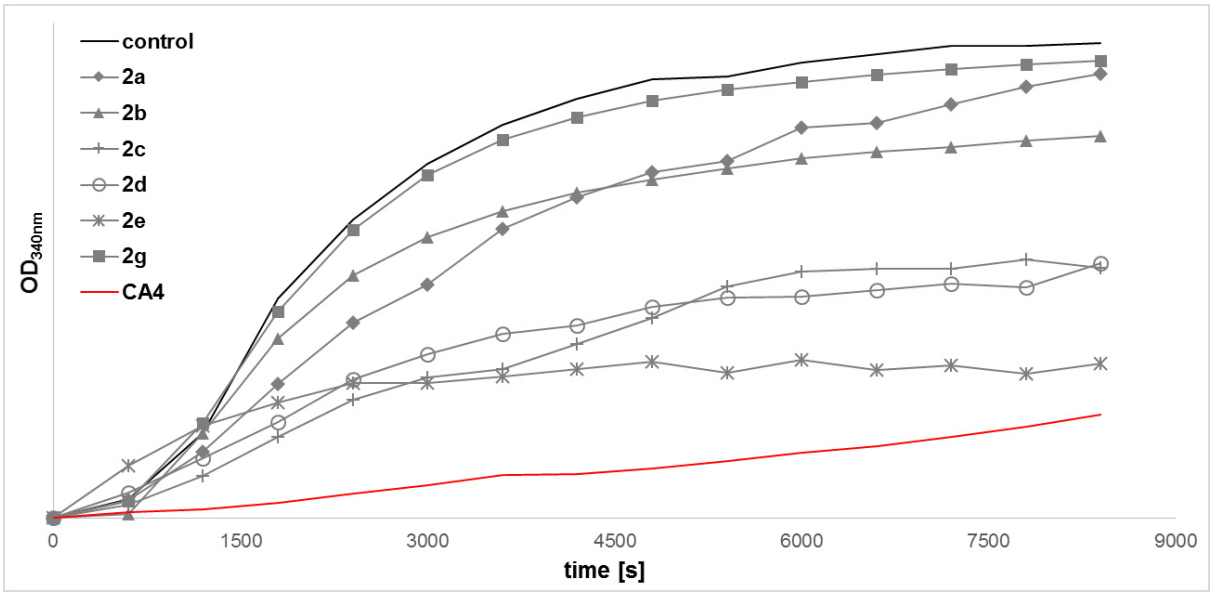

Figure 1S. Inhibition of tubulin polymerization by test compounds **2a-e** and **2g** (10 µM, each) as determined by a turbidimetric cell-free tubulin assay. CA4 (10 µM) was used as a positive control. Negative controls were treated with vehicle (DMSO). Data are representative of at least two independent experiments.

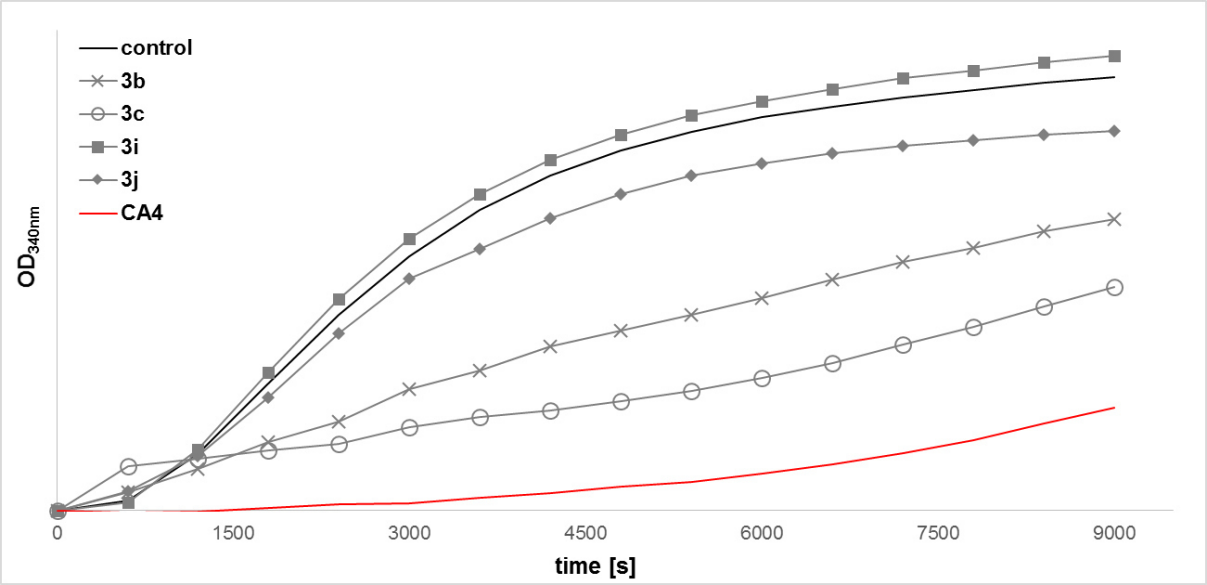

Figure 2S. Inhibition of tubulin polymerization by test compounds **3b-c** and **3i-j** (10 µM, each) as determined by a turbidimetric cell-free tubulin assay. CA4 (10 µM) was used as a positive control. Negative controls were treated with vehicle (DMSO). Data are representative of at least two independent experiments.

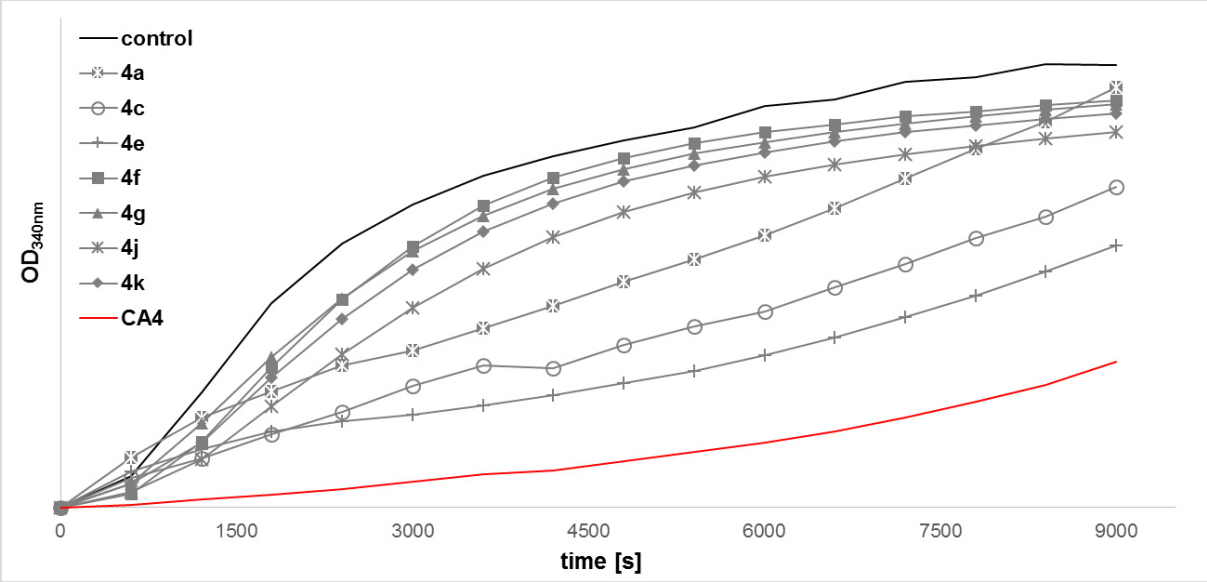

Figure 3S. Inhibition of tubulin polymerization by test compounds **4a, 4c, 4e-g** and **4j-k** (10 µM, each) as determined by a turbidimetric cell-free tubulin assay. CA4 (10 µM) was used as a positive control. Negative controls were treated with vehicle (DMSO). Data are representative of at least two independent experiments.

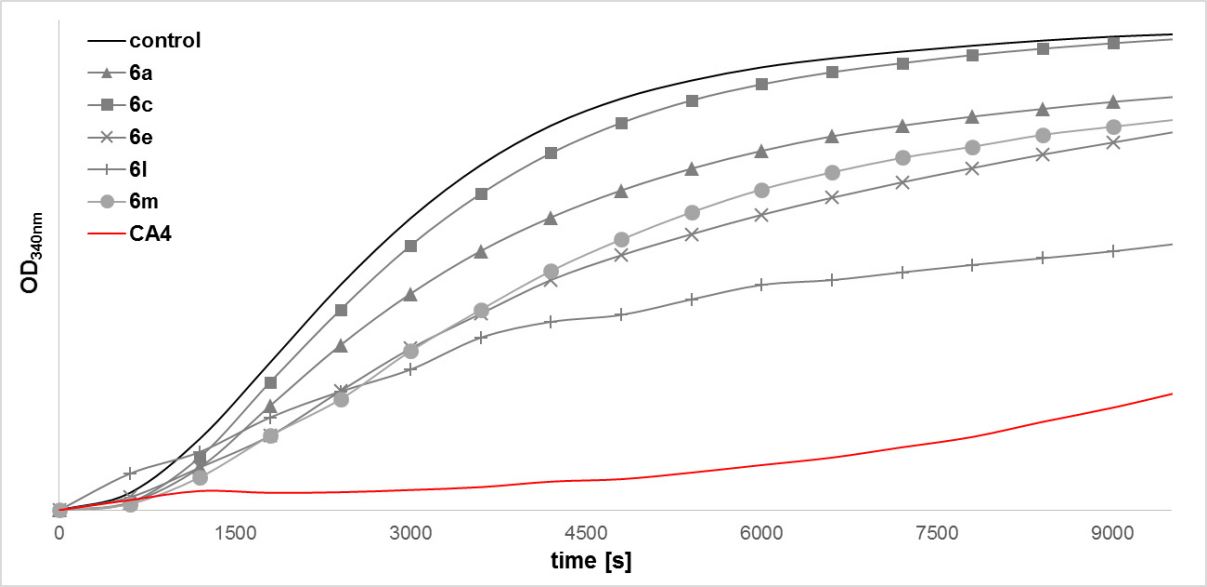

Figure 4S. Inhibition of tubulin polymerization by test compounds **6a, 6c, 6e** and **6l-m** (10 μM, each) as determined by a turbidimetric cell-free tubulin assay. CA4 (10 μM) was used as a positive control. Negative controls were treated with vehicle (DMSO). Data are representative of at least two independent experiments.

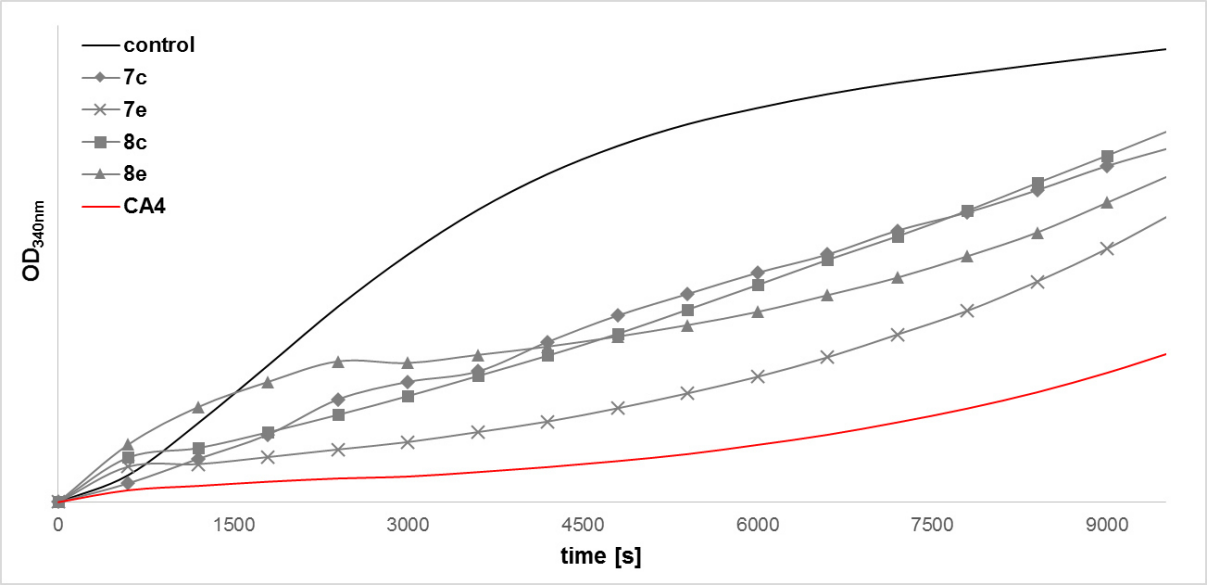

Figure 5S. Inhibition of tubulin polymerization by test compounds **7c/e** and **8c/e** (10 μM, each) as determined by a turbidimetric cell-free tubulin assay. CA4 (10 μM) was used as a positive control. Negative controls were treated with vehicle (DMSO). Data are representative of at least two independent experiments.

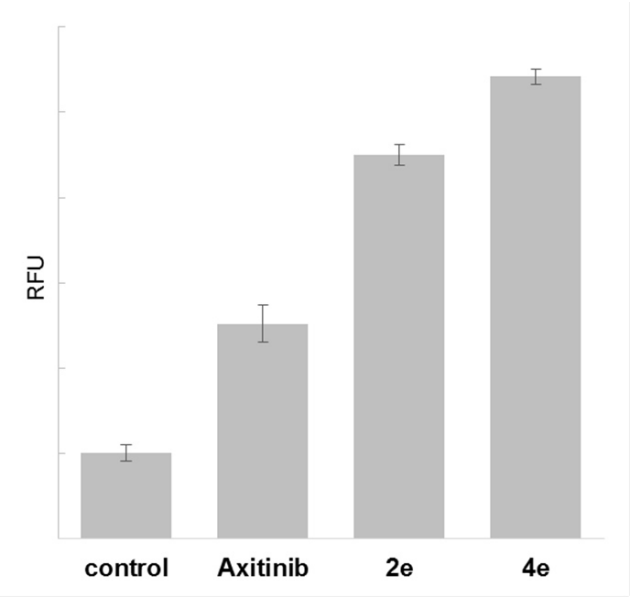

Figure 6S. Induction of caspase-3/7 activity in EA.hy926 endothelial hybrid cells after 21 h incubation with the test compounds **2e** and **4e** (5 µM). As a positive control the cells were treated with the known apoptosis inducing drug axitinib (5 µM). The negative controls were treated equally with neat solvent (DMSO).

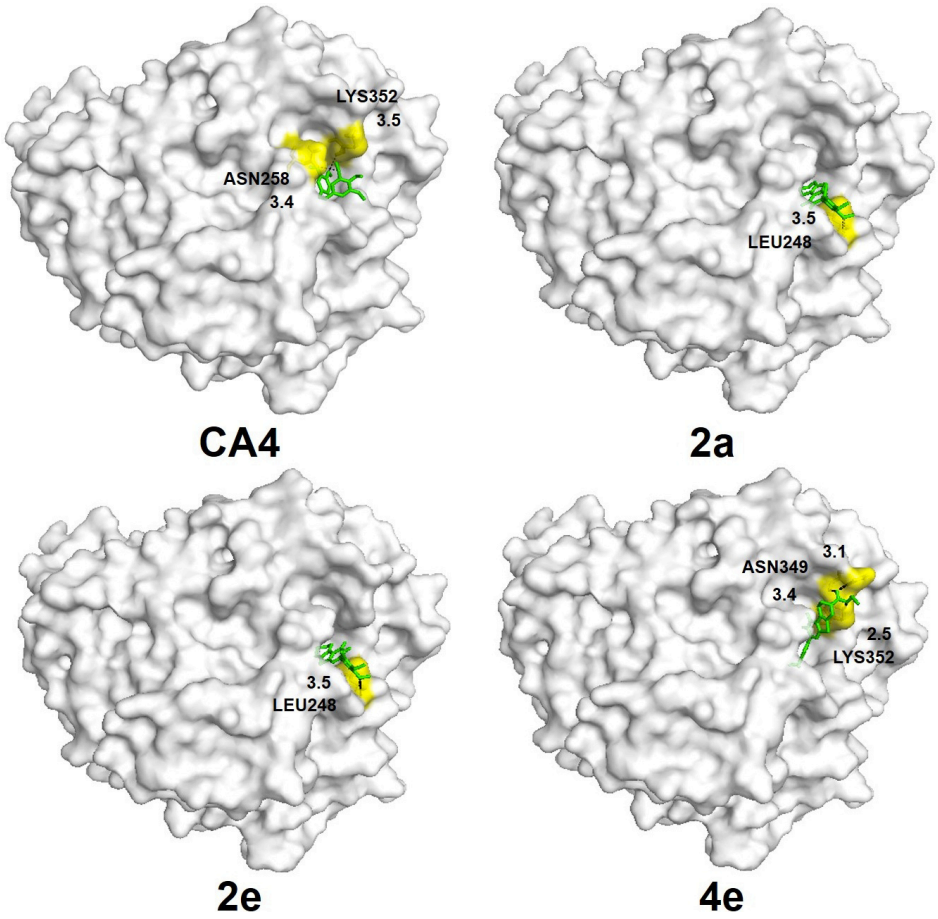

Figure 7S. Molecular docking of thienopyrimidines **2a, 2e** and **4e** into the colchicine binding site of ß-tubulin. CA4, which also binds to this site was used as positive control.

NMR spectra of new compounds

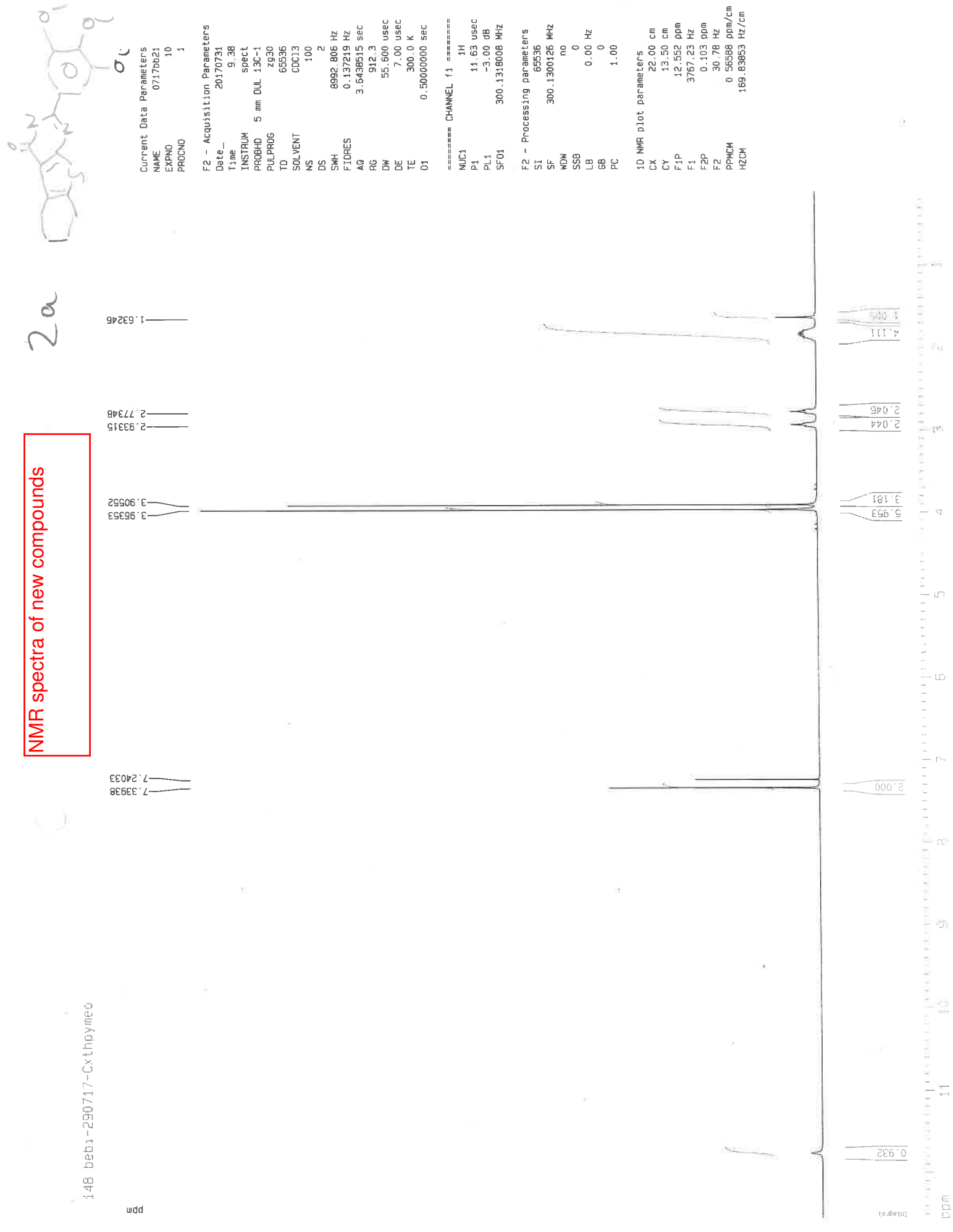

2a

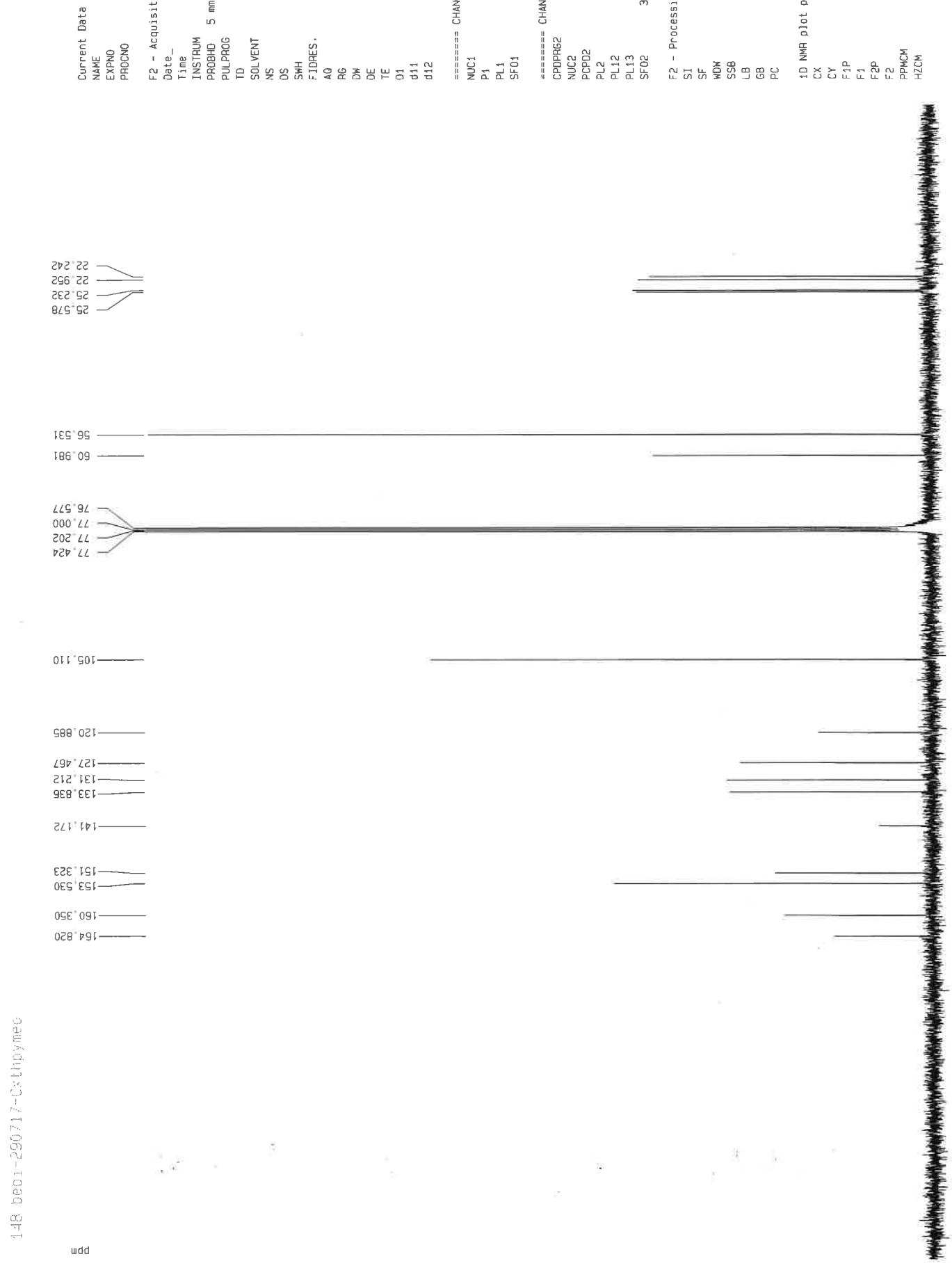
Current Data Parameters
NAME 0717bb21
EXPNO 11
PROCNO 1
F2 - Acquisition Parameters
Date_ 20170731
Time 9.47
INSTRUM spect
PROBHD 5 mm DUL 13C-1
PULPROG zgpg30
TD 32768
SOLVENT CDCl3
NS 10160
DS 4
SWH 18832.393 Hz
FIDRES 0.574719 Hz
AQ 0.8700404 sec
RG 18390.4
DW 26.550 usec
DE 20.00 usec
TE 300.0 K
D1 0.40000001 sec
d11 0.03000000 sec
d12 0.00002000 sec
======== CHANNEL f1 ========
NUC1 13C
P1 7.37 usec
PL1 5.00 dB
SFO1 75.4760505 MHz
======== CHANNEL f2 ========
CPDPRG2 waltz16
NUC2 1H
PCPD2 90.00 usec
PL2 -3.00 dB
PL12 14.77 dB
PL13 16.00 dB
SFO2 300.1312005 MHz
F2 - Processing parameters
SI 32768
SF 75.4677498 MHz
WDW EM
SSB 0
LB 1.00 Hz
GB 0
PC 1.40
1D NMR plot parameters
CX 22.00 cm
CY 15.00 cm
F1P 234.761 ppm
F1 17716.89 Hz
F2P -14.781 ppm
F2 -1115.50 Hz
PPMCM 11.34283 ppm/cm
HZCM 856.01782 Hz/cm
22.242
22.952
25.232
25.578
56.531
60.981
76.577
77.000
77.202
77.424
105.110
120.885
127.467
131.212
133.836
141.172
151.323
153.530
160.350
164.820
ppm
148 bea1-290717-Cxthpymec

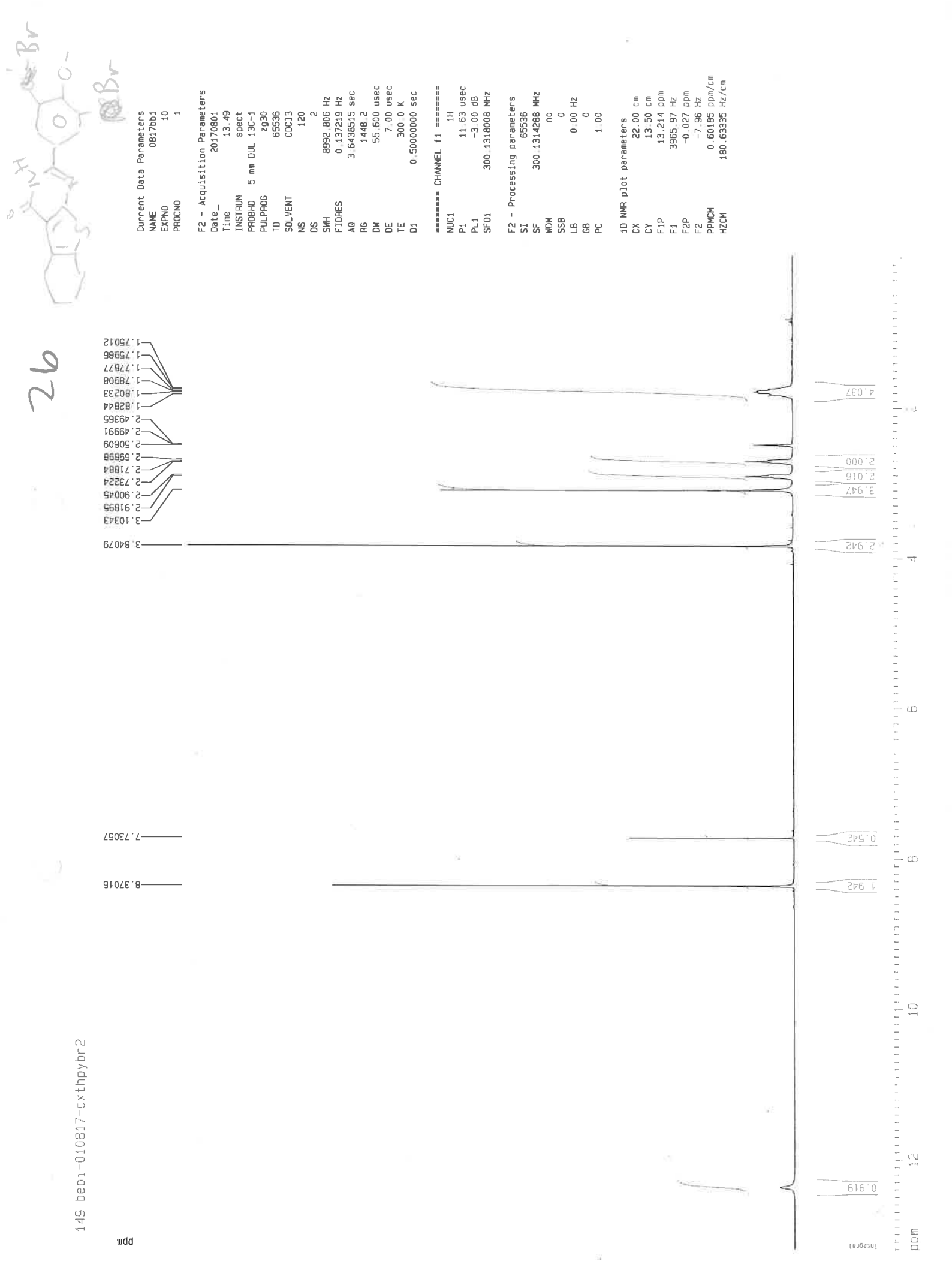
Current Data Parameters
NAME 0817bb1
EXPNO 10
PROCNO 1
F2 - Acquisition Parameters
Date_ 20170801
Time 13.49
INSTRUM spect
PROBHD 5 mm DUL 13C-1
PULPROG zg30
TD 65536
SOLVENT CDCl3
NS 120
DS 2
SWH 8992.806 Hz
FIDRES 0.137219 Hz
AQ 3.6438515 sec
RG 1448.2
DW 55.600 usec
DE 7.00 usec
TE 300.0 K
D1 0.50000000 sec
======== CHANNEL f1 ========
NUC1 1H
P1 11.63 usec
PL1 -3.00 dB
SFO1 300.1318008 MHz
F2 - Processing parameters
SI 65536
SF 300.1314288 MHz
WDW no
SSB 0
LB 0.00 Hz
GB 0
PC 1.00
1D NMR plot parameters
CX 22.00 cm
CY 13.50 cm
F1P 13.214 ppm
F1 3965.97 Hz
F2P -0.027 ppm
F2 -7.96 Hz
PPMCM 0.60185 ppm/cm
HZCM 180.63335 Hz/cm
1.75012
1.75986
1.77677
1.78908
1.80233
1.82844
2.49365
2.49991
2.50609
2.69698
2.71884
2.73224
2.90045
2.91895
3.10343
3.84079
7.73057
8.37015
4.037
2.000
2.016
3.947
2.942
0.542
1.942
0.919
integral
ppm
149 beb1-010817-cxthpybr2

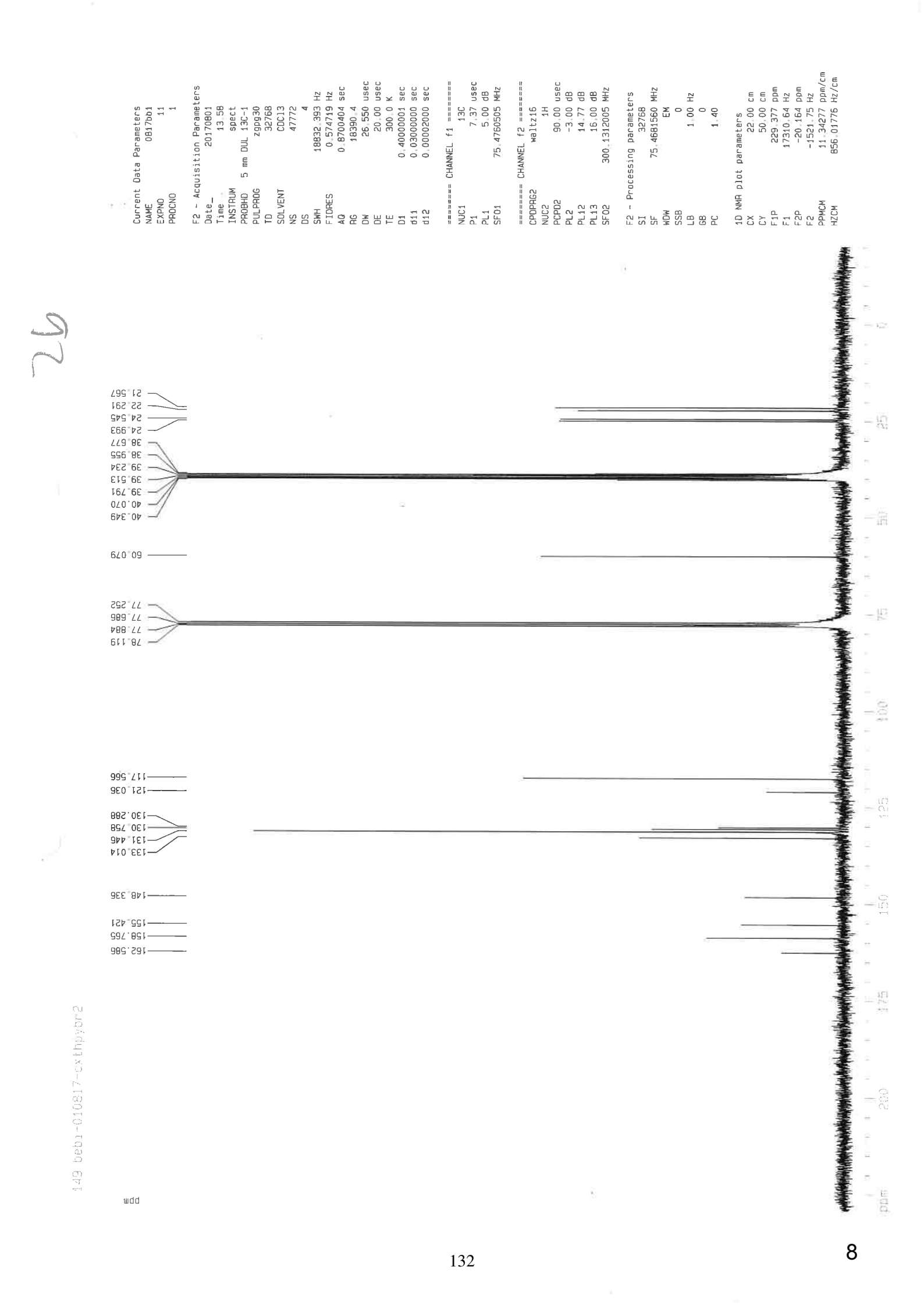
Current Data Parameters
NAME 0817bb1
EXPNO 11
PROCNO 1
F2 - Acquisition Parameters
Date_ 20170801
Time 13.58
INSTRUM spect
PROBHD 5 mm DUL 13C-1
PULPROG zgpg30
TD 32768
SOLVENT CDCl3
NS 47772
DS 4
SWH 18832.393 Hz
FIDRES 0.574719 Hz
AQ 0.8700404 sec
RG 18390.4
DW 26.550 usec
DE 20.00 usec
TE 300.0 K
D1 0.40000001 sec
d11 0.03000000 sec
d12 0.00002000 sec
======== CHANNEL f1 ========
NUC1 13C
P1 7.37 usec
PL1 5.00 dB
SFO1 75.4760505 MHz
======== CHANNEL f2 ========
CPDPRG2 waltz16
NUC2 1H
PCPD2 90.00 usec
PL2 -3.00 dB
PL12 14.77 dB
PL13 16.00 dB
SFO2 300.1312005 MHz
F2 - Processing parameters
SI 32768
SF 75.4681560 MHz
WDW EM
SSB 0
LB 1.00 Hz
GB 0
PC 1.40
1D NMR plot parameters
CX 22.00 cm
CY 50.00 cm
F1P 229.377 ppm
F1 17310.64 Hz
F2P -20.164 ppm
F2 -1521.75 Hz
PPMCM 11.34277 ppm/cm
HZCM 856.01776 Hz/cm
21.567
22.291
24.545
24.993
38.677
38.955
39.234
39.513
39.791
40.070
40.349
60.079
77.252
77.686
77.884
78.119
117.566
121.036
130.288
130.758
131.446
133.014
148.336
155.421
158.765
162.586
ppm
149 bebi-010817-exthybr2

2c

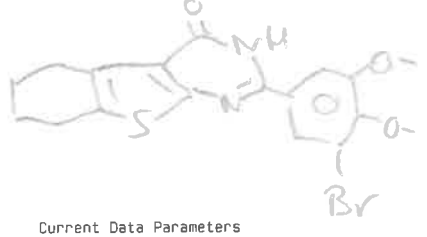

150 beb1-070817-cxtpbr

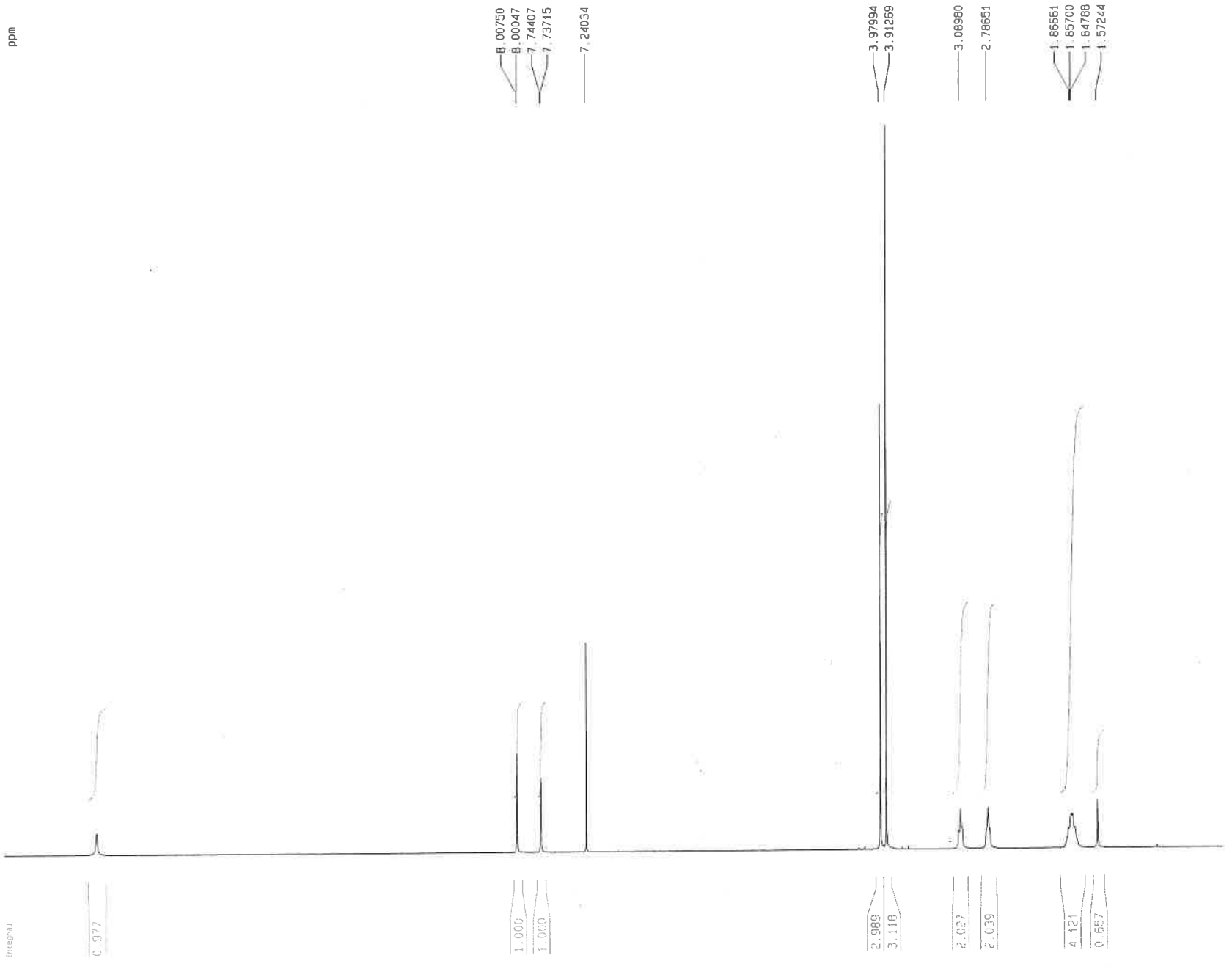

Current Data Parameters

NAME	0817bb8
EXPNO	10
PROCNO	1

F2 - Acquisition Parameters

Date_	20170807
Time	14.14
INSTRUM	spect
PROBHD	5 mm DUL 13C-1
PULPROG	zg30
TD	65536
SOLVENT	CDCl3
NS	92
DS	2
SWH	8992.806 Hz
FIDRES	0.137219 Hz
AQ	3.6438515 sec
RG	1149.4
DW	55.600 usec
DE	7.00 usec
TE	300.0 K
D1	0.50000000 sec

======== CHANNEL f1 ========

NUC1	1H
P1	11.63 usec
PL1	-3.00 dB
SFO1	300.1318008 MHz

F2 - Processing parameters

SI	65536
SF	300.1300126 MHz
WDW	no
SSB	0
LB	0.00 Hz
GB	0
PC	1.00

1D NMR plot parameters

CX	22.00 cm
CY	13.50 cm
F1P	13.686 ppm
F1	4107.63 Hz
F2P	0.182 ppm
F2	54.53 Hz
PPMCM	0.61384 ppm/cm
HZCM	184.23163 Hz/cm

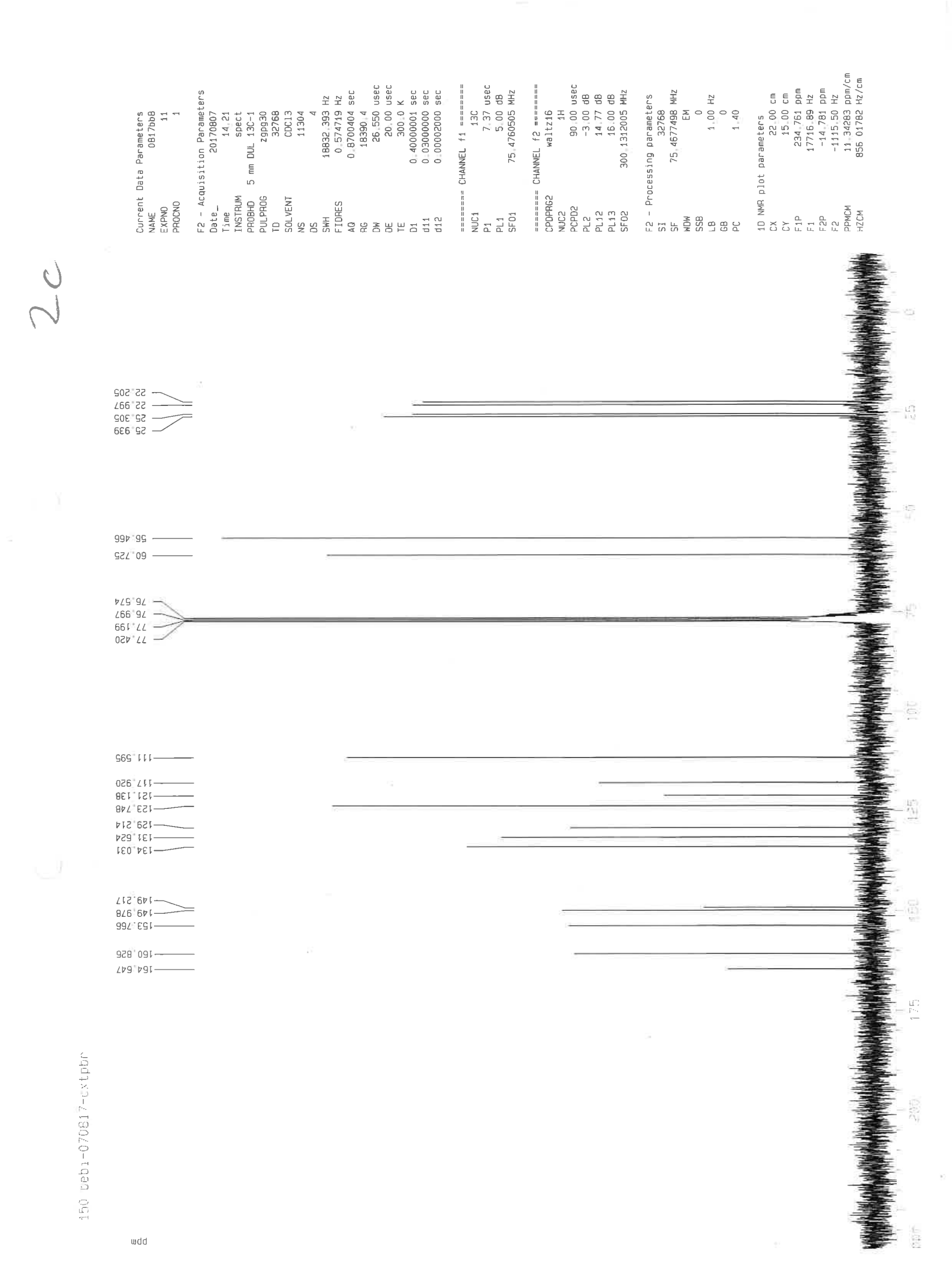
Current Data Parameters
NAME 0817bb8
EXPNO 11
PROCNO 1
F2 - Acquisition Parameters
Date_ 20170807
Time 14.21
INSTRUM spect
PROBHD 5 mm DUL 13C-1
PULPROG zgpg30
TD 32768
SOLVENT CDCl3
NS 11304
DS 4
SWH 18832.393 Hz
FIDRES 0.574719 Hz
AQ 0.8700404 sec
RG 18390.4
DW 26.550 usec
DE 20.00 usec
TE 300.0 K
D1 0.40000001 sec
d11 0.03000000 sec
d12 0.00002000 sec
======== CHANNEL f1 ========
NUC1 13C
P1 7.37 usec
PL1 5.00 dB
SFO1 75.4760505 MHz
======== CHANNEL f2 ========
CPDPRG2 waltz16
NUC2 1H
PCPD2 90.00 usec
PL2 -3.00 dB
PL12 14.77 dB
PL13 16.00 dB
SFO2 300.1312005 MHz
F2 - Processing parameters
SI 32768
SF 75.4677498 MHz
WDW EM
SSB 0
LB 1.00 Hz
GB 0
PC 1.40
1D NMR plot parameters
CX 22.00 cm
CY 15.00 cm
F1P 234.761 ppm
F1 17716.89 Hz
F2P -14.781 ppm
F2 -1115.50 Hz
PPMCM 11.34283 ppm/cm
HZCM 856.01782 Hz/cm
22.205
22.997
25.305
25.939
56.466
60.725
76.574
76.997
77.199
77.420
111.595
117.920
121.138
123.748
129.214
131.624
134.031
149.217
149.978
153.766
160.826
164.647
150 cebi-070817-extpbr
ppm

2c

2d

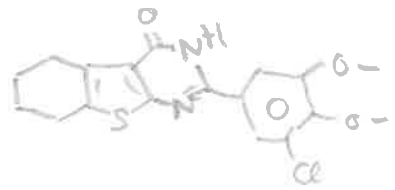

149 bebı-020817-chxtpcl

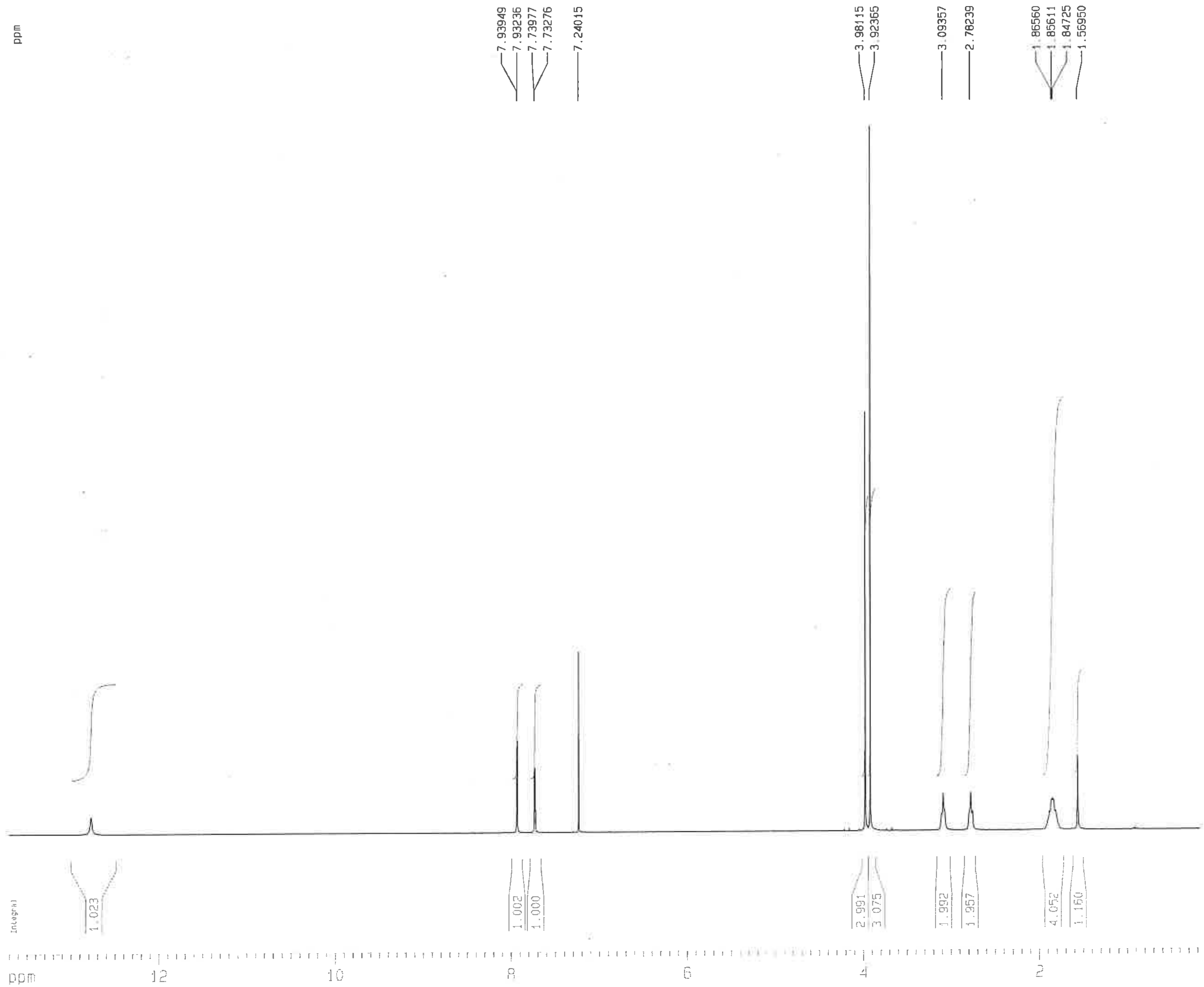

Current Data Parameters
NAME 0817bb3
EXPNO 10
PROCNO 1

F2 - Acquisition Parameters
Date_ 20170802
Time 15.46
INSTRUM spect
PROBHD 5 mm DUL 13C-1
PULPROG zg30
TD 65536
SOLVENT CDCl3
NS 100
DS 2
SWH 8992.806 Hz
FIDRES 0.137219 Hz
AQ 3.6438515 sec
RG 1149.4
DW 55.600 usec
DE 7.00 usec
TE 300.0 K
D1 0.50000000 sec

======== CHANNEL f1 ========
NUC1 1H
P1 11.63 usec
PL1 -3.00 dB
SFO1 300.1318008 MHz

F2 - Processing parameters
SI 65536
SF 300.1300126 MHz
WDW no
SSB 0
LB 0.00 Hz
GB 0
PC 1.00

1D NMR plot parameters
CX 22.00 cm
CY 13.50 cm
F1P 13.713 ppm
F1 4115.54 Hz
F2P 0.182 ppm
F2 54.53 Hz
PPMCM 0.61504 ppm/cm
HZCM 184.59145 Hz/cm

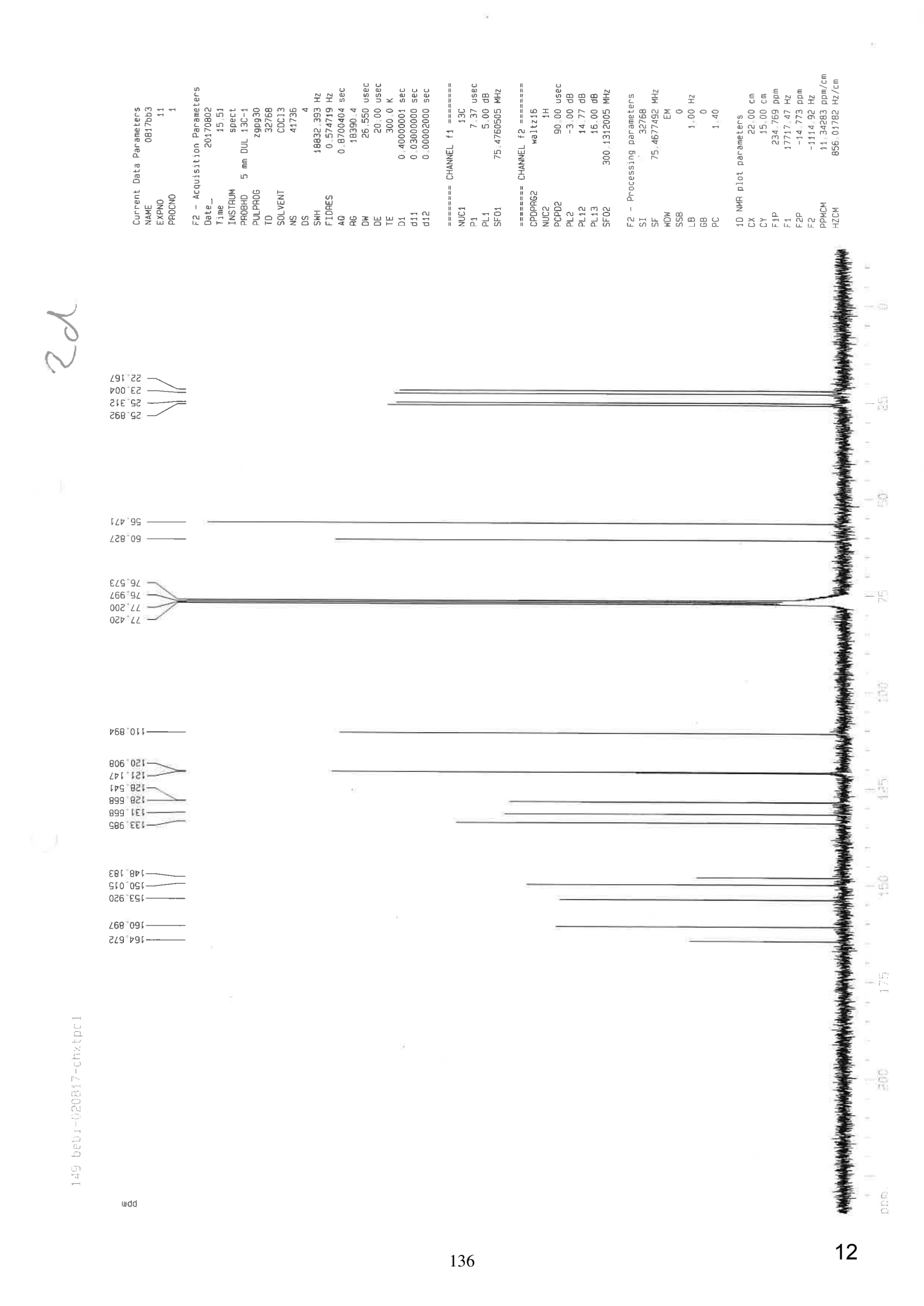
Current Data Parameters
NAME 0817bb3
EXPNO 11
PROCNO 1
F2 - Acquisition Parameters
Date_ 20170802
Time 15.51
INSTRUM spect
PROBHD 5 mm DUL 13C-1
PULPROG zgpg30
TD 32768
SOLVENT CDCl3
NS 41736
DS 4
SWH 18832.393 Hz
FIDRES 0.574719 Hz
AQ 0.8700404 sec
RG 18390.4
DW 26.550 usec
DE 20.00 usec
TE 300.0 K
D1 0.40000001 sec
d11 0.03000000 sec
d12 0.00002000 sec
======== CHANNEL f1 ========
NUC1 13C
P1 7.37 usec
PL1 5.00 dB
SFO1 75.4760505 MHz
======== CHANNEL f2 ========
CPDPRG2 waltz16
NUC2 1H
PCPD2 90.00 usec
PL2 -3.00 dB
PL12 14.77 dB
PL13 16.00 dB
SFO2 300.1312005 MHz
F2 - Processing parameters
SI 32768
SF 75.4677492 MHz
WDW EM
SSB 0
LB 1.00 Hz
GB 0
PC 1.40
1D NMR plot parameters
CX 22.00 cm
CY 15.00 cm
F1P 234.769 ppm
F1 17717.47 Hz
F2P -14.773 ppm
F2 -1114.92 Hz
PPMCM 11.34283 ppm/cm
HZCM 856.01782 Hz/cm
22.167
23.004
25.312
25.892
56.471
60.827
76.573
76.997
77.200
77.420
110.894
120.908
121.147
128.541
128.668
131.668
133.985
148.183
150.015
153.920
160.897
164.672
ppm
149 bebi-020817-chxtpcl

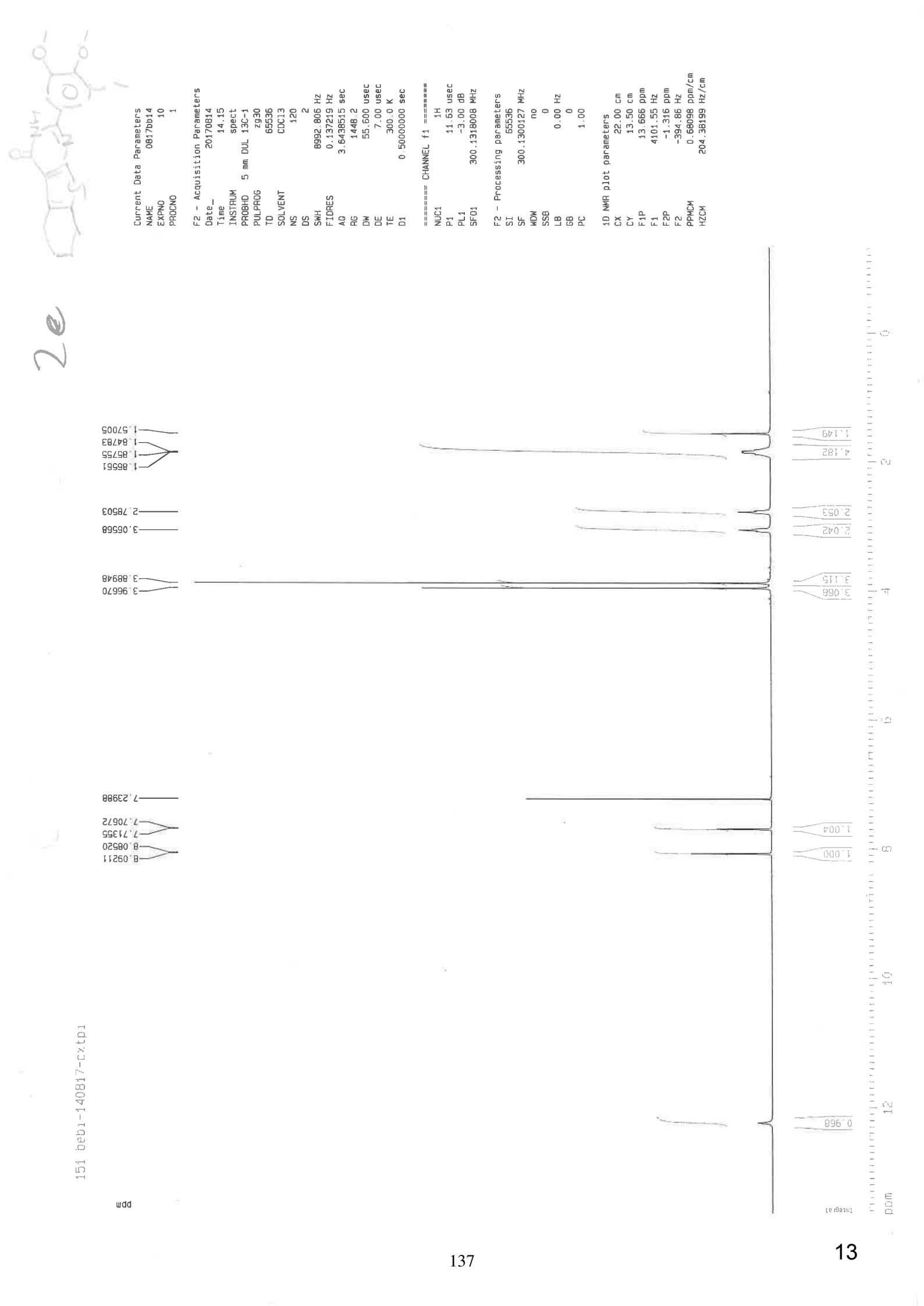
Current Data Parameters
NAME 0817bb14
EXPNO 10
PROCNO 1
F2 - Acquisition Parameters
Date_ 20170814
Time 14.15
INSTRUM spect
PROBHD 5 mm DUL 13C-1
PULPROG zg30
TD 65536
SOLVENT CDCl3
NS 120
DS 2
SWH 8992.806 Hz
FIDRES 0.137219 Hz
AQ 3.6438515 sec
RG 1448.2
DW 55.600 usec
DE 7.00 usec
TE 300.0 K
D1 0.50000000 sec
======== CHANNEL f1 ========
NUC1 1H
P1 11.63 usec
PL1 -3.00 dB
SFO1 300.1318008 MHz
F2 - Processing parameters
SI 65536
SF 300.1300127 MHz
WDW no
SSB 0
LB 0.00 Hz
GB 0
PC 1.00
1D NMR plot parameters
CX 22.00 cm
CY 13.50 cm
F1P 13.666 ppm
F1 4101.55 Hz
F2P -1.316 ppm
F2 -394.86 Hz
PPMCM 0.68098 ppm/cm
HZCM 204.38199 Hz/cm
1.57005
1.84783
1.85755
1.86561
2.78503
3.05568
3.88948
3.96670
7.23988
7.70672
7.71355
8.08520
8.09211
0.868
1.000
1.004
3.068
3.115
2.042
2.053
4.182
1.149
151 bebi-140817-cxtp1
ppm
Integral
PPM

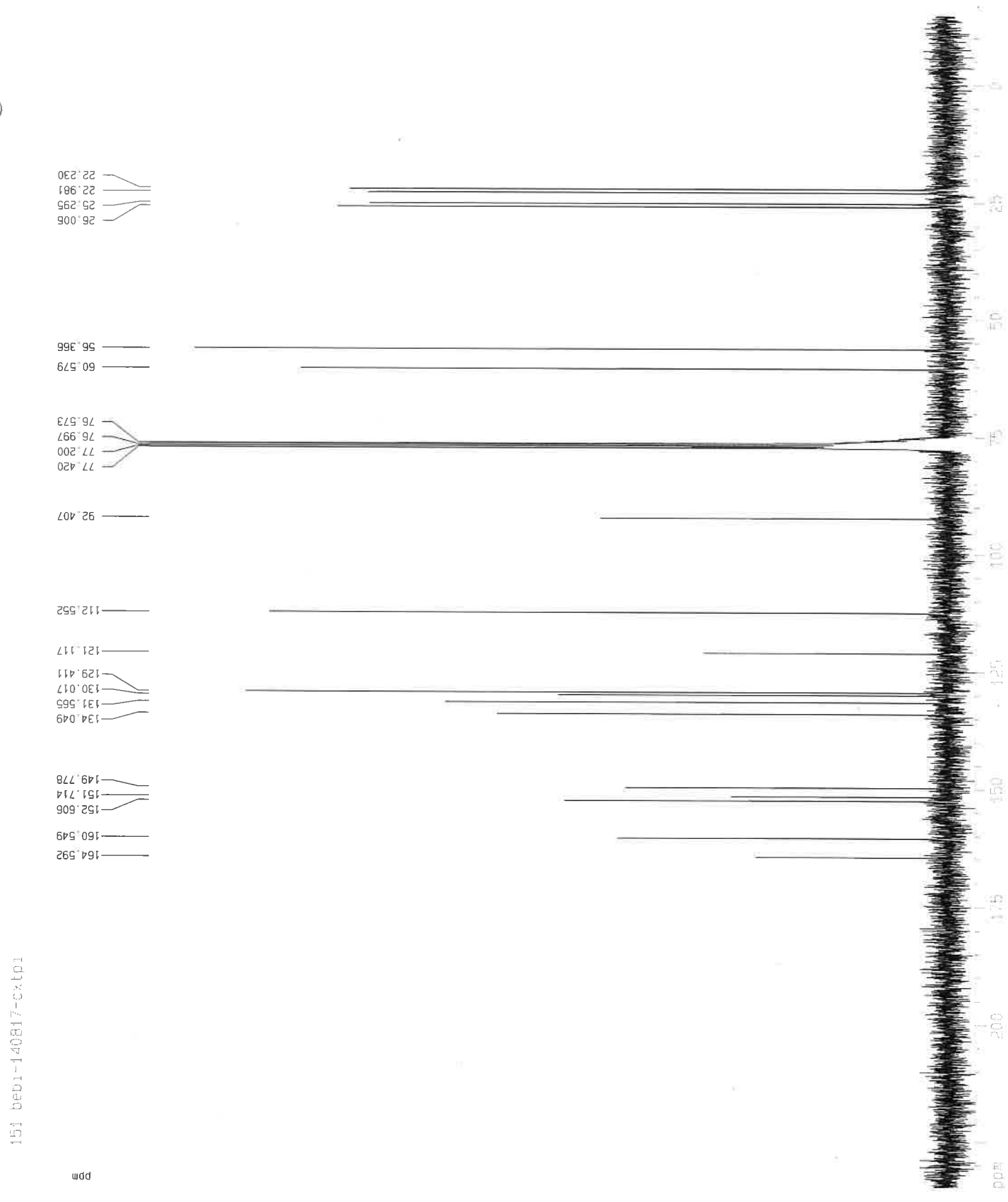
Current Data Parameters
NAME 0817bb14
EXPNO 20
PROCNO 1
F2 - Acquisition Parameters
Date_ 20170815
Time 6.41
INSTRUM spect
PROBHD 5 mm DUL 13C-1
PULPROG zgpg30
TD 32768
SOLVENT CDCl3
NS 28268
DS 4
SWH 18832.393 Hz
FIDRES 0.574719 Hz
AQ 0.8700404 sec
RG 18390.4
DW 26.550 usec
DE 20.00 usec
TE 300.0 K
D1 0.40000001 sec
d11 0.03000000 sec
d12 0.00002000 sec
======== CHANNEL f1 ========
NUC1 13C
P1 7.37 usec
PL1 5.00 dB
SFO1 75.4760505 MHz
======== CHANNEL f2 ========
CPDPRG2 waltz16
NUC2 1H
PCPD2 90.00 usec
PL2 -3.00 dB
PL12 14.77 dB
PL13 16.00 dB
SFO2 300.1312005 MHz
F2 - Processing parameters
SI 32768
SF 75.4677498 MHz
WDW EM
SSB 0
LB 1.00 Hz
GB 0
PC 1.40
1D NMR plot parameters
CX 22.00 cm
CY 15.00 cm
F1P 234.761 ppm
F1 17716.89 Hz
F2P -14.781 ppm
F2 -1115.50 Hz
PPMCM 11.34283 ppm/cm
HZCM 856.01782 Hz/cm
22.230
22.981
25.295
26.006
56.366
60.579
76.573
76.997
77.200
77.420
92.407
112.552
121.117
129.411
130.017
131.565
134.049
149.778
151.714
152.606
160.549
164.592
ppm
151 beb1-140817-extp1

2e

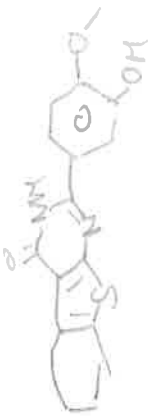

2f

```
Current Data Parameters
NAME          0817bb5
EXPNO              10
PROCNO              1

F2 - Acquisition Parameters
Date_        20170807
Time             7.09
INSTRUM          spect
PROBHD  5 mm DUL 13C-1
PULPROG            zg30
TD                65536
SOLVENT            MeOD
NS                  100
DS                    2
SWH            8992.806 Hz
FIDRES         0.137219 Hz
AQ             3.6438515 sec
RG                724.1
DW               55.600 usec
DE                7.00 usec
TE                300.0 K
D1             0.50000000 sec

======== CHANNEL f1 ========
NUC1                1H
P1              11.63 usec
PL1             -3.00 dB
SFO1       300.1318008 MHz

F2 - Processing parameters
SI                 65536
SF       300.1300053 MHz
WDW                   no
SSB                    0
LB              0.00 Hz
GB                     0
PC                  1.00

1D NMR plot parameters
CX              22.00 cm
CY              13.50 cm
F1P             8.435 ppm
F1              2531.68 Hz
F2P             0.048 ppm
F2              14.33 Hz
PPMCM         0.38125 ppm/cm
HZCM          114.42511 Hz/cm
```

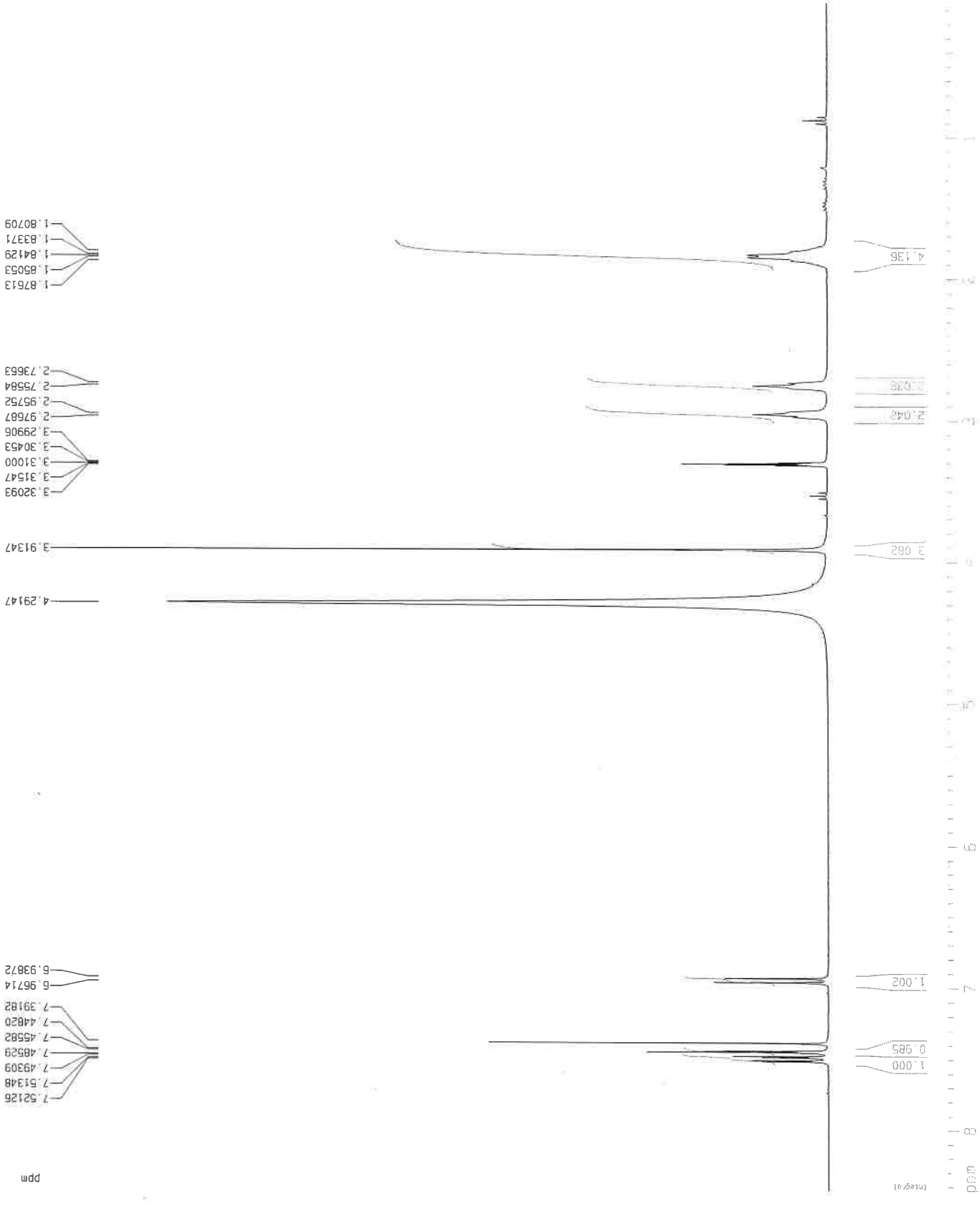

149 bebi-050817-cxtpiva

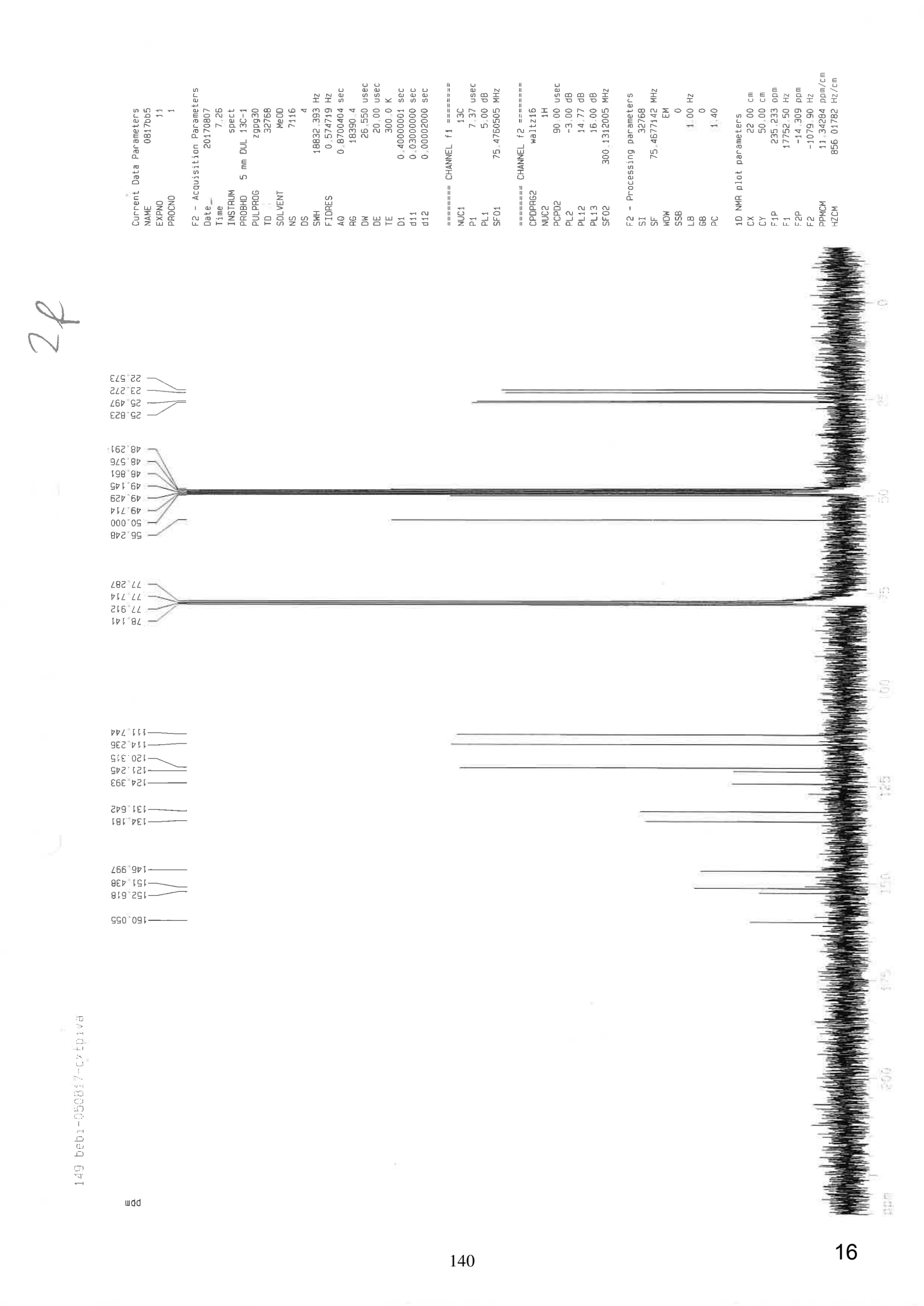
Current Data Parameters
NAME 0817bb5
EXPNO 11
PROCNO 1
F2 - Acquisition Parameters
Date_ 20170807
Time 7.26
INSTRUM spect
PROBHD 5 mm DUL 13C-1
PULPROG zgpg30
TD 32768
SOLVENT MeOD
NS 7116
DS 4
SWH 18832.393 Hz
FIDRES 0.574719 Hz
AQ 0.8700404 sec
RG 18390.4
DW 26.550 usec
DE 20.00 usec
TE 300.0 K
D1 0.40000001 sec
d11 0.03000000 sec
d12 0.00002000 sec
======== CHANNEL f1 ========
NUC1 13C
P1 7.37 usec
PL1 5.00 dB
SFO1 75.4760505 MHz
======== CHANNEL f2 ========
CPDPRG2 waltz16
NUC2 1H
PCPD2 90.00 usec
PL2 -3.00 dB
PL12 14.77 dB
PL13 16.00 dB
SFO2 300.1312005 MHz
F2 - Processing parameters
SI 32768
SF 75.4677142 MHz
WDW EM
SSB 0
LB 1.00 Hz
GB 0
PC 1.40
1D NMR plot parameters
CX 22.00 cm
CY 50.00 cm
F1P 235.233 ppm
F1 17752.50 Hz
F2P -14.309 ppm
F2 -1079.90 Hz
PPMCM 11.34284 ppm/cm
HZCM 856.01782 Hz/cm
22.573
23.272
25.497
25.823
48.291
48.576
48.861
49.145
49.429
49.714
50.000
56.248
77.287
77.714
77.912
78.141
111.744
114.236
120.315
121.245
124.393
131.642
134.181
146.997
151.438
152.618
160.055
149 bebi-050817-cxtbiva
ppm

2 Bg

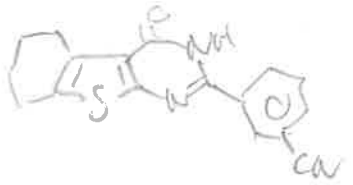

152 bebi-190817-cto3cn

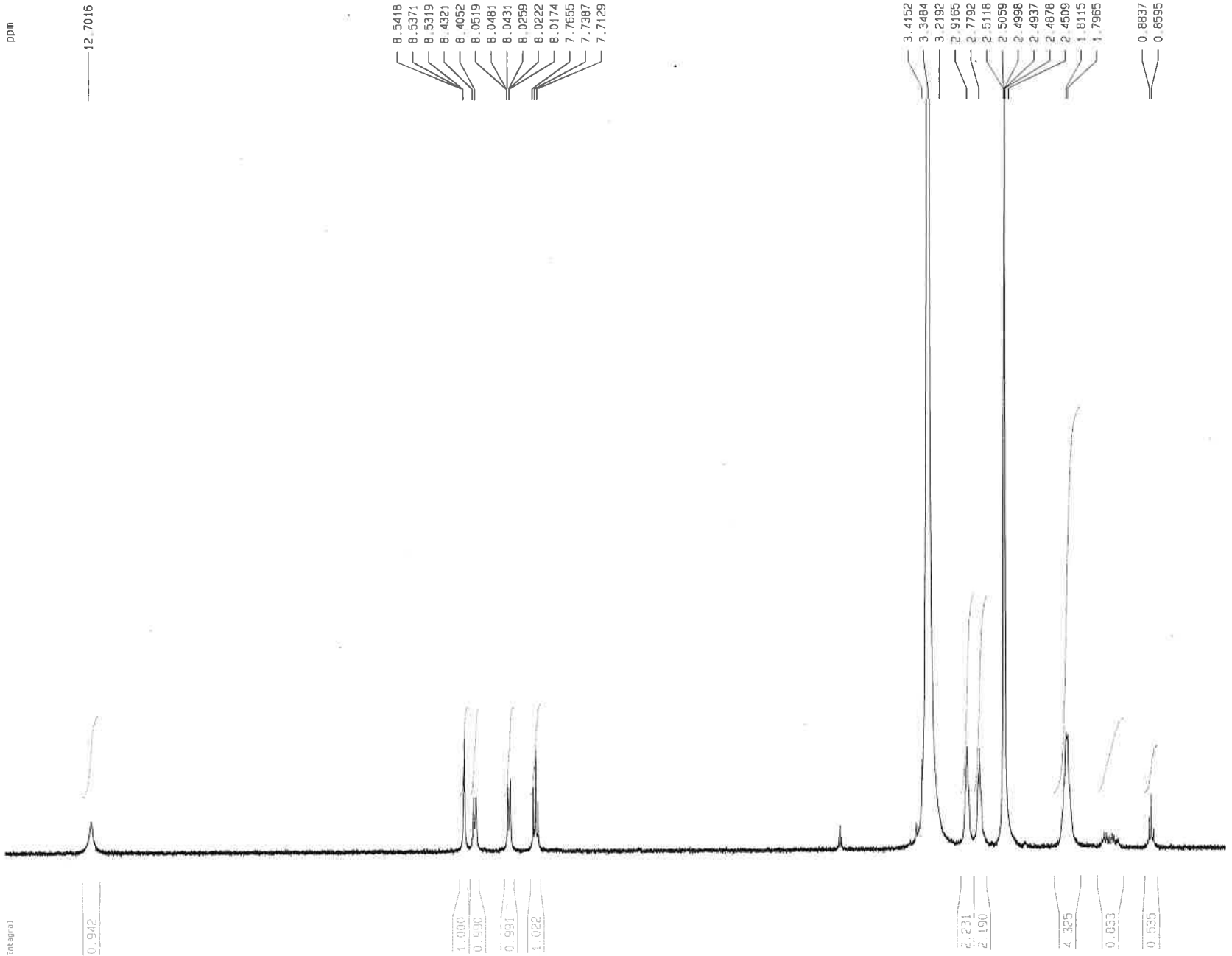

Current Data Parameters

NAME	0817bb20
EXPNO	10
PROCNO	1

F2 - Acquisition Parameters

Date_	20170821
Time	11.54
INSTRUM	spect
PROBHD	5 mm DUL 13C-1
PULPROG	zg30
TD	65536
SOLVENT	DMSO
NS	200
DS	2
SWH	8992.806 Hz
FIDRES	0.137219 Hz
AQ	3.6438515 sec
RG	1024
DW	55.600 usec
DE	7.00 usec
TE	300.0 K
D1	0.50000000 sec

======== CHANNEL f1 ========

NUC1	1H
P1	11.63 usec
PL1	-3.00 dB
SFO1	300.1318008 MHz

F2 - Processing parameters

SI	65536
SF	300.1300022 MHz
WDW	no
SSB	0
LB	0.00 Hz
GB	0
PC	1.00

1D NMR plot parameters

CX	22.00 cm
CY	300.00 cm
F1P	13.668 ppm
F1	4102.16 Hz
F2P	0.032 ppm
F2	9.48 Hz
PPMCM	0.61983 ppm/cm
HZCM	186.03076 Hz/cm

150 bebi-090817-cxtp3no

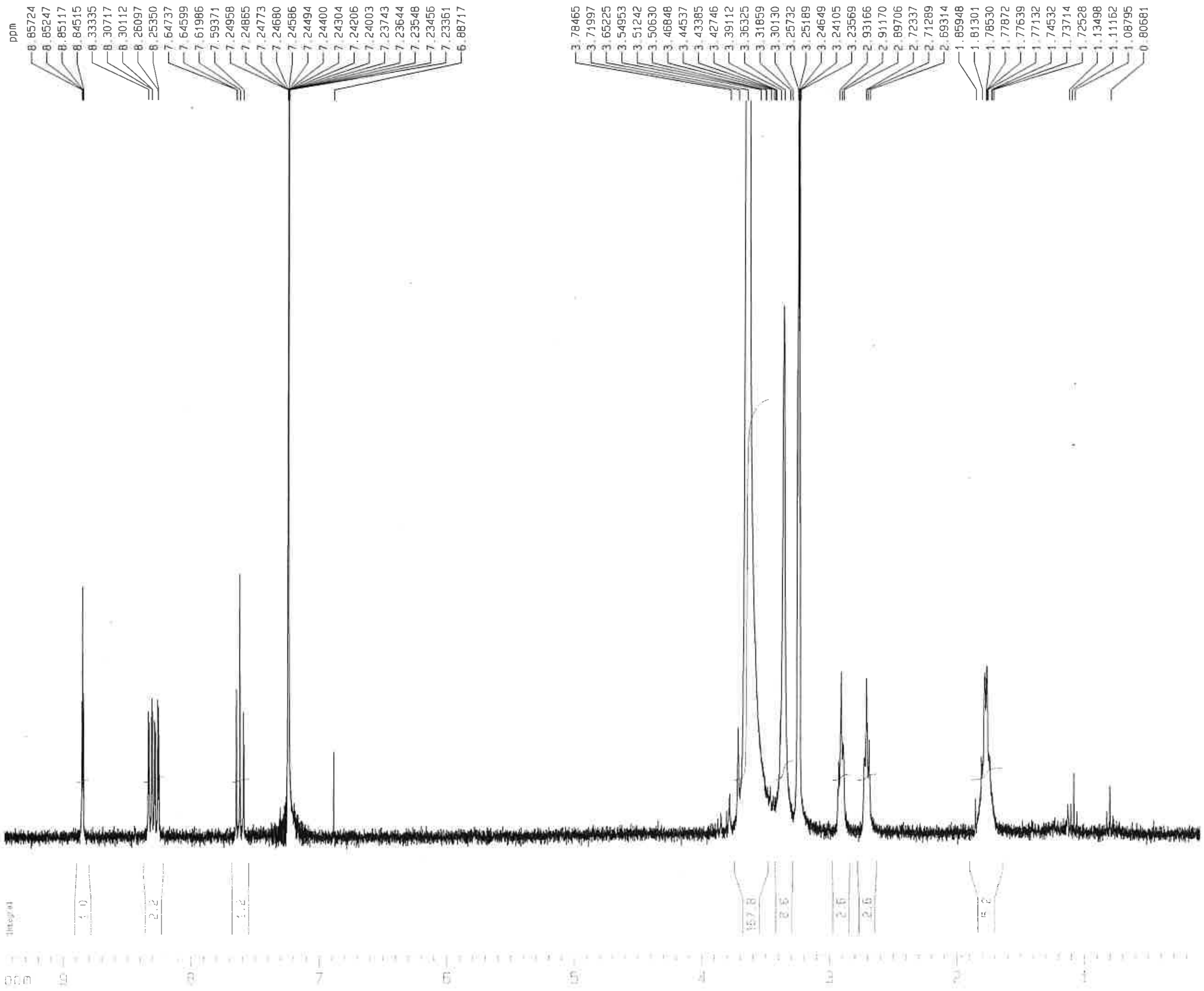

2h

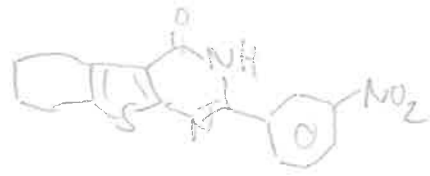

Current Data Parameters
NAME 0817bb10
EXPNO 1
PROCNO 1

F2 - Acquisition Parameters
Date_ 20170809
Time 13.25
INSTRUM spect
PROBHD 5 mm DUL 13C-1
PULPROG zg30
TD 65536
SOLVENT CDCl3
NS 400
DS 2
SWH 8992.806 Hz
FIDRES 0.137219 Hz
AQ 3.6438515 sec
RG 1149.4
DW 55.600 usec
DE 7.00 usec
TE 300.0 K
D1 0.50000000 sec

======== CHANNEL f1 ========
NUC1 1H
P1 11.63 usec
PL1 -3.00 dB
SFO1 300.1318008 MHz

F2 - Processing parameters
SI 65536
SF 300.1300123 MHz
WDW no
SSB 0
LB 0.00 Hz
GB 0
PC 1.00

1D NMR plot parameters
CX 22.00 cm
CY 600.00 cm
F1P 9.467 ppm
F1 2841.31 Hz
F2P 0.103 ppm
F2 31.05 Hz
PPMCM 0.42561 ppm/cm
HZCM 127.73872 Hz/cm

2i

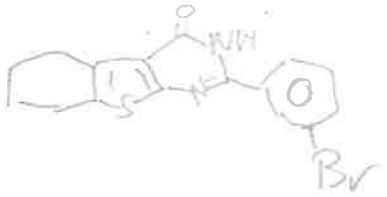

151 bebi-160817-cxtp3br

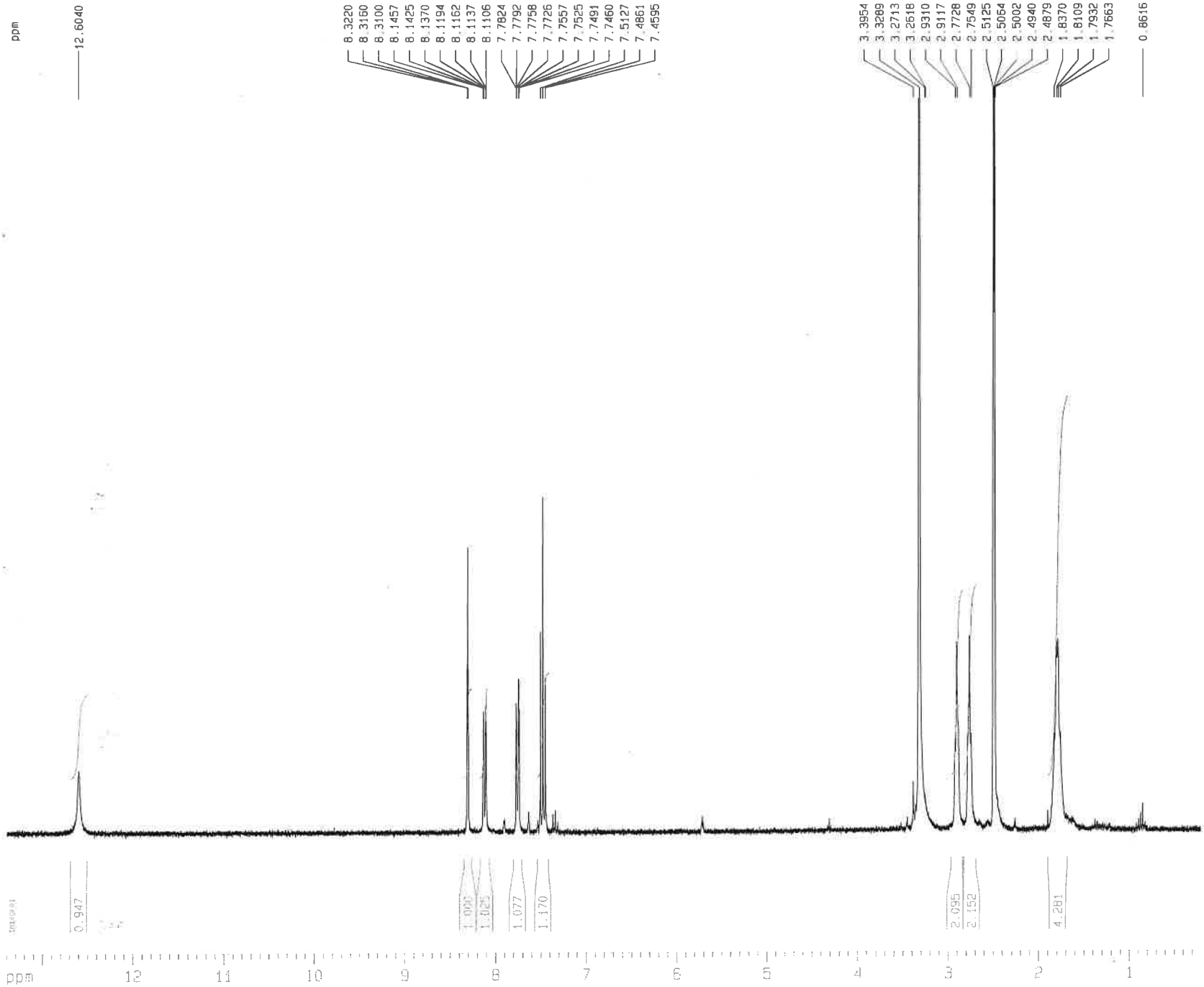

Current Data Parameters

NAME	0817bb17
EXPNO	1
PROCNO	1

F2 - Acquisition Parameters

Date_	20170816
Time	13.11
INSTRUM	spect
PROBHD	5 mm DUL 13C-1
PULPROG	zg30
TD	65536
SOLVENT	DMSO
NS	160
DS	2
SWH	8992.806 Hz
FIDRES	0.137219 Hz
AQ	3.6438515 sec
RG	1290.2
DW	55.600 usec
DE	7.00 usec
TE	300.0 K
D1	0.50000000 sec

======== CHANNEL f1 ========

NUC1	1H
P1	11.63 usec
PL1	-3.00 dB
SF01	300.1318008 MHz

F2 - Processing parameters

SI	65536
SF	300.1300021 MHz
WDW	no
SSB	0
LB	0.00 Hz
GB	0
PC	1.00

1D NMR plot parameters

CX	22.00 cm
CY	300.00 cm
F1P	13.405 ppm
F1	4023.13 Hz
F2P	0.217 ppm
F2	65.03 Hz
PPMCM	0.59945 ppm/cm
HZCM	179.91370 Hz/cm

2i

151 bebi-160817-cxtp3br

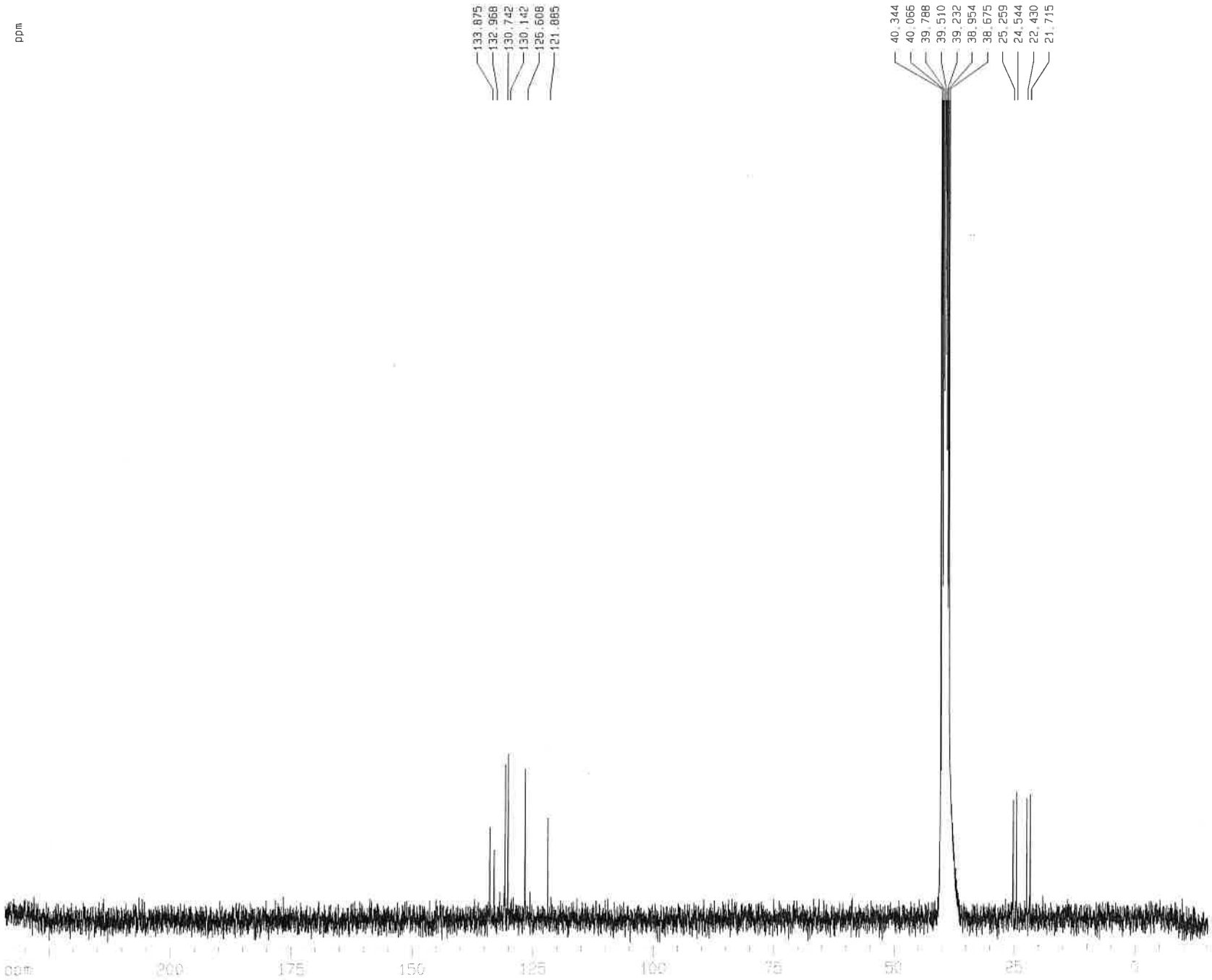

Current Data Parameters
NAME 0817bb17
EXPNO 2
PROCNO 1

F2 - Acquisition Parameters
Date_ 20170816
Time 15.07
INSTRUM spect
PROBHD 5 mm DUL 13C-1
PULPROG zgpg30
TD 32768
SOLVENT DMSO
NS 66684
DS 4
SWH 18832.393 Hz
FIDRES 0.574719 Hz
AQ 0.8700404 sec
RG 18390.4
DW 26.550 usec
DE 20.00 usec
TE 300.0 K
D1 0.40000001 sec
d11 0.03000000 sec
d12 0.00002000 sec

======== CHANNEL f1 ========
NUC1 13C
P1 7.37 usec
PL1 5.00 dB
SFO1 75.4760505 MHz

======== CHANNEL f2 ========
CPDPRG2 waltz16
NUC2 1H
PCPD2 90.00 usec
PL2 -3.00 dB
PL12 14.77 dB
PL13 16.00 dB
SFO2 300.1312005 MHz

F2 - Processing parameters
SI 32768
SF 75.4677876 MHz
WDW EM
SSB 0
LB 1.00 Hz
GB 0
PC 1.40

1D NMR plot parameters
CX 22.00 cm
CY 200.00 cm
F1P 234.259 ppm
F1 17679.02 Hz
F2P -15.283 ppm
F2 -1153.37 Hz
PPMCM 11.34282 ppm/cm
HZCM 856.01782 Hz/cm

150 bebi-100817-cxtp35df

2j

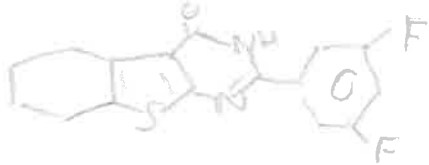

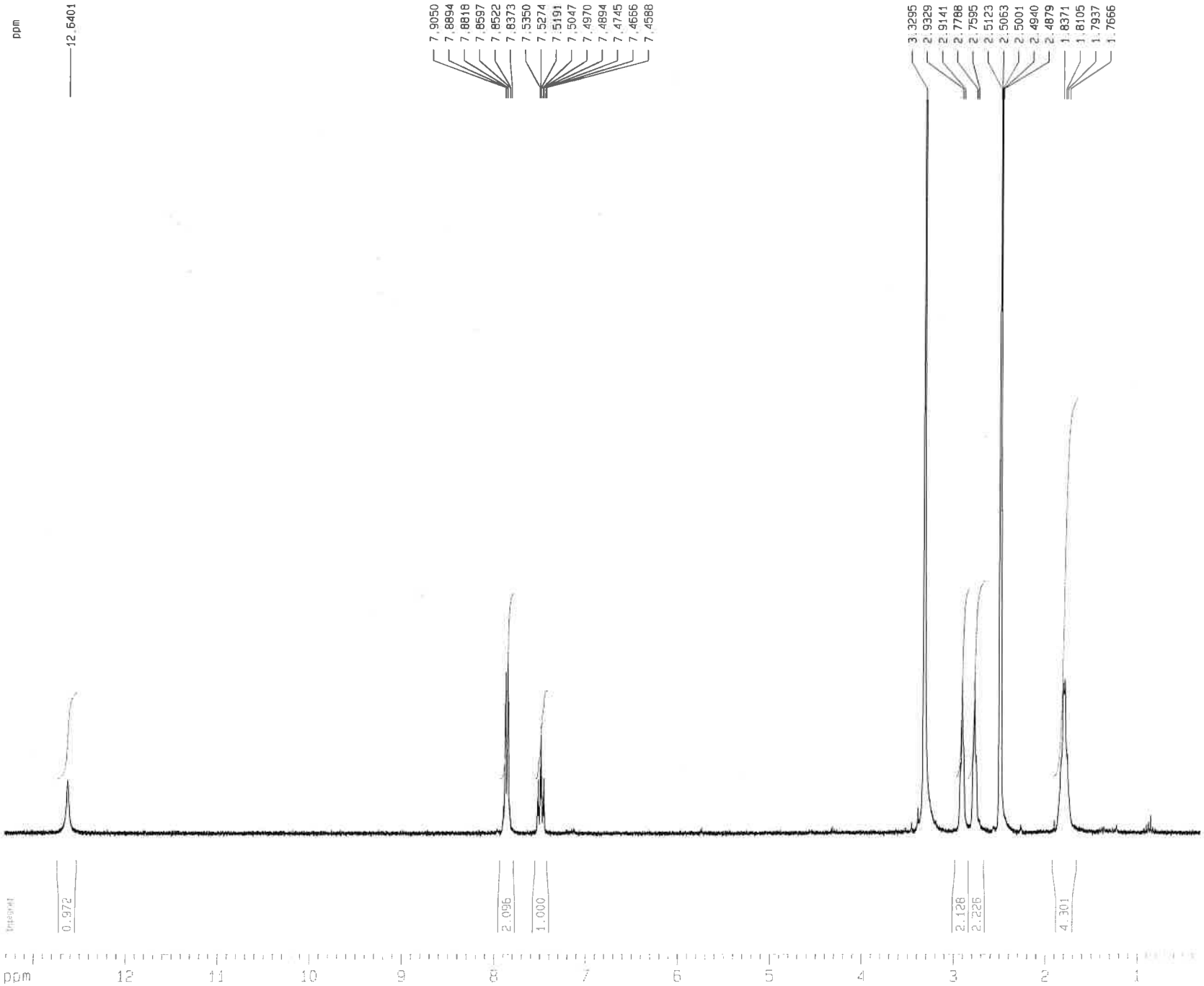

Current Data Parameters

NAME	0817bb11
EXPNO	1
PROCNO	1

F2 - Acquisition Parameters

Date_	20170810
Time	13.27
INSTRUM	spect
PROBHD	5 mm DUL 13C-1
PULPROG	zg30
TD	65536
SOLVENT	DMSO
NS	200
DS	2
SWH	8992.806 Hz
FIDRES	0.137219 Hz
AQ	3.6438515 sec
RG	1149.4
DW	55.600 usec
DE	7.00 usec
TE	300.0 K
D1	0.50000000 sec

======== CHANNEL f1 ========

NUC1	1H
P1	11.63 usec
PL1	-3.00 dB
SFO1	300.1318008 MHz

F2 - Processing parameters

SI	65536
SF	300.1300022 MHz
WDW	no
SSB	0
LB	0.00 Hz
GB	0
PC	1.00

1D NMR plot parameters

CX	22.00 cm
CY	200.00 cm
F1P	13.325 ppm
F1	3999.25 Hz
F2P	0.322 ppm
F2	96.56 Hz
PPMCM	0.59106 ppm/cm
HZCM	177.39491 Hz/cm

150 beb1-100817-cxtb35df

2j

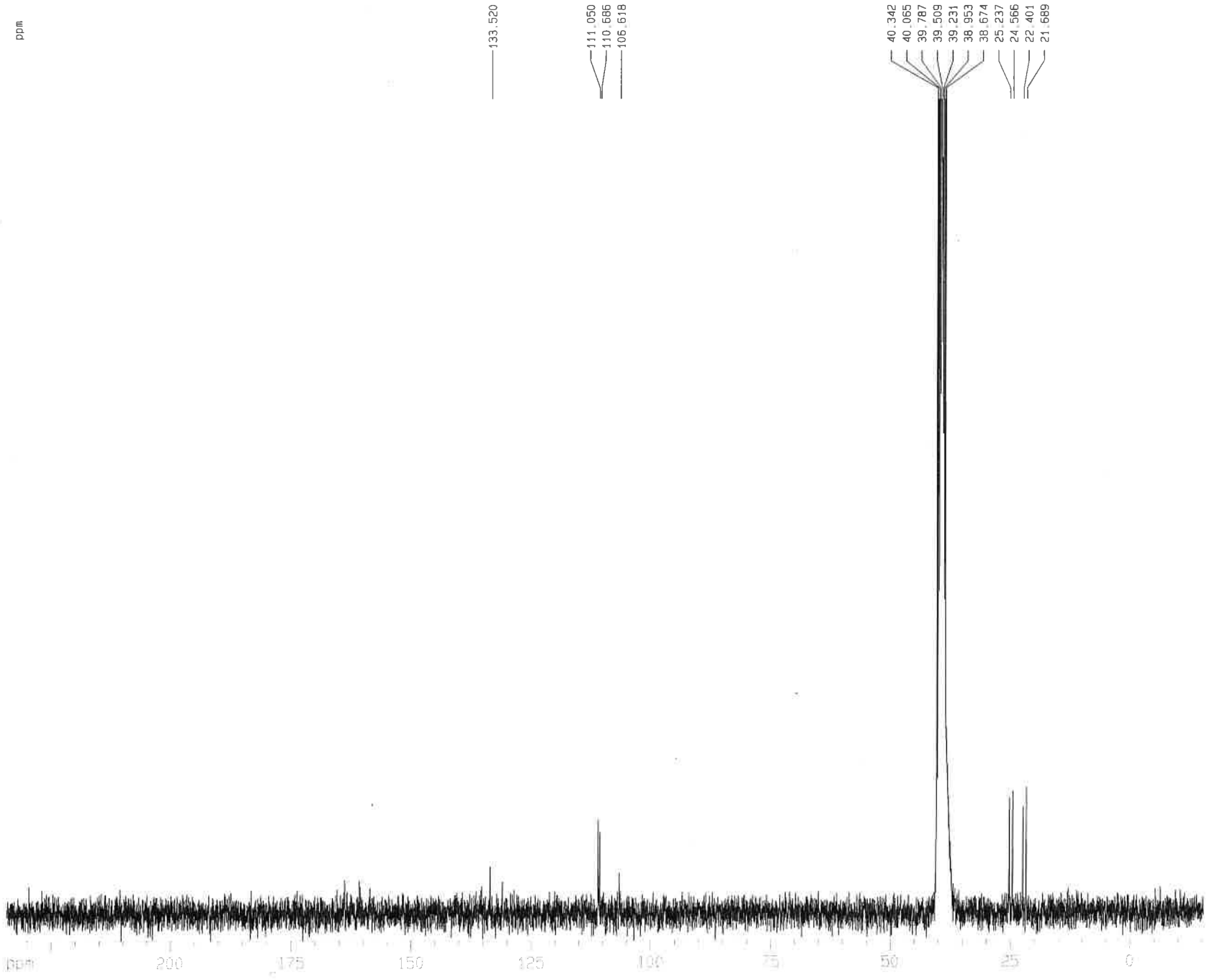

Current Data Parameters
NAME 0817bb11
EXPNO 2
PROCNO 1

F2 - Acquisition Parameters
Date_ 20170810
Time 14.59
INSTRUM spect
PROBHD 5 mm DUL 13C-1
PULPROG zgpg30
TD 32768
SOLVENT DMSO
NS 47444
DS 4
SWH 18832.393 Hz
FIDRES 0.574719 Hz
AQ 0.8700404 sec
RG 18390.4
DW 26.550 usec
DE 20.00 usec
TE 300.0 K
D1 0.40000001 sec
d11 0.03000000 sec
d12 0.00002000 sec

======== CHANNEL f1 ========
NUC1 13C
P1 7.37 usec
PL1 5.00 dB
SFO1 75.4760505 MHz

======== CHANNEL f2 ========
CPDPRG2 waltz16
NUC2 1H
PCPD2 90.00 usec
PL2 -3.00 dB
PL12 14.77 dB
PL13 16.00 dB
SFO2 300.1312005 MHz

F2 - Processing parameters
SI 32768
SF 75.4677876 MHz
WDW EM
SSB 0
LB 1.00 Hz
GB 0
PC 1.40

1D NMR plot parameters
CX 22.00 cm
CY 200.00 cm
F1P 234.259 ppm
F1 17679.02 Hz
F2P -15.283 ppm
F2 -1153.37 Hz
PPMCM 11.34282 ppm/cm
HZCM 856.01782 Hz/cm

36

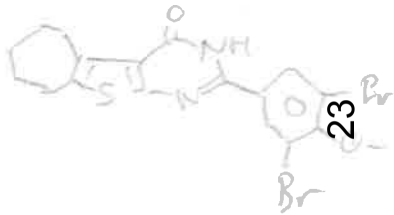

23

154 beb1-290817-cptpbr2

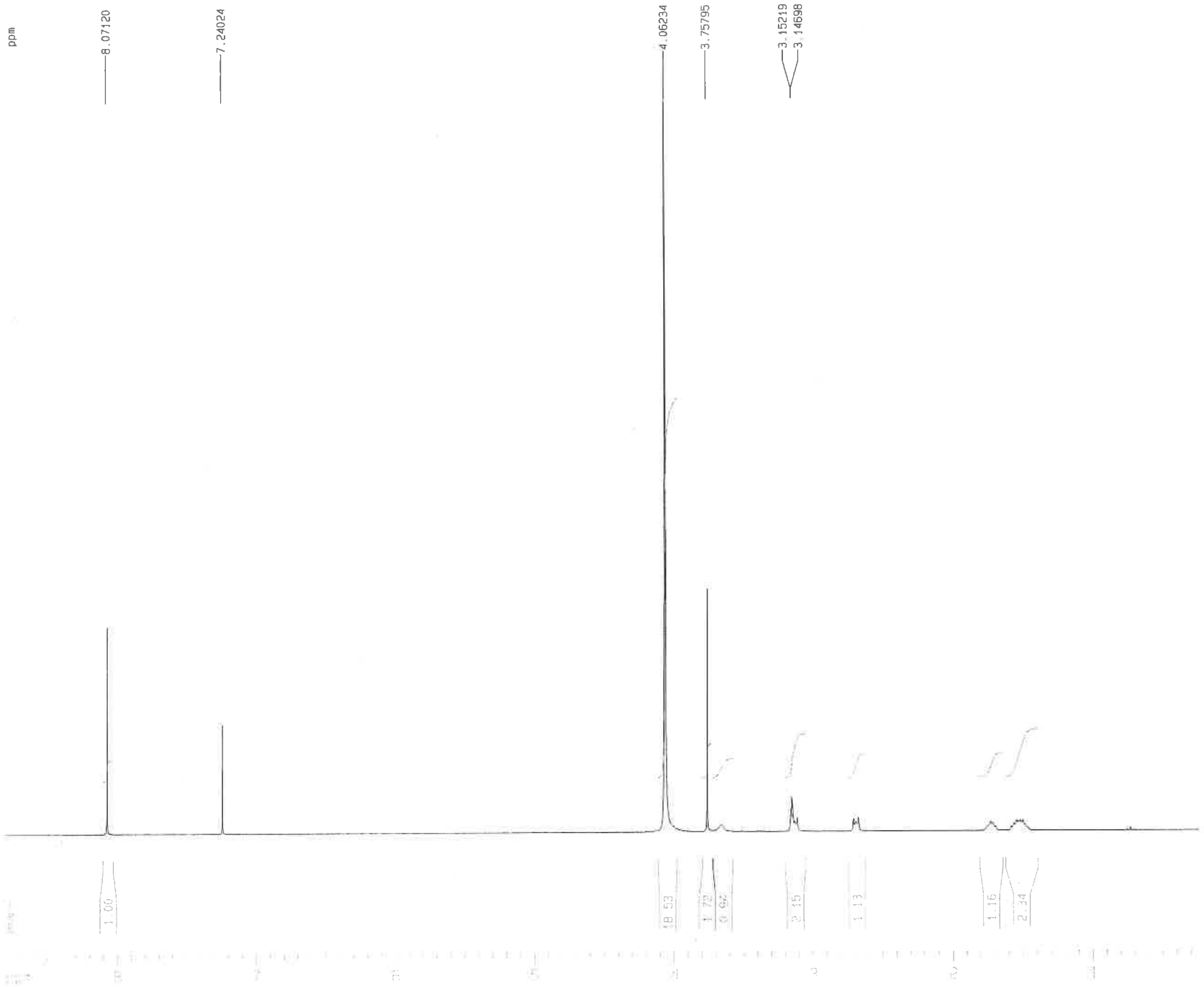

Current Data Parameters
NAME 0817bb27
EXPNO 10
PROCNO 1

F2 - Acquisition Parameters
Date_ 20170829
Time 13.10
INSTRUM spect
PROBHD 5 mm DUL 13C-1
PULPROG zg30
TD 65536
SOLVENT CDCl3 / MeOD
NS 200
DS 2
SWH 8992.806 Hz
FIDRES 0.137219 Hz
AQ 3.6438515 sec
RG 1149.4
DW 55.600 usec
DE 7.00 usec
TE 300.0 K
D1 0.50000000 sec

======== CHANNEL f1 ========
NUC1 1H
P1 11.63 usec
PL1 -3.00 dB
SFO1 300.1318008 MHz

F2 - Processing parameters
SI 65536
SF 300.1300121 MHz
WDW no
SSB 0
LB 0.00 Hz
GB 0
PC 1.00

1D NMR plot parameters
CX 22.00 cm
CY 13.50 cm
F1P 8.808 ppm
F1 2643.68 Hz
F2P 0.236 ppm
F2 70.91 Hz
PPMCM 0.38964 ppm/cm
HZCM 116.94389 Hz/cm

147

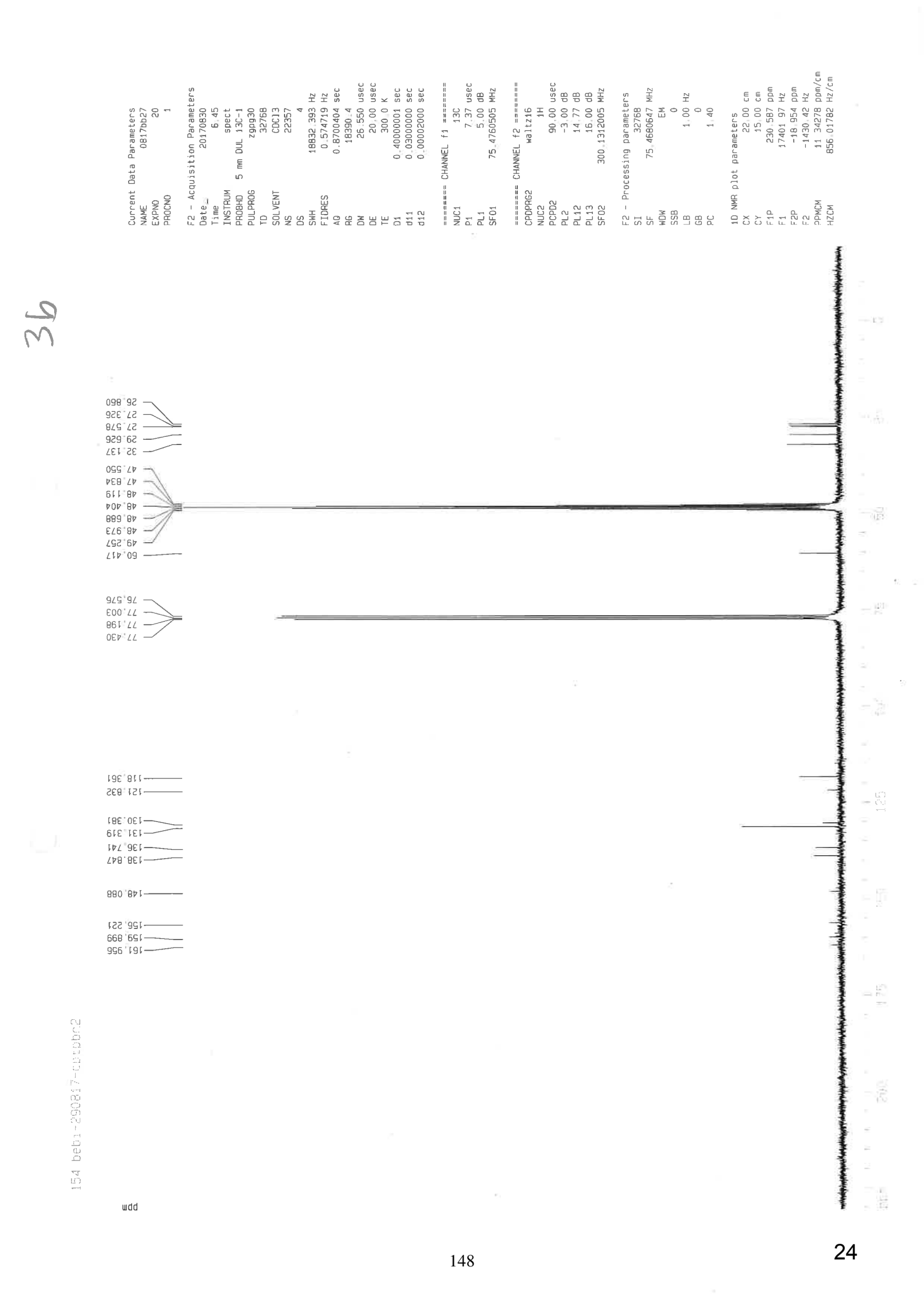
Current Data Parameters
NAME 0817bb27
EXPNO 20
PROCNO 1
F2 - Acquisition Parameters
Date_ 20170830
Time 6.45
INSTRUM spect
PROBHD 5 mm DUL 13C-1
PULPROG zgpg30
TD 32768
SOLVENT CDCl3
NS 22357
DS 4
SWH 18832.393 Hz
FIDRES 0.574719 Hz
AQ 0.8700404 sec
RG 18390.4
DW 26.550 usec
DE 20.00 usec
TE 300.0 K
D1 0.40000001 sec
d11 0.03000000 sec
d12 0.00002000 sec
======== CHANNEL f1 ========
NUC1 13C
P1 7.37 usec
PL1 5.00 dB
SFO1 75.4760505 MHz
======== CHANNEL f2 ========
CPDPRG2 waltz16
NUC2 1H
PCPD2 90.00 usec
PL2 -3.00 dB
PL12 14.77 dB
PL13 16.00 dB
SFO2 300.1312005 MHz
F2 - Processing parameters
SI 32768
SF 75.4680647 MHz
WDW EM
SSB 0
LB 1.00 Hz
GB 0
PC 1.40
1D NMR plot parameters
CX 22.00 cm
CY 15.00 cm
F1P 230.587 ppm
F1 17401.97 Hz
F2P -18.954 ppm
F2 -1430.42 Hz
PPMCM 11.34278 ppm/cm
HZCM 856.01782 Hz/cm
26.860
27.326
27.578
29.626
32.137
47.550
47.834
48.119
48.404
48.688
48.973
49.257
50.417
76.576
77.003
77.198
77.430
118.361
121.832
130.381
131.319
136.741
138.847
148.088
156.221
159.899
161.956
ppm
154 bebi-290817-curbbc2

36

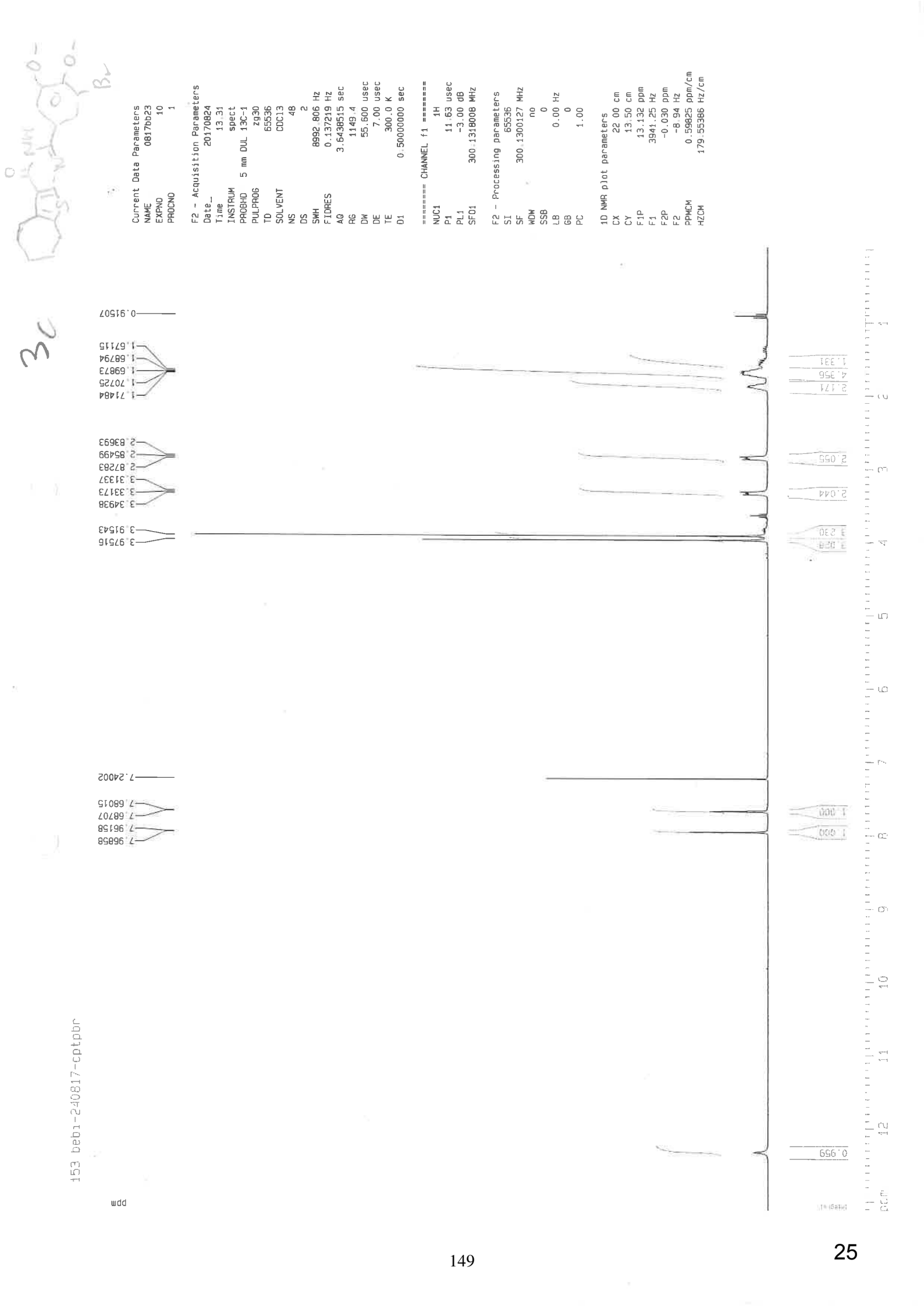
Current Data Parameters
NAME 0817bb23
EXPNO 10
PROCNO 1
F2 - Acquisition Parameters
Date_ 20170824
Time 13.31
INSTRUM spect
PROBHD 5 mm DUL 13C-1
PULPROG zg30
TD 65536
SOLVENT CDCl3
NS 48
DS 2
SWH 8992.806 Hz
FIDRES 0.137219 Hz
AQ 3.6438515 sec
RG 1149.4
DW 55.600 usec
DE 7.00 usec
TE 300.0 K
D1 0.50000000 sec
======== CHANNEL f1 ========
NUC1 1H
P1 11.63 usec
PL1 -3.00 dB
SFO1 300.1318008 MHz
F2 - Processing parameters
SI 65536
SF 300.1300127 MHz
WDW no
SSB 0
LB 0.00 Hz
GB 0
PC 1.00
1D NMR plot parameters
CX 22.00 cm
CY 13.50 cm
F1P 13.132 ppm
F1 3941.25 Hz
F2P -0.030 ppm
F2 -8.94 Hz
PPMCM 0.59825 ppm/cm
HZCM 179.55386 Hz/cm
0.91507
1.67115
1.68794
1.69873
1.70725
1.71484
2.83693
2.85499
2.87283
3.31337
3.33173
3.34938
3.91543
3.97516
7.24002
7.68015
7.68707
7.96158
7.96858
1.331
4.356
2.171
2.055
2.044
3.230
3.004
1.000
1.000
0.959
ppm
153 bebi-240817-cptpbr

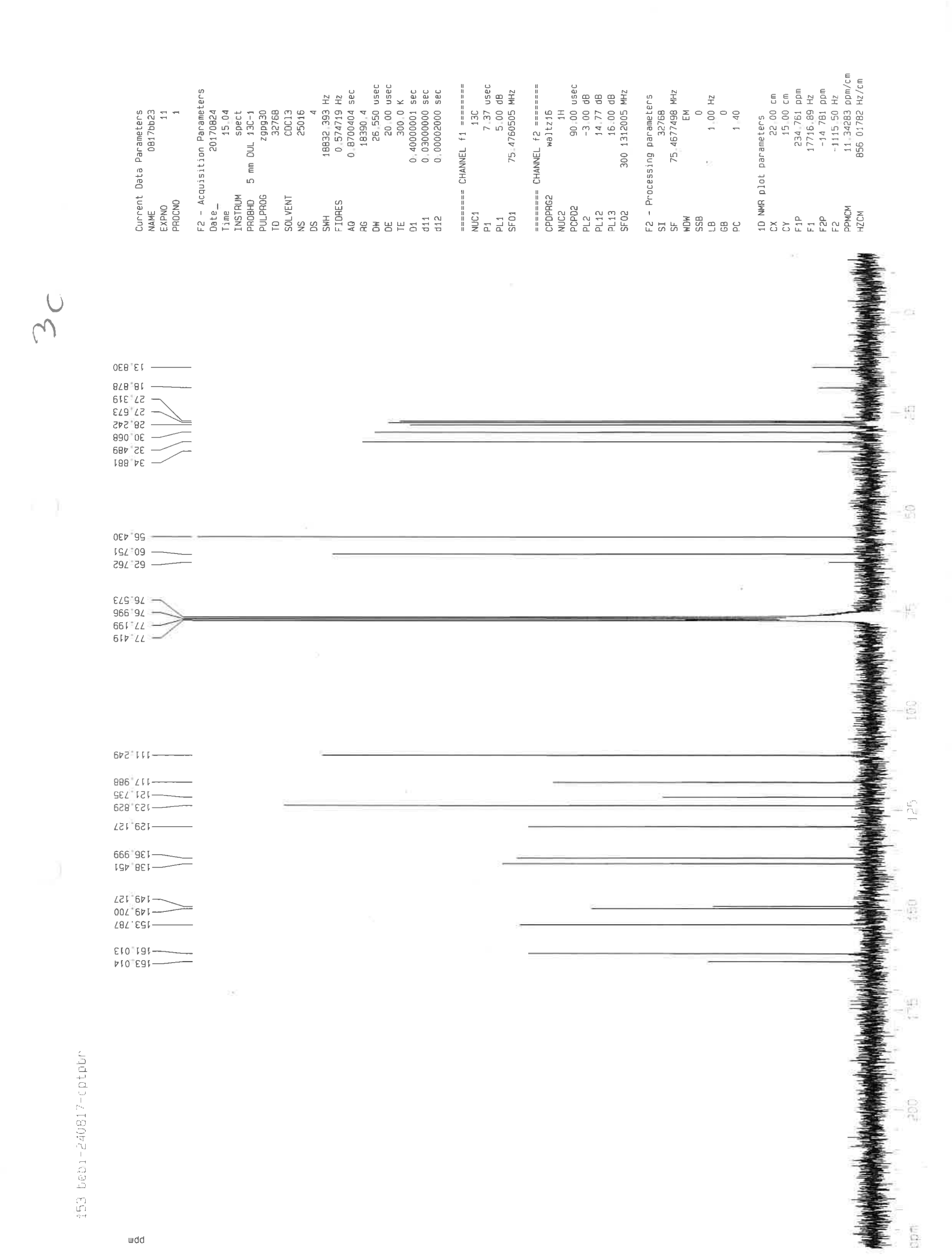
Current Data Parameters
NAME 0817bb23
EXPNO 11
PROCNO 1
F2 - Acquisition Parameters
Date_ 20170824
Time 15.04
INSTRUM spect
PROBHD 5 mm DUL 13C-1
PULPROG zgpg30
TD 32768
SOLVENT CDCl3
NS 25016
DS 4
SWH 18832.393 Hz
FIDRES 0.574719 Hz
AQ 0.8700404 sec
RG 18390.4
DW 26.550 usec
DE 20.00 usec
TE 300.0 K
D1 0.40000001 sec
d11 0.03000000 sec
d12 0.00002000 sec
======== CHANNEL f1 ========
NUC1 13C
P1 7.37 usec
PL1 5.00 dB
SFO1 75.4760505 MHz
======== CHANNEL f2 ========
CPDPRG2 waltz16
NUC2 1H
PCPD2 90.00 usec
PL2 -3.00 dB
PL12 14.77 dB
PL13 16.00 dB
SFO2 300.1312005 MHz
F2 - Processing parameters
SI 32768
SF 75.4677498 MHz
WDW EM
SSB 0
LB 1.00 Hz
GB 0
PC 1.40
1D NMR plot parameters
CX 22.00 cm
CY 15.00 cm
F1P 234.761 ppm
F1 17716.89 Hz
F2P -14.781 ppm
F2 -1115.50 Hz
PPMCM 11.34283 ppm/cm
HZCM 856.01782 Hz/cm
13.830
18.878
27.319
27.673
28.242
30.068
32.489
34.881
56.430
60.751
62.762
76.573
76.996
77.199
77.419
111.249
117.988
121.735
123.829
129.127
136.999
138.451
149.127
149.700
153.787
161.013
163.014
ppm
153 bebi-240817-optpdr

3C

3d

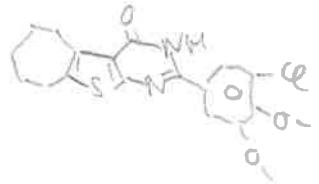

Acetone

10 bebi-270618-chptpcl

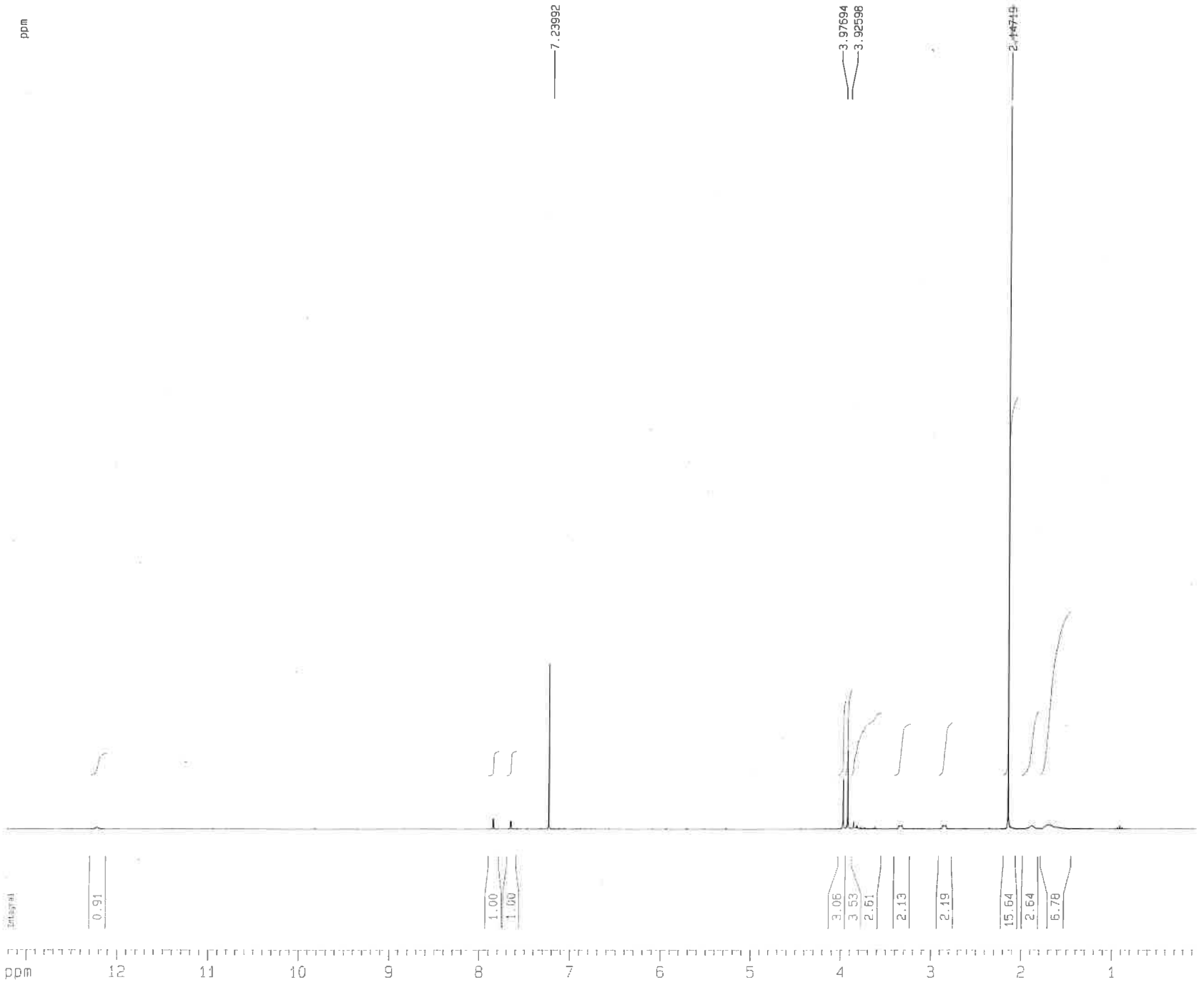

Current Data Parameters

NAME	0618bb51
EXPNO	10
PROCNO	1

F2 - Acquisition Parameters

Date_	20180627
Time	12.23
INSTRUM	spect
PROBHD	5 mm DUL 13C-1
PULPROG	zg30
TD	65536
SOLVENT	CDCl3
NS	100
DS	2
SWH	8992.806 Hz
FIDRES	0.137219 Hz
AQ	3.6438515 sec
RG	1024
DW	55.600 usec
DE	7.00 usec
TE	300.0 K
D1	0.50000000 sec

======== CHANNEL f1 ========

NUC1	1H
P1	11.63 usec
PL1	-3.00 dB
SFO1	300.1318008 MHz

F2 - Processing parameters

SI	65536
SF	300.1300127 MHz
WDW	no
SSB	0
LB	0.00 Hz
GB	0
PC	1.00

1D NMR plot parameters

CX	22.00 cm
CY	13.50 cm
F1P	13.236 ppm
F1	3972.46 Hz
F2P	0.061 ppm
F2	18.18 Hz
PPMCM	0.59887 ppm/cm
HZCM	179.74014 Hz/cm

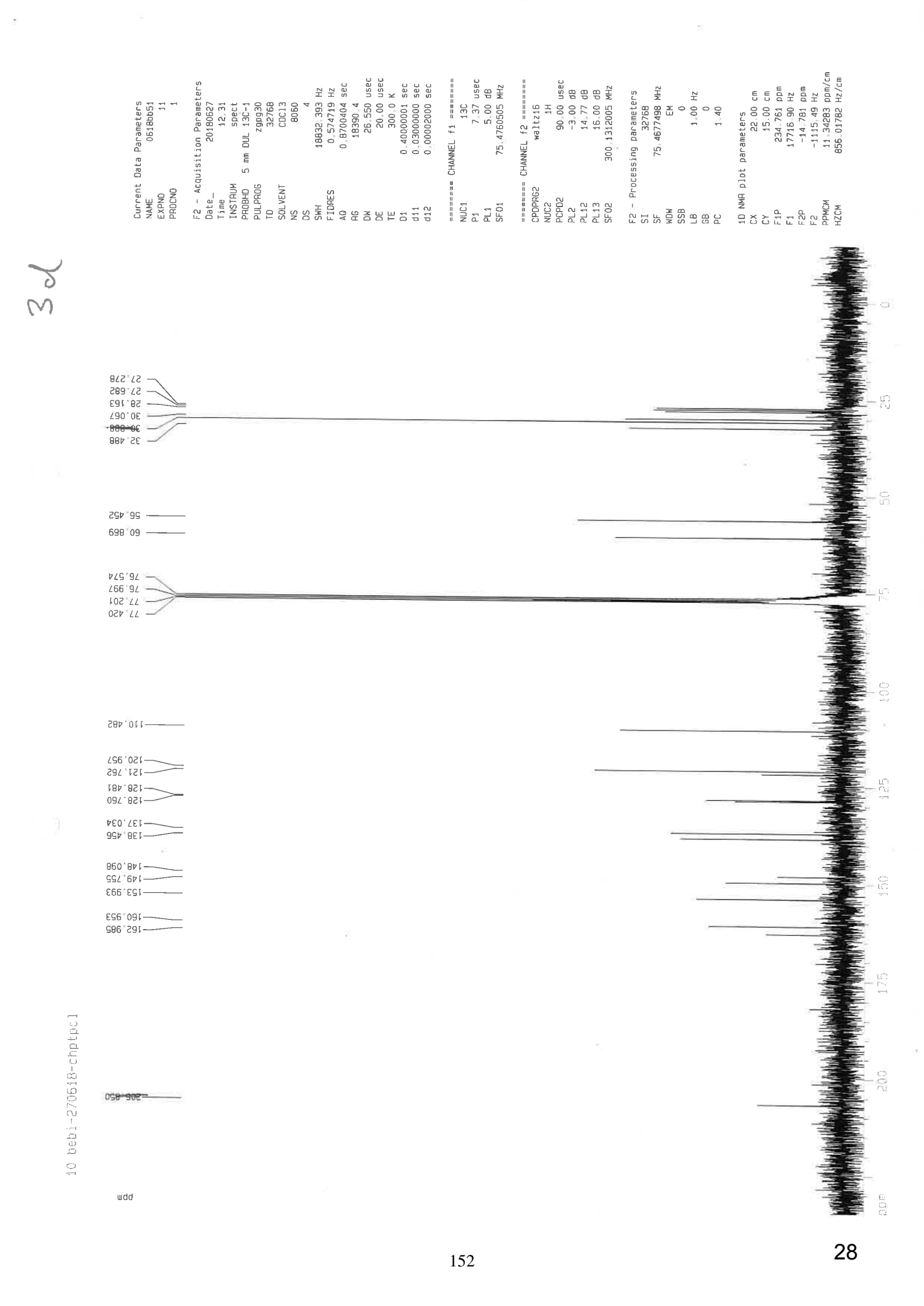
3d
Current Data Parameters
NAME 0618b51
EXPNO 11
PROCNO 1
F2 - Acquisition Parameters
Date_ 20180627
Time 12.31
INSTRUM spect
PROBHD 5 mm DUL 13C-1
PULPROG zgpg30
TD 32768
SOLVENT CDCl3
NS 8060
DS 4
SWH 18832.393 Hz
FIDRES 0.574719 Hz
AQ 0.8700404 sec
RG 18390.4
DW 26.550 usec
DE 20.00 usec
TE 300.0 K
D1 0.40000001 sec
d11 0.03000000 sec
d12 0.00002000 sec
======== CHANNEL f1 ========
NUC1 13C
P1 7.37 usec
PL1 5.00 dB
SFO1 75.4760505 MHz
======== CHANNEL f2 ========
CPDPRG2 waltz16
NUC2 1H
PCPD2 90.00 usec
PL2 -3.00 dB
PL12 14.77 dB
PL13 16.00 dB
SFO2 300.1312005 MHz
F2 - Processing parameters
SI 32768
SF 75.4677498 MHz
WDW EM
SSB 0
LB 1.00 Hz
GB 0
PC 1.40
1D NMR plot parameters
CX 22.00 cm
CY 15.00 cm
F1P 234.761 ppm
F1 17716.90 Hz
F2P -14.781 ppm
F2 -1115.49 Hz
PPMCM 11.34283 ppm/cm
HZCM 856.01782 Hz/cm
27.278
27.682
28.163
30.067
30.888
32.488
56.452
60.869
76.574
76.997
77.201
77.420
110.482
120.957
121.762
128.481
128.760
137.034
138.456
148.098
149.755
153.993
160.953
162.985
206.850
10 bebi-270618-chptpe1
ppm

3e

9 bbb1-210618-chptp1

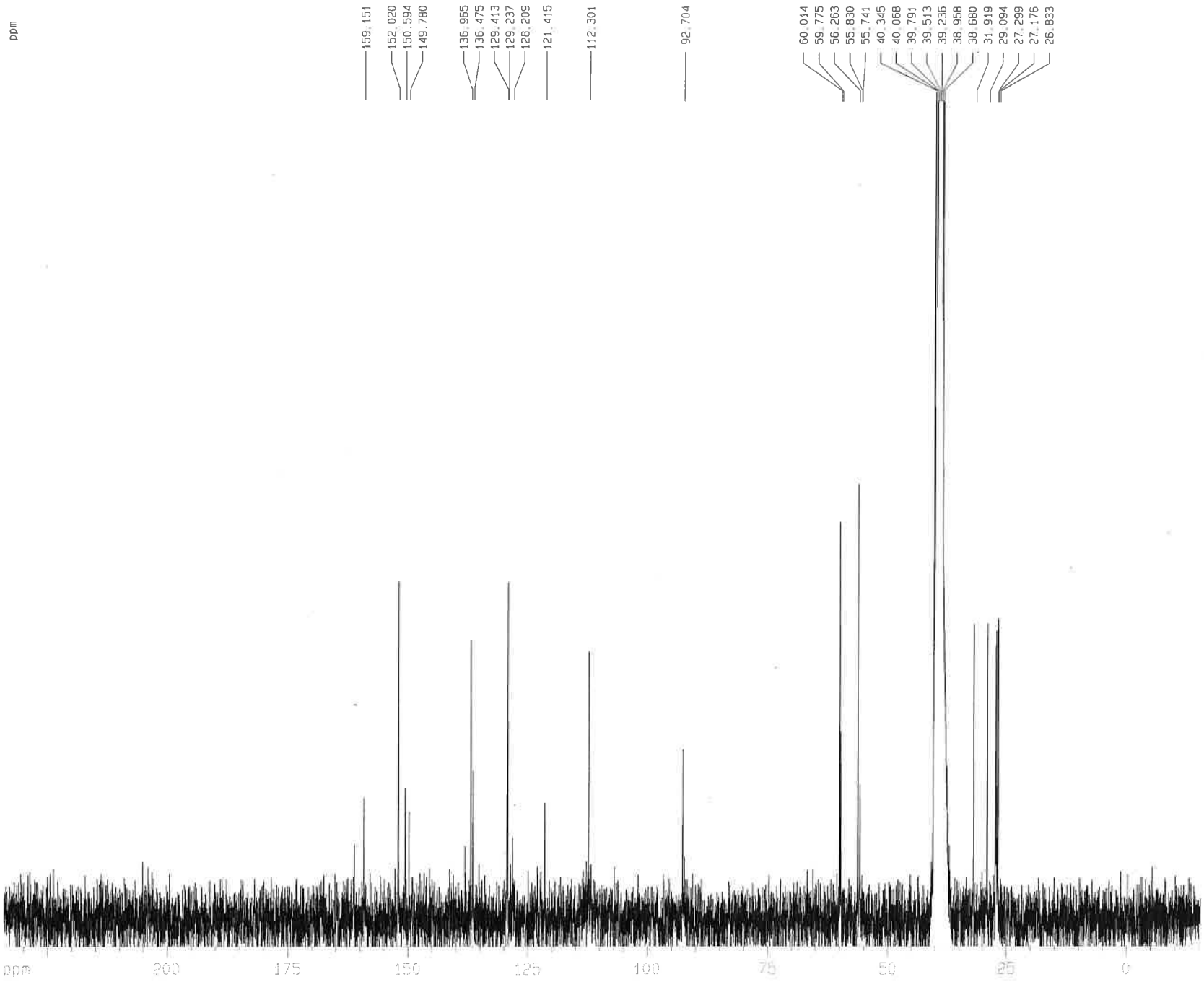

Current Data Parameters

NAME	0618bb41
EXPNO	11
PROCNO	1

F2 - Acquisition Parameters

Date_	20180621
Time	14.37
INSTRUM	spect
PROBHD	5 mm DUL 13C-1
PULPROG	zgpg30
TD	32768
SOLVENT	DMSO
NS	39580
DS	4
SWH	18832.393 Hz
FIDRES	0.574719 Hz
AQ	0.8700404 sec
RG	18390.4
DW	26.550 usec
DE	20.00 usec
TE	300.0 K
D1	0.40000001 sec
d11	0.03000000 sec
d12	0.00002000 sec

======== CHANNEL f1 ========

NUC1	13C
P1	7.37 usec
PL1	5.00 dB
SFO1	75.4760505 MHz

======== CHANNEL f2 ========

CPDPRG2	waltz16
NUC2	1H
PCPD2	90.00 usec
PL2	-3.00 dB
PL12	14.77 dB
PL13	16.00 dB
SFO2	300.1312005 MHz

F2 - Processing parameters

SI	32768
SF	75.4677876 MHz
WDW	EM
SSB	0
LB	1.00 Hz
GB	0
PC	1.40

1D NMR plot parameters

CX	22.00 cm
CY	8.00 cm
F1P	234.259 ppm
F1	17679.02 Hz
F2P	-15.283 ppm
F2	-1153.37 Hz
PPMCM	11.34282 ppm/cm
HZCM	856.01782 Hz/cm

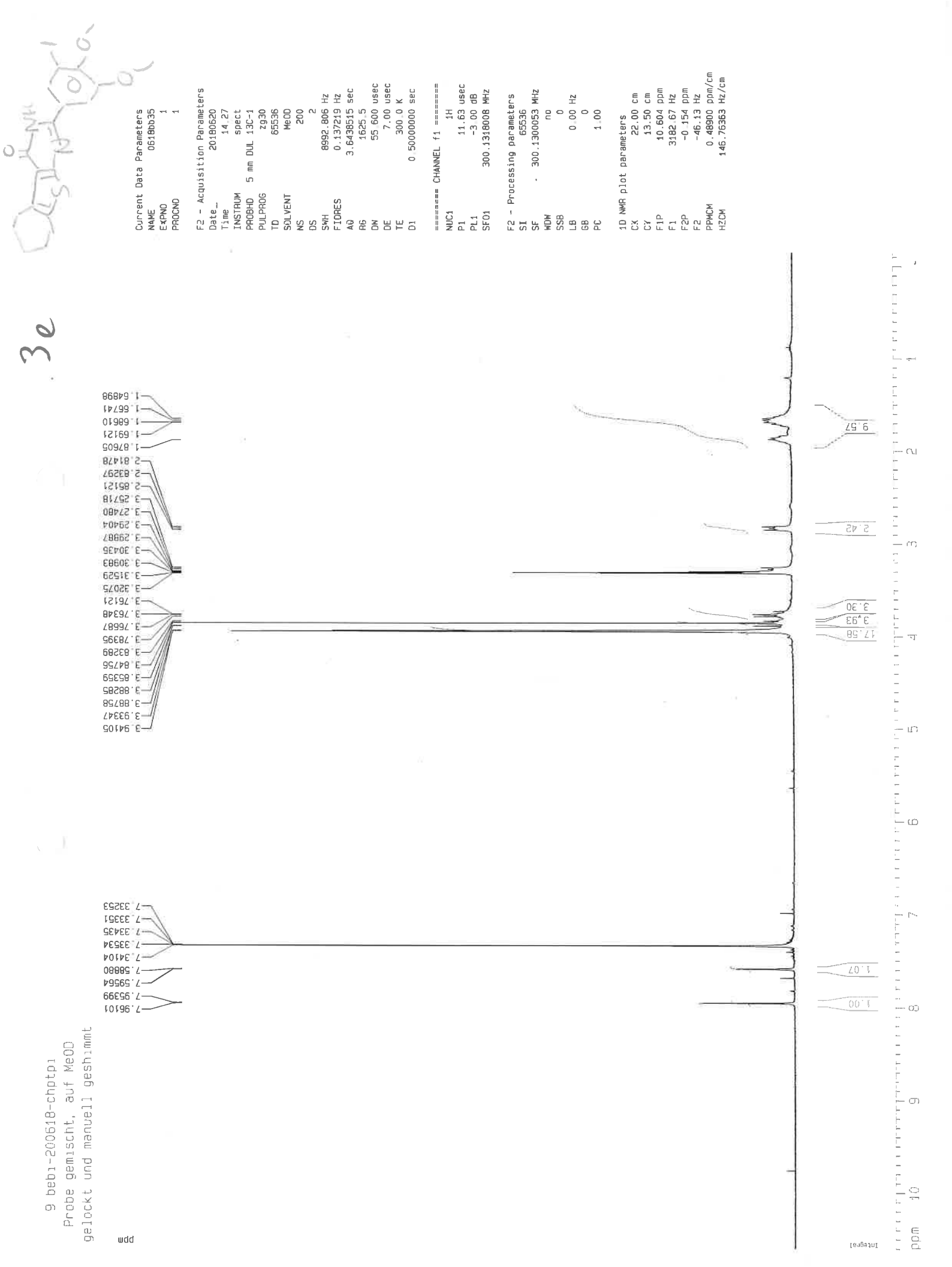
3e
Current Data Parameters
NAME 0618bb35
EXPNO 1
PROCNO 1
F2 - Acquisition Parameters
Date_ 20180620
Time 14.27
INSTRUM spect
PROBHD 5 mm DUL 13C-1
PULPROG zg30
TD 65536
SOLVENT MeOD
NS 200
DS 2
SWH 8992.806 Hz
FIDRES 0.137219 Hz
AQ 3.6438515 sec
RG 1625.5
DW 55.600 usec
DE 7.00 usec
TE 300.0 K
D1 0.50000000 sec
======== CHANNEL f1 ========
NUC1 1H
P1 11.63 usec
PL1 -3.00 dB
SFO1 300.1318008 MHz
F2 - Processing parameters
SI 65536
SF 300.1300053 MHz
WDW no
SSB 0
LB 0.00 Hz
GB 0
PC 1.00
1D NMR plot parameters
CX 22.00 cm
CY 13.50 cm
F1P 10.604 ppm
F1 3182.67 Hz
F2P -0.154 ppm
F2 -46.13 Hz
PPMCM 0.48900 ppm/cm
HZCM 146.76363 Hz/cm
1.64898
1.66741
1.68610
1.69121
1.87605
2.81478
2.83297
2.85121
3.25718
3.27480
3.29404
3.29987
3.30435
3.30983
3.31529
3.32075
3.76121
3.76348
3.76687
3.78395
3.83289
3.84756
3.85359
3.88285
3.88758
3.93347
3.94105
7.33253
7.33351
7.33435
7.33534
7.34104
7.58080
7.59564
7.95399
7.96101
9.57
2.42
3.30
3.93
17.58
1.07
1.00
9 bebi-200618-chptp1
Probe gemischt, auf MeOD
gelockt und manuell geshimmt
ppm
Integral
ppm

3g

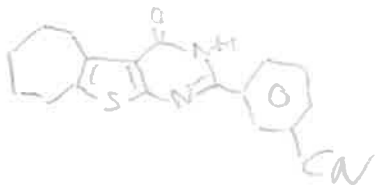

154 beb1-300817-cptp3cn

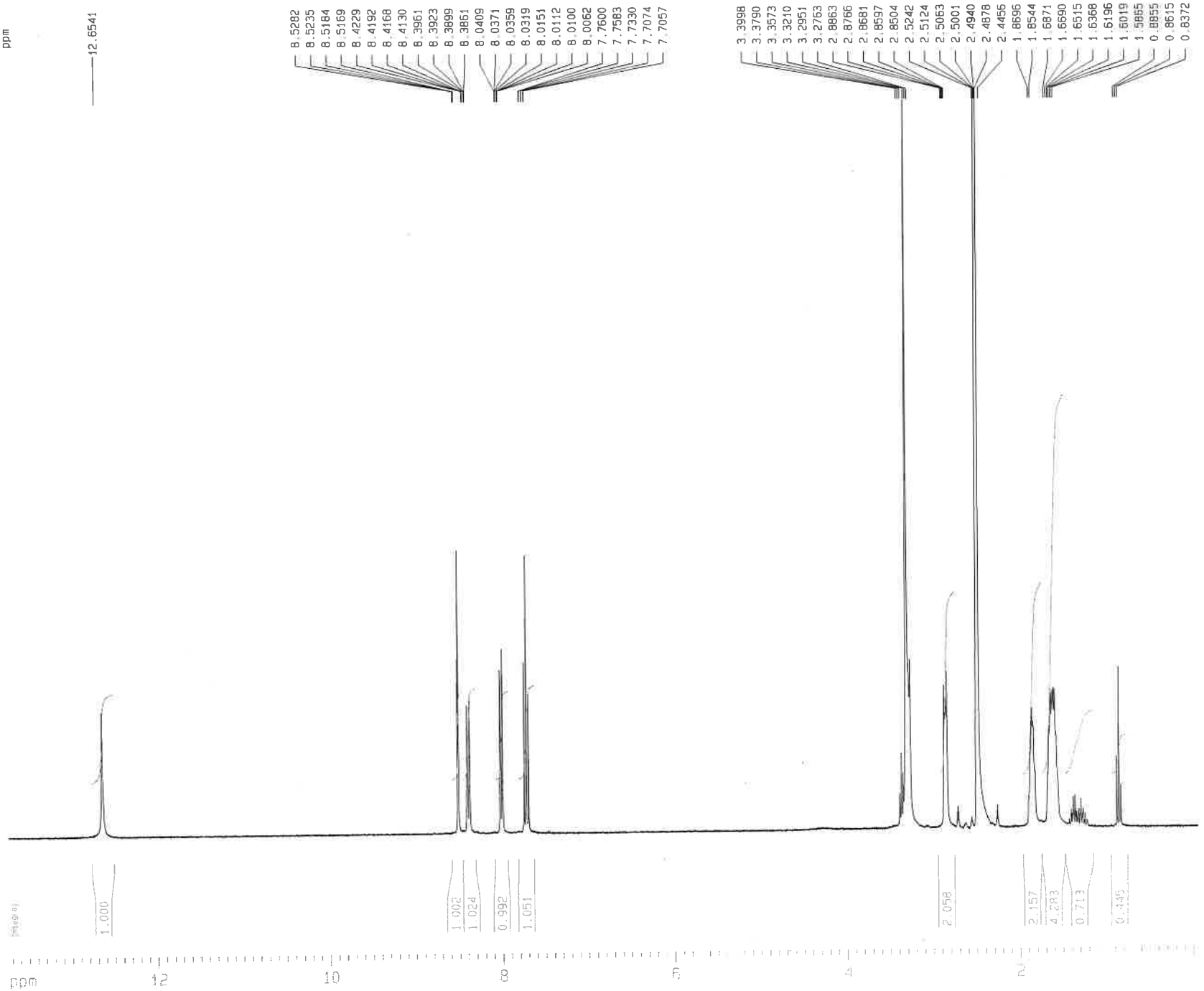

Current Data Parameters

NAME	0817bb28
EXPNO	10
PROCNO	1

F2 - Acquisition Parameters

Date_	20170830
Time	12.19
INSTRUM	spect
PROBHD	5 mm DUL 13C-1
PULPROG	zg30
TD	65536
SOLVENT	DMSO
NS	200
DS	2
SWH	8992.806 Hz
FIDRES	0.137219 Hz
AQ	3.6438515 sec
RG	1024
DW	55.600 usec
DE	7.00 usec
TE	300.0 K
D1	0.50000000 sec

======== CHANNEL f1 ========

NUC1	1H
P1	11.63 usec
PL1	-3.00 dB
SFO1	300.1318008 MHz

F2 - Processing parameters

SI	65536
SF	300.1300021 MHz
WDW	no
SSB	-0
LB	0.00 Hz
GB	0
PC	1.00

1D NMR plot parameters

CX	22.00 cm
CY	13.50 cm
F1P	13.748 ppm
F1	4126.04 Hz
F2P	-0.047 ppm
F2	-14.13 Hz
PPMCM	0.62703 ppm/cm
HZCM	188.18971 Hz/cm

3g

154 beb1-300817-cotu3cm

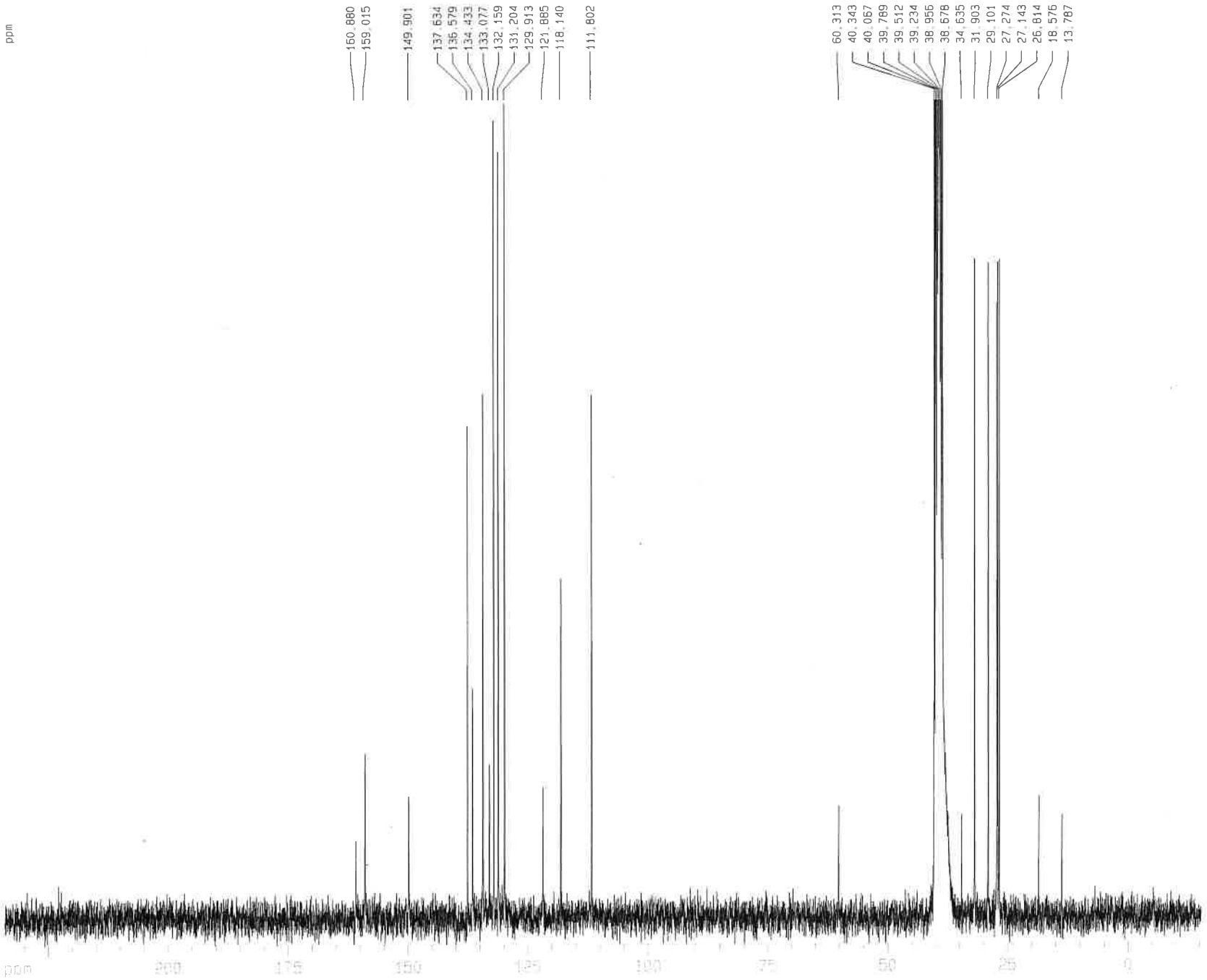

Current Data Parameters
NAME 0817bb28
EXPNO 11
PROCNO 1

F2 - Acquisition Parameters
Date_ 20170830
Time 13.36
INSTRUM spect
PROBHD 5 mm DUL 13C-1
PULPROG zgpg30
TD 32768
SOLVENT DMSO
NS 53660
DS 4
SWH 18832.393 Hz
FIDRES 0.574719 Hz
AQ 0.8700404 sec
RG 18390.4
DW 26.550 usec
DE 20.00 usec
TE 300.0 K
D1 0.40000001 sec
d11 0.03000000 sec
d12 0.00002000 sec

======== CHANNEL f1 ========
NUC1 13C
P1 7.37 usec
PL1 5.00 dB
SFO1 75.4760505 MHz

======== CHANNEL f2 ========
CPDPRG2 waltz16
NUC2 1H
PCPD2 90.00 usec
PL2 -3.00 dB
PL12 14.77 dB
PL13 16.00 dB
SFO2 300.1312005 MHz

F2 - Processing parameters
SI 32768
SF 75.4677882 MHz
WDW EM
SSB 0
LB 1.00 Hz
GB 0
PC 1.40

1D NMR plot parameters
CX 22.00 cm
CY 15.00 cm
F1P 234.252 ppm
F1 17678.45 Hz
F2P -15.291 ppm
F2 -1153.95 Hz
PPMCM 11.34282 ppm/cm
HZCM 856.01782 Hz/cm

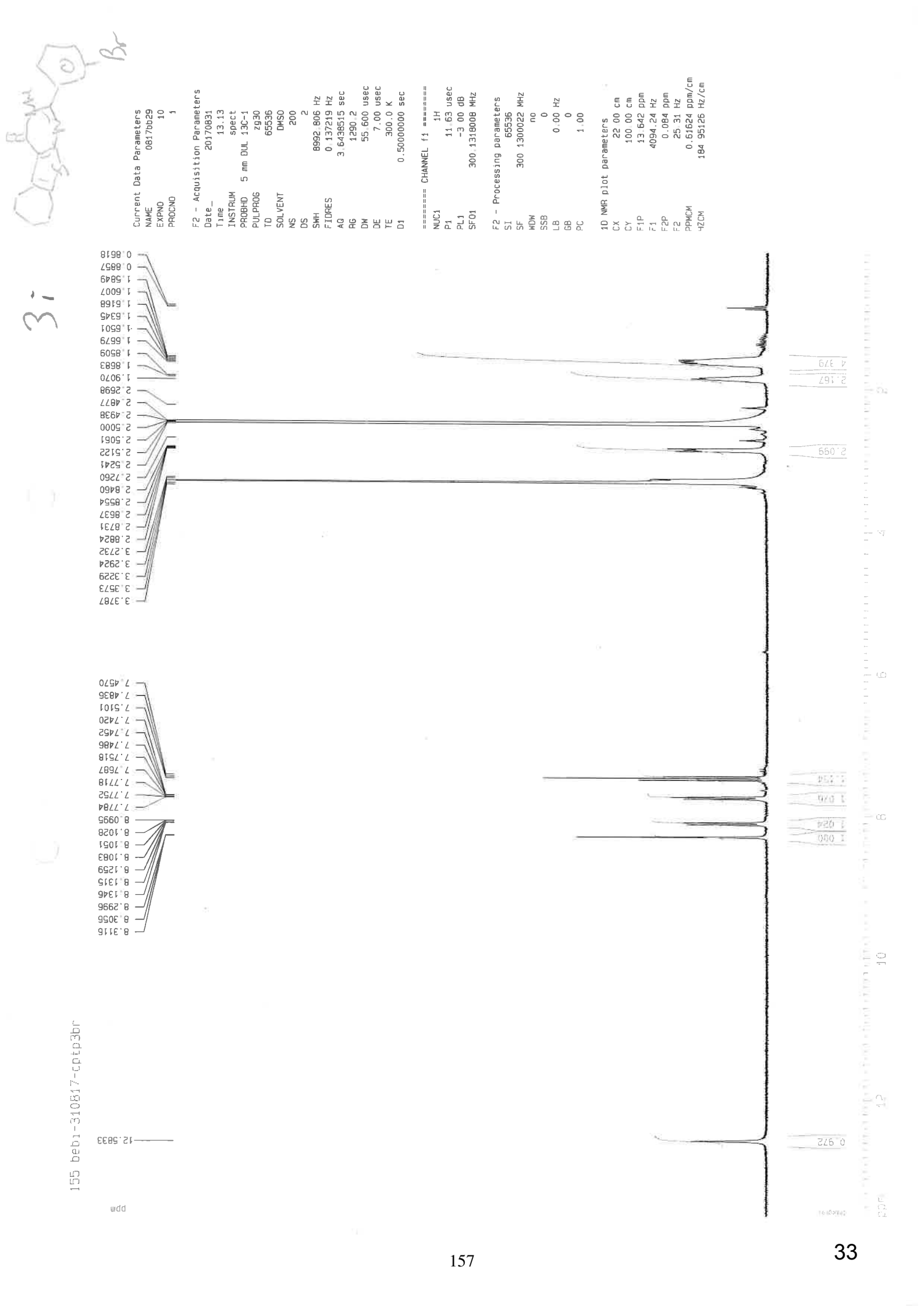
Current Data Parameters
NAME 0817bb29
EXPNO 10
PROCNO 1
F2 - Acquisition Parameters
Date_ 20170831
Time 13.13
INSTRUM spect
PROBHD 5 mm DUL 13C-1
PULPROG zg30
TD 65536
SOLVENT DMSO
NS 200
DS 2
SWH 8992.806 Hz
FIDRES 0.137219 Hz
AQ 3.6438515 sec
RG 1290.2
DW 55.600 usec
DE 7.00 usec
TE 300.0 K
D1 0.50000000 sec
======== CHANNEL f1 ========
NUC1 1H
P1 11.63 usec
PL1 -3.00 dB
SFO1 300.1318008 MHz
F2 - Processing parameters
SI 65536
SF 300.1300022 MHz
WDW no
SSB 0
LB 0.00 Hz
GB 0
PC 1.00
1D NMR plot parameters
CX 22.00 cm
CY 100.00 cm
F1P 13.642 ppm
F1 4094.24 Hz
F2P 0.084 ppm
F2 25.31 Hz
PPMCM 0.61624 ppm/cm
HZCM 184.95126 Hz/cm
0.8618
0.8857
1.5849
1.6007
1.6168
1.6345
1.6501
1.6579
1.8509
1.8683
1.9070
2.2698
2.4877
2.4938
2.5000
2.5061
2.5122
2.5241
2.7260
2.8460
2.8554
2.8637
2.8731
2.8824
3.2732
3.2924
3.3229
3.3573
3.3787
7.4570
7.4836
7.5101
7.7420
7.7452
7.7486
7.7518
7.7687
7.7718
7.7752
7.7784
8.0995
8.1028
8.1051
8.1083
8.1259
8.1315
8.1346
8.2996
8.3056
8.3116
12.5833
4.379
2.167
2.099
1.024
1.000
0.972
155 bebi-310817-cptp3br
ppm

155 bebi-310817-cptb3br

3i

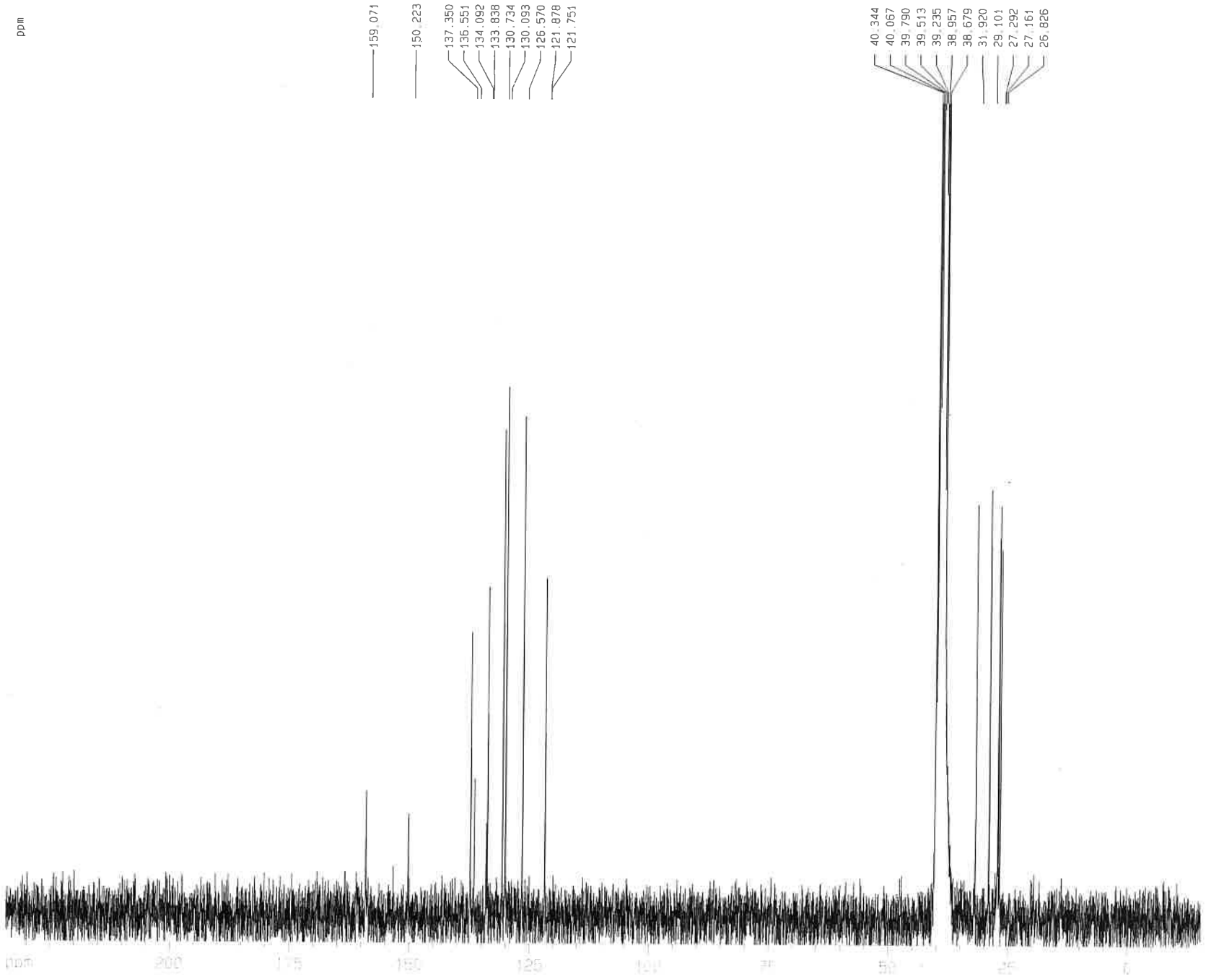

Current Data Parameters

NAME	0817bb29
EXPNO	20
PROCNO	1

F2 - Acquisition Parameters

Date_	20170831
Time	16.25
INSTRUM	spect
PROBHD	5 mm DUL 13C-1
PULPROG	zgpg30
TD	32768
SOLVENT	DMSO
NS	41324
DS	4
SWH	18832.393 Hz
FIDRES	0.574719 Hz
AQ	0.8700404 sec
RG	18390.4
DW	26.550 usec
DE	20.00 usec
TE	300.0 K
D1	0.40000001 sec
d11	0.03000000 sec
d12	0.00002000 sec

======== CHANNEL f1 ========

NUC1	13C
P1	7.37 usec
PL1	5.00 dB
SF01	75.4760505 MHz

======== CHANNEL f2 ========

CPDPRG2	waltz16
NUC2	1H
PCPD2	90.00 usec
PL2	-3.00 dB
PL12	14.77 dB
PL13	16.00 dB
SF02	300.1312005 MHz

F2 - Processing parameters

SI	32768
SF	75.4677876 MHz
WDW	EM
SSB	0
LB	1.00 Hz
GB	0
PC	1.40

1D NMR plot parameters

CX	22.00 cm
CY	10.00 cm
F1P	234.259 ppm
F1	17679.02 Hz
F2P	-15.283 ppm
F2	-1153.37 Hz
PPMCM	11.34282 ppm/cm
HZCM	856.01782 Hz/cm

158

34

3j

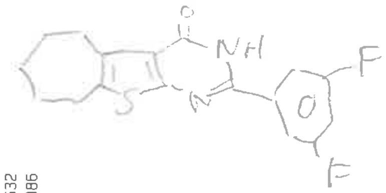

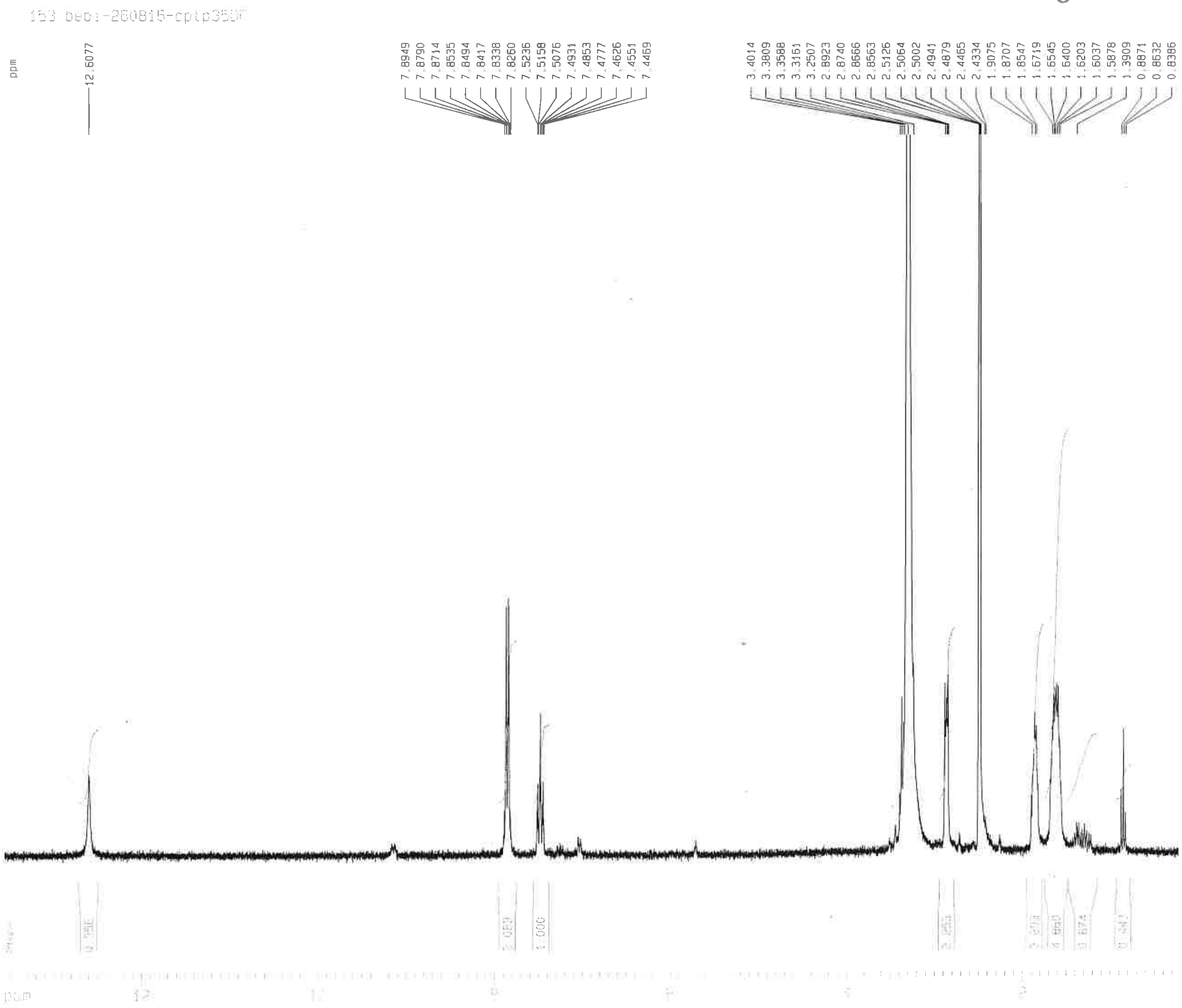

Current Data Parameters
NAME 0817bb24
EXPNO 1
PROCNO 1

F2 - Acquisition Parameters
Date_ 20170828
Time 8.51
INSTRUM spect
PROBHD 5 mm DUL 13C-1
PULPROG zg30
TD 65536
SOLVENT DMSO
NS 304
DS 2
SWH 8992.806 Hz
FIDRES 0.137219 Hz
AQ 3.6438515 sec
RG 1625.5
DW 55.600 usec
DE 7.00 usec
TE 300.0 K
D1 0.50000000 sec

======== CHANNEL f1 ========
NUC1 1H
P1 11.63 usec
PL1 -3.00 dB
SFO1 300.1318008 MHz

F2 - Processing parameters
SI 65536
SF 300.1300016 MHz
WDW no
SSB 0
LB 0.00 Hz
GB 0
PC 1.00

1D NMR plot parameters
CX 22.00 cm
CY 400.00 cm
F1P 13.565 ppm
F1 4071.18 Hz
F2P 0.245 ppm
F2 73.50 Hz
PPMCM 0.60545 ppm/cm
HZCM 181.71283 Hz/cm

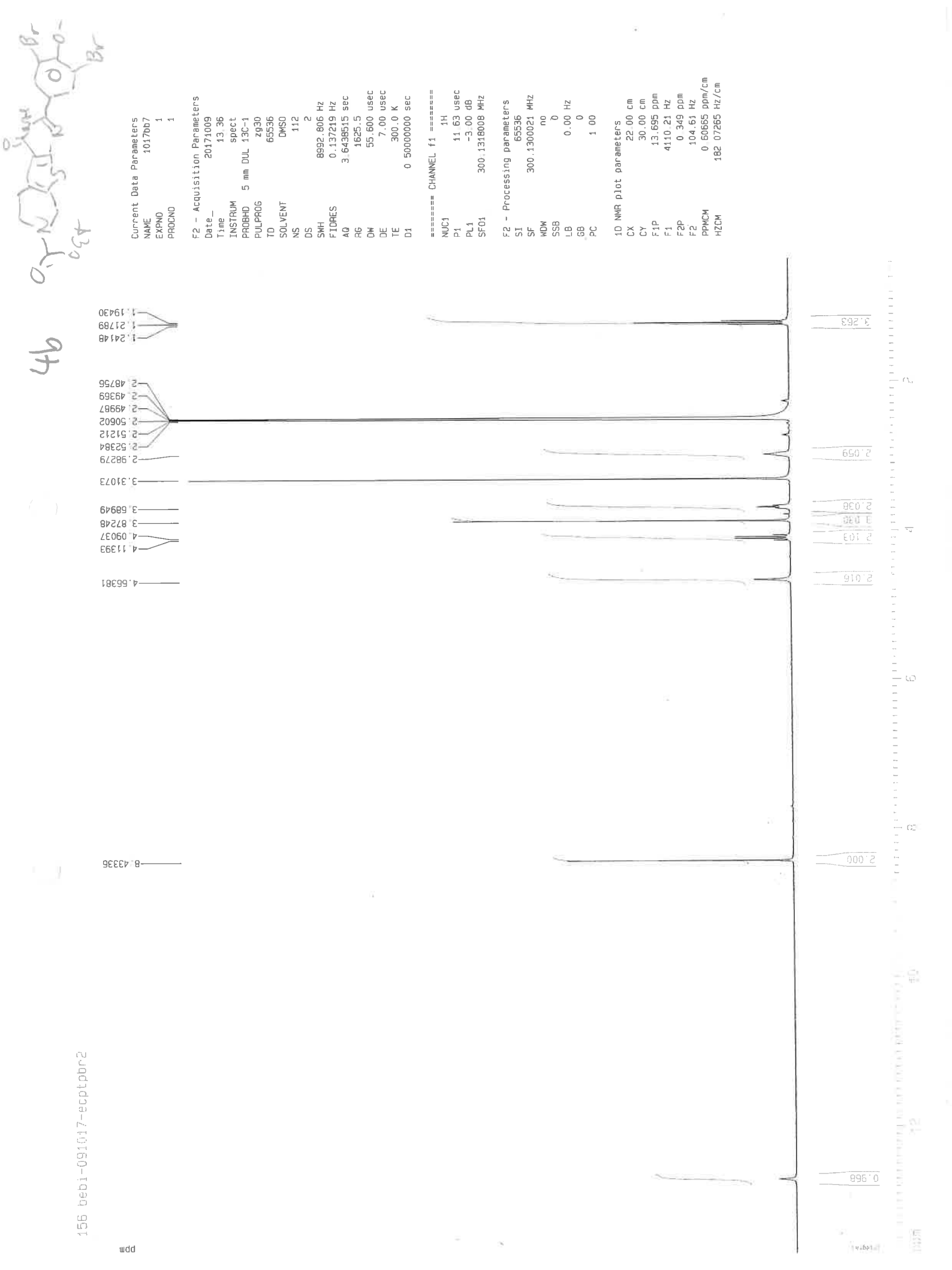
Current Data Parameters
NAME 1017bb7
EXPNO 1
PROCNO 1
F2 - Acquisition Parameters
Date_ 20171009
Time 13.36
INSTRUM spect
PROBHD 5 mm DUL 13C-1
PULPROG zg30
TD 65536
SOLVENT DMSO
NS 112
DS 2
SWH 8992.806 Hz
FIDRES 0.137219 Hz
AQ 3.6438515 sec
RG 1625.5
DW 55.600 usec
DE 7.00 usec
TE 300.0 K
D1 0.50000000 sec
======== CHANNEL f1 ========
NUC1 1H
P1 11.63 usec
PL1 -3.00 dB
SFO1 300.1318008 MHz
F2 - Processing parameters
SI 65536
SF 300.1300021 MHz
WDW no
SSB 0
LB 0.00 Hz
GB 0
PC 1.00
1D NMR plot parameters
CX 22.00 cm
CY 30.00 cm
F1P 13.695 ppm
F1 4110.21 Hz
F2P 0.349 ppm
F2 104.61 Hz
PPMCM 0.60665 ppm/cm
HZCM 182.07265 Hz/cm
1.19430
1.21789
1.24148
2.48756
2.49369
2.49987
2.50602
2.51212
2.52384
2.98279
3.31073
3.68949
3.87248
4.09037
4.11393
4.56381
8.43336
3.263
2.059
2.038
2.030
2.103
2.016
2.000
0.966
156 bebi-091017-ecptpbr2
ppm

158 bebi-091017-ecptpbr2

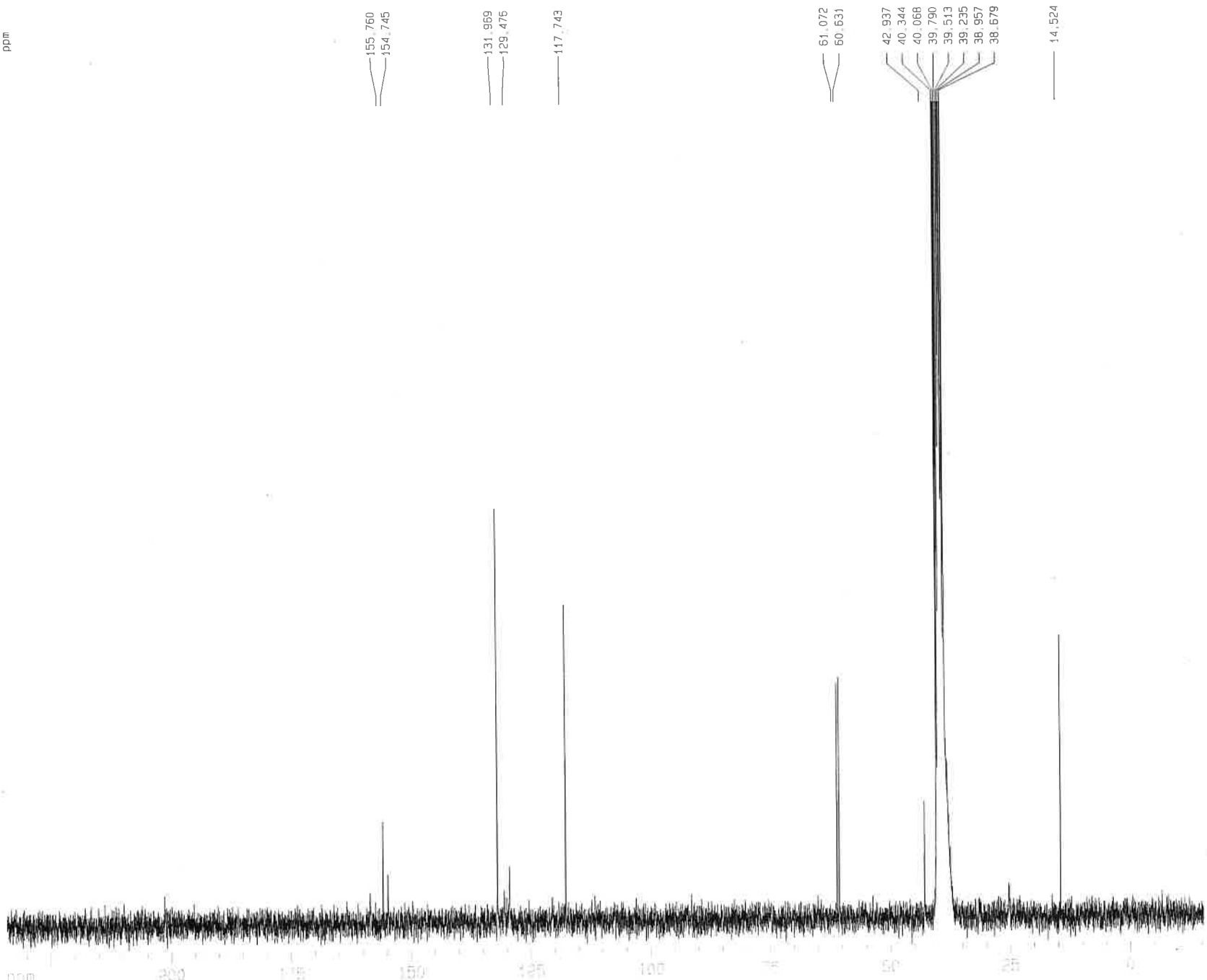

Current Data Parameters
NAME 1017bb7
EXPNO 2
PROCNO 1

F2 - Acquisition Parameters
Date_ 20171009
Time 13.45
INSTRUM spect
PROBHD 5 mm DUL 13C-1
PULPROG zgpg30
TD 32768
SOLVENT CDCl3
NS 47580
DS 4
SWH 18832.393 Hz
FIDRES 0.574719 Hz
AQ 0.8700404 sec
RG 18390.4
DW 26.550 usec
DE 20.00 usec
TE 300.0 K
D1 0.40000001 sec
d11 0.03000000 sec
d12 0.00002000 sec

======== CHANNEL f1 ========
NUC1 13C
P1 7.37 usec
PL1 5.00 dB
SFO1 75.4760505 MHz

======== CHANNEL f2 ========
CPDPRG2 waltz16
NUC2 1H
PCPD2 90.00 usec
PL2 -3.00 dB
PL12 14.77 dB
PL13 16.00 dB
SFO2 300.1312005 MHz

F2 - Processing parameters
SI 32768
SF 75.4677882 MHz
WDW EM
SSB 0
LB 1.00 Hz
GB 0
PC 1.40

1D NMR plot parameters
CX 22.00 cm
CY 200.00 cm
F1P 234.252 ppm
F1 17678.45 Hz
F2P -15.291 ppm
F2 -1153.95 Hz
PPMCM 11.34282 ppm/cm
HZCM 856.01782 Hz/cm

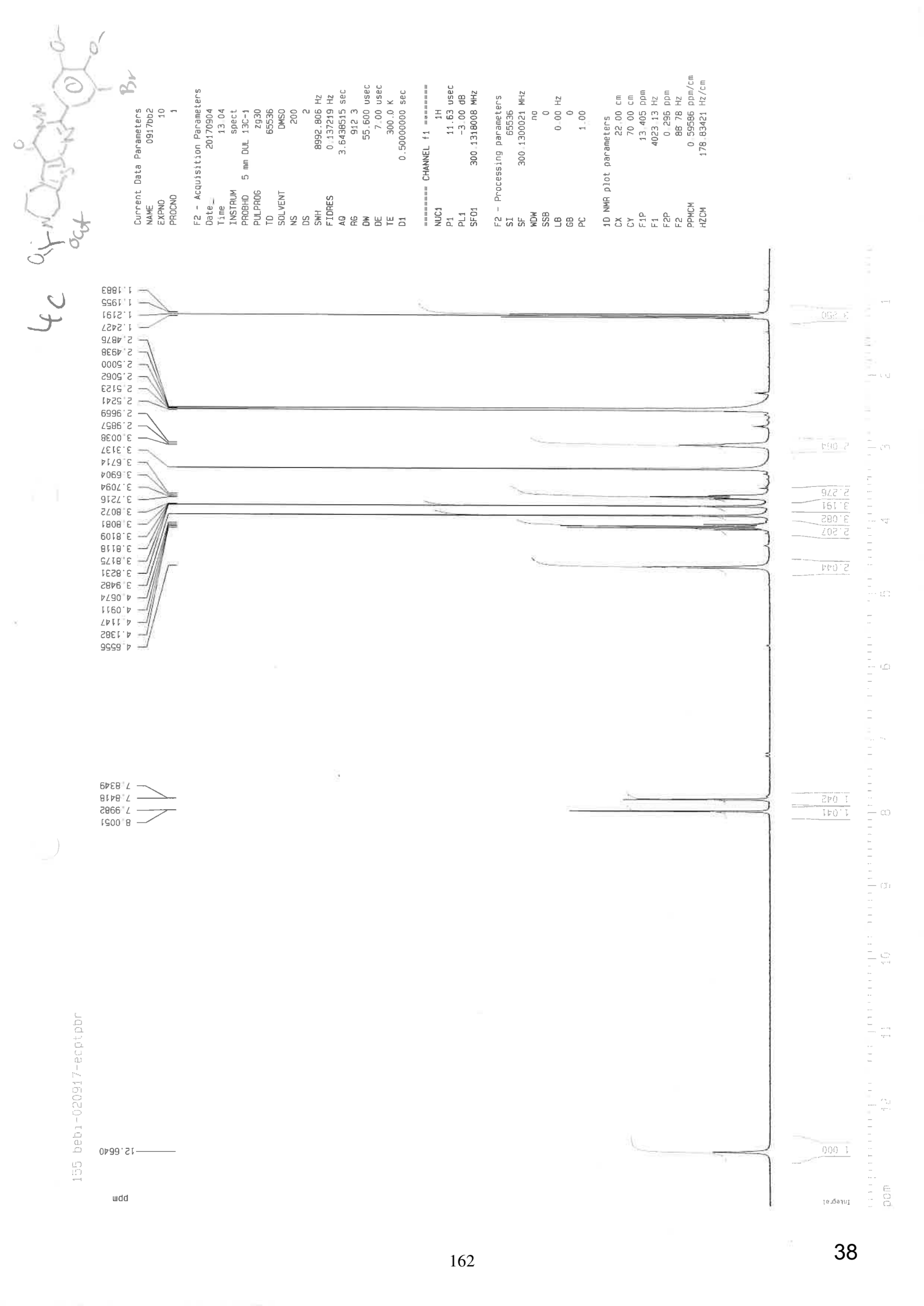
Current Data Parameters
NAME 0917bb2
EXPNO 10
PROCNO 1
F2 - Acquisition Parameters
Date_ 20170904
Time 13.04
INSTRUM spect
PROBHD 5 mm DUL 13C-1
PULPROG zg30
TD 65536
SOLVENT DMSO
NS 200
DS 2
SWH 8992.806 Hz
FIDRES 0.137219 Hz
AQ 3.6438515 sec
RG 912.3
DW 55.600 usec
DE 7.00 usec
TE 300.0 K
D1 0.50000000 sec
======== CHANNEL f1 ========
NUC1 1H
P1 11.63 usec
PL1 -3.00 dB
SFO1 300.1318008 MHz
F2 - Processing parameters
SI 65536
SF 300.1300021 MHz
WDW no
SSB 0
LB 0.00 Hz
GB 0
PC 1.00
1D NMR plot parameters
CX 22.00 cm
CY 70.00 cm
F1P 13.405 ppm
F1 4023.13 Hz
F2P 0.296 ppm
F2 88.78 Hz
PPMCM 0.59586 ppm/cm
HZCM 178.83421 Hz/cm
4c
1.1883
1.1955
1.2191
1.2427
2.4876
2.4938
2.5000
2.5062
2.5123
2.5241
2.9669
2.9857
3.0038
3.3137
3.6714
3.6904
3.7094
3.7216
3.8072
3.8081
3.8109
3.8118
3.8175
3.8231
3.9482
4.0674
4.0911
4.1147
4.1382
4.6556
7.8349
7.8418
7.9982
8.0051
12.6640
155 bebi-020917-ecptpbr
ppm
Integral

155 beb1-020917-ecpupbr

4c

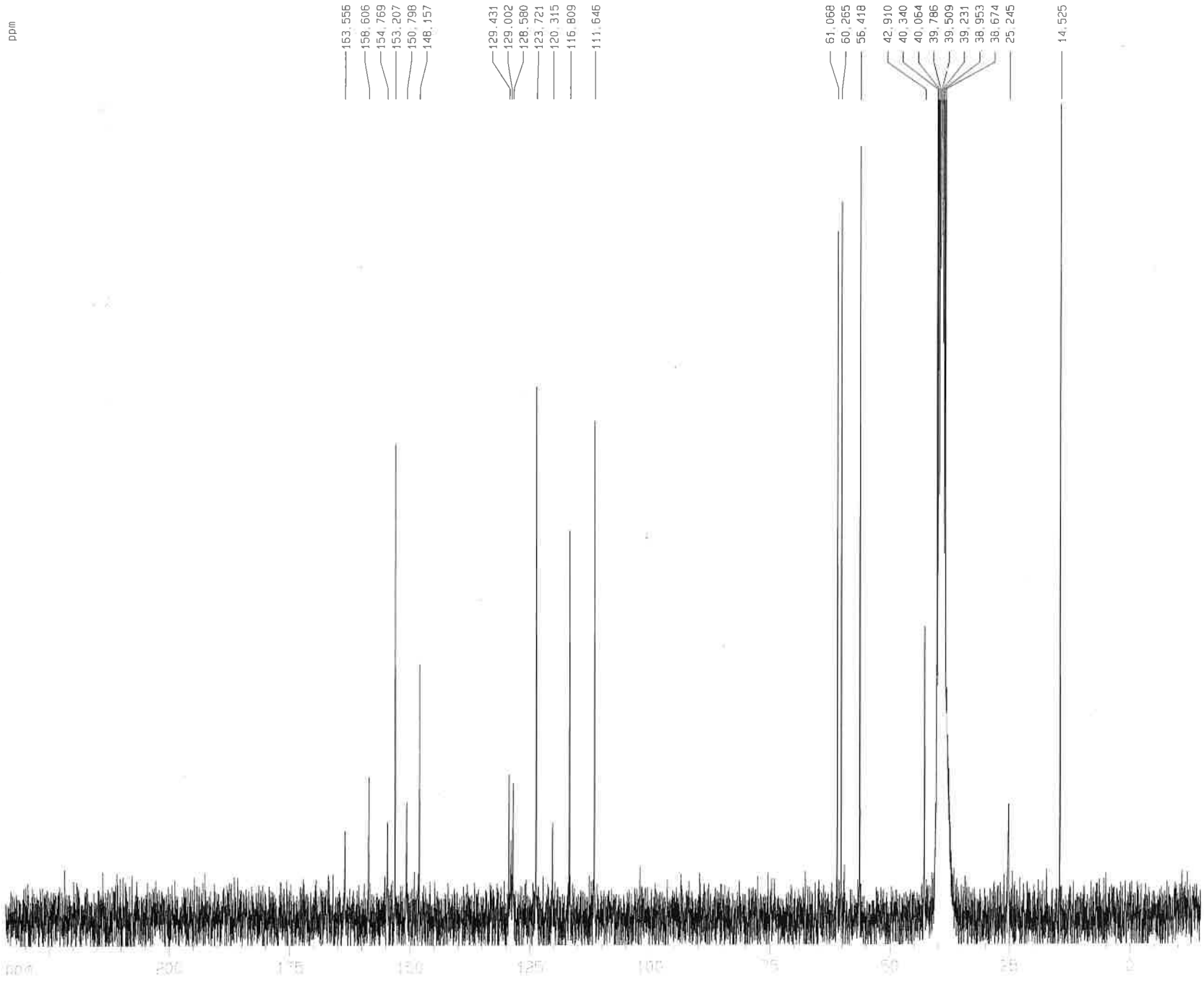

Current Data Parameters
NAME 0917bb2
EXPNO 20
PROCNO 1

F2 - Acquisition Parameters
Date_ 20170904
Time 13.35
INSTRUM spect
PROBHD 5 mm DUL 13C-1
PULPROG zgpg30
TD 32768
SOLVENT DMSO
NS 22616
DS 4
SWH 18832.393 Hz
FIDRES 0.574719 Hz
AQ 0.8700404 sec
RG 18390.4
DW 26.550 usec
DE 20.00 usec
TE 300.0 K
D1 0.40000001 sec
d11 0.03000000 sec
d12 0.00002000 sec

======== CHANNEL f1 ========
NUC1 13C
P1 7.37 usec
PL1 5.00 dB
SFO1 75.4760505 MHz

======== CHANNEL f2 ========
CPDPRG2 waltz16
NUC2 1H
PCPD2 90.00 usec
PL2 -3.00 dB
PL12 14.77 dB
PL13 16.00 dB
SFO2 300.1312005 MHz

F2 - Processing parameters
SI 32768
SF 75.4677882 MHz
WDW EM
SSB 0
LB 1.00 Hz
GB 0
PC 1.40

1D NMR plot parameters
CX 22.00 cm
CY 15.00 cm
F1P 234.771 ppm
F1 17717.65 Hz
F2P -14.771 ppm
F2 -1114.75 Hz
PPMCM 11.34283 ppm/cm
HZCM 856.01825 Hz/cm

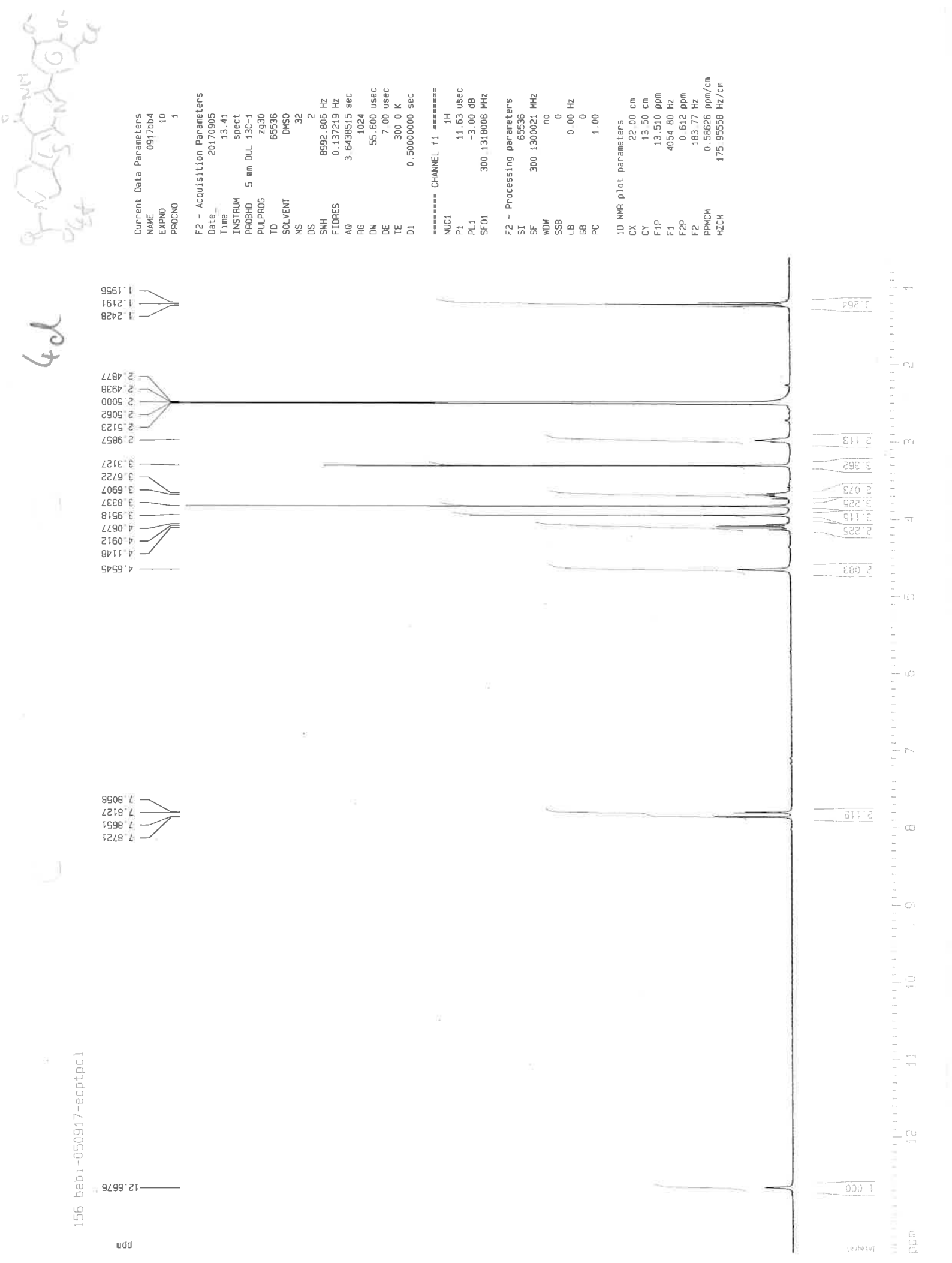
Current Data Parameters
NAME 0917bb4
EXPNO 10
PROCNO 1
F2 - Acquisition Parameters
Date_ 20170905
Time 13.41
INSTRUM spect
PROBHD 5 mm DUL 13C-1
PULPROG zg30
TD 65536
SOLVENT DMSO
NS 32
DS 2
SWH 8992.806 Hz
FIDRES 0.137219 Hz
AQ 3.6438515 sec
RG 1024
DW 55.600 usec
DE 7.00 usec
TE 300.0 K
D1 0.50000000 sec
======== CHANNEL f1 ========
NUC1 1H
P1 11.63 usec
PL1 -3.00 dB
SFO1 300.1318008 MHz
F2 - Processing parameters
SI 65536
SF 300.1300021 MHz
WDW no
SSB 0
LB 0.00 Hz
GB 0
PC 1.00
1D NMR plot parameters
CX 22.00 cm
CY 13.50 cm
F1P 13.510 ppm
F1 4054.80 Hz
F2P 0.612 ppm
F2 183.77 Hz
PPMCM 0.58626 ppm/cm
HZCM 175.95558 Hz/cm
1.1956
1.2191
1.2428
2.4877
2.4938
2.5000
2.5062
2.5123
2.9857
3.3127
3.6722
3.6907
3.8337
3.9518
4.0677
4.0912
4.1148
4.5545
7.8058
7.8127
7.8651
7.8721
12.6576
5.264
2.113
3.362
2.073
3.225
3.115
2.225
2.082
2.119
1.000
156 bebi-050917-ecptpc1
ppm
Integral

4d

156 beb1-050917-ecptpa1

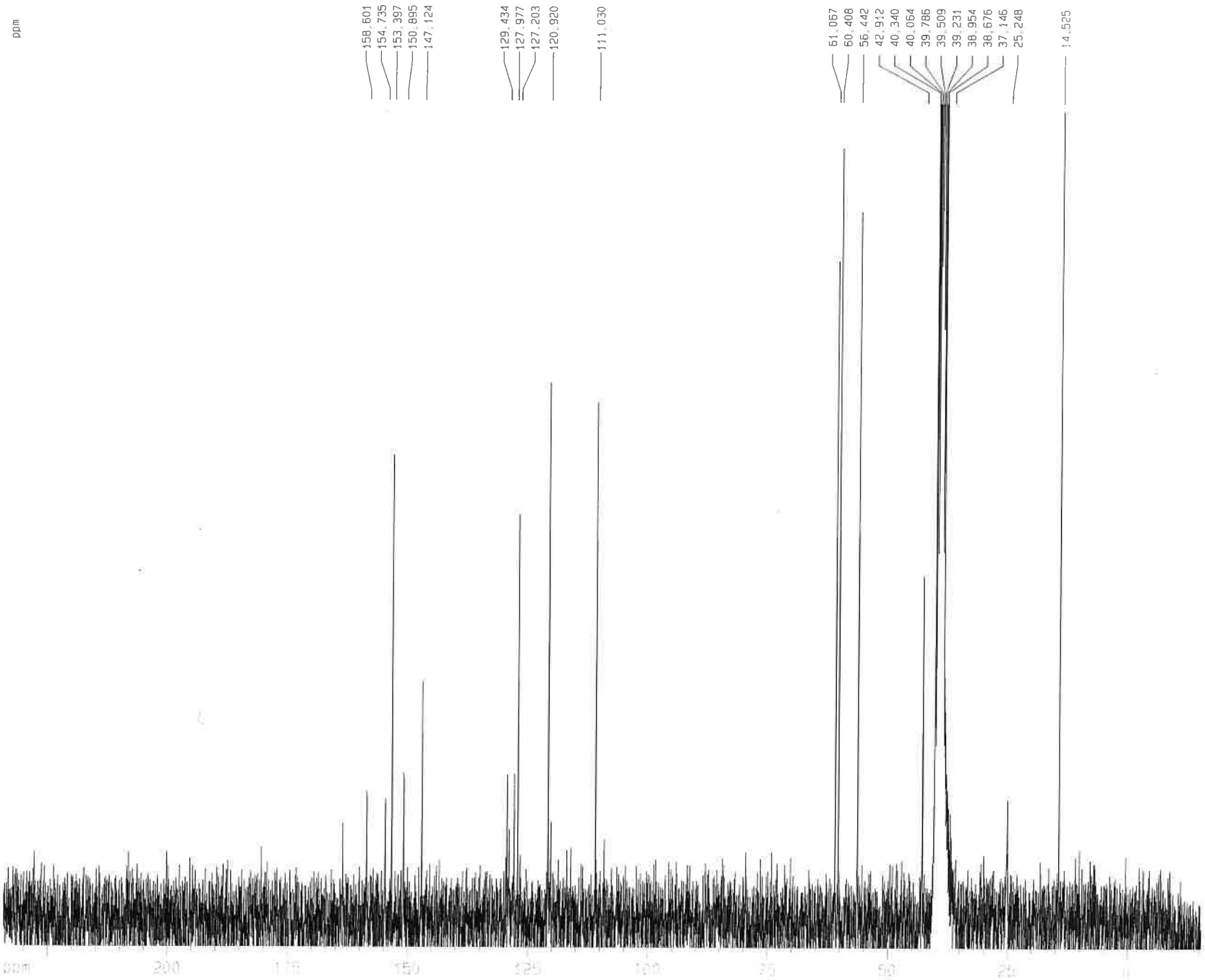

Current Data Parameters

NAME	0917bb4
EXPNO	11
PROCNO	1

F2 - Acquisition Parameters

Date_	20170905
Time	13.44
INSTRUM	spect
PROBHD	5 mm DUL 13C-1
PULPROG	zgpg30
TD	32768
SOLVENT	DMSO
NS	11304
DS	4
SWH	18832.393 Hz
FIDRES	0.574719 Hz
AQ	0.8700404 sec
RG	18390.4
DW	26.550 usec
DE	20.00 usec
TE	300.0 K
D1	0.40000001 sec
d11	0.03000000 sec
d12	0.00002000 sec

======== CHANNEL f1 ========

NUC1	13C
P1	7.37 usec
PL1	5.00 dB
SFO1	75.4760505 MHz

======== CHANNEL f2 ========

CPDPRG2	waltz16
NUC2	1H
PCPD2	90.00 usec
PL2	-3.00 dB
PL12	14.77 dB
PL13	16.00 dB
SFO2	300.1312005 MHz

F2 - Processing parameters

SI	32768
SF	75.4677882 MHz
WDW	EM
SSB	0
LB	1.00 Hz
GB	0
PC	1.40

1D NMR plot parameters

CX	22.00 cm
CY	15.00 cm
F1P	234.252 ppm
F1	17678.45 Hz
F2P	-15.291 ppm
F2	-1153.95 Hz
PPMCM	11.34282 ppm/cm
HZCM	856.01782 Hz/cm

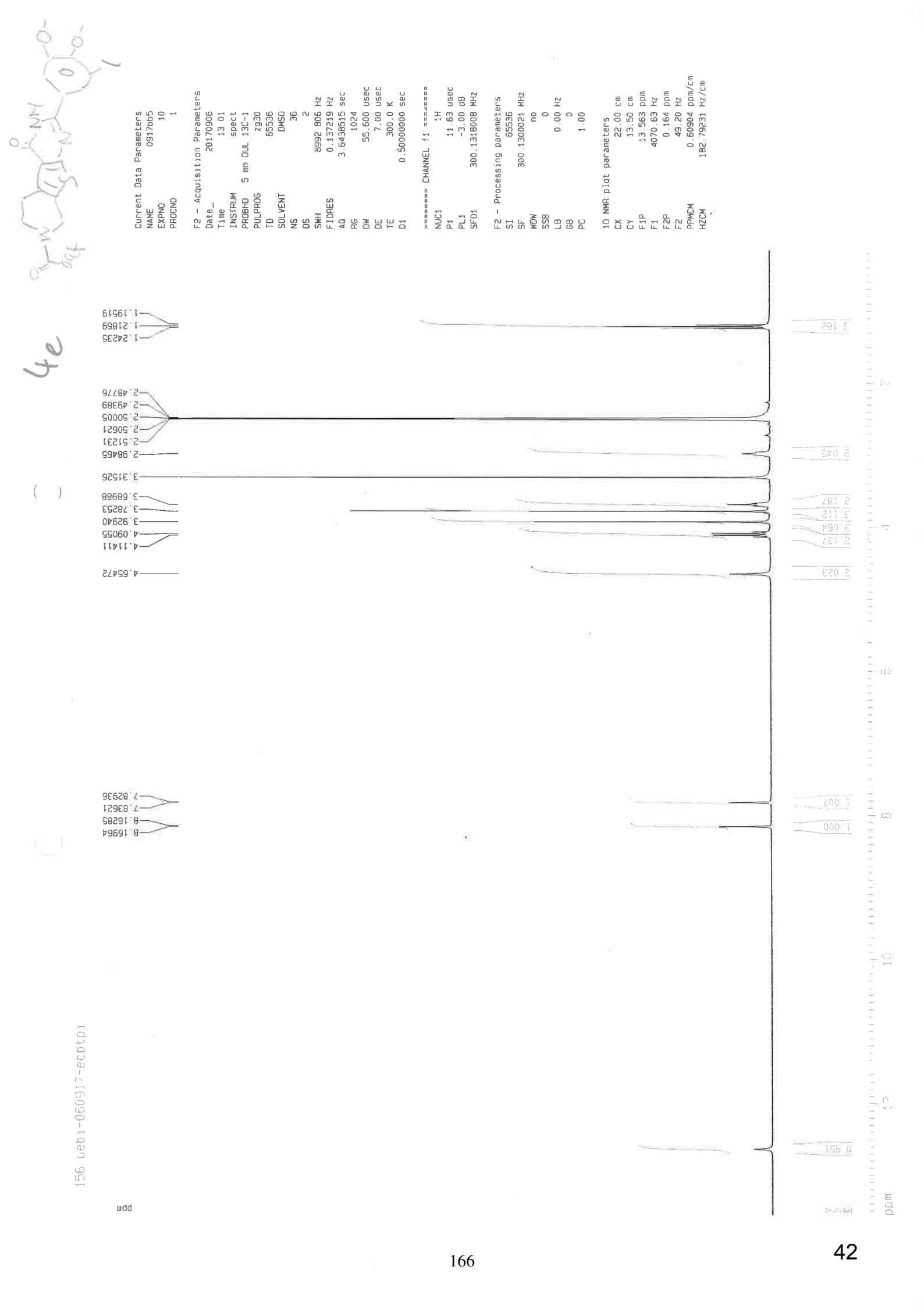
Current Data Parameters
NAME 0917bb5
EXPNO 10
PROCNO 1
F2 - Acquisition Parameters
Date_ 20170906
Time 13 01
INSTRUM spect
PROBHD 5 mm DUL 13C-1
PULPROG zg30
TD 65536
SOLVENT DMSO
NS 36
DS 2
SWH 8992.806 Hz
FIDRES 0.137219 Hz
AQ 3.6438515 sec
RG 1024
DW 55.600 usec
DE 7.00 usec
TE 300.0 K
D1 0.50000000 sec
======== CHANNEL f1 ========
NUC1 1H
P1 11.63 usec
PL1 -3.00 dB
SFO1 300.1318008 MHz
F2 - Processing parameters
SI 65536
SF 300.1300021 MHz
WDW no
SSB 0
LB 0.00 Hz
GB 0
PC 1.00
1D NMR plot parameters
CX 22.00 cm
CY 13.50 cm
F1P 13.563 ppm
F1 4070.63 Hz
F2P 0.164 ppm
F2 49.20 Hz
PPMCM 0.60904 ppm/cm
HZCM 182.79231 Hz/cm
1.19519
1.21869
1.24235
2.48776
2.49389
2.50005
2.50621
2.51231
2.98465
3.31526
3.68988
3.78253
3.92940
4.09055
4.11411
4.65472
7.82936
7.83621
8.16285
8.16964
3.186
2.045
2.187
3.115
3.064
2.137
2.023
1.007
1.000
0.951
156 ceb1-060917-eccptp1
ppm

4e

156 bea1-050917-ecptpi

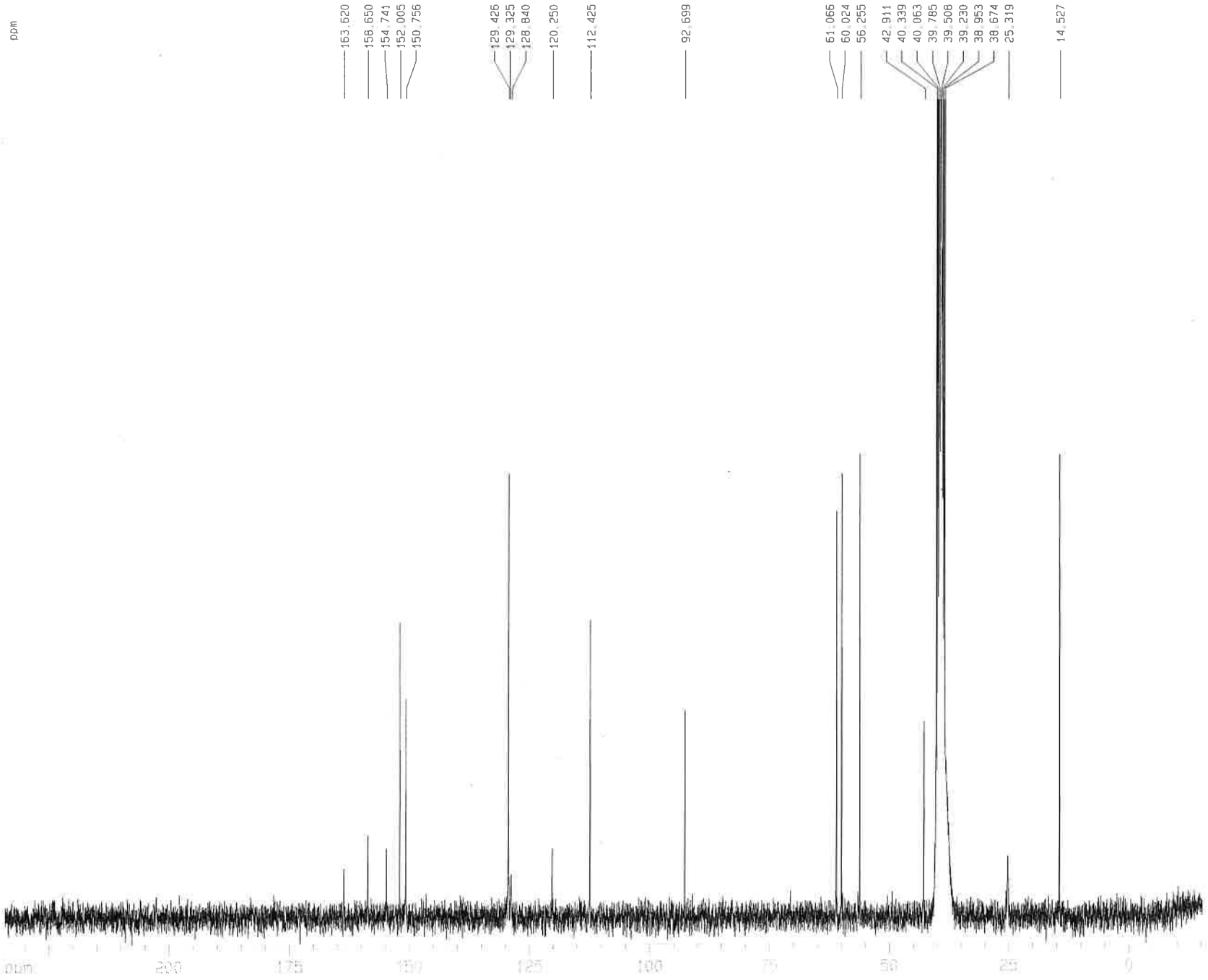

Current Data Parameters
NAME 0917bb5
EXPNO 2
PROCNO 1

F2 - Acquisition Parameters
Date_ 20170906
Time 14.26
INSTRUM spect
PROBHD 5 mm DUL 13C-1
PULPROG zgpg30
TD 32768
SOLVENT DMSO
NS 42408
DS 4
SWH 18832.393 Hz
FIDRES 0.574719 Hz
AQ 0.8700404 sec
RG 18390.4
DW 26.550 usec
DE 20.00 usec
TE 300.0 K
D1 0.40000001 sec
d11 0.03000000 sec
d12 0.00002000 sec

======== CHANNEL f1 ========
NUC1 13C
P1 7.37 usec
PL1 5.00 dB
SFO1 75.4760505 MHz

======== CHANNEL f2 ========
CPDPRG2 waltz16
NUC2 1H
PCPD2 90.00 usec
PL2 -3.00 dB
PL12 14.77 dB
PL13 16.00 dB
SFO2 300.1312005 MHz

F2 - Processing parameters
SI 32768
SF 75.4677882 MHz
WDW EM
SSB 0
LB 1.00 Hz
GB 0
PC 1.40

1D NMR plot parameters
CX 22.00 cm
CY 200.00 cm
F1P 234.252 ppm
F1 17678.45 Hz
F2P -15.291 ppm
F2 -1153.95 Hz
PPMCM 11.34282 ppm/cm
HZCM 856.01782 Hz/cm

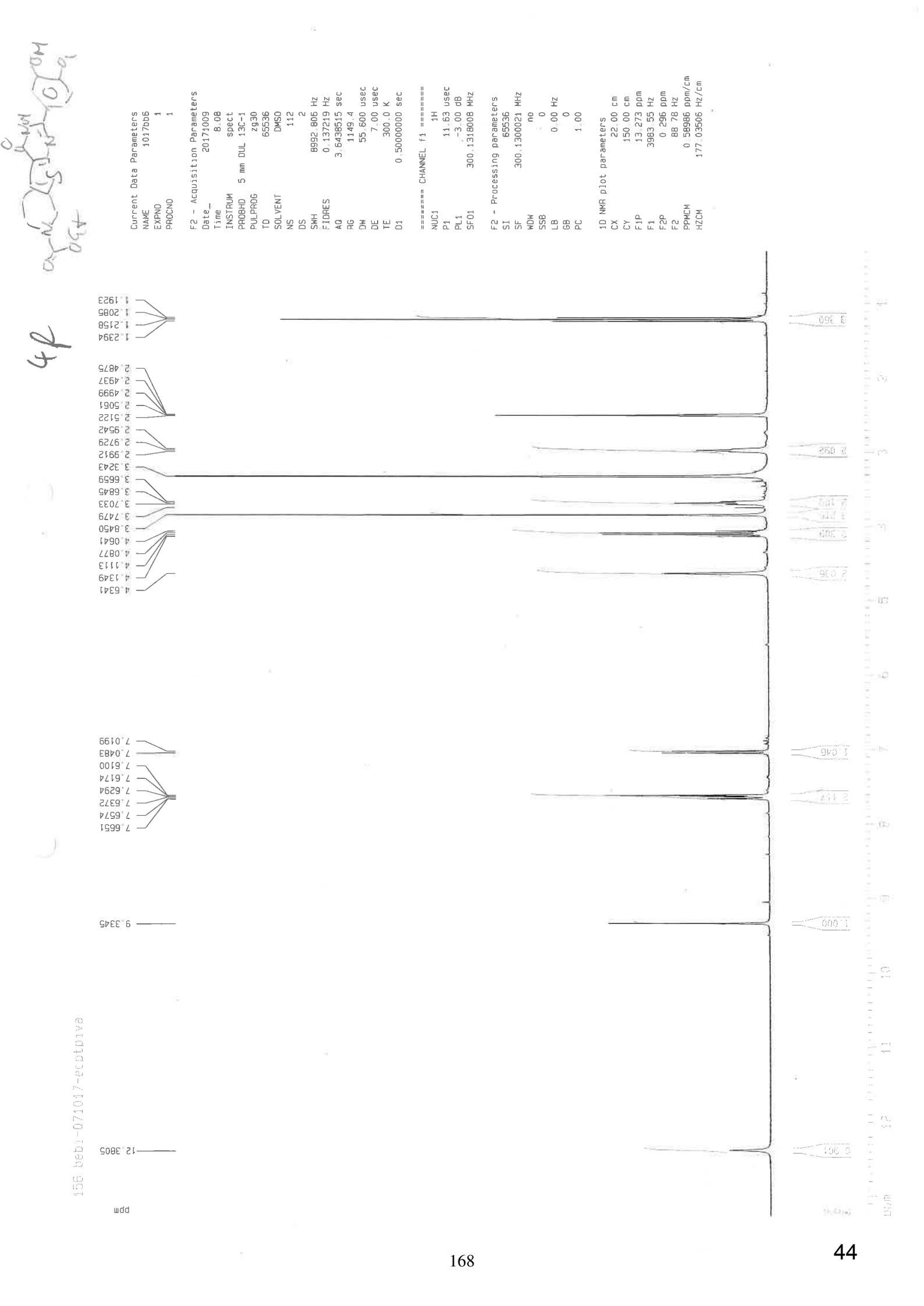
Current Data Parameters
NAME 1017bb6
EXPNO 1
PROCNO 1
F2 - Acquisition Parameters
Date_ 20171009
Time 8.08
INSTRUM spect
PROBHD 5 mm DUL 13C-1
PULPROG zg30
TD 65536
SOLVENT DMSO
NS 112
DS 2
SWH 8992.806 Hz
FIDRES 0.137219 Hz
AQ 3.6438515 sec
RG 1149.4
DW 55.600 usec
DE 7.00 usec
TE 300.0 K
D1 0.50000000 sec
======== CHANNEL f1 ========
NUC1 1H
P1 11.63 usec
PL1 -3.00 dB
SFO1 300.1318008 MHz
F2 - Processing parameters
SI 65536
SF 300.1300021 MHz
WDW no
SSB 0
LB 0.00 Hz
GB 0
PC 1.00
1D NMR plot parameters
CX 22.00 cm
CY 150.00 cm
F1P 13.273 ppm
F1 3983.55 Hz
F2P 0.296 ppm
F2 88.78 Hz
PPMCM 0.58986 ppm/cm
HZCM 177.03506 Hz/cm
1.1923
1.2085
1.2158
1.2394
2.4875
2.4937
2.4999
2.5061
2.5122
2.9542
2.9729
2.9912
3.3243
3.6659
3.6845
3.7033
3.7479
3.8450
4.0641
4.0877
4.1113
4.1349
4.6341
7.0199
7.0483
7.6100
7.6174
7.6294
7.6372
7.6574
7.6651
9.3345
12.3805
ppm

4f

156 bebi-071017-ecptpiva

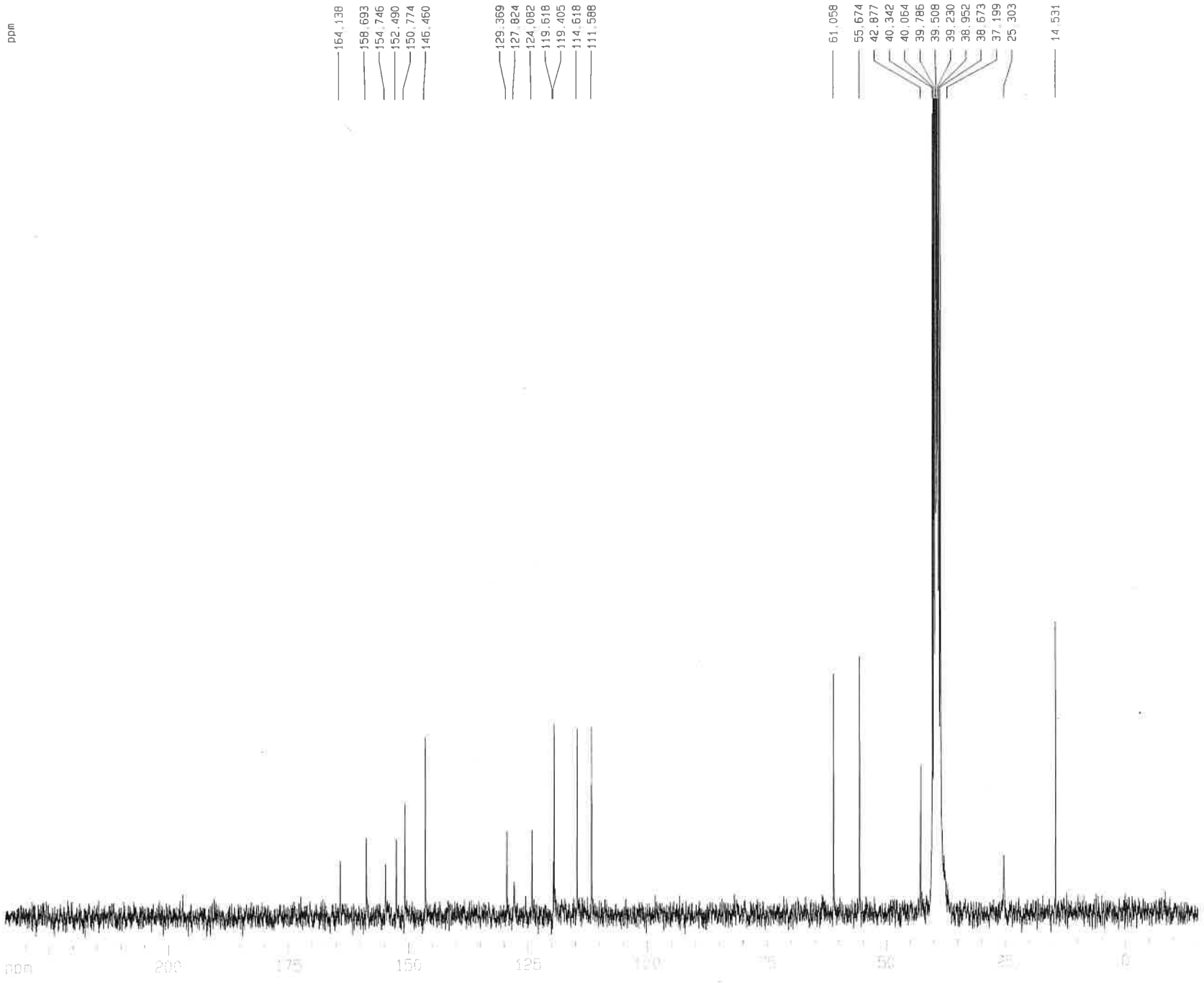

Current Data Parameters
NAME 1017bb6
EXPNO 2
PROCNO 1

F2 - Acquisition Parameters
Date_ 20171009
Time 8.17
INSTRUM spect
PROBHD 5 mm DUL 13C-1
PULPROG zgpg30
TD 32768
SOLVENT CDCl3
NS 14902
DS 4
SWH 18832.393 Hz
FIDRES 0.574719 Hz
AQ 0.8700404 sec
RG 18390.4
DW 26.550 usec
DE 20.00 usec
TE 300.0 K
D1 0.40000001 sec
d11 0.03000000 sec
d12 0.00002000 sec

======== CHANNEL f1 ========
NUC1 13C
P1 7.37 usec
PL1 5.00 dB
SFO1 75.4760505 MHz

======== CHANNEL f2 ========
CPDPRG2 waltz16
NUC2 1H
PCPD2 90.00 usec
PL2 -3.00 dB
PL12 14.77 dB
PL13 16.00 dB
SFO2 300.1312005 MHz

F2 - Processing parameters
SI 32768
SF 75.4677876 MHz
WDW EM
SSB 0
LB 2.00 Hz
GB 0
PC 1.40

1D NMR plot parameters
CX 22.00 cm
CY 100.00 cm
F1P 234.259 ppm
F1 17679.02 Hz
F2P -15.283 ppm
F2 -1153.37 Hz
PPMCM 11.34282 ppm/cm
HZCM 856.01782 Hz/cm

4g

bebi-130917-ecptp3cn-1H

Acquisition Time (sec)	3.2768	*Comment*	Group AK Schobert bebi-130917-ecptp3cn			*Date*	14 Sep 2017 05:01:20
Date Stamp	14 Sep 2017 05:01:20			*File Name*	\\132.180.48.106\AK_Schobert_NMR\Rehm_Tobias\bebi-130917-ecptp3cn\10\PDATA\1\1r		
Frequency (MHz)	500.13	*Nucleus*	1H	*Number of Transients*	16	*Origin*	spect
Original Points Count	32768	*Owner*	nmrsu	*Points Count*	65536	*Pulse Sequence*	zg30
Receiver Gain	32.00	*SW(cyclical) (Hz)*	10000.00	*Solvent*	DMSO-d6	*Spectrum Offset (Hz)*	3083.8975
Spectrum Type	STANDARD	*Sweep Width (Hz)*	9999.85	*Temperature (degree C)*	20.001		

^{1}H NMR (500 MHz, DMSO-d_6) δ ppm 1.22 (3 H, s), 2.93 - 3.07 (2 H, m), 3.60 - 3.79 (2 H, m), 4.04 - 4.18 (2 H, m), 4.57 - 4.76 (2 H, m), 7.66 - 7.82 (1 H, m), 7.98 - 8.09 (1 H, m), 8.33 - 8.48 (1 H, m), 8.49 - 8.63 (1 H, m), 12.72 - 12.91 (1 H, m)

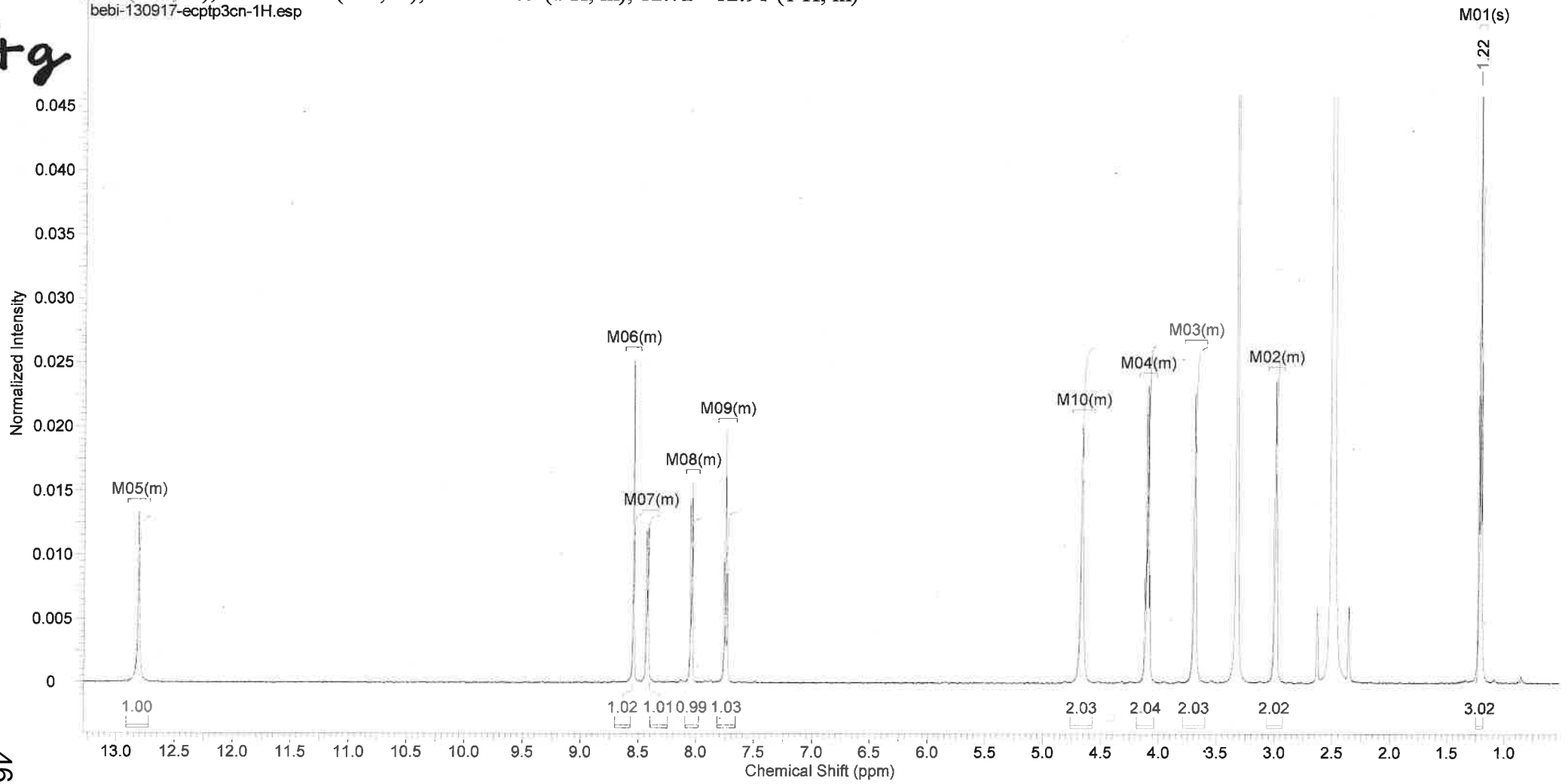

[redacted] 4g

bebi-130917-ecptp3cn-13C

Acquisition Time (sec)	1.1010	*Comment*	Group AK Schobert bebi-130917-ecptp3cn			*Date*	14 Sep 2017 05:56:48
Date Stamp	14 Sep 2017 05:56:48			*File Name*	\\132.180.48.106\AK_Schobert_NMR\Rehm_Tobias\bebi-130917-ecptp3cn\11\PDATA\1\1r		
Frequency (MHz)	125.76	*Nucleus*	13C	*Number of Transients*	1024	*Origin*	spect
Original Points Count	32768	*Owner*	nmrsu	*Points Count*	32768	*Pulse Sequence*	zgpg30
Receiver Gain	5.00	*SW(cyclical) (Hz)*	29761.90	*Solvent*	DMSO-d6	*Spectrum Offset (Hz)*	12575.1807
Spectrum Type	STANDARD	*Sweep Width (Hz)*	29761.00	*Temperature (degree C)*	20.002		

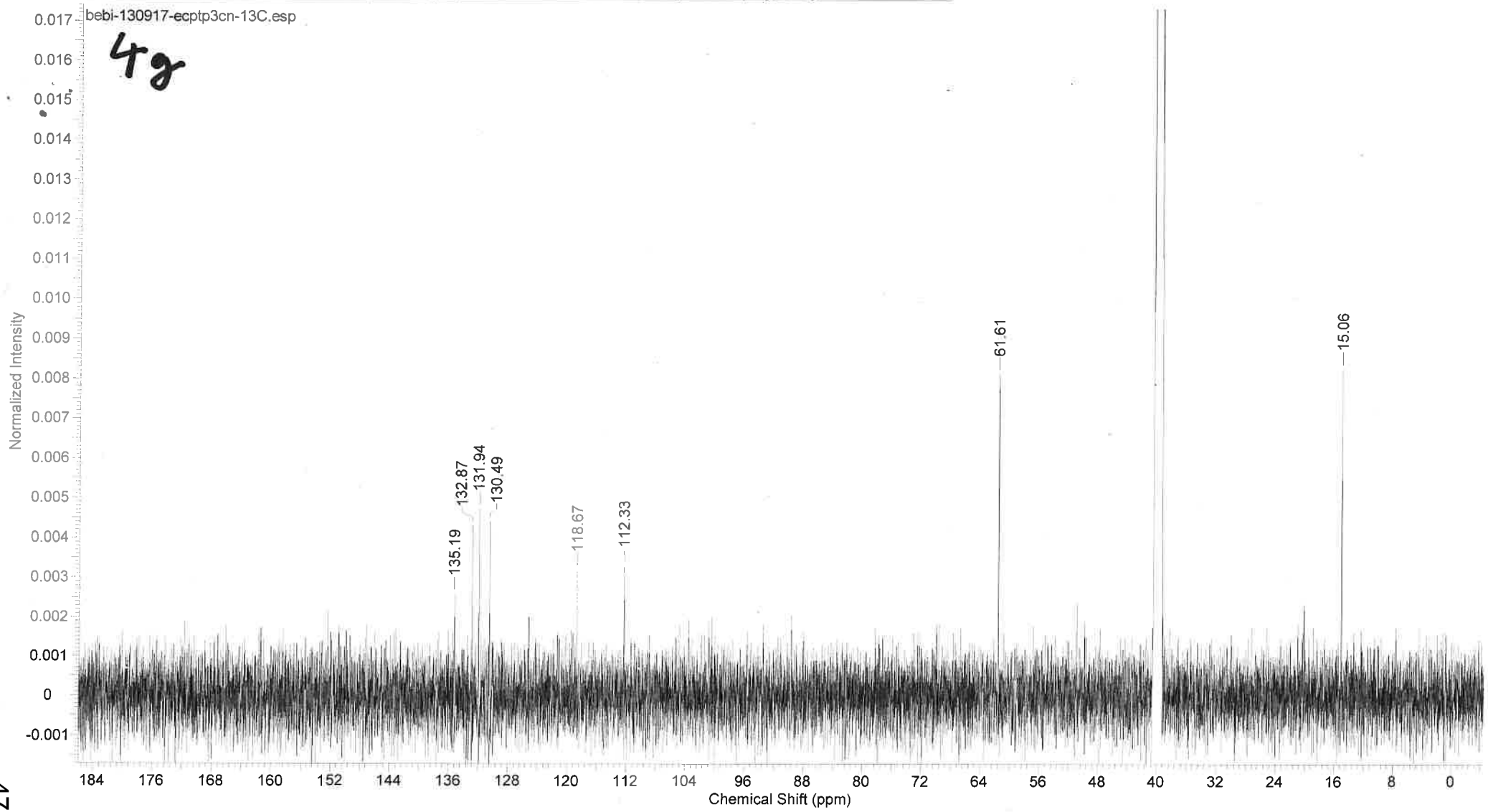

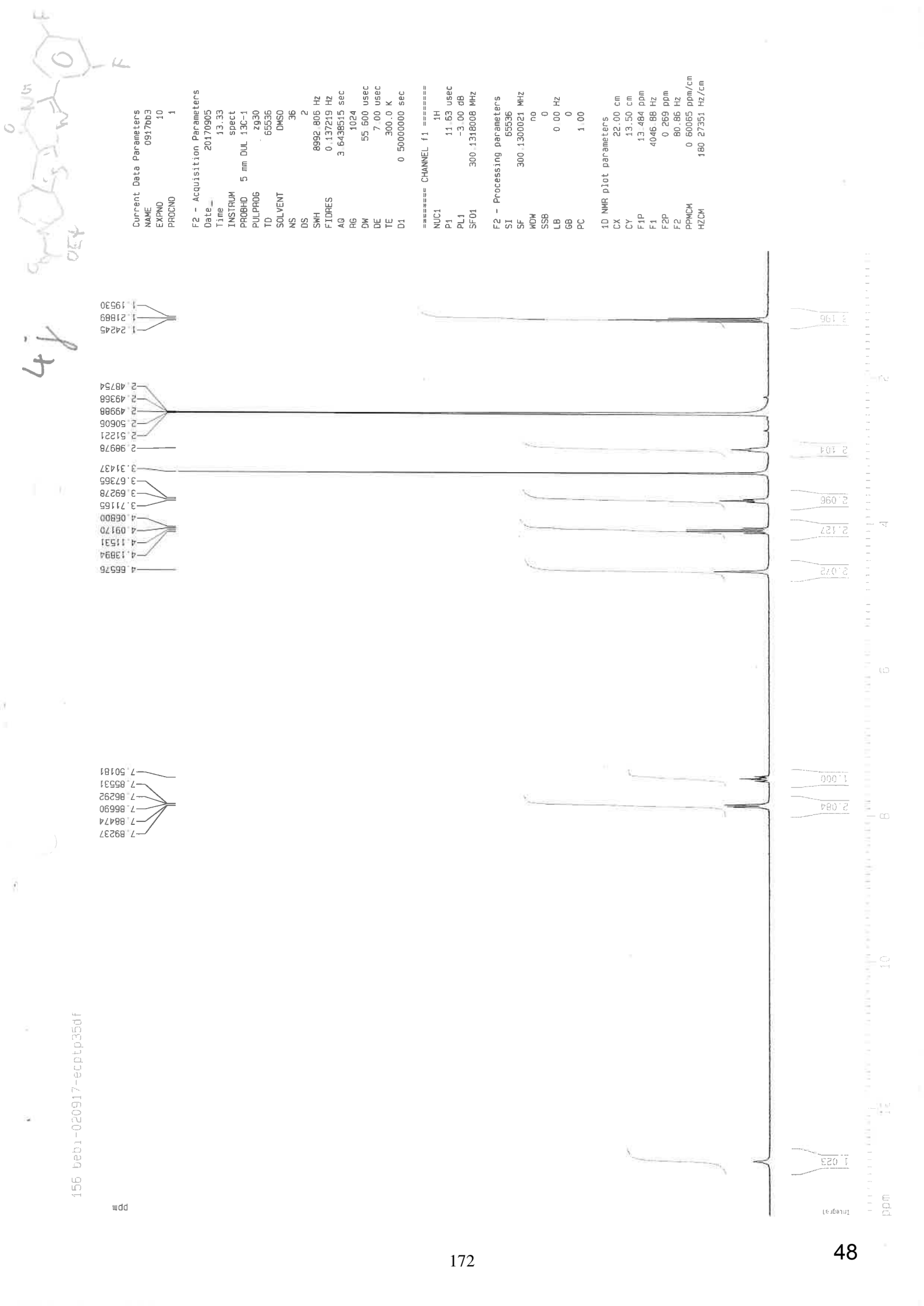
Current Data Parameters
NAME 0917bb3
EXPNO 10
PROCNO 1
F2 - Acquisition Parameters
Date_ 20170905
Time 13.33
INSTRUM spect
PROBHD 5 mm DUL 13C-1
PULPROG zg30
TD 65536
SOLVENT DMSO
NS 36
DS 2
SWH 8992.806 Hz
FIDRES 0.137219 Hz
AQ 3.6438515 sec
RG 1024
DW 55.600 usec
DE 7.00 usec
TE 300.0 K
D1 0.50000000 sec
======= CHANNEL f1 =======
NUC1 1H
P1 11.63 usec
PL1 -3.00 dB
SFO1 300.1318008 MHz
F2 - Processing parameters
SI 65536
SF 300.1300021 MHz
WDW no
SSB 0
LB 0.00 Hz
GB 0
PC 1.00
1D NMR plot parameters
CX 22.00 cm
CY 13.50 cm
F1P 13.484 ppm
F1 4046.88 Hz
F2P 0.269 ppm
F2 80.86 Hz
PPMCM 0.60065 ppm/cm
HZCM 180.27351 Hz/cm
1.19530
1.21889
1.24245
2.48754
2.49368
2.49988
2.50606
2.51221
2.98978
3.31437
3.67365
3.69278
3.71165
4.06800
4.09170
4.11531
4.13894
4.65576
7.50181
7.85531
7.86292
7.86690
7.88474
7.89237
1.196
2.104
2.096
2.127
2.072
1.000
2.084
1.025
ppm
156 bebi-020917-ecptp35df

lief 4 Stunden

4j

150 bebi-020917-ecptp35uf

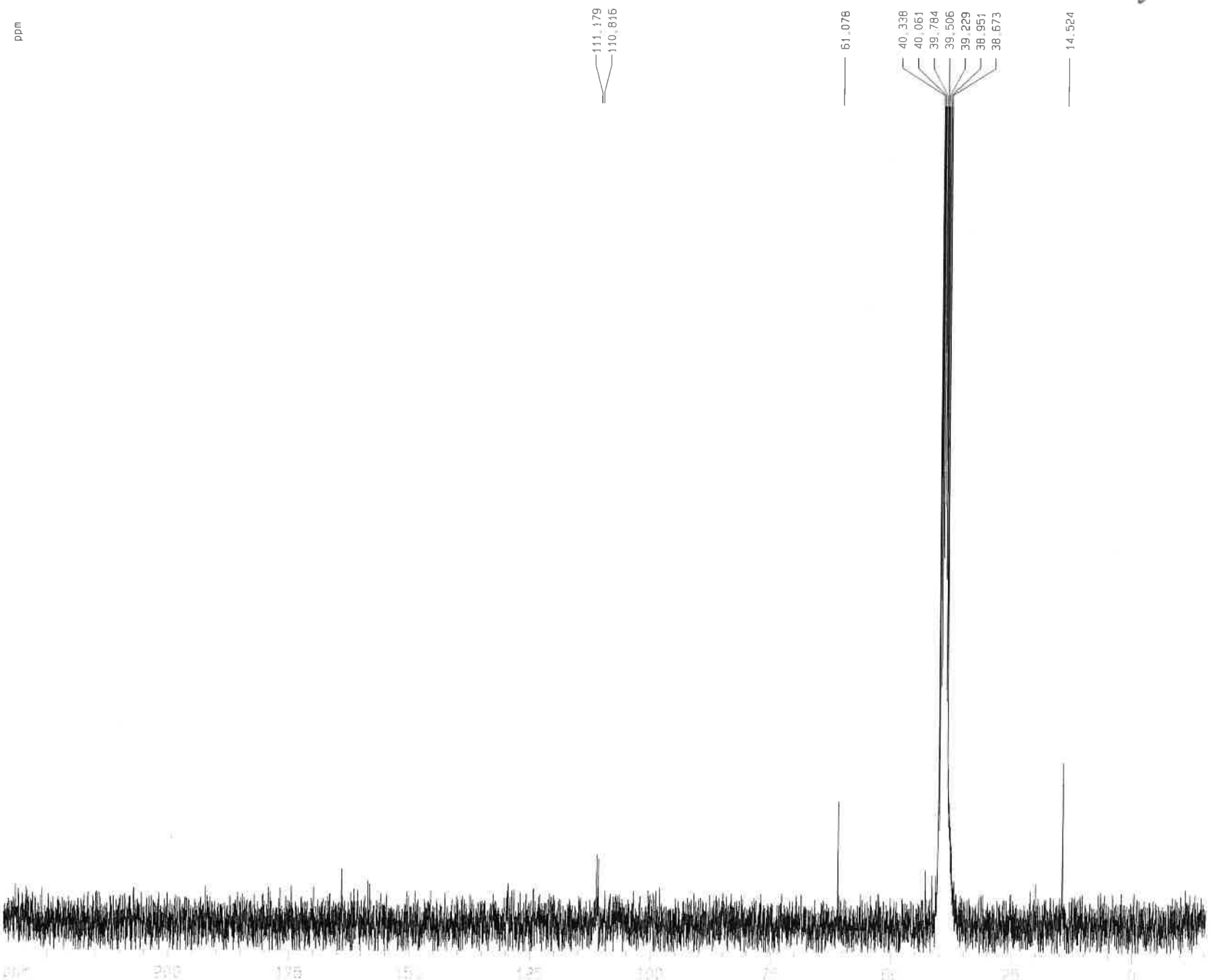

Current Data Parameters
NAME 0917bb3
EXPNO 20
PROCNO 1

F2 - Acquisition Parameters
Date_ 20170905
Time 21.51
INSTRUM spect
PROBHD 5 mm DUL 13C-1
PULPROG zgpg30
TD 32768
SOLVENT DMSO
NS 11304
DS 4
SWH 18832.393 Hz
FIDRES 0.574719 Hz
AQ 0.8700404 sec
RG 18390.4
DW 26.550 usec
DE 20.00 usec
TE 300.0 K
D1 0.40000001 sec
d11 0.03000000 sec
d12 0.00002000 sec

======== CHANNEL f1 ========
NUC1 13C
P1 7.37 usec
PL1 5.00 dB
SFO1 75.4760505 MHz

======== CHANNEL f2 ========
CPDPRG2 waltz16
NUC2 1H
PCPD2 90.00 usec
PL2 -3.00 dB
PL12 14.77 dB
PL13 16.00 dB
SFO2 300.1312005 MHz

F2 - Processing parameters
SI 32768
SF 75.4677882 MHz
WDW EM
SSB 0
LB 1.00 Hz
GB 0
PC 1.40

1D NMR plot parameters
CX 22.00 cm
CY 3.00 cm
F1P 234.252 ppm
F1 17678.45 Hz
F2P -15.291 ppm
F2 -1153.95 Hz
PPMCM 11.34282 ppm/cm
HZCM 856.01782 Hz/cm

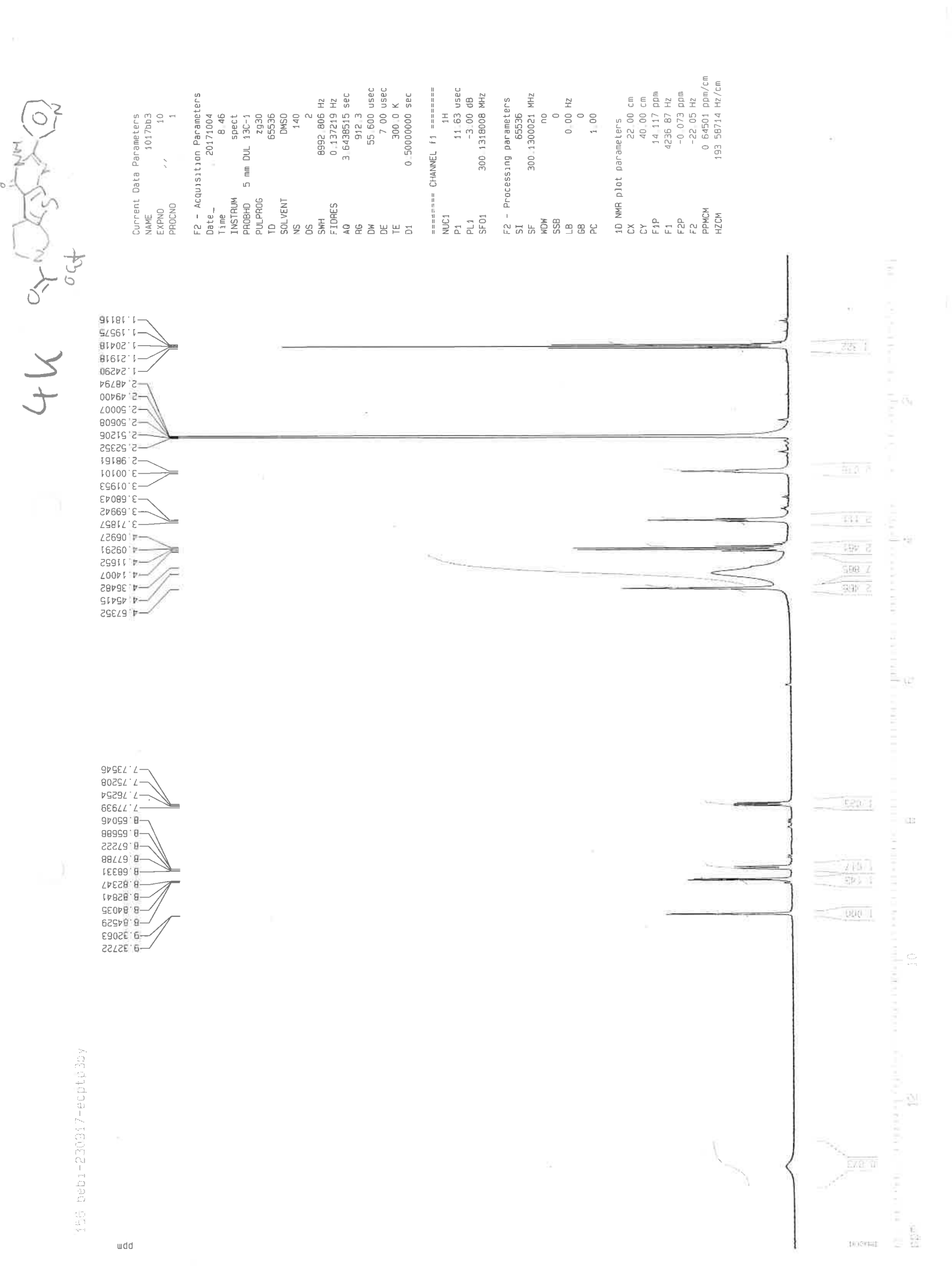
Current Data Parameters
NAME 1017bb3
EXPNO 10
PROCNO 1
F2 - Acquisition Parameters
Date_ 20171004
Time 8 46
INSTRUM spect
PROBHD 5 mm DUL 13C-1
PULPROG zg30
TD 65536
SOLVENT DMSO
NS 140
DS 2
SWH 8992 806 Hz
FIDRES 0 137219 Hz
AQ 3 6438515 sec
RG 912 3
DW 55 600 usec
DE 7 00 usec
TE 300 0 K
D1 0 50000000 sec
======== CHANNEL f1 ========
NUC1 1H
P1 11 63 usec
PL1 -3 00 dB
SF01 300 1318008 MHz
F2 - Processing parameters
SI 65536
SF 300 1300021 MHz
WDW no
SSB 0
LB 0 00 Hz
GB 0
PC 1 00
1D NMR plot parameters
CX 22 00 cm
CY 40 00 cm
F1P 14 117 ppm
F1 4236 87 Hz
F2P -0 073 ppm
F2 -22 05 Hz
PPMCM 0 64501 ppm/cm
HZCM 193 58714 Hz/cm
1.18116
1.19575
1.20418
1.21918
1.24290
2.48794
2.49400
2.50007
2.50608
2.51206
2.52352
2.98161
3.00101
3.01953
3.68043
3.69942
3.71857
4.06927
4.09291
4.11652
4.14007
4.36482
4.45415
4.67352
7.73546
7.75208
7.76254
7.77939
8.65046
8.65588
8.67222
8.67788
8.68331
8.82347
8.82841
8.84035
8.84529
9.32063
9.32722
ppm

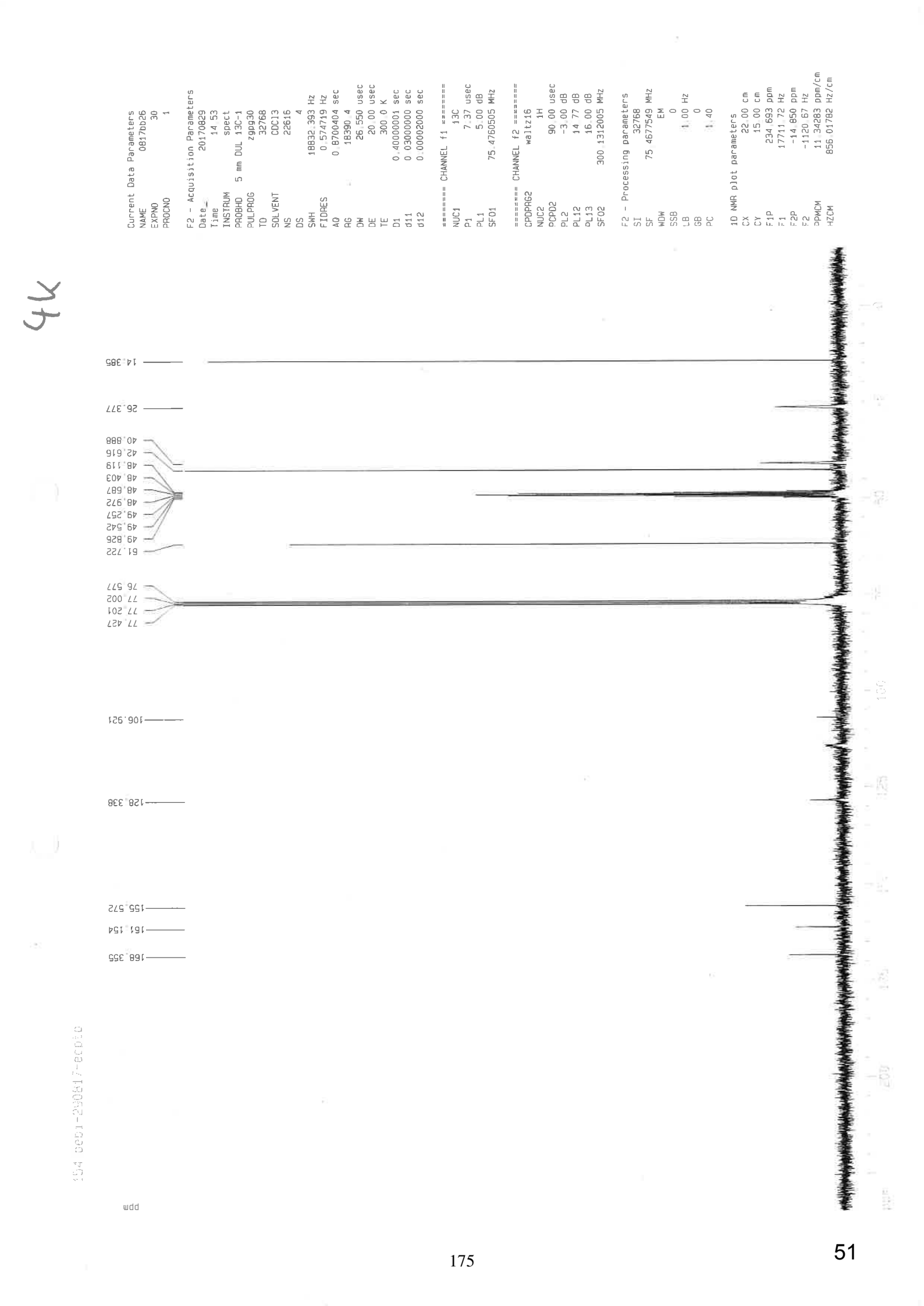
Current Data Parameters
NAME 0817bb26
EXPNO 30
PROCNO 1
F2 - Acquisition Parameters
Date_ 20170829
Time 14 53
INSTRUM spect
PROBHD 5 mm DUL 13C-1
PULPROG zgpg30
TD 32768
SOLVENT CDCl3
NS 22616
DS 4
SWH 18832.393 Hz
FIDRES 0.574719 Hz
AQ 0.8700404 sec
RG 18390.4
DW 26.550 usec
DE 20.00 usec
TE 300.0 K
D1 0.40000001 sec
d11 0.03000000 sec
d12 0.00002000 sec
======== CHANNEL f1 ========
NUC1 13C
P1 7.37 usec
PL1 5.00 dB
SFO1 75.4760505 MHz
======== CHANNEL f2 ========
CPDPRG2 waltz16
NUC2 1H
PCPD2 90.00 usec
PL2 -3.00 dB
PL12 14.77 dB
PL13 16.00 dB
SFO2 300.1312005 MHz
F2 - Processing parameters
SI 32768
SF 75.4677549 MHz
WDW EM
SSB 0
LB 1.00 Hz
GB 0
PC 1.40
1D NMR plot parameters
CX 22.00 cm
CY 15.00 cm
F1P 234.693 ppm
F1 17711.72 Hz
F2P -14.850 ppm
F2 -1120.67 Hz
PPMCM 11.34283 ppm/cm
HZCM 856.01782 Hz/cm
14.385
26.377
40.888
42.616
48.119
48.403
48.687
48.972
49.257
49.542
49.826
61.722
76.577
77.002
77.201
77.427
106.921
128.338
155.572
161.154
168.355
ppm

5a

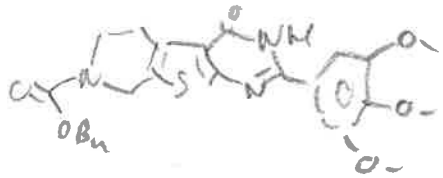

174 bebi-30011B-bcptptrim

ppm

7.37938
7.37564
7.37291
7.36392
7.36108
7.29302
7.24311
7.24215
7.24011

5.18085

3.95330
3.90246

5a
Known compd.

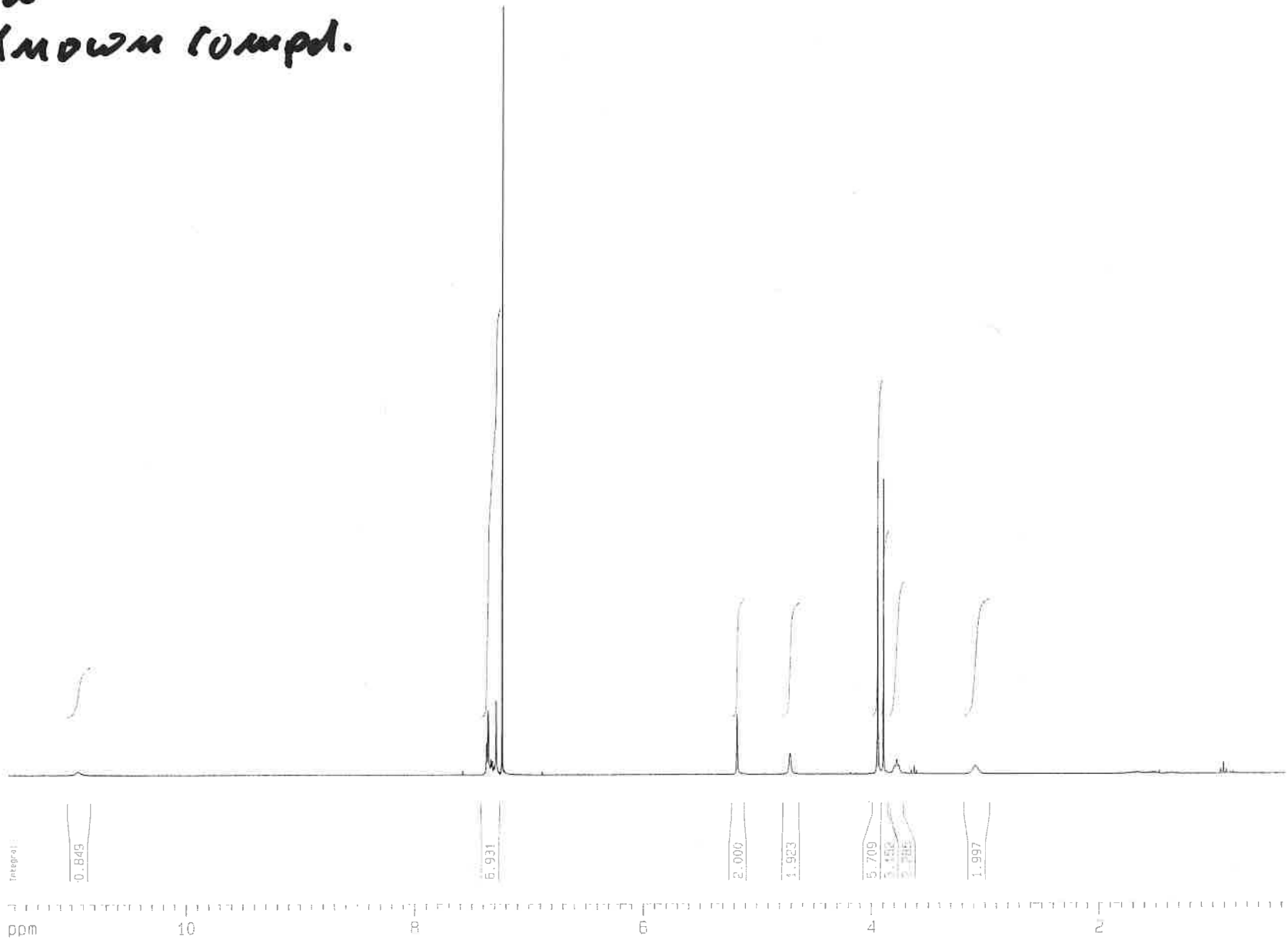

Current Data Parameters
NAME 0118bb32
EXPNO 10
PROCNO 1

F2 - Acquisition Parameters
Date_ 20180130
Time 13.49
INSTRUM spect
PROBHD 5 mm DUL 13C-1
PULPROG zg30
TD 65536
SOLVENT CDCl3
NS 200
DS 2
SWH 8992.806 Hz
FIDRES 0.137219 Hz
AQ 3.6438515 sec
RG 1625.5
DW 55.600 usec
DE 7.00 usec
TE 300.0 K
D1 0.50000000 sec

======== CHANNEL f1 ========
NUC1 1H
P1 11.63 usec
PL1 -3.00 dB
SFO1 300.1318008 MHz

F2 - Processing parameters
SI 65536
SF 300.1300126 MHz
WDW no
SSB 0
LB 0.00 Hz
GB 0
PC 1.00

1D NMR plot parameters
CX 22.00 cm
CY 13.50 cm
F1P 11.563 ppm
F1 3470.34 Hz
F2P 0.380 ppm
F2 113.99 Hz
PPMCM 0.50832 ppm/cm
HZCM 152.56169 Hz/cm

176

52

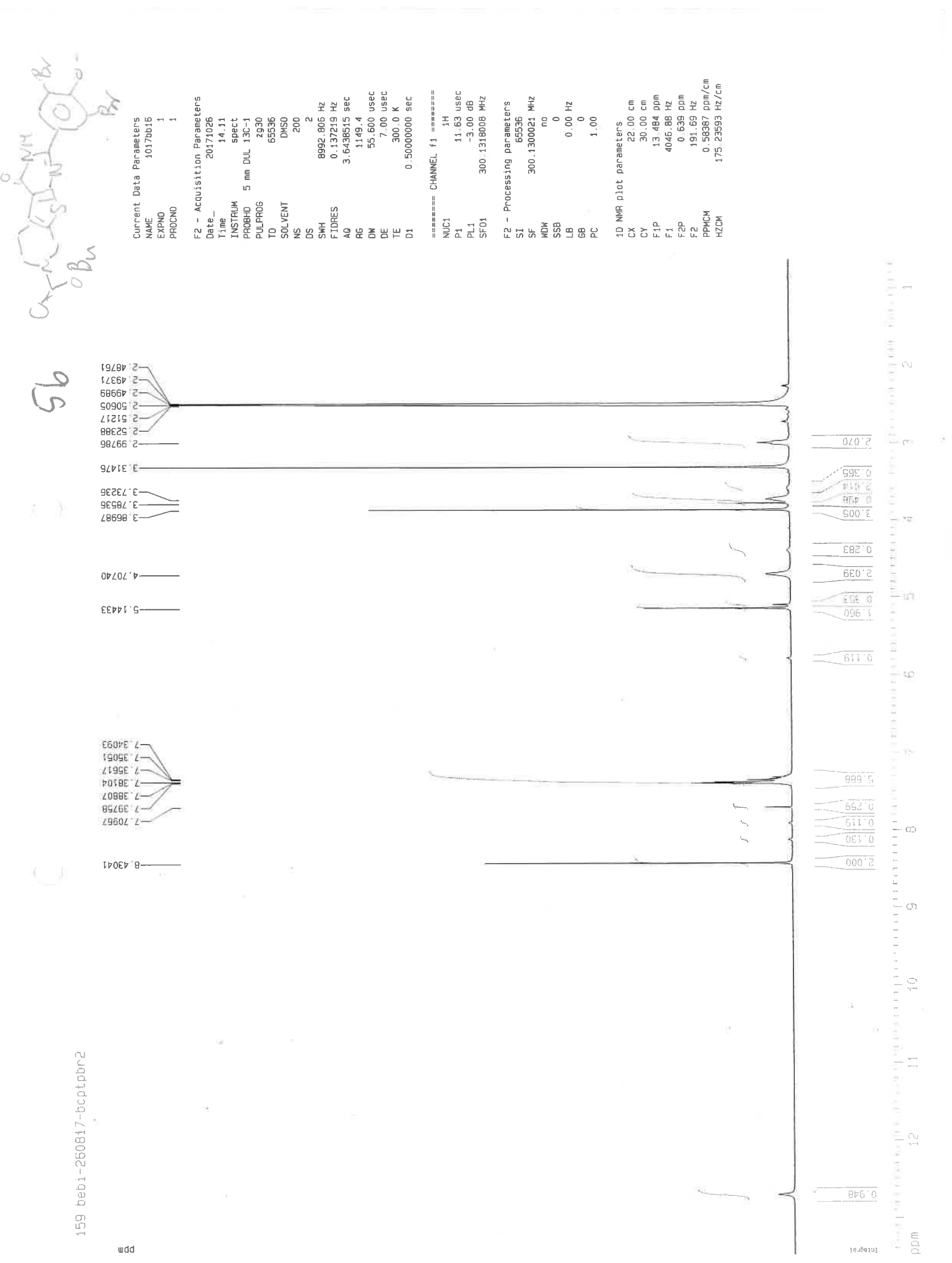
Current Data Parameters
NAME 1017bb16
EXPNO 1
PROCNO 1
F2 - Acquisition Parameters
Date_ 20171026
Time 14.11
INSTRUM spect
PROBHD 5 mm DUL 13C-1
PULPROG zg30
TD 65536
SOLVENT DMSO
NS 200
DS 2
SWH 8992.806 Hz
FIDRES 0.137219 Hz
AQ 3.6438515 sec
RG 1149.4
DW 55.600 usec
DE 7.00 usec
TE 300.0 K
D1 0.50000000 sec
======== CHANNEL f1 ========
NUC1 1H
P1 11.63 usec
PL1 -3.00 dB
SFO1 300.1318008 MHz
F2 - Processing parameters
SI 65536
SF 300.1300021 MHz
WDW no
SSB 0
LB 0.00 Hz
GB 0
PC 1.00
1D NMR plot parameters
CX 22.00 cm
CY 30.00 cm
F1P 13.484 ppm
F1 4046.88 Hz
F2P 0.639 ppm
F2 191.69 Hz
PPMCM 0.58387 ppm/cm
HZCM 175.23593 Hz/cm
159 bebi-260817-bcptpbr2
ppm
Integral

5b

159 beb1-260817-bcptpbr2

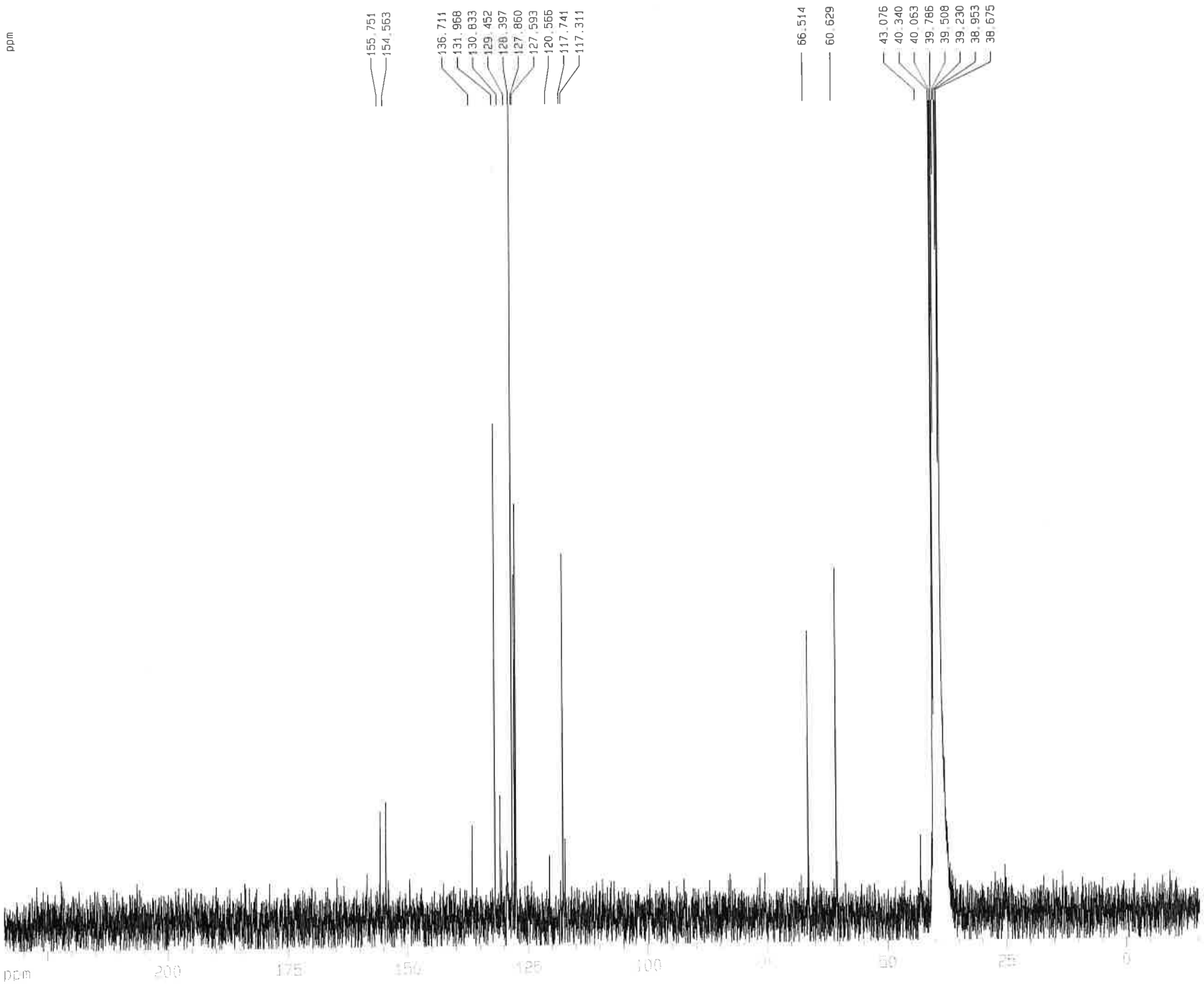

Current Data Parameters

NAME	1017bb16
EXPNO	10
PROCNO	1

F2 - Acquisition Parameters

Date_	20171026
Time	15.55
INSTRUM	spect
PROBHD	5 mm DUL 13C-1
PULPROG	zgpg30
TD	32768
SOLVENT	DMSO
NS	42168
DS	4
SWH	18832.393 Hz
FIDRES	0.574719 Hz
AQ	0.8700404 sec
RG	18390.4
DW	26.550 usec
DE	20.00 usec
TE	300.0 K
D1	0.40000001 sec
d11	0.03000000 sec
d12	0.00002000 sec

======== CHANNEL f1 ========

NUC1	13C
P1	7.37 usec
PL1	5.00 dB
SFO1	75.4760505 MHz

======== CHANNEL f2 ========

CPDPRG2	waltz16
NUC2	1H
PCPD2	90.00 usec
PL2	-3.00 dB
PL12	14.77 dB
PL13	16.00 dB
SFO2	300.1312005 MHz

F2 - Processing parameters

SI	32768
SF	75.4677882 MHz
WDW	EM
SSB	0
LB	1.00 Hz
GB	0
PC	1.40

1D NMR plot parameters

CX	22.00 cm
CY	15.00 cm
F1P	234.252 ppm
F1	17678.45 Hz
F2P	-15.291 ppm
F2	-1153.95 Hz
PPMCM	11.34282 ppm/cm
HZCM	856.01782 Hz/cm

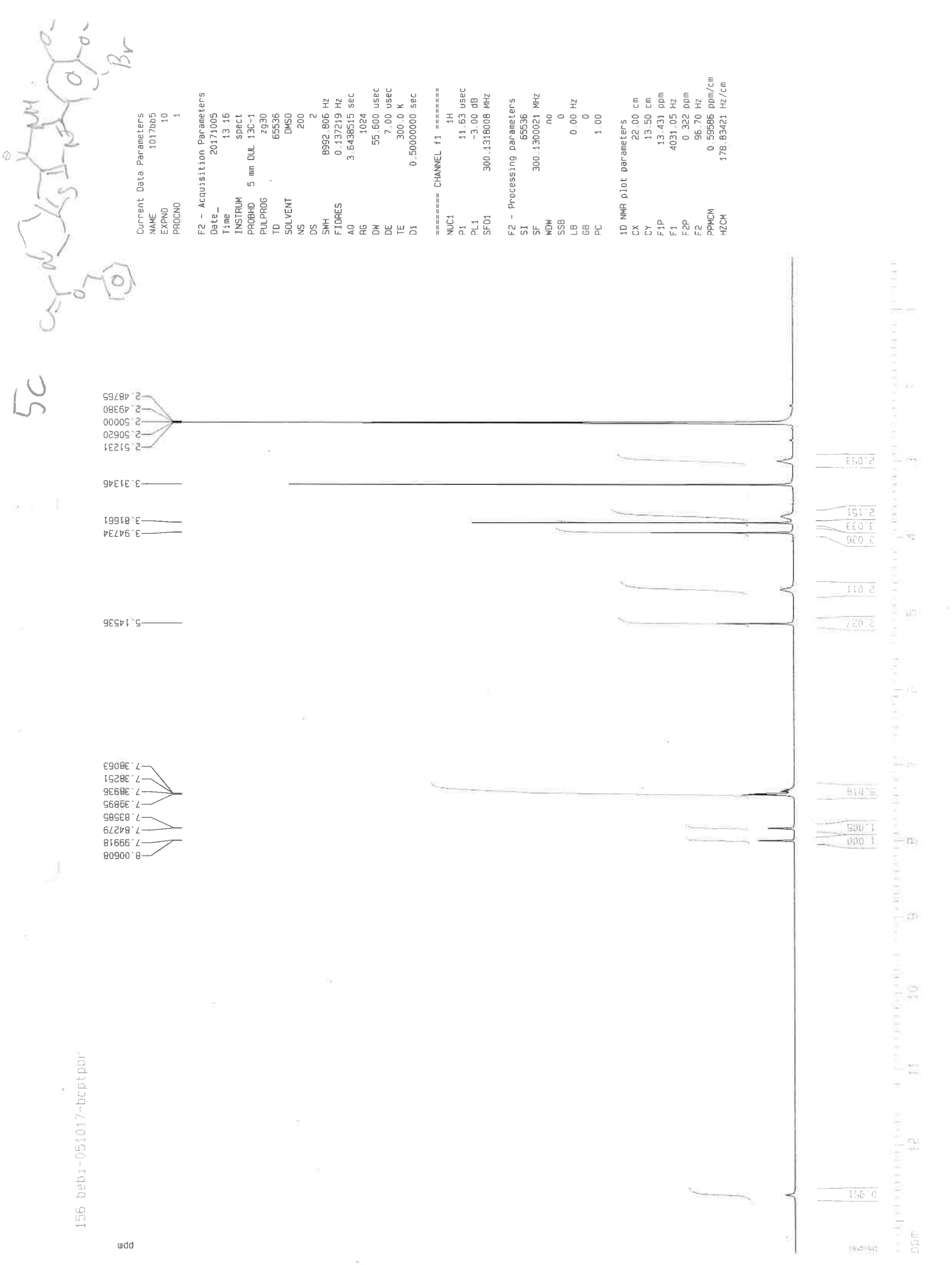
Br
5c
Current Data Parameters
NAME 1017bb5
EXPNO 10
PROCNO 1
F2 - Acquisition Parameters
Date_ 20171005
Time 13 16
INSTRUM spect
PROBHD 5 mm DUL 13C-1
PULPROG zg30
TD 65536
SOLVENT DMSO
NS 200
DS 2
SWH 8992 806 Hz
FIDRES 0 137219 Hz
AQ 3 6438515 sec
RG 1024
DW 55 600 usec
DE 7 00 usec
TE 300 0 K
D1 0 50000000 sec
======== CHANNEL f1 ========
NUC1 1H
P1 11 63 usec
PL1 -3 00 dB
SFO1 300 1318008 MHz
F2 - Processing parameters
SI 65536
SF 300 1300021 MHz
WDW no
SSB 0
LB 0 00 Hz
GB 0
PC 1 00
1D NMR plot parameters
CX 22 00 cm
CY 13 50 cm
F1P 13 431 ppm
F1 4031 05 Hz
F2P 0 322 ppm
F2 96 70 Hz
PPMCM 0 59586 ppm/cm
HZCM 178 83421 Hz/cm
2.48765
2.49380
2.50000
2.50620
2.51231
3.31346
3.81661
3.94734
5.14536
7.38063
7.38251
7.38936
7.39895
7.83585
7.84279
7.99918
8.00608
2.053
2.151
3.033
2.038
2.011
2.027
5.015
1.065
1.000
0.951
156 bebi-051017-bcptpor
ppm

5c

156 bebi-051017-bcptpar

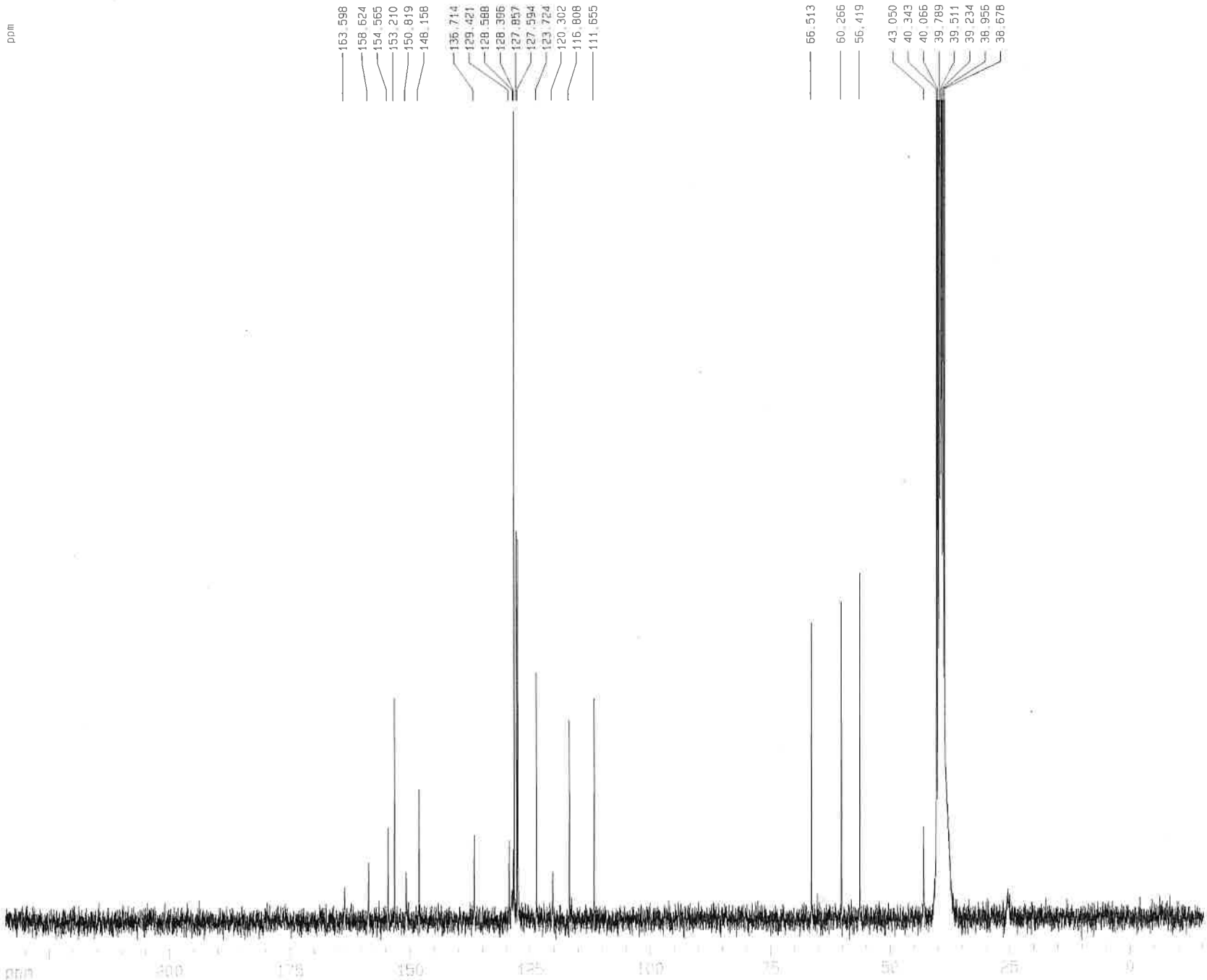

Current Data Parameters
NAME 1017bb5
EXPNO 11
PROCNO 1

F2 - Acquisition Parameters
Date_ 20171005
Time 15.08
INSTRUM spect
PROBHD 5 mm DUL 13C-1
PULPROG zgpg30
TD 32768
SOLVENT DMSO
NS 4B3B4
DS 4
SWH 18832.393 Hz
FIDRES 0.574719 Hz
AQ 0.8700404 sec
RG 18390.4
DW 26.550 usec
DE 20.00 usec
TE 300.0 K
D1 0.40000001 sec
d11 0.03000000 sec
d12 0.00002000 sec

======== CHANNEL f1 ========
NUC1 13C
P1 7.37 usec
PL1 5.00 dB
SFO1 75.4760505 MHz

======== CHANNEL f2 ========
CPDPRG2 waltz16
NUC2 1H
PCPD2 90.00 usec
PL2 -3.00 dB
PL12 14.77 dB
PL13 15.00 dB
SFO2 300.1312005 MHz

F2 - Processing parameters
SI 32768
SF 75.4677882 MHz
WDW EM
SSB 0
LB 1.00 Hz
GB 0
PC 1.40

1D NMR plot parameters
CX 22.00 cm
CY 15.00 cm
F1P 234.252 ppm
F1 17678.45 Hz
F2P -15.291 ppm
F2 -1153.95 Hz
PPMCM 11.34282 ppm/cm
HZCM 856.01782 Hz/cm

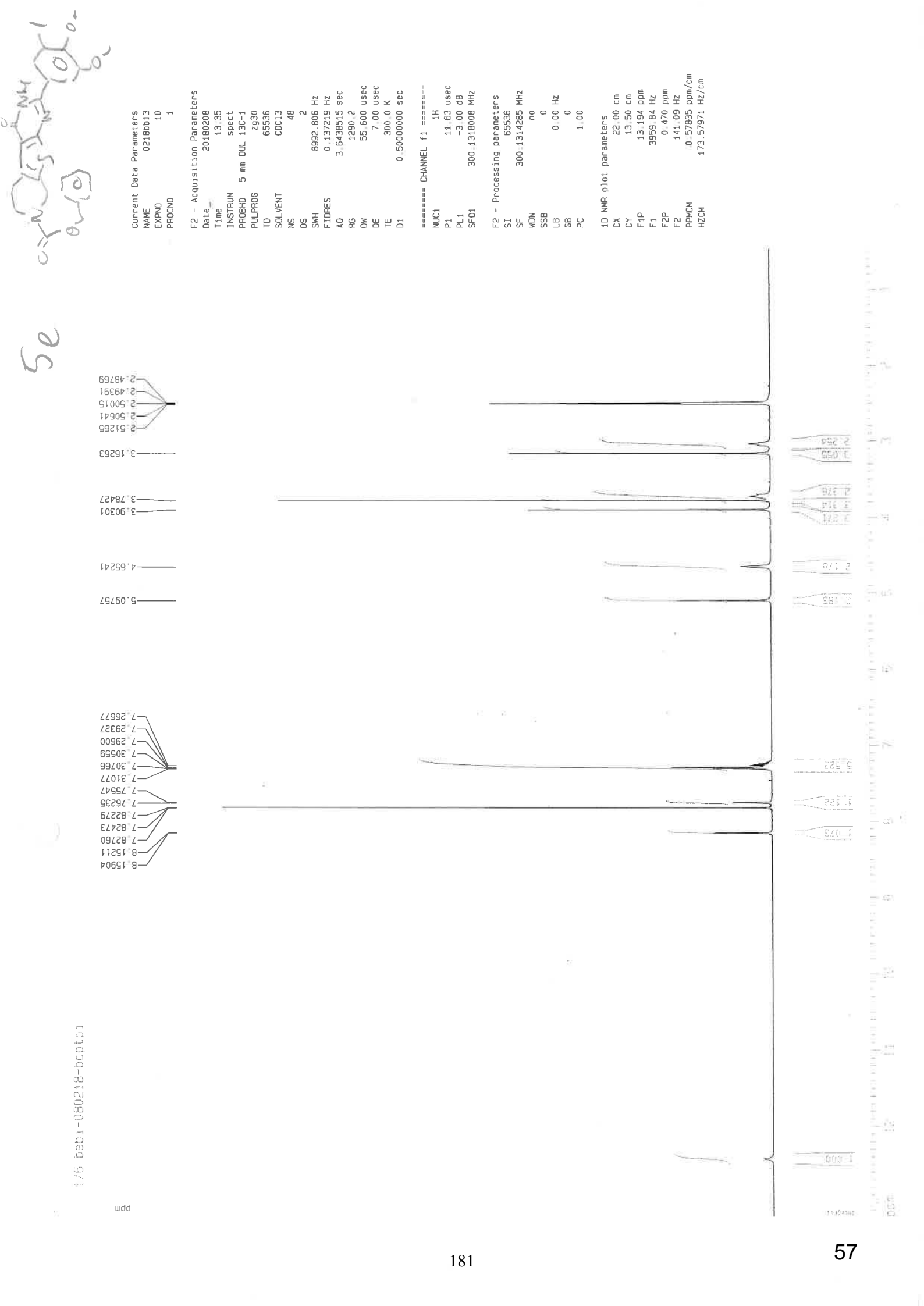
Current Data Parameters
NAME 0218bb13
EXPNO 10
PROCNO 1
F2 - Acquisition Parameters
Date_ 20180208
Time 13.35
INSTRUM spect
PROBHD 5 mm DUL 13C-1
PULPROG zg30
TD 65536
SOLVENT CDCl3
NS 48
DS 2
SWH 8992.806 Hz
FIDRES 0.137219 Hz
AQ 3.6438515 sec
RG 1290.2
DW 55.600 usec
DE 7.00 usec
TE 300.0 K
D1 0.50000000 sec
======== CHANNEL f1 ========
NUC1 1H
P1 11.63 usec
PL1 -3.00 dB
SFO1 300.1318008 MHz
F2 - Processing parameters
SI 65536
SF 300.1314285 MHz
WDW no
SSB 0
LB 0.00 Hz
GB 0
PC 1.00
1D NMR plot parameters
CX 22.00 cm
CY 13.50 cm
F1P 13.194 ppm
F1 3959.84 Hz
F2P 0.470 ppm
F2 141.09 Hz
PPMCM 0.57835 ppm/cm
HZCM 173.57971 Hz/cm
2.48769
2.49391
2.50015
2.50641
2.51265
3.16263
3.78427
3.90301
4.65241
5.09757
7.26677
7.29327
7.29600
7.30559
7.30766
7.31077
7.75547
7.76235
7.82279
7.82473
7.82760
8.15211
8.15904
ppm

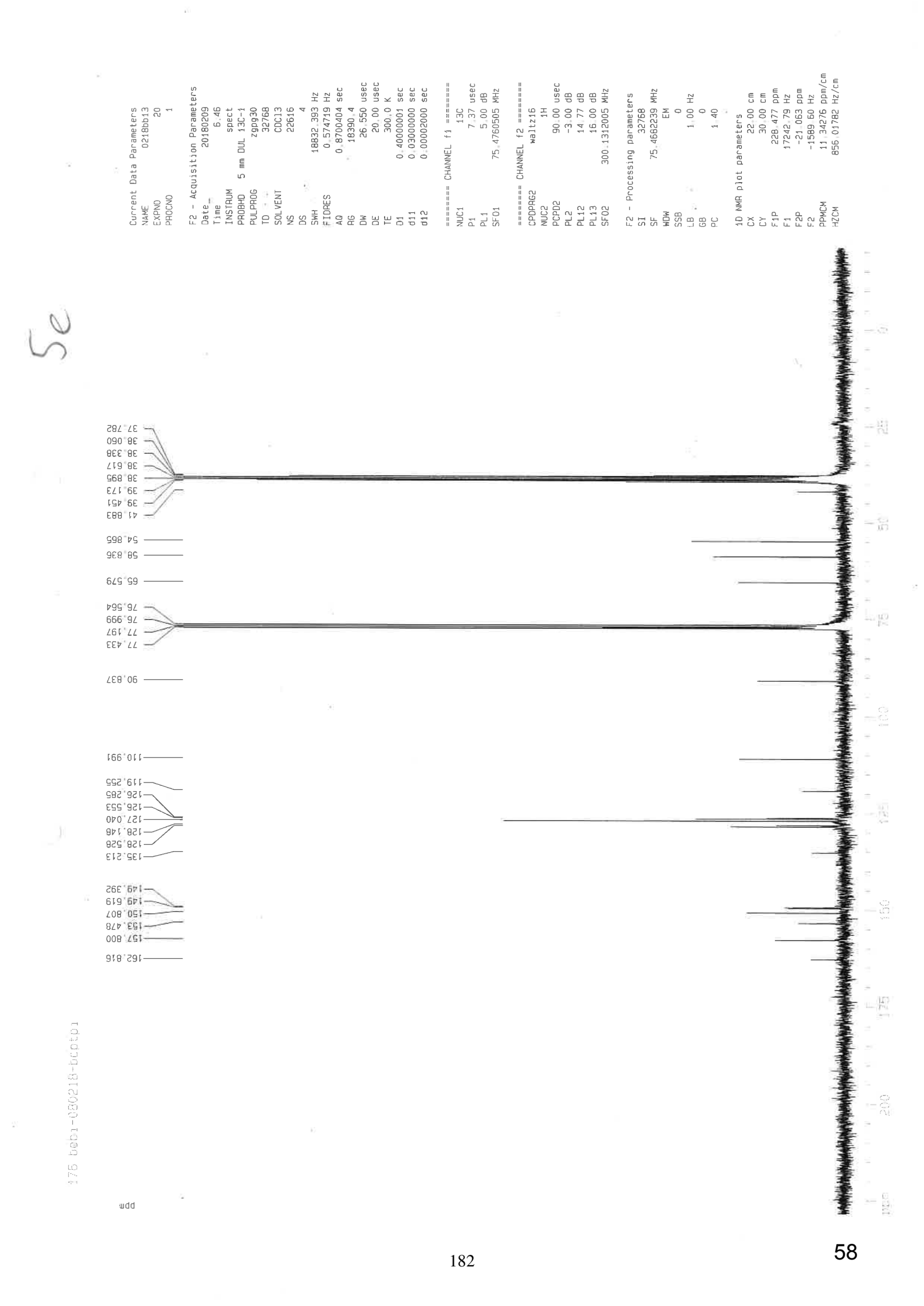
Current Data Parameters
NAME 0218bb13
EXPNO 20
PROCNO 1
F2 - Acquisition Parameters
Date_ 20180209
Time 6.46
INSTRUM spect
PROBHD 5 mm DUL 13C-1
PULPROG zgpg30
TD 32768
SOLVENT CDCl3
NS 22616
DS 4
SWH 18832.393 Hz
FIDRES 0.574719 Hz
AQ 0.8700404 sec
RG 18390.4
DW 26.550 usec
DE 20.00 usec
TE 300.0 K
D1 0.40000001 sec
d11 0.03000000 sec
d12 0.00002000 sec
======== CHANNEL f1 ========
NUC1 13C
P1 7.37 usec
PL1 5.00 dB
SFO1 75.4760505 MHz
======== CHANNEL f2 ========
CPDPRG2 waltz16
NUC2 1H
PCPD2 90.00 usec
PL2 -3.00 dB
PL12 14.77 dB
PL13 16.00 dB
SFO2 300.1312005 MHz
F2 - Processing parameters
SI 32768
SF 75.4662239 MHz
WDW EM
SSB 0
LB 1.00 Hz
GB 0
PC 1.40
1D NMR plot parameters
CX 22.00 cm
CY 30.00 cm
F1P 228.477 ppm
F1 17242.79 Hz
F2P -21.063 ppm
F2 -1589.60 Hz
PPMCM 11.34276 ppm/cm
HZCM 856.01782 Hz/cm
37.782
38.060
38.338
38.617
38.895
39.173
39.451
41.883
54.865
58.836
65.579
76.564
76.999
77.197
77.433
90.837
110.991
119.255
126.265
126.553
127.040
128.148
128.528
135.213
149.392
149.619
150.807
153.478
157.800
162.816
ppm
175 bccl-050218-bcptb1

58


Current Data Parameters
NAME 0418bb20
EXPNO 10
PROCNO 1
F2 - Acquisition Parameters
Date_ 20180423
Time 7.50
INSTRUM spect
PROBHD 5 mm DUL 13C-1
PULPROG zg30
TD 65536
SOLVENT DMSO
NS 200
DS 2
SWH 8992.806 Hz
FIDRES 0.137219 Hz
AQ 3.6438515 sec
RG 1024
DW 55.600 usec
DE 7.00 usec
TE 300.0 K
D1 0.50000000 sec
======== CHANNEL f1 ========
NUC1 1H
P1 11.63 usec
PL1 -3.00 dB
SFO1 300.1318008 MHz
F2 - Processing parameters
SI 65536
SF 300.1300021 MHz
WDW no
SSB 0
LB 0.00 Hz
GB 0
PC 1.00
1D NMR plot parameters
CX 22.00 cm
CY 130.00 cm
F1P 13.590 ppm
F1 4078.77 Hz
F2P 0.202 ppm
F2 60.71 Hz
PPMCM 0.60853 ppm/cm
HZCM 182.63919 Hz/cm
2 bBu-210418-bcptp3br
ppm
Integral

2 bebi-210418-bcpta3br

5i

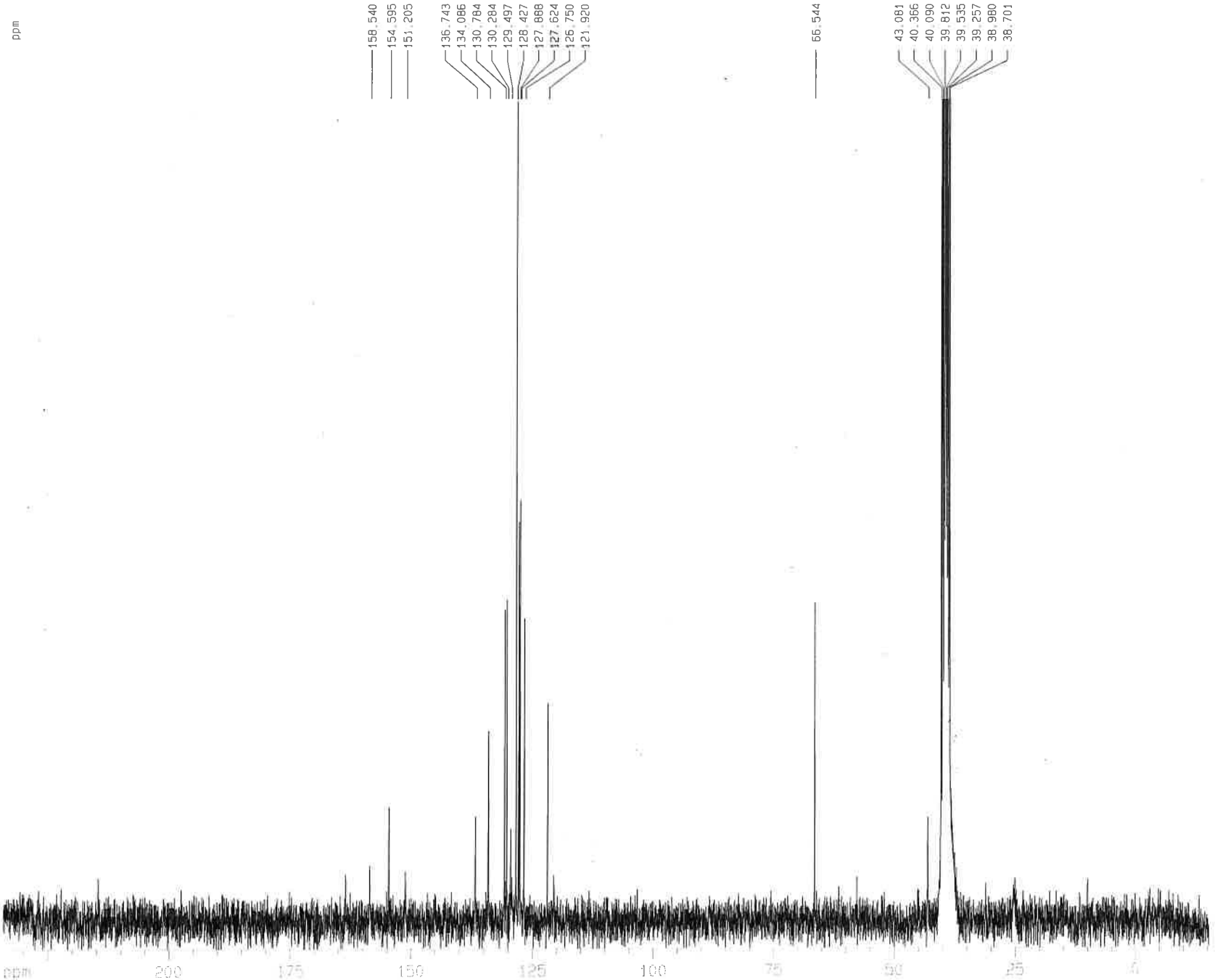

Current Data Parameters

NAME	0418bb20
EXPNO	11
PROCNO	1

F2 - Acquisition Parameters

Date_	20180423
Time	8.03
INSTRUM	spect
PROBHD	5 mm DUL 13C-1
PULPROG	zgpg30
TD	32768
SOLVENT	DMSO
NS	16800
DS	4
SWH	18832.393 Hz
FIDRES	0.574719 Hz
AQ	0.8700404 sec
RG	18390.4
DW	26.550 usec
DE	20.00 usec
TE	300.0 K
D1	0.40000001 sec
d11	0.03000000 sec
d12	0.00002000 sec

======== CHANNEL f1 ========

NUC1	13C
P1	7.37 usec
PL1	5.00 dB
SF01	75.4760505 MHz

======== CHANNEL f2 ========

CPDPRG2	waltz16
NUC2	1H
PCPD2	90.00 usec
PL2	-3.00 dB
PL12	14.77 dB
PL13	16.00 dB
SF02	300.1312005 MHz

F2 - Processing parameters

SI	32768
SF	75.4677859 MHz
WDW	EM
SSB	0
LB	1.00 Hz
GB	0
PC	1.40

1D NMR plot parameters

CX	22.00 cm
CY	15.00 cm
F1P	234.282 ppm
F1	17680.75 Hz
F2P	-15.260 ppm
F2	-1151.65 Hz
PPMCM	11.34282 ppm/cm
HZCM	856.01782 Hz/cm

5j

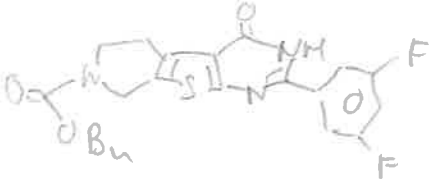

157 bebi-121017-bcptp35df

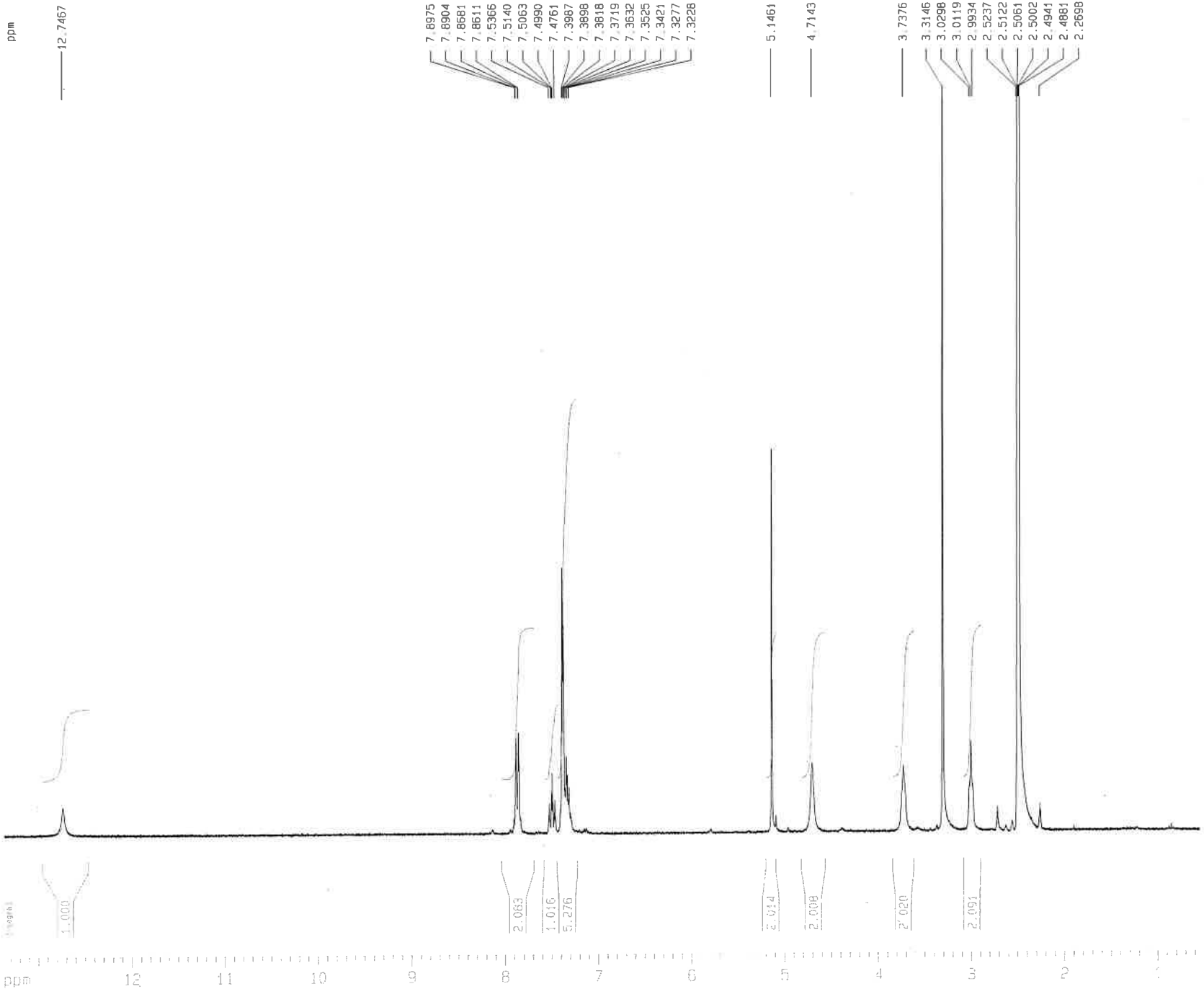

Current Data Parameters

NAME	1017bb9
EXPNO	1
PROCNO	1

F2 - Acquisition Parameters

Date_	20171012
Time	13.52
INSTRUM	spect
PROBHD	5 mm DUL 13C-1
PULPROG	zg30
TD	65536
SOLVENT	DMSO
NS	200
DS	2
SWH	8992.806 Hz
FIDRES	0.137219 Hz
AQ	3.6438515 sec
RG	1149.4
DW	55.600 usec
DE	7.00 usec
TE	300.0 K
D1	0.50000000 sec

======== CHANNEL f1 ========

NUC1	1H
P1	11.63 usec
PL1	-3.00 dB
SFO1	300.1318008 MHz

F2 - Processing parameters

SI	65536
SF	300.1300021 MHz
WDW	no
SSB	0
LB	0.00 Hz
GB	0
PC	1.00

1D NMR plot parameters

CX	22.00 cm
CY	80.00 cm
F1P	13.378 ppm
F1	4015.22 Hz
F2P	0.560 ppm
F2	167.94 Hz
PPMCM	0.58267 ppm/cm
HZCM	174.87611 Hz/cm

157 beb1-121017-bcctb35df

5j

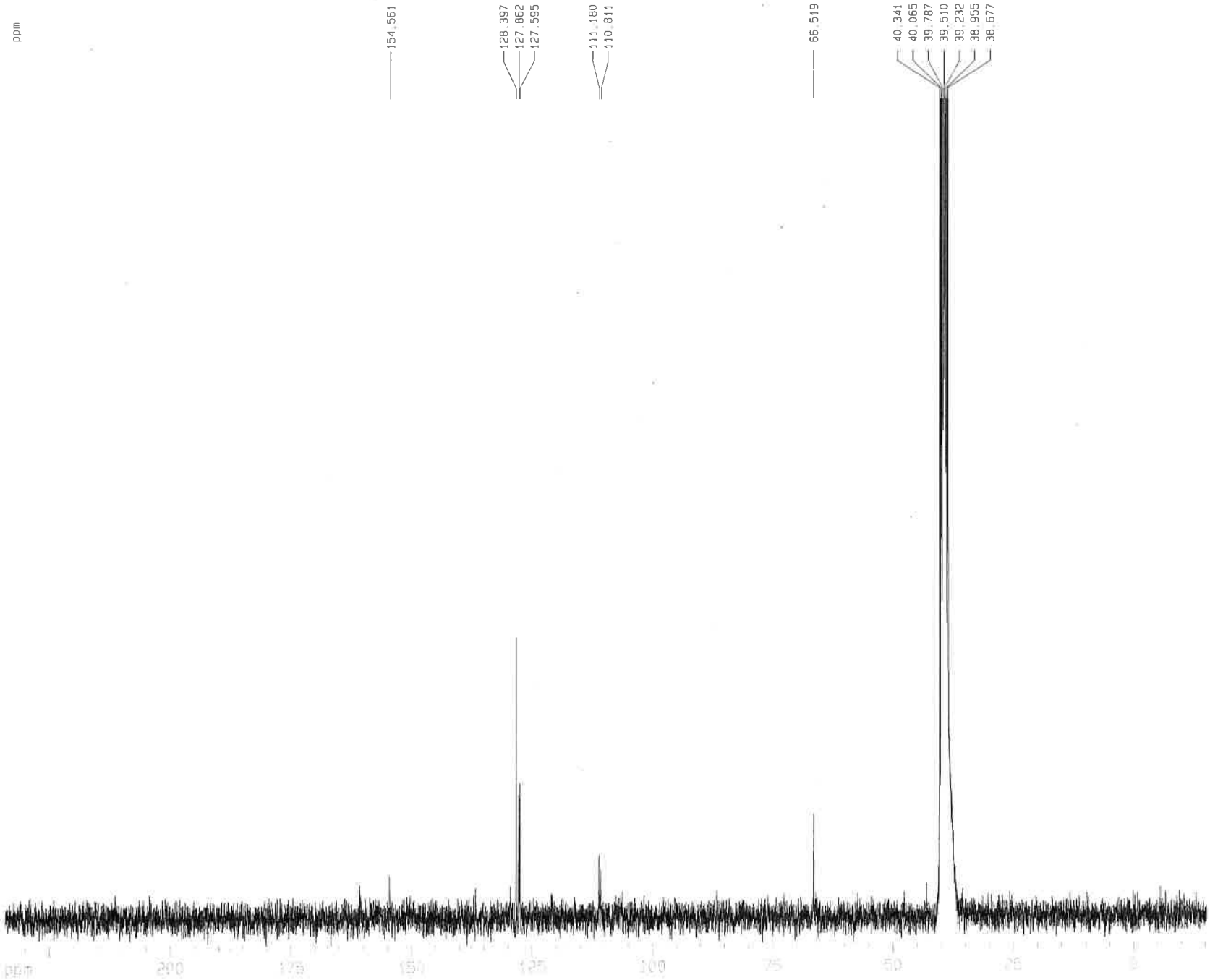

Current Data Parameters
NAME 1017bb9
EXPNO 2
PROCNO 1

F2 - Acquisition Parameters
Date_ 20171012
Time 14.52
INSTRUM spect
PROBHD 5 mm DUL 13C-1
PULPROG zgpg30
TD 32768
SOLVENT DMSO
NS 44528
DS 4
SWH 18832.393 Hz
FIDRES 0.574719 Hz
AQ 0.8700404 sec
RG 18390.4
DW 26.550 usec
DE 20.00 usec
TE 300.0 K
D1 0.40000001 sec
d11 0.03000000 sec
d12 0.00002000 sec

======== CHANNEL f1 ========
NUC1 13C
P1 7.37 usec
PL1 5.00 dB
SFO1 75.4760505 MHz

======== CHANNEL f2 ========
CPDPRG2 waltz16
NUC2 1H
PCPD2 90.00 usec
PL2 -3.00 dB
PL12 14.77 dB
PL13 16.00 dB
SFO2 300.1312005 MHz

F2 - Processing parameters
SI 32768
SF 75.4677882 MHz
WDW EM
SSB 0
LB 1.00 Hz
GB 0
PC 1.40

1D NMR plot parameters
CX 22.00 cm
CY 200.00 cm
F1P 234.252 ppm
F1 17678.45 Hz
F2P -15.291 ppm
F2 -1153.95 Hz
PPMCM 11.34282 ppm/cm
HZCM 856.01782 Hz/cm

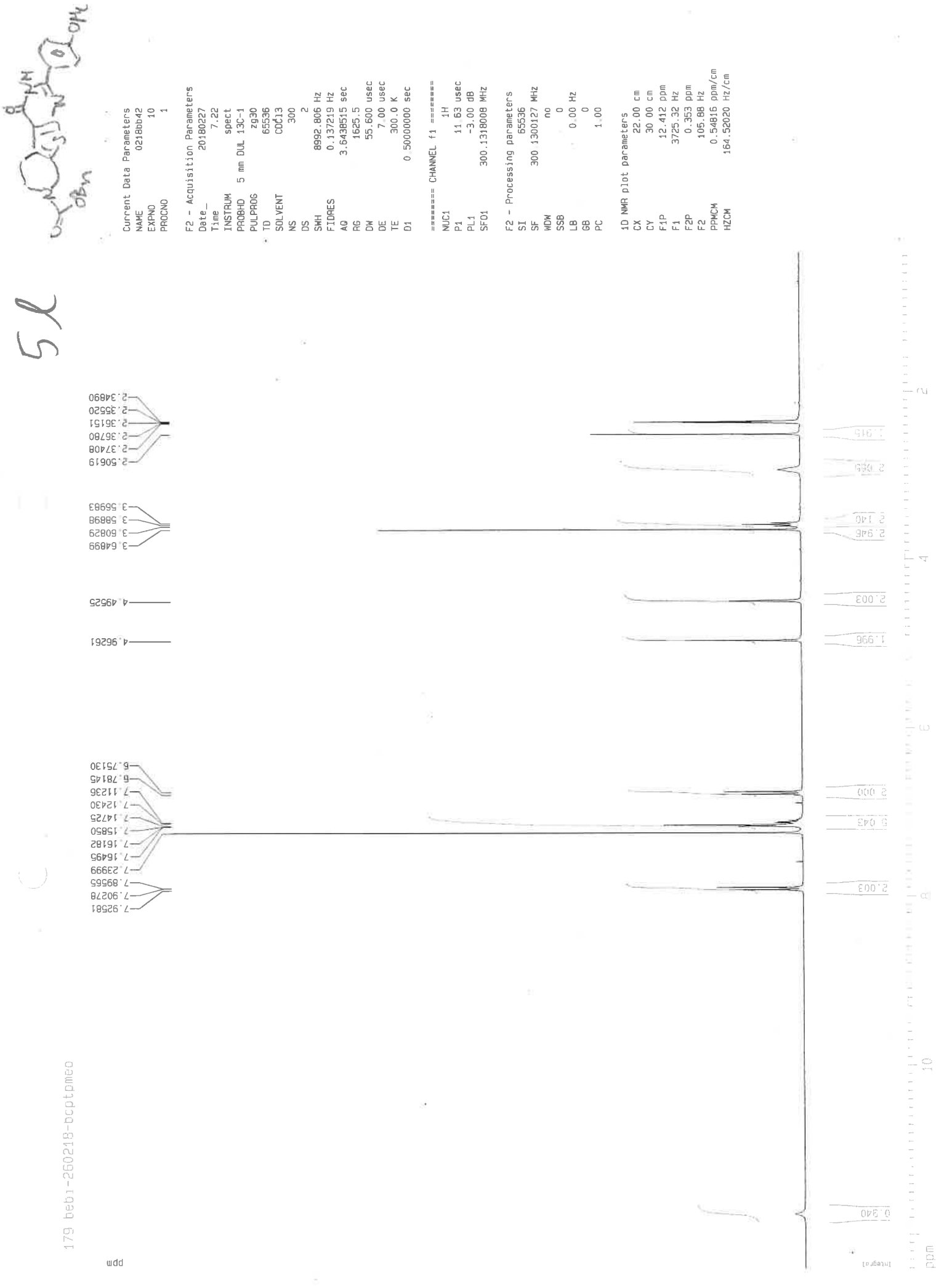
Current Data Parameters
NAME 0218bb42
EXPNO 10
PROCNO 1
F2 - Acquisition Parameters
Date_ 20180227
Time 7.22
INSTRUM spect
PROBHD 5 mm DUL 13C-1
PULPROG zg30
TD 65536
SOLVENT CDCl3
NS 300
DS 2
SWH 8992.806 Hz
FIDRES 0.137219 Hz
AQ 3.6438515 sec
RG 1625.5
DW 55.600 usec
DE 7.00 usec
TE 300.0 K
D1 0.50000000 sec
======== CHANNEL f1 ========
NUC1 1H
P1 11.63 usec
PL1 -3.00 dB
SFO1 300.1318008 MHz
F2 - Processing parameters
SI 65536
SF 300.1300127 MHz
WDW no
SSB 0
LB 0.00 Hz
GB 0
PC 1.00
1D NMR plot parameters
CX 22.00 cm
CY 30.00 cm
F1P 12.412 ppm
F1 3725.32 Hz
F2P 0.353 ppm
F2 105.88 Hz
PPMCM 0.54816 ppm/cm
HZCM 164.52020 Hz/cm
2.34890
2.35520
2.36151
2.36780
2.37408
2.50619
3.56983
3.58898
3.60829
3.64899
4.49525
4.96261
6.75130
6.78145
7.11236
7.12430
7.14725
7.15850
7.16182
7.16495
7.23999
7.89565
7.90278
7.92581
1.915
2.065
2.140
2.946
2.003
1.996
2.000
3.043
2.003
0.340
179 bebi-260218-bcptpmeo
ppm
Integral

5m

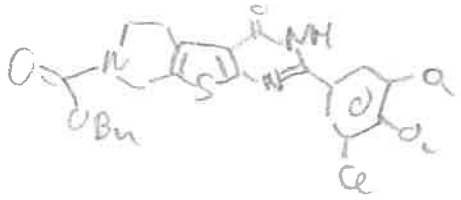

176 bebi-220218-hcptpcl

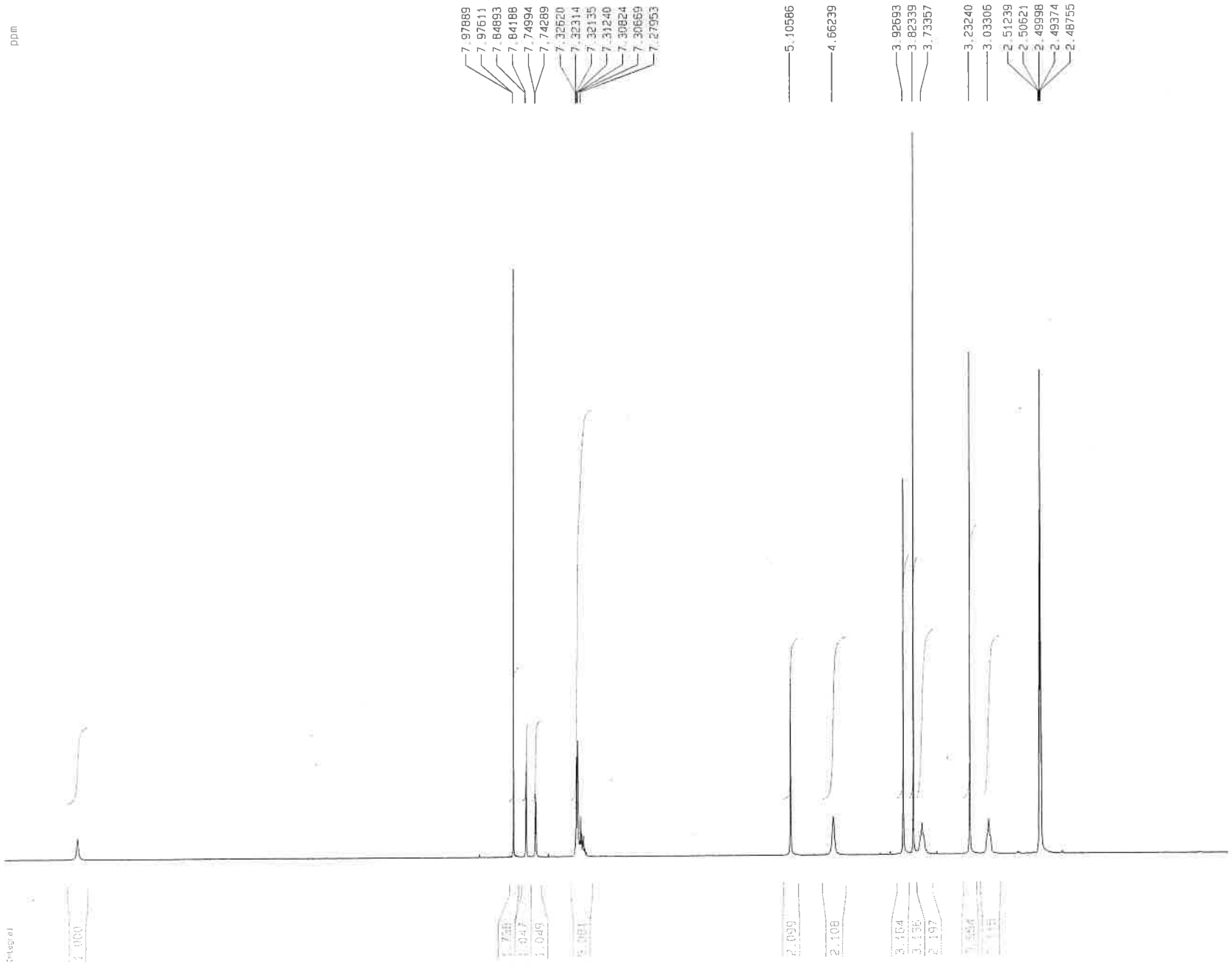

Current Data Parameters

NAME	0218bb34
EXPNO	10
PROCNO	1

F2 - Acquisition Parameters

Date_	20180222
Time	14.57
INSTRUM	spect
PROBHD	5 mm DUL 13C-1
PULPROG	zg30
TD	65536
SOLVENT	CDCl3
NS	200
DS	2
SWH	8992.806 Hz
FIDRES	0.137219 Hz
AQ	3.6438515 sec
RG	1149.4
DW	55.600 usec
DE	7.00 usec
TE	300.0 K
D1	0.50000000 sec

======== CHANNEL f1 ========

NUC1	1H
P1	11.63 usec
PL1	-3.00 dB
SFO1	300.1318008 MHz

F2 - Processing parameters

SI	65536
SF	300.1314284 MHz
WDW	no
SSB	0
LB	0.00 Hz
GB	0
PC	1.00

1D NMR plot parameters

CX	22.00 cm
CY	13.50 cm
F1P	13.247 ppm
F1	3975.93 Hz
F2P	0.550 ppm
F2	165.15 Hz
PPMCM	0.57714 ppm/cm
HZCM	173.21733 Hz/cm

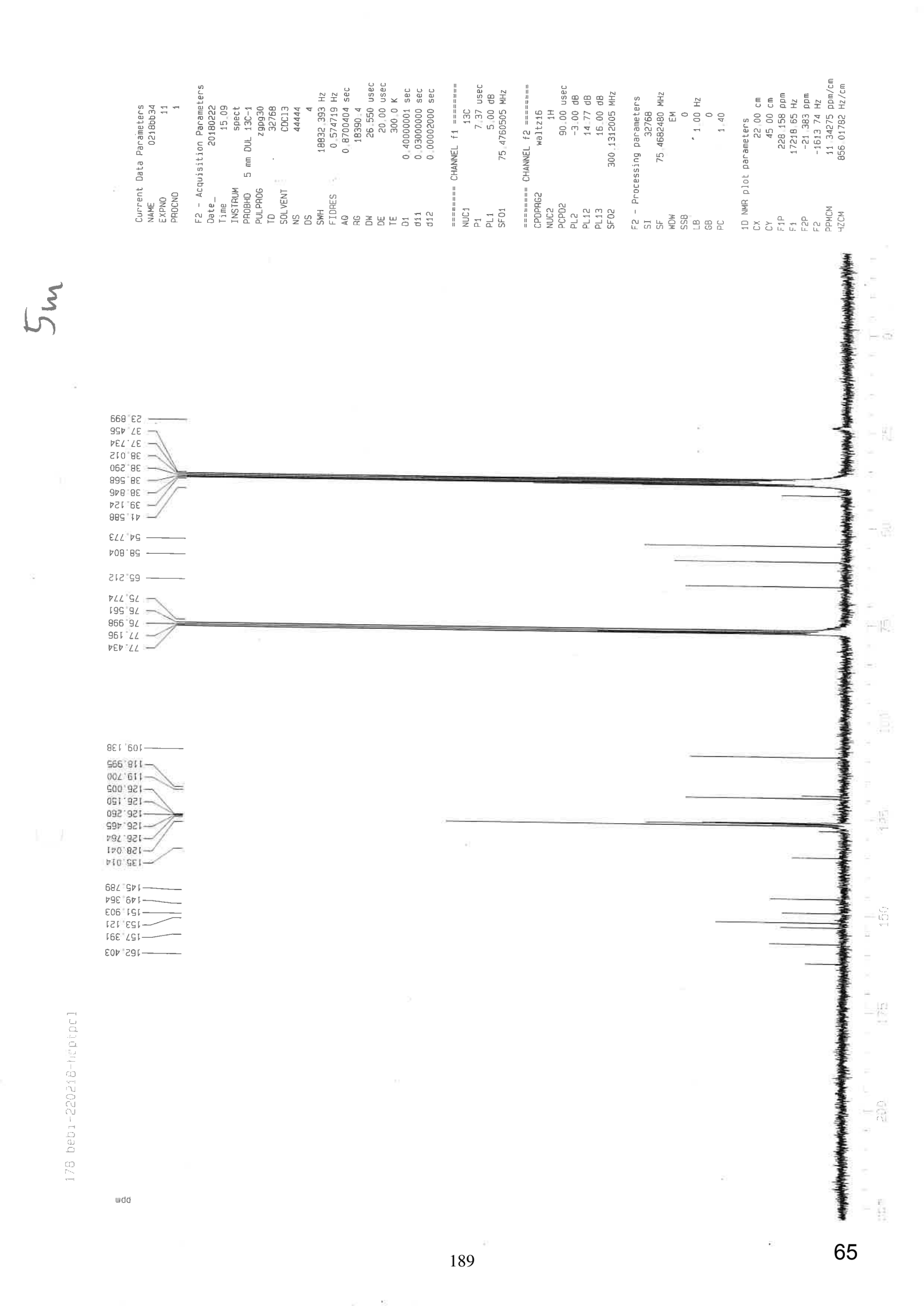
Current Data Parameters
NAME 0218bb34
EXPNO 11
PROCNO 1
F2 - Acquisition Parameters
Date_ 20180222
Time 15.09
INSTRUM spect
PROBHD 5 mm DUL 13C-1
PULPROG zgpg30
TD 32768
SOLVENT CDCl3
NS 44444
DS 4
SWH 18832.393 Hz
FIDRES 0.574719 Hz
AQ 0.8700404 sec
RG 18390.4
DW 26.550 usec
DE 20.00 usec
TE 300.0 K
D1 0.40000001 sec
d11 0.03000000 sec
d12 0.00002000 sec
======== CHANNEL f1 ========
NUC1 13C
P1 7.37 usec
PL1 5.00 dB
SFO1 75.4760505 MHz
======== CHANNEL f2 ========
CPDPRG2 waltz16
NUC2 1H
PCPD2 90.00 usec
PL2 -3.00 dB
PL12 14.77 dB
PL13 16.00 dB
SFO2 300.1312005 MHz
F2 - Processing parameters
SI 32768
SF 75.4682480 MHz
WDW EM
SSB 0
LB 1.00 Hz
GB 0
PC 1.40
1D NMR plot parameters
CX 22.00 cm
CY 45.00 cm
F1P 228.158 ppm
F1 17218.65 Hz
F2P -21.383 ppm
F2 -1613.74 Hz
PPMCM 11.34275 ppm/cm
HZCM 856.01782 Hz/cm
23.899
37.456
37.734
38.012
38.290
38.568
38.846
39.124
41.588
54.773
58.804
65.212
75.774
76.561
76.998
77.196
77.434
109.138
118.995
119.700
126.005
126.150
126.260
126.465
126.764
128.041
135.014
145.789
149.364
151.903
153.121
157.391
162.403
178 bebi-220218-1H.pipcp1
ppm

6a

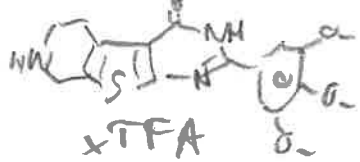

175 beb1-030218-hptptrim

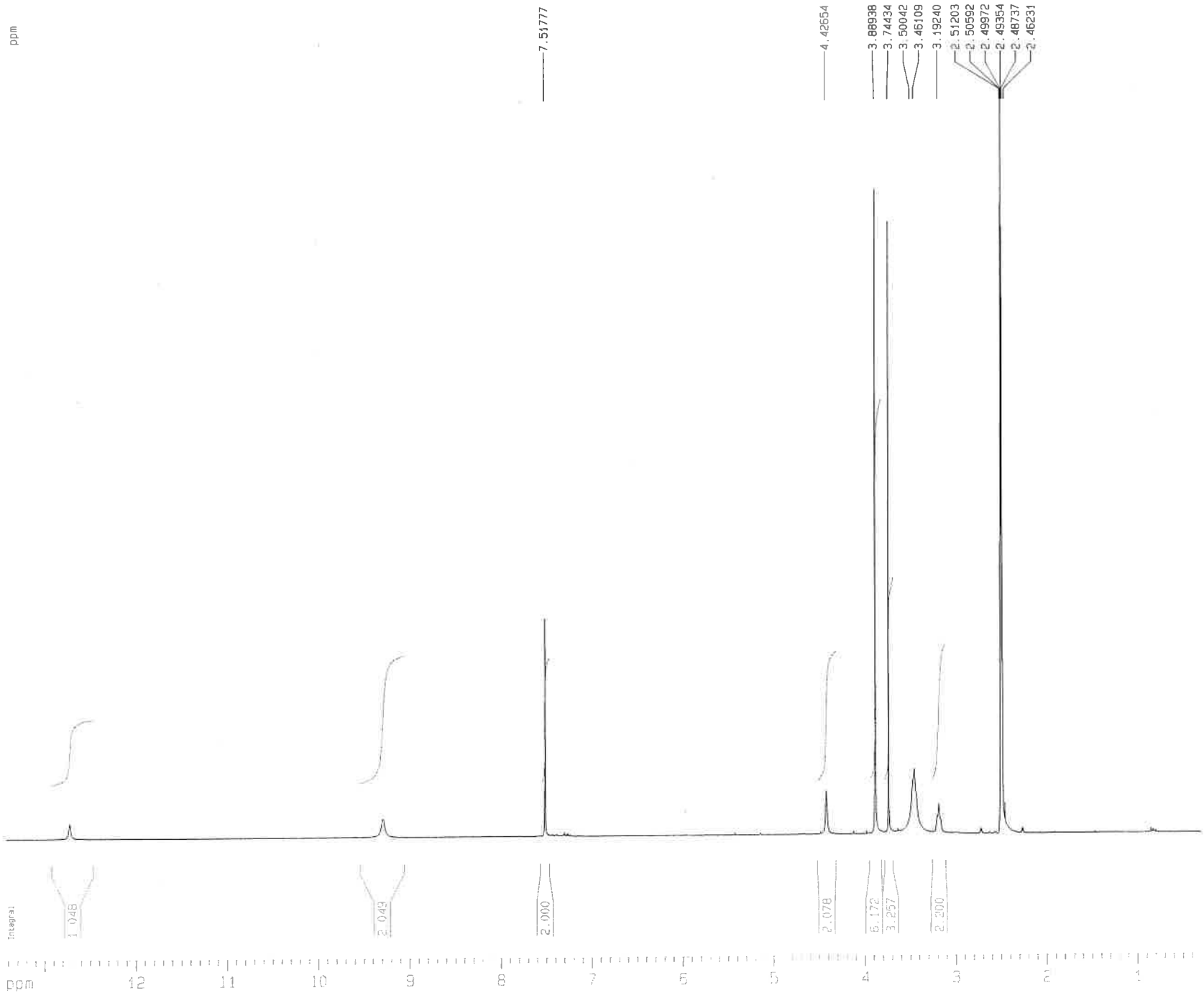

Current Data Parameters

NAME	0218bb7
EXPNO	10
PROCNO	1

F2 - Acquisition Parameters

Date_	20180205
Time	7.49
INSTRUM	spect
PROBHD	5 mm DUL 13C-1
PULPROG	zg30
TD	65536
SOLVENT	DMSO
NS	200
DS	2
SWH	8992.806 Hz
FIDRES	0.137219 Hz
AQ	3.6438515 sec
RG	1024
DW	55.600 usec
DE	7.00 usec
TE	300.0 K
D1	0.50000000 sec

======== CHANNEL f1 ========

NUC1	1H
P1	11.63 usec
PL1	-3.00 dB
SFO1	300.1318008 MHz

F2 - Processing parameters

SI	65536
SF	300.1300021 MHz
WDW	no
SSB	0
LB	0.00 Hz
GB	0
PC	1.00

1D NMR plot parameters

CX	22.00 cm
CY	16.00 cm
F1P	13.431 ppm
F1	4030.94 Hz
F2P	0.309 ppm
F2	92.60 Hz
PPMCM	0.59646 ppm/cm
HZCM	179.01540 Hz/cm

6a

175 oeb1-030218-natptrim

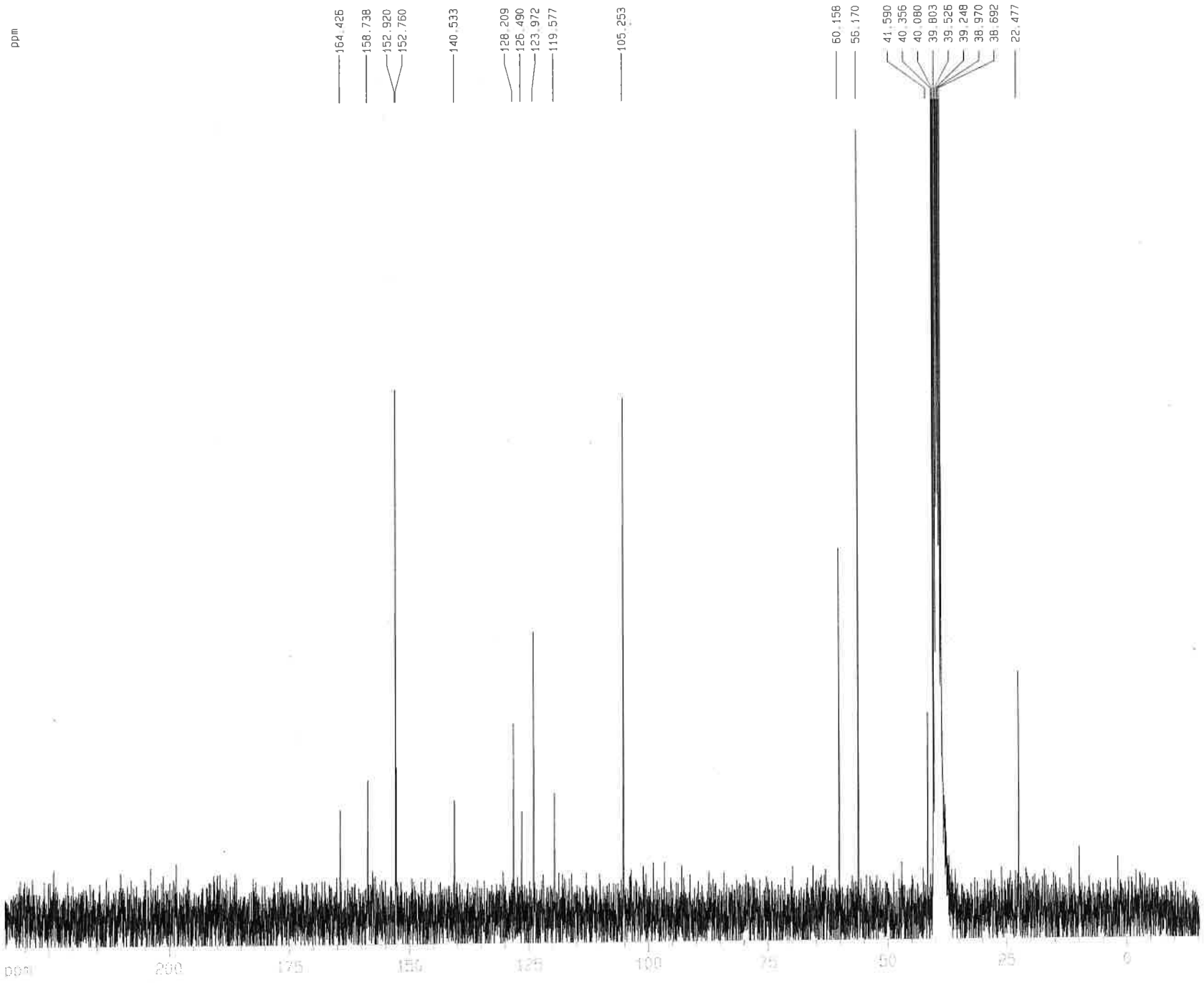

Current Data Parameters

NAME	0218bb7
EXPNO	11
PROCNO	1

F2 - Acquisition Parameters

Date_	20180205
Time	8.03
INSTRUM	spect
PROBHD	5 mm DUL 13C-1
PULPROG	zgpg30
TD	32768
SOLVENT	DMSO
NS	8400
DS	4
SWH	18832.393 Hz
FIDRES	0.574719 Hz
AQ	0.8700404 sec
RG	18390.4
DW	26.550 usec
DE	20.00 usec
TE	300.0 K
D1	0.40000001 sec
d11	0.03000000 sec
d12	0.00002000 sec

======== CHANNEL f1 ========

NUC1	13C
P1	7.37 usec
PL1	5.00 dB
SFO1	75.4760505 MHz

======== CHANNEL f2 ========

CPDPRG2	waltz16
NUC2	1H
PCPD2	90.00 usec
PL2	-3.00 dB
PL12	14.77 dB
PL13	16.00 dB
SFO2	300.1312005 MHz

F2 - Processing parameters

SI	32768
SF	75.4677865 MHz
WDW	EM
SSB	0
LB	1.00 Hz
GB	0
PC	1.40

1D NMR plot parameters

CX	22.00 cm
CY	15.00 cm
F1P	234.274 ppm
F1	17680.17 Hz
F2P	-15.268 ppm
F2	-1152.22 Hz
PPMCM	11.34282 ppm/cm
HZCM	856.01782 Hz/cm

6b

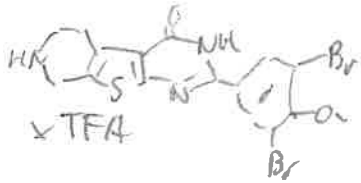

173 beb1-270118-hptpbr2

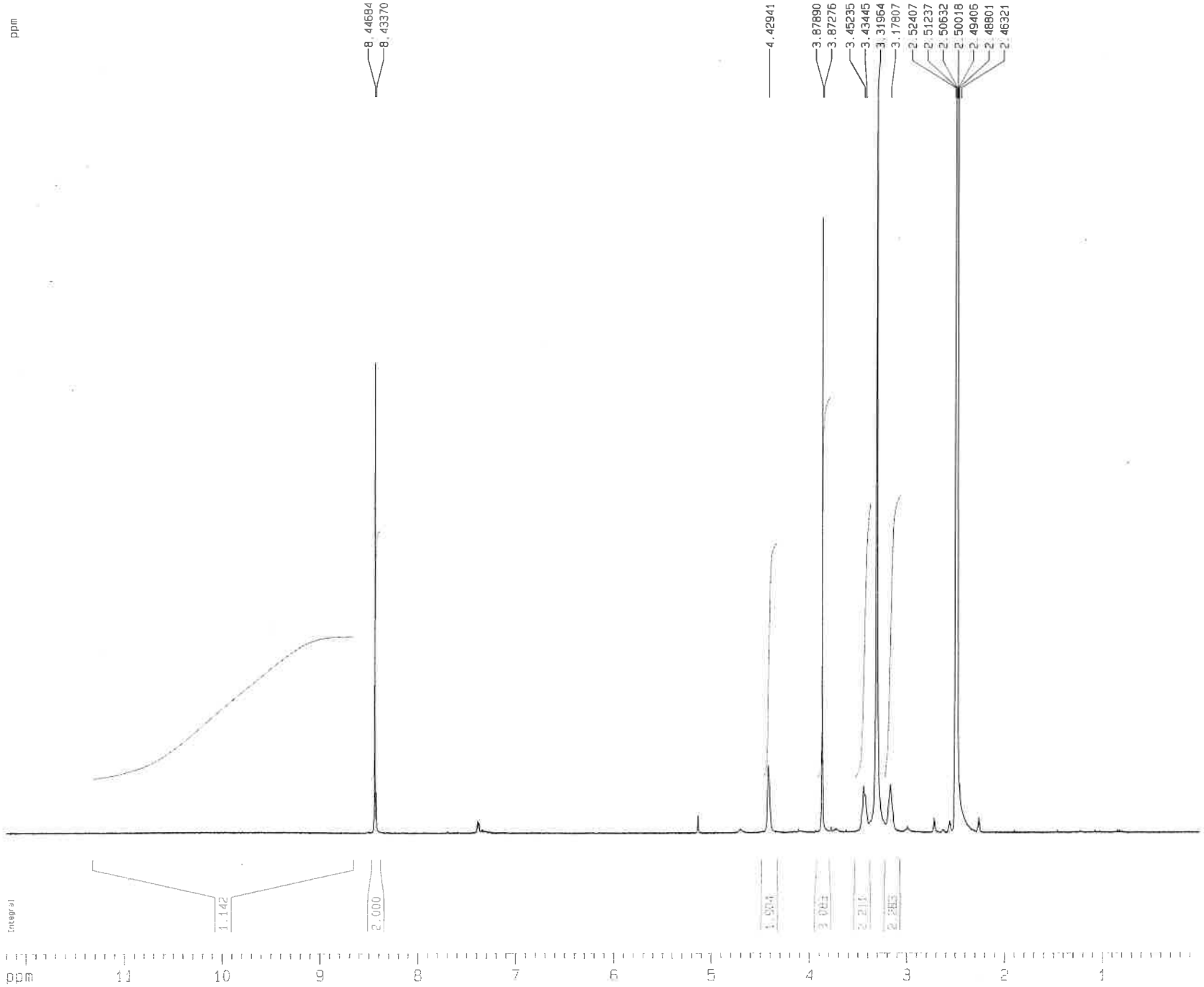

Current Data Parameters

NAME	0118bb29
EXPNO	10
PROCNO	1

F2 - Acquisition Parameters

Date_	20180129
Time	8.02
INSTRUM	spect
PROBHD	5 mm DUL 13C-1
PULPROG	zg30
TD	65536
SOLVENT	DMSO
NS	200
DS	2
SWH	8992.806 Hz
FIDRES	0.137219 Hz
AQ	3.6438515 sec
RG	1149.4
DW	55.600 usec
DE	7.00 usec
TE	300.0 K
D1	0.50000000 sec

======== CHANNEL f1 ========

NUC1	1H
P1	11.63 usec
PL1	-3.00 dB
SFO1	300.1318008 MHz

F2 - Processing parameters

SI	65536
SF	300.1300020 MHz
WDW	no
SSB	0
LB	0.00 Hz
GB	0
PC	1.00

1D NMR plot parameters

CX	22.00 cm
CY	13.50 cm
F1P	12.209 ppm
F1	3664.35 Hz
F2P	0.017 ppm
F2	5.04 Hz
PPMCM	0.55420 ppm/cm
HZCM	166.33212 Hz/cm

6b

173 bebi-270116-hptpbr2

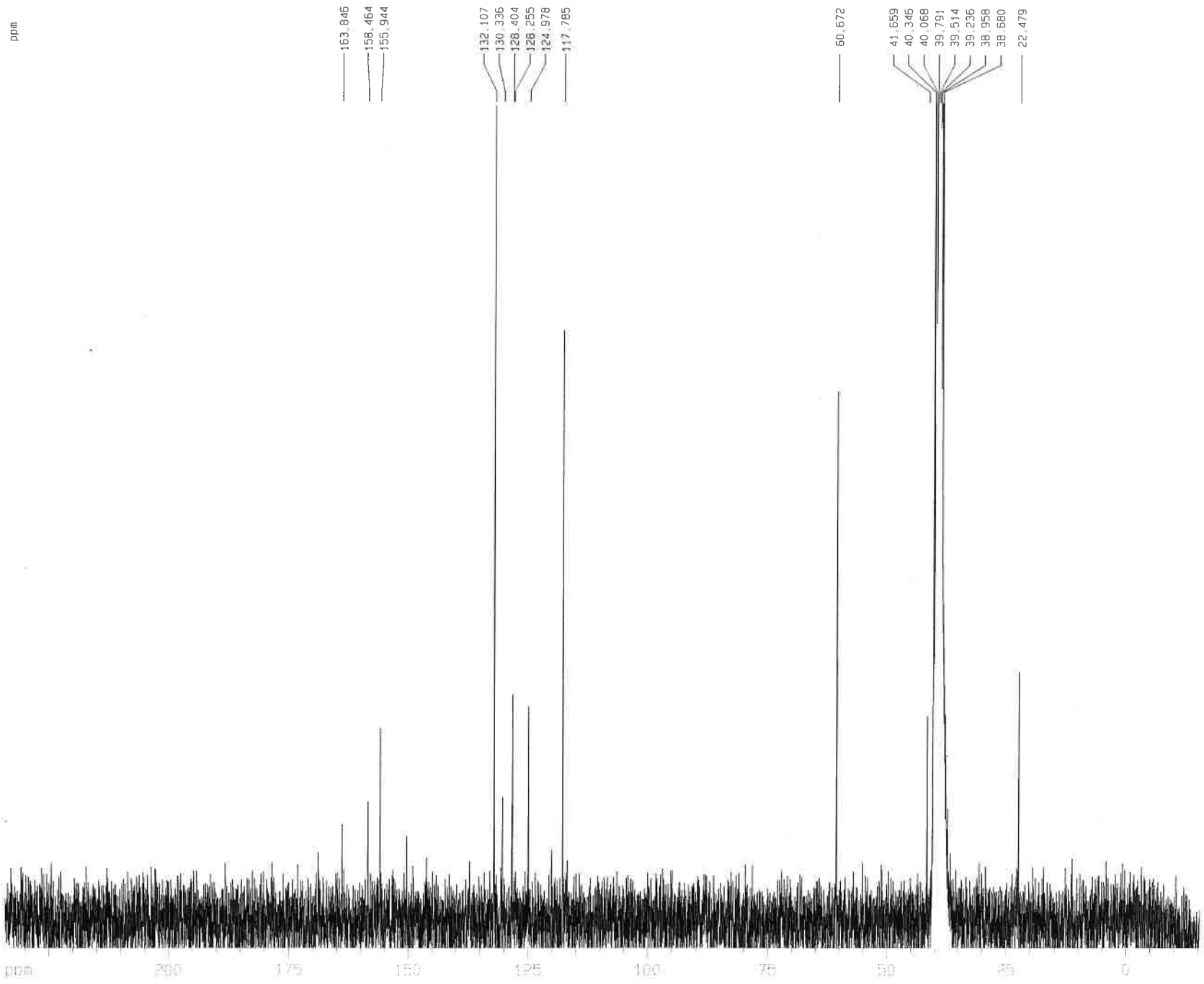

Current Data Parameters
NAME 0118bb29
EXPNO 20
PROCNO 1

F2 - Acquisition Parameters
Date_ 20180130
Time 7.06
INSTRUM spect
PROBHD 5 mm DUL 13C-1
PULPROG zgpg30
TD 32768
SOLVENT DMSO
NS 23124
DS 4
SWH 18832.393 Hz
FIDRES 0.574719 Hz
AQ 0.8700404 sec
RG 18390.4
DW 26.550 usec
DE 20.00 usec
TE 300.0 K
D1 0.40000001 sec
d11 0.03000000 sec
d12 0.00002000 sec

======== CHANNEL f1 ========
NUC1 13C
P1 7.37 usec
PL1 5.00 dB
SFO1 75.4760505 MHz

======== CHANNEL f2 ========
CPDPRG2 waltz16
NUC2 1H
PCPD2 90.00 usec
PL2 -3.00 dB
PL12 14.77 dB
PL13 16.00 dB
SFO2 300.1312005 MHz

F2 - Processing parameters
SI 32768
SF 75.4677876 MHz
WDW EM
SSB 0
LB 1.00 Hz
GB 0
PC 1.40

1D NMR plot parameters
CX 22.00 cm
CY 15.00 cm
F1P 234.259 ppm
F1 17679.02 Hz
F2P -15.283 ppm
F2 -1153.37 Hz
PPMCM 11.34282 ppm/cm
HZCM 856.01782 Hz/cm

6c

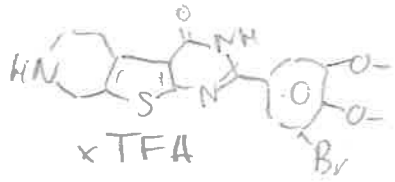

172 beb1-250118-hptpbr

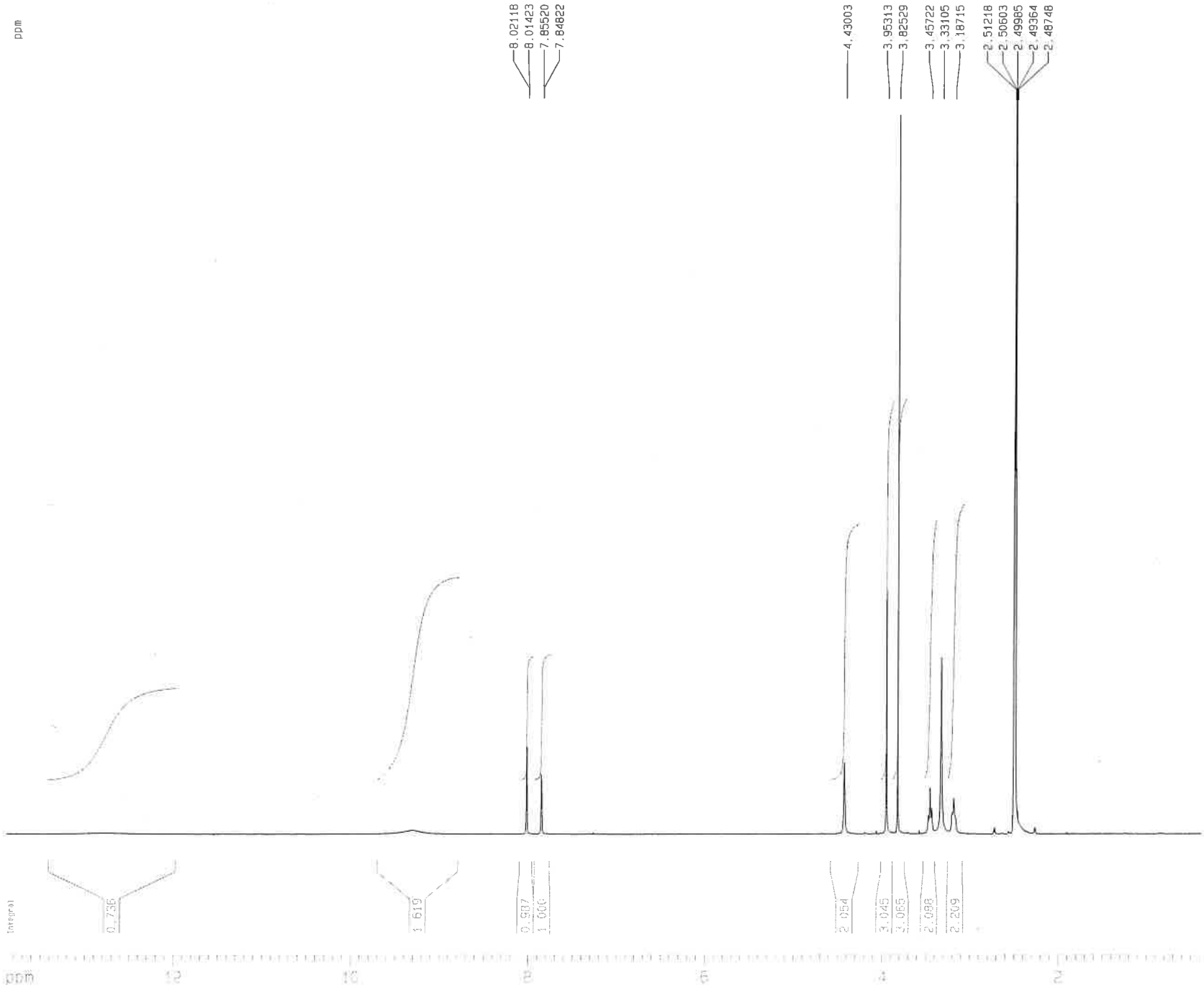

Current Data Parameters

NAME	0118bb28
EXPNO	10
PROCNO	1

F2 - Acquisition Parameters

Date_	20180125
Time	13.20
INSTRUM	spect
PROBHD	5 mm DUL 13C-1
PULPROG	zg30
TD	65536
SOLVENT	DMSO
NS	144
DS	2
SWH	8992.806 Hz
FIDRES	0.137219 Hz
AQ	3.6438515 sec
RG	1024
DW	55.600 usec
DE	7.00 usec
TE	300.0 K
D1	0.50000000 sec

======== CHANNEL f1 ========

NUC1	1H
P1	11.63 usec
PL1	-3.00 dB
SFO1	300.1318008 MHz

F2 - Processing parameters

SI	65536
SF	300.1300021 MHz
WDW	no
SSB	0
LB	0.00 Hz
GB	0
PC	1.00

1D NMR plot parameters

CX	22.00 cm
CY	13.50 cm
F1P	13.882 ppm
F1	4166.47 Hz
F2P	0.388 ppm
F2	116.52 Hz
PPMCM	0.61336 ppm/cm
HZCM	184.08870 Hz/cm

6c

172 bec1-250118-nptpbr

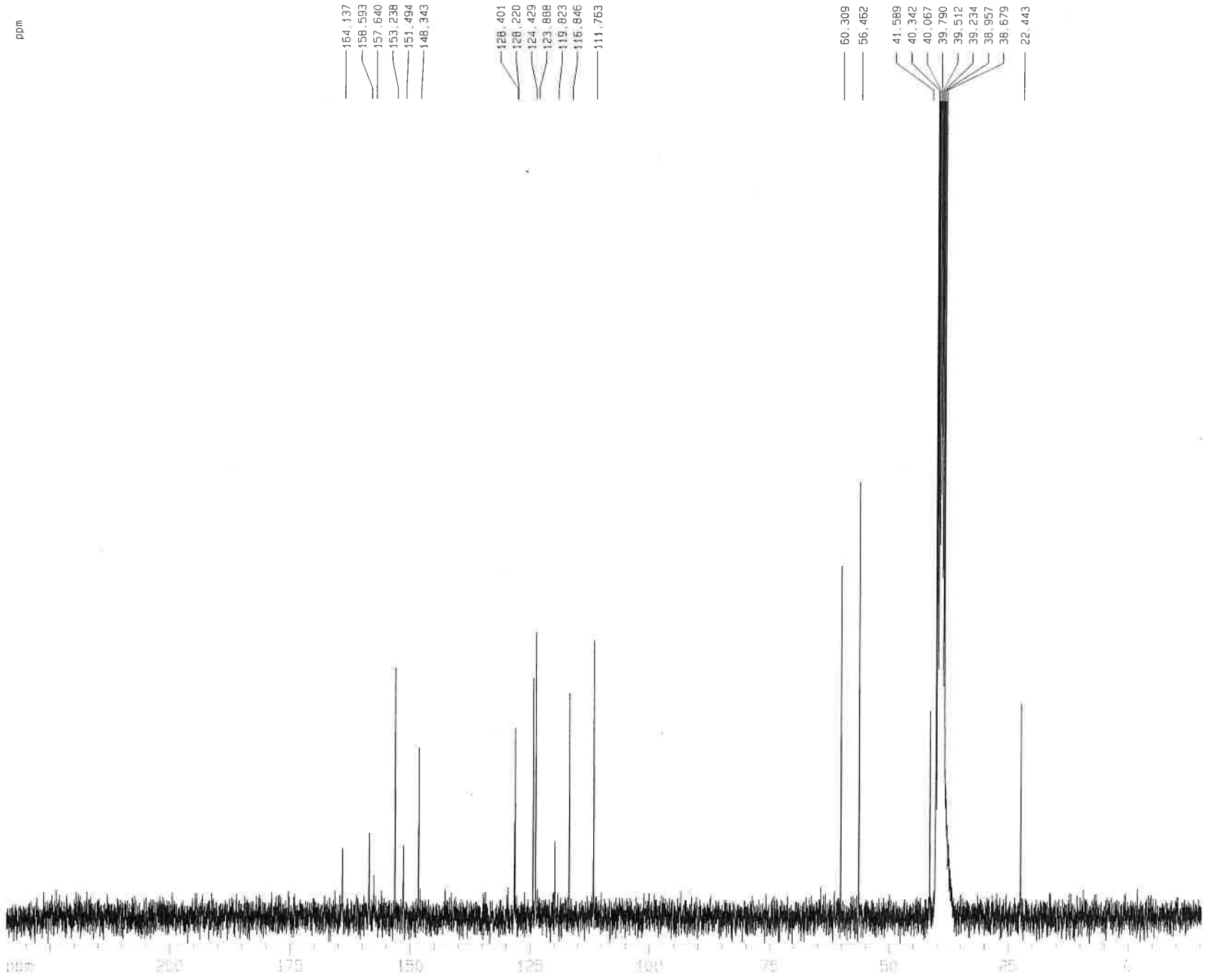

Current Data Parameters
NAME 0118bb2B
EXPNO 20
PROCNO 1

F2 - Acquisition Parameters
Date_ 20180125
Time 23.59
INSTRUM spect
PROBHD 5 mm DUL 13C-1
PULPROG zgpg30
TD 32768
SOLVENT DMSO
NS 22616
DS 4
SWH 18832.393 Hz
FIDRES 0.574719 Hz
AQ 0.8700404 sec
RG 18390.4
DW 26.550 usec
DE 20.00 usec
TE 300.0 K
D1 0.40000001 sec
d11 0.03000000 sec
d12 0.00002000 sec

======== CHANNEL f1 ========
NUC1 13C
P1 7.37 usec
PL1 5.00 dB
SFO1 75.4760505 MHz

======== CHANNEL f2 ========
CPDPRG2 waltz16
NUC2 1H
PCPD2 90.00 usec
PL2 -3.00 dB
PL12 14.77 dB
PL13 16.00 dB
SFO2 300.1312005 MHz

F2 - Processing parameters
SI 32768
SF 75.4677876 MHz
WDW EM
SSB 0
LB 1.00 Hz
GB 0
PC 1.40

1D NMR plot parameters
CX 22.00 cm
CY 8.00 cm
F1P 234.259 ppm
F1 17679.02 Hz
F2P -15.283 ppm
F2 -1153.37 Hz
PPMCM 11.34282 ppm/cm
HZCM 856.01782 Hz/cm

176 bebi-100218-hptpi

6e

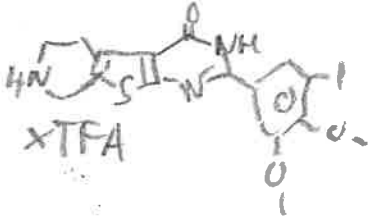

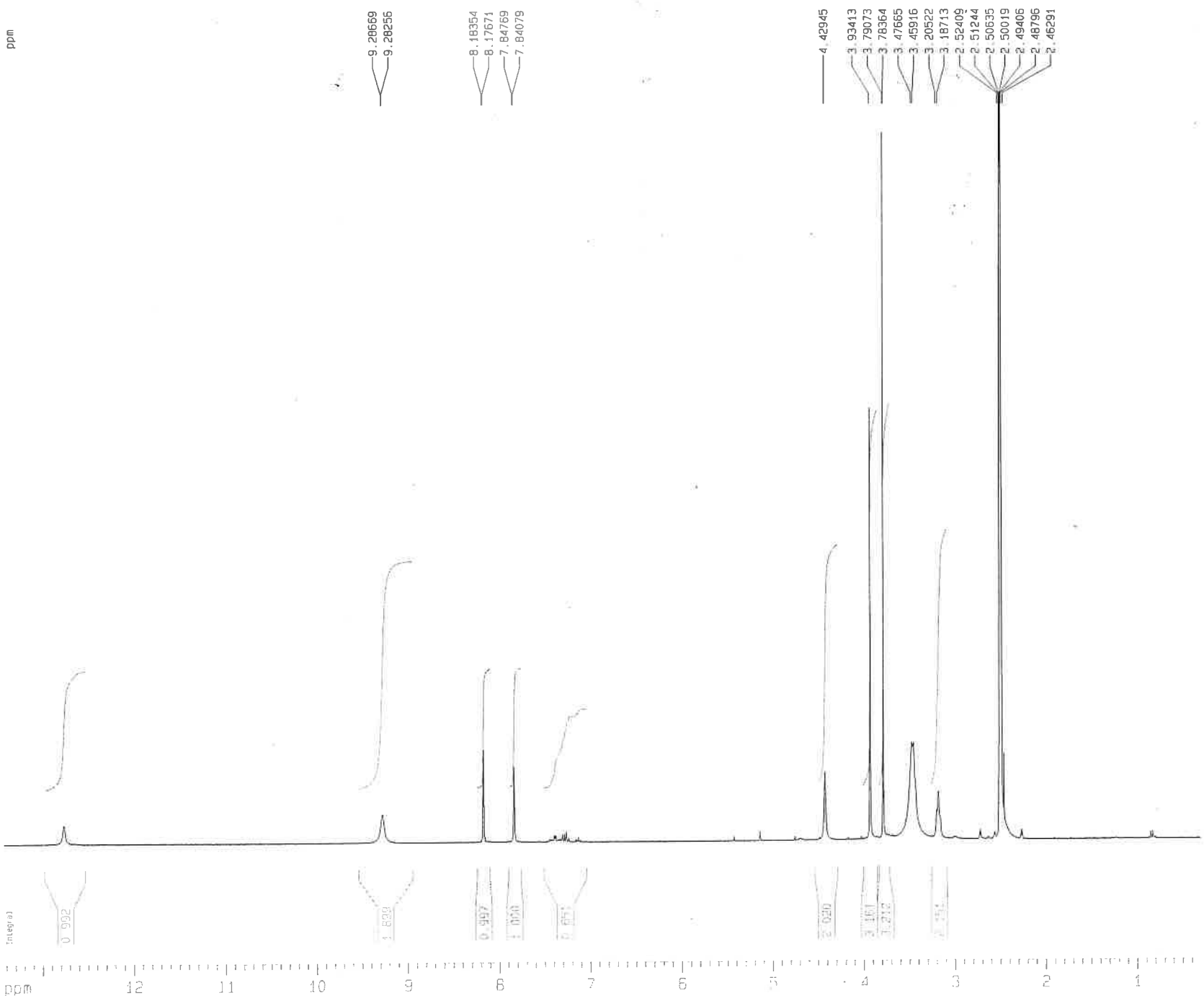

Current Data Parameters

NAME	0418bb16
EXPNO	10
PROCNO	1

F2 - Acquisition Parameters

Date_	20180212
Time	8.28
INSTRUM	spect
PROBHD	5 mm DUL 13C-1
PULPROG	zg30
TD	65536
SOLVENT	DMSO
NS	200
DS	2
SWH	8992.806 Hz
FIDRES	0.137219 Hz
AQ	3.6438515 sec
RG	1024
DW	55.600 usec
DE	7.00 usec
TE	300.0 K
D1	0.50000000 sec

======== CHANNEL f1 ========

NUC1	1H
P1	11.63 usec
PL1	-3.00 dB
SFO1	300.1318008 MHz

F2 - Processing parameters

SI	65536
SF	300.1300020 MHz
WDW	no
SSB	0
LB	0.00 Hz
GB	0
PC	1.00

1D NMR plot parameters

CX	22.00 cm
CY	30.00 cm
F1P	13.431 ppm
F1	4031.07 Hz
F2P	0.309 ppm
F2	92.74 Hz
PPMCM	0.59646 ppm/cm
HZCM	179.01540 Hz/cm

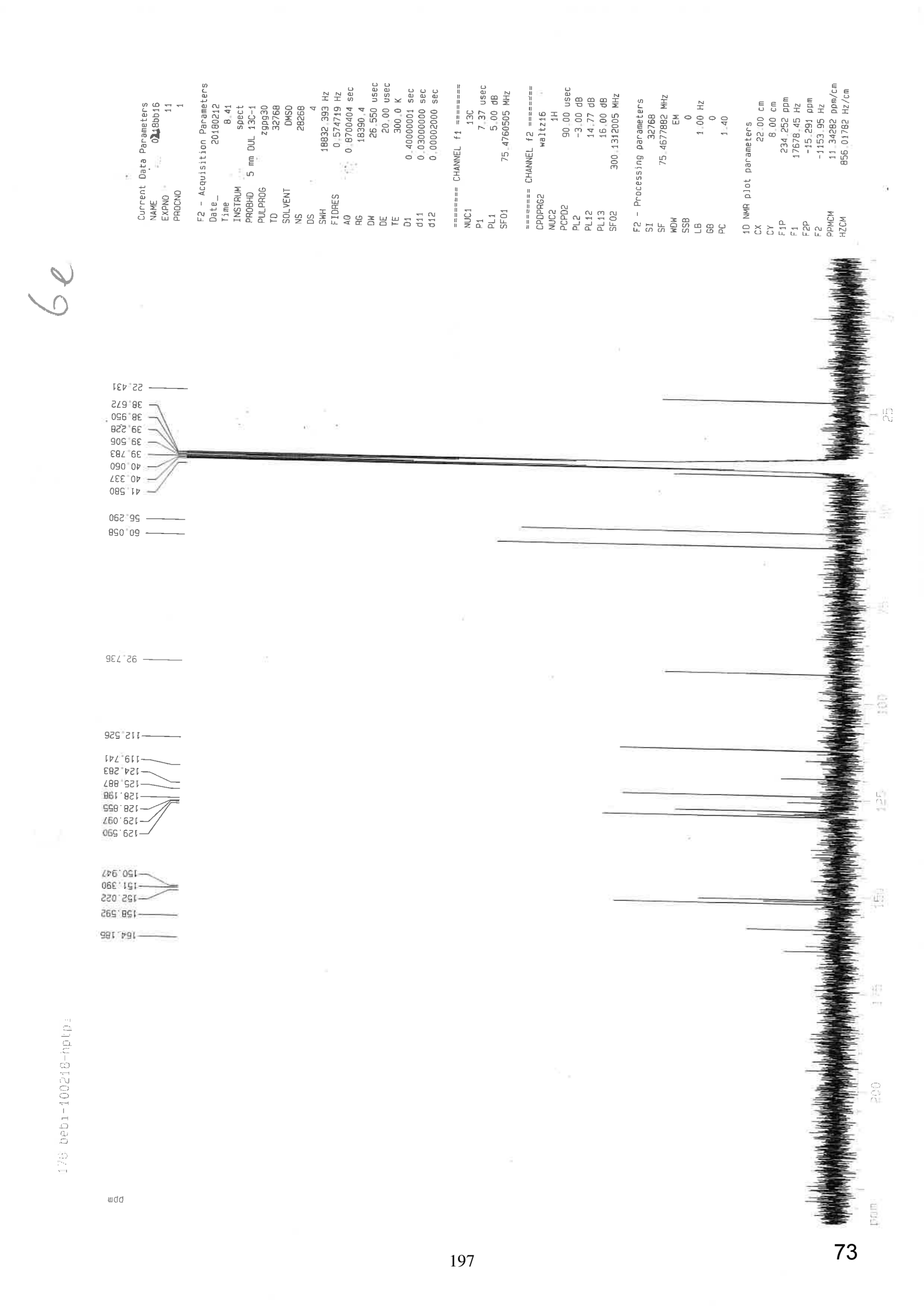
Current Data Parameters
NAME 0218b16
EXPNO 11
PROCNO 1
F2 - Acquisition Parameters
Date_ 20180212
Time 8.41
INSTRUM spect
PROBHD 5 mm DUL 13C-1
PULPROG zgpg30
TD 32768
SOLVENT DMSO
NS 28268
DS 4
SWH 18832.393 Hz
FIDRES 0.574719 Hz
AQ 0.8700404 sec
RG 18390.4
DW 26.550 usec
DE 20.00 usec
TE 300.0 K
D1 0.40000001 sec
d11 0.03000000 sec
d12 0.00002000 sec
======== CHANNEL f1 ========
NUC1 13C
P1 7.37 usec
PL1 5.00 dB
SFO1 75.4760505 MHz
======== CHANNEL f2 ========
CPDPRG2 waltz16
NUC2 1H
PCPD2 90.00 usec
PL2 -3.00 dB
PL12 14.77 dB
PL13 16.00 dB
SFO2 300.1312005 MHz
F2 - Processing parameters
SI 32768
SF 75.4677882 MHz
WDW EM
SSB 0
LB 1.00 Hz
GB 0
PC 1.40
1D NMR plot parameters
CX 22.00 cm
CY 8.00 cm
F1P 234.252 ppm
F1 17678.45 Hz
F2P -15.291 ppm
F2 -1153.95 Hz
PPMCM 11.34282 ppm/cm
HZCM 856.01782 Hz/cm
22.431
38.672
38.950
39.228
39.506
39.783
40.060
40.337
41.580
56.290
60.058
92.736
112.526
119.741
124.283
125.887
128.198
128.855
129.097
129.590
150.947
151.390
152.022
158.592
164.186
ppm

6i

104 bebi-011219-hptp3br

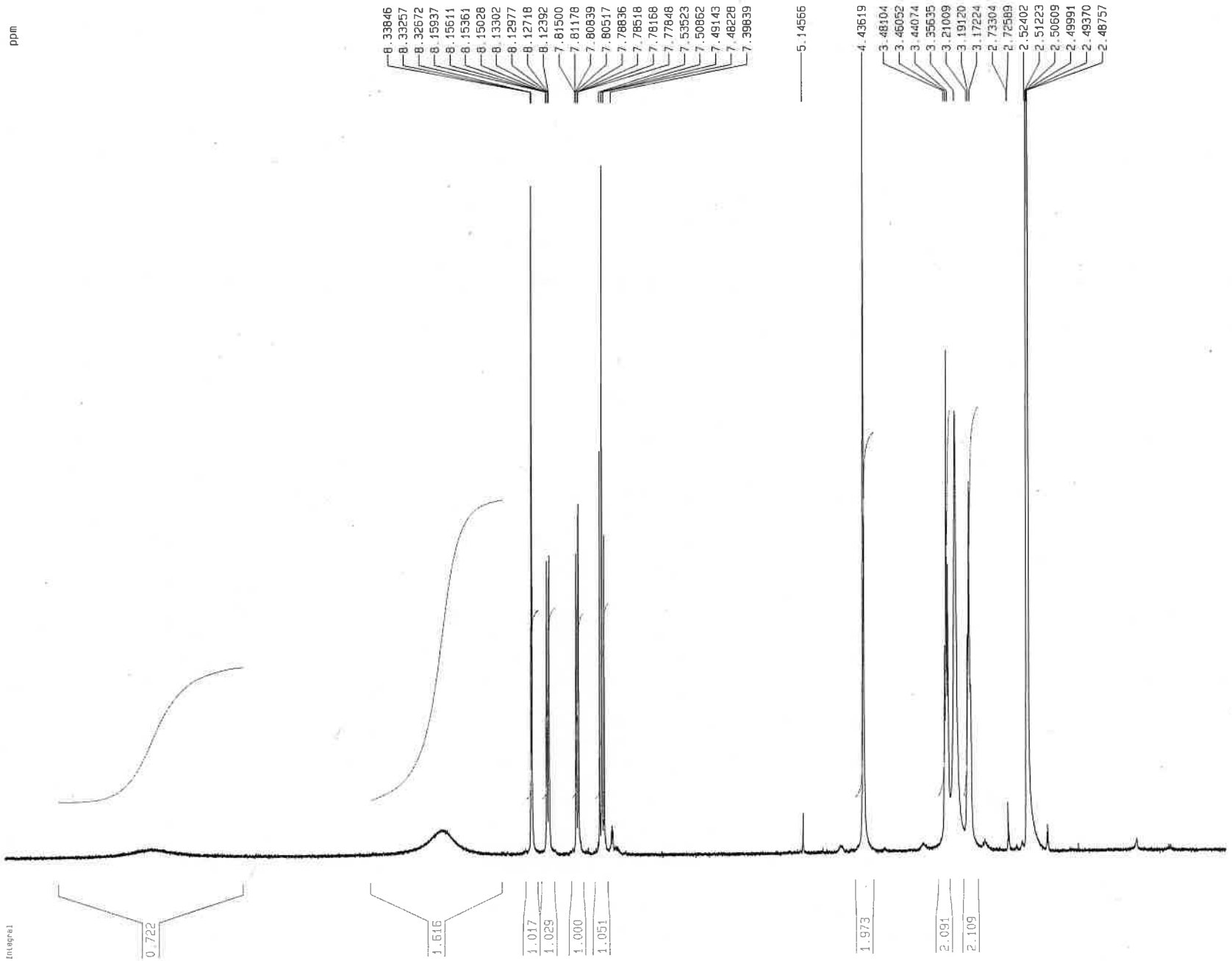

Current Data Parameters
NAME 1219bb1
EXPNO 10
PROCNO 1

F2 - Acquisition Parameters
Date_ 20191202
Time 7.22
INSTRUM. spect
PROBHD 5 mm DUL 13C-1
PULPROG zg30
TD 65536
SOLVENT DMSO
NS 200
DS 2
SWH 8992.806 Hz
FIDRES 0.137219 Hz
AQ 3.6438515 sec
RG 1149.4
DW 55.600 usec
DE 7.00 usec
TE 300.0 K
D1 0.50000000 sec

======== CHANNEL f1 ========
NUC1 1H
P1 11.63 usec
PL1 -3.00 dB
SF01 300.1318008 MHz

F2 - Processing parameters
SI 65536
SF 300.1300021 MHz
WDW no
SSB 0
LB 0.00 Hz
GB 0
PC 1.00

1D NMR plot parameters
CX 22.00 cm
CY 13.50 cm
F1P 14.520 ppm
F1 4357.80 Hz
F2P 0.176 ppm
F2 52.74 Hz
PPMCM 0.65200 ppm/cm
HZCM 195.68486 Hz/cm

6i

104 bebi-011219-hptp3br

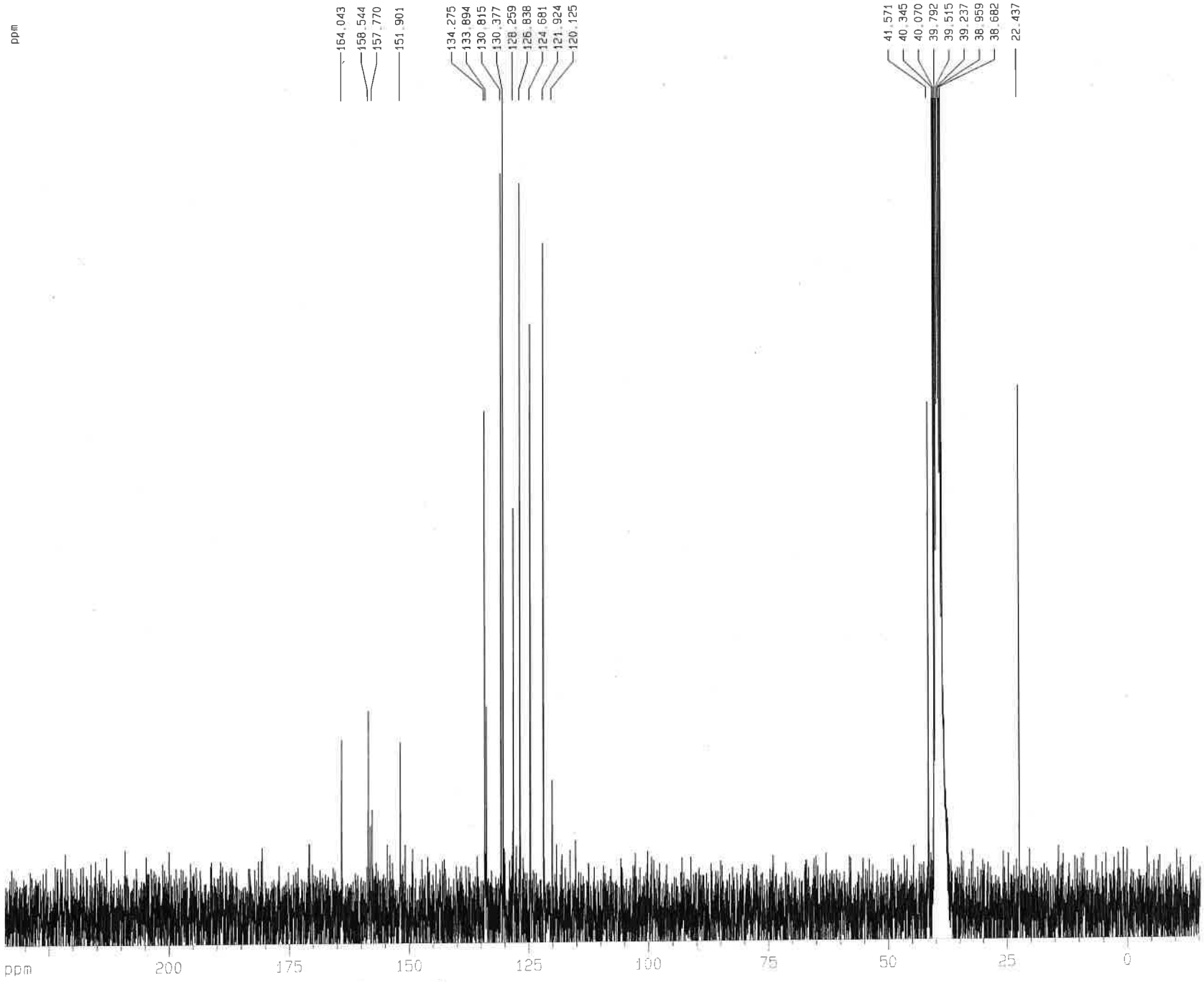

Current Data Parameters

NAME	1219bb1
EXPNO	20
PROCNO	1

F2 - Acquisition Parameters

Date_	20191202
Time	9.52
INSTRUM	spect
PROBHD	5 mm DUL 13C-1
PULPROG	zgpg30
TD	32768
SOLVENT	DMSO
NS	7276
DS	4
SWH	18832.393 Hz
FIDRES	0.574719 Hz
AQ	0.8700404 sec
RG	18390.4
DW	26.550 usec
DE	20.00 usec
TE	300.0 K
D1	0.40000001 sec
d11	0.03000000 sec
d12	0.00002000 sec

======== CHANNEL f1 ========

NUC1	13C
P1	7.37 usec
PL1	5.00 dB
SFO1	75.4760505 MHz

======== CHANNEL f2 ========

CPDPRG2	waltz16
NUC2	1H
PCPD2	90.00 usec
PL2	-3.00 dB
PL12	14.77 dB
PL13	16.00 dB
SFO2	300.1312005 MHz

F2 - Processing parameters

SI	32768
SF	75.4677871 MHz
WDW	EM
SSB	0
LB	1.00 Hz
GB	0
PC	1.40

1D NMR plot parameters

CX	22.00 cm
CY	15.00 cm
F1P	234.267 ppm
F1	17679.60 Hz
F2P	-15.275 ppm
F2	-1152.79 Hz
PPMCM	11.34282 ppm/cm
HZCM	856.01782 Hz/cm

6j

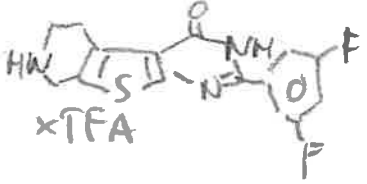

175 bebi-030218-hptp35df

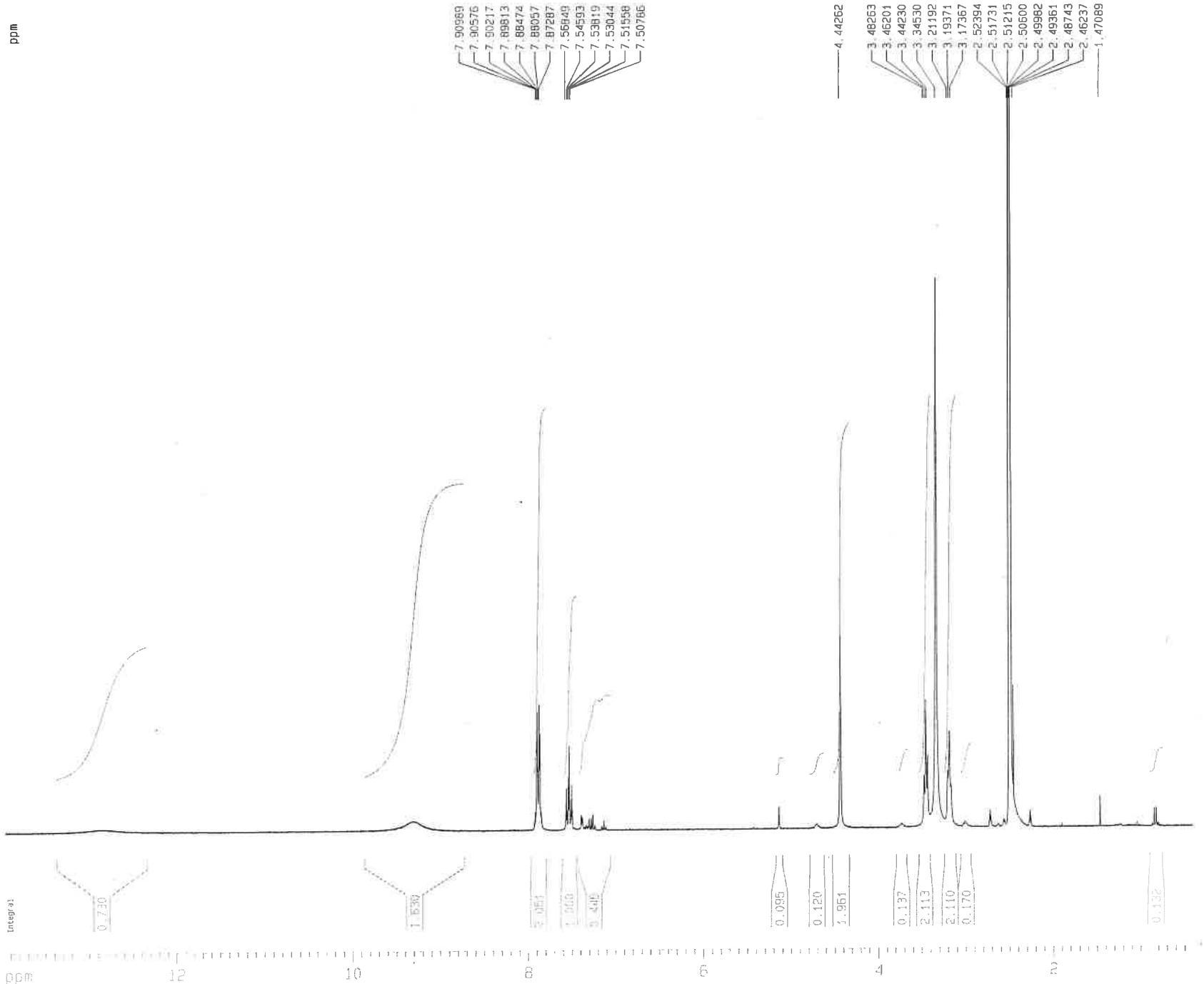

Current Data Parameters

NAME	0218bb6
EXPNO	10
PROCNO	1

F2 - Acquisition Parameters

Date_	20180205
Time	7.31
INSTRUM	spect
PROBHD	5 mm DUL 13C-1
PULPROG	zg30
TD	65536
SOLVENT	DMSO
NS	200
DS	2
SWH	8992.806 Hz
FIDRES	0.137219 Hz
AQ	3.6438515 sec
RG	1024
DW	55.600 usec
DE	7.00 usec
TE	300.0 K
D1	0.50000000 sec

======== CHANNEL f1 ========

NUC1	1H
P1	11.63 usec
PL1	-3.00 dB
SFO1	300.1318008 MHz

F2 - Processing parameters

SI	65536
SF	300.1300021 MHz
WDW	no
SSB	0
LB	0.00 Hz
GB	0
PC	1.00

1D NMR plot parameters

CX	22.00 cm
CY	50.00 cm
F1P	13.962 ppm
F1	4190.38 Hz
F2P	0.415 ppm
F2	124.49 Hz
PPMCM	0.61578 ppm/cm
HZCM	184.81346 Hz/cm

6j

175 debi-030218-hptp35at

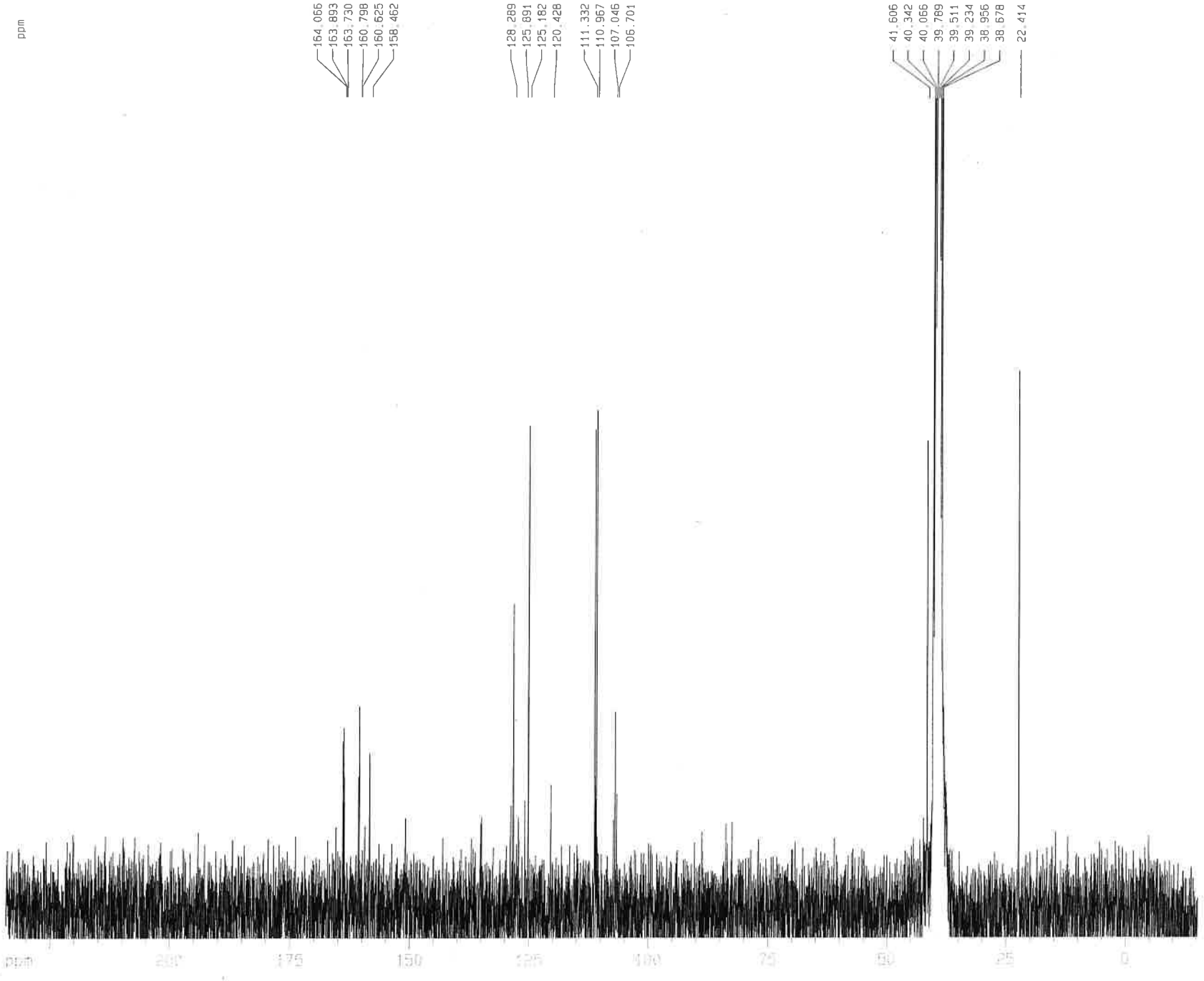

Current Data Parameters
NAME 0218bb6
EXPNO 20
PROCNO 1

F2 - Acquisition Parameters
Date_ 20180205
Time 14.06
INSTRUM spect
PROBHD 5 mm DUL 13C-1
PULPROG zgpg30
TD 32768
SOLVENT DMSO
NS 11181
DS 4
SWH 18832.393 Hz
FIDRES 0.574719 Hz
AQ 0.8700404 sec
RG 18390.4
DW 26.550 usec
DE 20.00 usec
TE 300.0 K
D1 0.40000001 sec
d11 0.03000000 sec
d12 0.00002000 sec

======== CHANNEL f1 ========
NUC1 13C
P1 7.37 usec
PL1 5.00 dB
SFO1 75.4760505 MHz

======== CHANNEL f2 ========
CPDPRG2 waltz16
NUC2 1H
PCPD2 90.00 usec
PL2 -3.00 dB
PL12 14.77 dB
PL13 16.00 dB
SFO2 300.1312005 MHz

F2 - Processing parameters
SI 32768
SF 75.4677876 MHz
WDW EM
SSB 0
LB 1.00 Hz
GB 0
PC 1.40

1D NMR plot parameters
CX 22.00 cm
CY 10.00 cm
F1P 234.259 ppm
F1 17679.02 Hz
F2P -15.283 ppm
F2 -1153.37 Hz
PPMCM 11.34282 ppm/cm
HZCM 856.01782 Hz/cm

6l

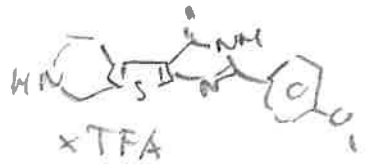

180 bebi-030318-hptparis

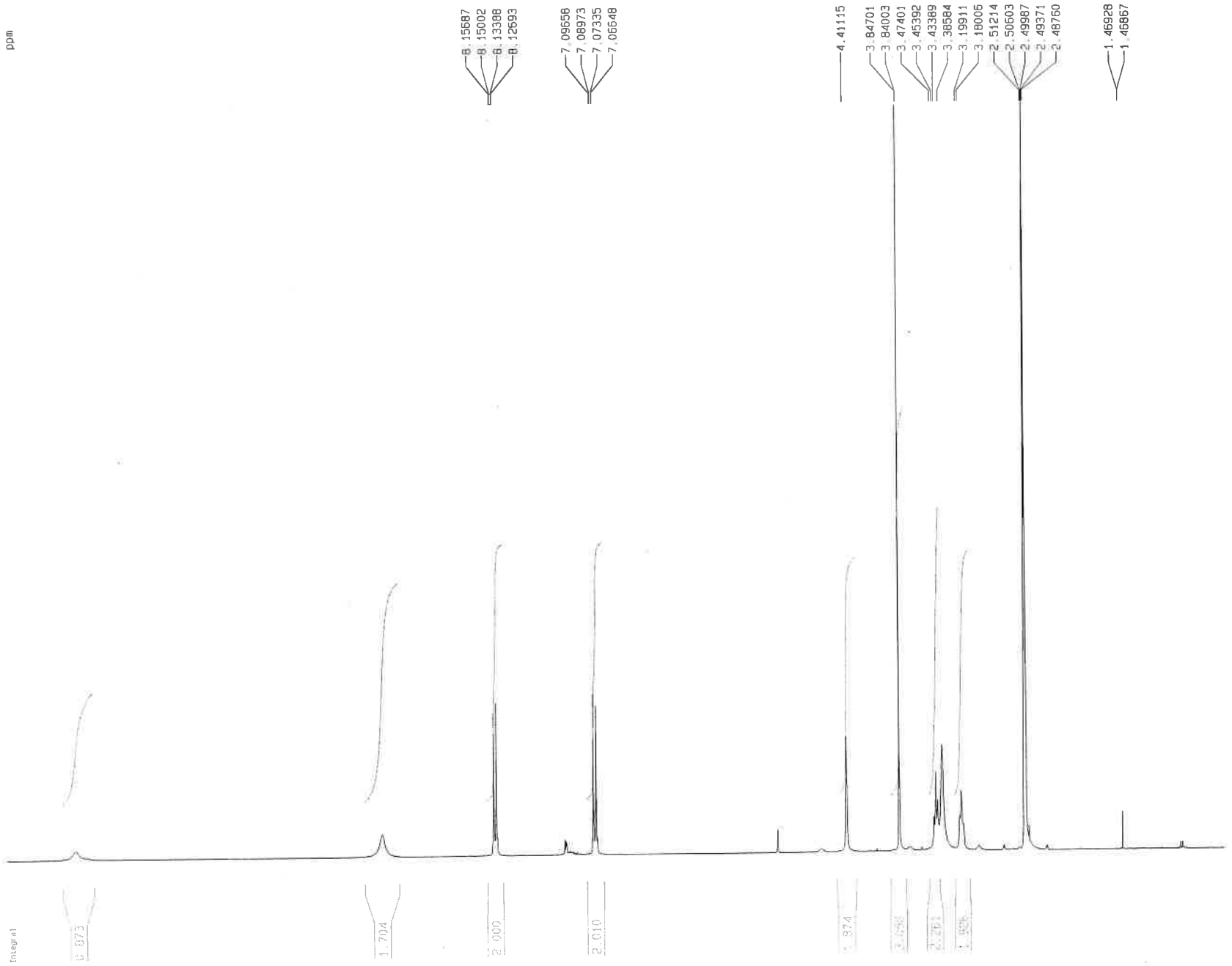

Current Data Parameters

NAME	0318bb3
EXPNO	1
PROCNO	1

F2 - Acquisition Parameters

Date_	20180305
Time	6.47
INSTRUM	spect
PROBHD	5 mm DUL 13C-1
PULPROG	zg30
TD	65536
SOLVENT	DMSO
NS	200
DS	2
SWH	8992.806 Hz
FIDRES	0.137219 Hz
AQ	3.6438515 sec
RG	812.7
DW	55.600 usec
DE	7.00 usec
TE	300.0 K
D1	0.50000000 sec

======== CHANNEL f1 ========

NUC1	1H
P1	11.63 usec
PL1	-3.00 dB
SFO1	300.1318008 MHz

F2 - Processing parameters

SI	65536
SF	300.1300021 MHz
WDW	no
SSB	0
LB	0.00 Hz
GB	0
PC	1.00

1D NMR plot parameters

CX	22.00 cm
CY	16.00 cm
F1P	13.324 ppm
F1	3999.05 Hz
F2P	0.388 ppm
F2	116.52 Hz
PPMCM	0.58801 ppm/cm
HZCM	176.47874 Hz/cm

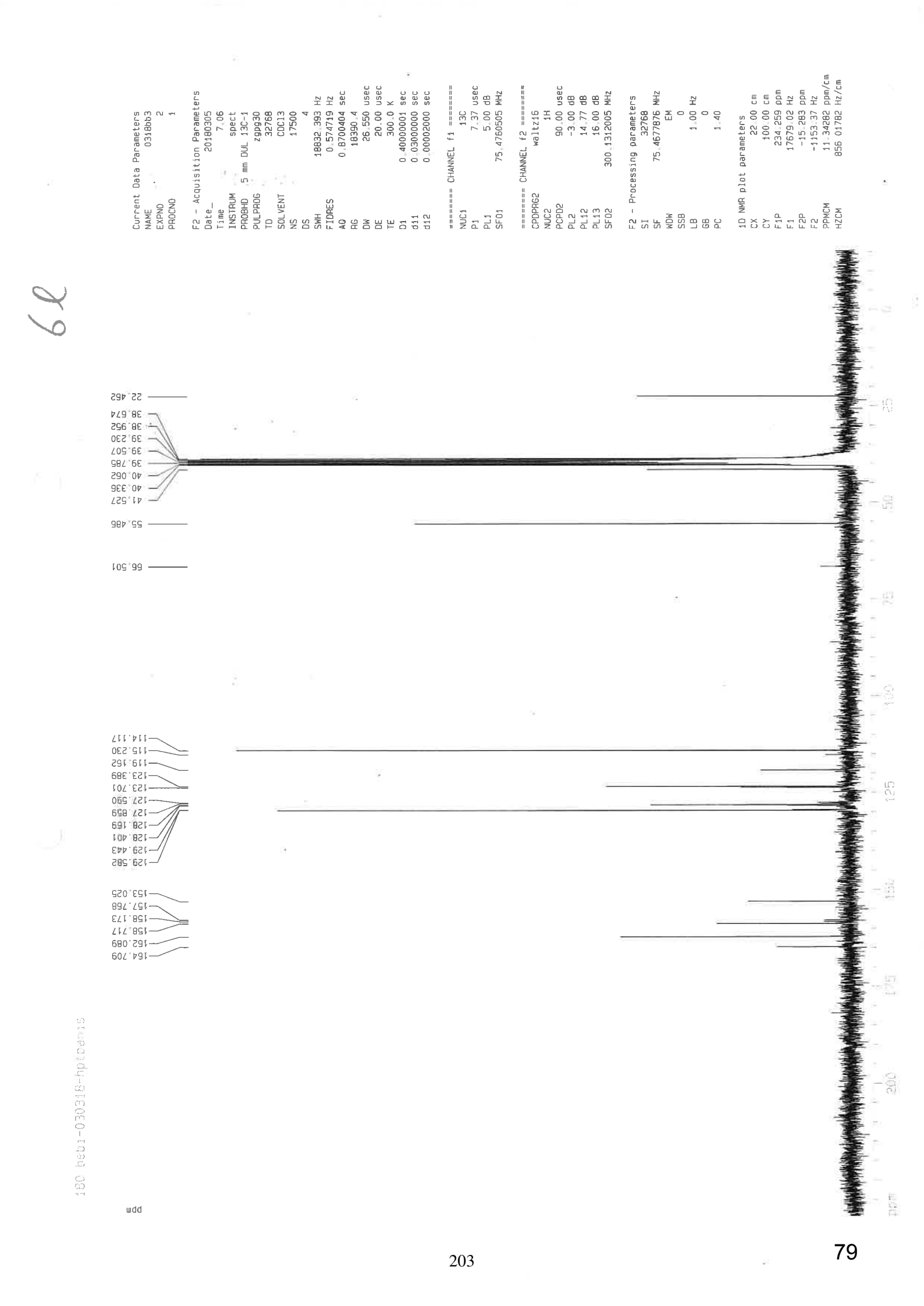
Current Data Parameters
NAME 0318bb3
EXPNO 2
PROCNO 1
F2 - Acquisition Parameters
Date_ 20180305
Time 7.06
INSTRUM spect
PROBHD 5 mm DUL 13C-1
PULPROG zgpg30
TD 32768
SOLVENT CDCl3
NS 17500
DS 4
SWH 18832.393 Hz
FIDRES 0.574719 Hz
AQ 0.8700404 sec
RG 18390.4
DW 26.550 usec
DE 20.00 usec
TE 300.0 K
D1 0.40000001 sec
d11 0.03000000 sec
d12 0.00002000 sec
======= CHANNEL f1 =======
NUC1 13C
P1 7.37 usec
PL1 5.00 dB
SFO1 75.4760505 MHz
======= CHANNEL f2 =======
CPDPRG2 waltz16
NUC2 1H
PCPD2 90.00 usec
PL2 -3.00 dB
PL12 14.77 dB
PL13 16.00 dB
SFO2 300.1312005 MHz
F2 - Processing parameters
SI 32768
SF 75.4677876 MHz
WDW EM
SSB 0
LB 1.00 Hz
GB 0
PC 1.40
1D NMR plot parameters
CX 22.00 cm
CY 100.00 cm
F1P 234.259 ppm
F1 17679.02 Hz
F2P -15.283 ppm
F2 -1153.37 Hz
PPMCM 11.34282 ppm/cm
HZCM 856.01782 Hz/cm
22.462
38.674
38.952
39.230
39.507
39.785
40.062
40.336
41.527
55.486
66.501
114.117
115.230
119.162
123.389
123.701
127.590
127.859
128.169
128.401
129.443
129.582
153.025
157.768
158.173
158.717
162.089
164.709
ppm
180 bebi-030318-npteams

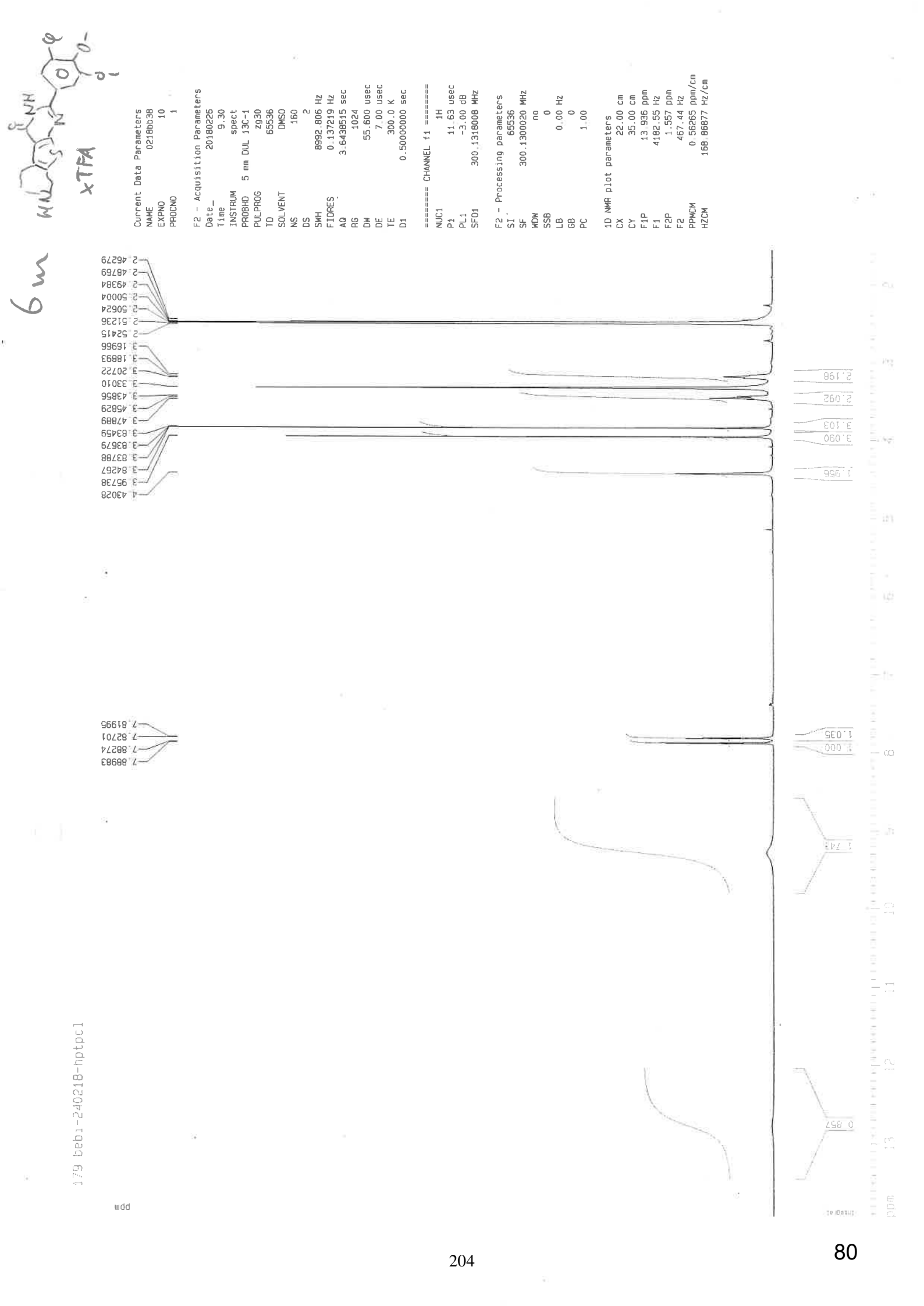
xTFA
6m
Current Data Parameters
NAME 0218bb38
EXPNO 10
PROCNO 1
F2 - Acquisition Parameters
Date_ 20180226
Time 9.30
INSTRUM spect
PROBHD 5 mm DUL 13C-1
PULPROG zg30
TD 65536
SOLVENT DMSO
NS 160
DS 2
SWH 8992.806 Hz
FIDRES 0.137219 Hz
AQ 3.6438515 sec
RG 1024
DW 55.600 usec
DE 7.00 usec
TE 300.0 K
D1 0.50000000 sec
======= CHANNEL f1 =======
NUC1 1H
P1 11.63 usec
PL1 -3.00 dB
SFO1 300.1318008 MHz
F2 - Processing parameters
SI 65536
SF 300.1300020 MHz
WDW no
SSB 0
LB 0.00 Hz
GB 0
PC 1.00
1D NMR plot parameters
CX 22.00 cm
CY 35.00 cm
F1P 13.936 ppm
F1 4182.55 Hz
F2P 1.557 ppm
F2 467.44 Hz
PPMCM 0.56265 ppm/cm
HZCM 168.86877 Hz/cm
2.46279
2.48769
2.49384
2.50004
2.50624
2.51236
2.52415
3.16966
3.18893
3.20722
3.33010
3.43856
3.45829
3.47889
3.83459
3.83679
3.83788
3.84267
3.95738
4.43028
7.80983
7.80274
7.80701
7.81995
2.198
2.092
3.103
3.090
1.956
1.035
1.000
1.747
0.857
179 bebi-240218-hptpc1
ppm

6m

179 bebi-240218-rptocl

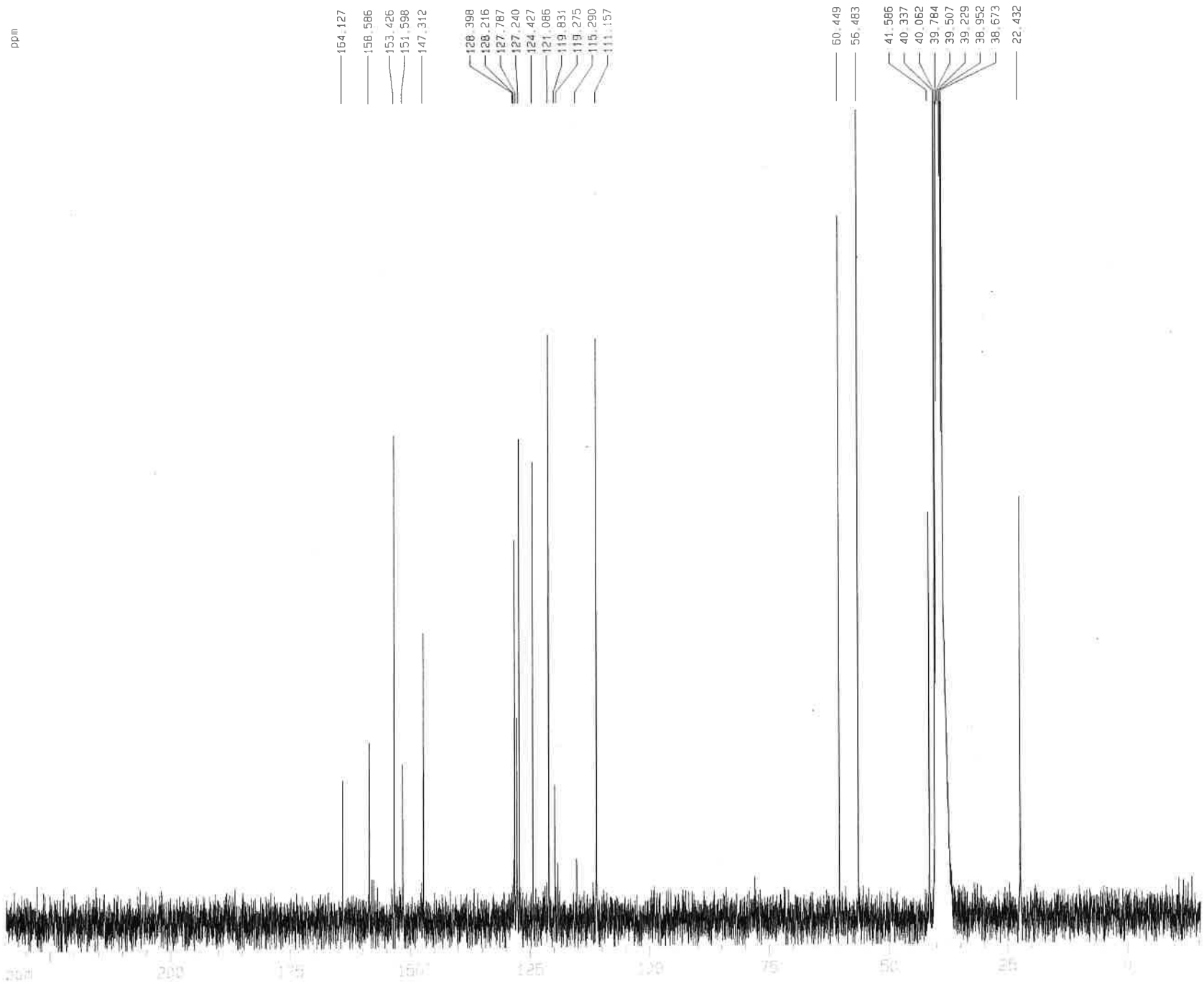

Current Data Parameters

NAME	0218bb38
EXPNO	11
PROCNO	1

F2 - Acquisition Parameters

Date_	20180226
Time	9.38
INSTRUM	spect
PROBHD	5 mm DUL 13C-1
PULPROG	zgpg30
TD	32768
SOLVENT	DMSO
NS	56548
DS	4
SWH	18832.393 Hz
FIDRES	0.574719 Hz
AQ	0.8700404 sec
RG	18390.4
DW	26.550 usec
DE	20.00 usec
TE	300.0 K
D1	0.40000001 sec
d11	0.03000000 sec
d12	0.00002000 sec

======== CHANNEL f1 ========

NUC1	13C
P1	7.37 usec
PL1	5.00 dB
SFO1	75.4760505 MHz

======== CHANNEL f2 ========

CPDPRG2	waltz16
NUC2	1H
PCPD2	90.00 usec
PL2	-3.00 dB
PL12	14.77 dB
PL13	16.00 dB
SFO2	300.1312005 MHz

F2 - Processing parameters

SI	32768
SF	75.4677882 MHz
WDW	EM
SSB	0
LB	1.00 Hz
GB	0
PC	1.40

1D NMR plot parameters

CX	22.00 cm
CY	15.00 cm
F1P	234.252 ppm
F1	17678.45 Hz
F2P	-15.291 ppm
F2	-1153.95 Hz
PPMCM	11.34282 ppm/cm
HZCM	856.01782 Hz/cm

7c

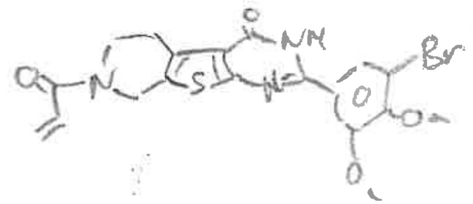

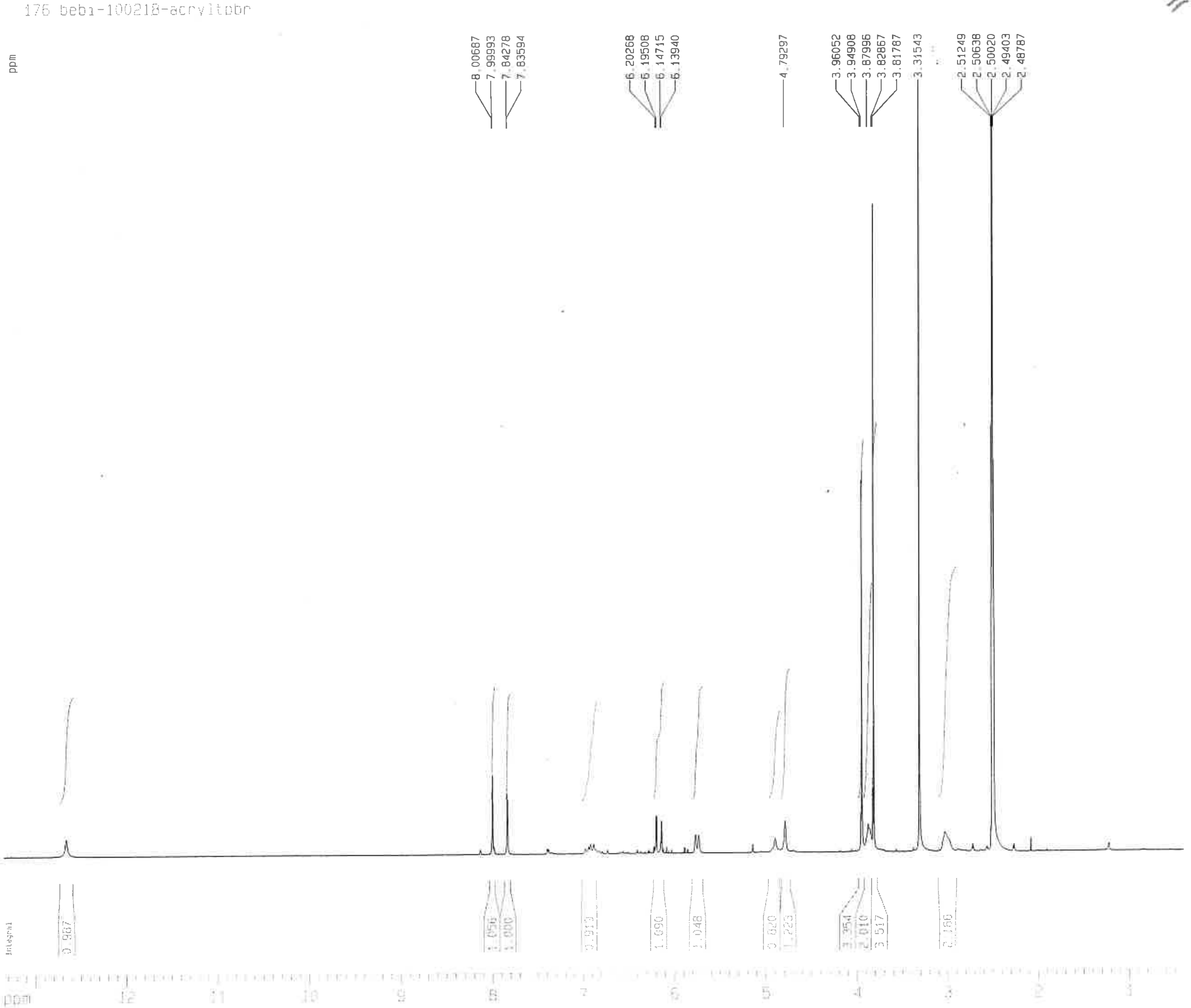

Current Data Parameters	
NAME	0418bb15
EXPNO	10
PROCNO	1
F2 - Acquisition Parameters	
Date_	20180212
Time	8.09
INSTRUM	spect
PROBHD	5 mm DUL 13C-1
PULPROG	zg30
TD	65536
SOLVENT	DMSO
NS	200
DS	2
SWH	8992.806 Hz
FIDRES	0.137219 Hz
AQ	3.6438515 sec
RG	1024
DW	55.600 usec
DE	7.00 usec
TE	300.0 K
D1	0.50000000 sec
======== CHANNEL f1 ========	
NUC1	1H
P1	11.63 usec
PL1	-3.00 dB
SFO1	300.1318008 MHz
F2 - Processing parameters	
SI	65536
SF	300.1300020 MHz
WDW	no
SSB	0
LB	0.00 Hz
GB	0
PC	1.00
1D NMR plot parameters	
CX	22.00 cm
CY	25.00 cm
F1P	13.351 ppm
F1	4007.16 Hz
F2P	0.415 ppm
F2	124.63 Hz
PPMCM	0.58801 ppm/cm
HZCM	176.47874 Hz/cm

176 bcbi-100218-acryltabb

7c

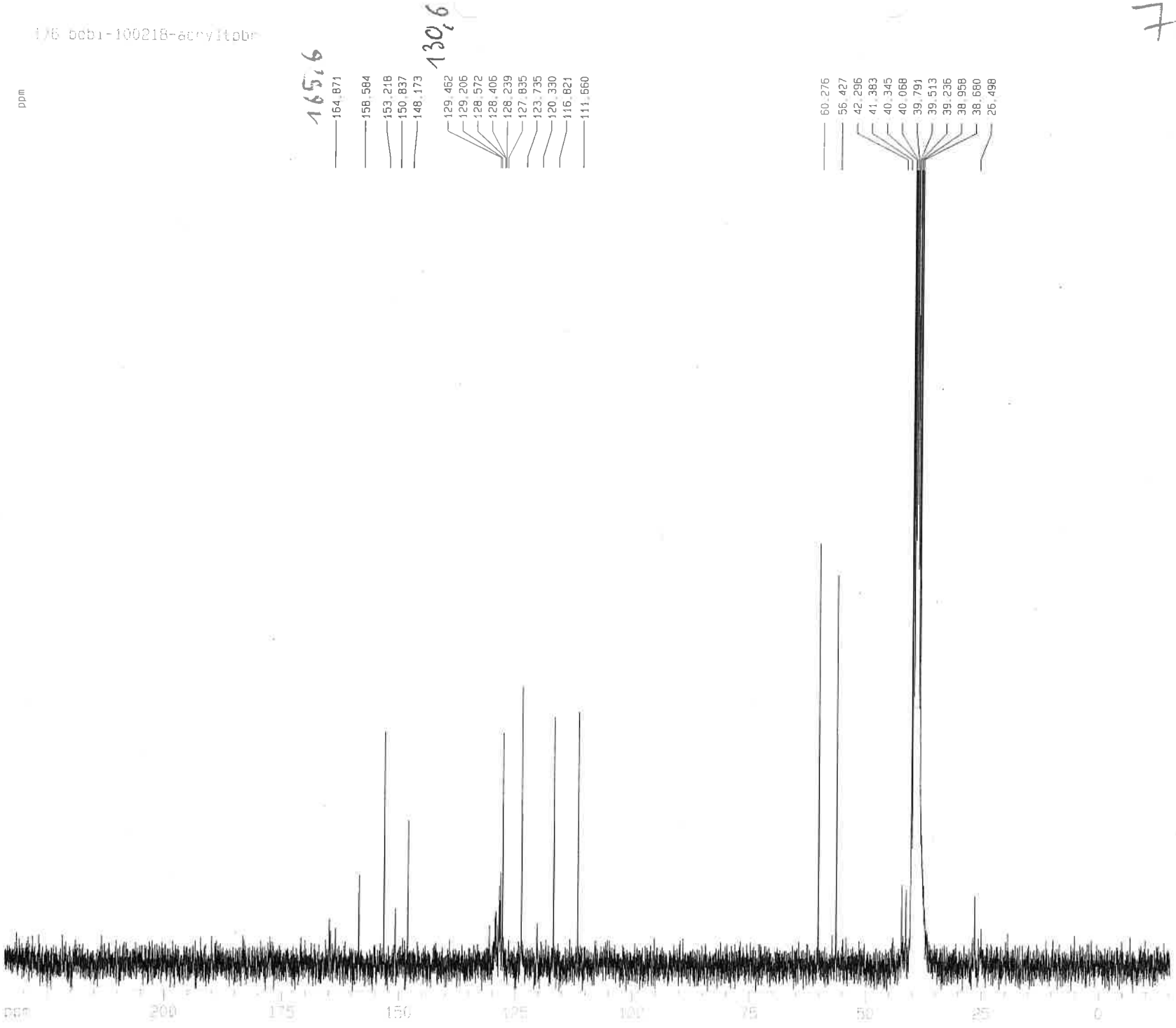

Current Data Parameters
NAME 0218bb15
EXPNO 20
PROCNO 1

F2 - Acquisition Parameters
Date_ 20180213
Time 4.45
INSTRUM spect
PROBHD 5 mm DUL 13C-1
PULPROG zgpg30
TD 32768
SOLVENT DMSO
NS 28268
DS 4
SWH 18832.393 Hz
FIDRES 0.574719 Hz
AQ 0.8700404 sec
RG 18390.4
DW 26.550 usec
DE 20.00 usec
TE 300.0 K
D1 0.40000001 sec
d11 0.03000000 sec
d12 0.00002000 sec

======== CHANNEL f1 ========
NUC1 13C
P1 7.37 usec
PL1 5.00 dB
SFO1 75.4760505 MHz

======== CHANNEL f2 ========
CPDPRG2 waltz16
NUC2 1H
PCPD2 90.00 usec
PL2 -3.00 dB
PL12 14.77 dB
PL13 16.00 dB
SFO2 300.1312005 MHz

F2 - Processing parameters
SI 32768
SF 75.4677876 MHz
WDW EM
SSB 0
LB 1.00 Hz
GB 0
PC 1.40

1D NMR plot parameters
CX 22.00 cm
CY 8.00 cm
F1P 234.259 ppm
F1 17679.02 Hz
F2P -15.283 ppm
F2 -1153.37 Hz
PPMCM 11.34282 ppm/cm
HZCM 856.01782 Hz/cm

12,65

8,16
7,83
6,8-7,0
6,16 d J=15,3Hz
5,5-5,8
4,7-4,9
3,92-3,99
3,77
2,9-3,1
2,72
2,59

7e

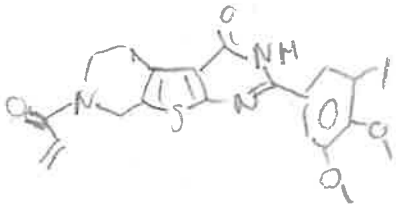

SpinWorks 3: no title

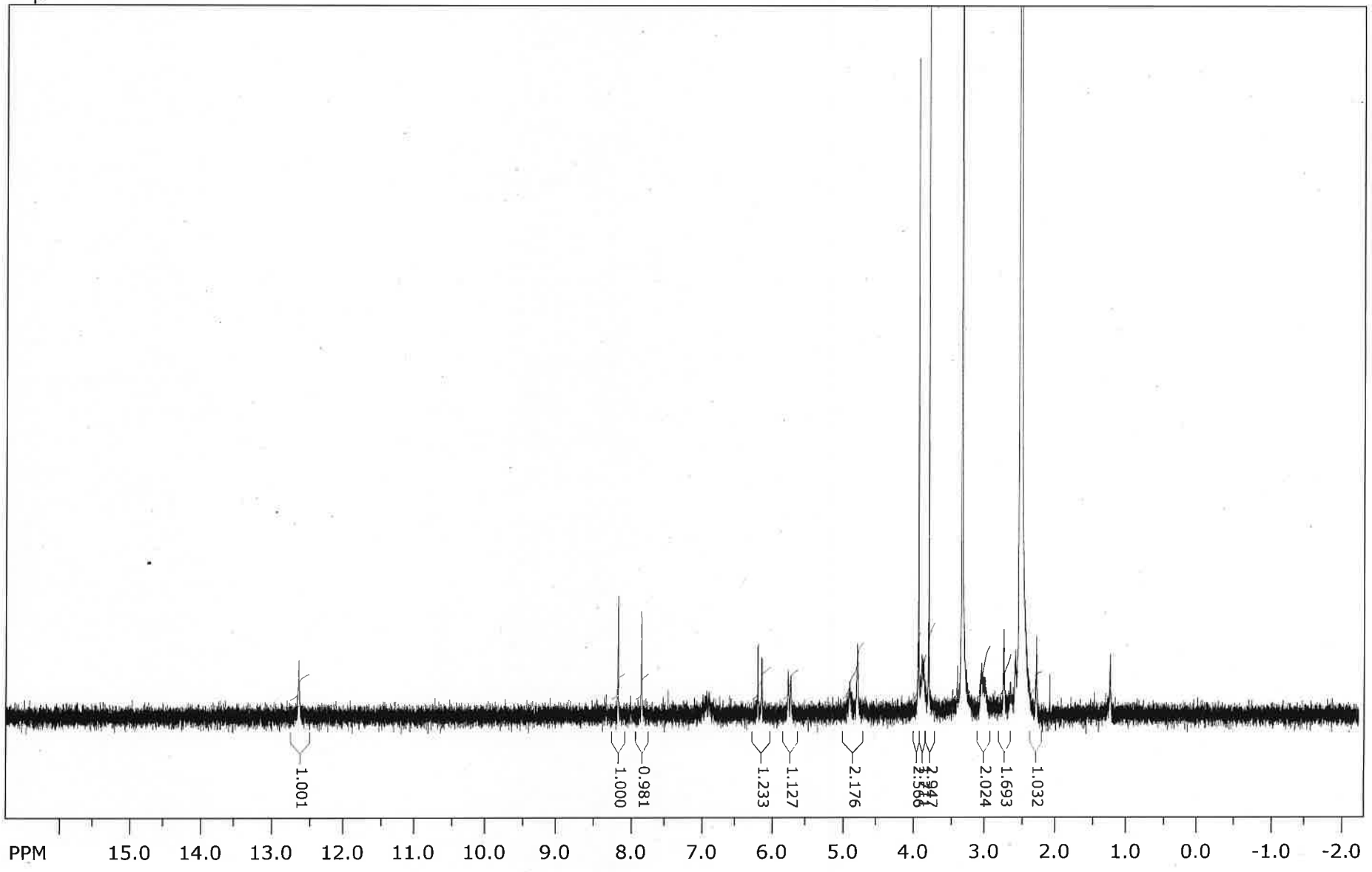

file: C:\bebi090518acryltpi\1\fid expt: <zg30>
transmitter freq.: 300.131801 MHz

DMSO

freq. of 0 ppm: 300.130005 MHz
processed size: 65536 complex points

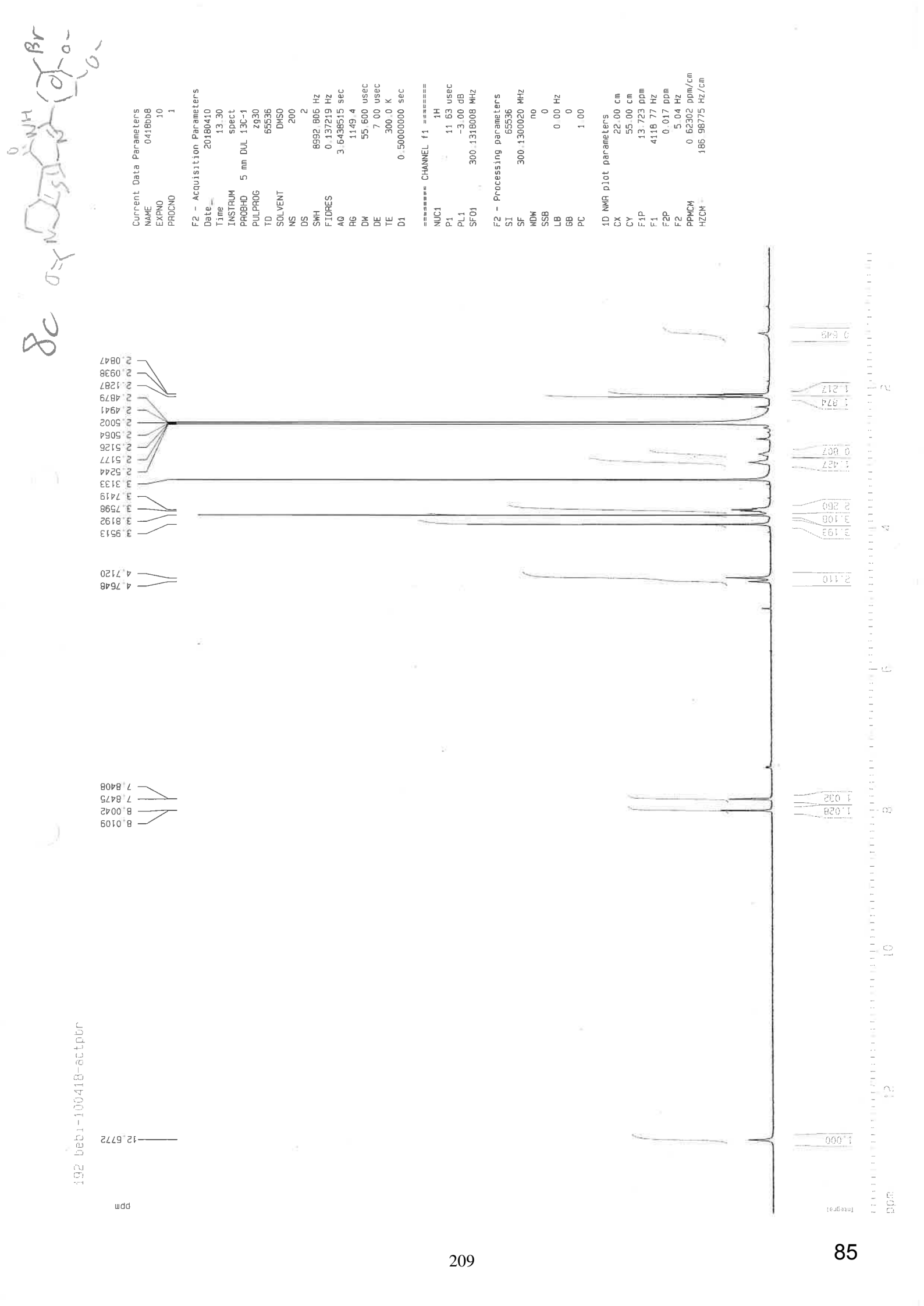
Current Data Parameters
NAME 0418bd8
EXPNO 10
PROCNO 1
F2 - Acquisition Parameters
Date_ 20180410
Time 13.30
INSTRUM spect
PROBHD 5 mm DUL 13C-1
PULPROG zg30
TD 65536
SOLVENT DMSO
NS 200
DS 2
SWH 8992.806 Hz
FIDRES 0.137219 Hz
AQ 3.6438515 sec
RG 1149.4
DW 55.600 usec
DE 7.00 usec
TE 300.0 K
D1 0.50000000 sec
======== CHANNEL f1 ========
NUC1 1H
P1 11.63 usec
PL1 -3.00 dB
SFO1 300.1318008 MHz
F2 - Processing parameters
SI 65536
SF 300.1300020 MHz
WDW no
SSB 0
LB 0.00 Hz
GB 0
PC 1.00
1D NMR plot parameters
CX 22.00 cm
CY 55.00 cm
F1P 13.723 ppm
F1 4118.77 Hz
F2P 0.017 ppm
F2 5.04 Hz
PPMCM 0.62302 ppm/cm
HZCM 186.98775 Hz/cm
2.0847
2.0938
2.1287
2.4879
2.4941
2.5002
2.5064
2.5126
2.5177
2.5244
3.3133
3.7419
3.7598
3.8192
3.9513
4.7120
4.7648
7.8408
7.8475
8.0042
8.0109
12.6772
192 beb-180418-actpbr
ppm
Integral

192 bec1-100418-actpbr
addfid 11+20

8c

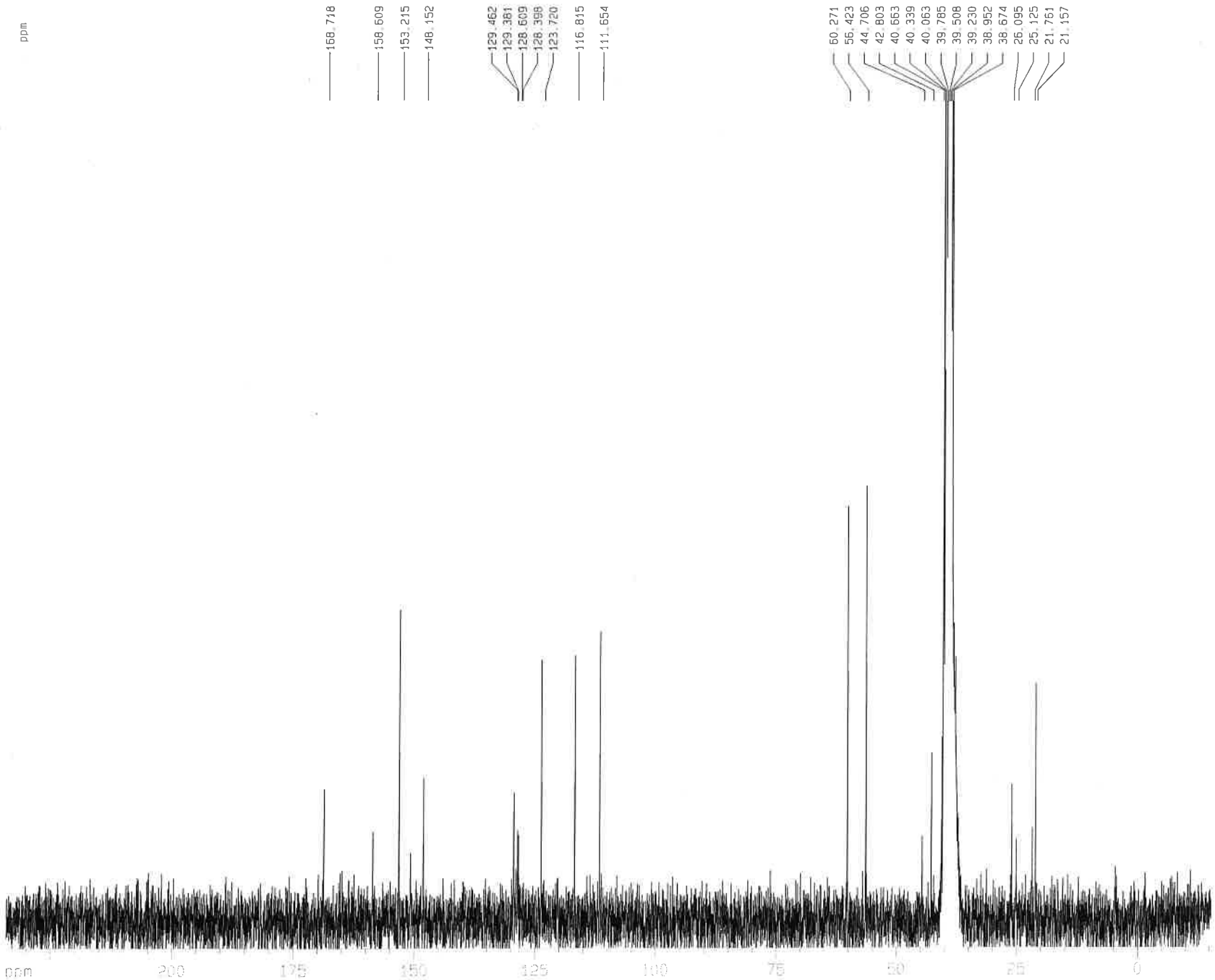

Current Data Parameters
NAME 0418bb8
EXPNO 21
PROCNO 1

F2 - Acquisition Parameters
Date_ 20180410
Time 13.50
INSTRUM spect
PROBHD 5 mm DUL 13C-1
PULPROG zgpg30
TD 32768
SOLVENT DMSO
NS 5916
DS 4
SWH 18832.393 Hz
FIDRES 0.574719 Hz
AQ 0.8700404 sec
RG 18390.4
DW 26.550 usec
DE 20.00 usec
TE 300.0 K
D1 0.40000001 sec
d11 0.03000000 sec
d12 0.00002000 sec
NUC1 13C
P1 7.37 usec
PL1 5.00 dB
SFO1 75.4760505 MHz
CPDPRG2 waltz16
NUC2 1H
PCPD2 90.00 usec
PL2 -3.00 dB
PL12 14.77 dB
PL13 16.00 dB
SFO2 300.1312005 MHz

F2 - Processing parameters
SI 32768
SF 75.4677882 MHz
WDW EM
SSB 0
LB 1.00 Hz
GB 0
PC 1.40

1D NMR plot parameters
CX 22.00 cm
CY 8.00 cm
F1P 234.252 ppm
F1 17678.45 Hz
F2P -15.291 ppm
F2 -1153.95 Hz
PPMCM 11.34282 ppm/cm
HZCM 856.01782 Hz/cm

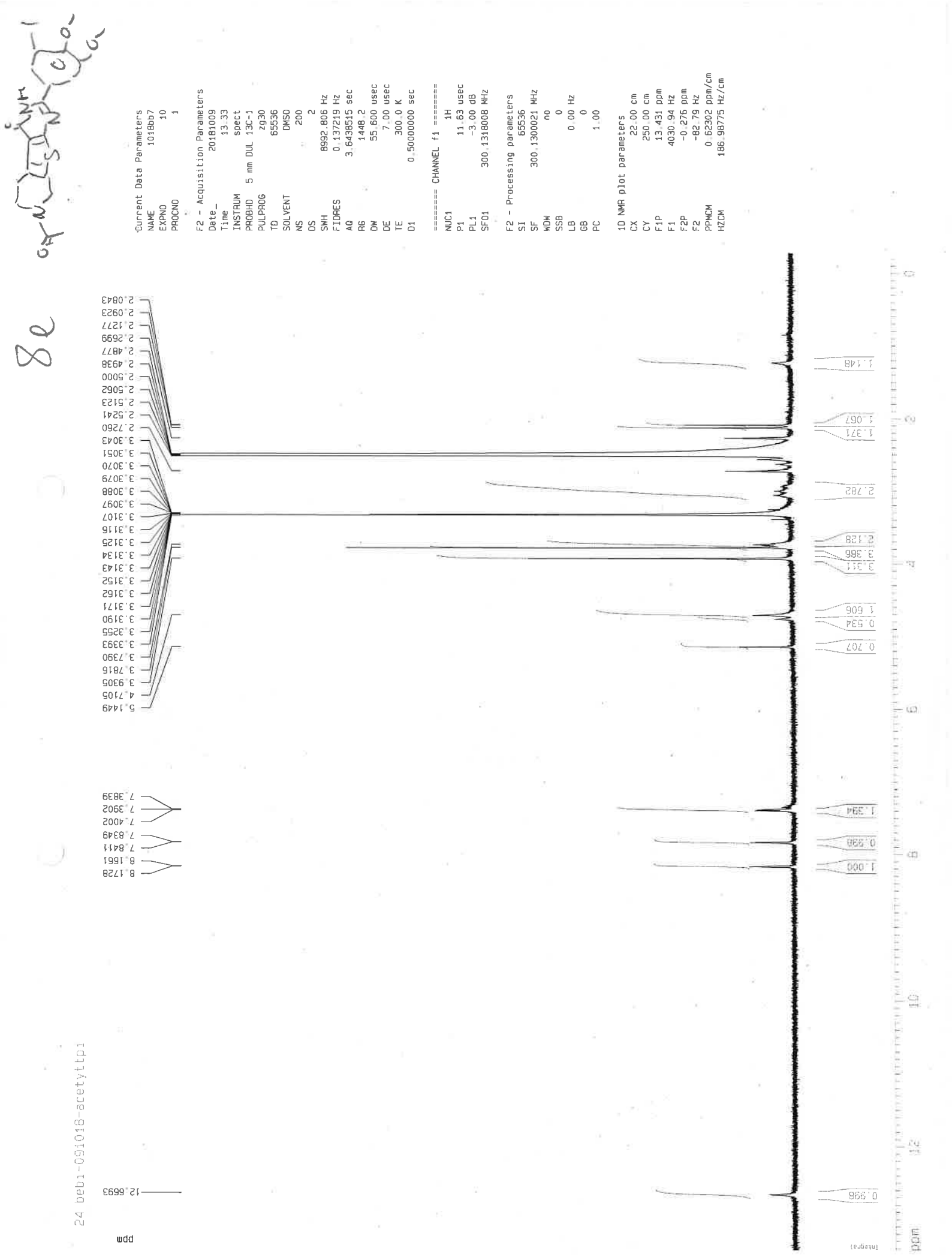
8e
Current Data Parameters
NAME 1018bb7
EXPNO 10
PROCNO 1
F2 - Acquisition Parameters
Date_ 20181009
Time 13.33
INSTRUM spect
PROBHD 5 mm DUL 13C-1
PULPROG zg30
TD 65536
SOLVENT DMSO
NS 200
DS 2
SWH 8992.806 Hz
FIDRES 0.137219 Hz
AQ 3.6438515 sec
RG 1448.2
DW 55.600 usec
DE 7.00 usec
TE 300.0 K
D1 0.50000000 sec
======== CHANNEL f1 ========
NUC1 1H
P1 11.63 usec
PL1 -3.00 dB
SFO1 300.1318008 MHz
F2 - Processing parameters
SI 65536
SF 300.1300021 MHz
WDW no
SSB 0
LB 0.00 Hz
GB 0
PC 1.00
1D NMR plot parameters
CX 22.00 cm
CY 250.00 cm
F1P 13.431 ppm
F1 4030.94 Hz
F2P -0.276 ppm
F2 -82.79 Hz
PPMCM 0.62302 ppm/cm
HZCM 186.98775 Hz/cm
2.0843
2.0923
2.1277
2.2699
2.4877
2.4938
2.5000
2.5062
2.5123
2.5241
2.7260
3.3043
3.3051
3.3070
3.3079
3.3088
3.3097
3.3107
3.3116
3.3125
3.3134
3.3143
3.3152
3.3162
3.3171
3.3190
3.3255
3.3393
3.7390
3.7816
3.9305
4.7105
5.1449
7.3839
7.3902
7.4002
7.8349
7.8411
8.1661
8.1728
12.5693
1.148
1.067
1.371
2.782
2.128
3.386
3.311
1.606
0.534
0.707
1.394
0.998
1.000
0.996
24 bebi-091018-acetyttpi
ppm
Integral

5.5. Publikation IV

Guided Antitumoral Drugs: (Imidazol-2-ylidene)(L)goldI Complexes Seeking Cellular Targets Controlled by the Nature of Ligand L

Sofia I. Bär, Madeleine Gold, Sebastian W. Schleser, Tobias Rehm, Alexander Bär, Leonhard Köhler, Lucas R. Carnell, Bernhard Biersack, Rainer Schobert*

Organic Chemistry Laboratory, University of Bayreuth, Universitaetsstrasse 30, 95440 Bayreuth, Germany

* Corresponding author, Email address: Rainer.Schobert@uni-bayreuth.de

Chemistry **2021,** 27, 5003-5010.

Reprinted with permission from Chemistry – A European Journal published by Wiley-VCH GmbH 2020, 27, 5003, *Guided Antitumoral Drugs: (Imidazol-2-ylidene)(L)gold I Complexes Seeking Cellular Targets Controlled by the Nature of Ligand L.* S.I. Bär, M. Gold, S.W. Schleser, T. Rehm, A. Bär, L. Köhler, L.R. Carnell, B. Biersack, R. Schobert. Doi: 10.1002/chem.202005451.

Ligand Effects

Guided Antitumoural Drugs: (Imidazol-2-ylidene)(L)gold(I) Complexes Seeking Cellular Targets Controlled by the Nature of Ligand L

Sofia I. Bär[+], Madeleine Gold[+], Sebastian W. Schleser, Tobias Rehm, Alexander Bär, Leonhard Köhler, Lucas R. Carnell, Bernhard Biersack, and Rainer Schobert*[a]

Abstract: Three [1,3-diethyl-4-(*p*-methoxyphenyl)-5-(3,4,5-trimethoxyphenyl)imidazol-2-ylidene](L)gold(I) complexes, **4a** (L = Cl), **5a** (L = PPh_3), and **6a** (L = same N-heterocyclic carbene (NHC)), and their fluorescent [4-(anthracen-9-yl)-1,3-diethyl-5-phenylimidazol-2-ylidene](L)gold(I) analogues, **4b**, **5b**, and **6b**, respectively, were studied for their localisation and effects in cancer cells. Despite their identical NHC ligands, the last three accumulated in different compartments of melanoma cells, namely, the nucleus (**4b**), mitochondria (**5b**), or lysosomes (**6b**). Ligand L was also more decisive for the site of accumulation than the NHC ligand because the couples **4a**/**4b**, **5a**/**5b**, and **6a**/**6b**, carrying different NHC ligands, afforded similar results in cytotoxicity tests, and tests on targets typically found at their sites of accumulation, such as DNA in nuclei, reactive oxygen species and thioredoxin reductase in mitochondria, and lysosomal membranes. Regardless of the site of accumulation, cancer cell apoptosis was eventually induced. The concept of guiding a bioactive complex fragment to a particular subcellular target by secondary ligand L could reduce unwanted side effects.

Introduction

Although N-heterocyclic carbene (NHC) complexes have been much used as catalysts, their medicinal relevance was recognised surprisingly late, given their chemical stability under physiological conditions and their structural flexibility.[1,2] Unlike cisplatin (CDDP) and related platinum coordination complexes, which all lead to DNA adducts, resulting in an inhibition of the cancer cell cycle and eventually in apoptotic cancer cell death,[3] NHC complexes of various metals may address a broader array of molecular targets. Complexes with the character of delocalised lipophilic cations (DLCs) were found to selectively accumulate in mitochondria, which can be explained by their negative inner transmembrane potential.[4,5] Because cancer cells have a more hyperpolarised mitochondrial membrane potential (MMP) than normal cells, the selective accumulation of metal–carbene complexes with DLC character in cancer cells can be expected.[5,6] With the detection of antitumour activity of the antirheumatic gold(I) compound auranofin, (2,3,4,6-tetra-*O*-acetyl-1-thio-β-D-glucopyranosato)(triethylphosphane)gold, gold complexes came to the fore as potential anticancer drug candidates.[7] Auranofin mainly acts through the inhibition of mitochondrial thioredoxin reductase (TrxR) and by enhancing the mitochondrial permeability.[8,9] Through the inhibition of TrxR activity, the intracellular levels of reactive oxygen species (ROS) rise, which damages predominantly cancer cells because of their elevated ROS levels compared with healthy cells.[10] As a result, cytochrome c is released into the cytosol, triggering apoptotic cell death.[11] Due to their stability, NHC ligands can also be annulated and substituted in multifarious ways, allowing the mimicking or combinatorial attachment of pharmacophores to afford pleiotropic drugs.[12] Herein, we report on NHC gold(I) complexes **4a**–**6a**, carrying a 1,3-diethyl-4-(4-methoxyphenyl)-5-(3,4,5-trimethoxyphenyl)imidazol-2-ylidene ligand, akin to the natural antimitotic combretastatin A4 (CA-4), and differing only in the second ligand on the gold atom (Scheme 1). Preliminary studies had shown strong cytotoxicity against cancer cells with IC_{50} values in the low triple- to double-digit nanomolar range for complex **6a**, but its actual mechanism of action remained unclear.[13] A second series of complexes **4b**–**6b**, bearing the same "second ligands L", yet a better detectable fluorescent 1,3-diethyl-4-(anthracen-9-yl)-5-phenylimidazol-2-ylidene ligand, were synthesised and studied for their intracellular accumulation and their modes of anticancer action. The aim of this study was to find out whether ligand L could be used to set the site of accumulation, and thus, the targets and nature of antitumour effects of gold complexes with identical or closely related NHC li-

[a] S. I. Bär,[+] M. Gold,[+] S. W. Schleser, Dr. T. Rehm, A. Bär, L. Köhler, L. R. Carnell, Dr. B. Biersack, Prof. Dr. R. Schobert
Organic Chemistry Laboratory, University Bayreuth
Universitaetsstr. 30, 95447 Bayreuth (Germany)
E-mail: Rainer.Schobert@uni-bayreuth.de

[+] These authors contributed equally to this work.

Supporting information and the ORCID identification numbers for the authors of this article can be found under: https://doi.org/10.1002/chem.202005451.

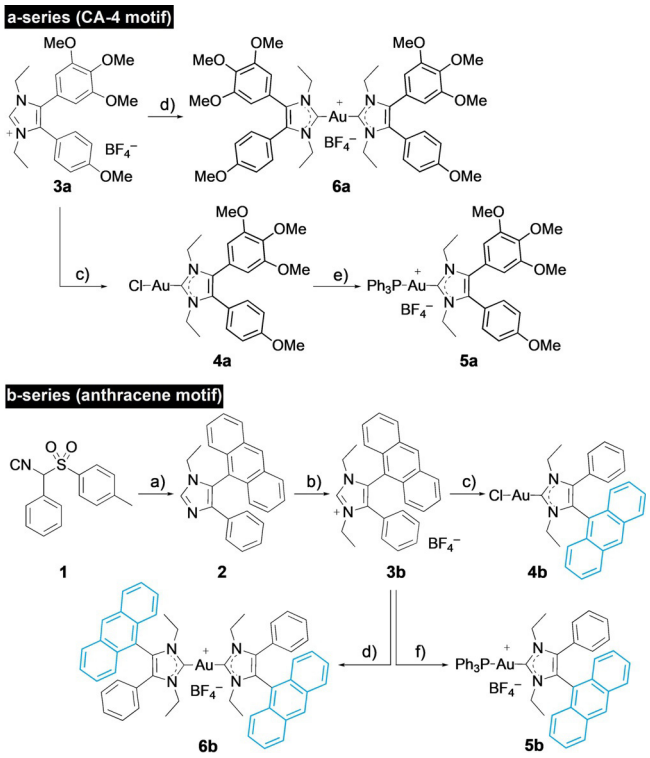

Scheme 1. Syntheses of complexes **4**–**6**: a) 9-formylanthracene, $EtNH_2$/THF, AcOH, EtOH, reflux, 2 h, then **1**, K_2CO_3, reflux 6 h, 61%; b) 1) EtI, MeCN, reflux, 48 h; 2) $NaBF_4$, acetone, RT, 1 h, 95%; c) Ag_2O (0.5 equiv), CH_2Cl_2, RT, 5 h, then $[AuCl(SMe_2)]$ (1 equiv), LiCl, RT, 24 h, 92%; d) Ag_2O (0.5 equiv), CH_2Cl_2, RT, 5 h, then $[AuCl(SMe_2)]$ (0.5 equiv), RT, 24 h, 88%; e) PPh_3, $NaBF_4$, CH_2Cl_2, RT, 24 h, 79%; f) $[AuCl(PPh_3)]$, KO*t*Bu, CH_2Cl_2, RT, 24 h, 70%.

gands. This was particularly tempting because similar *cis*-[{bis(1,3-dibenzylimidazol-2-ylidene)Cl(L)}Pt^{II}] complexes were previously shown by us to always accumulate in mitochondria, regardless of the charge of the complex and nature of ligands L.[14] Likewise, Ott et al. reported a triad of (1,3-diethylbenzimidazol-2-ylidene)(L)gold(I) complexes with the same ligands (L = Cl, PPh_3, NHC), which all localised in the mitochondria, albeit to different degrees.[15]

Results and Discussion

Synthesis

The new gold(I) NHC complexes were prepared from imidazolium salts **3a** and **3b** (Scheme 1). Compound **3b** was synthesised analogously to known compound **3a** by the van Leusen reaction of toluenesulfonylmethyl isocyanide (TosMIC) reagent **1** with 9-formylanthracene, followed by N-alkylation and anion exchange of the resulting imidazole **2**. Reactions of **3a** and **3b** with Ag_2O and transmetalation of the corresponding silver carbene complexes with different amounts of $[AuCl(SMe_2)]$ afforded mono- and bis-carbene gold(I) complexes **4a/b** and **6a/b** analogously to literature procedures.[12,13] New cationic complex **5a** was prepared by the reaction of complex **4a** with triphenylphosphane. Complex **5b** was obtained by diprotonation of **3b** and reaction of the free carbene with $[AuCl(PPh_3)]$. The stability of all complexes **4**–**6** in aqueous solution was ascertained by ^{1}H NMR spectroscopic monitoring over a period of 72 h (see the Supporting Information).

Cytotoxicity against cancer cells

All complexes **4**–**6** had an antiproliferative effect, with IC_{50} values in the three-digit nanomolar to low double-digit micromolar range, on cells of the human cancer cell lines HCT-116^{wt}, its p53 knockout mutant HCT-116$^{p53-/-}$ (both colon cancer), 518A2 (melanoma), HeLa, and multi-drug-resistant KB-V1^{Vbl} (both cervical carcinoma; Table 1). For complexes **4a**, **5a** and **6a** bearing a CA-4 analogous NHC ligand, we found that the cytotoxicity increased with their DLC character, that is, in the order **4a** < **5a** < **6a**, except for the KB-V1^{Vbl} cells. A similar trend was observed for the anthracenyl complexes (**4b** < **5b** < **6b**), with the exception of bis-NHC complex **6b**, which is less active than phosphane complex **5b** in 518A2 melanoma and HeLa cervical carcinoma cells. This conformity of cytotoxicities of the **a** and **b** series of complexes suggests similar mechanisms of action. Interestingly, all tested gold complexes, including auranofin, were more active against the p53-knockout mutant HCT-116$^{p53-/-}$, if compared with its wild-type analogue HCT-116^{wt} expressing functional p53 protein. We assume that complexes **4**–**6** induce cancer cell death in a way that is inde-

Table 1. Inhibitory concentrations, IC_{50}[a] [μM], of complexes **4**–**6** upon application to cells of HCT-116^{wt} and HCT-116$^{p53-/-}$ knockout mutant colon carcinomas, 518A2 melanoma, HeLa and mdr KB-V1^{Vbl} cervical carcinomas, and human adult dermal fibroblast cells HDFa.

	IC_{50} [μM][a]					
	HCT-116^{wt}	HCT-116 p$^{53-/-}$	518A2	HeLa	KB-V1^{Vbl}	HDFa
4a	6.6 ± 0.8	2.2 ± 0.4	19.8 ± 2.0	12.4 ± 0.5	> 50	24.6 ± 3.4
4b	16.4 ± 0.2	8.4 ± 0.3	7.9 ± 0.8	23.7 ± 1.1	5.9 ± 1.3	9.0 ± 1.3
5a	1.1 ± 0.3	0.6 ± 0.1	5.0 ± 0.3	3.6 ± 0.7	0.6 ± 0.2	5.8 ± 0.9
5b	1.3 ± 0.6	0.4 ± 0.1	2.9 ± 0.5	1.8 ± 0.4	2.2 ± 0.2	5.9 ± 0.2
6a	0.2 ± 0.02	0.05 ± 0.001	0.4 ± 0.1	0.3 ± 0.02	4.6 ± 0.2	1.4 ± 0.2
6b	0.3 ± 0.03	0.2 ± 0.05	5.5 ± 0.4	3.6 ± 0.4	0.7 ± 0.2	3.2 ± 0.4
auranofin	11.9 ± 0.4	5.0 ± 0.2	1.8 ± 0.03	2.6 ± 0.4	n.d.[b]	13.7 ± 1.0

[a] Values are the means ± standard deviation (SD) determined in four independent experiments and derived from dose–response curves after 72 h incubation by using the 3-(4,5-dimethylthiazol-2-yl)-2,5-diphenyltetrazolium bromide (MTT) assay. [b] Not determined.

pendent of p53, as already shown for auranofin[16,17] and for related (1,3-diethylbenzimidazol-2-ylidene)gold(I) complexes.[18] Complexes **4b**, **5** and **6** were also quite active against the multi-drug-resistant cell line KB-V1^{Vbl}, which expresses high levels of Pg-p, an ATP-dependent efflux pump, capable of expelling a variety of xenobiotics. Complexes **5a** and **6b** appear to have a particularly low affinity for Pg-p. Cationic complexes **5b** and **6a** showed some selectivity for cancer over non-malignant cells and are particularly interesting candidates for further studies.

Intracellular localisation

The fluorescent complexes **4b**, **5b** and **6b** were synthesised as easy-to-track analogues of complexes **4a**, **5a** and **6a**, respectively. Well-observable, flat 518A2 melanoma cells were treated with the **b** complexes, then counterstained with dyes specifically accumulating in particular cancer-relevant cellular organelles, and eventually fixed and examined through confocal microscopy (Figure 1). By counterstaining with Nuclear Green, neutral chloride complex **4b** could be localised in the area of the nucleus and to a minor degree in the cytoplasm. This is in line with reports on the nuclear accumulation of neutral gold(I) complexes bearing an aryl-substituted NHC ligand.[19,20] Many established first-line anticancer drugs target cancer cell nuclei,[21] yet suffer from therapeutic shortcomings, including off-target side effects and an early onset of resistance, owing to insufficient nuclear accumulation.[22] Against this background, the enrichment of new (NHC)Au^{I}Cl complex **4b** predominantly in cancer cell nuclei is remarkable. Cationic phosphane complex **5b** accumulated in the mitochondria, as demonstrated by counterstaining of treated 518A2 cells with red mitochondria-selective MitoTracker (Figure 1). Apparently, the DLC character of this complex favours accumulation in the negatively charged mitochondrial compartments over any potential DNA intercalation of the planar anthracene residue. Mitochondria are considered to be promising targets for cancer therapy. A distinct disruption of the MMP typically results in the induction of apoptosis. One of the pro-apoptotic stimuli is an increased mitochondrial ROS production, which, in turn, causes disruption of the MMP.[23] Cationic bis-NHC complex **6b** accumulated mainly in lysosomes within the cytoplasm. It

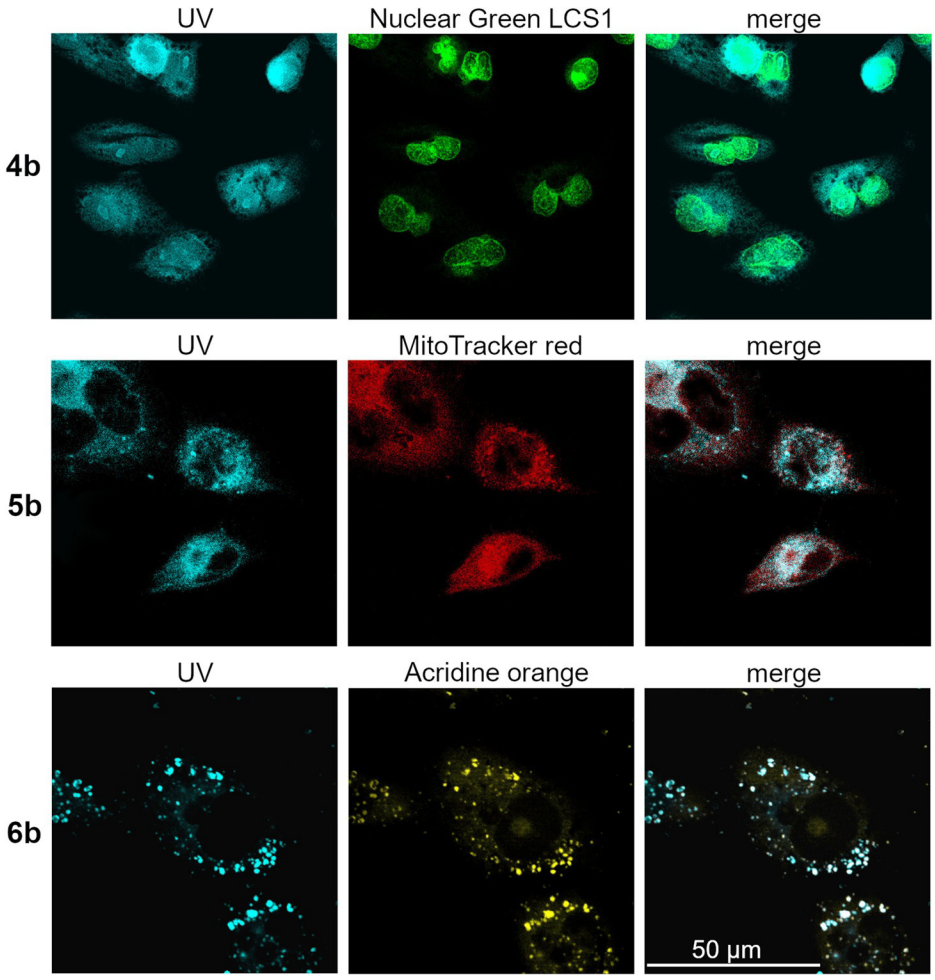

Figure 1. Confocal fluorescence microscopy images of 518A2 melanoma cells incubated for 30 min with 30 µM of complexes **4b**–**6b** (λ_{ex} = 350 nm and λ_{em} = 420–480 nm). The nuclei were counterstained with Nuclear Green LCS1 (abcam; λ_{ex} = 514 nm and λ_{em} = 520–535 nm), the mitochondria with MitoTracker^{TM} (Thermo Fisher; λ_{ex} = 580 nm and λ_{em} = 595–610 nm) and the lysosomes with acridine orange solution (5 µg mL^{-1}, ABCR GmbH; λ_{ex} = 350 nm and λ_{em} = 600–660 nm). Images are representative of at least four independent experiments; 2000-fold magnification.

should be noted that Gust et al. found an accumulation of all three [1,3-diethyl-4,5-di(*p*-fluorophenyl)imidazol-2-ylidene](L)-gold(I) analogues of complexes **4a**, **5a** and **6a** in the nuclei of MCF-7 and HT-29 cells upon a 24 h long exposure.[24] So, the organelle-selective accumulation of our **a** complexes after only 30 min might be a kinetic effect. The bottom row of Figure 1 shows confocal fluorescence microscopy images of 518A2 melanoma cells treated with complex **6b** and lysotropic acridine orange, as well as the good match of the blue fluorescence of **6b** (UV) with the orange fluorescence of the counterstained lysosomes. Lysosomes are the recycling centres of the cell and are involved in cellular digestion processes, such as autophagy, endocytosis and phagocytosis. Moreover, the release of lysosomal hydrolases, so called cathepsins, is involved in the induction of cell death.[25,26] Cathepsins mediate caspase- and mitochondrion-independent cell death, especially in cancer cells with mutations in genes involved in the classic apoptotic pathway, for example, the TP53 tumour suppressor gene.[27]

Induction of cancer cell apoptosis

The majority of p53 mutations are missense mutations, as in the case of 518A2 melanoma cells,[28] leading to the expression of dysfunctional p53 proteins with oncogenic activities intensifying malignant properties of cancer cells, such as clinical drug resistance.[29] Because the p53-independent induction of cancer cell apoptosis had been reported for auranofin[17,30] and for (1,3-diethylbenzimidazol-2-ylidene)gold(I) complexes,[18] we investigated if complexes **4**–**6** also lead to an activation of apoptosis (Figure 2). Upon treatment of 518A2 melanoma cells with these complexes, the activation of effector caspases-3 and -7 was observed, which we assumed to be p53 independent, given the results from our cytotoxicity studies. The treated cells showed the typical morphological signs of apoptosis, as well as translocalisation of phosphatidylserines to the outer leaflet of the plasma membrane, which indicated early rather than late apoptosis or necrosis (see the Supporting Information). Because about 50% of all human tumours bear p53 mutations, drugs that induce p53-independent programmed cell death are of particular interest.[31,32]

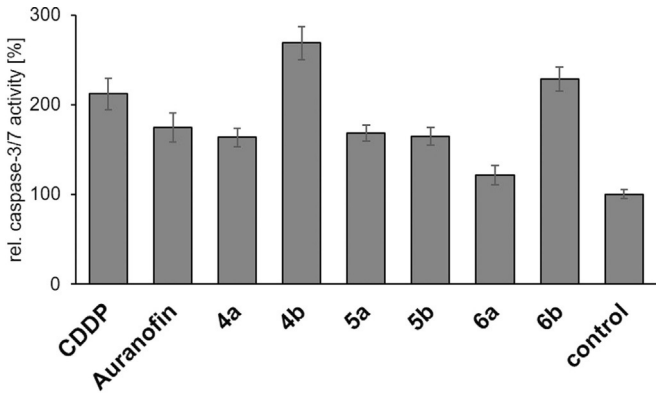

Figure 2. Induction of effector caspase-3/-7 activity in 518A2 melanoma cells after treatment with 5 μM **4**–**6** for 6 h, measured by means of the Apo-ONE® Homogenous Caspase-3/7 Assay Kit (Promega). CDDP was used as a positive control. The vitality of cells was simultaneously tested by MTT assays and was >80% for all experiments, except for complex **6a** (70%). All experiments were performed in triplicate and results quoted as means ± SD. The solvent-treated negative control was set to 100%.

Mechanism of action of complexes 4a and 4b in the nucleus

The antiproliferative effect of CDDP and other platinum complexes is based mainly on their interaction with cellular DNA.[3b,33] Because of the localisation of neutral complex **4b** in the nuclear area, a potential DNA interaction of **4b** and its close structural analogue **4a** was examined by ethidium bromide (EtdBr) saturation assays (Figure 3) and electrophoretic mobility shift assays (EMSAs; Figure 4).

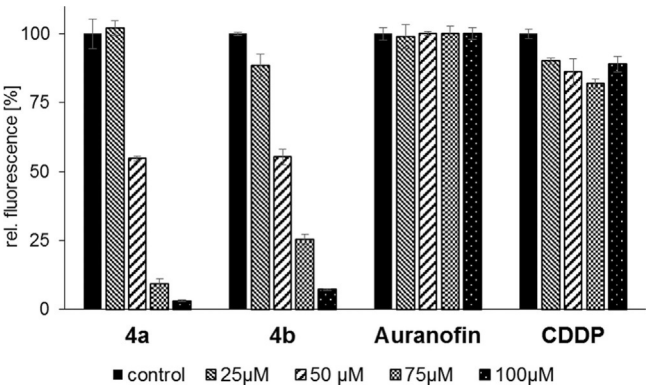

Figure 3. EtdBr saturation assays with 25, 50, 75 and 100 μM **4a**, **4b** and auranofin. CDDP was used as a positive control. Negative controls were treated with an equivalent amount of solvent (DMF or H_2O). All experiments were carried out in triplicate with negative controls set to 100%.

Addition of complexes **4a** or **4b** to linear, double-stranded salmon sperm DNA led to a distinct concentration-dependent displacement, and thus, to a reduction of the fluorescence of intercalated EtdBr, exceeding that caused by CDDP by far. This suggests a strong interaction of both complexes **4** with this DNA form, possibly associated with an alteration of the DNA morphology. Auranofin showed no such effect (Figure 3). In the EMSA with circular plasmid DNA, a slight relaxation, that is, despiralisation, of the covalently closed circular (ccc) DNA form for the benefit of the open circular (oc) form was observed after incubation with complex **4a**, and a stronger relaxation after treatment with complex **4b** (Figure 4). In contrast to CDDP, gold NHC complexes are known to bind non-covalently to DNA, which may be the reason for their weaker effects in the EMSA.[34]

Although auranofin had previously been reported to interact neither with linear DNA nor with circular plasmid DNA,[35] various other gold(I) complexes with readily displaceable ligands (e.g., Cl^-) had shown affinity to different types of DNA.[35,36] Irreparable DNA damage induces apoptosis, normally triggered by the tumour suppressor protein p53. However, apoptosis as a consequence of DNA damage caused by metal complexes had also been reported to proceed independently of p53,[37,38] through the mitogen-activated protein kinase (MAPK) signal-

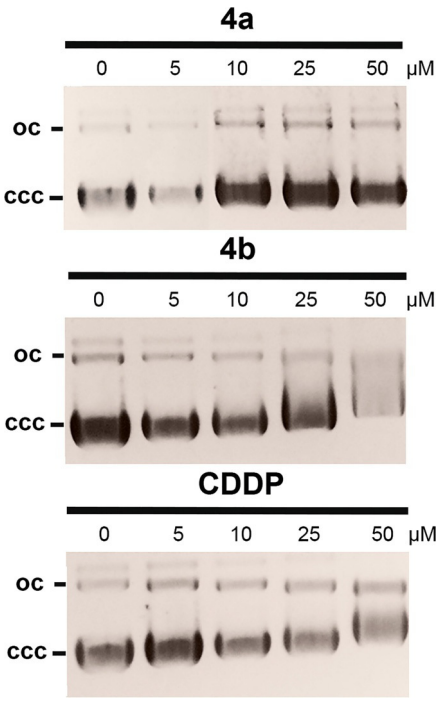

Figure 4. EMSAs with circular pBR322 plasmid DNA after 24 h treatment with complexes **4a** or **4b**, as visualised by UV radiation. CDDP was used as a positive control. Images are representative of at least two independent experiments.

ling pathway involving JNK, p38 and ERK1/2.[37,18] Whether complexes **4**, which we have found to induce cancer cell apoptosis and to be cytotoxic independently of functional p53, operate by a similar mechanism remains to be shown. At present, we cannot exclude that their reactions with further biologically relevant macromolecules might also play a role.[39]

Mechanism of action of complexes 5a and 5b in mitochondria

Because cationic triphenylphosphane complex **5b** was localised in the mitochondria of 518A2 melanoma cells, we anticipated a mitochondria-associated mode of action for **5b** and closely related complex **5a**. The anticancer effect of auranofin, and several other gold(I) complexes, mainly relies on the inhibition of TrxR.[40,41] TrxRs, which catalyse the reduced nicotinamide adenine dinucleotide phosphate (NADPH)-dependent reduction of the redox protein thioredoxin (Trx) and other compounds, are key enzymes for cellular protection against oxidative stress.[42] To date, three different isoforms of TrxR are known: cytosolic TrxR1, mitochondrial TrxR2 and testis-specific TrxR3.[43] Gold complexes, such as auranofin, are thought to inhibit TrxRs by releasing monovalent Au^{I} species, which bind to selenocysteine residues in the active site of the enzyme.[44] This is in line with reports that mono-NHC gold(I) complexes with good leaving groups, such as halides or phosphanes, are better TrxR inhibitors than bis-NHC complexes.[45] For instance, sub-micromolar IC_{50} values were reported by Gust et al. for donor-substituted (1,3-diethyl-4,5-diarylimidazol-2-ylidene)(PPh_3)gold(I) complexes,[24] and by Ott et al. for benzimidazol-2-ylidene analogues,[15,46] whereas few inhibitory bis(1,3-diarylimidazol-2-ylidene) complexes have been reported, to date.[45,47]

If applied in low sub-micromolar concentrations, complexes **5a** and **5b** strongly inhibited the panTrxR activity in colorimetric TrxR microplate assays with 5,5′-dithiobis(2-dinitrobenzoic acid (DTNB; Ellman's reagent) as a substrate (Figure 5). Because many tumours have elevated TrxR levels,[43] and tumour cells are more sensitive to oxidative stress, due to their a priori high intracellular ROS levels relative to non-malignant cells, TrxR are interesting targets for selective antitumour therapy.

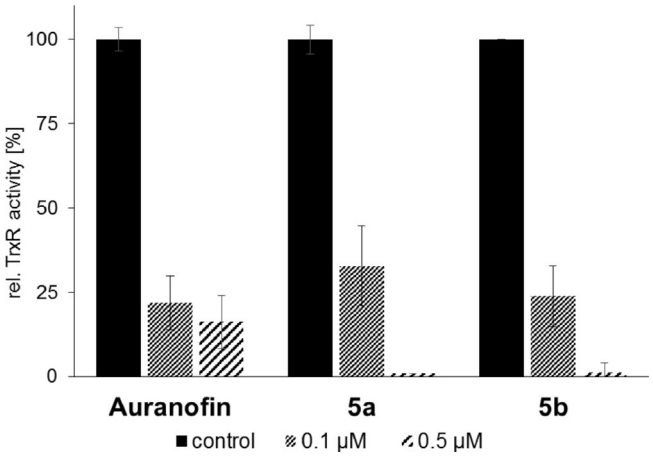

Figure 5. Concentration-dependent inhibition of TrxR activity in cell lysates of 518A2 melanoma cells by gold(I) complexes **5a** and **5b**, and auranofin as a positive control. TrxR-independent substrate reduction was accounted for by experiments in the presence and absence of the specific TrxR inhibitor aurothiomalate. All values are means ± SD of at least three independent experiments with negative controls set to 100%.

TrxR inhibition generally leads to an accumulation of oxidised Trx and ROS in mitochondria, resulting in an increase of mitochondrial permeability.[40] Upon treatment of 518A2 melanoma cells with complexes **5a** and **5b**, we observed a distinct reduction of the MMP through a fluorescence-based microplate assay (Figure 6), exceeding that induced by auranofin, which is in keeping with their stronger TrxR inhibition.

We confirmed these results by an assessment of the intracellular ROS concentrations after treatment of 518A2 melanoma cells with auranofin, CCCP and complexes **5a** and **5b** using the cell permeant, fluorogenic dye 2′,7′-dichlorofluorescein diacetate (DCFH-DA). After diffusion into the cells, DCFH-DA is deacetylated by cellular esterases to a non-fluorescent compound, which is later oxidised by hydroxyl, peroxyl or other ROS to the intensely fluorescent 2′,7′-dichlorofluorescein (DCF), detectable by fluorescence spectroscopy (Figure 7).

We conclude that the cytotoxicity of complexes **5** originates mainly from their inhibition of TrxR in the mitochondria of cancer cells and the subsequent alteration of the intracellular ROS equilibrium.[40] Elevated concentrations of hydrogen peroxide and oxidised Trx2 affect further intra-mitochondrial targets, leading to the opening of the mitochondrial permeability

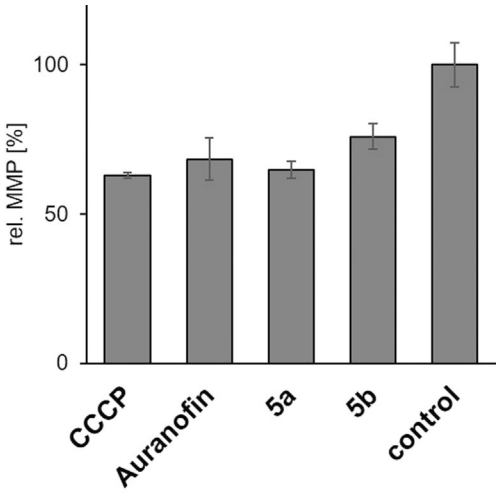

Figure 6. Relative MMP in 518A2 melanoma cells after treatment (45 min) with complexes **5a** and **5b** (10 μM each). Carbonylcyanide-*m*-chlorophenylhydrazone (CCCP) and auranofin (10 μM, each) were used as positive controls and solvent-treated negative controls were set to 100%. Assays were carried out in triplicate.

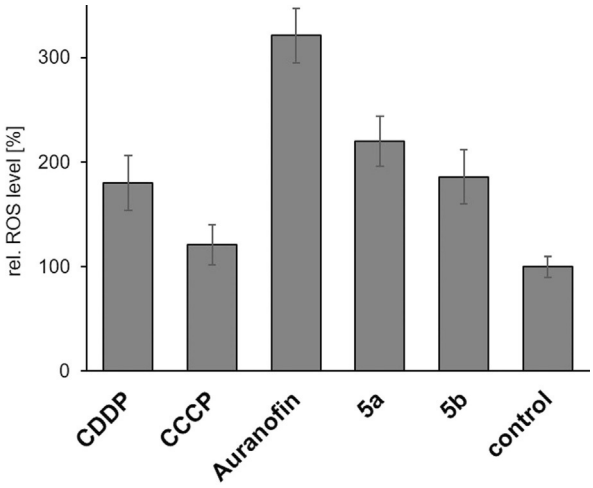

Figure 7. Influence of gold(I) complexes **5a** and **5b**, and auranofin (10 μM each), as well as CCCP (10 μM) as a positive control, on the levels of ROS in 518A2 melanoma cells, as determined by fluorescence-based DCFH-DA assays after an incubation time of 1 h. Negative controls were treated identically with solvent. All values are mean values ± SD from at least four independent experiments with negative controls set to 100%.

transition pore and/or to an increase of the permeability of the outer membrane.[9,48] As a result, hydrogen peroxide is released into the cytosol where it oxidises cytosolic Trx1 irreversibly, due to the inhibition of TrxRs. The elevated levels of hydrogen peroxide and oxidised Trx in the cytosol then activate various signalling pathways, eventually leading to apoptosis, which is likely to be dependent on p38/ERK1/2, rather than p53, as shown for auranofin.[40,49] Because cancer cells, unlike non-malignant cells, are not normally susceptible to mitochondrial membrane permeability transition, the induction of this condition by mitochondria-targeting complexes, such as **5**, could be exploited in a therapeutic context.[50]

Mechanism of action of complexes 6a and 6b in lysosomes

The cationic bis-NHC complex **6b** was localised in the lysosomes of 518A2 melanoma cells. Lysosomes mediate the degradation of macromolecules of intracellular origin or those that are internalised by endocytosis or phagocytosis.[51] These single-membrane acidic organelles (pH 4.5–4.8) are involved in various cellular pathways and different types of cell death, and their functionality is thus inevitable for cellular homeostasis.[51] Various forms of cellular stress lead to lysosomal swelling and lysosomal membrane permeabilisation (LMP), resulting in the release of intralysosomal cargo into the cytoplasm.[51] Amongst others, cathepsins B and D are released into the cytoplasm under stress, where they induce different forms of cell death, including the p53-independent, lysosome-dependent apoptotic cell death.[26,31,51,52] To detect a potential induction of LMP by complexes **6**, we performed a time-dependent staining of lysosomes in solvent- and complex-treated 518A2 melanoma cells (Figure 8). Because the cytotoxicity of both complexes against 518A2 cells in MTT assays was quite different (IC_{50}(**6a**) = 0.4 μM, IC_{50}(**6b**) = 5.5 μM), we adjusted their concentrations accordingly to ensure a sufficient cell viability. The incubation with either complex **6a** or **6b** led to an induction of LMP. The lysotropic orange dye used in this assay selectively accumulates in intact acidic lysosomes. If LMP occurs, the dye is released into the cytosol and the fluorescence of defined lysosomal compartments disappears. As expected, complex **6a**, which had proved to be more active in MTT assays, also led to faster lysosomal disruption after only 2 h of incubation. Cells treated with **6b** showed first signs of LMP only after 4 h of treatment.

Conclusion

The [4-(anthracen-9-yl)-1,3-diethyl-5-phenylimidazol-2-ylidene](L)gold(I) complexes **4b**, **5b**, and **6b** accumulated quickly in different compartments of 518A2 melanoma cells, that is, neutral chlorido complex **4b** in the nuclei, cationic phosphane complex **5b** in mitochondria and large delocalised cationic bis-NHC complex **6b** in the lysosomes. The analogous **a** series of complexes carried a slightly different 4,5-diarylimidazol-2-ylidene ligand. The fact that all couples **4a**/**4b**, **5a**/**5b** and **6a**/**6b** afforded similar results in cytotoxicity tests with cancer cells, and in tests on targets typically found at the identified sites of accumulation, supports the assumption that **a** complexes localise similarly to the **b** complexes, and that the nature of ligand L, which is responsible for the charge, size and lipophilicity of the complex, is decisive for the site of accumulation. However, this phenomenon might be limited to divalent gold(I)–NHC or even to (imidazol-2-ylidene)gold(I) complexes because a comparable series of *cis*-[bis(1,3-dibenzylimidazol-2-ylidene)]Cl(L)Pt^{II}[14] and (1,3-diethylbenzimidazol-2-ylidene)(L)gold(I) complexes,[15] carrying the same ligands L (Cl, PPh_3 or the same NHC ligand), were previously shown to accumulate in mitochondria, regardless of the charge of the complex and the nature of ligand L. The different distributions of DLC complexes **5** (in mitochondria) and **6** (in lysosomes) is explicable by the higher molecular weight and steric demand of

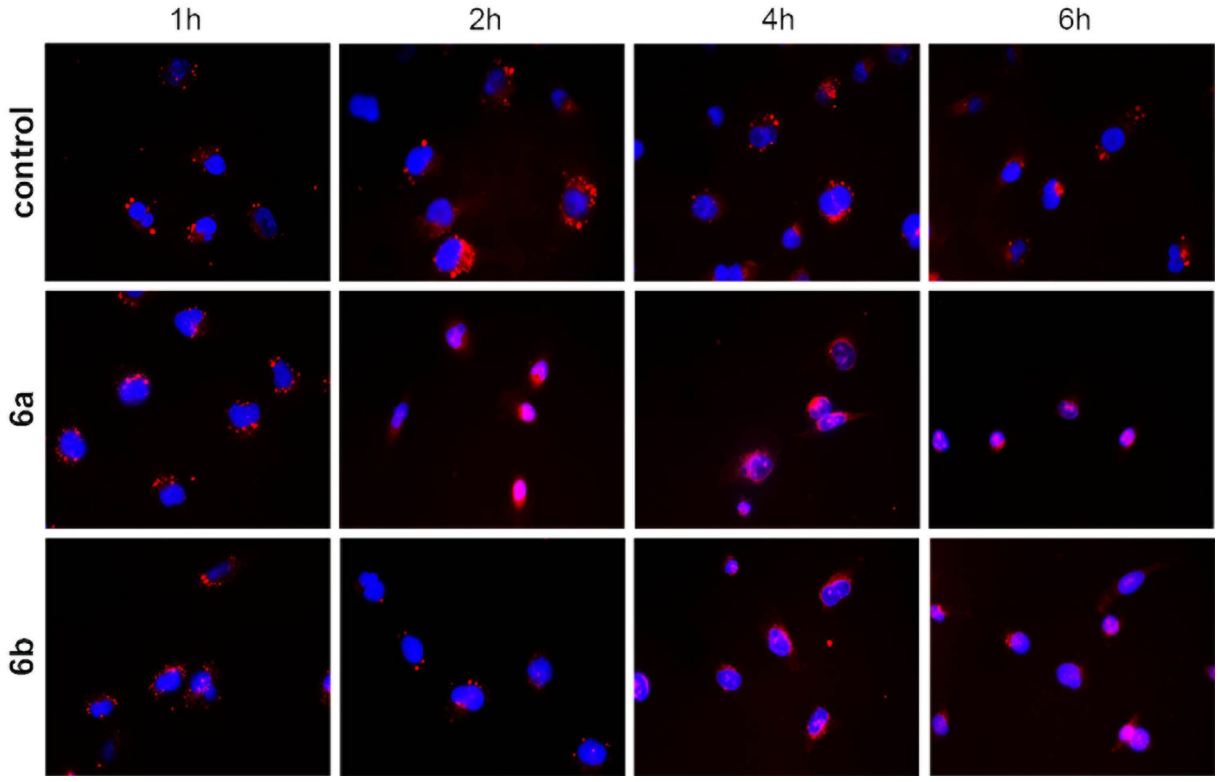

Figure 8. Fluorescence microscopy images of 518A2 melanoma cells treated with solvent (DMF), or complexes **6a** (0.4 μM) or **6b** (5.5 μM), for 1, 2, 4 or 6 h under standard cell-culture conditions; 30 min before each time interval ended, cells were stained with Lysosomal Staining Reagent Orange (Abcam). Nuclear counterstaining was performed by using blue 4′,6-diamidino-2-phenylindole (DAPI). Images are representative of at least ten independent measurements at 400-fold magnification.

the latter, which are too large for embedding in the mitochondrial membrane, and thus, are dealt with by the cellular "waste-to-energy plants", the lysosomes. Once fully understood, the concept of controlling the intracellular distribution of metallodrugs by the choice of secondary ligands and charge of the complex could be exploited in rational drug design.

For the mode of action of new complexes **4**–**6**, we found an eventual induction of p53-independent apoptotic cell death, which was initiated by different effects of the three complex types at their respective sites of accumulation.

Acknowledgements

We thank the Deutsche Forschungsgemeinschaft (DFG) for a grant (Scho 402/12-2). Furthermore, we would like to thank Luisa Kober for her support in identifying the target structures of the compounds, and Dr. Julienne K. Münzner and Dr. Matthias Rothemund for preliminary tests. Open access funding enabled and organized by Projekt DEAL.

Conflict of interest

The authors declare no conflict of interest.

Keywords: cancer · drug discovery · gold · metallodrugs · subcellular localisation

[1] L.-A. Schaper, S. J. Hock, W. A. Herrmann, F. E. Kühn, *Angew. Chem. Int. Ed.* **2013**, *52*, 270 – 289; *Angew. Chem.* **2013**, *125*, 284 – 304.
[2] M.-L. Teyssot, A.-S. Jarrousse, M. Manin, A. Chevry, S. Roche, F. Norre, C. Beaudoin, L. Morel, D. Boyer, R. Mahiou, A. Gautier, *Dalton Trans.* **2009**, 6894 – 6902.
[3] a) B. Rosenberg, L. VanCamp, *Cancer Res.* **1970**, *30*, 1799 – 1802; b) J. Reedijk, P. H. Lohman, *Pharm. Weekbl. Sci.* **1985**, *7*, 173 – 180; c) M. H. Hanigan, P. Devarajan, *Cancer Ther.* **2003**, *1*, 47 – 61; d) C. M. Sorenson, M. A. Barry, A. Eastman, *J. Natl. Cancer Inst.* **1990**, *82*, 749 – 755.
[4] a) J. S. Modica-Napolitano, J. R. Aprille, *Adv. Drug Delivery Rev.* **2001**, *49*, 63 – 70; b) C. I. Yeo, K. K. Ooi, E. R. T. Tiekink, *Molecules* **2018**, *23*, 1410.
[5] S. B. Aher, P. N. Muskawar, K. Thenmozhi, P. R. Bhagat, *Eur. J. Med. Chem.* **2014**, *81*, 408 – 419.
[6] a) L. Oehninger, R. Rubbiani, I. Ott, *Dalton Trans.* **2013**, *42*, 3269 – 3284; b) C. Hu, X. Li, W. Wang, R. Zhang, L. Deng, *Curr. Med. Chem.* **2014**, *21*, 1220 – 1230; c) A. Gautier, F. Cisnetti, *Metallomics* **2012**, *4*, 23 – 32.
[7] a) M. Chaffman, R. N. Brogden, R. C. Heel, T. M. Speight, G. S. Avery, *Drugs* **1984**, *27*, 378 – 424; b) V. Gandin, A. P. Fernandes, M. P. Rigobello, B. Dani, F. Sorrentino, F. Tisato, M. Björnstedt, A. Bindoli, A. Sturaro, R. Rella, C. Marzano, *Biochem. Pharmacol.* **2010**, *79*, 90 – 101.
[8] S. Gromer, L. D. Arscott, C. H. Williams, R. H. Schirmer, K. Becker, *J. Biol. Chem.* **1998**, *273*, 20096 – 20101.
[9] M. P. Rigobello, G. Scutari, R. Boscolo, A. Bindoli, *Br. J. Pharmacol.* **2002**, *136*, 1162 – 1168.
[10] G.-Y. Liou, P. Storz, *Free Radical Res.* **2010**, *44*, 479 – 496.
[11] X. Jiang, X. Wang, *Annu. Rev. Biochem.* **2004**, *73*, 87 – 106.
[12] L. Kaps, B. Biersack, H. Müller-Bunz, K. Mahal, J. Münzner, M. Tacke, T. Mueller, R. Schobert, *J. Inorg. Biochem.* **2012**, *106*, 52 – 58.

[13] J. K. Muenzner, B. Biersack, H. Kalie, I. C. Andronache, L. Kaps, D. Schuppan, F. Sasse, R. Schobert, *ChemMedChem* **2014**, *9*, 1195 – 1204.
[14] M. Rothemund, S. I. Bär, T. Rehm, H. Kostrhunova, V. Brabec, R. Schobert, *Dalton Trans.* **2020**, *49*, 8901 – 8910.
[15] R. Rubbiani, S. Can, I. Kitanovic, H. Alborzinia, M. Stefanopoulou, M. Kokoschka, S. Mönchgesang, W. S. Sheldrick, S. Wölfl, I. Ott, *J. Med. Chem.* **2011**, *54*, 8646 – 8657.
[16] E. Hedström, S. Eriksson, J. Zawacka-Pankau, E. S. J. Arnér, G. Selivanova, *Cell Cycle* **2009**, *8*, 3584 – 3591.
[17] S.-H. Park, J. H. Lee, J. S. Berek, M. C.-T. Hu, *Int. J. Oncol.* **2014**, *45*, 1691 – 1698.
[18] X. Cheng, P. Holenya, S. Can, H. Alborzinia, R. Rubbiani, I. Ott, S. Wölfl, *Molecular Cancer* **2014**, *13*, 221.
[19] B. Bertrand, A. de Almeida, E. P. M. van der Burgt, M. Picquet, A. Citta, A. Folda, M. P. Rigobello, P. Le Gendre, E. Bodio, A. Casini, *Eur. J. Inorg. Chem.* **2014**, 4532 – 4536.
[20] A. Citta, E. Schuh, F. Mohr, A. Folda, M. L. Massimino, A. Casini, M. P. Rigobello, *Metallomics* **2013**, *5*, 1006 – 1015.
[21] a) D. Ingato, J. A. Edson, M. Zakharian, Y. J. Kwon, *ACS Nano* **2018**, *12*, 9568 – 9577; b) L. H. Hurley, *Nat. Rev. Cancer* **2002**, *2*, 188 – 200.
[22] a) A. L. B. Seynhaeve, B. M. Dicheva, S. Hoving, G. A. Koning, T. L. M. ten Hagen, *J. Controlled Release* **2013**, *172*, 330 – 340; b) M. A. Fuertes, C. Alonso, J. M. Pérez, *Chem. Rev.* **2003**, *103*, 645 – 662.
[23] S. Fulda, L. Galluzzi, G. Kroemer, *Nat. Rev. Drug Discovery* **2010**, *9*, 447 – 464.
[24] W. Liu, K. Bensdorf, M. Proetto, A. Hagenbach, U. Abram, R. Gust, *J. Med. Chem.* **2012**, *55*, 3713 – 3724.
[25] a) U. T. Brunk, J. Neuzil, J. W. Eaton, *Redox Rep.* **2001**, *6*, 91 – 97; b) T. Cirman, K. Oresić, G. D. Mazovec, V. Turk, J. C. Reed, R. M. Myers, G. S. Salvesen, B. Turk, *J. Biol. Chem.* **2004**, *279*, 3578 – 3587.
[26] P. Boya, K. Andreau, D. Poncet, N. Zamzami, J.-L. Perfettini, D. Metivier, D. M. Ojcius, M. Jäättelä, G. Kroemer, *J. Exp. Med.* **2003**, *197*, 1323 – 1334.
[27] M. Jäättelä, *Oncogene* **2004**, *23*, 2746 – 2756.
[28] S. F. Zerp, A. van Elsas, L. T. Peltenburg, P. I. Schrier, *Br. J. Cancer* **1999**, *79*, 921 – 926.
[29] A. Parrales, T. Iwakuma, *Front. Oncol.* **2015**, *5*, 288.
[30] B. Tessoulin, G. Descamps, C. Dousset, M. Amiot, C. Pellat-Deceunynck, *Front. Oncol.* **2019**, *9*, 128.
[31] H. Erdal, M. Berndtsson, J. Castro, U. Brunk, M. C. Shoshan, S. Linder, *Proc. Natl. Acad. Sci. USA* **2005**, *102*, 192 – 197.
[32] a) C. Béroud, T. Soussi, *Nucleic Acids Res.* **1998**, *26*, 200 – 204; b) L. Bouaoun, D. Sonkin, M. Ardin, M. Hollstein, G. Byrnes, J. Zavadil, M. Olivier, *Hum. Mutat.* **2016**, *37*, 865 – 876.
[33] D. P. Bancroft, C. A. Lepre, S. J. Lippard, *J. Am. Chem. Soc.* **1990**, *112*, 6860 – 6871.
[34] Ö. Karaca, S. M. Meier-Menches, A. Casini, F. E. Kühn, *Chem. Commun.* **2017**, *53*, 8249 – 8260.
[35] C. K. Mirabelli, C.-M. Sung, J. P. Zimmerman, D. T. Hill, S. Mong, S. T. Crooke, *Biochem. Pharmacol.* **1986**, *35*, 1427 – 1433.
[36] a) C. E. Blank, J. C. Dabrowiak, *J. Inorg. Biochem.* **1984**, *21*, 21 – 29; b) S. Urig, K. Fritz-Wolf, R. Réau, C. Herold-Mende, K. Tóth, E. Davioud-Charvet, K. Becker, *Angew. Chem. Int. Ed.* **2006**, *45*, 1881 – 1886; *Angew. Chem.* **2006**, *118*, 1915 – 1920.
[37] S. L. R. Silva, I. R. S. Baliza, R. B. Dias, C. B. S. Sales, C. A. G. Rocha, M. B. P. Soares, R. S. Correa, A. A. Batista, D. P. Bezerra, *Sci. Rep.* **2019**, *9*, 11094.
[38] a) N. C. de Carvalho, S. P. Neves, R. B. Dias, L. de F. Valverde, C. B. S. Sales, C. A. G. Rocha, M. B. P. Soares, E. R. dos Santos, R. M. M. Oliveira, R. M. Carlos, P. C. L. Nogueira, D. P. Bezerra, *Cell Death Dis.* **2018**, *9*, 79; b) M. Altaf, M. Monim-Ul-Mehboob, A.-N. Kawde, G. Corona, R. Larcher, M. Ogasawara, N. Casagrande, M. Celegato, C. Borghese, Z. H. Siddik, D. Aldinucci, A. A. Isab, *Oncotarget* **2017**, *8*, 490 – 505.
[39] L. Ronconi, D. Fregona, *Dalton Trans.* **2009**, 10670 – 10680.
[40] A. Bindoli, M. P. Rigobello, G. Scutari, C. Gabbiani, A. Casini, L. Messori, *Coord. Chem. Rev.* **2009**, *253*, 1692 – 1707.
[41] a) C. Marzano, V. Gandin, A. Folda, G. Scutari, A. Bindoli, M. P. Rigobello, *Free Radical Biol. Med.* **2007**, *42*, 872 – 881; b) A. Meyer, C. P. Bagowski, M. Kokoschka, M. Stefanopoulou, H. Alborzinia, S. Can, D. H. Vlecken, W. S. Sheldrick, S. Wölfl, I. Ott, *Angew. Chem. Int. Ed.* **2012**, *51*, 8895 – 8899; *Angew. Chem.* **2012**, *124*, 9025 – 9030; c) M. G. Fabbrini, D. Cirri, A. Pratesi, L. Ciofi, T. Marzo, A. Guerri, S. Nistri, A. Dell'Accio, T. Gamberi, M. Severi, A. Bencini, L. Messori, *ChemMedChem* **2019**, *14*, 182 – 188.
[42] D. Mustacich, G. Powis, *Biochem. J.* **2000**, *346*, 1 – 8.
[43] S. Urig, K. Becker, *Semin. Cancer Biol.* **2006**, *16*, 452 – 465.
[44] D. Parsonage, F. Sheng, K. Hirata, A. Debnath, J. H. McKerrow, S. L. Reed, R. Abagyan, L. B. Poole, L. M. Podust, *J. Struct. Biol.* **2016**, *194*, 180 – 190.
[45] C. Zhang, C. Hemmert, H. Gornitzka, O. Cuvillier, M. Zhang, R. W.-Y. Sun, *ChemMedChem* **2018**, *13*, 1218 – 1229.
[46] R. Rubbiani, L. Salassa, A. de Almeida, A. Casini, I. Ott, *ChemMedChem* **2014**, *9*, 1205 – 1210.
[47] J. F. Arambula, R. McCall, K. J. Sidoran, D. Magda, N. A. Mitchell, C. W. Bielawski, V. M. Lynch, J. L. Sessler, K. Arumugam, *Chem. Sci.* **2016**, *7*, 1245 – 1256.
[48] A. G. Cox, K. K. Brown, E. S. J. Arner, M. B. Hampton, *Biochem. Pharmacol.* **2008**, *76*, 1097 – 1109.
[49] S.-J. Park, I.-S. Kim, *Br. J. Pharmacol.* **2005**, *146*, 506 – 513.
[50] G. Kroemer, L. Galluzzi, C. Brenner, *Physiol. Rev.* **2007**, *87*, 99.
[51] F. Wang, R. Gómez-Sintes, P. Boya, *Traffic* **2018**, *19*, 918 – 931.
[52] a) F. Wang, A. Salvati, P. Boya, *Open Biol.* **2018**, *8*, 170271; b) S. Aits, M. Jäättelä, *J. Cell Sci.* **2013**, *126*, 1905 – 1912.

Manuscript received: December 23, 2020
Accepted manuscript online: December 28, 2020
Version of record online: February 8, 2021

Chemistry–A European Journal

Supporting Information

Guided Antitumoural Drugs: (Imidazol-2-ylidene)(L)gold(I) Complexes Seeking Cellular Targets Controlled by the Nature of Ligand L

Sofia I. Bär[+], Madeleine Gold[+], Sebastian W. Schleser, Tobias Rehm, Alexander Bär, Leonhard Köhler, Lucas R. Carnell, Bernhard Biersack, and Rainer Schobert*[a]

Author Contributions

S.B. Formal analysis: Lead; Investigation: Lead; Methodology: Lead; Project administration: Lead; Writing – original draft: Lead
M.G. Formal analysis: Equal; Investigation: Equal; Methodology: Equal; Project administration: Equal; Writing – original draft: Equal
S.S. Formal analysis: Supporting; Investigation: Supporting; Methodology: Supporting
T.R. Formal analysis: Supporting; Investigation: Supporting; Methodology: Supporting
A.B. Formal analysis: Supporting; Investigation: Supporting; Methodology: Supporting
L.K. Formal analysis: Supporting; Investigation: Supporting; Methodology: Supporting
L.C. Formal analysis: Supporting; Methodology: Supporting
B.B. Formal analysis: Supporting; Investigation: Supporting; Methodology: Supporting; Project administration: Supporting.

Table of Contents

Experimental Procedures

Chemical Synthesis and Analytics

General.

Melting points (uncorrected): GALLENKAMP; IR spectra: PERKIN-ELMER Spectrum One FT-IR spectrophotometer with ATR sampling unit; Nuclear magnetic resonance (NMR) spectra: BRUKER DRX 500 Hz spectrometer, chemical shifts are given in parts per million (δ) downfield from tetramethylsilane as internal standard for ^{1}H and ^{13}C; Mass spectra: VARIAN MAT 311A (EI), WATERS UPLC-Q-TOF (ESI), ThermoFisher UPLC/Orbitrap MS system (HRMS-ESI); All starting compounds were purchased from ALDRICH and used without further purification. The known compounds **3a**[1], **4a**[1] and **6a**[1] were prepared according to literature procedures.

5-(Anthracen-9-yl)-1-ethyl-4-phenylimidazole (2). A solution of 9-formylanthracene (700 mg, 3.39 mmol) in ethanol (50 mL) was treated with 2M $EtNH_2$/THF (8.49 mL, 17.0 mmol). Acetic acid (970 μL) was added and the reaction mixture was refluxed for 2 h. After cooling to room temperature, phenyl-TosMIC **1** (1.39 g, 5.09 mmol) and K_2CO_3 (1.88 g, 13.6 mmol) were added and refluxed again for 6 h. The solvent was evaporated, the residue was dissolved in ethyl acetate (100 mL) and washed with water (100 mL) and brine (100 mL), dried over Na_2SO_4, filtered and the filtrate was concentrated in vacuum. The residue was purified by column chromatography (silica gel 60; EtOAc/MeOH: 97/3). Yield: 726 mg (2.08 mmol, 61%); yellow solid; R_f = 0.64; ν_{max}/cm^{-1}: 3053, 2977, 2931, 1623, 1599, 1517, 1501, 1458, 1442, 1398, 1373, 1352, 1343, 1314, 1244, 1224, 1175, 1163, 1135, 1117, 1056, 1067, 1011, 983, 951, 917, 899, 852, 813, 799, 771, 744, 715, 728, 692; ^{1}H NMR (500 MHz, $CDCl_3$): δ 1.01 (3 H, t, J = 7.3 Hz), 3.45 (2 H, q, J = 7.3 Hz), 6.96-6.98 (3 H, m), 7.29-7.31 (2 H, m), 7.38-7.41 (2 H, m), 7.48-7.51 (2 H, m) 7.64 (2 H, d, J = 8.7 Hz), 7.91 (1 H, s), 8.10 (2 H, d, J = 8.7 Hz), 8.64 (1 H, s); ^{13}C NMR (126 MHz, $CDCl_3$): δ 16.4, 40.1, 123.9, 124.5, 125.4, 125.6, 125.7, 126.1, 126.9, 128.1, 128.8, 128.9, 131.5, 134.0, 134.5, 136.8, 140.0.

4-(Anthracen-9-yl)-1,3-diethyl-5-phenylimidazolium tetrafluoroborate (3b).

Compound **2** (500 mg, 1.43 mmol) was dissolved in acetonitrile (100 mL) and iodoethane (6.34 mL) was added. The reaction mixture was stirred at 85 °C for 48 h. The solvent was evaporated and the remainder was crystallised from CH_2Cl_2/*n*-hexane at 4 °C. Yield: 689 mg (1.37 mmol, 95%); yellow solid; ν_{max}/cm^{-1}: 3420, 3118, 3027, 2979, 1622, 1592, 1556, 1520, 1499, 1443, 1386, 1348, 1263, 1193, 1159, 1091, 1074, 1023, 1012, 962, 932, 897, 854, 794, 774, 740, 700; ^{1}H NMR (500 MHz, $CDCl_3$): ^{1}H NMR (500 MHz, $CDCl_3$): δ 1.28 (3 H, t, J = 7.3 Hz), 1.68 (3 H, t, J = 7.3 Hz), 3.91 (2 H, q, J = 7.3 Hz), 4.52 (2 H, q, J = 7.3 Hz), 7.13-7.23 (5 H, m), 7.50-7.55 (2 H, m), 7.59 (2 H, t, J = 8.1 Hz), 7.65 (2 H, d, J = 8.7 Hz) 8.06 (2 H, d, J = 8.4 Hz), 8.62 (1 H, s), 10.83 (1 H, s);^{13}C NMR (126 MHz, $CDCl_3$): δ 15.8, 15.9, 43.6, 44.1, 117.0, 124.4, 124.9, 126.0, 128.3, 128.4, 129.1, 129.2, 129.4, 130.4, 131.0, 131.2, 132.0, 133.9. The resulting 4-(anthracen-9-yl)-1,3-diethyl-5-phenylimidazolium iodide (41 mg, 0.081 mmol) was dissolved in acetone (10 mL) and $NaBF_4$ (13 mg, 0.122 mmol) was added. The reaction mixture was stirred at room temperature for 24 h. After filtration through Mg_2SO_4 the filtrate was concentrated in vacuum and dried. Yield: 38 mg (0.081 mmol, 100%); yellow solid; ν_{max}/cm^{-1}: 3464, 3039, 2982, 1622, 1557, 1520, 1499, 1444, 1387, 1349, 1333, 1305, 1263, 1193, 1065, 1023, 963, 932, 897, 854, 774, 740, 727, 700; ^{1}H NMR (300 MHz, $CDCl_3$): δ 1.24 (3 H, t, J = 7.3 Hz), 1.65 (3 H, t, J = 7.3 Hz), 3.88 (2 H, q, J = 7.3 Hz), 4.49 (2 H, q, J = 7.3 Hz), 7.0-7.2 (5 H, m), 7.4-7.6 (4 H, m), 7.67 (2 H, d, J = 8.6 Hz), 8.01 (2 H, d, J = 8.4 Hz), 8.58 (1 H, s), 10.66 (1 H, s); ^{13}C NMR (75.5 MHz, $CDCl_3$): δ 15.7, 15.8, 43.5, 44.0, 117.0, 124.3, 124.9, 125.8, 128.2, 128.3, 129.0, 129.1, 129.4, 130.2, 130.9, 131.0, 131.9, 133.9, 137.2; ^{11}B NMR (96.3 MHz, $CDCl_3$): δ -0.76.

Chlorido-[4-(anthracen-9-yl)-1,3-diethyl-5-phenylimidazol-2-ylidene]gold(I) (4b).

Compound **3b** (100 mg, 0.198 mmol) was dissolved in CH_2Cl_2 (5 mL) and treated with Ag_2O (27.6 mg, 0.119 mmol). The mixture was stirred in darkness at room temperature for 5 h. Chloro(dimethylsulfide)gold(I) (64.2 mg, 0.218 mmol) and LiCl (84 mg, 1.98 mmol) were added and the reaction mixture was stirred for additional 24 h. The crude product was crystallised from CH_2Cl_2/*n*-hexane at 4 °C. Yield: 111 mg (0.182 mmol, 92%); yellowish solid of of mp > 250 °C (dec.); ν_{max} (ATR)/cm^{-1}: 3051, 2976, 2933, 1622, 1500, 1461, 1427, 1443, 1414, 1344, 1294, 1213, 1115, 1088, 1025, 1013, 997, 962, 933, 896, 851, 819, 775, 757, 727, 699, 652, 607, 582; ^{1}H NMR(500 MHz, $CDCl_3$): δ 0.98 (3 H, t, J = 7.2 Hz), 1.45 (3 H, t, J = 7.1 Hz), 3.81 (2 H, q, J = 7.2 Hz), 4.37 (2 H, q, *J* = 7.2 Hz), 7.07-7.16 (5 H, m), 7.45-7.55 (4 H, m), 7.60 (2 H, d, J = 8.4 Hz), 8.00-8.05 (2 H, m), 8.55 (1 H, s); ^{13}C NMR (125 MHz, $CDCl_3$): δ 17.0, 17.2, 44.7, 44.8, 120.4, 124.7, 125.7, 127.0, 127.5, 127.6, 128.7, 129.1, 129.2, 129.3, 129.4, 130.2, 131.1, 132.0, 133.0, 170.3; *m/z* (ESI, %) 614.2 [M^++CH_3CN] (100). HRMS (ESI) m/z ((M-Cl+MeCN)$^+$) found 614.18508; calcd. 614.18650.

[1,3-Diethyl-5-(4-methoxyphenyl)-4-(3,4,5-trimethoxyphenyl)imidazol-2-ylidene](triphenylphosphane)gold(I) tetrafluoroborate (5a).

Complex **4a** (112 mg, 0.178 mmol) was dissolved in acetone (10 mL) and $NaBF_4$ (36 mg, 0.33 mmol) and triphenylphosphane (61 mg, 0.23 mmol) were added. The reaction mixture was stirred at room temperature for 24 h. The suspension was filtered, the filtrate concentrated in vacuum, and the residue recrystallized from acetone/*n*-hexane. Yield: 132 mg (0.14 mmol, 79%); colorless solid of mp = 107-110 °C; Elemental analysis ($C_{41}H_{43}AuBF_4N_2O_4P$, %) found C 52.14 H 4.47 N 2.93; calcd. C 52.25, H 4.60, N 2.97. ν_{max} (ATR)/cm^{-1}: 3056, 2936, 2836, 1607, 1581, 1516, 1504, 1463, 1437, 1415, 1331, 1292, 1248, 1179, 1124, 1099, 1050, 1024, 997, 887, 839, 811, 748, 711, 693 ^{1}H NMR (500 MHz, $CDCl_3$): δ 1.42 (3H, t, *J* = 7.3 Hz), 1.49 (3H, *J* = 7.2 Hz), 3.76 (3 H, s), 3.82 (3 H, s), 3.85 (3 H, s), 4.27 (2 H, q, *J* = 7.1 Hz), 4.35 (2 H, q, J = 7.1 Hz), 6.44 (3 H, s), 6.92 (6H, vd); 7.21 (3H, vd) 7.46 (15H, m) ^{13}C NMR

(125 MHz, $CDCl_3$): δ 17.5, 17.8, 44.3, 44.6, 55.3, 56.3, 60.9, 107.7, 114.3, 128.8, 128.9, 130.8, 131.9, 133.9, 134.0; ^{31}P NMR (202 MHz, $CDCl_3$): δ 33.8; *m/z* (ESI, %) 855.0 (100) [M^+], 721.4 (22). HRMS (ESI) m/z (M^+) found 855.2577; calcd. 855.2620.

[4-(Anthracen-9-yl)-1,3-diethyl-5-phenylimidazol-2-ylidene](triphenylphosphane)gold(I) tetrafluoroborate (5b).
Compound **3b** (100 mg, 0.198 mmol) in dry CH_2Cl_2 (5 mL) was treated with KO*t*Bu (27 mg, 0.238 mmol) and $(PPh_3)AuCl$ (98 mg, 0.198 mmol). The mixture was stirred at room temperature for 24. The crude product was filtered and crystallised from CH_2Cl_2/*n*-hexane at 4 °C. Yield: 166 mg (0.191 mmol, 96%); white solid of of mp = 165 °C; ν_{max} (ATR)/cm^{-1}: 3051, 2981, 1977, 1622, 1464, 1432, 1345, 1262, 1095, 1025, 895, 849, 775, 737, 690, 607, 565;^1H NMR (500 MHz, $CDCl_3$): δ 1.14 (3 H, t, J = 7.2 Hz), 1.59 (3 H, t, J = 7.2 Hz), 3.92 (2 H, q, J = 7.2 Hz), 4.55 (2 H, q, *J* = 7.2 Hz), 7.10-7.16 (3 H, m), 7.19-7.21 (2 H, m), 7.35-7.39 (6 H, m), 7.42-7.45 (3 H, m), 7.48-7.52 (8 H, m), 7.56-7.59 (2 H, m), 7.73 (2 H, d, J = 8.4 Hz), 8.03 (2 H, d, J = 8.4 Hz), 8.57 (1H, s); ^{13}C NMR (125 MHz, $CDCl_3$): δ 17.6, 17.8, 44.8, 45.1, 120.2, 125.0, 125.7, 127.4, 127.7, 128.8, 128.9, 129.0, 129.4, 129.6, 130.2, 130.6, 131.1, 132.1, 132.2, 133.4 133.9, 134.0, 134.1, 183.9; ^{31}P NMR (202 MHz, $CDCl_3$): δ 30.3; *m/z* (ESI, %) 949.4 (100), 835.2 (7) [M^+], 721.2 (40). HRMS (ESI) m/z (M^+) found 835.2476; calcd. 835.2511.

Bis[4-(anthracen-9-yl)-1,3-diethyl-5-phenylimidazol-2-ylidene]gold(I) tetrafluoroborate (6b).
Compound **3b** (100 mg, 0.198 mmol) was dissolved in CH_2Cl_2/methanol (1:1, 80 mL) and Ag_2O (50.1 mg, 0.216 mmol) was added. The reaction mixture was stirred in the dark at room temperature for 5 h. Chloro(dimethylsulfide)gold(I) (33.9 mg, 0.115 mmol) was added and the reaction mixture was stirred for additional 24 h. The suspension was filtered, the filtrate was concentrated in vacuum and the residue was redissolved in CH_2Cl_2, filtered over $MgSO_4$/Celite, and the filtrate was concentrated in vacuum and the residue dried in vacuum. Yield: 79 mg (0.080 mmol, 88%); reddish solid of mp > 250 °C (dec.); ν_{max}/cm^{-1}: 3052, 2965, 2924, 1623, 1595, 1520, 1498, 1460, 1443, 1407, 1378, 1345, 1294, 1260, 1218, 1161, 1088, 1050, 1012, 988, 961, 917, 896, 852, 774, 757, 737, 698; ^1H NMR (500 MHz, $CDCl_3$): δ 1.13 (6 H, t, J = 7.2 Hz), 1.59 (6 H, t, J = 7.2 Hz), 3.88 (4 H, q, J = 7.2 Hz), 4.49 (4 H, q, J = 7.2 Hz), 7.08-7.22 (10 H, m), 7.51 (4 H, t, J = 8.7 Hz), 7.58 (4 H, t, J = 8.7 Hz), 7.68 (4 H, d, J = 8.4 Hz), 8.04 (4 H, d, J = 8.4 Hz), 8.58 (2 H, s); ^{13}C NMR (126 MHz, $CDCl_3$): δ 17.6, 17.8, 44.7, 44.8, 119.8, 124.6, 124.7, 125.8, 127.1, 127.8, 127.9, 128.9, 129.1, 129.4, 129.5, 129.6, 130.4, 131.1, 131.2, 132.2, 134.0, 183.6; *m/z* (ESI, %) 949.4 [M^+] (100). HRMS (ESI) m/z (M^+) found 949.35035; calcd. 949.35390.

NMR Spectra

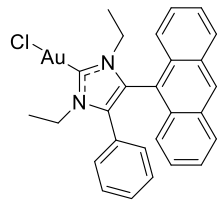

4b

Figure 1:^1H NMR (500 MHz, $CDCl_3$) spectrum of **4b.**

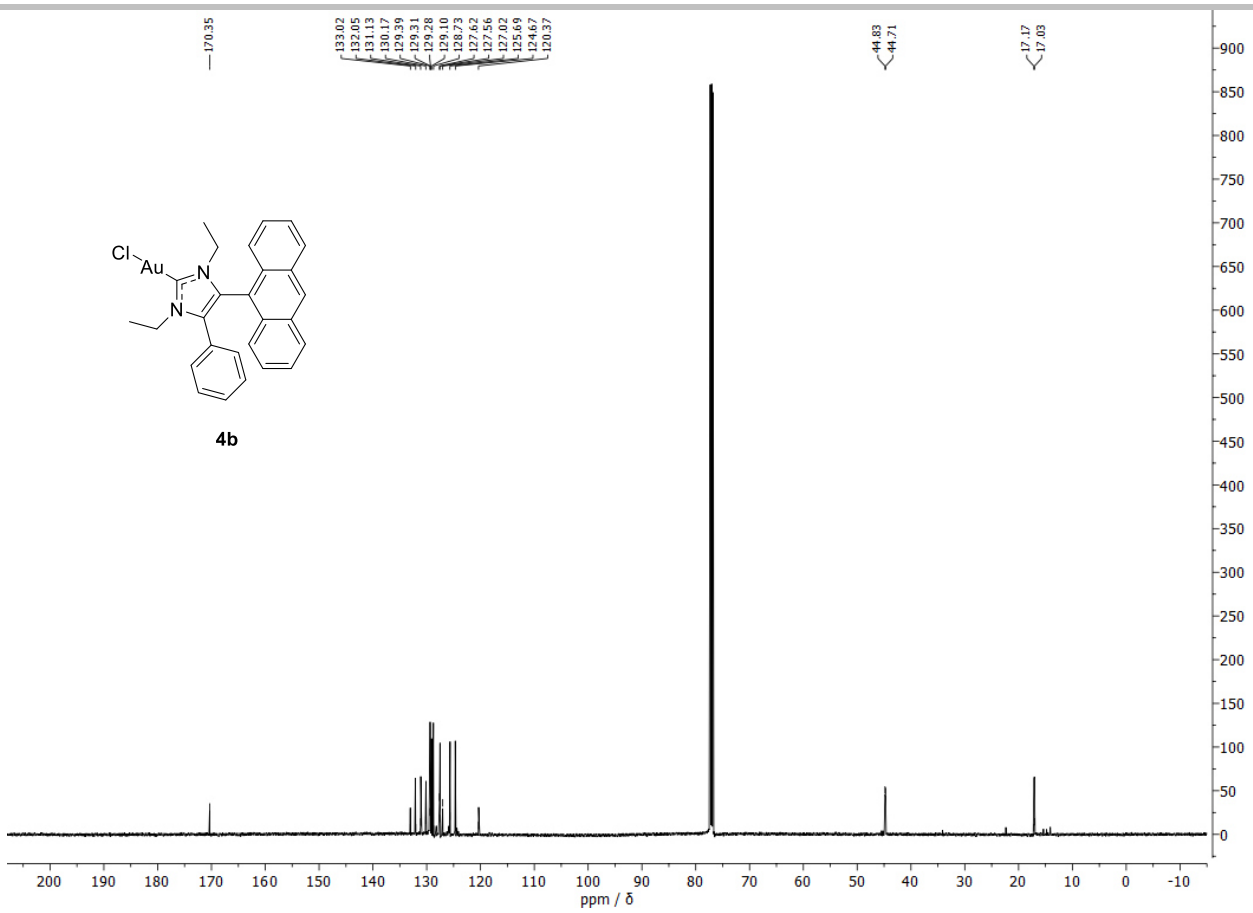

Figure 2: ^{13}C NMR (125 MHz, $CDCl_3$) spectrum of **4b.**

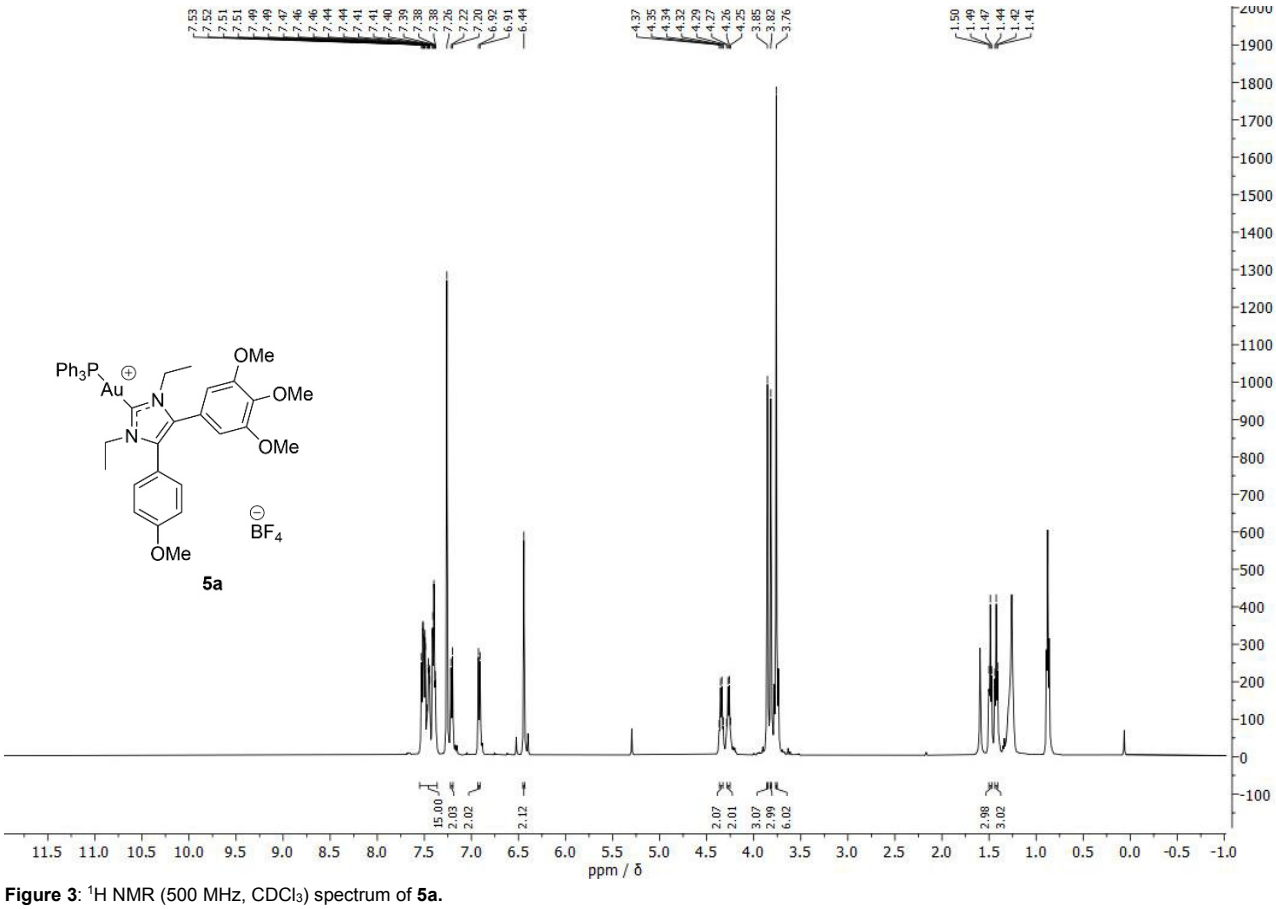

Figure 3: ^{1}H NMR (500 MHz, $CDCl_3$) spectrum of **5a.**

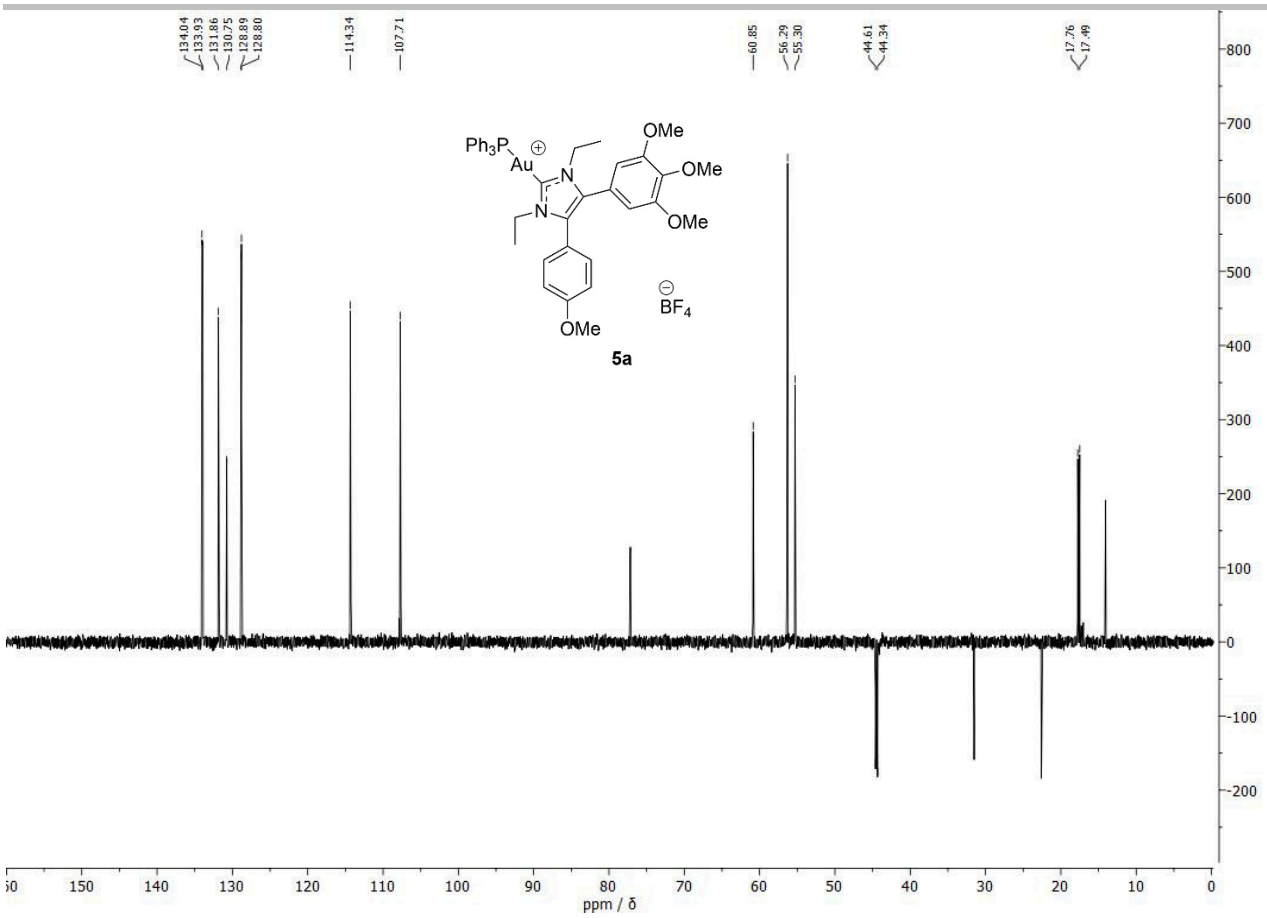

Figure 4: ^{13}C NMR (125 MHz, $CDCl_3$) spectrum of **5a.**

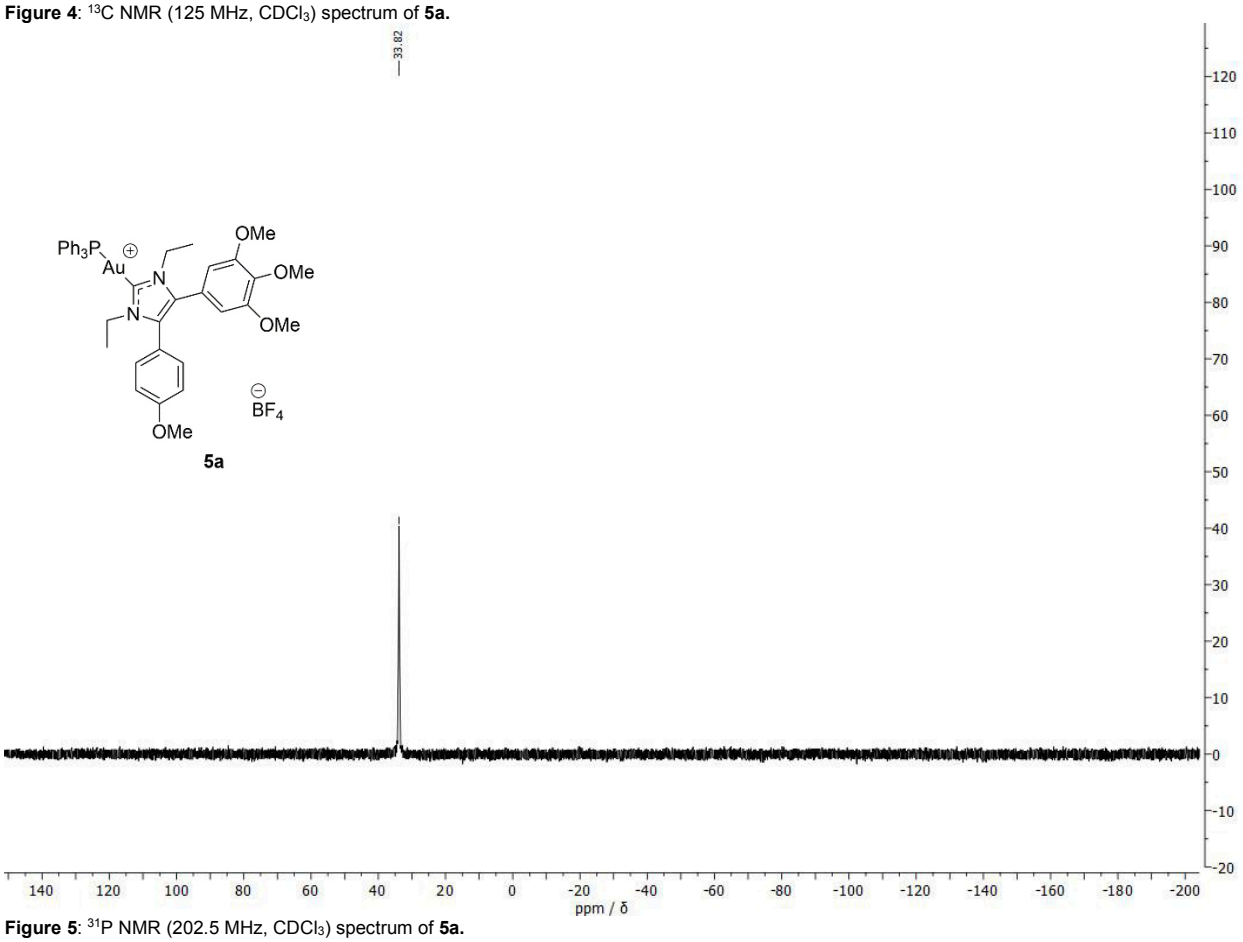

Figure 5: ^{31}P NMR (202.5 MHz, $CDCl_3$) spectrum of **5a.**

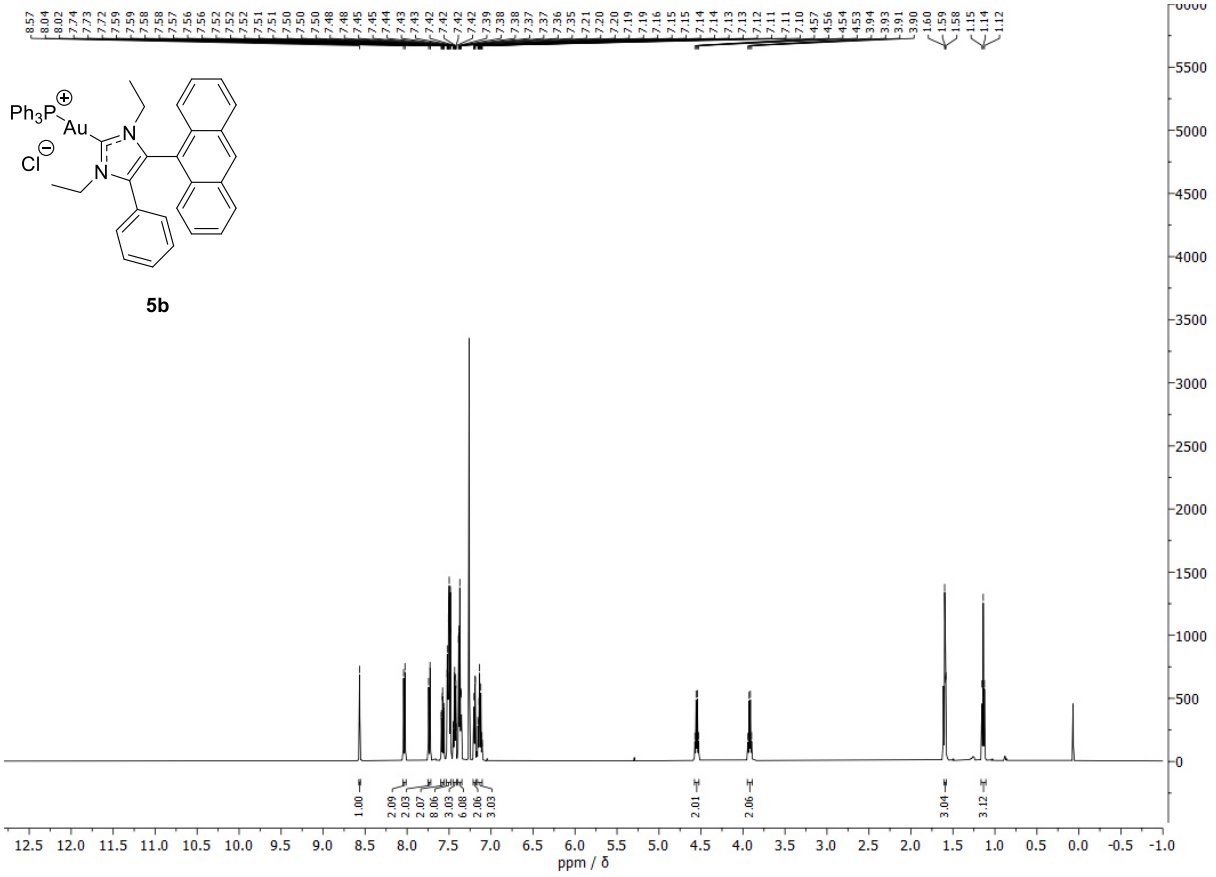

Figure 6: ^{1}H NMR (500 MHz, $CDCl_3$) spectrum of **5b.**

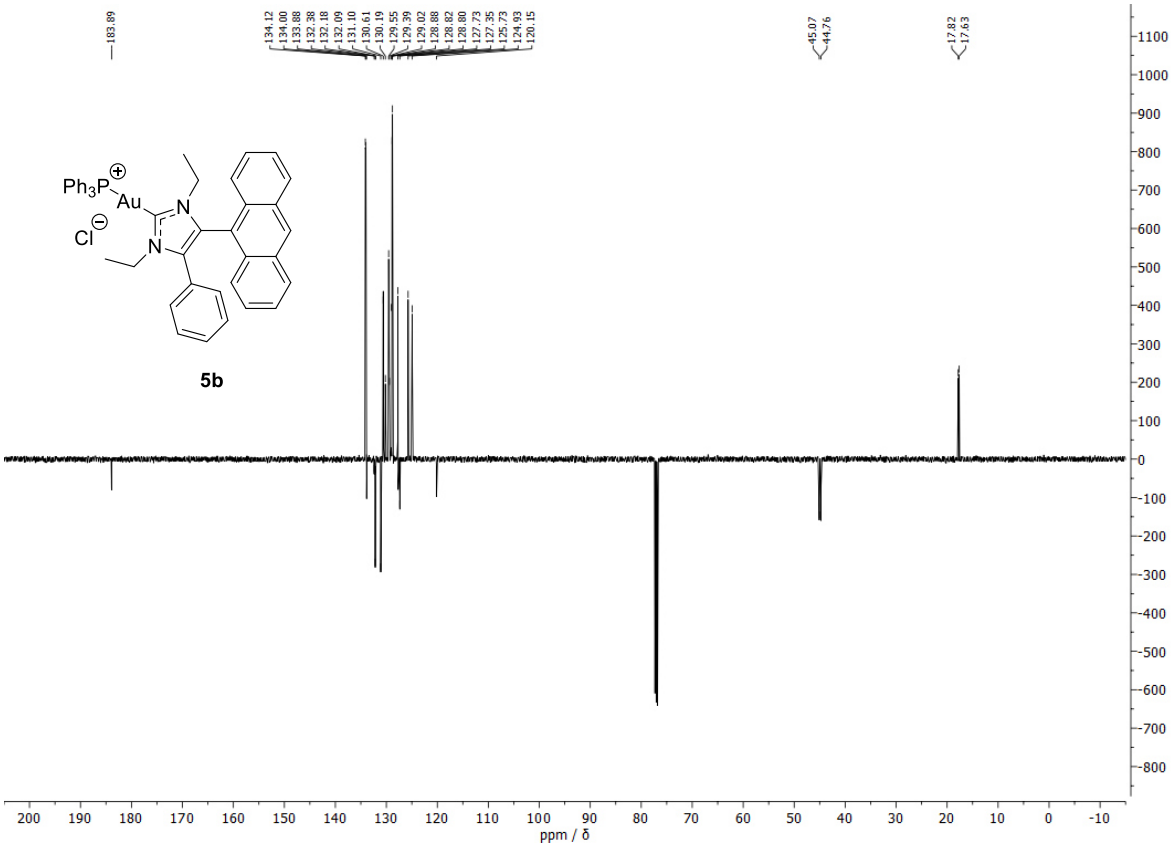

Figure 7: ^{13}C NMR (125 MHz, $CDCl_3$) spectrum of **5b.**

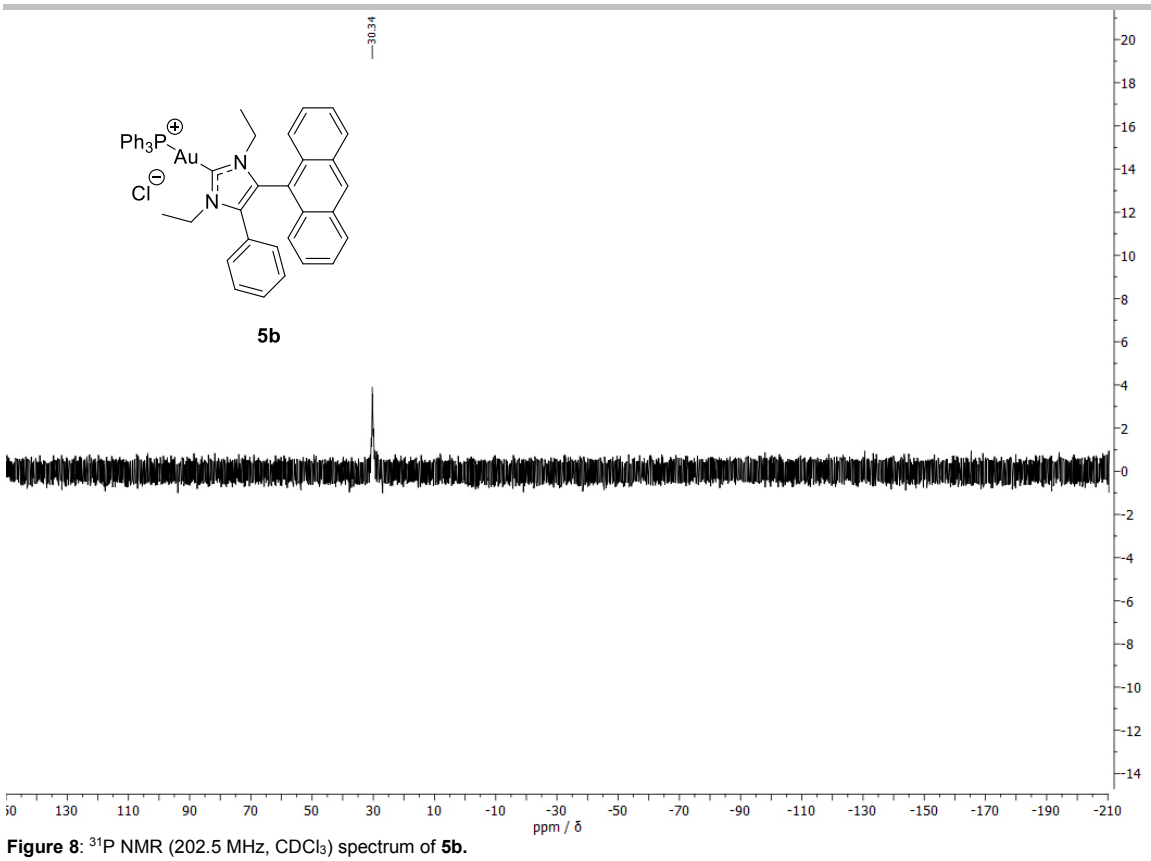

Figure 8: ^{31}P NMR (202.5 MHz, $CDCl_3$) spectrum of **5b.**

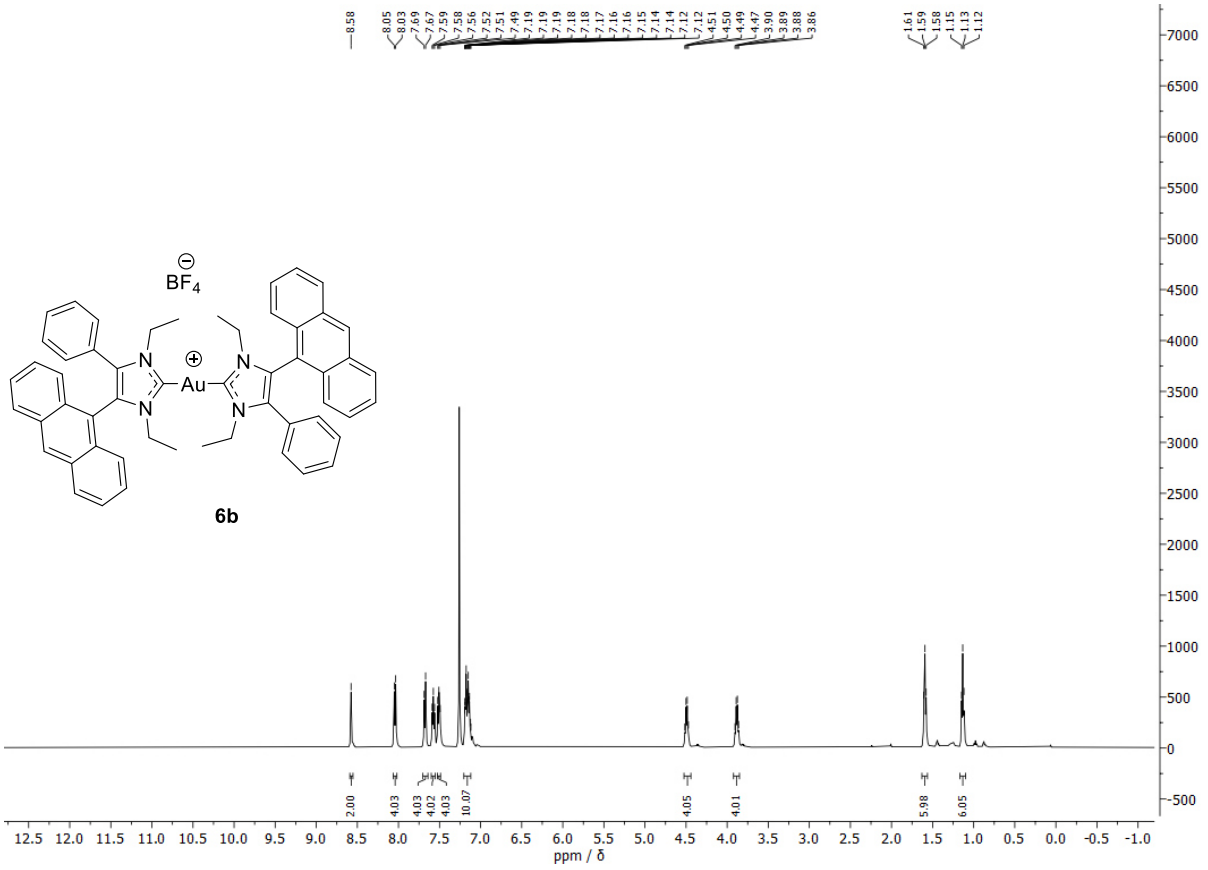

Figure 9: ^{1}H NMR (500 MHz, $CDCl_3$) spectrum of **6b.**

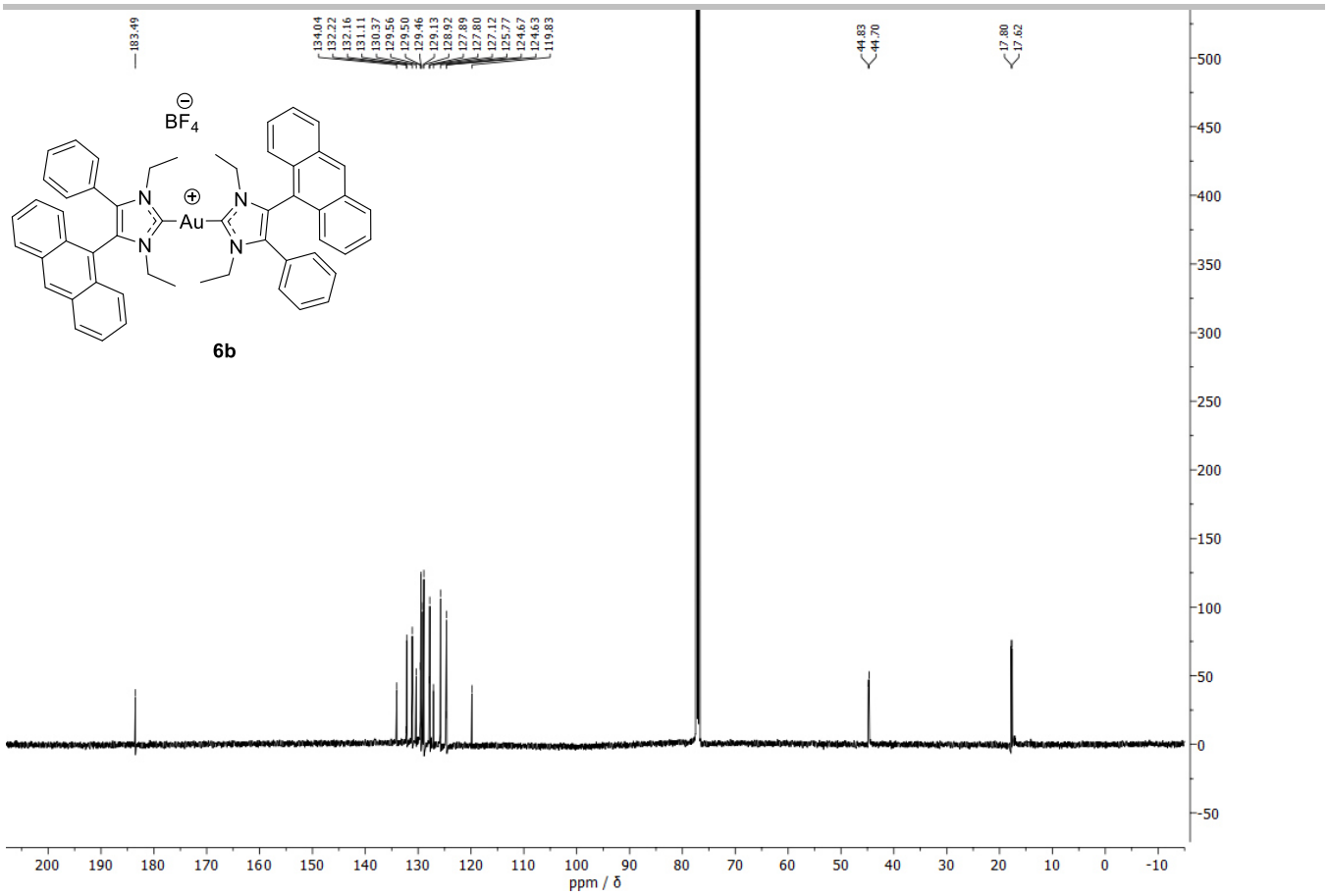

Figure 10: ^{13}C NMR (125 MHz, $CDCl_3$) spectrum of **6b.**

Biochemical Evaluation

Stock solutions of all test compounds were prepared (10 mM in DMF) and stored for at most one week at -20 °C. They were diluted, assay-depending, in ddH_2O, cell culture medium, or buffer.

Cell lines and culture conditions.

518A2 (Department of Radiotherapy and Radiobiology, University Hospital Vienna) human melanoma cells, HCT-116 (ACC-581) human colon carcinoma cells, as well as its p53 knockout mutant cell line HCT-116$^{p53-/-}$, HeLa cervix carcinoma, KB-V1^{Vbl} multi-drug resistant cervix carcinoma cells, and HDFa (ATCC® PCS-201-012™) human dermal fibroblasts were grown in Dulbecco´s Modified Eagle Medium (DMEM; Biochrom) supplemented with 10% (v/v) fetal bovine serum (FBS; Biochrom) and 1% (v/v) Antibiotic-Antimycotic solution (Gibco). The cells were incubated at 37 °C, 5% CO_2, 95% humidified atmosphere and were serially passaged following trypsinisation by using 0.05% trypsin/0.02% EDTA (w/v; Biochrom GmbH, Berlin, Germany). The maximum-tolerated dose of vinblastine was added to the cell culture medium 24 h after every cell passage to keep the KB-V1^{Vbl} cells resistant. The 518A2 melanoma cells are not available from cell banks, yet easily identified by their large size and flattened, spread-out morphology. Mycoplasma contamination was frequently monitored, and only mycoplasma-free cultures were used.

Inhibition of cell growth (MTT assay).[2]

The cytotoxic effect upon treatment with gold complexes **4**–**6** and auranofin for 72 h was determined by standard MTT assays. The tetrazolium salt 3-(4,5-dimethylthiazol-2-yl)-2,5-diphenyltetrazolium bromide (MTT; ABCR) is reduced by viable cells to a violet, water-soluble formazan. 518A2 melanoma cells, colon carcinoma cells HCT-116 and HCT-116$^{p53-/-}$, mdr KB-V1^{Vbl} and HeLa cervix carcinoma cells (5×10^4 cells mL^{-1}, 100 µL/well), as well as HDFa cells (10×10^4 cells mL^{-1}, 100 µL/well) were seeded in 96-well tissue culture plates and cultured for 24 h at 37 °C, 5% CO_2 and 95% humidity. After treatment with the test compounds incubation of cells was continued for 72 h. Blank and solvent controls were treated identically. After addition of a 5 mg mL^{-1} MTT stock solution in phosphate buffered saline (PBS), microplates were incubated for 2 h at 37 °C, centrifuged at 300 g, 4 °C for 5 min and the supernatant was discarded. The precipitate of formazan crystals was then redissolved in a 10% (w/v) solution of sodium dodecylsulfate (SDS; Carl Roth) in DMSO containing 0.6% (v/v) acetic acid. To ensure complete dissolution of the formazan, the microplates were incubated for at least 1 h in the dark. Finally the absorbance at λ = 570 and 630 nm (background) was measured using a microplate reader (Tecan F200). All experiments were carried out in quadruplicate and the percentage of viable cells was calculated as the mean ± SD with controls set to 100%.

Intracellular localisation of gold complexes.

518A2 melanoma cells (500 µL/well, 0.5×10^5 cells/mL) were seeded on glass coverslips in 24-well plates and incubated under cell culture conditions for 24 h. The medium was aspirated and the cells were washed once with PBS. Nuclear counterstaining was performed with Nuclear Green LCS1 (5 µM; abcam) with an incubation time of 15 min under standard cell culture conditions. MitoTracker™ (Thermo Fisher) was used for mitochondrial staining, and the cells were incubated with this dye for 30 min. For lysosomal staining, the cells were incubated 20 min in an acridine orange solution (5 µg/mL, 400 µL/well). The cells were then washed twice with PBS and fresh DMEM was added. Then the cells were treated with the test compounds at a concentration of 30 µM and incubated for 30 min at standard cell culture conditions. The cells were fixed for 20 min at rt after a washing step with PBS in 3.7% formaldehyde solution in PBS, then washed three times and the coverslips were mounted in ProLong™ Gold Antifade Mountant (Invitrogen). The localisation of the test compounds was documented using confocal microscopy (Leica Confocal TCS SP5, 1000× magnification).

Caspase-3/7 activation assay.

For caspase activity measurements the Apo-ONE® Homogenous Caspase-3/7 Assay Kit (Promega Corp., Wisconsin, USA) was used. 518A2 melanoma cells (67.5 µL/well; 2×10^5 cells mL^{-1}) were grown in black 96-well plates for 24 h (37 °C, 5% CO_2 and 95% humidity). After incubation with different concentrations of the test compounds or solvent for 24 h under cell culture conditions, fluorogenic 1× caspase-3/7 substrate solution was added to each well and the substrate transformation by activated caspase-3/7 was performed for 45 min at rt. The fluorescence intensity (λ_{ex}: 485 ± 20 nm, λ_{em}: 530 ± 25 nm) was measured using a microplate reader (Tecan F200). Blank values (caspase-3/7 substrate solution plus test compound/solvent) were subtracted to reduce background signals, and a potential loss of cell viability after the incubation with the test compounds was taken into account by performing an MTT-assay as described above. The caspase-3/7 activity of the remaining vital cells was calculated as means ± SD with solvent controls set to 100%. All experiments were carried out at least in quadruplicate.

Detection of morphological signs of apoptosis.

518A2 melanoma cells (3 mL/well, 5×10^4 cells mL^{-1}) were grown in 6-well plates for 24 h (37 °C, 5% CO_2 and 95% humidity). After incubation with IC_{50} concentrations of the test compounds (staurosporine: 500 nM, **4a**: 19.8 µM, **4b**: 7.9 µM, **5a**: 5.0 µM, **5b**: 2.9 µM, **6a**: 0.4 µM, **6b**: 5.5 µM) or solvent for 2.5 h under cell culture conditions, morphological changes of the cells were documented via brightfield microscopy (ZEISS Axiovert 135 and AxioVert MRc5, 100× magnification).

Annexin-V-FITC/PI staining.

For Annexin-V-FITC staining the TACS® Annexin-V-FITC Apoptosis Detection Kit (Trevigen, Maryland, USA) was used. 518A2 melanoma cells were seeded on glass coverslips (500 µL/well, 5×10^4 cells mL^{-1}) in 24-well plates, incubated under cell culture conditions (37 °C, 5% CO_2 and 95% humidity) for 24 h and treated with IC_{50} concentrations of the test compounds (staurosporine: 500 nM, CDDP: 7.8 µM,[3] **4a**: 19.8 µM, **4b**: 7.9 µM, **5a**: 5.0 µM, **5b**: 2.9 µM, **6a**: 0.4 µM, **6b**: 5.5 µM) or solvent for a further 45 min under cell culture conditions. Afterwards the medium was aspirated and the cells were stained with 150 µL of Annexin-V-FITC/PI staining solution for 15 min according to the manufacturer´s instruction. Apoptosis-induced exposure of phosphatidylserine on the outer leaflet of the cytoplasmic membrane was documented by fluorescence microscopy (ZEISS Imager A1 AX10, 200× magnification). For differentiation between early apoptotic and late apoptotic/necrotic cells (which have lost membrane integrity), cells were counterstained with PI (propidium iodide).

Ethidium bromide saturation assay.

A potential DNA interaction of complexes **4**–**6** was assessed by a fluorescence-based ethidium bromide (EtdBr) staining assay. Salmon sperm DNA (SS-DNA, Sigma-Aldrich) in TE buffer (10 mM Tris-HCl, 1 mM EDTA, pH 8.5) was pipetted into a black 96-well plate to reach a final amount of 1 µg/100 µL assay volume and incubated with varying concentrations of test compounds for 2 h at 37 °C. Afterwards, 100 µL of EtdBr solution (10 µg mL^{-1} in TE buffer) was added to each well. The fluorescence (λ_{ex} = 535 nm, λ_{em} = 595 nm) was measured using a microplate reader (Tecan F200) after 5 min of incubation. Each fluorescence value was corrected for intrinsic compound and EtdBr background fluorescence. A decreased fluorescence indicates an interaction between DNA and test compound which prevents the intercalation of EtdBr molecules into the double-stranded SS-DNA. All experiments were carried out in triplicate and the relative EtdBr fluorescence was quoted as means ± standard deviation with solvent controls set to 100%.

Electrophoretic mobility shift assay (EMSA).

Circular pBR322 plasmid DNA (1.5 µg; Thermoscientific) was incubated with dilution series (0, 25, 50, 75, 100 µM) of the test compounds or CDDP in TE-buffer (10 mM Tris-HCl, 1 mM EDTA, pH 8.5) for 24 h at 37 °C (20 µL total sample volume). Afterwards the DNA samples were subjected to DNA gel electrophoresis using 1% agarose gel in 0.5× TBE-buffer (89 mM Tris, 89 mM boric acid, 25 mM EDTA, pH 8.3). After staining the gels with an EtdBr solution (10 µg mL^{-1} in 0.5× TBE-buffer) for 30 min, DNA bands were visualized using UV excitation. All experiments were performed at least in duplicate.

Inhibition of thioredoxin reductase (TrxR) activity.

For the measurement of thioredoxin reductase (TrxR) activity the TrxR Colorimetric Assay Kit (Cayman Chemical) was used according to manufacturer´s instructions. 1×10^8 518A2 melanoma cells were harvested using a cell scraper, homogenised in 5 mL cold lysis buffer (50 mM K_3PO_4, 1 mM EDTA, pH 7.4) on ice and centrifuged for 15 min (4 °C, 10000×g). The protein concentration of the supernatant was determined via Bradford assays. Then, 10 µL Protease Inhibitor Cocktail Plus (Carl Roth) were added to 1 mL of the cell lysate which was either used for the assay right away or stored at -80 °C. Prior to use, the Assay Buffer was warmed to rt and the cell lysates, NADPH, aurothiomalate (ATM; specific TrxR inhibitor) and rat liver TrxR enzyme were thawed and kept on ice. After determination of the amount of cell lysate to use for optimum TrxR activity, all components were pipetted into the wells of a clear 96 well plate and the enzymatic reactions were initiated by addition of NADPH and 5,5´-dithio-bis(2-dinitrobenzoic acid) (DTNB). Then the absorbance at 405 nm was measured once every minute using a plate reader (Tecan F200) at at least ten time points. The TrxR activity was measured in the presence and absence of ATM. It is established that gold compounds such as ATM are highly specific inhibitors of mitochondrial TrxR.[4] Therefore, in presence of ATM an inhibition of TrxR can be assumed which allows a correction for TrxR-independent DTNB reduction (e.g. via glutathione). The difference between the two results renders the DTNB reduction due to TrxR activity. By plotting the average absorbance values as a function of time the slope of the linear portion of the curve was obtained, and the change of absorbance (ΔA_{405}) per minute could be determined. The values were corrected for unspecific DTNB reduction and the TrxR activity was calculated using the following formula: TrxR activity [µmol/min/mL] = [corrected ΔA/min (sample) / 7.92 mM^{-1}] × [0.2 mL / 0.02 mL] × sample dilution. The assay was conducted at 22 °C. All experiments were performed in triplicate and the solvent-treated negative controls were set to 100%.

Mitochondrial membrane potential.

518A2 melanoma cells (100 µL/well, 0.25×10^6 cells/mL) were seeded in transparent (for viability control via MTT) and black 96-well plates, followed by an incubation period of 24 h under cell culture conditions. The medium was replaced by 90 µL/well standard assay buffer (80 mM NaCl, 75 mM KCl, 25 mM D-Glucose, 25 mM HEPES, pH 7.4 in ddH_2O) and the cells were treated with a volume of 10 µL of various concentrations of test compounds or solvent (DMF). CCCP (10 µM) served as a positive control. The cells were incubated for a further 45 min under standard cell culture conditions. Then 10 µL/well of a TMRM (tetramethylrhodamine methyl ester; Cayman Chemicals) solution were added (2 µM in standard assay buffer), followed by an incubation period of 10 min under exclusion of light. The cells were washed three times (160 µL PBS per well) and the fluorescence signal was measured after adding 100 µL PBS per well (Tecan F200, $\lambda_{ex}/\lambda_{em}$: 535/590 nm). The fluorescence signal was correlated to viability, determined by corresponding MTT assays.

Determination of intracellular concentration of reactive oxygen species (DCFH-DA assay).

518A2 melanoma cells were seeded in black 96 well plates (100 µL/well, 0.1×10^6 cells/mL) and incubated for 24 h under standard cell culture conditions. The medium was replaced by serum-free medium containing 20 µM DCFH-DA, followed by a further incubation periode of 30 min. Cells were washed twice with PBS (100 µL/well) and fresh medium without FBS was added (100 µL/well). After treatment with 10 µM of the test compounds or solvent, the cells were incubated for 1 h under standard cell culture conditions and subsequently washed twice with PBS. The cells were kept in PBS and the fluorescence was measured (Tecan F200, $\lambda_{ex}/\lambda_{em}$: 485/535 nm). Solvent-treated cells were taken as negative controls and their fluorescence was set to 100%.

Lysosomal integrity.

518A2 melanoma cells (500 µL/well, 0.05×10^6 cells/mL) were seeded on glass coverslips in 24 well plates and incubated for 24 h under standard cell culture conditions. Then the cells were treated with the test compounds at IC_{50} concentrations and incubated for 1, 2, 4 or 6 h under standard cell culture conditions. 30 min before each time interval ended, cells were stained with Lysosomal Staining Kit Orange - Cytopainter (Abcam). To this end, medium was aspirated and the cells were washed once with 1 mL HHBS (Hanks Buffer with HEPES; 140 mM NaCl, 5 mM KCl, 1 mM $CaCl_2$, 0.4 mM $MgSO_4 \times 7H_2O$, 0.5 mM $MgCl_2 \times 6H_2O$, 0.3 mM $Na_2HPO_4 \times 2H_2O$, 0.4 mM KH_2PO_4, 6 mM D-glucose, 20 mM HEPES, pH 7.0). The cells were treated with 300 µL staining solution, incubated for 30 min under standard cell culture conditions, washed twice with 1 mL HHBS and fixed for 10 min at rt in 1 mL/well 3.7% formaldehyde in PBS. After three further washing steps, the coverslips were washed with 500 µL ddH_20 and embedded on glass slides with ProLong Gold™ (Invitrogen) containing 1 µg/mL DAPI. Lysosomal and nuclear staining was documented using a fluorescence microscope (Zeiss Imager A1 AX10, 400-fold magnification).

Stability testing via NMR spectroscopy.

Solutions of the test compounds were freshly prepared corresponding to stock solutions in dimethylformamide-d_7, 5 vol-% water-d_2 were added. ^1H NMR (500 MHz) spectra (16 scans) were measured at 0 h, 24 h, 48 h and 72 h to demonstrate the stability of the complexes in solution in the presence of water.

Tubulin polymerisation assay.

Purified porcine brain tubulin protein [5 mg/mL in Brinkley´s buffer 80 (BRB80)] containing 10% glycerol and 1.5 mM guanosine 5´-triphosphate (GTP)] was pipetted in a black 96-well half-area plate and mixed with the test compounds or solvent (DMSO) to a final concentration of 10 µM. The microplate was immediately placed in the pre-heated microplate reader (Tecan F200) and polymerisation was measured turbidimetrically at 37 °C by recording the absorption at 340 nm for 2 h in intervals of 20 s. All experiments were at least carried out in duplicate.

Cell cycle analysis.

518A2 melanoma cells (3 mL/well; 5×10^4 cells mL^{-1}) were grown on 6-well tissue culture plates for 24 h (37 °C, 5% CO_2, 95% humidity) and treated with different concentrations of the test compounds or solvent for another 24 h (37 °C, 5% CO_2, 95% humidity). The cells were harvested by trypsinisation and fixed in ice-cold 70% EtOH (1 h, 4 °C). After RNA digestion and propidium iodide (PI; Carl Roth) staining with PI staining solution (50 µg mL^{-1} PI, 0.1% sodium citrate, 50 µg mL^{-1} RNAse A in PBS) for 30 min at 37 °C to quantitatively stain DNA, the fluorescence intensity of 10 000 single cells was measured at λ_{em} = 570 nm (λ_{ex} = 488 nm laser source) with a Beckmann Coulter Cytomics FC500 flow cytometer. The percentage of cells in the different phases of the cell cycle (G1, S and G2/M phase) was determined by CXP software (Beckmann Coulter). The percentage of apoptotic and necrotic cells was derived from sub-G1 peaks.

Results

Influence on cellular morphology

To confirm induction of apoptosis after treatment of 518A2 melanoma cells with complexes **4-6** we additionally documented morphological alterations via brightfield microscopy (Fig. 11).

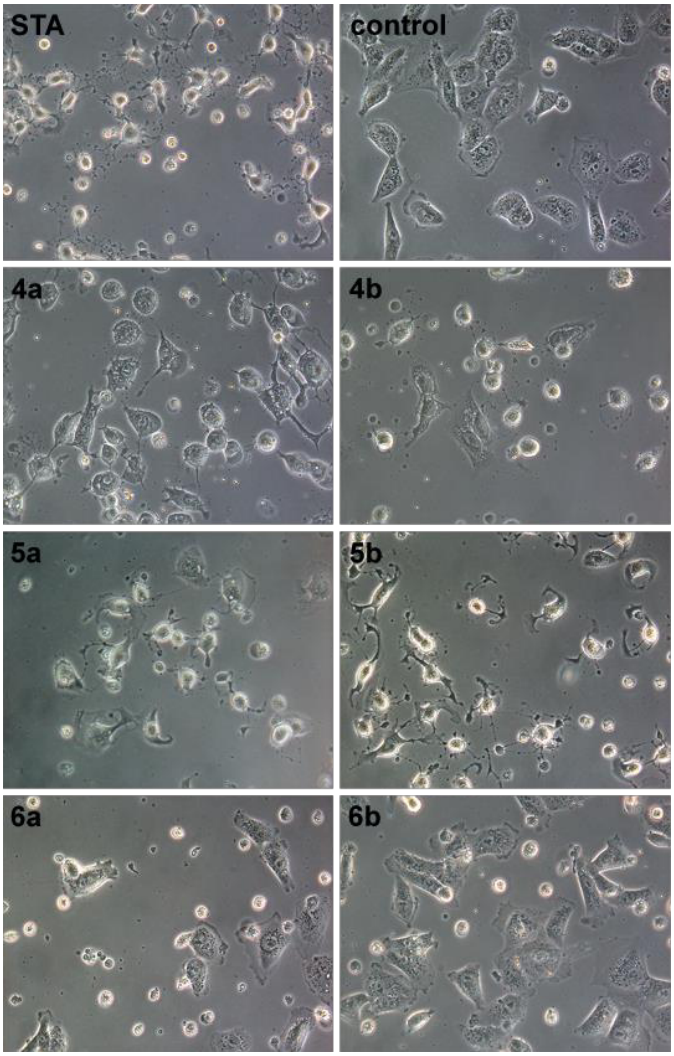

Figure 11: Morphological signs of apoptosis of 518A2 melanoma cells after incubation with staurosporine (STA; 500 nM) as well as IC_{50} concentrations of gold complexes **4-6** for 2.5 h. (**4a**: 19.8 µM, **4b**: 7.9 µM, **5a**: 5.0 µM, **5b**: 2.9 µM, **6a:** 0.4 µM, **6b**: 5.5 µM). Documented using brightfield microscopy, 100× magnification. Images are representative of at least three independent experiments.

Apoptosis detection using Annexin V-FITC and PI

Early apoptotic events upon treatment of 518A2 melanoma cells with gold complexes **4-6** were detected by staining of phosphatitylserines on the outer surface of the cytoplasmic membrane with Annexin-V-FITC. Early apoptotic and late apoptotic/necrotic cells could be differentiated by counterstaining with propidium iodide (PI), which can only enter cells lacking membrane integrity. Results were documented via fluorescence microscopy (Fig. 12).

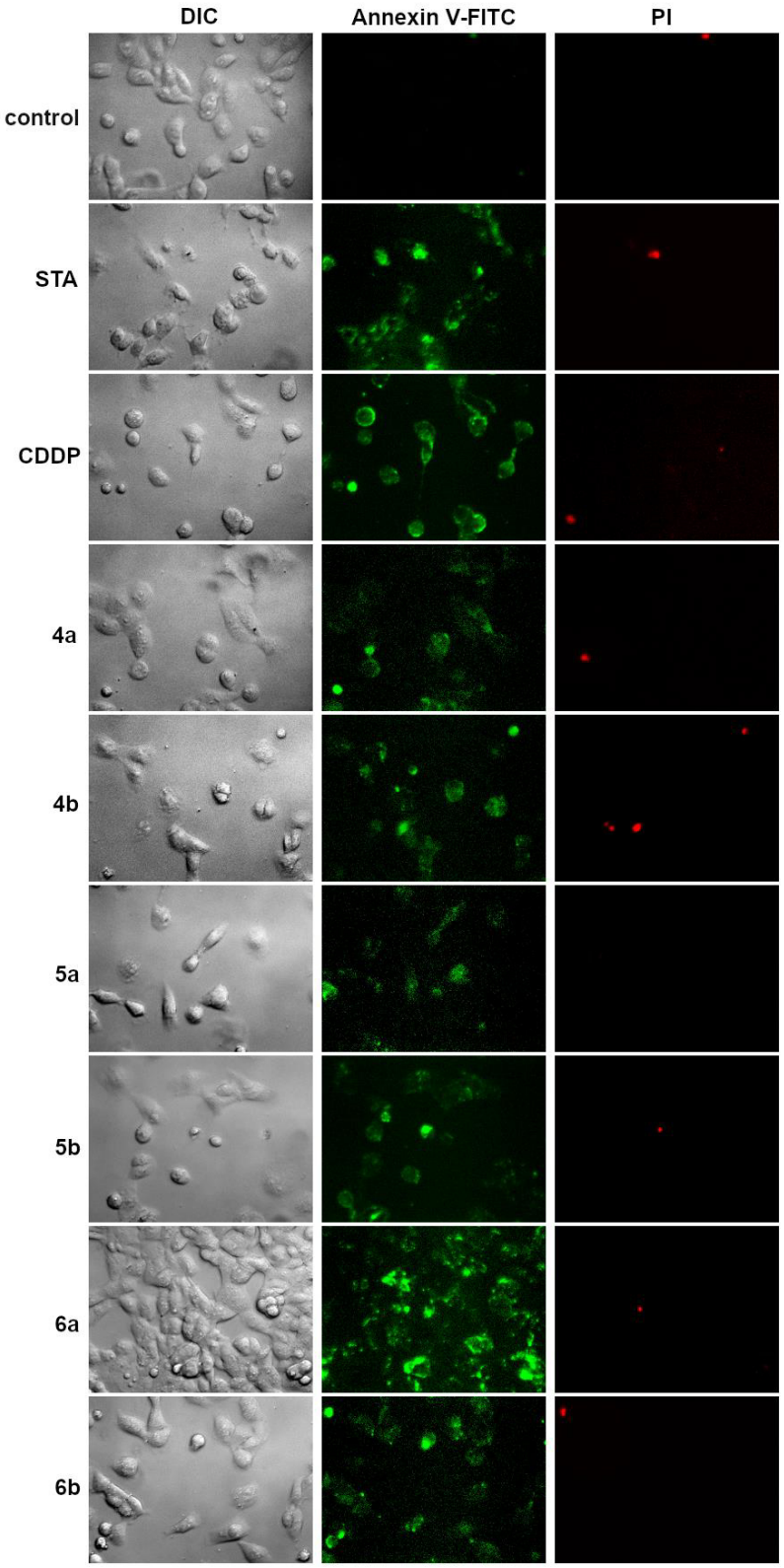

Figure 12: Annexin-V-FITC/PI staining of 518A2 melanoma cells treated with staurosporine (STA; 500 nM), CDDP (7.8 µM) as well as IC_{50} concentrations of gold complexes **4-6** for 45 min. (**4a**: 19.8 µM, **4b**: 7.9 µM, **5a**: 5.0 µM, **5b**: 2.9 µM, **6a**: 0.4 µM, **6b**: 5.5 µM). Documented using fluorescence microscopy, 200× magnification. Images are representative for at least three independent experiments.

Stability testing via NMR spectroscopy

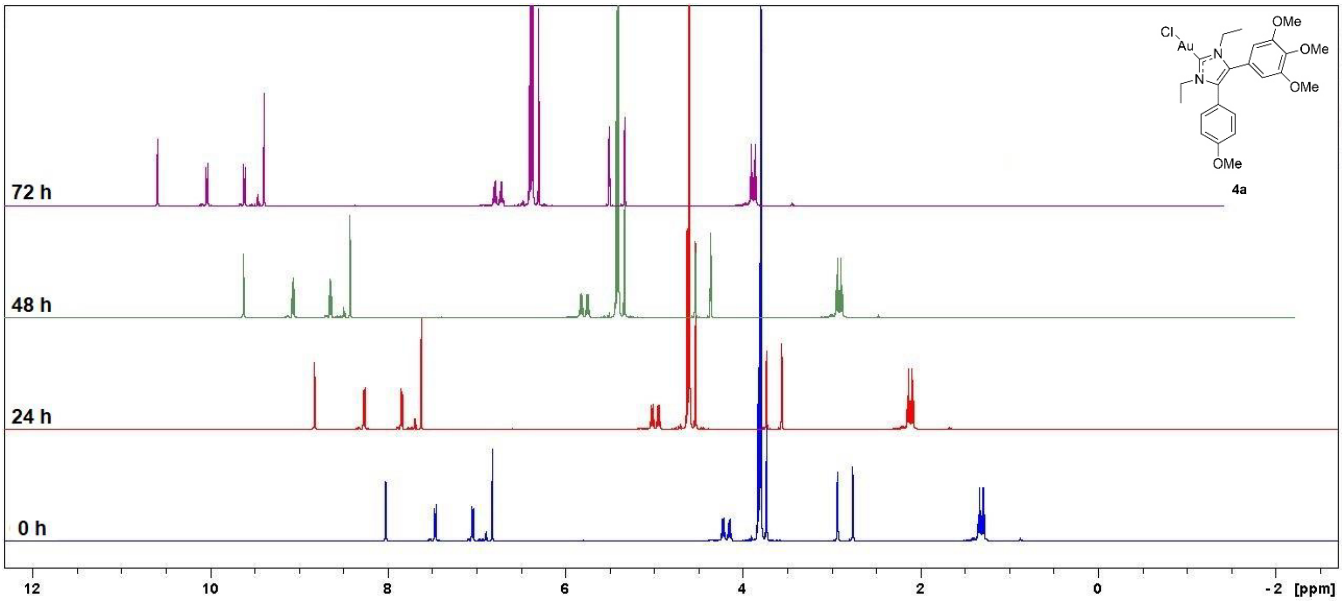

Figure 13: ^{1}H NMR (500 MHz, dimethylformamide-d_7, 5 vol-% water-d_2) spectra of **4a**; 0 h, 24 h, 48 h and 72 h after preparing of stock solution.

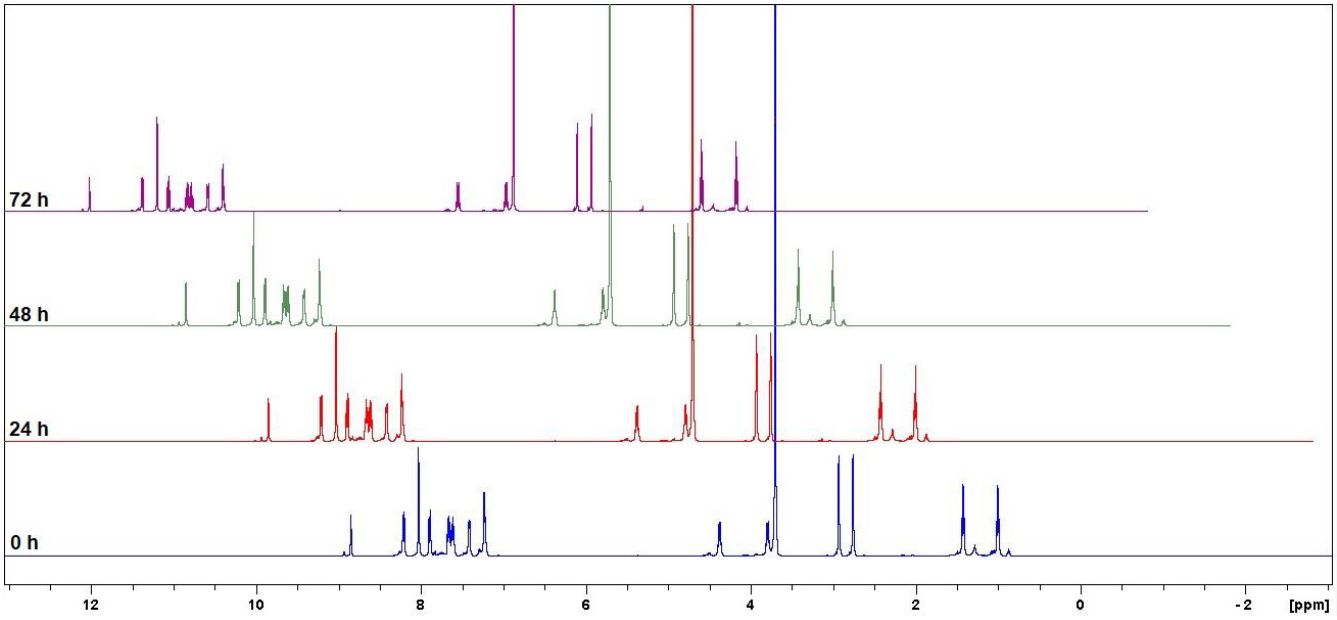

Figure 14: ^{1}H NMR (500 MHz, dimethylformamide-d_7, 5 vol-% water-d_2) spectra of **4b**; 0 h, 24 h, 48 h and 72 h after preparing of stock solution.

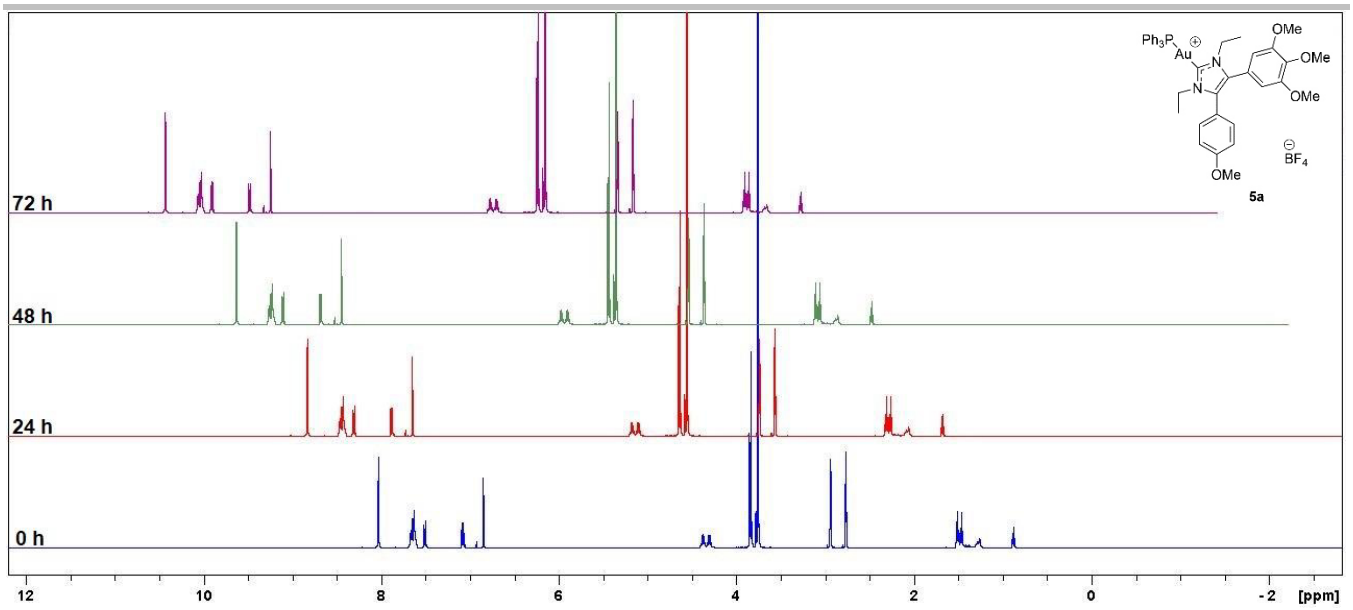

Figure 15: ^{1}H NMR (500 MHz, dimethylformamide-d_7, 5 vol-% water-d_2) spectra of **5a**; 0 h, 24 h, 48 h and 72 h after preparing of stock solution.

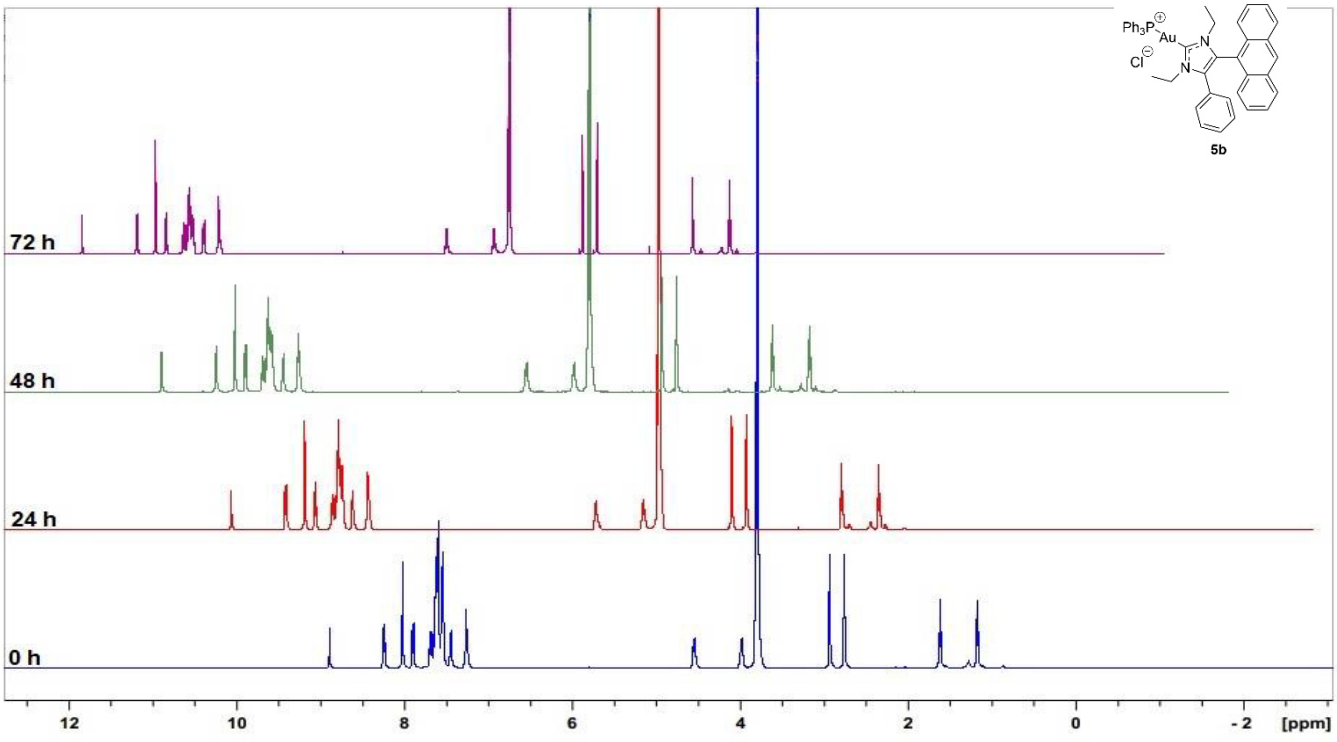

Figure 16: ^{1}H NMR (500 MHz, dimethylformamide-d_7, 5 vol-% water-d_2) spectra of **5b**; 0 h, 24 h, 48 h and 72 h after preparing of stock solution.

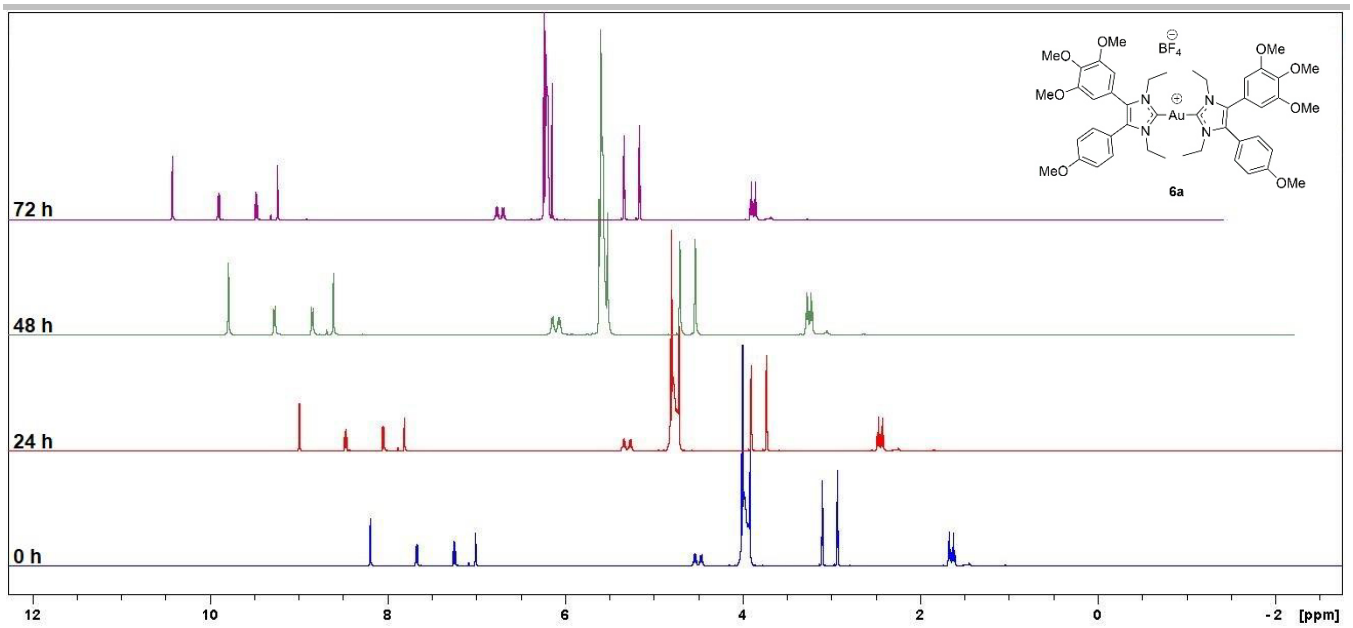

Figure 17: ^{1}H NMR (500 MHz, dimethylformamide-d_7, 5 vol-% water-d_2) spectra of **6a**; 0 h, 24 h, 48 h and 72 h after preparing of stock solution.

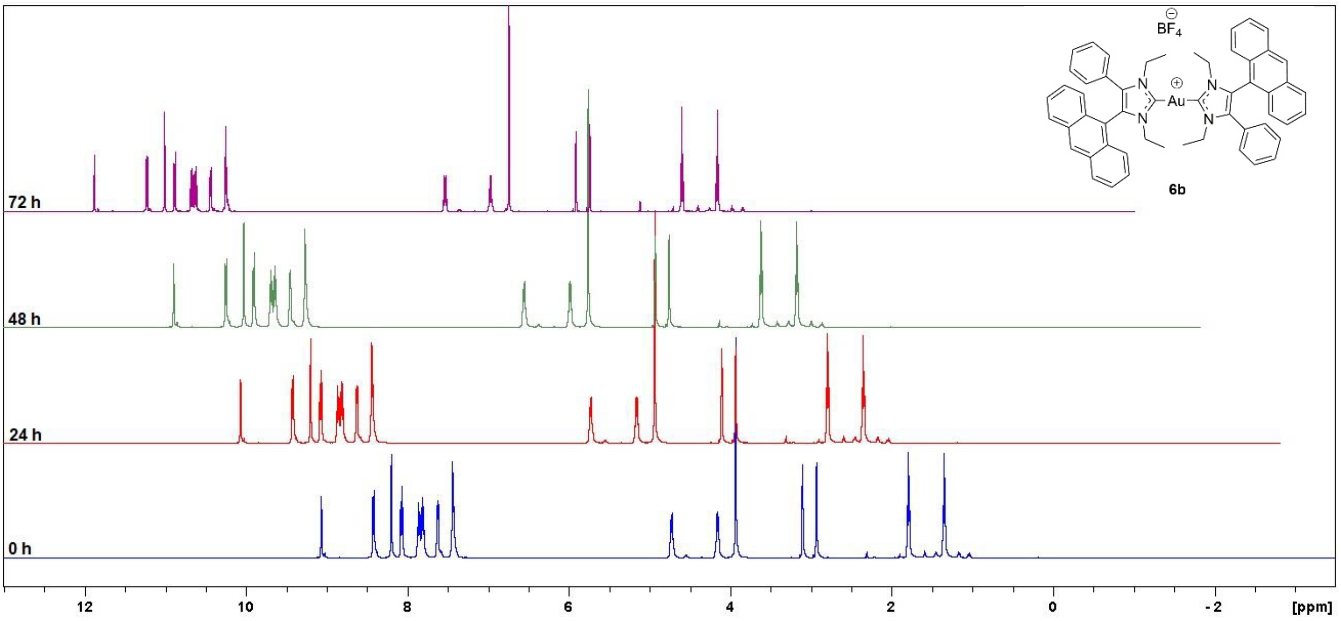

Figure 18: ^{1}H NMR (500 MHz, dimethylformamide-d_7, 5 vol-% water-d_2) spectra of **6b**; 0 h, 24 h, 48 h and 72 h after preparing of stock solution.

Interaction with tubulin

Figure 19 shows the results from tubulin polymerization assays with complexes **4-6**. The known microtubule-destabilizing compound combretastatin A-4 (CA-4) was used as a positive control. With the exception of complexes **5**, which induce a slight inhibition of tubulin polymerization, no effects could be observed for the other test compounds **4** and **6**.

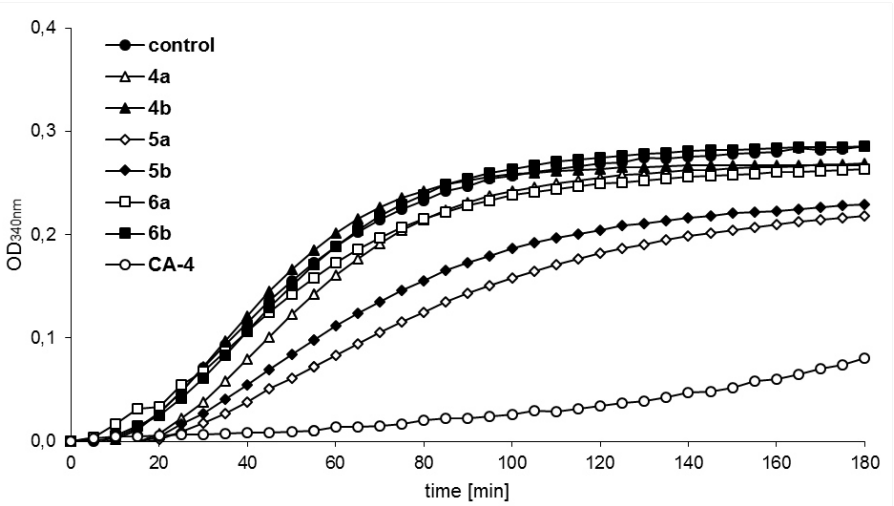

Figure 19: Turbidimetric measurement (OD at 340 ± 20 nm) of the polymerization of monomeric tubulin under the influence of the test compounds **4-6** at a final concentration of 10 µM. DMF was used as negative control, CA-4 at 10 µM was used as positive control. Values are representative of at least two independent measurements.

Influence on the cell cycle of 518A2 melanoma cells

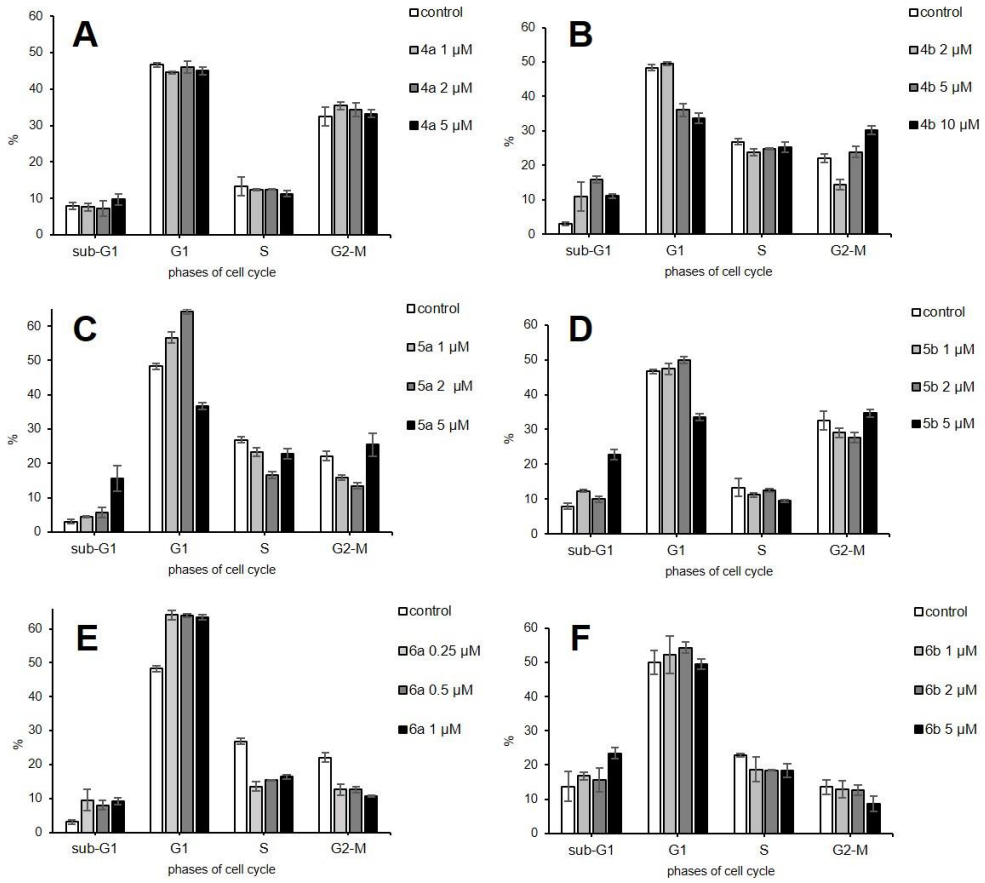

Figure 20. Influence of different concentrations of the test compounds **4a** (A), **4b** (B), **5a** (C), **5b** (D), **6a** (E) and **6b** (F) on the cell cycle of 518A2 melanoma cells measured via flow cytometry and PI staining; as a control the respective volume of solvent was used. Concentrations were adjusted to the IC_{50} values of the compounds for 518A2 melanoma cells in MTT assays. Values are means ± standard deviation derived from three independent assays.

References

[1] J. K. Muenzner, B. Biersack, H. Kalie, I. C. Andronache, L. Kaps, *et al*., *Chem. Med. Chem.* **2014**, *9*, 1195-1204.
[2] T. Mosmann, *J. Immunol. Methods* **1983**, *65*, 55-63.
[3] M. Gold, Y. Mujahid, K. Ahmed, H. Kostrhunova, J. Kasparkova, *et al., J. Biol. Inorg. Chem*. **2019**, 24, 647-657.
[4] M. P. Rigobello, L. Messori, G. Marcon, M. A. Cinellu, M. Bragadin, *et al*, *J. Inorg. Biochem*. **2004**, 98, 1634-1641

Author Contributions

S. I. Bär: Experimental studies and data acquisition (biochemical assays and stability tests), formal analysis, chemical analysis, project administration, writing of original draft, creation of graphics and art work; degree: lead, equal to M. Gold;
M. Gold: Experimental studies and data acquisition (biochemical assays and elemental analyses), formal analysis, project administration, writing of original draft, creation of graphics and art work; degree: lead, equal to S. I. Bär;
S. W. Schleser: Synthesis of gold(I) complexes, chemical analysis; degree: supporting;
T. Rehm: Synthesis of gold(I) complexes, chemical analyses; degree: supporting;
A. Bär: Synthesis of gold(I) complexes, writing of original draft; degree: supporting;
B. Biersack: Synthesis of gold(I) complexes, writing of original draft; degree: supporting;
L. Köhler: Experimental studies (EMSA); degree: supporting;
L. R. Carnell: Experimental studies (biochemical assays); degree: supporting;
R. Schobert: Project supervision, writing of original draft, funding acquisition, project coordination; degree: corresponding author;

5.5. Publikation V

Monitoring of circulating epithelial tumor cells (CETCs) by the Maintrac® method and its potential benefit for the therapy of patients with colorectal cancer

Madeleine Gold,[a] Katharina Pachmann,[b] Alexander Kiani,[c] Rainer Schobert*[a]

[a] Organic Chemistry Laboratory, University of Bayreuth, Universitaetsstrasse 30, 95440 Bayreuth, Germany

[b] Transfusion Centre Bayreuth, SIMFO GmbH Bayreuth, Kurpromenade 2, 95448 Bayreuth, Germany

[c] Department of Oncology and Hematology, Klinikum Bayreuth GmbH, Preuschwitzer Strasse 101, 95445 Bayreuth, Germany

* Corresponding author, Email address: Rainer.Schobert@uni-bayreuth.de

Molecular and Clinical Oncology
2021, 15, 201.

Reprinted with permission from Molecular and Clinical Oncology published by Spandidos Publications 2021, 15, 201, *Monitoring of circulating epithelial tumor cells (CETCs) by the Maintrac® method and its potential benefit for the therapy of patients with colorectal cancer.* M. Gold, K. Pachmann, A. Kiani, R. Schobert. Doi: 10.3892/mco.2021.2363.

Monitoring of circulating epithelial tumor cells using the Maintrac® method and its potential benefit for the treatment of patients with colorectal cancer

MADELEINE GOLD[1], KATHARINA PACHMANN[2], ALEXANDER KIANI[3,4] and RAINER SCHOBERT[1]

[1]Department of Chemistry, University of Bayreuth, D-95440 Bayreuth; [2]Transfusion Centre Bayreuth, SIMFO GmbH Bayreuth, D-95448 Bayreuth; [3]Department of Oncology and Hematology, Klinikum Bayreuth GmbH, D-95445 Bayreuth; [4]Comprehensive Cancer Center Erlangen-EMN (CCC ER-EMN), D-91054 Erlangen, Germany

Received February 11, 2021; Accepted July 13, 2021

DOI: 10.3892/mco.2021.2363

Abstract. Circulating tumor cells are an important link between primary tumors and metastases. A longitudinal monitoring of their numbers and properties can provide valuable information on therapy response and disease progression for patients with colorectal cancer. As several techniques for the detection of circulating tumor cells are notorious for yielding low detection rates in patients with non-metastatic colorectal cancer, the present study aimed to perform a proof-of-principle study using the Maintrac® approach for an assessment of circulating epithelial tumor cells (CETCs) in patients with colorectal cancer receiving neoadjuvant and/or adjuvant radio/chemotherapy (R/CT). CETCs in the peripheral blood of 22 patients with colorectal cancer were quantified by fluorescence image analysis (Maintrac®) before and after the first cycle of a neoadjuvant and/or adjuvant R/CT, as well as before and after surgical resection of the primary tumor. To determine that blood-borne CETCs originate from tumor tissues, spheres were cultured from CETCs as well as from primary tumor tissue and compared with the expression of tumor-specific antigens. Within the scope of this study, it was demonstrated that the Maintrac® method allows for the precise detection and characterization of CETCs in the blood of patients with colorectal cancer independent of tumor stage. Furthermore, correlations between CETC parameters and patients' response to neoadjuvant and/or adjuvant R/CT that have been described in previous literature could be reproduced. Whether the observed trends are of a general nature and suitable as an auxiliary criterion for prognosis and treatment decisions remains to be shown. Patients with rectal cancer may benefit from CETC monitoring as a method to select suitable patients for adjuvant therapy.

Correspondence to: Professor Rainer Schobert, Department of Chemistry, University of Bayreuth, Universitaetsstrasse 30, D-95440 Bayreuth, Germany
E-mail: rainer.schobert@uni-bayreuth.de

Abbreviations: CETCs, circulating epithelial tumor cells; EGF, epidermal growth factor; EpCAM, epithelial cell adhesion molecule; FBS, fetal bovine serum; PD-L1, programmed death-ligand 1

Key words: circulating tumor cells, circulating epithelial tumor cells, Maintrac®, colorectal cancer

Introduction

For both sexes, colorectal cancer is the second leading cause of cancer-related death, globally (9.2%) (1). The growing incidence, especially in industrialized countries, can be attributed to a change in lifestyle connected with obesity, physical inactivity, alcohol consumption and high red meat intake (2). Colorectal cancer is the result of a stepwise transition from normal mucosa to an invasive tumor, comprising several intermediate stages of premalignant or invasive lesions. As this process often drags on for years, cancer prevention and early diagnosis through screening programs represent a mainstay in colon cancer assessment and avoidance (3). Symptoms are generally associated with large tumors or advanced disease stages, and in most cases are relatively unspecific, so that the majority of colorectal cancers go unnoticed in early stages (3). Therapeutic options for the treatment of malignant tumors are resection, radiation and/or chemotherapy, depending on tumor stage and patient characteristics (3-5).

In the last 30 years, the survival of patients suffering from colorectal cancer has increased markedly, owing mainly to the introduction of screening programs and of new therapeutic agents (6). Conventional cytotoxic chemotherapy is the backbone of treatment for colorectal cancer patients with lymph node positive disease (7). Over the last decade, targeted therapies came to the fore with genomic markers enabling the selection of appropriate patients, who generally represent a minority among the whole patient population (8). But with the latest results regarding total neoadjuvant therapy (TNT), also cytotoxic chemotherapy gains in importance again. Both, the RAPIDO-, as well as the PRODIGE 23-study showed a significant and clinically relevant extension of disease-free survival after TNT instead of conventional, neoadjuvant RCT (9,10). Although some prognostic indicators

for the probable response to conventional chemotherapy were identified, most of the proposed biomarkers and predictive assays are not currently used in the clinic, because of lacking validation, practicability and scalability, and of long turnaround times, or extensive costs (8,11-13). Altogether, there is a great demand for analytical methods easy-to-apply, which may support physicians with therapy decisions, and help to protect patients from under- or over-treatment.

Circulating tumor cells, readily accessible from blood samples of patients with solid tumors, are an important link between primary tumors and metastases. A longitudinal monitoring of their numbers and properties can provide valuable information on therapy response and disease progression. Various studies demonstrated a correlation between circulating tumor cells and metastases, survival and therapy response for patients with different types of cancer (14-18).

Ki-67 is a non-histone nuclear protein, which is expressed in actively proliferating cells throughout the cell cycle, but not in quiescent (G0) cells (19). Besides its detection in primary tumors, Ki-67 was also shown to be expressed in circulating tumor cells (20), and so might constitute a biomarker for identifying patients at a high risk of metastatic relapse.

While circulating tumor cells were shown to have prognostic potential for tumors of different entities (14-18), their clinical importance in colorectal cancer remained unclear. Our study was designed to use the immunofluorescence-based Maintrac® method to identify and quantify circulating epithelial tumor cells (CETCs) in the blood of patients with colorectal carcinoma (ICD10: C18/20) before and during neoadjuvant and/or adjuvant R/CT. Moreover, the ratio of CETCs expressing the proliferation marker Ki-67 was determined during the course of therapy.

Materials and methods

Patient and inclusion criteria. A total of 22 patients, diagnosed with colorectal cancer, were enrolled in this study between October 2018 und August 2020. Before treatment, all patients passed a complete clinical evaluation including clinical history, physical examination, rectoscopy/colonoscopy, relevant blood examination and chest/abdominal computed tomography. Local stage was determined according to the TNM classification of the UICC (21). The recruitment criteria were as follows: Histologically confirmed, invasive colorectal carcinoma (ICD10: C18/C20); primary diagnosis. The characteristics of all patients enrolled in this study are shown in Table I. All patients were treated according to current treatment guidelines for colon (ICD10: C18) or rectal (ICD10: C20) cancer (22). Long term R/CT for rectal cancer was performed as follows: Radiation dose: 50.4 Gy (single dose 1.8 Gy); target volume: Rectal cancer and region of pelvic lymphatic drainage; chemotherapy: 5-Fluorouracil (10 patients), Capecitabine (1 patient), 5-Fluouracil/Oxaliplatin (3 patients). Individual therapy decisions were within the discretion of the attending physician and independent of any data collected in the course of this study. For patients receiving neoadjuvant therapy, 7.5 ml peripheral blood samples were obtained 1-7 days before initiation of R/CT, 17±3 days after the first cycle of R/CT, and after the completion of R/CT (1-7 days before surgery). For patients with only or additional adjuvant therapy, blood samples were obtained 1-7 days before surgery, 6-8 weeks after surgery (before initiation of adjuvant therapy), 17±3 days after the first cycle of adjuvant chemotherapy, and on the last day of therapy, respectively.

The study was based on the Ethics Declaration of Helsinki and was approved by the Ethics Committee of the University of Bayreuth. Participants provided their written informed consent to participate in this study.

Assessment of tumor regression after neoadjuvant therapy. For all rectal cancer patients, treatment responses were assessed according to the pathological results after surgery, and graded by histological evaluation of the surgical specimens according to the criteria described by Dworak *et al* (23). The grade of tumor regression was defined as follows: Grade 0: No regression; Grade 1: Dominant tumor mass with obvious fibrosis and/or vasculopathy; Grade 2: Dominantly fibrotic changes with few tumor cells or groups (easy to find); Grade 3: Very few tumor cells (difficult to find microscopically) in fibrotic tissue with or without mucous substance; Grade 4: No tumor cells, only fibrotic mass (total regression/response).

For a proper assessment of therapy response, we additionally compared the tumor size and lymph node status as assessed by computed tomography and/or endosonography of each patient before and after neoadjuvant R/CT. According to Dworak regression grade, as well as TNM re-staging, each patient was individually assigned either to the group of good or poor responders to neoadjuvant R/CT (Table II).

Blood collection and Maintrac® analysis. Peripheral blood (7.5 ml) from 22 patients with colorectal cancer at different stages of disease was drawn into blood count tubes containing ethylenediaminetetraacetic acid (EDTA) as an anticoagulant and processed 24 h after collection.

The Maintrac® approach was used for identification, quantification and further characterization of CETCs (22). To this end, 1 ml of EDTA-blood was subjected to red blood cells lysis at 4˚C for 15 min using 14 ml erythrocyte lysis buffer (Qiagen GmbH). Remaining cells were spun down at 700 x g for 7 min at rt and resuspended in 500 μl of PBS/EDTA buffer. Immunostaining was performed by adding 4 μl fluorescein-isothiocyanate (FITC)-conjugated anti-human epithelial cell adhesion molecule (EpCAM) antibody (clone HEA-125; Miltenyi Biotec GmbH) to 25 μl of the cell suspension (about 10^7 cells/100 μl) and incubation for 20 min at 4˚C in the dark. The corresponding isotype control for EpCAM (mouse IgG1 K FITC; Miltenyi Biotec) was used at the same final concentration. In case of co-staining of Ki-67, additional 2.5 μl of phycoerythrin (PE)-conjugated anti-Ki-67 antibody (clone B56; BD Biosciences) was added prior to incubation. Subsequently, all samples were diluted in PBS/EDTA buffer to a total volume of 250 μl. A defined volume of the cell suspension and propidium iodide (PI; Sigma-Aldrich; Merck KGaA) was transferred to the wells of ELISA-plates (Greiner Bio-one). Co-staining of cells with Ki-67 was performed without PI. Red and green fluorescence of the cells was examined using a Fluorescence Scanning Microscope ScanR (Olympus), enabling detection and relocation of cells for visual examination of EpCAM-, PI- or Ki-67-positive cells.

Table I. Clinicopathological characteristics of patients with colon (C18) and rectal (C20) cancer included in this study.

Clinicopathological characteristics	Number of patients with colon cancer, n (%)	Number of patients with rectal cancer, n (%)
Total	6 (27)	16 (73)
Age, years		
>60	5 (23)	11 (50)
≤60	1 (4)	5 (23)
Sex		
Female	3 (14)	6 (27)
Male	3 (14)	10 (45)
Tumor size[a]		
T1	0 (0)	0 (0)
T2	1 (4)	3 (14)
T3	4 (18)	11 (50)
T4	1 (4)	2 (9)
Lymph node status[a]		
Positive	6 (27)	4 (18)
Negative	0 (0)	12 (54)
Distant metastasis		
Positive	1 (4)	1 (4)
Negative	5 (23)	15 (68)
Neoadjuvant therapy	1 (17)[b]	14 (64)
Adjuvant therapy	6 (27)	3 (14)

[a]Obtained by histopathological examination of a surgical specimen; [b]one patient with carcinoma of the colon ascendens also had rectal cancer, for which neoadjuvant radiochemotherapy had been performed prior to study entry.

For quantification of CETCs, only vital CETCs with intact cell morphology and without PI staining were counted. For daily verification of optical components and detectors of the microscope, fluorospheres (Flow-Check 770; Beckman Coulter) were used.

Culture of spheres from peripheral blood. Only a small subpopulation of CETCs possessing additional stem cell properties is able to grow into metastases. By enumeration of CETCs able to clonally grow into CETC microspheres under specific conditions, we specified and quantified this subpopulation. Therefore, CETCs and leukocytes were isolated from peripheral blood as described earlier, plated at a density of $2x10^5$ cells/ml in RPMI-1640 supplemented with l-glutamine, HEPES, penicillin/streptomycin and growth factors such as EGF, insulin and hydrocortisone, and incubated under standard cell culture conditions (37˚C, 5% CO_2) in a sterile incubator. Every five days, the cultures were inspected under an inverted light microscope (PrimoVert) and fresh culture medium was added. Between days 21 and 28 of incubation, spheres were collected from the culture flasks, pelleted (250 x g, 7 min), and resuspended in 500 μl PBS. Immunostaining of spheres was performed using FITC-conjugated mouse anti-human EpCAM-antibody (clone HEA-125; Miltenyi Biotec GmbH), PE-conjugated mouse anti-human CD44-antibody (BD Biosciences) or mouse anti-human CD133-antibody (clone 7; BioLegend) for 20 min at 4˚C in the dark. The samples were then diluted in PBS/EDTA and transferred into the wells of a 96-well microtiter plate (Greiner Bio-one). Analysis of fluorescence was performed using a fluorescence scanning microscope (ScanR; Olympus). To verify vitality, PI staining of spheres was performed before the analysis. Finally, only vital CTC spheres with intact morphology and without PI staining were counted.

Primary culture from tumor tissue. In case of surgery of the primary tumor, a small piece of tissue from the middle of the tumor (ø depending on the size of the tumor) was obtained in a sterile falcon in 10 ml transportation medium (RPMI-1640, 5% FBS, 5 μg/ml insulin, 2.75 μg/ml transferrin, 20 mM sodium selenite, 55 μg/ml sodium pyruvate, 1 μM hydrocortisone, 1,000 U/ml penicillin, 1,000 μg/ml streptomycin, 250 mg/ml amphotericin B, 15 mM HEPES, 100 μg/ml gentamycin, 5 μg/ml metronidazole) directly from the operating theater and kept at 4˚C for transportation. All samples were processed within 24 h after withdrawal. For further processing, the tumor tissue was washed 3-5 times in PBS by extensive shaking and put into a sterile petri dish. Before the tissue was chopped into small pieces of about 1 mm in diameter by anti-parallel movement of two scalpels, it was covered with a small amount of sphere culture medium (RPMI-1640 supplemented with l-glutamine, HEPES, penicillin/streptomycin and growth factors such as EGF, insulin and hydrocortisone). After one more washing step with PBS, the tissue was enzymatically homogenized with Accumax™ solution (Sigma-Aldrich; Merck KGaA) for 45 min under continuous mixing at rt. Then the cell suspension was filtered using a cell strainer (mesh size 0.44 μm; Greiner Bio-one) to eliminate bigger cell clumps and centrifuged at 240 x g for 10 min at rt. The resulting cell pellet was resuspended in 1 ml of culture medium and the number of vital cells was determined by bromophenol blue staining. Finally, the cells were plated in a concentration of approximately $0.6x10^6$ vital cells/ml in culture medium in 6-well plates and incubated at standard cell culture conditions (37˚C, 5% CO_2) for several weeks. All cultures were checked for bacterial infections daily and in the case of a minor infection isolated and treated with additional antibiotics, or in case of a major infection, discarded. If primary tumor spheres were detectable after a few weeks, a small amount of the culture was harvested and immunostained for further characterization and documentation.

Statistical analysis. Statistical analysis was performed using SigmaPlot (version 14.0; Systat Software Inc.) for Windows. Comparisons between variables were performed using ANOVA (analysis of variance) followed by a post hoc test for parametric data, or Kruskal-Wallis test followed by Dunn's test for nonparametric data. The significance level was set at $P<0.05$.

Results

General. A total of 22 patients with histologically confirmed colorectal cancer (16 patients with rectal cancer, 6 patients

Table II. Responses of patients with rectal cancer (C20) after receiving neoadjuvant R/CT.

Patient number	TNM		Regression grade	Response category
	Before R/CT	After R/CT		
1	μ, T2; μ, N0	yp, T3b; yp, N1	1	Poor
2	μ, T2; c, T3; μ, N1	yp, T2; yp, N0	3	Good
3	μ, T3; μ, N+	yp, T2; yp, N0	2	Good
4	μ, T3; μ, N0	yp, T2; yp, N0	3	Good
5	μ, T3; μ, N1; c, M1HEP	yp, T3; yp, N0	3	Good
6	c, T4; c, N2b	yp, T3b; yp, N0	3	Good
7	c, T3; c, N+	yp, T3a; yp, N1b	3	Good
8	μ, T3; μ, N+	yp, T3a; yp, N0	3	Good
9	μ, T3; μ, N0	yp, T3b; yp, N0	1	Poor
10	μ, T2; μ, N+	yp, T3; yp, N0	2	Poor
11	c, T3; c, N1	yp, T4a; yp, N1b	3	Poor
12	μ, T2; μ, N+	yp, T3a; p, N0	1	Poor
13	μ, T3; μ, N1	yp, T3b; yp, N0	1	Poor
14	μ, T3; μ, N1; c, M1aPUL	yp, T4a; yp, N0; c, M1a	1	Poor

Patients with rectal cancer (C20) were assigned to either the group of good or poor responders according to Dworak regression grade and TNM re-staging. μ, stage determined by ultrasonography; c, stage determined by clinical examination; y, stage assessed after R/CT; p, stage given by histopathological examination of a surgical specimen; TNM, tumor node metastasis; R/CT, radio/chemotherapy.

with colon cancer) were enrolled in this study. Patients' characteristics are given in Table I.

Considering all patients (ICD10: C18 and C20), 1 patient was at stage I (4%), 7 patients were at stage II (32%), 12 patients were at stage III (55%), and 2 patients were at stage IV (9%). Six patients (27%) suffered from colon cancer and 16 (73%) from rectal cancer. The age of the patients ranged from 51 to 80 years (median 65.5 years). The median number of CETCs of all 22 patients with colorectal cancer was 55 CETCs per 100 μl cell suspension (ranging from 0 to 640) from which colon cancer patients (ICD10: C18) had a median CETC number per 100 μl of 45 (ranging from 0 to 145), and rectal cancer patients (ICD10: C20) of 65 (range from 0 to 640). No statistically significant differences in CETC numbers were observed in correlation to tumor size, lymph node status or distant metastasis (data not shown).

CETC quantification. Using the Maintrac® method we detected CETCs in 100% of colorectal cancer patients included in this study. CETC numbers of all patients during the course of therapy are specified in Table SI. In addition to epithelial characteristics as assigned by immunostaining, we could demonstrate proliferative and stemness properties of CETCs under specific conditions, which were identical to those of cells derived from the primary tumor itself (Fig. 1).

CETC characterization. CETCs from patient #1 were investigated for their proliferative activity by growing non-adhesive suspension cultures. Formation of EpCAM-positive spheres was observed after the first cycle of neoadjuvant R/CT (5 spheres/100 μl blood). Interestingly, CETCs from all other samples did not show any sphere formation. During surgery of patient 1, a small piece of tumor tissue was set aside and stored on ice until further processing. After separation and washing, primary tumor cells were cultured under the same conditions as CETCs, also resulting in the formation of spherical structures. Both, spheres from the primary tumor, as well as spheres from the peripheral blood of patient #1 were further characterized by immunostaining (Fig. 1). The viability of the spheres was ensured by counterstaining with PI (propidium iodide), which cannot permeate live cells. Expression patterns in primary tumor spheres of specific stem cell markers, which are regularly over-expressed in colorectal tumors (CD44 and CD133), correlated with those in spheres from peripheral blood. Moreover, primary tumor spheres expressed high levels of PD-L1.

Response to neoadjuvant R/CT in rectal cancer patients. 14 patients with rectal cancer received neoadjuvant R/CT, 7 (50%) of whom showed a good response (Fig. 2) and 7 (50%) did not or only partially respond to the therapy (Fig. 3). In the group of good responders, the mean CETC number before R/CT was 105 CETCs/100 μl of cell suspension. After the first cycle of the R/CT it decreased to 47 per 100 μl. With a P-value of 0.543, the differences between the three time points did not reach statistical significance likely due to the small sample size. Nevertheless, the results show a trend. In detail, the CETC numbers declined in 5 of 7 patients (71%) and increased in only 2 patients (29%) with good response to neoadjuvant R/CT (Fig. 2). In the group of poor responders (7 patients), the mean CETC number was initially 40 CETCs/100 μl cell suspension, and increased continuously from 73 after the first cycle of the R/CT to 210 CETCs/100 μl cell suspension before surgery (Fig. 3). Again, the small number of participants (n=7) might be the major cause for the lack of statistical significance (P=0.428).

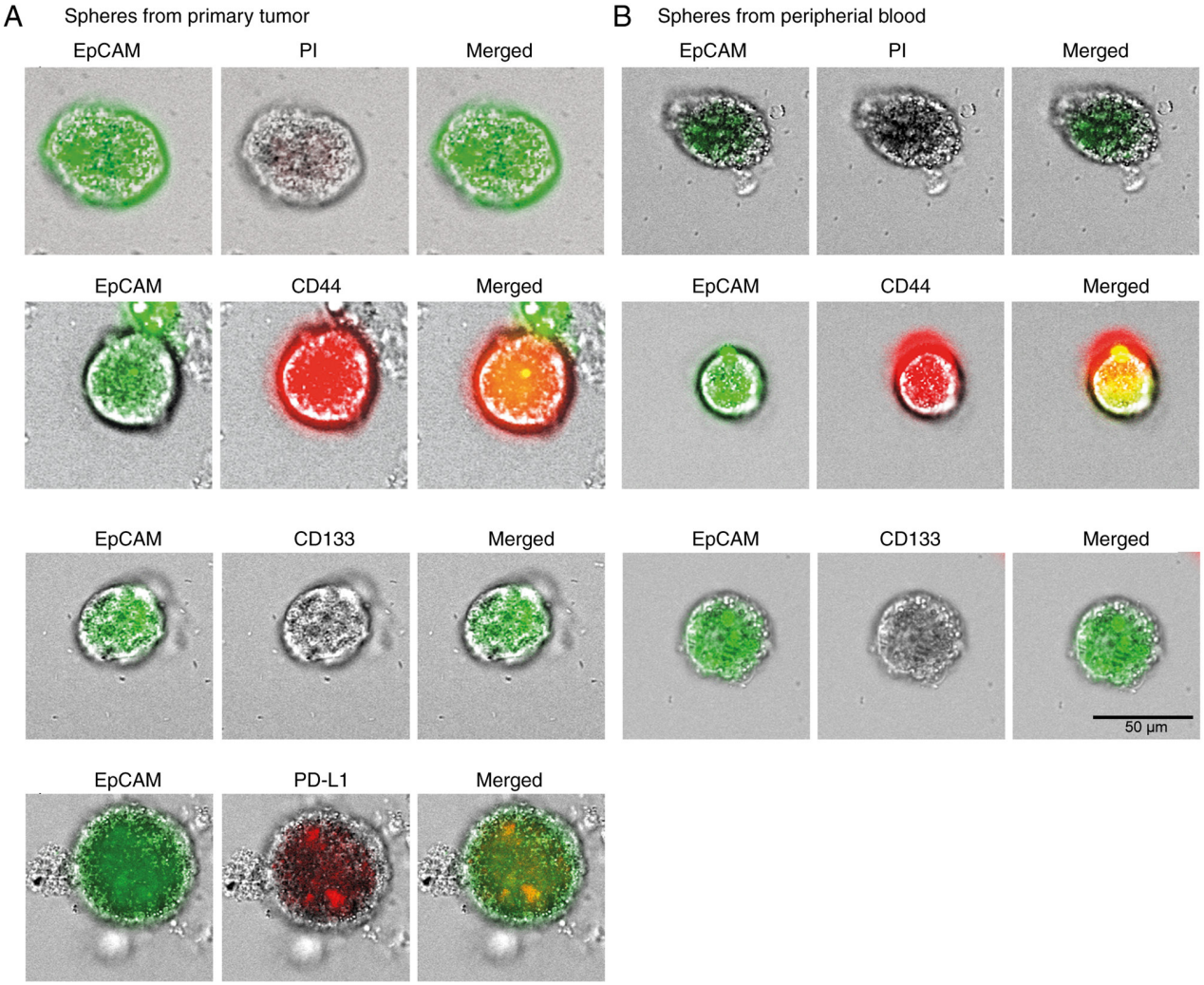

Figure 1. 3-Dimensional spheres cultured from peripheral blood or primary tumor tissue from patient #1. Immunostaining of spheres cultured from (A) primary tumor tissue or (B) CETCs from peripheral blood from patient #1. The epithelial origin of the spheres was identified by staining with anti-EpCAM antibody. PI was used as a vitality marker. Additionally, EpCAM-positive spheres were investigated for the expression of specific stem cell markers (CD44, CD133) and PD-L1. EpCAM, epithelial cell adhesion molecule; PI, propidium iodide; PD-L1, programmed death-ligand 1; CETC, circulating epithelial tumor cell.

Response to adjuvant therapy in colorectal cancer patients. 9 patients (41%; 6 patients with colon cancer and 3 patients with rectal cancer) received adjuvant chemotherapy and CETCs were quantified before surgery, before the beginning of chemotherapy and after the first cycle of adjuvant therapy (Fig. 4). Before surgery the median CETC number was 55/100 μl cell suspension, 6-8 weeks after surgery (before the beginning of the adjuvant CT) the median value was 65, and after the first cycle of CT the median was 20 CETCs/100 μl cell suspension. The difference between the mean values of the three time points was not statistically significant (P=0.114).

Interestingly, all patients showed decreasing CETC numbers under adjuvant chemotherapy.

Expression of the proliferation marker Ki-67 during therapy. Ki-67-positive CETCs were detected in 20 patients (91%) and the percentage ranged from 0-100 (median: 25 Ki-67-positive CETCs/100 μl cell suspension). The median of Ki-67-positive CETCs/100 μl cell suspension in colon cancer patients was 18 (ranging from 0 to 170), and in rectal cancer patients 25 (ranging from 0 to 169). Although the differences in the Ki-67-positive CETCs at the three time points were not statistically significant neither for patients with neoadjuvant R/CT (P=0.202), nor in the group of patients with adjuvant CT (P=0.151), there was a trend in the number of Ki-67-positive CETCs to decrease under adjuvant CT, and to increase in patients receiving neoadjuvant R/CT (Fig. 5).

Case report. Fig. 6 shows an example of a serial analysis of the CETC numbers during the therapy of a 63-year-old patient with stage III (T3, N1, M0; G2) rectal cancer. The patient was treated with neoadjuvant R/CT (Dworak 1, poor response), followed by surgery (R0-resection) and additional adjuvant chemotherapy. During neoadjuvant therapy the CETC numbers increased significantly and reached their maximum (225 CETCs/100 μl cell suspension) before surgical removal of the primary tumor. Eight weeks after surgery the CETC number had fallen to a level similar to that at the beginning of the R/CT. It continued to decrease until there were no residual CETCs detectable at the last day of the adjuvant CT. Until 9 months after completion of the adjuvant therapy, this patient has remained free of relapse.

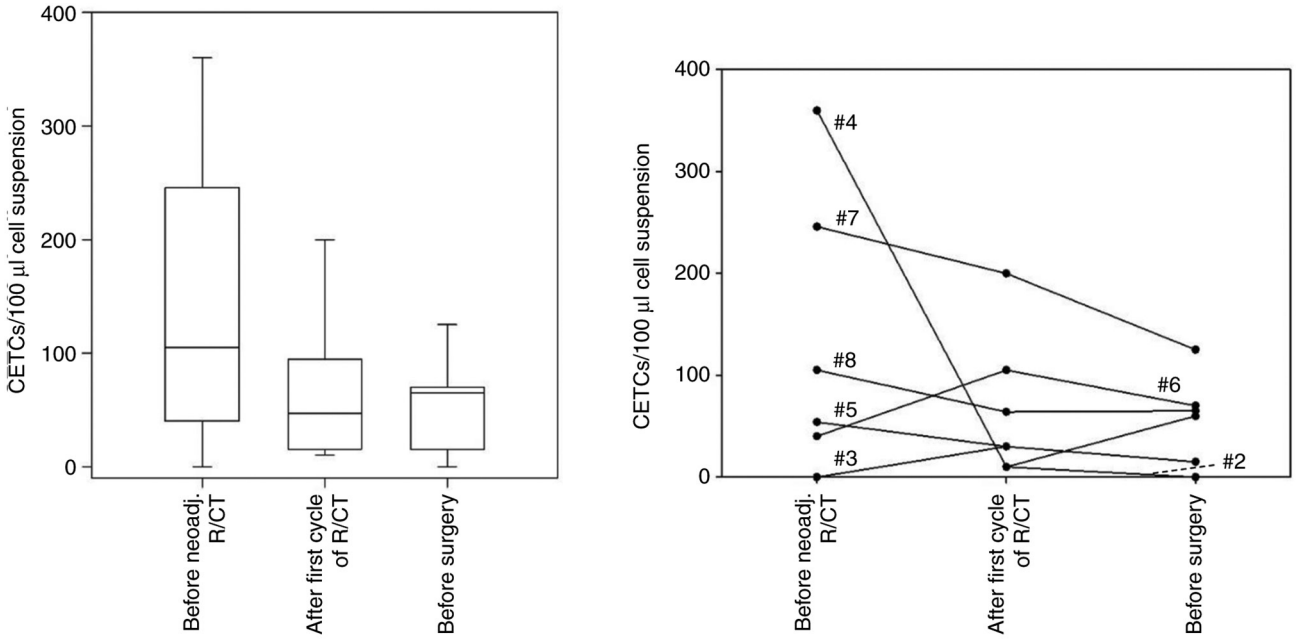

Figure 2. Number of CETCs in the blood of patients with rectal cancer with good response to neoadj. R/CT. Blood samples were drawn before R/CT, after the first cycle of R/CT and after completion of R/CT immediately before surgery. Left, boxplot with median CETC values, quartiles and variability at each time point; right, individual CETC numbers at all time points, each line represents one patient. Patient #4 (360/10/60 CETC/100 μl), patient #7 (246/200/125 CETC/100 μl), patient #8 (105/64/65 CETC/100 μl), patient #5 (54/30/n.d. CETC/100 μl), patient #6 (40/105/70 CETC/100 μl), patient #3 (0/30/15 CETC/100 μl), patient #2 (n.d./10/0 CETC/100 μl). Assignment of patients in Tables II and SI. n.d., not defined; CETC, circulating epithelial tumor cell; neoadj., neoadjuvant; R/CT, radio/chemotherapy.

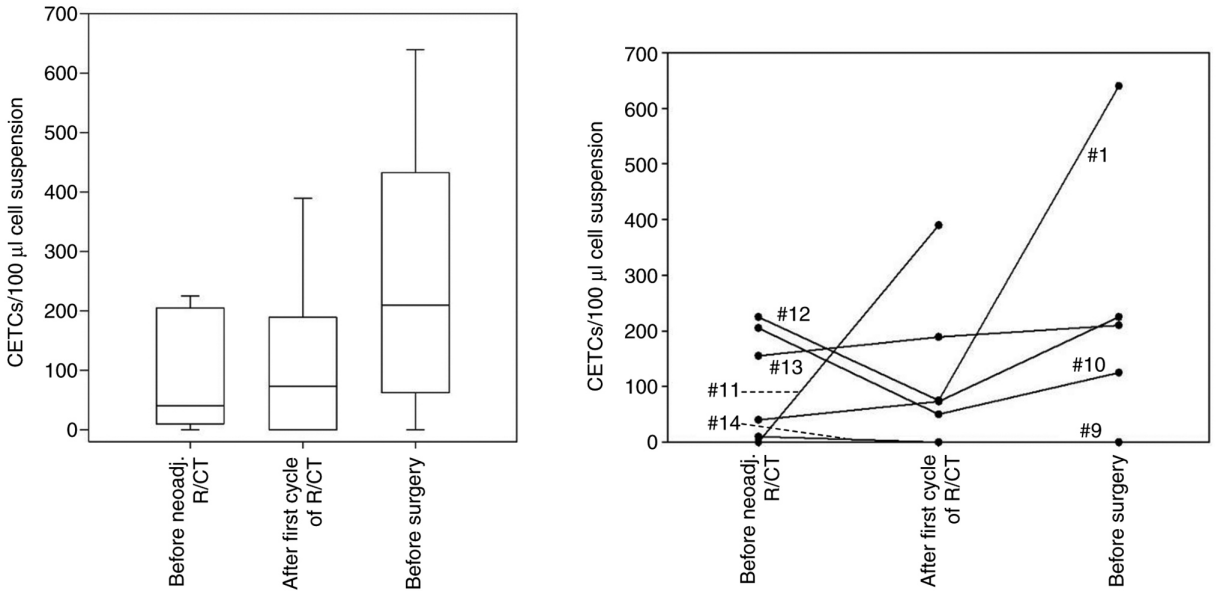

Figure 3. Number of CETCs in the blood of patients with rectal cancer with poor response to neoadj. R/CT. Blood samples were drawn before R/CT, after the first cycle of R/CT and after completion of R/CT immediately before surgery. Left, boxplot with median CETC values, quartiles and variability at each time point; right, individual CETC numbers at all time points, each line represents one patient. Patient #1 (40/73/225 CETC/100 μl), patient #9 (10/0/0 CETC/100 μl), patient #10 (205/50/125 CETC/100 μl), patient #11 (0/390/n.d. CETC/100 μl), patient #12 (225/75/640 CETC/100 μl), patient #13 (155/189/210 CETC/100 μl), patient #14 (10/0/n.d. CETC/100 μl). Assignment of patients in Tables II and SI. n.d., not defined; CETC, circulating epithelial tumor cell; neoadj., neoadjuvant; R/CT, radio/chemotherapy.

Discussion

Although disseminated tumor cells play a major role in the metastatic process of tumors, their detection and monitoring does not play a decisive role in standard clinical procedures. Monitoring of circulating tumor cells in the blood of cancer patients during therapy has already been shown to be a powerful prognostic tool for tumors of different entities including colorectal tumors (15,24-26). From a clinical perspective, assessment of patients' response to antitumoral therapy by detection of circulating tumor cells in the peripheral blood appears comfortable, both for the physician (time- and

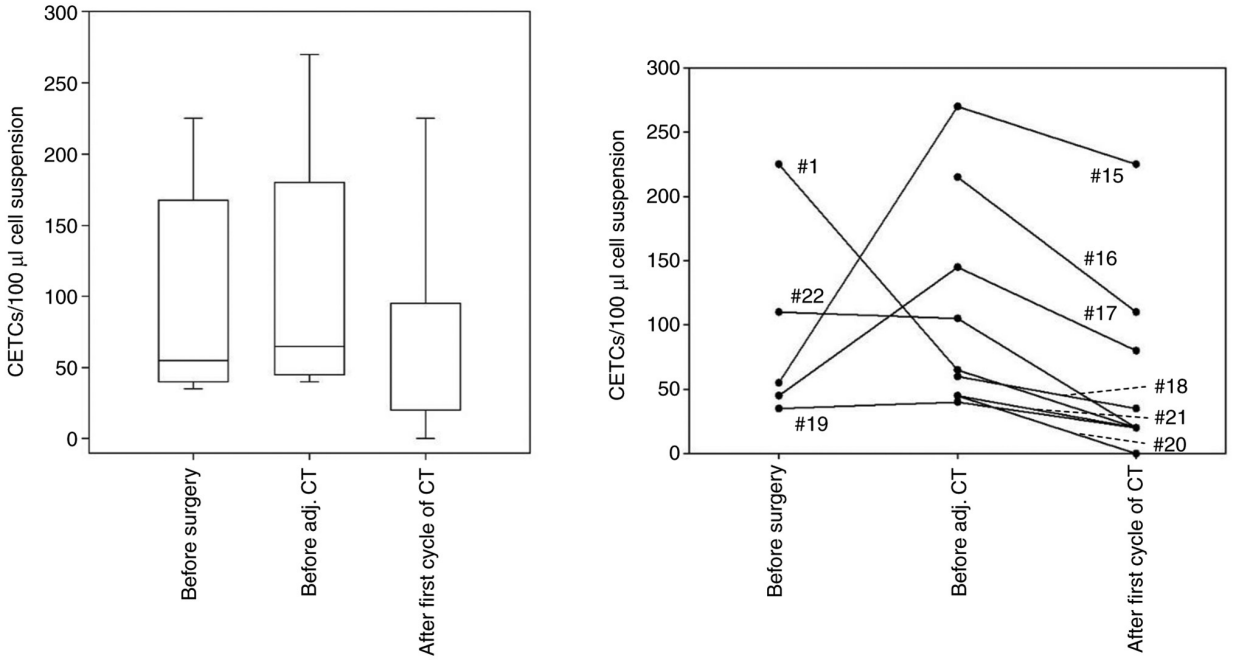

Figure 4. Number of CETCs in the blood of patients with colorectal cancer with adj. CT. Blood samples were drawn directly before surgery, 6-8 weeks after surgery and after the first cycle of adj. CT. Left, boxplot with median CETC values, quartiles and variability at each time point; right, individual CETC numbers at all time points, each line represents one patient. Patient #1 (C20; 225/65/20 CETC/100 μl), patient #15 (C20; 55/270/225 CETC/100 μl), patient #16 (C20; n.d./215/110 CETC/100 μl), patient #17 (C18; 45/145/80 CETC/100 μl), patient #18 (C18; n.d./60/35 CETC/100 μl), patient #19 (C18; 35/40/20 CETC/100 μl), patient #20 (C18; n.d./45/0 CETC/100 μl), patient #21 (C18; n.d./45/20 CETC/100 μl), patient #22 (C18; 110/105/20 CETC/100 μl). Assignment of patients in Table SI. n.d., not defined; CETC, circulating epithelial tumor cell; adj., adjuvant; CT, chemotherapy; C18, colon carcinoma; C20, rectum carcinoma.

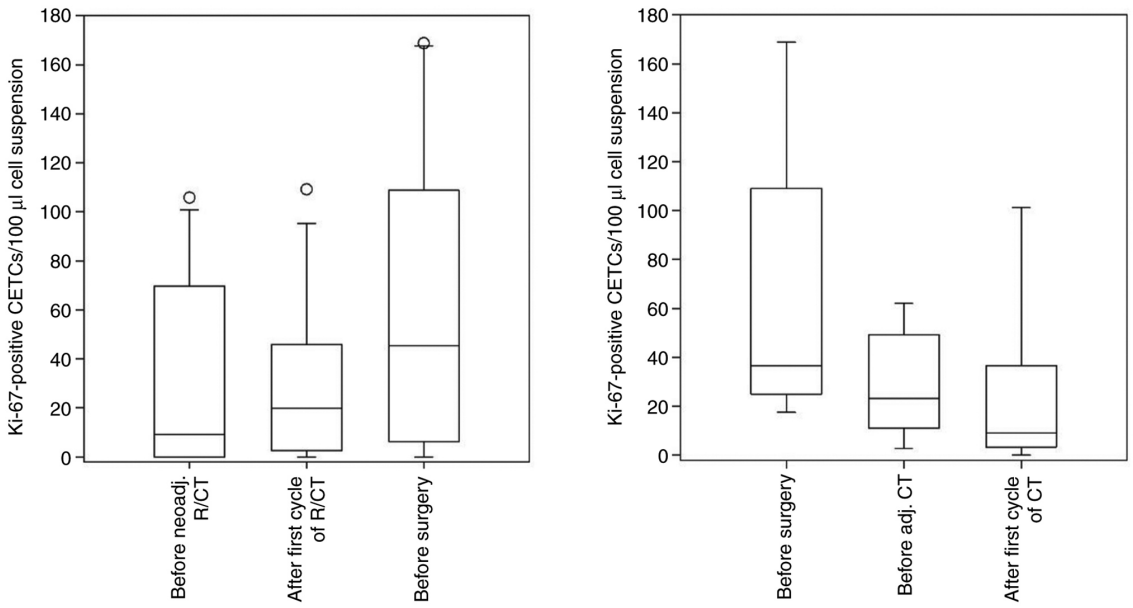

Figure 5. Boxplots with median values, quartiles and variabilities of Ki-67-positive CETCs in the blood of patients with colorectal cancer. Left, patients with neoadj. R/CT; blood samples were drawn before the beginning of the neoadj. R/CT, after the first cycle of R/CT and after completion of R/CT (before surgery). Right, patients with adj. CT; blood samples were drawn directly before surgery, 6-8 weeks after surgery and after the first cycle of CT. CETC, circulating epithelial tumor cell; neoadj., neoadjuvant; adj., adjuvant; CT, chemotherapy; R/CT, radio/chemotherapy.

cost-efficient), as well as for the patients (non-invasive, neither toxic nor painful), and may be easily repeated as a monitoring tool without great efforts.

In recent years, different techniques have been described for the detection of circulating tumor cells (27-32). Various studies demonstrated that their detection via CellSearch system could be used to predict treatment responses and long-term prognosis for stage IV colorectal cancer patients (33,34). But in the case of non-metastatic patients, the detection rate via CellSearch system is too low (11-25%) to further analyze the correlation between circulating tumor cells and patients' characteristics and treatment responses (35). In the present *proof-of-principle*

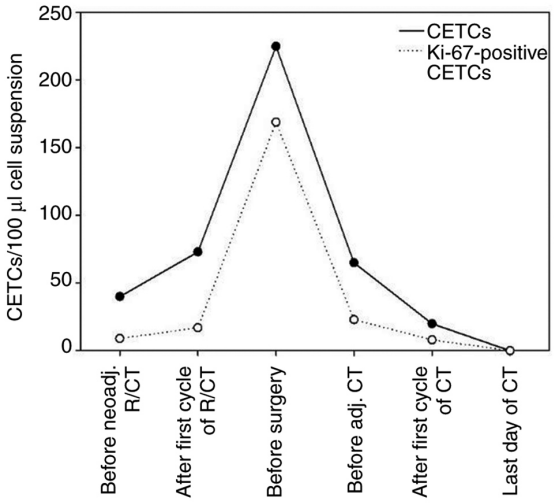

Figure 6. Number of CETCs and Ki-67-positive CETCs in the blood of patient #1 with rectal cancer receiving neoadj. R/CT, as well as adj. CT after surgical removal of the primary tumor (R0-resection). Blood samples were drawn prior to the neoadj. R/CT (40 CETCs/100 μl), after the first cycle of R/CT (73 CETCs/100 μl), immediately before surgery (225 CETCs/100 μl), 6-8 weeks after surgery/before the beginning of adj. CT (65 CETCs/100 μl), after the first cycle of adj. CT (20 CETCs/100 μl) and on the last day of adj. CT (0 CETCs/100 μl). CETC, circulating epithelial tumor cell; neoadj., neoadjuvant; adj., adjuvant; CT, chemotherapy; R/CT, radio/chemotherapy.

study with a small group of colorectal cancer patients of all stages using the Maintrac® method for CETC identification, we detected CETCs in the peripheral blood of 100% of the patients. Moreover, we were able to show that some of the cells, which have been quantified, possess proliferative and stemness characteristics matching those found in the primary tumor.

Up until now, only a few studies investigated the role of circulating tumor cells for evaluating the response to neoadjuvant R/CT for patients with rectal cancer. In a study by Zitt *et al* the circulating tumor cells were investigated during neoadjuvant R/CT in 26 patients with locally advanced rectal cancer using a non-quantitative RT-PCR-based method (36). Sun *et al* used a size-dependent detection method to analyze changes in circulating tumor cell numbers during neoadjuvant R/CT within a collective of 115 rectal cancer patients (37). Keeping in mind the respective drawbacks of each method, both studies agreed, that responders had an obvious decrease of the numbers of circulating tumor cells after neoadjuvant R/CT, while there was no noticeable alteration after treatment in non-responders. These results were confirmed by other studies (38,39). In our study, applying the Maintrac® approach for CETC detection, we allocated 14 rectal cancer patients either to the group of good or poor responders to neoadjuvant R/CT, based upon alterations in TNM staging before and after R/CT and on Dworak regression grades of their surgical specimens. For both groups we confirmed that a decrease in CETC numbers correlates with, and thus indicates, a good response, whereas an increase of CETC numbers is rather indicative of a poor response to neoadjuvant R/CT using the Maintrac® approach for CETC detection. Whether this observation is of general relevance, and thus a potential prognostic tool for the clinician, must be clarified by extended studies with larger collectives of patients. As all patients in our study experienced a decline of CETCs under adjuvant treatment, it would be interesting to know if and when individual rectal cancer patients benefit from an adjuvant chemotherapy after neoadjuvant R/CT. Moreover, it would also be interesting to see, if CETC monitoring may also be able to identify individual rectal cancer patients, which benefit from TNT. The latest results of the PRODIGE 23 and RAPIDO phase III clinical studies have shown that TNT is able to extent disease free survival, as well as to improve the pathological complete remission (pCR) rate, organ preservation and local control in patients with locally advanced rectal cancer in comparison to conventional, neoadjuvant/adjuvant therapy regimes (9,10).

As discussed above, we observed a heterogenic reaction of the CETC profile for patients receiving neoadjuvant R/CT. In contrast, a constant decrease in CETC numbers during adjuvant therapy was found. A potential explanation for this discrepancy may be the tumor burden in the adjuvant versus the neoadjuvant situation. While the neoadjuvant therapy targets the whole, intact tumor, in the adjuvant situation the tumor burden is low, because only microscopic tumor residues remain in the patient after surgery which may be more sensitive to chemotherapy and radiation. In addition, because of the reduced number of tumor cells, the development of resistance is less likely when compared to the neoadjuvant situation (40,41).

The proliferation marker Ki-67 is widely utilized in routine clinical diagnostic of breast cancer patients (42). Lumachi *et al* suggested Ki-67 as a predictive parameter for colorectal cancer, as they found an inverse correlation between Ki-67 expression and overall survival in a small retrospective study (43). However, its prognostic value for colorectal tumors remains controversial. While some studies completely failed to demonstrate its prognostic significance in the case of colorectal tumors (44), others found Ki-67 overexpression indicating a good clinical outcome for colorectal cancer patients (45). In our study, we observed that the Ki-67 index, and thus the proliferative activity, of CETCs from the blood of colorectal cancer patients increased during neoadjuvant R/CT, and decreased during adjuvant CT. Considering the above mentioned findings from literature, these results cannot be interpreted regarding a good or poor prognosis for the patients. On a cellular level, one possible explanation for the rise in Ki-67 expression under neoadjuvant R/CT may be the radiotherapy-induced inflammation, which in turn induces an increase of the proliferating activity of tumor cells, and consequently of circulating tumor cells (46,47).

Finally, the general trends reported in this study could be exemplified by a case report of a rectal cancer patient (#1) receiving neoadjuvant R/CT, as well as adjuvant CT. This patient seemed to benefit from the surgery and from the additional adjuvant CT as CETC numbers decreased continuously after surgery to reach zero level on the last day of adjuvant therapy. This patient has remained free of relapse until nine months after the completion of therapy.

Acknowledgements

Not applicable.

Funding

The present study was supported by a PhD fellowship from the Bayerische Eliteförderungsgesetz (BayEFG).

Availability of data and materials

The datasets used and/or analyzed during the current study are available from the corresponding author on reasonable request.

Authors' contributions

RS, AK, KP and MG contributed to the design of the present study and developed the methodology. MG collected the bioinformatics data, performed the experiments, analyzed the results and wrote the manuscript. AK contributed to the collection of patient data. RS, AK and KP critically revised the manuscript and approved the final version to be published. All authors agreed to be accountable for all aspects of the study. All authors have read and approved the final manuscript. MG and RS confirm the authenticity of all the raw data.

Ethics approval and consent to participate

The present study was approved by the Ethics Committee of the University of Bayreuth (approval no. O 1305/1-GB; Bayreuth, Germany). Written informed consent was obtained from all patients.

Patient consent for publication

Not applicable.

Competing interests

Katharina Pachmann holds a patent protecting the Maintrac® method used in the present study (patent no. EP 3128325 B1; dated February 8th, 2017). The other authors declare that they have no competing interests.

References

1. Bray F, Ferlay J, Soerjomataram I, Siegel RL, Torre LA and Jemal A: Global cancer statistics 2018: GLOBOCAN estimates of incidence and mortality worldwide for 36 cancers in 185 countries. CA Cancer J Clin 68: 394-424, 2018.
2. Kerr J, Anderson C and Lippman SM: Physical activity, sedentary behaviour, diet, and cancer: An update and emerging new evidence. Lancet Oncol 18: e457-e471, 2017.
3. Argilés G, Tabernero J, Labianca R, Hochhauser D, Salazar R, Iveson T, Laurent-Puig P, Quirke P, Yoshino T, Taieb J, *et al*: Localised colon cancer: ESMO clinical practice guidelines for diagnosis, treatment and follow-up. Ann Oncol 31: 1291-1305, 2020.
4. Glynne-Jones R, Wyrwicz L, Tiret E, Brown G, Rödel C, Cervantes A and Arnold D; ESMO Guidelines Committee: Rectal cancer: ESMO clinical practice guidelines for diagnosis, treatment and follow-up. Ann Oncol 28 (Suppl 4): iv22-iv40, 2017.
5. van Cutsem E, Nordlinger B and Cervantes A; ESMO Guidelines Working Group: Advanced colorectal cancer: ESMO clinical practice guidelines for treatment. Ann Oncol 21 (Suppl 5): v93-v97, 2010.
6. Boussios S, Ozturk MA, Moschetta M, Karathanasi A, Zakynthinakis-Kyriakou N, Katsanos KH, Christodoulou DK and Pavlidis N: The developing story of predictive biomarkers in colorectal cancer. J Pers Med 9: 12, 2019.
7. Moertel CG, Fleming TR, Macdonald JS, Haller DG, Laurie JA, Goodman PJ, Ungerleider JS, Emerson WA, Tormey DC and Glick JH: Levamisole and fluorouracil for adjuvant therapy of resected colon carcinoma. N Engl J Med 322: 352-358, 1990.
8. Punt CJA, Koopman M and Vermeulen L: From tumour heterogeneity to advances in precision treatment of colorectal cancer. Nat Rev Clin Oncol 14: 235-246, 2017.
9. Bahadoer RR, Dijkstra EA, van Etten B, Marijnen CAM, Putter H, Kranenbarg EM, Roodvoets AGH, Nagtegaal ID, Beets-Dan RGH, Blomqvist L, *et al*: Short-course radiotherapy followed by chemotherapy before total mesorectal excision (TME) versus preoperative chemoradiotherapy, TME, and optional adjuvant chemotherapy in locally advanced rectal cancer (RAPIDO): A randomised, open-label, phase 3 trial. Lancet Oncol 22: 29-42, 2021.
10. Conroy T, Lamficheck N, Etienne PL, Rio E, Francois E, Mesgouez-Nebout N, Vendrely V, Artignan X, Bouché O, Gargot D, *et al*: Total neoadjuvant therapy with mFOLFIRINOX versus preoperative chemoradiation in patients with locally advanced rectal cancer: Final results of PRODIGE 23 phase III trial, a UNICANCER GI trial. J Clin Oncol 38: S4007, 2020.
11. Ebert MPA, Tänzer M, Balluff B, Burgermeister E, Kretzschmar AK, Hughes DJ, Tetzner R, Lofton-Day C, Rosenberg R, Reinacher-Schick AC, *et al*: TFAP2E-DKK4 and chemoresistance in colorectal cancer. N Engl J Med 366: 44-53, 2012.
12. Friedman AA, Letai A, Fisher DE and Flaherty KT: Precision medicine for cancer with next-generation functional diagnostics. Nat Rev Cancer 15: 747-756, 2015.
13. Garnett MJ, Edelman EJ, Heidorn SJ, Greenman CD, Dastur A, Lau KW, Greninger P, Thompson R, Luo X, Soares J, *et al*: Systematic identification of genomic markers of drug sensitivity in cancer cells. Nature 483: 570-575, 2012.
14. Wang L, Zhou S, Zhang W, Wang J, Wang M, Hu X, Liu F, Zhang Y, Jiang B and Yuan H: Circulating tumor cells as an independent prognostic factor in advanced colorectal cancer: A retrospective study in 121 patients. Int J Colorectal Dis 34: 589-597, 2019.
15. Yang C, Chen F, Wang S and Xiong B: Circulating tumor cells in gastrointestinal cancers: Current status and future perspectives. Front Oncol 9: 1427, 2019.
16. Kapeleris J, Kulasinghe A, Warkiani ME, Vela I, Kenny L, O'Byrne K and Punyadeera C: The prognostic role of circulating tumor cells (CTCs) in lung cancer. Front Oncol 8: 311, 2018.
17. Banys-Paluchowski M, Krawczyk N and Fehm T: Potential role of circulating tumor cell detection and monitoring in breast cancer: A review of current evidence. Front Oncol 6: 255, 2016.
18. Xun Y, Cao Q, Zhang J, Guan B and Wang M: Clinicopathological and prognostic significance of circulating tumor cells in head and neck squamous cell carcinoma: A systematic review and meta-analysis. Oral Oncol 104: 104638, 2020.
19. Schlüter C, Duchrow M, Wohlenberg C, Becker MH, Key G, Flad HD and Gerdes J: The cell proliferation-associated antigen of antibody Ki-67: A very large, ubiquitous nuclear protein with numerous repeated elements, representing a new kind of cell cycle-maintaining proteins. J Cell Biol 123: 513-522, 1993.
20. Pizon M, Schott DS, Pachmann U and Pachmann K: B7-H3 on circulating epithelial tumor cells correlates with the proliferation marker, Ki-67, and may be associated with the aggressiveness of tumors in breast cancer patients. Int J Oncol 53: 2289-2299, 2018.
21. Union for International Cancer Control (UICC): Colon and Rectum. In: TNM classification of malignant tumours. Brierley J, Gospodarowicz MK and Wittekind C (eds) John Wiley & Sons Ltd., Chichester, pp73-76, 2017.
22. Pox C: Update der S3-leitlinie zum kolorektalen karzinom. Best Pract Onkol 13: 254-262, 2018 (In German).
23. Dworak O, Keilholz L and Hoffmann A: Pathological features of rectal cancer after preoperative radiochemotherapy. Int J Colorectal Dis 12: 19-23, 1997.
24. Pachmann K, Willecke-Hochmuth R, Schneider K and Kaatz M: Circulating epithelial tumor cells as a prognostic tool for malignant melanoma. Melanoma Res 28: 37-43, 2018.
25. Krebs MG, Sloane R, Priest L, Lancashire L, Hou JM, Greystoke A, Ward TH, Ferraldeschi R, Hughes A, Clack G, *et al*: Evaluation and prognostic significance of circulating tumor cells in patients with non-small-cell lung cancer. J Clin Oncol 29: 1556-1563, 2011.
26. Rahbari NN, Aigner M, Thorlund K, Mollberg N, Motschall E, Jensen K, Diener MK, Büchler MW, Koch M and Weitz J: Meta-analysis shows that detection of circulating tumor cells indicates poor prognosis in patients with colorectal cancer. Gastroenterology 138: 1714-1726, 2010.

27. Nagrath S, Sequist LV, Maheswaran S, Bell DW, Irimia D, Ulkus L, Smith MR, Kwak EL, Digumarthy S, Muzikansky A, *et al*: Isolation of rare circulating tumour cells in cancer patients by microchip technology. Nature 450: 1235-1239, 2007.
28. Lara O, Tong X, Zborowski M and Chalmers JJ: Enrichment of rare cancer cells through depletion of normal cells using density and flow-through, immunomagnetic cell separation. Exp Hematol 32: 891-904, 2004.
29. Park JM, Lee JY, Lee JG, Jeong H, Oh JM, Kim YJ, Park D, Kim MS, Lee HJ, Oh JH, *et al*: Highly efficient assay of circulating tumor cells by selective sedimentation with a density gradient medium and microfiltration from whole blood. Anal Chem 84: 7400-7407, 2012.
30. Pachmann K: Current and potential use of MAINTRAC method for cancer diagnosis and prediction of metastasis. Expert Rev Mol Diagn 15: 597-605, 2015.
31. Desitter I, Guerrouahen BS, Benali-Furet N, Wechsler J, Jänne PA, Kuang Y, Yanagita M, Wang L, Berkowitz JA, Distel RJ and Cayre YE: A new device for rapid isolation by size and characterization of rare circulating tumor cells. Anticancer Res 31: 427-441, 2011.
32. Wang L, Balasubramanian P, Chen AP, Kummar S, Evrard YA and Kinders RJ: Promise and limits of the cellSearch platform for evaluating pharmacodynamics in circulating tumor cells. Semin Oncol 43: 464-475, 2016.
33. Cohen SJ, Punt CJA, Iannotti N, Saidman BH, Sabbath KD, Gabrail NY, Picus J, Morse M, Mitchell E, Miller MC, *et al*: Relationship of circulating tumor cells to tumor response, progression-free survival, and overall survival in patients with metastatic colorectal cancer. J Clin Oncol 26: 3213-3221, 2008.
34. Tol J, Koopman M, Miller MC, Tibbe A, Cats A, Creemers GJM, Vos AH, Nagtegaal ID, Terstappen LWMM and Punt CJA: Circulating tumour cells early predict progression-free and overall survival in advanced colorectal cancer patients treated with chemotherapy and targeted agents. Ann Oncol 21: 1006-1012, 2010.
35. Sastre J, Maestro ML, Puente J, Veganzones S, Alfonso R, Rafael S, Gracía-Saenz JA, Vidaurreta M, Martín M, Arroyo M, *et al*: Circulating tumor cells in colorectal cancer: Correlation with clinical and pathological variables. Ann Oncol 19: 935-938, 2008.
36. Zitt M, Zitt M, Müller HM, Dinnewitzer AJ, Schwendinger V, Goebel G, De Vries A, Amberger A, Weiss H, Margreiter R, *et al*: Disseminated tumor cells in peripheral blood: A novel marker for therapy response in locally advanced rectal cancer patients undergoing preoperative chemoradiation. Dis Colon Rectum 49: 1484-1491, 2006.
37. Sun W, Li G, Wan J, Zhu J, Shen W and Zhang Z: Circulating tumor cells: A promising marker of predicting tumor response in rectal cancer patients receiving neoadjuvant chemo-radiation therapy. Oncotarget 7: 69507-69517, 2016.
38. Magni E, Botteri E, Ravenda PS, Cassatella MC, Bertani E, Chiappa A, Luca F, Zorzino L, Bianchi PP, Adamoli L, *et al*: Detection of circulating tumor cells in patients with locally advanced rectal cancer undergoing neoadjuvant therapy followed by curative surgery. Int J Colorectal Dis 29: 1053-1059, 2014.
39. Hinz S, Röder C, Tepel J, Hendricks A, Schafmayer C, Becker T and Kalthoff H: Cytokeratin 20 positive circulating tumor cells are a marker for response after neoadjuvant chemoradiation but not for prognosis in patients with rectal cancer. BMC Cancer 15: 953, 2015.
40. Imyanitov EN and Yanus GA: Neoadjuvant therapy: Theoretical, biological and medical consideration. Chin Clin Oncol 7: 55, 2018.
41. Leary A, Cowan R, Chi D, Kehoe S and Nankivell M: Primary surgery or neoadjuvant chemotherapy in advanced ovarian cancer: The debate continue. Am Soc Clin Oncol Educ Book 35: 153-162, 2016.
42. Inwald EC, Klinkhammer-Schalke M, Hofstädter F, Zeman F, Koller M, Gerstenhauer M and Ortmann O: Ki-67 is a prognostic parameter in breast cancer patients: Results of a large population-based cohort of a cancer registry. Breast Cancer Res Treat 139: 539-552, 2013.
43. Lumachi F, Orlando R, Marino F, Chiara GB and Basso SMM: Expression of p53 and Ki-67 as prognostic factors for survival of men with colorectal cancer. Anticancer Res 32: 3965-3967, 2012.
44. Ghiţă C, Vîlcea ID, Dumitrescu M, Vîlcea AM, Mirea CS, Aşchie M and Vasilescu F: The prognostic value of the immunohistochemical aspects of tumor suppressor genes p53, bcl-2, PTEN and nuclear proliferative antigen Ki-67 in resected colorectal carcinoma. Rom J Morphol Embryol 53: 549-556, 2012.
45. Melling N, Kowitz CM, Simon R, Bokemeyer C, Terracciano L, Sauter G, Izbicki JR and Marx AH: High Ki67 expression is an independent good prognostic marker in colorectal cancer. J Clin Pathol 69: 209-214, 2016.
46. Kiraly O, Gong G, Olipitz W, Muthupalani S and Engelward BP: Inflammation-induced cell proliferation potentiates DNA damage-induced mutations in vivo. PLOS Genet 11: e1004901, 2015.
47. Di Maggio FM, Minafra L, Forte GI, Cammarata FP, Lio D, Messa C, Gilardi MC and Bravatà V: Portrait of inflammatory response to ionizing radiation treatment. J Inflamm 12: 14, 2015.

-Supplementary data-

Monitoring of circulating epithelial tumor cells (CETCs) by the Maintrac® method and its potential benefit for the therapy of patients with colorectal cancer

Madeleine Gold,[a] Katharina Pachmann,[b] Alexander Kiani[c] and Rainer Schobert[a]

[a] Organic Chemistry Laboratory, University of Bayreuth, Universitaetsstrasse 30, 95440 Bayreuth, Germany.

[b] Transfusion Centre Bayreuth, Kurpromenade 2, 95448 Bayreuth, Germany.

[c] Klinikum Bayreuth GmbH, Department of Oncology and Hematology, Preuschwitzer Strasse 101, 95445 Bayreuth, Germany.

Corresponding Author: Rainer Schobert, Tel.: +49 921/552679, Email: Rainer.schobert@uni-bayreuth.de

Table SI. Number of CETCs of all patients during the treatment course.

Patient number	ICD10	Number of CETCs					Tumor location
		Before neoadj. R/CT	After first cycle of R/CT	Before surgery	Before adj. CT	After first cycle of CT	
1	C20	40	73	225	65	20	Rectum
2	C20	n.d.	10	0	n.d.	n.d.	Rectum
3	C20	0	30	15	n.d.	n.d.	Rectum
4	C20	360	10	60	n.d.	n.d.	Rectum
5	C20	54	30	n.d.	n.d.	n.d.	Rectum
6	C20	40	105	70	n.d.	n.d.	Rectum
7	C20	246	200	125	n.d.	n.d.	Rectum
8	C20	105	64	65	n.d.	n.d.	Rectum
9	C20	10	0	0	n.d.	n.d.	Rectum
10	C20	205	50	125	n.d.	n.d.	Rectum
11	C20	0	390	n.d.	n.d.	n.d.	Rectum
12	C20	225	75	640	n.d.	n.d.	Rectum
13	C20	155	189	210	n.d.	n.d.	Rectum
14	C20	10	0	n.d.	n.d.	n.d.	Rectum
15	C20	n.d.	n.d.	55	270	225	Rectum
16	C20	n.d.	n.d.	n.d.	215	110	Rectum
17	C18	n.d.	n.d.	45	145	80	Colon ascendens
18	C18	n.d.	n.d.	n.d.	60	35	Colon sigmoideum
19	C18	n.d.	n.d.	35	40	20\	Colon sigmoideum
20	C18	n.d.	n.d.	n.d.	45	0	Colon sigmoideum
21	C18	n.d.	n.d.	n.d.	45	20	Colon ascendens[a]
22	C18	n.d.	n.d.	110	105	20	Coecum

[a]Patient had a simultaneous rectal cancer, for which neoadjuvant radiochemotherapy had been performed prior to study entry; C18, diagnosed with colon carcinoma; C20, diagnosed with rectum carcinoma; n.d., not defined; CETC, circulating epithelial tumor cell; neoadj., neoadjuvant; adj., adjuvant; CT, chemotherapy; R/CT, radio/chemotherapy.

6. Liste weiterer Publikationen im Rahmen der Dissertation

Fluoro and pentafluorothio analogs of the antitumoral curcuminoid EF24 with superior antiangiogenic and vascular-disruptive effects

Florian Schmitt, Madeleine Gold, Gerrit Begemann, Ion Andronache, Bernhard Biersack, Rainer Schobert

Bioorganic & Medicinal Chemistry, 25 (2017) 4894-4903; doi: 10.1016/j.bmc.2017.07.039.

Bioorganic & Medicinal Chemistry 25 (2017) 4894–4903

Contents lists available at ScienceDirect

Bioorganic & Medicinal Chemistry

journal homepage: www.elsevier.com/locate/bmc

Fluoro and pentafluorothio analogs of the antitumoral curcuminoid EF24 with superior antiangiogenic and vascular-disruptive effects

Florian Schmitt [a], Madeleine Gold [a], Gerrit Begemann [b], Ion Andronache [c], Bernhard Biersack [a], Rainer Schobert [a,*]

[a] Organic Chemistry Laboratory, University of Bayreuth, Universitaetsstrasse 30, 95447 Bayreuth, Germany
[b] Developmental Biology, University of Bayreuth, Universitaetsstrasse 30, 95447 Bayreuth, Germany
[c] University of Bucharest, Research Center for Integrated Analysis and Territorial Management, 4-12, Regina Elisabeta Avenue, Bucharest, 3rd district, 030018, Romania

Abstract

A series of 14 analogs of the curcuminoid EF24, (3*E*,5*E*)-3,5-bis[(2-fluorophenyl)methylene]-4-piperidinone, bearing fluorine or pentafluorothio substituents, were prepared and tested for antiproliferative, vascular-disruptive, and antiangiogenic activity, as well as for their influence on other cancer-relevant targets. They proved antiproliferative against eight cancer cell lines with IC_{50} values in the low single-digit micromolar to triple-digit nanomolar range. Like EF24, the hexafluoro **3c** and **3d** and bis(pentafluorothio) **4f** derivatives arrested HT-29 colon carcinoma cells in G2/M phase of the cell cycle, yet inhibited angiogenesis, e.g. in zebrafish larvae, to a much greater extent. The antimigratory effects in 518A2 melanoma cells of **3c**, its regioisomer **3d**, and of **4f**, originate from an inhibition of NF-κB translocation. Moreover, **3c** and **3d** showed potential as vascular-disruptive agents in chorio-allantoic/vitelline membrane (CA/VM) assays.

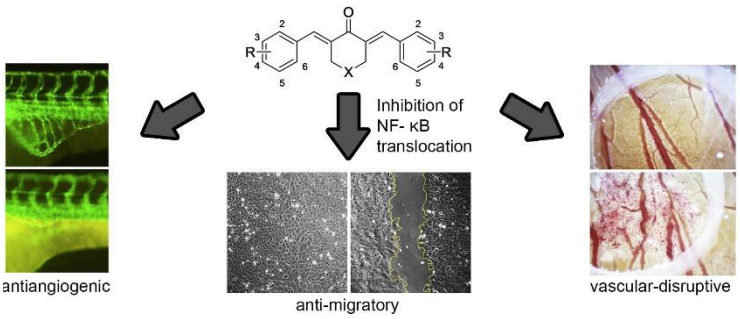

[Abstract and graphical abstract reprinted with permission from Elsevier]

New naphthopyran analogues of LY290181 as potential tumor vascular-disrupting agents

Florian Schmitt, Madeleine Gold, Matthias Rothemund, Ion Andronache, Bernhard Biersack, Rainer Schobert, Thomas Mueller

European Journal of Medicinal Chemistry, 163 (2019) 160-168;
doi: 10.1016/j.ejmech.2018.11.055.

European Journal of Medicinal Chemistry
journal homepage: www.elsevier.com

New Naphthopyran Analogues of LY290181 as Potential Tumor Vascular-disrupting Agents

Florian Schmitt[a], Madeleine Gold[a], Matthias Rothemund[a], Ion C. Andronache[b], Bernhard Biersack[a], Rainer Schobert[a,*], Thomas Mueller[c]

[a] *Department of Chemistry, University Bayreuth, Universitaetsstrasse 30, 95440 Bayreuth, Germany.*
[b] *University of Bucharest, Research Center for Integrated Analysis and Territorial Management, 4-12, Regina Elisabeta Avenue, Bucharest, 3rd district, 030018, Romania.*
[c] *Department of Internal Medicine IV, Oncology/Hematology, Martin Luther University Halle-Wittenberg, Ernst-Grube-Straße 40, 06120 Halle, Germany.*

Abstract

A series of 19 analogues of the antiproliferative naphthopyran LY290181 were prepared for structure-activity relationship studies. We found the best activities for test compounds bearing small substituents at the meta position of the phenyl ring. The mode of action of LY290181 and eight new analogues was studied in detail. The compounds were highly anti-proliferative with IC_{50} values in the sub-nanomolar to triple-digit nanomolar range. The new analogues led to G2/M arrest due to interruption of the microtubule dynamics. In 518A2 melanoma cells they caused a mitotic catastrophe which eventually led to apoptosis. The naphthopyrans also induced a disruption of the vasculature in the chorioallantoic membrane (CAM) of fertilized chicken eggs as well as in xenograft tumors in mice. In a preliminary therapy trial, the difluoro derivative **2b** retarded the growth of resistant xenograft tumors in mice.

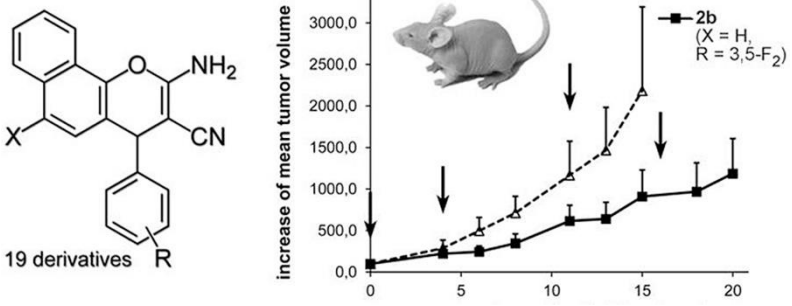

[Abstract and graphical abstract reprinted with permission from Elsevier]

Luminescent Gold(I) Complexes of 1-Pyridyl-3-anthracenylchalcone Inducing Apoptosis in Colon Carcinoma Cells and Antivascular Effects

Juan Jesús González, Enrique Ortega-Forte, Matthias Rothemund, Madeleine Gold, Consuelo Vicente, Concepción de Haro, Delia Bautista, Rainer Schobert, Jose Ruiz

Inorganic Chemistry, 58 (2019) 12954-12963; doi: 10.1021/acs.inorgchem.9b01901.

Inorganic Chemistry Article

Cite This: *Inorg. Chem.* 2019, 58, 12954−12963 pubs.acs.org/IC

Luminescent Gold(I) Complexes of 1-Pyridyl-3-anthracenylchalcone Inducing Apoptosis in Colon Carcinoma Cells and Antivascular Effects

Juan Jesús González,[†] Enrique Ortega,[†] Matthias Rothemund,[‡] Madeleine Gold,[‡] Consuelo Vicente,[†] Concepción de Haro,[†] Delia Bautista,[§] Rainer Schobert,[*,‡] and José Ruiz[*,†]

[†]Departamento de Química Inorgánica, Facultad de Química, Biomedical Research Institute of Murcia (IMIB-Arrixaca-UMU), Universidad de Murcia, E-30071 Murcia, Spain

[‡]Organic Chemistry Laboratory, University Bayreuth, Universitaetsstrasse 30 95440 Bayreuth, Germany

[§]SAI, Universidad de Murcia, E-30071 Murcia, Spain

Supporting Information

Abstract

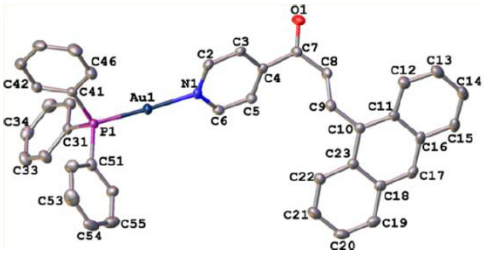

Chalcone gold conjugates are located in the mitochondria.
They are quite active towards colon carcinoma cells lacking p53.
Increase quickly the production of ROS.
Exhibit *in vivo* antivascular effects on the CAM.

The luminescent chalcone gold(I) conjugates [Au(PPh$_3$)(AN3*E*)]PF$_6$ (**1**) and [Au(SIMes)(AN3*E*)]PF$_6$ (**2**) (AN3*E* = (*E*)-3-(9-anthracenyl)-1-(4-pyridyl)propenone; SIMes = *N,N′*-dimesitylimidazolidin-2-ylidene; Mes = 2,4,6-trimethylphenyl) were prepared and characterized; complex **1** was also characterized by X-ray crystallography. In MTT assays against a panel of three human colon, a melanoma and a breast cancer cell lines both complexes were antiproliferative with low micromolar IC$_{50}$ values. It is noteworthy that HCT116$^{p53-/-}$ colon carcinoma cells lacking functional p53 (a vital tumor suppressor) were more susceptible to them than the wildtype parent cell line. In flow cytometry analyses, the gold conjugates induced a significant arrest in G2/M phase primarily. Complexes **1** and **2** quickly increased the production of reactive oxygen species (ROS) and induced mitochondrial membrane potential depolarization, higher ROS values being obtained after coadministration with enzymatic inhibitors. The free chalcone AN3*E* and its gold(I) complex conjugates located in the cell mitochondria according to confocal microscopy. In addition, complexes **1** and **2** showed *in vivo*

antivascular effects on the chorioallantoic membrane (CAM) of fertilized specific-pathogen-free (SPF) chicken eggs.

[Abstract and graphical abstract reprinted with permission of the American Chemical Society]

Monitoring circulating epithelial tumor cells (CETCs) in patients with locally advanced colorectal cancer during therapy as a tool to predict therapy response

Madeleine Gold, Katharina Pachmann, Rainer Schobert

Tagungsbeitrag: ESMO 22nd World Congress on Gastrointestinal Cancer, 2020 (Virtual)

Annals of Oncology, 31 (2020) S172; doi: 10.1016/j.annonc.2020.04.335.

P-253 **Monitoring circulating epithelial tumor cells (CETCs) in patients with locally advanced colorectal cancer during therapy as a tool to predict therapy response**

M. Gold[1], K. Pachmann[2], R. Schobert[1]

[1]*University of Bayreuth, Bayreuth, Germany;* [2]*Simfo GmbH, Bayreuth, Germany*

Background: Since the first results of the CAO/ARO/AIO-94 trial were published, a combination of neoadjuvant therapy with subsequent total mesorectal excision (TME) has been established as a standard treatment for patients suffering from locally advanced (stage II and III) rectal cancer. Replacing the postoperative by a preoperative (chemo-) radiotherapy (C/RT) led to an impressive improvement in the rates of local tumor recurrence (6% vs. 13%) and of toxicity (27% vs. 40%). Significant decreases in metastatic relapses, the main reason for therapy failure, have not been achieved, resulting in a poorer outcome in patients with rectal vs. colon cancer. Circulating epithelial tumor cells (CETCs) are an important link between primary tumors and metastases and provide a readily accessible source of tumor material from patients with solid cancer.

Methods: Our study was designed to use the immunofluorescence-based maintrac® method to identify and quantify CETCs in the blood of patients with colorectal carcinoma (C18/C20) before an during neoadjuvant and/or adjuvant C/RT. Moreover, the ratio of CETCs expressing the proliferation marker Ki-67 was determined during the course of therapy. Sample size of the study is 18 patients and still recruiting.

Results: Stage II and III colon cancer patients were predominantly treated with surgery followed by adjuvant chemotherapy, whereas patients with locally advanced rectum cancer (stage II and III) received neoadjuvant C/RT. The CETC numbers, as well as the ratio of Ki-67 positive CETCs decreased in blood samples of patients with colon cancer during adjuvant therapy. In rectal cancer patients, the number of CETCs before initiation of neoadjuvant chemotherapy correlated with lymph node involvement. Overall, 71% of patients with locally advanced rectal cancer (stage II and III) did not or only partially respond to neoadjuvant C/RT; 60% of the latter had increasing CETC numbers during therapy.

Conclusion: The presence of cells from the tumor circulating in the blood is assumed to be a prerequisite for metastasis formation. Changes in the number of CETCs during neoadjuvant C/RT could directly reflect response to therapy. This rationale is supported by an improvement of therapy results by

additional adjuvant chemotherapy following surgery in patients with rectal cancer. The clinical relevance of our findings needs to be analyzed.

Editorial acknowledgement: Writing and editorial assistance was provided by M. Pizon and D. Schott of Simfo GmbH (Bayreuth, Germany).

Legal entity responsible for the study: The authors.

Funding: BayEFG postgraduate scholarship.

Disclosure: Madeleine Gold has an affiliation with Grant/Research Support: Simfo GmbH.

7. Danksagung

Mein besonderer Dank gilt zunächst meinem Betreuer Prof. Dr. Rainer Schobert sowohl für die interessante Themenstellung als auch die wissenschaftliche Förderung während meiner Promotion. Vielen Dank für Ihre Diskussionsbereitschaft, das Vertrauen in meine Arbeit und den akademischen Freiraum.

Darüber hinaus möchte ich Dr. Bernhard Biersack für die Synthese zahlreicher im Rahmen dieser Arbeit untersuchten Verbindungen danken. Mein Dank geht auch an Tobias Rehm, Alexander Bär und Sebastian Schleser für die Synthese der Gold(I)-NHC-Komplexe, sowie an Katja Dankhoff und Andreas Dürrmann vom Lehrstuhl AC1 für die Synthese und Charakterisierung der Kupfer(II)-Komplexe.

Prof. Dr. Brabec und seinen Mitarbeitern gilt mein Dank für ihre Studien bezüglich der DNA-Bindung und zellulären Aufnahme diverser Metallkomplexe. Auch bei Ion C. Andronache möchte ich mich für die gute Zusammenarbeit im Rahmen mehrerer Projekte bedanken. Ebenso bei Prof. Dr. Birgit Weber für die gute Zusammenarbeit.

Mein ganz besonderer Dank gilt Prof. Dr. Katharina Pachmann, Dr. Ulrich Pachmann, sowie allen Mitarbeitern der Simfo GmbH und des Labors Pachmann für die gute Zusammenarbeit, die zahlreichen Diskussionen und guten Ratschläge. Dorothea Schott, Dr. Monika Pizon und Erika Schill danke ich für die viele guten Tipps und ihre ständige Hilfsbereitschaft.

Darüber hinaus möchte ich mich bei Prof. Dr. Gerrit Begemann, sowie seinen Mitarbeitern dafür bedanken, dass ich die *in vivo* Tests an Zebrafischembryonen unter Verwendung der dortigen Ressourcen und Mitbenutzung aller Gerätschaften durchführen konnte. Vielen Dank insbesondere an Heidrun Draut und Thomas Liebenstein für eure Hilfsbereitschaft, die zahlreichen lustigen Gespräche und Tierbesichtigungen. Weiterhin geht mein Dank an Prof. Dr. Stemmann und seine Mitarbeiter für die Mitbenutzung verschiedener Geräte und Räumlichkeiten. Besonders bedanken möchte ich mich bei Markus Hermann für zahlreiche Antikörperlösungen, Hilfe bei mikroskopischen und durchfluss-zytometrischen Problemen, sowie auch für die zahlreichen lustigen Kaffeerunden.

Weiterhin möchte ich mich bei Prof. Dr. Alexander Kiani vom Klinikum Bayreuth und seinen an der CETC-Studie beteiligten Mitarbeitern und Kollegen bedanken. Nicht zu vergessen, auch bei allen an der Studie beteiligten Patienten, sowie deren Angehörigen. Ohne euch wäre dieses Projekt nicht möglich gewesen! Auch bei den Mitarbeitern des Institutes für Pathologie des Klinikums Bayreuth möchte ich mich für ihre stete Hilfsbereitschaft und die unkomplizierte Zusammenarbeit herzlich bedanken!

Besonders bedanken möchte ich mich auch bei meinen Arbeitskollegen der OCI:
Bei meinen ehemaligen und aktuellen S1-Kollegen Dr. Florian Schmitt, Dr. Matthias Rothemund, Sofia Bär und Leonhard Köhler: Danke für die angenehme Arbeitsatmosphäre im S1-Labor, für Diskussionen

und Ratschläge, die vielen lustigen Kaffeerunden und Pizzabestellungen! Es war eine unvergessliche Zeit! Ich möchte mich hier auch bei allen Praktikanten, Bachelor- und Master-Studenten bedanken, die ich während meiner Promotion betreuen durfte. Für eure Unterstützung bin ich euch sehr dankbar!
Auch bei Dr. Thomas Schmalz, Dr. Ulrike Lacher, Silvia Kastner, André Wetzel, Kerstin Hannemann, sowie allen anderen Lehrstuhlangehörigen möchte ich mich für die Hilfe bei organisatorischen, analytischen, technischen und bürokratischen Angelegenheiten bedanken. Danke an alle aktuellen und ehemaligen Doktoranden des Lehrstuhls OCI für diverse wissenschaftliche Ratschläge, Unterstützung und ein gutes Miteinander.

Natürlich bedanke ich mich auch bei allen, die während meiner Promotion an der Universität Bayreuth eine wichtige Rolle gespielt haben und hier nicht namentlich erwähnt oder vergessen wurden. Vielen Dank!

Ein besonderes Dankeschön geht an meine Familie, welche mich während meines Studiums und meiner Promotion immer unterstützt hat! Danke.

8. Eidesstattliche Versicherungen und Erklärungen des Verfassers

(§ 9 Satz 2 Nr. 3 PromO BayNAT)

Hiermit versichere ich eidesstattlich, dass ich die Arbeit selbstständig verfasst und keine anderen als die von mir angegebenen Quellen und Hilfsmittel benutzt habe (vgl. Art. 64 Abs. 1 Satz 6 BayHSchG).

(§ 9 Satz 2 Nr. 3 PromO BayNAT)

Hiermit erkläre ich, dass ich die Dissertation nicht bereits zur Erlangung eines akademischen Grades eingereicht habe und dass ich nicht bereits diese oder eine gleichartige Doktorprüfung endgültig nicht bestanden habe.

(§ 9 Satz 2 Nr. 4 PromO BayNAT)

Hiermit erkläre ich, dass ich Hilfe von gewerblichen Promotionsberatern bzw. -vermittlern oder ähnlichen Dienstleistern weder bisher in Anspruch genommen habe noch künftig in Anspruch nehmen werde.

(§ 9 Satz 2 Nr. 7 PromO BayNAT)

Hiermit erkläre ich mein Einverständnis, dass die elektronische Fassung meiner Dissertation unter Wahrung meiner Urheberrechte und des Datenschutzes einer gesonderten Überprüfung unterzogen werden kann.

(§ 9 Satz 2 Nr. 8 PromO BayNAT)

Hiermit erkläre ich mein Einverständnis, dass bei Verdacht wissenschaftlichen Fehlverhaltens Ermittlungen durch universitätsinterne Organe der wissenschaftlichen Selbstkontrolle stattfinden können.

……

Ort, Datum Unterschrift (Madeleine Gold)